



Synthetic Nano- and Microfibers

Editors: R. Martijn Wagterveld, Jan C.M. Marijnissen, Leon Gradoń and Arkadiusz Moskal

Synthetic Nano- and Microfibers

Editors: R. Martijn Wagterveld, Jan C.M. Marijnissen, Leon Gradoń and Arkadiusz Moskal



PUBLISHED BY WETSUS, EUROPEAN CENTRE OF EXCELLENCE FOR SUSTAINABLE WATER TECHNOLOGY
[HTTPS://WWW.WETSUS.NL](https://www.wetsus.nl)

Copyright © 2020 R. Martijn Wagterveld

This work is licensed under the Creative Commons Attribution-NonCommercial 4.0 International License. To view a copy of the license, visit <https://creativecommons.org/licenses/by-nc/4.0/>.



ISBN: 978-1-71663-242-6

Front cover image: Artistic representation of plastic microfibers versus microparticles (from: freeimages.com, by Sorin Luca).

Book design by R. Martijn Wagterveld.

PRINTED BY GLASSTREE ACADEMIC PUBLISHING

First printing, September 2020

Preface

xi

Day One

1 Plastic and the Planet: How to take care of the next generation 3
By: Maria Westerbos

2 Micro- and nanofibers: aerodynamics and physicochemical aspect 5
By: Arkadiusz Moskal, Tomasz R. Sosnowski

2.1 Introduction 5

2.2 Fiber dynamics in the viscous fluid 5

2.3 Modeling of the dynamics of fibrous particles in viscous fluid 11

2.4 Micro- and nanofibers on the air/liquid interface 12

2.5 Fibrous-like particles and lung fluids 14

2.6 Conclusions 16

**3 Production of nano- and microfibers from synthetic and natural polymers -
 Nanofibers technology 19**
By: Michał Wojasiński, Tomasz Ciach

3.1 Introduction 19

3.2 Meltblowing 20

3.3 Electrospinning 21

3.4 Solution blow spinning 24

3.5 Centrifugal spinning 27

3.6 Conclusion 28

3.7 Acknowledgement 29

4	Questions and answers about synthetic fibers in wastewater treatment	35
	<i>By: Heather A. Leslie, Edited by R. Martijn Wagterveld</i>	
5	Measurement of nano- and microfibers in water and air: Physical and chemical methods.	37
	<i>By: Louk Peffer, R. Martijn Wagterveld, Jan. C.M. Marijnissen</i>	
6	Measurement of nanofibers in the breathing air	41
	<i>By: George Biskos, Jan C.M. Marijnissen</i>	
6.1	Introduction	41
6.2	Online physical characterization of nanofibers	42
6.2.1	Optical Sizing	42
6.2.2	Electrostatic Classification	43
6.2.3	The Fibre Aerosol Monitor	46
6.2.4	Aerodynamic classification	46
6.3	Integrated systems for determining the size and shape of aerosol nanoparticles	47
6.4	Online chemical analysis	49
6.5	Conclusions and future perspectives	50
7	A human risk banding scheme for high aspect-ratio materials	55
	<i>By: Dirk Broßell, Asmus Meyer-Plath, Kerstin Kämpf, Sabine Pnitzko, Wendel Wohlleben, Burkhard Stahlmecke, Martin Wiemann, Andrea Haase</i>	
7.1	Introduction	56
7.2	Risk banding and material properties required for HARM risk banding	57
7.2.1	Length	59
7.2.2	Respirability	61
7.2.3	Thickness (Rigidity)	61
7.2.4	Biopersistence	65
7.2.5	Release propensity (dustiness)	66
7.2.6	Dust agglomeration	67
7.2.7	WHO-fiber concentration	68
7.3	Summary of human risk banding for high aspect-ratio materials	71
7.4	Matrix for risk banding	71
7.5	Application in risk prediction for MWCNT	73
7.6	Conclusions and outlook	74
7.7	Acknowledgements	75
8	Deposition of synthetic fibers in human respiratory tract	81
	<i>By: Yung Sung Cheng, Wei-Chung Su, Yue Zhou</i>	
8.1	Introduction	81
8.2	Materials and Methods	83
8.2.1	Human nasal airway cast	83
8.2.2	Human respiratory airway casts	83
8.2.3	Fiber materials	84

8.3	Experimental setup	88
8.4	Sample preparation, fiber counting and length measurement	90
8.5	Results and discussion	91
8.5.1	Fiber deposition efficiency in the human nasal airway	91
8.5.2	Comparison of nasal deposition between fibers and compact particles	93
8.5.3	Fiber Deposition in the Human Oral Airway	95
8.5.4	Fiber deposition in the tracheobronchial airways	98
8.5.5	Empirical model for fiber deposition in the nasal airway	100
8.5.6	Empirical model for fiber deposition in the oral airway	101
8.5.7	Empirical model for fiber deposition in the tracheobronchial airway	102
8.5.8	Fiber exposure index	103
8.6	Conclusions	104

Day Two

9	Micro and nanoplastics in the aquatic environment with special reference to synthetic fibers	111
	<i>By: A. Dick Vethaak, C. Martínez-Gómez</i>	
9.1	Introduction	111
9.2	Sources, pathways and sinks	112
9.2.1	Major sources of MNPs	112
9.2.2	Sources of fibrous MNPs	113
9.2.3	Pathways and sinks	113
9.3	Composition of aquatic micro- and nanoplastic debris	113
9.3.1	Debris polymers	114
9.3.2	Chemical additives	114
9.3.3	Adsorption of chemical contaminants	114
9.3.4	Eco-corona, biofilm and biofouling	115
9.4	Factors that control degradation and fate of polymeric material	115
9.5	Physical and chemical quantification and characterization of MNPs	116
9.5.1	Analysis of microplastics in aquatic matrices	116
9.5.2	Analysis of microplastic fibers and nanoplastics	117
9.5.3	Uncertainties in aquatic MNP measurements	117
9.6	Occurrence of microplastics in aquatic systems	118
9.6.1	Microplastics in abiotic matrices	118
9.6.2	Microplastics in aquatic biota	119
9.7	Uptake and effects of MNPs on aquatic biota	122
9.7.1	Uptake	122
9.7.2	Physical effects	123
9.7.3	Chemical-mediated effects of MNPs	128
9.7.4	Microbial effects of MNPs	129
9.7.5	Potential ecological effects of MNPs	130
9.7.6	Field evidence and ecological relevance of laboratory studies	130

9.8	Key conclusions	130
9.9	Key knowledge gaps and research priorities	131
10	Micro(nano)plastics in aquatic organisms, transferability of knowledge from nanowires	147
	<i>By: Martina G. Vijver, Willie Peijnenburg, Fazel Abdolapur Monikh</i>	
10.1	Introduction	147
10.2	Aims of the chapter	148
10.3	Human exposure to micro(nano)plastics through food	148
10.4	Responses attributed to additives in micro(nano)plastics	149
10.5	Understanding responses attributed to MNPs in laboratory setting	149
10.6	Transferability of knowledge on nanowires to micro(nano)fibers	151
10.7	To summarize and recommend	153
11	Health effects of synthetic fibers and nanoparticles: Advanced electron microscopy to determine nanoparticle and nanoplastic <i>in vivo</i>	157
	<i>By: Uschi M. Graham, Günter Oberdörster</i>	
11.1	Introduction	157
11.2	Background	158
11.3	Analytical imaging techniques for nanoparticles/fibers in tissues	159
11.4	Select case studies of nanoparticle-tissue interactions	164
11.5	Synopsis	171
12	The intake of synthetic fibers into the human body, by food, water and air ...	175
	<i>By: Ingeborg M. Kooter, Heleen Lanfers, Wilma Middel, Harrie Buist</i>	
12.1	Introduction	175
12.1.1	The origin of plastics	175
12.1.2	Plastics, blessing or curse	175
12.1.3	What are microplastics and microfibers	175
12.1.4	Are microplastics and synthetic microfibers a threat to human health?	176
12.1.5	Reading guide	177
12.2	Sources of synthetic microfibers	178
12.3	External exposure to synthetic microfibers	182
12.3.1	Introduction	182
12.3.2	Air	182
12.3.3	Water	183
12.4	Human exposure routes	187
12.4.1	Introduction	187
12.4.2	Inhalation pathway	187
12.4.3	Oral pathway	187
12.4.4	Dermal pathway	190

12.5	Internal exposure and human uptake routes	190
12.5.1	Introduction	190
12.5.2	Uptake via inhalation	191
12.5.3	Uptake via ingestion	193
12.5.4	Uptake via the skin	194
12.6	Conclusion	194
13	An overview of the effects of synthetic micro(nano)fibers following exposure, with a focus on humans	201
	<i>By: Stephanie Wright</i>	
13.1	Introduction	201
13.2	Inferences from fiber toxicology	201
13.3	Plausible toxic properties of synthetic fibers	202
13.4	Occupational epidemiology of synthetic fibers	204
13.5	<i>In vivo</i> evidence	205
13.5.1	Mammalian models	205
13.5.2	Human studies	205
13.6	A potential for chemical effects?	206
13.7	Discussion	206
13.8	Conclusions, limitations and future work	207
14	Mechanics of fibrous particles immersed in selected flow conditions	211
	<i>By: Rafał Przekop, Leon Gradoń</i>	
14.1	Introduction	211
14.2	Modelling of fibrous particle deposition in a fibrous filter	213
14.2.1	The effect of gas velocity and fibre orientation on deposition efficiency	214
14.2.2	The effect of particle volume and slenderness ratio on the deposition efficiency	215
14.2.3	Effect of collectors orientation	217
14.2.4	Flexible aggregate model	217
14.3	Lattice-Boltzmann modelling	220
14.4	Results and discussion	221
14.5	Conclusions	222
15	Cleaning water from nano- and microfibers	227
	<i>By: R. Martijn Wagterveld, Inez J.T. Dinkla</i>	
15.1	Introduction	227
15.2	Nano- and microfibers in aquatic ecosystems	227
15.3	Techniques to remove nano- and microfibers	229
15.3.1	Separation at source	229
15.3.2	Waste water treatment plants	230
15.3.3	Alternatives to conventional treatment techniques	231
15.3.4	Approaches for nanofiber removal	234
15.4	Future perspective for waste water treatment	235

15.5	Conclusion	235
16	Workshop Summary and Conclusions	237
	<i>By: Stephanie Wright, Uschi M. Graham, Arkadiusz Moskal</i>	
	Index	241

Global production of fibrous material is significantly growing with expectation of reaching 145 million metric tons in 2030. Production includes mostly synthetic polymers fibers, cotton fibers and man-made cellulosic (viscose) fibers. A smaller contribution comes from animal-made fibers (wool, silk). The main uses of fibrous material are in clothing, household and furnishing, industrial construction, automotive and other.

Increasing consumption of fabric material causes the accumulation of single fibers into the natural environment. Significant numbers of fibers are discharged via wastewater from washing clothes, deposition from atmosphere or by other ways of transport. Fibers are now the most prevalent type of anthropogenic particles found by microplastic pollution surveys around the world. Substantial concentration of fibers have been detected in surface water, deep-sea and fresh water ecosystems. As a consequence fibers are present in food, drinking water, human lungs and digestive tracts of aquatic animals. Currently, there is great concern for the release of plastic nano- and micro fibers and microparticles (microplastics) to the natural environment for which nobody knows, so far, the ultimate consequences for health and ecological homeostasis.

The potential risk introduced by the presence of fibers in the environment induces significant interest of researchers in this problem as becomes clear from the increasing number of publications related to microplastics. For example, a comprehensive study of microfibers in oceanic surface water was recently published here: <https://advances.sciencemag.org>. The aforementioned challenges were the source of inspiration for organizing our workshop.

During November 4th and 5th, 2019, a group of scientists from different parts of the world met at Wetsus, the European Centre of Excellence for Sustainable Water Technology in Leeuwarden, The Netherlands, to discuss all known aspects of synthetic nano- and microfibers. This included the morphology, physicochemical properties, production and origin of nano/micro fibers entering the atmosphere, water and food chain; the potential consequences of inhalation and ingestion for human health, and exposure and ingress via life cycle for aquatic biota; analytical and measurement methods; techniques to clean air and water, and protection means against inhalation or other ways to enter the human body.

This workshop is the fifth in a series of very specialized workshops on aerosol particles and human health. The four former workshops were held in the Jablonna Palace near Warsaw, Poland. Now the fifth workshop, for the first time in Leeuwarden, the Netherlands, dealt with particles, in this case fibers, in both air and water. A group of top-experts from different disciplines, but all involved with small fibers, gathered to share their view from scientific, technical, and health perspective, presented their subject of expertise, and contributed to the discussion.

The chapters in this book have been placed in a logical sequence starting with the statement of the problem, properties of small fibers, fibrous particle identification, via environmental and health issues, and ending with possible cleaning methods. It is very evident that still much is not known and that in each discipline more must be investigated. For almost each sub-research program, reliable on-line measuring techniques are indispensable. We assume that this workshop presented the state of the art and will give directions on how to proceed to answer the many remaining questions. It is indisputable that it is essential to work together with all involved subdisciplines.

As mentioned, the workshop was held at Wetsus, in their very attractive, impressive and modern research centre. To make this workshop in line with the former four, which were held in the beautiful Jablonna Palace near Warsaw, the participants stayed for the nights in "Het Stadhouders Hof " (a former Stadtholder (Governor) Palace) in

Leeuwarden. The splendid dining room, completely decorated with paintings of the former noble inhabitants, served as venue for the workshop dinner. Besides the excellent food for the body, the participants were treated with food for the mind, with a special musical event. In the darkened hall at Wetsus, under blue light, the participants could almost feel themselves as suspended fibers in the sea as they were submerged by a marvellous performance by Jetje van Wijk (piano), Astrid Schijns (cello) and Rogier de Pijper (flute), of the very intriguing composition, “The Voice of the Whale” from the American composer George Crumb.

We would like to express our appreciation to Wetsus for making this workshop possible, providing the financial means, the location and support, before and during the workshop, with special thanks to ms. Linda van der Ploeg for her efficient and pleasant assistance.

Jan C.M. Marijnissen	Formerly Delft University of Technology/Wetsus
Leon Gradoń	Warsaw University of Technology
R. Martijn Wagterveld	Wetsus, European Centre of Excellence for Sustainable Technology
Arkadiusz Moskal	Warsaw University of Technology

Part I.
Day One

1. Plastic and the Planet: How to take care of the next generation

By: Maria Westerbos¹

1 – Plastic Soup Foundation, Sumatrakade 1537, 1019 RS Amsterdam, The Netherlands

Plastic is everywhere: in our kitchens and bathrooms, in our clothing, in our gardens. We've grown so accustomed to the convenience and all the advantages of plastic, you could even call it a worldwide addiction. And as a result, we have a worldwide environmental disaster on our hands. That's because plastic is not fully degradable and never actually decays. All the plastic that ever entered our environment is still there in one form or another. It's floating in our air, mixed into our groundwater, and sinks to the bottom of the ocean. Plastic is truly everywhere and it is penetrating our ecosystem, with a variety of negative consequences. Welcome to the **Plasticene**.

Despite all we already know about plastic's downsides, the production of polymer-based synthetic materials is still increasing. Economics prevails over ecology. If, in 2050, we produce the projected amount of over 1124 million tons – as compared to the 2020 production level of 420 million tons – we will emit nearly three times more plastic into our environment than we emit now. Once plastic is out there in the environment, it breaks up into countless miniscule particles. In the years ahead, we will see an exponential increase in the amount of microparticles and nanoparticles in particular. Even if 'only' three percent of that ends up in the ocean, soil or air, we're talking about 33 Milliard kilos of plastic.

We have created a plastic soup, and we've done so in a time span shorter than an average human being's life. The fast-growing world population is not good at dealing with this miracle product we call plastic. We're allowing it to pollute the planet at an unprecedented speed. In January 2019, the then just 16-year-old Greta Thunberg addressed the World Economic Forum in Davos, and said this:

"Adults keep saying 'we owe it to the young people to give them hope.' But I don't want your hope. I don't want you to be hopeful. I want you to panic. I want you to feel the fear I feel every day. And then I want you to act. I want you to act as you would in a crisis. I want you to act as if our house is on fire. Because it is."

Sir David Attenborough, also speaking in Davos, was just as provocative when he said, *"Global business, international co-operation and the striving for ideals: these are all possible because for millennia, on a global scale, nature has been largely predictable and stable. Now, in the space of one human lifetime – indeed in the space of my lifetime – all that has changed. The Holocene has ended. The Garden of Eden is no more..."*

Both of them, this famous young woman and even more famous old man, are right. Our planet is warming up and being choked by waste. Biodiversity is declining rapidly. The relationship between the plastic soup and climate

1. *Plastic and the Planet: How to take care of the next generation*

change has been proven. And yet, industry keeps finding ways to deny the seriousness of these threats and looks at the global crisis as an opportunity for ‘green’ growth.

To make matters worse, plastic is not only endangering our environment, but probably jeopardizing our health, too. We eat, drink and breathe plastic, which means tiny pieces of plastic are entering our bodies and – maybe - staying there. We also know the chemicals that are added to plastic can physically harm us, some of them very seriously. There appears to be a link between plastic in the human body and fertility problems, language acquisition problems, cancer, obesity and ADHD, though the causal relationship has not yet been conclusively proven.

That’s why we need to answer some urgent questions:

- How dangerous are plastic and plastic additives?
- Might our unborn children be in danger?
- Will plastic be our undoing in the future, if we continue along this path?
- How can plastic particles penetrate into our bodies?
- What role do size, shape and composition of the plastics play?
- Are there any discernable effects from pathogenic micro-organisms that attach themselves to plastics, and where in the body might we see these health effects?

The most prevalent microplastics and nanoplastics in our environment come from the clothing we wear and textiles we use. That’s because over 60% of our clothing is synthetic and this percentage continues to grow. A typical washing machine load weighing five kilos releases an average of nine million tiny fibers that enter the environment by way of our sewage systems. A recent study showed that every ten square centimeters of our ocean floors are littered with nearly 40 microplastics, most of which are microfibers.

It’s not just in the water. Another study, published in the scientific journal *Environment International* in late 2019, showed that our air is gradually being permeated by clothing fibers, too. The study revealed that London had the highest concentrations of airborne microplastics of all locations measured. The vast majority of those particles, 92%, are fibers originating from synthetic garments and carpets.

How was this study conducted? Twice per week over the course of a month, researchers counted the microplastics that landed on the roof of a nine-story building. Every sample contained more microplastics than were found in Paris or the Chinese city of Dongguan. London is probably the source of these particles, which are carried by the wind to a wider surrounding area. But it is difficult to establish precisely where these tiny fibers come from.

High concentrations of plastic dust cause all kinds of health problems. That’s why this study also points out that while there are worldwide efforts to reduce fine particle emissions from automotive traffic and wood-burning, hardly any initiatives exist to diminish airborne microfiber pollution.

Due to the annual growth in our plastic use and synthetic textiles in particular, the share of synthetic fibers in airborne dust will continue to increase. Therefore, we need more basic research to help us better understand how microplastics in general and micro-, nano-fibers in particular contribute to particulate matter-related health problems. Dr. Stephanie Wright of King’s College, who led the **research** in London, said, “An important next step in predicting risk is to estimate human exposure to airborne microplastics.”

To answer questions like this, we need – now more than ever – independent scientists who accelerate our discussion and sharpen our understanding of the problems we’re facing. An impressive number of such scientists contributed to this valuable book. I applaud their work.

Maria Westerbos
Founder and Director, Plastic Soup Foundation

2.

Chapter

Micro- and nanofibers: aerodynamics and physicochemical aspect

By: Arkadiusz Moskal¹, Tomasz R. Sosnowski¹

1 – Warsaw University of Technology, Faculty of Chemical and Process Engineering, ul. Waryńskiego 1, 00-645 Warsaw, Poland

2.1 Introduction

Fibrous micro- and nanoparticles are very common pollutants of the environment and they pose a real threat for health of living organisms, including human beings. The proper understanding of peculiar properties of fine fibers and their behavior in gases and liquids is a necessary condition of their effective removal from these media. At the same time, the knowledge on physical chemistry of nano- and microfibers helps to evaluate their toxic potential and to identify the pathways of specific material- and size-dependent interactions of fibers with organisms.

In this chapter we discuss the properties of fiber-like particles in a viscous fluid and indicate the potential impact of these properties on the processes of fibers removal from the aerosol. In the second part we focus on physicochemical interactions of fibers with wet deposition surfaces. Such analysis becomes important, e.g., in the assessment of toxic potential of inhaled fibers in the respiratory system which runs via their interactions with the bronchial mucus and the lung surfactant.

2.2 Fiber dynamics in the viscous fluid

The need for extremely clean air and water for many modern applications requires careful design of cleaning devices. The common solution for this problem is use of the oldest process in industry – filtration. Briefly speaking, the idea of filtration is to force contaminated fluid to flow through the porous structure, which may be built by cylindrical collectors (fibers). During the flow the particles suspended in fluid deposit on the surface of fibers. This process may ensure high filtration efficiency for given characteristics of particles simultaneously with a low pressure drop. However, only good understanding of particles dynamics during flow around cylindrical collector may give us proper designed filters because the transport properties (e.g. diffusion coefficient, mass transfer coefficient etc.) of particles strongly affect the filtration process. An important class of particle – fluid interactions involves transport and deformation of flexible fibers or elongated particles. Such systems are particularly challenging to study because the suspended fibers have many degrees of freedom in deformations. Globally, the dynamics of any particles in fluid may be described by the well-known Newton second law of dynamics. However, the detailed shape of the description depends on four crucial issues which should be taken into account during considerations, namely:

- (i) scale (size) of the particle comparing to the whole system under consideration;
- (ii) particle morphology;

2. Micro- and nanofibers: aerodynamics and physicochemical aspect

- (iii) intensiveness of the interactions with viscous fluid;
- (iv) material properties of the particle;

First of all, one should compare characteristic length of the particle to the scale of the system (Fig. 2.1).

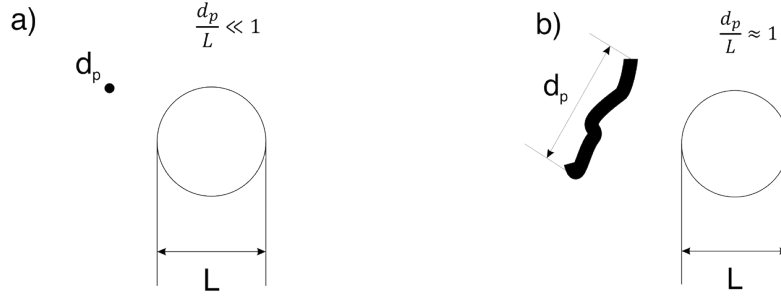


Figure 2.1.: The scale of the particle comparing to the scale of the collector; a) the particle is much smaller than the collector b) the particle size is similar to the collector.

If particle size is much smaller than scale of the system 2.1, then the particle during consideration may be reduced to the material point and its dynamics in viscous fluid is reduced to the ordinary differential equation for linear acceleration of particle mass center and may be described using equation called the generalized Baaset – Boussinesq – Oseen (BBO) equation [1–3]:

$$m_p \frac{d\mathbf{v}}{dt} = 3\pi\mu d_p (\mathbf{u} - \mathbf{v}) + \frac{1}{2}m_f \frac{d(\mathbf{u} - \mathbf{v})}{dt} + m_f \frac{D\mathbf{u}}{Dt} + \frac{3}{2}d_p^2 \sqrt{\pi\mu\rho} \int_0^t \frac{1}{\sqrt{t-\tau}} \frac{d(\mathbf{u} - \mathbf{v})}{d\tau} d\tau + \mathbf{F}^{EXT} \quad (2.1)$$

where \mathbf{v} is a vector of particle velocity¹, \mathbf{u} is vector of fluid velocity, μ and ρ are fluid viscosity and density, respectively. The first term on the right-hand side of this equation is the resultant *viscous drag and resistant force*². The second term (*virtual added mass force*) denotes the force necessary to accelerate half of the fluid mass m_f displaced by the particle. The third term is the force caused by pressure gradient created in the particle surrounding by accelerating fluid. The fourth term (*Basset force*) accounts for the whole history of the unsteadiness of the particle motion. The last term in equation 2.1 includes all other *external forces* acting on the particle (e.g., gravity, electrostatic interactions, etc.). The integration of the equation 2.1 allows to predict the trajectory of the particle in a given fluid flow field and predict the probability of collection on cylindrical obstacle in the filter structure. If scale of the particle is similar to the scale of the system (Fig. 2.1b), the morphology of the particle must be taken into account during description of its dynamics. One of the measures describing the morphology of the particle can be the fractal dimension [4]. Generally speaking, fractals are mathematical objects characterized by self-similarity. For our purpose, when the real particles are not the fractals in mathematical sense, we can treat the fractal dimension as the information about the distribution of mass in particle relative to its center of gravity (Fig. 2.2).

One may distinguish the relation: smaller fractal dimension describes the structures more open and in the limiting case when $D_f \rightarrow 1.0$ we have fiber-like particles. On the other hand, higher value of fractal dimension describes the structures more compact and in the limiting case when $D_f \rightarrow 3.0$ we have sphere like particles. In these cases, where morphology of particles should be taken into account to describe dynamics of particles in fluid flow, the description of linear translation of mass center is not enough. The particle is able to rotate over its center of mass so one should add the equation for angular acceleration of the entire particle. The set of the equations describing the dynamics of

¹The particle is assumed to be a sphere with diameter d_p , but only the translational acceleration of its center of mass is under consideration.

²We take into consideration only laminar flow of the fluid, so Stokes law is fulfilled.

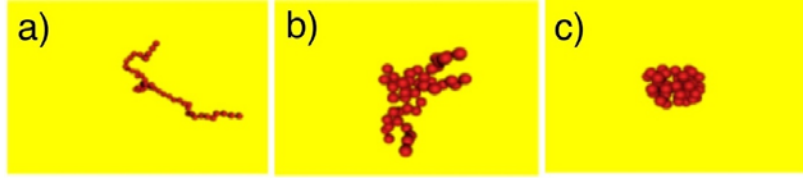


Figure 2.2.: Example of aggregates built by 50 identical primary particles. The distribution of mass relative to the center of gravity is described by different value of fractal dimension a) $D_f = 1.2$ b) $D_f = 1.6$ c) $D_f = 2.2$.

particle becomes as follows:

$$\frac{d\mathbf{v}}{dt} = \frac{1}{m} \sum \mathbf{F} \quad (2.2)$$

$$\frac{d\boldsymbol{\omega}}{dt} = \mathbf{J} \sum \mathbf{M}_G \quad (2.3)$$

where the m is particle mass, $\boldsymbol{\omega}$ is angular velocity, \mathbf{F} is a sum of all forces acting on the particle, \mathbf{M}_G is a sum of all moments relative to particles center of gravity, and \mathbf{J} is a symmetric second order tensor called *angular mobility around the mass center* calculated using the tensor of inertia about particle mass center, \mathbf{A} , as follows:

$$\mathbf{J} = \mathbf{A}^{-1} \quad (2.4)$$

$$\mathbf{A} = \begin{bmatrix} I_{xx} & -I_{xy} & -I_{xz} \\ -I_{xy} & I_{yy} & -I_{yz} \\ -I_{xz} & -I_{yz} & I_{zz} \end{bmatrix} \quad (2.5)$$

In many cases the morphology of particles can be described using well known geometrical shapes which allow to easily calculate its tensor of inertia. For solid sphere of radius r and mass m :

$$\mathbf{A} = \begin{bmatrix} \frac{2}{5}mr^2 & 0 & 0 \\ 0 & \frac{2}{5}mr^2 & 0 \\ 0 & 0 & \frac{2}{5}mr^2 \end{bmatrix} \quad (2.6)$$

and for slender rod along y-axis of length l and mass m rotating about center of mass:

$$\mathbf{A} = \begin{bmatrix} \frac{1}{12}ml^2 & 0 & 0 \\ 0 & 0 & 0 \\ 0 & 0 & \frac{1}{12}ml^2 \end{bmatrix} \quad (2.7)$$

In all this cases, the mass distribution relative to the center of gravity affects the dynamics of the particles. The integration of the set of equations 2.2 and 2.3 allows to predict trajectory of the particle in a given fluid flow field but to do so, first one should describe all forces in the system. The dominant forces in our case are the forces of particle

2. Micro- and nanofibers: aerodynamics and physicochemical aspect

interactions with viscous fluid [5]. If we assume that the particle is immersed in Newtonian fluid of (temperature T , shear viscosity μ) that is moving with strain rate $\dot{\gamma}$, and the inertial forces can be neglected³, we can distinguish four main interactions which are at play:

Brownian forces:

$$\mathbf{F}_B \sim \frac{k_B T}{d_p} \quad (2.8)$$

Drag forces:

$$\mathbf{F}_D \sim \mu \dot{\gamma} d_p^2 \quad (2.9)$$

Elasticity forces:

$$\mathbf{F}_E \sim \frac{E}{d_p^2} \quad (2.10)$$

And gravitational forces:

$$\mathbf{F}_G = m\mathbf{g} \quad (2.11)$$

where the flexural rigidity $E = YI$ (Y is the material Young's modulus and I is the areal moment of inertia⁴), k_B is Boltzmann constant, and g is gravitational acceleration. To assess the contribution of individual forces, one can calculate the value of characteristic numbers which illustrate the process, such as Peclet number:

$$\text{Pe} = \frac{8\pi\mu\dot{\gamma}d_p^3}{k_B T} \quad (2.12)$$

which gives us an information about the intensity of particles transport by viscous convection comparing to transport by Brownian diffusion, and

$$l_p = \frac{E}{k_B T} \quad (2.13)$$

being the persistence length of the fiber against thermal fluctuations. For fibers with length of a few micrometers submersed in water of temperature 25 °C which flows with strain rate equal to 1.0 s⁻¹, the value of Pe is in the range of few hundred which means that the viscous drag forces govern the transport process and the Brownian diffusion may be neglected during considerations. However, when the characteristic length of fiber decreases, especially into submicron region, the Peclet number decreases and the stochastic Brownian forces become important and affect the dynamics of the fiber. The crucial parameter become the persistence length of the fiber against thermal fluctuations which gives the information about elastic deformation of fiber versus Brownian excitation. For synthetic fibers with material modulus Y about 1 GPa and aspect ratio⁵ $\varepsilon = 10^{-2}$ immersed in water, $\frac{l_p}{d_p} \sim 10^{-2}$ which means that the Brownian forces can be neglected comparing to elastic forces. However, for semi-flexible polymers as well as actin filaments with aspect ratio reduced to $\varepsilon = 10^{-3}$ and material modulus Y equal to 0.1 GPa, the $\frac{l_p}{d_p} \sim 1$ so the

³This assumption is valid for colloidal systems;

⁴In the case of cylindrical fiber $I = \frac{\pi r^4}{4}$ where the r is the radius of perpendicular cross section of the fiber.

⁵Geometric aspect of the fiber is the ratio of the radius of perpendicular cross section of the fiber to the length of the fiber.

Brownian excitations should be taken into account because they strongly affect the fiber dynamics. It means that the material and size of the fiber strongly determine its behavior in fluid. In the case of stiff particles, as a limit situation, one may assume that the particle is perfectly rigid which makes the description of the dynamics much simpler but still not easy. When the Brownian interactions are significant, one has the relation between the diffusion tensor and the hydrodynamic properties of a rigid body that provides a linear relationship between velocities and angular velocities to forces and torques acting on the particle. This relationship allows us in many cases to describe the morphology of the fiber by simple geometrical shapes, such as spheres, spheroids, cylinders, for which the elements of diffusion tensor are known. In the simplest case, when the particle may be described as a sphere and one should take into account the stochastic Brownian interactions, the eq. 2.1 transforms into stochastic differential equation known as *Langevin equation*⁶. Implementation of the numerical methods of the Brownian motion simulations using *Langevin equation* yields several different Brownian Dynamics algorithms [6] which allow to predict the stochastic trajectory of the particle in a given system and elements of diffusion tensor using the trajectory sampling method [7]. It should be borne in mind that in any case of random particle motion the computational cost is much higher than for deterministic particle motion as the simulations have to be performed for a large ensemble of particles to obtain statistically significant averaged results. In the case when the morphology of the particles can be described by spheroid shape (Fig. 2.3), the elements of the diffusion tensor are easy to establish:

$$D_a = \frac{k_B T \left[\ln \left(\frac{d_p}{r} \right) - 0.5 \right]}{2\pi\mu d_p} \quad (2.14)$$

$$D_b = \frac{k_B T \left[\ln \left(\frac{d_p}{r} \right) - 0.5 \right]}{4\pi\mu d_p} \quad (2.15)$$

$$D_\theta = \frac{3k_B T \left[\ln \left(\frac{d_p}{r} \right) - 0.5 \right]}{2\pi\mu d_p^3} \quad (2.16)$$

where d_p and r denote the length and radius of the spheroid ($d_p \gg r$).

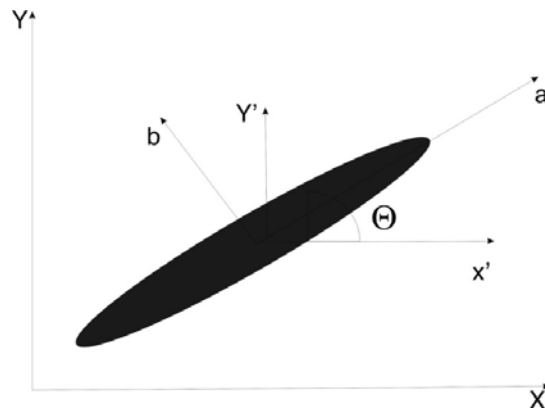


Figure 2.3.: Brownian movement of the spheroid particle, D_a , D_b denote the translational diffusion coefficients along and perpendicular to the particle's main axis, D_θ is the rotational diffusion perpendicular to the main axis of the particle.

⁶in such case the right hand side of the equation 2.1 contains only drag and resistance force, external forces and stochastic Brownian force.

2. Micro- and nanofibers: aerodynamics and physicochemical aspect

The problem becomes more complicated when one should characterize the diffusion transport (for small particles) or convective transport (for large particles) of flexible elongated objects, such as nanofilaments, long molecular chains or synthetic or natural fibers. There are not just translational and rotational motion of the objects which should be analyzed but also multifunctional shape variation. There is no unique method for characterizing the diffusivity of such objects because the internal and external mechanical interactions affect the process together with the shape and particle geometry. In general, the set of partial differential equations must be used to describe the dynamics of such an object. The interesting mathematical approach to describe flexible objects dynamics was presented by Podgórski, Gradoń, and Grzybowski [8] but this approach was limited only to two cases: the perfect rigid body and the perfect flexible fiber, i.e. the elongated inextensible body having no stiffness for bending. Even for this ideal case the integration of set of partial differential equations is very difficult and time-consuming. Hence, it is necessary to introduce several simplifications to build models more useful and suitable for predictions of particles behavior at reasonable costs and time. The numerical analysis of the process can be supported by the experimental observations of the dynamics of fibers. There are many experimental works mainly based on the microscopic observations of fibers in microfluidic flow under different conditions [9–11]. To reduce the complexity of the mathematical description of the flexible particles one can use the most common approach, proposed by Kratky and Porod [12] in which the complex shape variations of an object are described by a chain of spherical subunits (Fig. 2.4).

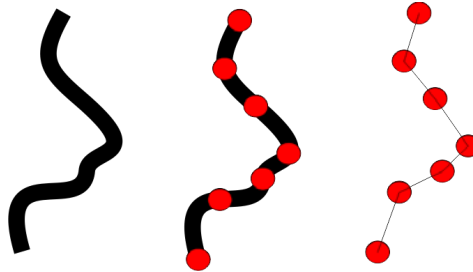


Figure 2.4.: The idea of describing the fiber as a chain of spherical subunits connected by springs.

Its dynamic structure may be regarded as a behavior of elements connected by springs where the internal force between elements can be described as follows:

$$F_{ij}^s = -k_s (r_{ij} - r_{ij}^0) - f_d \frac{dr_{ij}}{dt} \quad (2.17)$$

where k_s is a spring constant and f_d is a dumping factor of oscillations, indexes i, j denoting i^{th} and j^{th} subunit in chain. Using this simple idea, Żywczyk and Moskal [13] introduced the model of the behavior of flexible particles in a flow of viscous fluid. However, in their model the internal interactions between spherical subunits were extended by adding the bending force, torque force and inversion force to get more realistic behavior. In the case, when the fiber is described by chain containing N primary spherical subunits, the dynamics of such system is written in sets of ordinary differential equations in a form:

$$m_i \frac{dv_i}{dt} = \phi_i (U - v_i) + F_i^B + \sum_{i=1}^N F_{ij}^s + \sum_{i=1}^N F_{ij}^{bending} + \sum_{i=1}^N F_{ij}^{torque} + \sum_{i=1}^N F_{ij}^{inversion} + f_d v_i \quad (2.18)$$

where m_i is mass of subunit, ϕ_i is a drag and resistance coefficient for subunit, U is fluid velocity in a place occupied by subunit, F^B is Brownian force acting on subunit. The integration of those equations in a given fluid flow field gives the information about the trajectory of the particles in the system.

2.3 Modeling of the dynamics of fibrous particles in viscous fluid

To demonstrate the influence of the morphology and material properties of the particles on their dynamics during the transport in viscous fluids two important examples may be recalled: filtration of elongated particles in fibrous filters and the sedimentation of fibers. Saggiorato, Elgeti, Winkler, and Gompper [14] investigated the influence of the flexibility of the fiber on its sedimentation. The material properties were introduced into parameter B :

$$B = \frac{F_g d_p^2}{E} \quad (2.19)$$

where F_g is gravitational force. For stiff fibers (small B) only small bending into V shape occurred (Fig. 2.5). For more flexible fiber, one can see the drift of the fiber sideways. For even more flexible fiber, the symmetries are spontaneously broken, and the fiber rotates following a helical trajectory. The residence time in the system increases for flexible fibers which means that such fibers are more difficult to sediment in a given volume of the apparatus comparing to the stiff fibers or to the equivalent spherical particles.

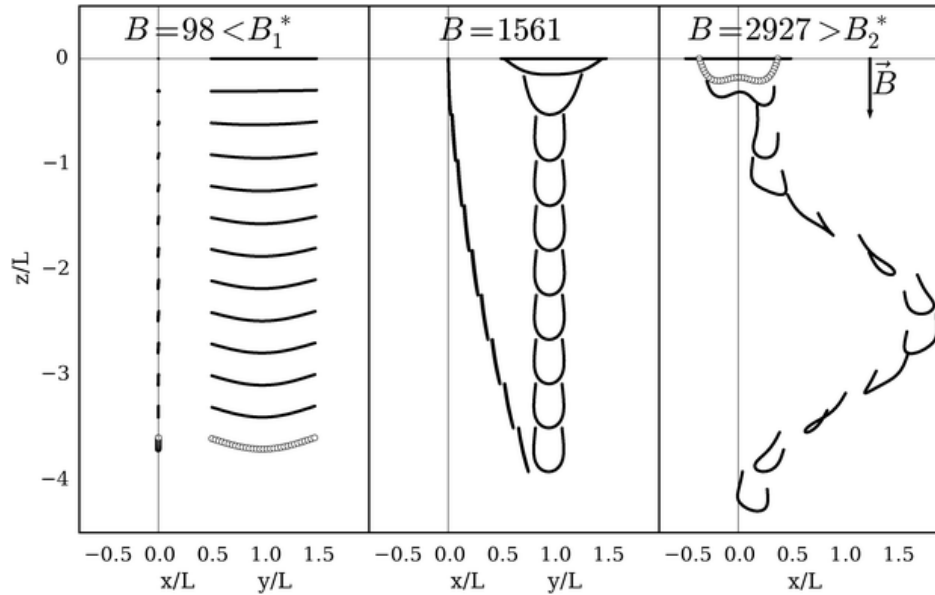


Figure 2.5.: Sedimentation of single fiber for different values of parameter B . (From: Saggiorato, Elgeti, Winkler, and Gompper [14].)

Using the equation 2.18, Żywczyk and Moskal [13], performed numerical simulations of the filtration process of flexible aggregates collected by spherical primary particles with different fractal dimensions on a single fiber placed in the Kuwbara cell. The results obtained during calculations are presented in Figs 2.6 and 2.7. As one can see in Fig. 2.6, decreasing the fractal dimension of the aggregates (when aggregates shape looks more like a fiber) leads to the decrease in filtration efficiency, which means that the filtration of fiber particles is more difficult than of spherical ones. The explanation of this phenomenon is difficult but, briefly speaking, fibers have higher possibility to follow the streamlines in the system which allows them to avoid the deposition.

In Fig. 2.7 one can see another important result: increasing the velocity of fluid decreases the deposition efficiency of the particles. This phenomenon may be explained by the fact that higher deformation which takes place in stronger flows results in a higher probability of particle penetration through the filter. The presented data are similar to those obtained by Podgórski [6]. As a conclusion, one can say that the filtration of fibers and elongated aggregates (with

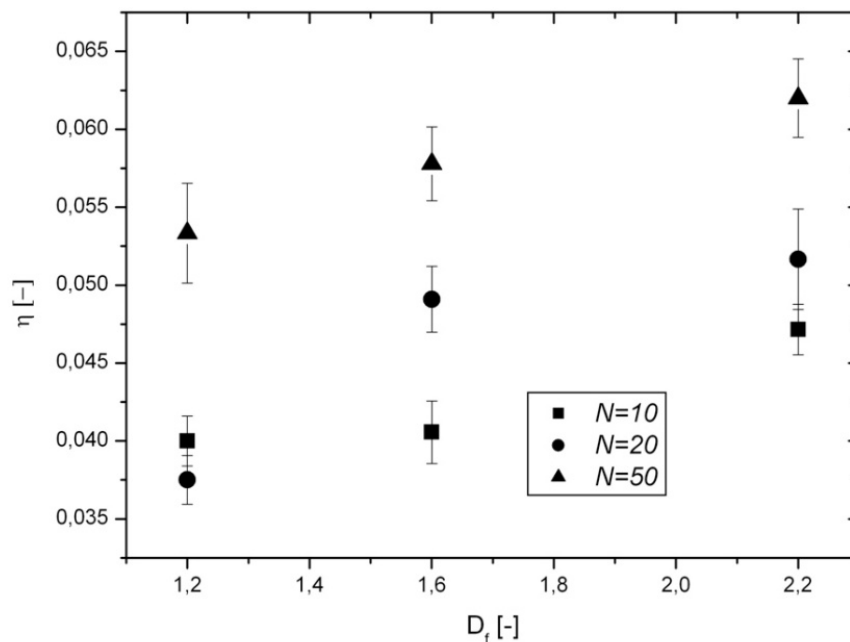


Figure 2.6.: The filtration efficiency for different flexible particles as a function of their morphology described by fractal dimension. N denotes number of primary spherical particles in aggregate.

small fractal dimension) is more difficult which means that such an object are more hazardous and can penetrate into human body via inhalation. In such situation they land on the wet surface of the lungs and this initiates fibers interactions with the liquid which will be addressed in the next sections.

2.4 Micro- and nanofibers on the air/liquid interface

In the micro- and nanoscale, surface interactions often predominate over other forces. Therefore, the fate of fibers after they touch the gas/liquid interface, depends mainly on the capillary forces. The orientation of fibers that is achieved on the fluid interface minimizes the energy of surface interactions. The equilibrium state requires some immersion of the fiber, and it depends on fiber weight (density) and wetting properties. In general, fibers and needles are lying flat on the liquid surface, however high concentration of fibers favors both more tilted orientation and fiber aggregation on the interface [15]. It has been also demonstrated that flat orientation of nanofibers on the fluid-fluid interface makes them act as stabilizers of two-phase dispersions (emulsions or foams) [16]. Small fibers which arrive with the gas are immobilized on the surface of liquid due to the capillary forces, unless they are not too heavy, which means that they are characterized by the small value of Bond number: $Bo = \frac{r^2 \Delta \rho g}{\sigma}$ (where r – particle radius, σ - the surface tension). In such conditions, as discussed by Binks and Horozov [17], the free energy of the detachment of idealized rod-like particle with rounded ends (Fig. 2.8a) from the planar interface is expressed by:

$$\Delta G = \sigma \pi r^2 (1 - \cos \theta)^2 \left[1 + \frac{4 \left(\frac{a}{r} - 1 \right) (\sin \theta - \theta \cos \theta)}{\pi (1 - \cos \theta)^2} \right] \quad (2.20)$$

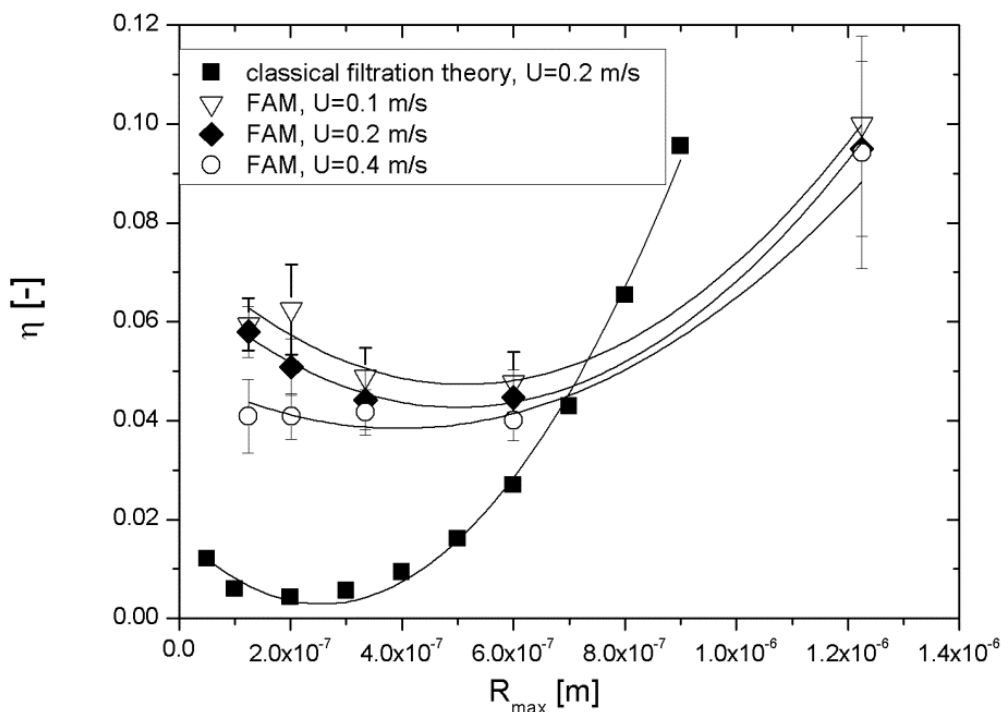


Figure 2.7.: The filtration efficiency for different flexible particles as a function of their maximal radius for different values of fluid velocity. Black squares indicate the results obtained for spherical particles with equivalent mass using classical filtration theory.

Considering this, it is clear that the spontaneous detachment of such idealized fibers from the air/liquid interface requires the input of energy which is a few orders of magnitude higher than the energy of thermal fluctuations of fluid molecules. However, the detachment (sinking) of fibers having density greater than water is favored if fibers are hydrophilic and the surface tension of liquid is low. Obviously, mechanical disturbances of the interface also facilitate their displacement to the liquid phase. An important issue for fiber stability at the fluid/fluid interface is the effective contact angle which defines fiber wettability. It is known, that even materials which are hydrophilic in a macroscopic sense, can be poorly wetted by water in a micro- or nanoscale due to structural features of the surface. Microscopically rough surface of a fiber allow to trap air bubbles making the fiber more hydrophobic, Fig. 2.9 (e.g., Wang, Elimelech, and Lin [18]). This effect can influence the forces of adhesion of deposited fibers to the air-water interface.

Obviously, only fibers made of materials with the density higher than water can sink and be distributed in the volume of the aqueous phase. Polymeric fibers which are sometimes lighter than water (e.g., PE - density: 0.88 g cm^{-3} to 0.92 g cm^{-3} , PP - density: 0.86 g cm^{-3} to 0.95 g cm^{-3}) will not sink, but in the real world they may be colonized by microorganisms (e.g., Dussud, Hudec, George, Fabre, Higgs, Bruzard, Delort, Eyheraguibel, Meistertzheim, Jacquin, et al. [19]). This increases the effective density of such structures and help them to sink. The fibers in the environment also undergo ageing which changes their properties and allow them to be more easily distributed in the aqueous phase. However, another question arises: if and how fibers which have already got fully immersed and distributed in water, e.g. in the sea/ocean, can be transferred to the gaseous phase (the air). The only explanation is that they have to be contained in droplets which are formed by splashing, for instance by waves and bubbles formed in the sea due to

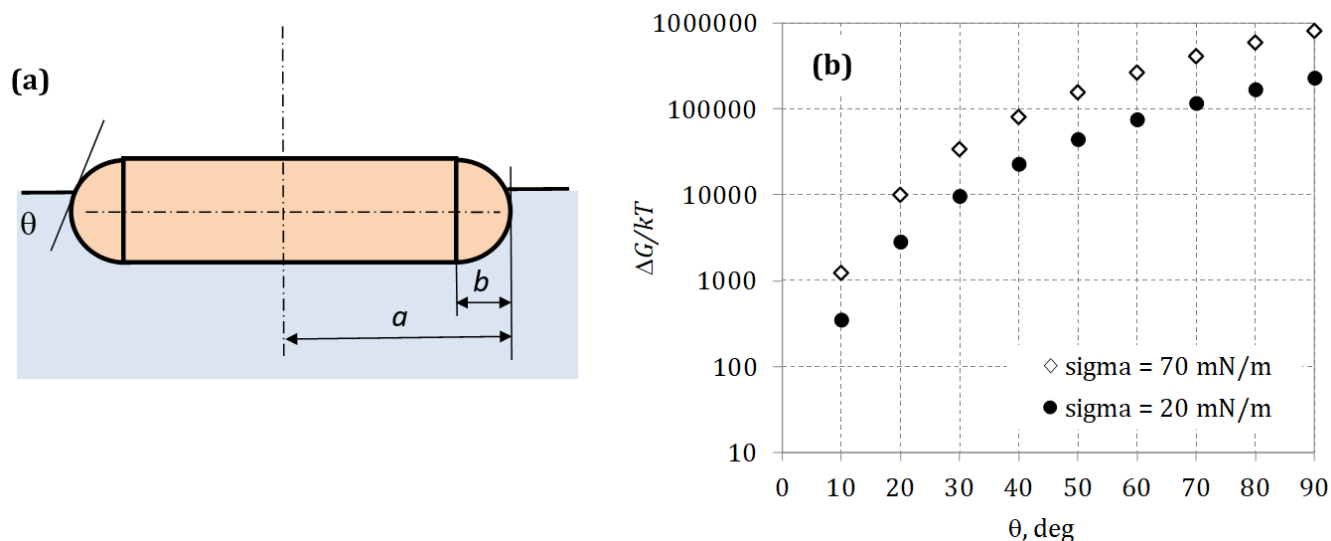


Figure 2.8.: Equilibrium position of rod-like particle at air/liquid interface (modified after Binks and Horozov [17]); (b) Normalized free energy of particle detachment from air/liquid interface for different contact angles θ and two values of the surface tension. Calculated from Eq. 2.20, for particle radius 50 nm and aspect ratio, $\frac{a}{b} = 5$.

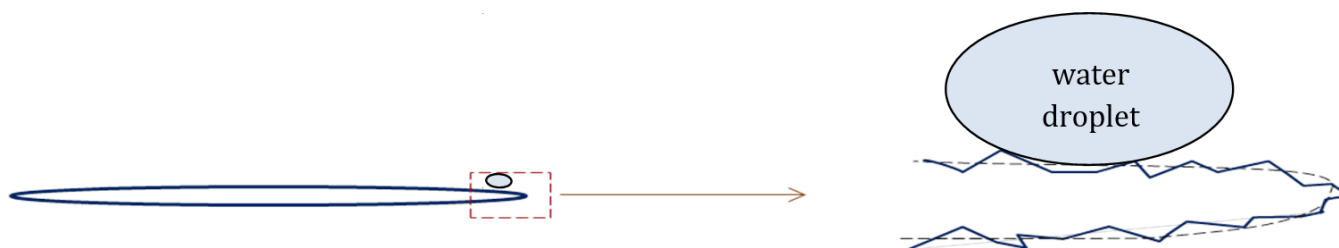


Figure 2.9.: Surface roughness as a factor in the effective wettability of fibers.

wind. These droplets evaporate in the air, so eventually the aerosol of free fibers can be formed. Accordingly, fibers which form the contamination of surface water may be released and spread in the atmosphere, so they can spread and deposit even in distant locations [20]. If fibers contained in the air are small enough, they may be also inhaled by humans [21].

2.5 Fibrous-like particles and lung fluids

The conducting ducts of the respiratory tract (naso-oro-pharynx and bronchial tree) act as a filter for inhaled particulates, however it is known that fibrous particles easily penetrate to the deep lungs (pulmonary region), [22]. Fibers deposited in bronchi are captured by mucus and removed by the mucocilliary clearance. The bronchial mucus is a layer of viscous gel-like liquid, so the fibers have very low chance to penetrate across this protective blanket and reach the epithelial cells. On the other hand, fibers which reach the pulmonary part of the lungs, land on the ultrathin layer of the alveolar liquid that contains the lung surfactant (LS). LS is composed of lipids and proteins so all deposited particles will directly contact with these compounds. The interactions of particles with LS may be modeled by in vitro experiments which allow to trace the important physicochemical effects at the air/liquid interface of the lungs. Such investigations allow to study LS dynamics during breathing cycle, i.e., during periodical variations of the pulmonary are, and the numerical analysis of experimental results may be facilitated by the application of 2D rheology

[23, 24]. Disturbance in the rheological properties of the air/liquid interface of LS are associated with the alterations of mass transfer processes in the pulmonary region [23–25]. Recent data demonstrated that elongated (fiber-like) particles can notably change the apparent rheological properties of the oscillated air-liquid interface of the LS solution. The results showed that these effects depend on some geometrical factors, including the particle specific surface area, the wettability and the total concentration of the particles [26]. Fig. 2.10 shows that the influence of carbon nanowires (nanotubes) on the dynamic properties of the air/liquid interface in a model LS system is concentration-dependent, however other properties of these nanomaterials should not be neglected. The figure shows that even if the specific surface area of particles Type I and II is similar ($400 \text{ m}^2 \text{ g}^{-1}$ to $450 \text{ m}^2 \text{ g}^{-1}$), the difference in the effects can depend e.g., on the particle aspect ratio. The aspect ratio of Type I nanotubes is much higher ($\sim 10^3$) than of Type II (below 30). It seen that surface viscosity is only slightly changed with particle concentration, however surface elasticity is notably altered, increasing to 160 and 250% of the control value (in “pure” LS) for 1 mg ml^{-1} of Type I and Type II nanotubes, respectively. This means that the nanotubes cause a stiffening of the air/liquid interface which probably can be attributed to formation of particle-surfactant complexes or particle aggregates at the liquid surface [27, 28]. Such variations in surface elasticity and viscosity are related to changes in the surface tension hysteresis which is recognized to be an indicator of the natural dynamics of healthy lungs (e.g., [23, 24, 29]). Therefore, the effects of elongated micro-/nanoparticles on the surface activity of LS may result in the adverse changes in the lung physiology, including breathing mechanics and pulmonary mass transfer. This suggests that inhaled elongated particles may create a health risk even if they are not recognized to be directly toxic.

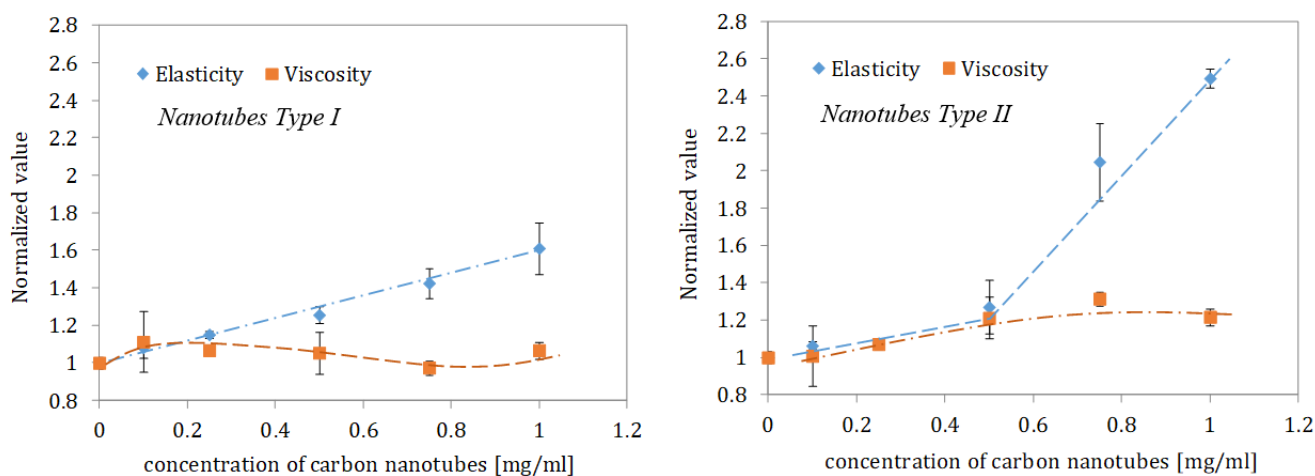


Figure 2.10.: Normalized value of the surface elasticity and surface viscosity of the air/liquid interface of LS solution (Survanta[®]) with different concentrations of two types of carbon nanotubes. Unit values correspond to LS without nanoparticles. Surface oscillation rate: 0.25 Hz, $T = 36.8 \pm 0.2 \text{ }^\circ\text{C}$.

Molecular modeling of nanotubes behavior at the air/liquid interface of the lung surfactant system confirmed that surfactant components can form a “corona” on the particle surface [30]. This event results in both the modification of particle surface properties and depletion of the local concentration of surface active molecules on the lung surface. These mechanisms cause that fiber-like particles become wetted and more immersed in the pulmonary fluid. At the same time they can induce a disturbance the interfacial phenomena in the LS system. Discussion of fibers interaction with the pulmonary surface must also account for the size of deposited fibers in relation to the dimensions of alveolar structures. As shown in Fig. 2.11, fiber diameter may be larger than the depth of the alveolar liquid. In such situations the above discussed phenomena related to fiber immersion and floatability become less important.

Large fibers can touch the tissue without sensing any barrier effect of the surfactant layer and this can explain their direct impact on the alveolar cells. Geometrical dimensions may also reduce the possibility of fiber neutralization by

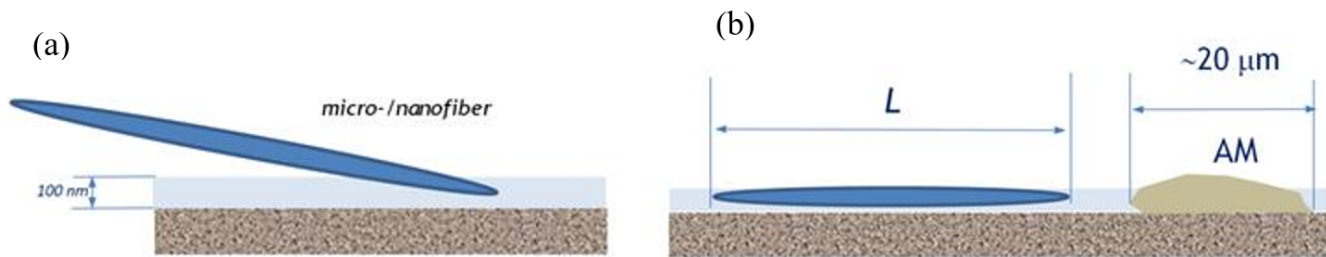


Figure 2.11.: Long fibers or needles may be not fully immersed in the pulmonary fluid (a) and they can also avoid neutralization by alveolar macrophages – AMs (b).

alveolar macrophages (AMs) on the pulmonary surface and this will extend the retention time of deposited fibers. Moreover, long fibers can also cause destruction of AMs with a release of lysosomal fluid, inducing the inflammation in the alveoli [31].

2.6 Conclusions

In this chapter we discussed the specific behavior of fibrous particles in the air taking into account the specific mechanical conditions of their movement in fluids. The important consequence of fibers shape and deformability is that they are more difficult to remove from the fluid phase by conventional mechanisms which are more effective for particles of compact shapes. The analysis of the physicochemical behavior of elongated particles present on the air-liquid interface showed that such particles strongly adhere to the liquid surface, and that this process is dependent on fiber wettability, density and aspect ratio. Fibers concentration may influence their aggregation and reorientation on the interface, and the fibers will sink more easily if the surface tension of liquid is low. Such situation can be observed in the lungs where the surface tension is significantly reduced by the lung surfactant. Elongated particles (e.g., nanotubes) may be wetted also due to adsorption of surfactant molecules to the particle surface. This process, in turn, can reduce local concentration of the surfactant in the lung fluid, inducing undesirable effects for health. The information highlighted in this chapter should help to recognize the specific properties and behavior of fiber-like particles in selected environmental and health-related aspects.

References

- [1] A. B. Basset. *A treatise on hydrodynamics: with numerous examples*. Volume 2. Deighton, Bell and Company, 1888 (cited on page 6).
- [2] J. Boussinesq. *Théorie analytique de la chaleur mise en harmonie avec la thermodynamique et avec la théorie mécanique de la lumière: Tome I-[II]...* Volume 2. Gauthier-Villars, 1903 (cited on page 6).
- [3] C. W. Oseen. “Neuere methoden und ergebnisse in der hydrodynamik”. In: *Leipzig: Akademische Verlagsgesellschaft mb H.* (1927) (cited on page 6).
- [4] B. B. Mandelbrot. “Self-affine fractals and fractal dimension”. In: *Physica scripta* 32.4 (1985), page 257 (cited on page 6).
- [5] O. Du Roure, A. Lindner, E. N. Nazockdast, and M. J. Shelley. “Dynamics of flexible fibers in viscous flows and fluids”. In: *Annual Review of Fluid Mechanics* 51 (2019), pages 539–572 (cited on page 8).
- [6] A. Podgórski. “On the transport, deposition and filtration of aerosol particles in fibrous filters: Selected problems”. In: *Prace Wydziału Inżynierii Chemicznej i Procesowej Politechniki Warszawskiej* 28.1 (2002), pages 3–207 (cited on pages 9, 11).
- [7] A. Moskal and A. Payatakes. “Estimation of the diffusion coefficient of aerosol particle aggregates using Brownian simulation in the continuum regime”. In: *Journal of aerosol science* 37.9 (2006), pages 1081–1101 (cited on page 9).

- [8] A. Podgórski, L. Gradoń, and P. Grzybowski. “Theoretical study on deposition of flexible and stiff fibrous aerosol particles on a cylindrical collector”. In: *The Chemical Engineering Journal and the Biochemical Engineering Journal* 58.2 (1995), pages 109–121 (cited on page 10).
- [9] J. Gross, S. Sayle, A. R. Karow, U. Bakowsky, and P. Garidel. “Nanoparticle tracking analysis of particle size and concentration detection in suspensions of polymer and protein samples: influence of experimental and data evaluation parameters”. In: *European Journal of Pharmaceutics and Biopharmaceutics* 104 (2016), pages 30–41 (cited on page 10).
- [10] V. Filipe, A. Hawe, and W. Jiskoot. “Critical evaluation of Nanoparticle Tracking Analysis (NTA) by NanoSight for the measurement of nanoparticles and protein aggregates”. In: *Pharmaceutical research* 27.5 (2010), pages 796–810 (cited on page 10).
- [11] D. Mukhija and M. J. Solomon. “Translational and rotational dynamics of colloidal rods by direct visualization with confocal microscopy”. In: *Journal of colloid and interface science* 314.1 (2007), pages 98–106 (cited on page 10).
- [12] O. Kratky and G. Porod. “Röntgenuntersuchung gelöster fadenmoleküle”. In: *Recueil des Travaux Chimiques des Pays-Bas* 68.12 (1949), pages 1106–1122 (cited on page 10).
- [13] Ł. Żywczyk and A. Moskal. “Modelling of deposition of flexible fractal-like aggregates on cylindrical fibre in continuum regime”. In: *Journal of Aerosol Science* 81 (2015), pages 75–89 (cited on pages 10, 11).
- [14] G. Saggiorato, J. Elgeti, R. G. Winkler, and G. Gompper. “Conformations, hydrodynamic interactions, and instabilities of sedimenting semiflexible filaments”. In: *Soft matter* 11.37 (2015), pages 7337–7344 (cited on page 11).
- [15] E. L. Sharp, H. Al-Shehri, T. S. Horozov, S. D. Stoyanov, and V. N. Paunov. “Adsorption of shape-anisotropic and porous particles at the air–water and the decane–water interface studied by the gel trapping technique”. In: *RSC advances* 4.5 (2014), pages 2205–2213 (cited on page 12).
- [16] I. Kalashnikova, H. Bizot, B. Cathala, and I. Capron. “New Pickering emulsions stabilized by bacterial cellulose nanocrystals”. In: *Langmuir* 27.12 (2011), pages 7471–7479 (cited on page 12).
- [17] B. P. Binks and T. S. Horozov. *Colloidal particles at liquid interfaces*. Cambridge University Press, 2006 (cited on pages 12, 14).
- [18] Z. Wang, M. Elimelech, and S. Lin. “Environmental applications of interfacial materials with special wettability”. In: *Environmental science & technology* 50.5 (2016), pages 2132–2150 (cited on page 13).
- [19] C. Dussud, C. Hudec, M. George, P. Fabre, P. Higgs, S. Bruzard, A.-M. Delort, B. Eyheraguibel, A.-L. Meistertzheim, J. Jacquin, et al. “Colonization of non-biodegradable and biodegradable plastics by marine microorganisms”. In: *Frontiers in microbiology* 9 (2018), page 1571 (cited on page 13).
- [20] S. Allen, D. Allen, V. R. Phoenix, G. Le Roux, P. D. Jiménez, A. Simonneau, S. Binet, and D. Galop. “Atmospheric transport and deposition of microplastics in a remote mountain catchment”. In: *Nature Geoscience* 12.5 (2019), pages 339–344 (cited on page 14).
- [21] J. Gasperi, S. L. Wright, R. Dris, F. Collard, C. Mandin, M. Guerrouache, V. Langlois, F. J. Kelly, and B. Tassin. “Microplastics in air: are we breathing it in?” In: *Current Opinion in Environmental Science & health* 1 (2018), pages 1–5 (cited on page 14).
- [22] M. Lippmann. “Effects of fiber characteristics on lung deposition, retention, and disease.” In: *Environmental health perspectives* 88 (1990), pages 311–317 (cited on page 14).
- [23] T. R. Sosnowski. “Particles on the lung surface-physicochemical and hydrodynamic effects”. In: *Current opinion in colloid & interface science* 36 (2018), pages 1–9 (cited on page 15).
- [24] T. R. Sosnowski, K. Jabłczyńska, M. Odziomek, W. K. Schlage, and A. K. Kuczaj. “Physicochemical studies of direct interactions between lung surfactant and components of electronic cigarettes liquid mixtures”. In: *Inhalation toxicology* 30.4-5 (2018), pages 159–168 (cited on page 15).
- [25] T. R. Sosnowski. “Influence of insoluble aerosol deposits on the surface activity of the pulmonary surfactant: a possible mechanism of alveolar clearance retardation?” In: *Aerosol Science & Technology* 32.1 (2000), pages 52–60 (cited on page 15).
- [26] D. Kondej and T. R. Sosnowski. “Interactions of Carbon Nanotubes and Carbon Nanohorns with a Model Membrane Layer and Lung Surfactant In Vitro”. In: *Journal of Nanomaterials* 2019 (2019) (cited on page 15).
- [27] J. Melbourne, A. Clancy, J. Seiffert, J. Skepper, T. D. Tetley, M. S. Shaffer, and A. Porter. “An investigation of the carbon nanotube–Lipid interface and its impact upon pulmonary surfactant lipid function”. In: *Biomaterials* 55 (2015), pages 24–32 (cited on page 15).
- [28] E. Guzmán and E. Santini. “Lung surfactant-particles at fluid interfaces for toxicity assessments”. In: *Current Opinion in Colloid & Interface Science* 39 (2019), pages 24–39 (cited on page 15).
- [29] R. H. Notter. *Lung surfactants: basic science and clinical applications*. CRC Press, 2000 (cited on page 15).

- [30] Y. Xu, Z. Luo, S. Li, W. Li, X. Zhang, Y. Y. Zuo, F. Huang, and T. Yue. “Perturbation of the pulmonary surfactant monolayer by single-walled carbon nanotubes: a molecular dynamics study”. In: *Nanoscale* 9.29 (2017), pages 10193–10204 (cited on page 15).
- [31] T. Padmore, C. Stark, L. A. Turkevich, and J. A. Champion. “Quantitative analysis of the role of fiber length on phagocytosis and inflammatory response by alveolar macrophages”. In: *Biochimica et Biophysica Acta (BBA)-General Subjects* 1861.2 (2017), pages 58–67 (cited on page 16).

Production of nano- and microfibers from synthetic and natural polymers - Nanofibers technology

By: Michał Wojasiński¹, Tomasz Ciach¹

1 – Warsaw University of Technology, Faculty of Chemical and Process Engineering, Waryńskiego 1, 00-645 Warsaw, Poland

3.1 Introduction

Nanoscale, falling in between a classic mechanic's scale and a quantum mechanics scale, describes a class of materials with properties changing in the way that slips away from the description by both approaches. In this way, nanofibrous non-woven materials have advantages over microfibers of low weight, small pore size with high porosity, high specific area (about $10^3 \text{ m}^2 \text{ g}^{-1}$), even though their mean size falls in the range from few nanometers to about one micrometer - a slight extension of the nanoscale [1]. In terms of environment protection application, nanoscale level functionality of nanofibrous materials relies on their high permeability, on top of the properties mentioned above. Hence, the main nanofibrous materials characteristics that require consideration during design and production include: 1) mean fiber size/distribution, 2) mean pore size/distribution, 3) porosity, 4) non-woven thickness and 5) connectivity of pores [2].

In filtration processes where the filtration media consists of fibrous materials, particles are removed from the fluid stream by following mechanisms: sieving, inertial impaction, interception, diffusion, and electrostatic attraction. The filtration process relies on parameters of non-woven filtration material, such as filtration efficiency, pressure drop, flux, and mechanical stability [2]. The non-slip flow mechanism dominates filtration with conventional high-efficiency particulate filters, composed of microfibers. While fibers size decreases, however, the slip mechanism becomes predominant. Slip flow is the type of flow, where the fluid velocity on the surface of the fiber is not equal to zero. This effect leads to lower the pressure drop, and increase of the diffusion, interception, and inertial impaction efficiencies [3]. Using meltblown synthetic fibers, Podgórski et al. [4] the increased filtration efficiency of nanoparticulate aerosol (10-500 nm) within micro/nanofibrous materials with an increased number of nanofibers [4].

Currently, the most popular technology in the production of non-woven conventional filters exhibiting a fractional number of nanofibers in between microfibrillar structure is meltblowing [5, 6]. However, in order to increase the number of nanofibers within the non-woven material, numerous groups proposed novel technologies of producing mostly/only nanofibers. Such technologies, listing the most productive and have the highest potential to be applied in industrial scale, include electrospinning, solution blow spinning, and centrifugal spinning. Other laboratory level technologies include magnetospinning, templating, drawing to name a few [7-9]. There are possibilities to produce micro- and nanofibrous materials with both synthetic and natural polymers, including natural polymers, being a byproduct, or waste from other processes (zein, soybean proteins, and the like) using technologies listed above [10]. However, the need for one efficient and sustainable production technology for nanofibrous materials remains unmet. This review aims at summarizing research published in the subject of the most currently developed efficient technologies for nanofibers production, and at proposing the most pressing problems that need to be addressed.

3.2 Meltblowing

The inception of the concept of meltblowing dates back to 1954 when the Naval Research Laboratory in the United States of America invented the technology. Van Wente et al. [11] developed the technology for the production of fine fibers using molten polymers extruded through dies right into the high-speed stream of hot air (or other gas) [11, 12]. Then, Exxon laboratories developed meltblowing technology and submitted the patent application in 1973 (Fig. 3.1) [13]. After licensing the patent and adaptation of the technology by several companies meltblowing became a common process for the production of non-woven fibrous materials, covering the vast majority of the market of such materials [14].

Meltblowing process can be defined as a ‘one-step process in which high-velocity fluid, normally air blows molten thermoplastic resin from an extruder die tip onto a conveyor, or take-up screen, or substrate to form a fine fibered self-bonded web’ [14]. This process results in fine fibers from thermoplastic polymers, with diameters in a range from submicrometric to more than 10 micrometers [15]. Regardless of the application of fibrous materials, the most significant property of such materials is the mean fiber size and fibers size distribution. Most research identifies two main groups of parameters affecting the mean fiber size, not only in the meltblowing process but in almost all fibers producing processes mentioned in the previous subchapter: 1) material parameters; and 2) process parameters. In meltblowing, the first group consists of polymer molecular weight and its melting temperature. The second group includes pressure in the die, a temperature of hot gas (mostly air), a flow rate of hot gas, offset of the die tip, and die-tip-to-collector distance [16]. According to Jarecki et al. [17], the viscosity of molten polymer used in the meltblowing process depends on the polymer molecular weight and process temperature, and those parameters should be adjusted to achieve a narrow operability window for the process [17].

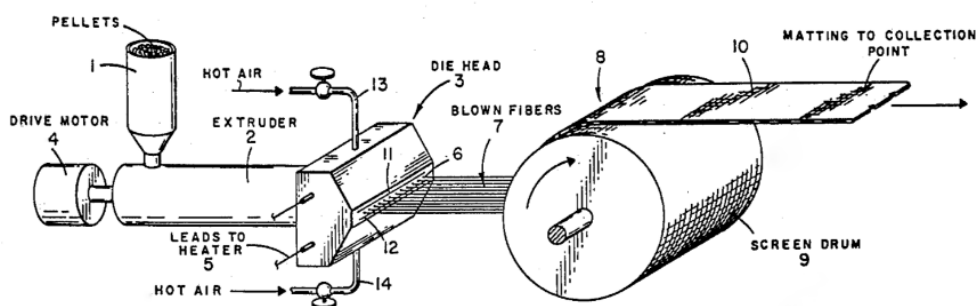


Figure 3.1.: Schematic of typical meltblowing system. Die head construction uses an air-blade technique for increasing hot air velocity to the subsonic regime [13]

Based on the above presented approach of Jarecki et al. [17], it is possible to determine the proper operability window for various polymers, and such a window requires consideration of process parameters like temperature, the temperature of hot gas affecting the temperature and rheological properties of the stretched polymer filament that forms a fiber [17]. All of those parameters affect the formation of fibers that solidify on the surface of the collector. According to Gradoń et al. [18], the mentioned parameters collected into the mathematical model allow determination of the fiber size [18]. Moreover, Jarecki et al. [17] reported that reduction of molten polymer viscosity results in fibrous materials with lower minimum size, while Ellison et al. [19] reported possibilities to produce fibers from polystyrene (mean fiber size of $0.38 \mu\text{m}$), polypropylene ($0.30 \mu\text{m}$), and poly(butylene terephthalate) ($0.44 \mu\text{m}$) by reducing viscosities of polymers using higher temperatures [17, 19]. Another parameter pointed out by Gradoń et al. [18] that affects the size of meltblown fibers during the meltblowing process is the velocity of the stretching gas [18]. Zachara et al. [20] and Jarecki et al. [17], in their series of papers, investigated the dynamics of the airflow in a meltblowing device, and its influence on fiber size [17, 20]. They showed that increasing the air velocity from about 30 m s^{-1} to the subsonic region (about 300 m s^{-1}) significantly decreases the diameter of polymer filament in

the meltblowing process, which should result in fibers with diameters reduced from about 350 μm to about 10 μm [20–22].

Even though the meltblowing process and non-woven materials produced in meltblowing found an application in various industries and scientific research fields, the choice of polymers for fibers production is limited. Limiting factors include not only the melting temperature of the polymer but also the rheological behavior of polymer melts, especially in conditions similar to those during the meltblowing process. Nevertheless, since the introduction of this technique, various polymers, mostly synthetic, were used for the production of non-woven materials in the meltblowing process: polyethylene (PE), polypropylene (PP), poly(ethylene terephthalate) (PET), poly(methyl methacrylate) (PMMA), poly(butylene terephthalate) (PBT), polyamides (PA), and polystyrene (PS) [5, 12, 19, 23–29]. Despite quite a narrow choice of polymers for meltblowing, products from this technique found applications in a vast number of industries. To name a few, polymeric non-woven materials produced in the meltblowing process can be applied as membranes in 1) separation processes, like filtration [4, 28, 30, 31], 2) batteries [13, 32], and as materials for medical and hygiene purposes, like medical garments [33, 34], surgical masks [35], filtration membranes contacting with blood [36], and in some applications in tissue engineering and regenerative medicine field [37].

Still, the main drawback of the meltblowing process - narrow choice of polymers, limited to mostly synthetic polymers - limits possibilities to produce non-woven fibrous materials from biodegradable and natural polymers using meltblowing.

3.3 Electrospinning

It was in the eighteenth century when Bose introduced theoretical foundations and presented experimental details showing the liquid behavior upon application of high electric potential [38]. Application of the electrostatic forces to produce a material, especially fibrous threads from artificial materials, was described by Fomhals [39]. His patent is now considered a first-ever mention of the electrospinning-like process in the technical literature. Further development of the electrospinning process and the field of submicron fibrous materials became possible since the popularization of the scanning electron microscope, which allows observing objects with dimensions lower than 100 nm. From 1990, the term ‘electrospinning’ and ‘nanofiber’ started to appear in the scientific literature more often, leading to a rapid growth up until now [40]. LF Nascimento et al. [40] showed that the end of the twentieth century and the beginning of the twenty-first century were the times of the significant development of the electrospinning [40]. The technique became the subject of not only scientific papers but also patents, leading to the birth of the new branch of the fibrous materials industry [41].

The simple electrospinning system, most commonly used in the experimental setups described in the literature, consists of the nozzle, grounded collector, high-voltage power supply, and a device to control the flow rate of the spinning material - either polymer solution or polymer melt [42]. During the electrospinning process, polymer solution or melt charged and stretched by electrostatic forces from the electrostatic field produced between the nozzle and grounded collector dries (polymer solution) or solidifies (polymer melt) into the form of the fiber. During the stretching process, fiber diameter decreases, mostly due to electrostatic forces acting on the jet and bending instabilities caused by imbalanced charges on the surface of the jet. The next step for production fibers composed of more than one material, apart from emulsion electrospinning [43], is coaxial electrospinning [44]. Using two coaxially placed nozzles for supplying the polymers for the electrospinning process, one can produce core-shell fibers (Fig. 3.2). Increasing the number of nozzles in the electrospinning systems, called multi-needle electrospinning or multiple jet electrospinning, leads to an increase in the yield of production of the fibers [45]. Other approaches to multi-jet electrospinning, without the usage of the multiple nozzles, included multihole electrospinning [46], and free surface electrospinning [47]. Figure 3.2 summarizes the evolution of the electrospinning setups used in described approaches. Now, machines offering automated production of the submicron fibrous polymeric materials are commercially available, like 4SPIN by Contipro a.s., NanoSpider™ by Elmarco s.r.p., and Nanospinner24 by

3. Production of nano- and microfibers from synthetic and natural polymers - Nanofibers technology

Inovenso Inc., to name a few.

Processing parameters in polymer solution electrospinning fall into categories depending on the origin of the parameter. One can group parameters in electrospinning into following categories: 1) polymer and solvent properties (in case of melt electrospinning - polymer only), 2) processing parameters from the system, and 3) ambient conditions (in some electrospinning systems, ambient conditions could also be controlled by the operator) [48]. Even though the control over all parameters can provide precise conditions to prepare fibers with designed properties, several parameters are the most important for the stable production of fibers with specified mean fiber diameter and fibers size distribution. For the polymer and solvent properties, it is mostly polymer molecular weight and ability of the solvent to dissolve the polymer [49]. They are especially important to create a polymer solution with spinnable properties. From the processing parameters point of view, the most important is the polymer concentration, thus polymer solution viscosity, the voltage applied to the polymer solution, polymer solution feed rate, working distance, and the type of the collector [50]. Meaning, processing parameters are the critical parameters in electrospinning for obtaining the designed and desired fibrous materials from spinnable polymer solutions, among all groups of parameters in the electrospinning. In some cases, the control over properties of polymer fibers from electrospinning was put to the control of the ambient parameters. However, only the humidity can affect the process in the most significant way, preventing electrospinning from starting for a highly humid atmosphere [51].

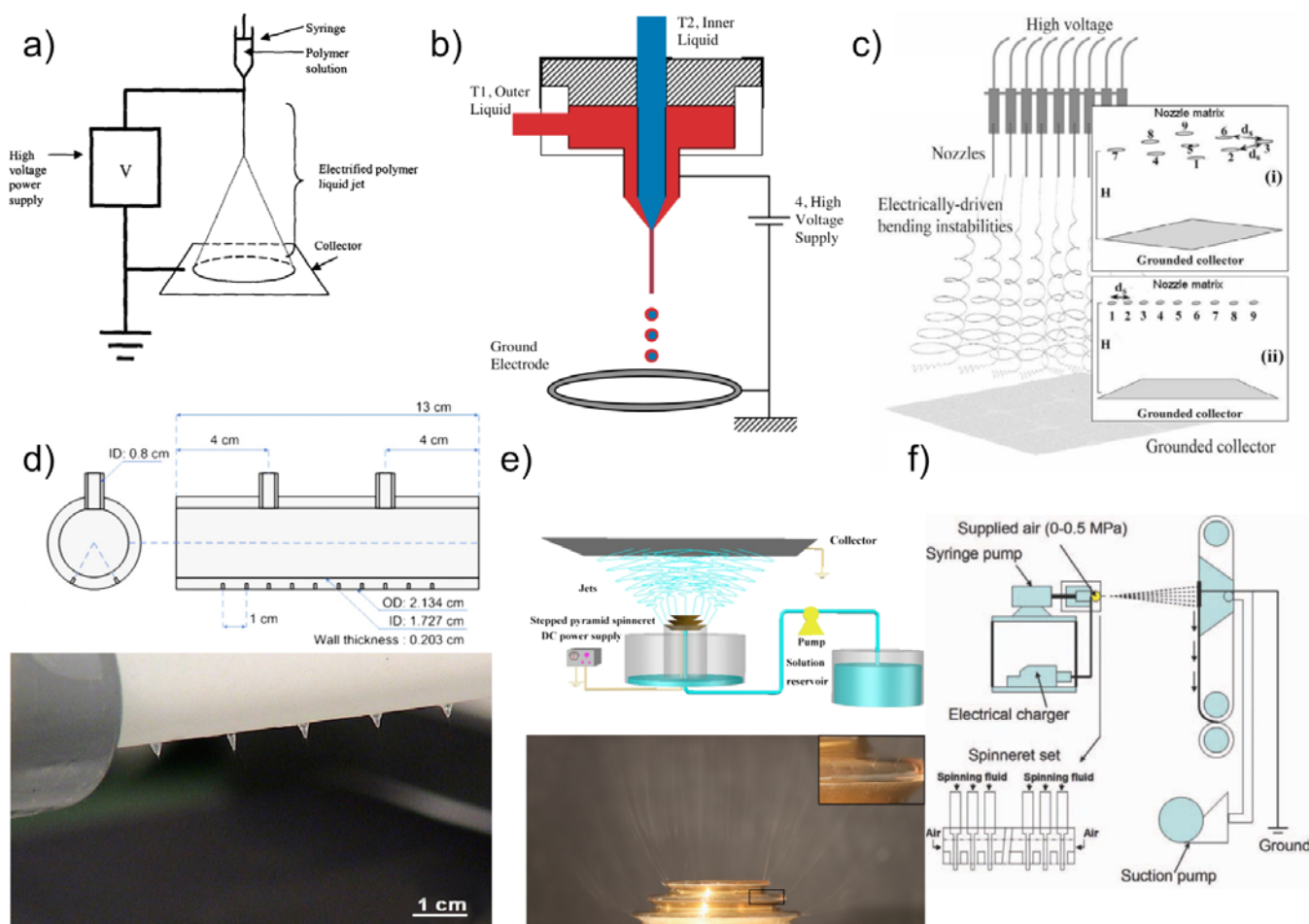


Figure 3.2.: Evolution of the electrospinning system: a) single-jet electrospinning system [52]; b) coaxial electrospinning [44]; c) multi-nozzle/multi-needle electrospinning [53]; d) multijet/multihole electrospinning [54]; e) free surface electrospinning [47]; f) blow-assisted electrospinning [55]

Environmental protection, involving various ways to separate solid particles from fluids, requires materials with the high surface-to-volume ratio, similar to this of micro and especially nanofibrous materials. Simple electrospinning of poly(ethylene oxide) (PEO), polycarbonate (PC), and polyurethane (PU) resulted in filtration materials exhibiting filtration efficiency of nanoparticles (about 100 nm) from the air over 80% [56]. Further development of the air filters builds in the electrospinning process involved applications of polyacrylonitrile (PAN) and polysulfone (PSU) - electrospun in the co-electrospinning system [57]. As prepared, the fibrous material with PAN fibers with mean fibers size of about 300 nm and PSU mean fibers size of about 1300 nm showed a filtration efficiency of nanoparticles (300 to 500 nm NaCl particles) from the air over 70%. Zhang et al. [57] developed their system even further, by electrospinning of PAN on the surface of the polyethylene substrate, they prepared filters with the filtration efficiency of the same NaCl nanoparticles over 95% [58]. Changing materials from synthetic polymers into silk, Wang et al. [59] produced electrospun air filters with extreme lightness, comparing to the synthetic materials [59]. They achieved the filtration efficiency of nanoparticles (100 - 400 nm) over 80%, using submicron silk fibers with a mean fiber diameter of about 500 nm. What is more, they presented that such a submicron mat can be doped with silver nanoparticles to provide the antimicrobial properties of the filtration material.

Filtration with an application of submicron fibers also extends to water purification. Gopal et al. [60] presented poly(vinylidene fluoride) (PVDF) submicron fibers with a mean fiber diameter of about 400 nm, building a mat with pore sizes within the range of 4 to 10 μm and thickness of 300 μm . Such a material, subjected to test of separation of polystyrene (PS) beads from the water stream resulted in filtration efficiency of 98% for 1 μm beads, 91% for 5 μm beads, and 96% for 10 μm beads [60]. Increased wettability of the filtration material should lead to increased penetration of the water impurities into such material. Huang et al. [61] used this assumption, and after electrospinning of PAN and PSU submicron fibrous materials for water filtration, they used a polydopamine coating to increase the wettability of their materials. Resulting submicron fibrous mats, with the mean fiber diameter of about 300 nm and about 500 nm, respectively, exhibited increased water permeation and improved mechanical properties [61].

Environmental protection using submicron fibrous materials extends over the filtration process. Bae et al. [62], electrospun highly porous poly(methyl methacrylate) (PMMA) fibers are building highly porous mat. Their material exhibited great adsorption potential for phenol and especially iodine, serving as an absorber for the removal of those substances, suggesting that this type of material can serve in the removal of organic and inorganic pollutants from water. The high surface area makes the submicron fibrous material a perfect candidate as a catalyst [62]. Since the carbon dioxide removal from the air is mostly realized during electrochemical reduction, Kumar et al. [63] proposed a replacement of the noble metal catalyst by submicron carbon fibers. Using electrospinning followed by carbonization at 1050 $^{\circ}\text{C}$, they prepared carbon submicron fibrous materials with a mean fiber diameter of about 500 nm, which increased the electrostatic potential of the reduction device about 13 times, comparing to bulk silver metal catalyst [63].

Electrospinning shows several significant limitations in the scale-up of the production process. Even though researchers propose improvements of the production rate, mostly based on the multiplication of the single jet electrospinning into 1) multi-needle electrospinning, 2) needleless electrospinning, and 3) free surface electrospinning, the rate of polymer solution processed into the fibers remains low, comparing to the capabilities of meltblowing technology. The increase of the production rate by multiplication of the jets resulted in the increase of the polymer solution feed rate from about 1 mg h^{-1} to only about 300 mg h^{-1} (Tab. 3.1) [64]. Associated with production rate limitation is the source of the driving force of the electrospinning process. The high voltage necessary for supplying of the electrostatic field between nozzles or polymer solution surface and collector remains a drawback of the electrospinning process. Mainly, the necessity of the high voltage in this process creates a danger for personnel. Secondly, the electrostatic field induces instabilities in the electrospinning process when the number of jets increases [45]. High voltage, necessary for the generation of the electrostatic field in the electrospinning system, introduces another limitation of the technique. In the majority of reports, the counter electrode in the electrospinning system plays the role of a collector. This type of setup limits forms and materials for collectors to plates, rotating drums, rotating discs, and several meshes made of metals, especially aluminum [65].

3. Production of nano- and microfibers from synthetic and natural polymers - Nanofibers technology

Table 3.1.: Comparison of productivity among nanofibers production technologies.

Technology	Single nozzle productivity	Jet multiplication productivity	Stage
Electrospinning	1 to 100 mg h ⁻¹	~ 300 g h ⁻¹ (needleless)	industrial
Solution blow spinning	0.5 to 1.0 g h ⁻¹	~ 400 g h ⁻¹ (multi-jet)	prototype
Centrifugal spinning	1 to 50 g h ⁻¹	~ 500 g h ⁻¹ (multi-jet)	test

All the limitations of the electrospinning process inspired another approach to the entirely controlled production of submicron fibrous structures. Approaches, where high production rates can be achieved, the driving force does not require dangerous sources, and where the structure of the resulting submicron fibrous material can be fully determined and tailored for a particular application.

3.4 Solution blow spinning

Foundations for the electrospinning process laid down in the seventeenth and eighteenth century by Bose, combined with the technological development of the process and other processes, like meltblowing, served as a steppingstone for the development of following way for producing fibers - solution blow spinning. The solution blow spinning, developed and published probably for the first time in 2009, operates using polymer solutions, with properties similar to those used in electrospinning, and transforms those solutions into fibrous structures based on the technological means similar to meltblowing nozzles. The first appearance of this technology came from two teams working separately: 1) Brazilian team led by Mattoso developed the process because they were looking for a more robust way to produce submicron fibrous materials from polymer solutions than electrospinning, and 2) Canadian team led by Laroche needed a system as a solution to the particular problem – a production of submicron fibers on the inner surface of vascular prostheses, which was not possible using meltblowing and electrospinning [66, 67].

Since the introduction of the solution blow spinning in the scientific literature, the technology gathered great attention. In the last decade, reviews on fibers spinning technologies have included not only a brief introduction to a solution blow spinning or similar techniques [8, 68]. Other review papers described the solution blow spinning as an emerging technology with great potential for a scale up to the industrial level [10, 69]. In a review paper published in 2016, Daristotle et al. [70] pointed out that the solution blow spinning gets more and more traction, resulting in the rapid growth of the scientific papers about the technology. They listed about 75 papers for the time of publishing their review [70]. Currently, the process of formation of submicron fibers from polymer solutions using compressed air as a source of the stretching force dynamically acting on such a solution became even more popular.

Examples of the different systems for blowing of polymer solutions to the form of fibers that result in different names for the process are presented in Figure 3.3. Throughout this work, the process for a formation of submicron polymeric fibers in the way described above will be named ‘solution blow spinning’. The mutual governing principle of all modifications of the solution blow spinning process involves an application of the concentric nozzles system, where generally a polymer solution is supplied through the inner nozzle, and the compressed carrier gas (in most of the applications, the carrier gas is air) is supplied through the outer nozzle. As the compressed air exits the outer nozzle, the pressure instantly drops, increasing the kinetic energy of the stream, increasing the air velocity [67]. This increase of air velocity creates a driving force for deformation of the polymer solution by induction of the shearing and elongating forces acting on the polymer solution at the air/jet interface. Resulting forces are responsible for polymer solution deformation and creation of the conical shape at the apex of the inner nozzle (the effect similar to the effect known in the literature as Taylor’s cone for electrospinning) [16]. When the driving force overcomes the surface tension force of the polymer solution at the apex of the inner nozzle, the jet of the solution erupts from the polymer solution drop. While in flight, the solvent rapidly evaporates from the stream, and the formation of the fibers occurs.

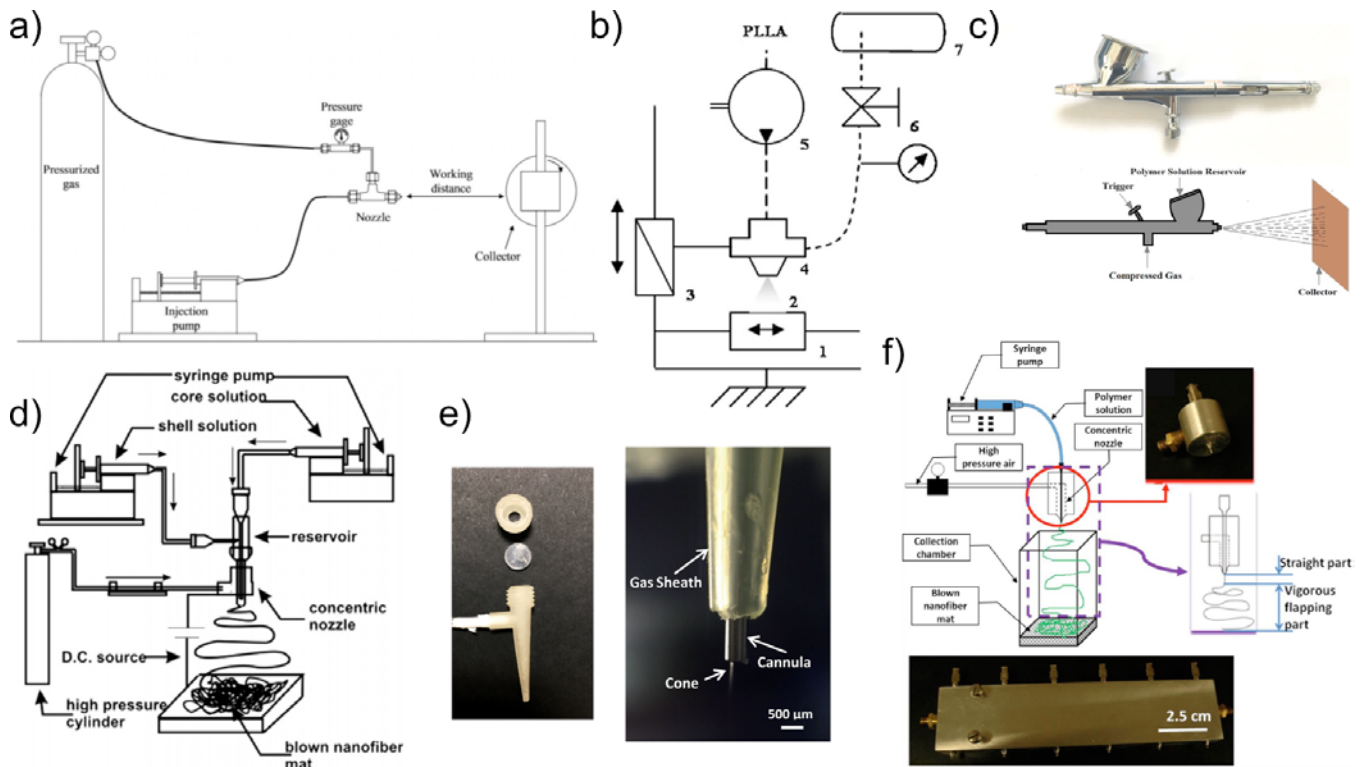


Figure 3.3.: Evolution of the solution blow spinning system from a) simple one nozzle device [67], through b) an air spinning system for vascular prostheses modifications [66], c) airbrushing device for solution blowing of fibers [71], d) co-axial system for solution blowing of core-shell submicron fibers [72], e) 3D-printed solution blow spinning single nozzle system [73], to f) multi-jet solution blow spinning device for industrial production of the soy submicron fibers [74].

What is more, the bending instabilities of the jet cause further stretching of the fibers to submicron dimensions. On the contrary to the electrospinning process, where elongation of fibers occurs due to bending instabilities resulting from forces acting on charged polymer solution jet, bending instabilities in solution blow spinning result from turbulent deformations caused by the turbulent flow of the carrier gas in the process [75].

Generally, the solution blow spinning setup consists of four main elements: 1) concentric nozzles system or any modification of such allowing generation of fibers using a principle described above, 2) source of the compressed carrier gas, 3) a device for controlled supply of the polymer solution to the nozzles system, and 4) a system for fibers collection, which mostly consists of a rotational or stationary surface for collection of the submicron polymeric fibers (Fig. 3.3) [76]. Apart from research on the single nozzle solution blow spinning process (Fig. 3.3a to c), several research groups work on the development of the more advanced systems for blowing fibers with even more advanced properties (Fig. 3.3d to f).

A review of the currently used solution blow spinning systems leads to the conclusion that not only the process fundamental phenomena but the system used for the process generates processing parameters that can influence the properties of the final product. However, comparing to the electrospinning - currently, the most popular and widely employed fiber fabrication technique - solution blow spinning has fewer requirements and variables affecting fibers properties [70]. Like in the electrospinning process description, the mean fiber diameter and fiber size distribution are here considered as the most important characteristics defining properties of the solution blow spun submicron fibrous materials. So similarly like in the case of the electrospinning, processing parameters affecting fibers properties in the solution blow spinning process can be divided into following categories: 1) polymer and solvent properties, and

3. Production of nano- and microfibers from synthetic and natural polymers - Nanofibers technology

2) processing parameters from the system [8, 10, 70]. The ambient conditions of the atmosphere surrounding the solution blow spinning system can be neglected, because of the shielding properties of the carrier gas, protecting formed fibers from the influence of the conditions like relative humidity, or ambient temperature [77]. What is more, the solution blow spinning process is an isothermal method for submicron fibers production [67, 72].

The most apparent application of the submicron fibrous mats produced using solution blow spinning is a filtration process. Since solution blow spun fibers tend to have higher porosities and less densely packed fibers within the non-woven structure comparing to electrospinning, the pressure drop occurring in filtration processes using submicron scale filtration mats can be reduced. Hence, several approaches to the production of high-efficient filters appeared in the literature. Srinivasan et al. [78] reported the production of superoleophobic membranes built from poly(methyl methacrylate) (PMMA). They tested the bacteria adhesion to such membrane and stated that solution blow spun submicron fibrous membrane from PMMA exhibit anti-biofouling properties and can be used in wastewater treatment [78]. Building on that, Zhuang et al. [79] proposed a PVDF solution blow spun membranes for microfiltration. With fibers diameters in the range from 60 nm to 280 nm and porosity up to 95.8%, their materials provided excellent filtration properties with high water flux under low pressures [79]. Wastewater treatment remained the vital subject, and the removal of oil spills on the surfaces of the large water reservoirs inspired in situ formations of polystyrene (PS) or PCL/PS blend solution blow spun fibers for the oil removal [71, 80]. In order to offer excellent filtration efficiency, solution blow spun fibers composed of nylon 6, calcinated zirconium dioxide, calcinated titanium dioxide (both with PVP as a precursor), alumina, and yttria-stabilized zirconium dioxide were produced by several groups [81–84].

With a high surface-to-volume ratio, solution blow spun offers excellent adsorption properties. Hsiao et al. [55] exploited this characteristic of the solution blow spun fibers by preparing polyacrylonitrile (PAN) non-woven for carbon dioxide removal. However, their fibrous material required post-processing in order to provide enough activated carbon on the surface of the adsorbent. Nevertheless, PAN submicron fibrous CO₂ adsorber worked with high efficiency and remained active after three regeneration cycles [55]. Polyaniline and polyimide blend used by Wang et al. [85] in submicron fibrous mat allowing adsorption of the chromium (VI), and biopolymers reinforced with nylon 6 by [74] allowed heavy metal removal from the wastewater [74, 85]. Further, the addition of graphene oxide to the PMMA allowed Mercante et al. [86] to design and produce solution blow spun membrane for adsorption and removal of the organic impurities from the wastewater. Considering a presented review of the adsorption application of the solution blow spun materials, the composition of the non-woven plays a more important role than the structure (however, the high surface-to-volume ratio and high porosity remain required) [86].

The same advantages that enable the application of solution blow spun submicron fibers in the filtration and adsorption processes allow the application of such fibers to the photocatalytic processes. They especially find applications in the processes that are associated with wastewater treatment and, in general, impurities removal. Such applications involve submicron composite fibers produced from soy protein reinforced with silver nanoparticles and poly(vinyl acetamide) with titanium dioxide nanoparticles [87–89]. Using sol-gel solution blow spinning, followed by a calcination process, Ghosh et al. [90] produced a vanadium oxide-titanium oxide submicron fibrous structure in order to perform a photocatalytic removal of impurities in the visible light [90]. Another approach to photocatalysis for environmental protection purposes, proposed by Li et al. [91], involved PAN fibers modified to perform a Fenton reaction for photocatalytic removal of organic substances [91].

Since the driving force of the solution blow spinning process differs from the one driving the electrospinning process, the limitations of efficiency, and a processing setup involving a high electrostatic field become mute. Solution blow spinning allows productivities from about 0.5 to about 1 g h⁻¹ for single nozzle systems and about 400 g h⁻¹ for multi-jet systems (Tab. 3.1) [7].

3.5 Centrifugal spinning

The centrifugal spinning process relies on a mechanical driving force that stretches the molten polymer or polymer solution into the fibrous structure. First mentions of the process and the design of a system for centrifugal spinning of fibers was an American Patent granted to Hooper [92]. Since then, the process went through the several phases of development which resulted with refinement of the system and slight changes of the process name, including centrifugal spinning, forcespinning, and rotary jet-spinning [93–95]. In general, the basic centrifugal system consists of two parts 1) a rotating nozzle providing the centrifugal driving force, and 2) a collector surrounding the nozzle [96]. The spinning process occurs when the centrifugal force overcomes the surface tension force of molten polymer or polymer solution. After the jet ejection from the nozzle, the centrifugal force and air friction elongate the jet into the micro- and nanofibers by subsequent stretching leading to their deposition on the collectors.

Table 3.2.: Parameters in centrifugal spinning divided into categories of origin.

Polymer and solvent properties	Nozzle geometry	Processing parameters Polymer
Polymer:	Nozzle radius	Rotational speed
- molecular weight	Orifice radius	Nozzle-collector distance
- melting temperature		
Solvent:		
- surface tension		
- vapor pressure		
- ability to dissolve the polymer	Nozzle radius	

In centrifugal spinning, control over the mean fiber size and their distribution, leading to control over the structural properties of a fibrous structure, comes from three groups of parameters 1) molten polymer or polymer solution properties, 2) nozzle geometry, and 3) processing parameters. Like in electrospinning and solution blow spinning, the molten polymer or polymer solution properties involve polymer molecular weight and type of solvent, leading to appropriate viscosity and viscoelastic properties [97, 98]. A detailed list of all parameters affecting the structural properties of the centrifugal spun fibers is presented in Table 3.2.

Although the mathematical description and models for prediction of the fibers size and distribution in centrifugal spinning developed significantly during last few years, the system for the process did not change in such significant manner (Fig. 3.4) [98, 101]. The system consists of a nozzle with an appropriate number of orifices for releasing the molten polymer or polymer solution (Fig. 3.4a). However, in some cases, needles replace the orifices to achieve controllable dimensions of the nozzle outlet (Fig. 3.4b).

Up until now, the centrifugal spinning investigation lead to successful formation of fibers from polymers like hybrid poly(2,5-bis(2'-ethyl-hexyl)-1,4-phenylenevinylene) (BEH-PPV) and poly(ethylene oxide) (PEO), as well as pristine PEO, and polyacrylonitrile (PA6) with sizes in the submicron range, depending on the rotational speed of the centrifugal spinning nozzle [99, 102, 103]. With poly-L-lactic acid (PLLA), several groups managed to produce nanofibers with mean fiber size in the range from about 250 to about 850 nm, as well as microfibers with sizes up to 2 μm [93, 100]. Ren et al. [96] suggested the use of the PLLA blended with polyvinylpyrrolidone (PLLA/PVP) in order to increase the porosity of resulting fibrous materials. They achieved a mean fibrous size in the range from about 100 nm up to 7 μm [96]. All examples of PLLA-based micro- and nanofibrous structures listed above were designed for tissue engineering applications. As for environmental protection of centrifugally spun nanofibers, the polyvinylidene fluoride (PVDF) production resulted in nanofibers with mean size from about 300 to 900 nm, while the range for microfibers size ranged from about 1 to about 1.7 μm [94].

Centrifugal spinning achieves superior fiber productivity because of the presence of the centrifugal force caused by high-speed rotation. This high throughput is obtained without the need for a high voltage electric field or compressed

3. Production of nano- and microfibers from synthetic and natural polymers - Nanofibers technology

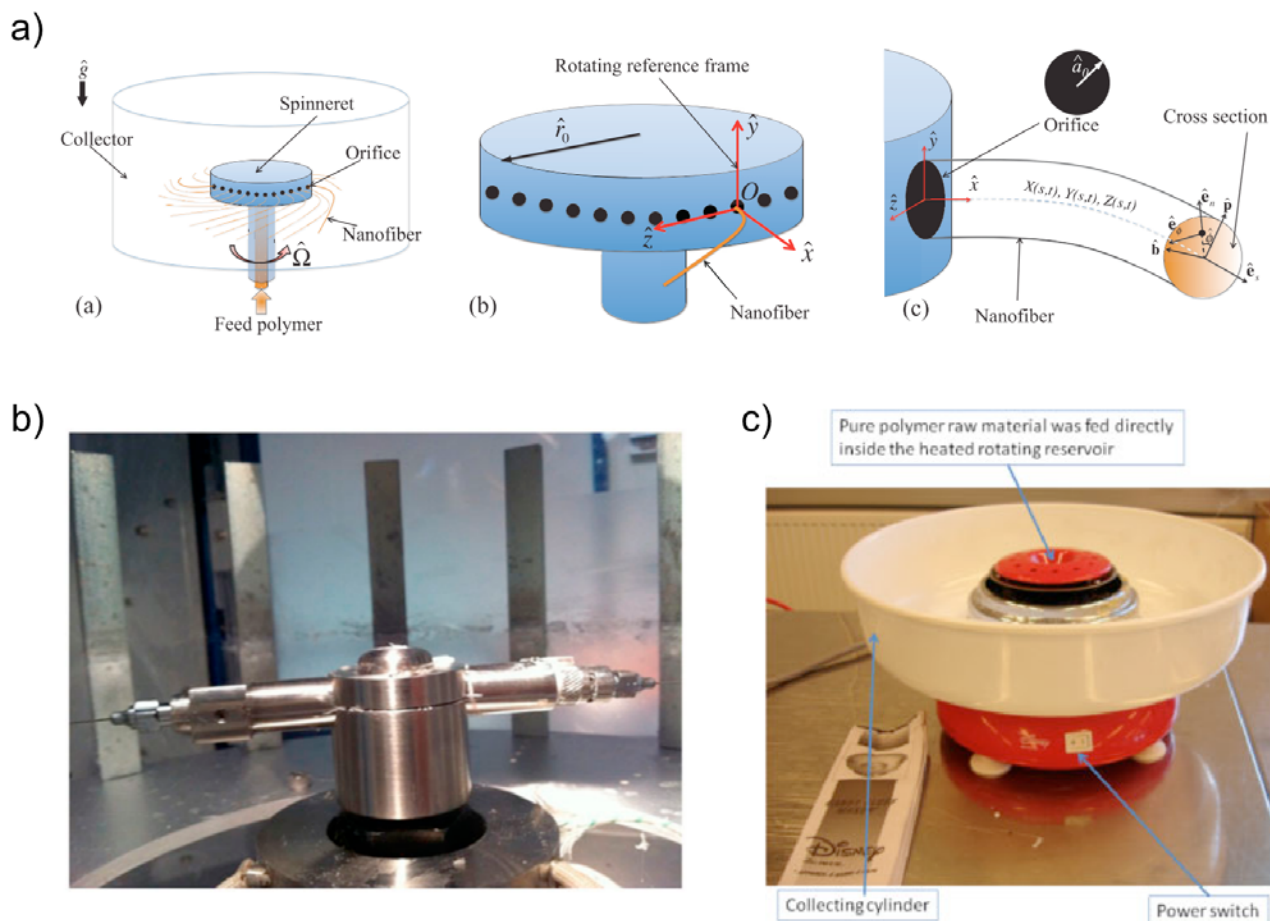


Figure 3.4.: Centrifugal spinning systems a) schematic representation [98], b) nozzles-based system [99], and c) cotton candy machine-based system [100].

air stream, comparing to electrospinning and solution blow spinning. What is more, it allows high productivity (about 500 gh^{-1}) in the spinning of biodegradable polymers (Tab. 3.1). Centrifugal spinning easily produces aligned nanofibers because the centrifugal force stretches the jet along one unique direction. However, centrifugal spinning produces fibers with higher average diameters compared to electrospinning and is limited to cylindrical collecting systems surrounding the rotating nozzle (in the most straightforward systems) [7].

3.6 Conclusion

Solution blow spinning and centrifugal spinning with their output and efficiency offer the industrial level of productivity scale of nanofibrous materials, especially non-woven materials. Both techniques allow spinning from synthetic biodegradable polymers as well as natural polymers, which are frequently by-products from other industries. The versatility of collectors and nozzles possible to use in solution blow spinning opens the formation of nanofibrous layers on top of different substrates, including biodegradable microfibrous filtering materials. This way, with controlled rate and placement of produced fibers, one can produce not only simple nanofibrous filtration systems for water and air filtration, but also in situ water cleaning systems, and transparent window protection systems, and the like. Comparing to meltblowing, where hot air can introduce damage to synthetic biodegradable polymers or natural

polymers, solution blow spinning produces nanofibers from such polymers without significant degradation of their molecular and physical structure. However, the need for polymer solution formation, in some cases using organic solvents, requires a limitation of solution blow spinning. The work on (1) in-line adsorption systems to remove volatile organic solvents from the exhaust from solution blow spinning system; (2) application of water-soluble degradable polymers; and (3) substitution of volatile organic solvents with less harmful substances like carbonates is now a vital point before the industrial implementation of solution blow spinning.

3.7 Acknowledgement

Authors acknowledge the financial support by the National Science Centre, Poland, within the project entitled: Investigation and modeling of the polymer solution cone formation in solution blow spinning process. National Science Centre/Preludium/2014/13/N/ST8/01690.

References

- [1] E. Tan and C. Lim. “Mechanical characterization of nanofibers—a review”. In: *Composites Science and Technology* 66.9 (2006), pages 1102–1111 (cited on page 19).
- [2] X. Qin and S. Subianto. “Electrospun nanofibers for filtration applications”. In: *Electrospun Nanofibers*. Elsevier, 2017, pages 449–466 (cited on page 19).
- [3] K. Graham, M. Ouyang, T. Raether, T. Grafe, B. McDonald, and P. Knauf. “Polymeric nanofibers in air filtration applications”. In: *5th Annual Technical Conference & Expo of the American Filtration & Separations Society, Galveston, Texas*. 2002 (cited on page 19).
- [4] A. Podgórski, A. Bałazy, and L. Gradoń. “Application of nanofibers to improve the filtration efficiency of the most penetrating aerosol particles in fibrous filters”. In: *Chemical Engineering Science* 61.20 (2006), pages 6804–6815 (cited on pages 19, 21).
- [5] R. Nayak, I. L. Kyrtziz, Y. B. Truong, R. Padhye, L. Arnold, G. Peeters, L. Nichols, and M. O’Shea. “Fabrication and characterisation of nanofibres by meltblowing and melt electrospinning”. In: *Advanced Materials Research*. Volume 472. Trans Tech Publ, 2012, pages 1294–1299 (cited on pages 19, 21).
- [6] S. Xin and X. Wang. “Mechanism of fiber formation in melt blowing”. In: *Industrial & engineering chemistry research* 51.32 (2012), pages 10621–10628 (cited on page 19).
- [7] Y. Huang, J. Song, C. Yang, Y. Long, and H. Wu. “Scalable manufacturing and applications of nanofibers”. In: *Materials Today* (2019) (cited on pages 19, 26, 28).
- [8] E. Stojanovska, E. Canbay, E. S. Pampal, M. D. Calisir, O. Agma, Y. Polat, R. Simsek, N. S. Gundogdu, Y. Akgul, and A. Kilic. “A review on non-electro nanofibre spinning techniques”. In: *RSC advances* 6.87 (2016), pages 83783–83801 (cited on pages 19, 24, 26).
- [9] A. Tokarev, O. Trotsenko, I. M. Griffiths, H. A. Stone, and S. Minko. “Magnetospinning of Nano- and Microfibers”. In: *Advanced Materials* 27.23 (2015), pages 3560–3565 (cited on page 19).
- [10] A. Kakoria and S. Sinha-Ray. “A review on biopolymer-based fibers via electrospinning and solution blowing and their applications”. In: *Fibers* 6.3 (2018), page 45 (cited on pages 19, 24, 26).
- [11] A. Van Wente, E. Boone, and C. Fluharty. *Manufacture of superfine organic fibers*. Technical report. Naval research lab Washington DC, 1954 (cited on page 20).
- [12] A. Van Wente. “Superfine thermoplastic fibers”. In: *Industrial & Engineering Chemistry* 48.8 (1956), pages 1342–1346 (cited on pages 20, 21).
- [13] R. R. Buntin. “Battery separators made from polymeric fibers”. Aug. 1976 (cited on pages 20, 21).
- [14] J. G. McCulloch. “The history of the development of melt blowing technology”. In: *International Nonwovens Journal* 1 (1999), 1558925099OS–800123 (cited on page 20).
- [15] L. Jarecki, S. Blonski, A. Blim, and A. Zachara. “Modeling of pneumatic melt spinning processes”. In: *Journal of applied polymer science* 125.6 (2012), pages 4402–4415 (cited on page 20).
- [16] A. L. Yarin, B. Pourdeyhimi, and S. Ramakrishna. *Fundamentals and applications of micro- and nanofibers*. Cambridge University Press, 2014 (cited on pages 20, 24).

- [17] L. Jarecki, A. Ziabicki, Z. Lewandowski, and A. Blim. “Dynamics of air drawing in the melt blowing of nonwovens from isotactic polypropylene by computer modeling”. In: *Journal of applied polymer science* 119.1 (2011), pages 53–65 (cited on page 20).
- [18] L. Gradoń, A. Podgórski, and A. Balazy. “Filtration of nanoparticles in the nanofibrous filters”. In: *Filtech Europa* (2005), pages 178–85 (cited on page 20).
- [19] C. J. Ellison, A. Phatak, D. W. Giles, C. W. Macosko, and F. S. Bates. “Melt blown nanofibers: Fiber diameter distributions and onset of fiber breakup”. In: *Polymer* 48.11 (2007), pages 3306–3316 (cited on pages 20, 21).
- [20] A. Zachara and Z. Lewandowski. “Mathematical modelling of pneumatic melt spinning of isotactic polypropylene. Part I. Modelling of the air jet dynamics”. In: *relation* 8.10 (2008), page 10 (cited on pages 20, 21).
- [21] L. Jarecki and A. Ziabicki. “Mathematical modelling of the pneumatic melt spinning of isotactic polypropylene. Part II. Dynamic model of melt blowing”. In: *Fibres Text. East. Eur* 16.5 (2008), pages 17–24 (cited on page 21).
- [22] L. Jarecki and Z. Lewandowski. “Mathematical modelling of the pneumatic melt spinning of isotactic polypropylene. Part III. Computations of the process dynamics”. In: *Fibres Textiles Eastern Eur* 17.1 (2009), pages 75–80 (cited on page 21).
- [23] T. Chen, L. Li, and X. Huang. “Fiber diameter of polybutylene terephthalate melt-blown nonwovens”. In: *Journal of applied polymer science* 97.4 (2005), pages 1750–1752 (cited on page 21).
- [24] M. W. Milligan and B. D. Haynes. “Empirical models for melt blowing”. In: *Journal of applied polymer science* 58.1 (1995), pages 159–163 (cited on page 21).
- [25] D. H. Tan, C. J. Ellison, F. S. Bates, and C. W. Macosko. “Impact of rheology on meltblown polymer nanofibers”. In: *AIP Conference Proceedings*. Volume 1027. 1. American Institute of Physics. 2008, pages 72–74 (cited on page 21).
- [26] M. A. Uyttendaele and R. L. Shambaugh. “Melt blowing: General equation development and experimental verification”. In: *AIChE Journal* 36.2 (1990), pages 175–186 (cited on page 21).
- [27] X. Wang and Q. Ke. “Experimental investigation of adhesive meltblown web production using accessory air”. In: *Polymer Engineering & Science* 46.1 (2006), pages 1–7 (cited on page 21).
- [28] Y. Yesil and G. S. Bhat. “Porosity and barrier properties of polyethylene meltblown nonwovens”. In: *The Journal of the Textile Institute* 108.6 (2017), pages 1035–1040 (cited on page 21).
- [29] R. Zhao and L. C. Wadsworth. “Study of polypropylene/poly (ethylene terephthalate) bicomponent melt-blowing process: The fiber temperature and elongational viscosity profiles of the spinline”. In: *Journal of applied polymer science* 89.4 (2003), pages 1145–1150 (cited on page 21).
- [30] T. Ciach and L. Gradoń. “Highly efficient filtering materials”. In: *Journal of Aerosol Science* 27 (1996), S613–S614 (cited on page 21).
- [31] G. Ward. “Nanofibres: media at the nanoscale”. In: *Filtration & Separation* 42.7 (2005), pages 22–24 (cited on page 21).
- [32] T. Kanno, Y. Matsushima, and M. Suzuki. “High-strength non-woven fabric, method of producing same and battery separator constituted thereby”. Feb. 1992 (cited on page 21).
- [33] L. H. McAmish, T. O. Addy, and G. F. Lee. “Nonwoven medical fabric”. 1986 (cited on page 21).
- [34] M. T. Morman, T. W. Odorzynski, W. W. Jackson, and G. T. Sudduth. “Personal care articles with abrasion resistant meltblown layer”. 2000 (cited on page 21).
- [35] C. Grier-Idris. “Conformable surgical face mask”. 1987 (cited on page 21).
- [36] S. Guo, Q. Ke, H. Wang, X. Jin, and Y. Li. “Poly (butylene terephthalate) electrospun/melt-blown composite mats for white blood cell filtration”. In: *Journal of applied polymer science* 128.6 (2013), pages 3652–3659 (cited on page 21).
- [37] S. Sahoo, H. Ouyang, J. C.-H. Goh, T. Tay, and S. Toh. “Characterization of a novel polymeric scaffold for potential application in tendon/ligament tissue engineering”. In: *Tissue engineering* 12.1 (2006), pages 91–99 (cited on page 21).
- [38] G. M. Bose. *Recherches sur la cause et sur la veritable theorie de l'electricite publies par George Mathias Bose prof. en physique*. de l'imprimerie de Jean Fred. Slomac, 1745 (cited on page 21).
- [39] A. Fomhals. *Process and apparatus for preparing artificial threads: US, 1975504*. 1934 (cited on page 21).
- [40] M. LF Nascimento, E. S Araujo, E. R Cordeiro, A. HP de Oliveira, and H. P de Oliveira. “A literature investigation about electrospinning and nanofibers: historical trends, current status and future challenges”. In: *Recent patents on nanotechnology* 9.2 (2015), pages 76–85 (cited on page 21).
- [41] D. Li and Y. Xia. “Electrospinning of nanofibers: reinventing the wheel?” In: *Advanced materials* 16.14 (2004), pages 1151–1170 (cited on page 21).
- [42] J. Doshi and D. H. Reneker. “Electrospinning process and applications of electrospun fibers”. In: *Conference Record of the 1993 IEEE Industry Applications Conference Twenty-Eighth IAS Annual Meeting*. IEEE, 1993, pages 1698–1703 (cited on page 21).

- [43] J. Rafalowska, D. Sulejczak, S. J. Chrapusta, R. Gadamski, A. Taraszewska, P. Nakielski, T. Kowalczyk, and D. Dziejulska. “Non-woven nanofiber mats—a new perspective for experimental studies of the central nervous system?” In: *Folia neuropathologica* 52.4 (2014), pages 407–416 (cited on page 21).
- [44] I. G. Loscertales, A. Barrero, I. Guerrero, R. Cortijo, M. Marquez, and A. M. Ganan-Calvo. “Micro/nano encapsulation via electrified coaxial liquid jets”. In: *Science* 295.5560 (2002), pages 1695–1698 (cited on pages 21, 22).
- [45] M. Wojasiński, J. Goławski, and T. Ciach. “Blow-assisted multi-jet electrospinning of poly-L-lactic acid nanofibers”. In: *Journal of Polymer Research* 24.5 (2017), page 76 (cited on pages 21, 23).
- [46] F.-L. Zhou, R.-H. Gong, and I. Porat. “Mass production of nanofibre assemblies by electrostatic spinning”. In: *Polymer International* 58.4 (2009), pages 331–342 (cited on page 21).
- [47] G. Jiang, S. Zhang, and X. Qin. “High throughput of quality nanofibers via one stepped pyramid-shaped spinneret”. In: *Materials Letters* 106 (2013), pages 56–58 (cited on pages 21, 22).
- [48] N. Bhardwaj and S. C. Kundu. “Electrospinning: a fascinating fiber fabrication technique”. In: *Biotechnology advances* 28.3 (2010), pages 325–347 (cited on page 22).
- [49] C. J. Buchko, L. C. Chen, Y. Shen, and D. C. Martin. “Processing and microstructural characterization of porous biocompatible protein polymer thin films”. In: *Polymer* 40.26 (1999), pages 7397–7407 (cited on page 22).
- [50] M. Borrotti, E. Lanzarone, F. Manganini, S. Ortelli, A. Pievatolo, and C. Tonetti. “Defect minimization and feature control in electrospinning through design of experiments”. In: *Journal of applied polymer science* 134.17 (2017) (cited on page 22).
- [51] S. De Vrieze, T. Van Camp, A. Nelvig, B. Hagström, P. Westbroek, and K. De Clerck. “The effect of temperature and humidity on electrospinning”. In: *Journal of materials science* 44.5 (2009), pages 1357–1362 (cited on page 22).
- [52] S. Ramakrishna. *An introduction to electrospinning and nanofibers*. World Scientific, 2005 (cited on page 22).
- [53] S. Theron, A. Yarin, E. Zussman, and E. Kroll. “Multiple jets in electrospinning: experiment and modeling”. In: *Polymer* 46.9 (2005), pages 2889–2899 (cited on page 22).
- [54] J. Varabhas, G. G. Chase, and D. Reneker. “Electrospun nanofibers from a porous hollow tube”. In: *Polymer* 49.19 (2008), pages 4226–4229 (cited on page 22).
- [55] H.-Y. Hsiao, C.-M. Huang, M.-Y. Hsu, and H. Chen. “Preparation of high-surface-area PAN-based activated carbon by solution-blowing process for CO₂ adsorption”. In: *Separation and purification technology* 82 (2011), pages 19–27 (cited on pages 22, 26).
- [56] P. P. Tsai, H. Schreuder-Gibson, and P. Gibson. “Different electrostatic methods for making electret filters”. In: *Journal of electrostatics* 54.3-4 (2002), pages 333–341 (cited on page 23).
- [57] S. Zhang, H. Liu, X. Yin, J. Yu, and B. Ding. “Anti-deformed polyacrylonitrile/polysulfone composite membrane with binary structures for effective air filtration”. In: *ACS applied materials & interfaces* 8.12 (2016), pages 8086–8095 (cited on page 23).
- [58] S. Zhang, H. Liu, F. Zuo, X. Yin, J. Yu, and B. Ding. “A Controlled Design of Ripple-Like Polyamide-6 Nanofiber/Nets Membrane for High-Efficiency Air Filter”. In: *Small* 13.10 (2017), page 1603151 (cited on page 23).
- [59] C. Wang, S. Wu, M. Jian, J. Xie, L. Xu, X. Yang, Q. Zheng, and Y. Zhang. “Silk nanofibers as high efficient and lightweight air filter”. In: *Nano Research* 9.9 (2016), pages 2590–2597 (cited on page 23).
- [60] R. Gopal, S. Kaur, Z. Ma, C. Chan, S. Ramakrishna, and T. Matsuura. “Electrospun nanofibrous filtration membrane”. In: *Journal of Membrane Science* 281.1-2 (2006), pages 581–586 (cited on page 23).
- [61] L. Huang, J. T. Arena, S. S. Manickam, X. Jiang, B. G. Willis, and J. R. McCutcheon. “Improved mechanical properties and hydrophilicity of electrospun nanofiber membranes for filtration applications by dopamine modification”. In: *Journal of Membrane Science* 460 (2014), pages 241–249 (cited on page 23).
- [62] H.-S. Bae, A. Haider, K. K. Selim, D.-Y. Kang, E.-J. Kim, and I.-K. Kang. “Fabrication of highly porous PMMA electrospun fibers and their application in the removal of phenol and iodine”. In: *Journal of Polymer Research* 20.7 (2013), page 158 (cited on page 23).
- [63] B. Kumar, M. Asadi, D. Pisasale, S. Sinha-Ray, B. A. Rosen, R. Haasch, J. Abiade, A. L. Yarin, and A. Salehi-Khojin. “Renewable and metal-free carbon nanofibre catalysts for carbon dioxide reduction”. In: *Nature communications* 4.1 (2013), pages 1–8 (cited on page 23).
- [64] O. Akampumuza, H. Gao, H. Zhang, D. Wu, and X.-H. Qin. “Raising nanofiber output: The progress, mechanisms, challenges, and reasons for the pursuit”. In: *Macromolecular Materials and Engineering* 303.1 (2018), page 1700269 (cited on page 23).

- [65] A. Baji, Y.-W. Mai, S.-C. Wong, M. Abtahi, and P. Chen. “Electrospinning of polymer nanofibers: effects on oriented morphology, structures and tensile properties”. In: *Composites science and technology* 70.5 (2010), pages 703–718 (cited on page 23).
- [66] S. François, N. Chakfé, B. Durand, and G. Laroche. “A poly (L-lactic acid) nanofibre mesh scaffold for endothelial cells on vascular prostheses”. In: *Acta Biomaterialia* 5.7 (2009), pages 2418–2428 (cited on pages 24, 25).
- [67] E. S. Medeiros, G. M. Glenn, A. P. Klamczynski, W. J. Orts, and L. H. Mattoso. “Solution blow spinning: A new method to produce micro-and nanofibers from polymer solutions”. In: *Journal of applied polymer science* 113.4 (2009), pages 2322–2330 (cited on pages 24–26).
- [68] C. J. Luo, S. D. Stoyanov, E. Stride, E. Pelan, and M. Edirisinghe. “Electrospinning versus fibre production methods: from specifics to technological convergence”. In: *Chemical Society Reviews* 41.13 (2012), pages 4708–4735 (cited on page 24).
- [69] C. T. Lim. “Nanofiber technology: current status and emerging developments”. In: *Progress in Polymer Science* 70 (2017), pages 1–17 (cited on page 24).
- [70] J. L. Daristotle, A. M. Behrens, A. D. Sandler, and P. Kofinas. “A review of the fundamental principles and applications of solution blow spinning”. In: *ACS applied materials & interfaces* 8.51 (2016), pages 34951–34963 (cited on pages 24–26).
- [71] X. Zhang, J. Lv, X. Yin, Z. Li, Q. Lin, and L. Zhu. “Nanofibrous polystyrene membranes prepared through solution blow spinning with an airbrush and the facile application in oil recovery”. In: *Applied Physics A* 124.5 (2018), page 362 (cited on pages 25, 26).
- [72] S. Sinha-Ray, A. Yarin, and B. Pourdeyhimi. “The production of 100/400 nm inner/outer diameter carbon tubes by solution blowing and carbonization of core–shell nanofibers”. In: *Carbon* 48.12 (2010), pages 3575–3578 (cited on pages 25, 26).
- [73] C. Chen, A. D. Townsend, S. A. Sell, and R. S. Martin. “Microchip-based 3D-cell culture using polymer nanofibers generated by solution blow spinning”. In: *Analytical methods* 9.22 (2017), pages 3274–3283 (cited on page 25).
- [74] A. Kolbasov, S. Sinha-Ray, A. L. Yarin, and B. Pourdeyhimi. “Heavy metal adsorption on solution-blown biopolymer nanofiber membranes”. In: *Journal of Membrane Science* 530 (2017), pages 250–263 (cited on pages 25, 26).
- [75] D. H. Reneker, A. L. Yarin, H. Fong, and S. Koombhongse. “Bending instability of electrically charged liquid jets of polymer solutions in electrospinning”. In: *Journal of Applied physics* 87.9 (2000), pages 4531–4547 (cited on page 25).
- [76] E. S. Medeiros, G. M. Glenn, A. P. Klamczynski, W. J. Orts, and L. H. Mattoso. “Solution blow spinning”. 2014 (cited on page 25).
- [77] S. Sinha-Ray, S. Sinha-Ray, A. L. Yarin, and B. Pourdeyhimi. “Theoretical and experimental investigation of physical mechanisms responsible for polymer nanofiber formation in solution blowing”. In: *Polymer* 56 (2015), pages 452–463 (cited on page 26).
- [78] S. Srinivasan, S. S. Chhatre, J. M. Mabry, R. E. Cohen, and G. H. McKinley. “Solution spraying of poly (methyl methacrylate) blends to fabricate microtextured, superoleophobic surfaces”. In: *Polymer* 52.14 (2011), pages 3209–3218 (cited on page 26).
- [79] X. Zhuang, L. Shi, K. Jia, B. Cheng, and W. Kang. “Solution blown nanofibrous membrane for microfiltration”. In: *Journal of membrane science* 429 (2013), pages 66–70 (cited on page 26).
- [80] J. Lv, X. Yin, R. Li, J. Chen, Q. Lin, and L. Zhu. “Superhydrophobic PCL/PS composite nanofibrous membranes prepared through solution blow spinning with an airbrush for oil adsorption”. In: *Polymer Engineering & Science* 59.S1 (2019), E171–E181 (cited on page 26).
- [81] A. Abdal-Hay, A. S. Hamdy, and J. H. Lim. “Facile preparation of titanium dioxide micro/nanofibers and tubular structures by air jet spinning”. In: *Ceramics International* 40.10 (2014), pages 15403–15409 (cited on page 26).
- [82] B. Cheng, X. Tao, L. Shi, G. Yan, and X. Zhuang. “Fabrication of ZrO₂ ceramic fiber mats by solution blowing process”. In: *Ceramics International* 40.9 (2014), pages 15013–15018 (cited on page 26).
- [83] L. Li, W. Kang, X. Zhuang, J. Shi, Y. Zhao, and B. Cheng. “A comparative study of alumina fibers prepared by electro-blown spinning (EBS) and solution blowing spinning (SBS)”. In: *Materials Letters* 160 (2015), pages 533–536 (cited on page 26).
- [84] H. Wang, S. Lin, S. Yang, X. Yang, J. Song, D. Wang, H. Wang, Z. Liu, B. Li, M. Fang, et al. “High-temperature particulate matter filtration with resilient yttria-stabilized ZrO₂ nanofiber sponge”. In: *Small* 14.19 (2018), page 1800258 (cited on page 26).
- [85] N. Wang, Y. Chen, J. Ren, X. Huang, X. Chen, G. Li, and D. Liu. “Electrically conductive polyaniline/polyimide microfiber membrane prepared via a combination of solution blowing and subsequent in situ polymerization growth”. In: *Journal of Polymer Research* 24.3 (2017), page 42 (cited on page 26).

- [86] L. A. Mercante, M. H. Facure, D. A. Locilento, R. C. Sanfelice, F. L. Migliorini, L. H. Mattoso, and D. S. Correa. "Solution blow spun PMMA nanofibers wrapped with reduced graphene oxide as an efficient dye adsorbent". In: *New Journal of Chemistry* 41.17 (2017), pages 9087–9094 (cited on page 26).
- [87] A. Abdal-hay, A. S. Hamdy, K. A. Khalil, and J. H. Lim. "A novel simple one-step air jet spinning approach for deposition of poly (vinyl acetate)/hydroxyapatite composite nanofibers on Ti implants". In: *Materials Science and Engineering: C* 49 (2015), pages 681–690 (cited on page 26).
- [88] M. Gonzalez-Abrego, A. Hernandez-Granados, C. Guerrero-Bermea, A. M. de la Cruz, D. Garcia-Gutierrez, S. Sepulveda-Guzman, and R. Cruz-Silva. "Mesoporous titania nanofibers by solution blow spinning". In: *Journal of Sol-Gel Science and Technology* 81.2 (2017), pages 468–474 (cited on page 26).
- [89] Y. Zhang, M. W. Lee, S. An, S. Sinha-Ray, S. Khansari, B. Joshi, S. Hong, J.-H. Hong, J.-J. Kim, B. Pourdeyhimi, et al. "Antibacterial activity of photocatalytic electrospun titania nanofiber mats and solution-blown soy protein nanofiber mats decorated with silver nanoparticles". In: *Catalysis Communications* 34 (2013), pages 35–40 (cited on page 26).
- [90] M. Ghosh, J. Liu, S. S. Chuang, and S. C. Jana. "Fabrication of hierarchical V₂O₅ nanorods on TiO₂ nanofibers and their enhanced photocatalytic activity under visible light". In: *ChemCatChem* 10.15 (2018), pages 3305–3318 (cited on page 26).
- [91] L. Li, W. Kang, F. Li, Z. Li, J. Shi, Y. Zhao, and B. Cheng. "Coaxial solution blowing of modified hollow polyacrylonitrile (PAN) nanofiber Fe complex (Fe-AO-CSB-HPAN) as a heterogeneous Fenton photocatalyst for organic dye degradation". In: *RSC Advances* 5.84 (2015), pages 68439–68445 (cited on page 26).
- [92] J. P. Hooper. "Centrifugal spinneret". July 1924 (cited on page 27).
- [93] M. R. Badrossamay, H. A. McIlwee, J. A. Goss, and K. K. Parker. "Nanofiber assembly by rotary jet-spinning". In: *Nano letters* 10.6 (2010), pages 2257–2261 (cited on page 27).
- [94] B. Vazquez, H. Vasquez, and K. Lozano. "Preparation and characterization of polyvinylidene fluoride nanofibrous membranes by forcespinningTM". In: *Polymer Engineering & Science* 52.10 (2012), pages 2260–2265 (cited on page 27).
- [95] X. Zhang and Y. Lu. "Centrifugal spinning: an alternative approach to fabricate nanofibers at high speed and low cost". In: *Polymer Reviews* 54.4 (2014), pages 677–701 (cited on page 27).
- [96] L. Ren, V. Pandit, J. Elkin, T. Denman, J. A. Cooper, and S. P. Kotha. "Large-scale and highly efficient synthesis of micro- and nano-fibers with controlled fiber morphology by centrifugal jet spinning for tissue regeneration". In: *Nanoscale* 5.6 (2013), pages 2337–2345 (cited on page 27).
- [97] K. Sarkar, C. Gomez, S. Zambrano, M. Ramirez, E. de Hoyos, H. Vasquez, and K. Lozano. "Electrospinning to forcespinningTM". In: *Materials today* 13.11 (2010), pages 12–14 (cited on page 27).
- [98] S. Taghavi and R. Larson. "Regularized thin-fiber model for nanofiber formation by centrifugal spinning". In: *Physical Review E* 89.2 (2014), page 023011 (cited on pages 27, 28).
- [99] M. A. Hammami, M. Krifa, and O. Harzallah. "Centrifugal force spinning of PA6 nanofibers—processability and morphology of solution-spun fibers". In: *the Journal of the Textile Institute* 105.6 (2014), pages 637–647 (cited on pages 27, 28).
- [100] M. Huttunen and M. Kellomäki. "A simple and high production rate manufacturing method for submicron polymer fibres". In: *Journal of tissue engineering and regenerative medicine* 5.8 (2011), e239–e243 (cited on pages 27, 28).
- [101] P. Mellado, H. A. McIlwee, M. R. Badrossamay, J. A. Goss, L. Mahadevan, and K. Kit Parker. "A simple model for nanofiber formation by rotary jet-spinning". In: *Applied Physics Letters* 99.20 (2011), page 203107 (cited on page 27).
- [102] S. Padron, R. Patlan, J. Gutierrez, N. Santos, T. Eubanks, and K. Lozano. "Production and characterization of hybrid BEH-PPV/PEO conjugated polymer nanofibers by forcespinningTM". In: *Journal of applied polymer science* 125.5 (2012), pages 3610–3616 (cited on page 27).
- [103] S. Padron, A. Fuentes, D. Caruntu, and K. Lozano. "Experimental study of nanofiber production through forcespinning". In: *Journal of applied physics* 113.2 (2013), page 024318 (cited on page 27).

4.

Chapter

Questions and answers about synthetic fibers in wastewater treatment

By: Heather A. Leslie¹, Edited by R. Martijn Wagterveld²

- 1 – Dept. of Environment and Health, VU Amsterdam, the Netherlands
- 2 – Wetsus, European Centre of Excellence for Sustainable Water Technology, Oostergoweg 9, 8911 MA Leeuwarden, The Netherlands
e-mail: martijn.wagterveld@wetsus.nl

In chapter 9 and 12 is mentioned that in the order of 10 million tonnes per year of persistent plastic waste leaks into rivers and waterways, and ultimately into the oceans [1, 2], from a large number of land based sources [3]. It is estimated that around 2 million tons is in the form of macro- and micro-plastic [4]. Wastewater treatment plants are significant sources of microplastics in river catchments with concentrations reaching up to 125 particles per liter [5]. In addition to this, sea-based sources of plastic litter (beach littering, shipping and fisheries) and atmospheric transport and deposition of micro and nanoplastics (MNPs), may also be important pathways [3, 6, 7].

Chapter 1 highlights that air is also being permeated by fibers; 92% are fibers originating from synthetic garments and carpets. Although little information is available in literature some deposition numbers can be found, which are in the order of 100 fibers $m^{-2} d^{-1}$ (outdoor) and 10 fibers m^{-3} (indoor), see chapter 12.

Sewage treatment plants (STPs) collect the debris of consumer society and biological waste that go down our drains and into our sewers in the Netherlands. They receive synthetic fibers from washing machine effluents, house dust we clean off our shelves and rinse down the drain, from atmospheric deposition and other diffuse sources of plastic microdebris.

What is the real role of wastewater treatment in mitigation of emissions of synthetic fibers to the environment?

Wastewater treatment is an end-of-pipe infrastructure that is available to about 20% of the world's total human population. Over 6 billion people do not have access to wastewater treatment so obviously this is a 'solution' that is available strictly to the richest communities on Earth. One thing that ca. 7.7 billion humans do have in common is that they are all wearing synthetic clothing and using synthetic fiber textiles. And this means they are emitting microfibrils and microfilaments every single day through normal use of these products.

STPs are not designed to digest plastic, as these materials are highly resistant to biodegradation. A large fraction of the plastic particles are however contained in the sludge. The sludge is then converted to microplastic-enriched biosolids for use as fertilizer, or incinerated. It is no longer legal to dump sewage sludge at sea. In our study of Dutch STPs over 70% of the microplastics were retained in the sludge. The treated wastewater effluents always contained microplastics, varying in concentrations from 9 to 91 particles per liter. The majority of the particles

detected were filaments of synthetic fibers. The Amsterdam surface waters receiving these effluents were also enriched in microplastics, as were the suspended particulate matter samples collected from the Rhine and Meuse rivers.

Chapter 9 will also show that car wear and tear, consisting largely of elongated particles of rubber polymers [8], significantly contribute to the flow of (micro)plastics into the aquatic environment with a relative contribution of 5–10% of total global oceanic plastic.

The water sector is activated to determine to what extent it can mitigate the emissions of plastic. Chapter 15 discusses alternative treatment techniques. In light of all the above we can ask ourselves if the wastewater treatment sector is the best place to invest resources to this end. There is a strong case for cleaner, production of textiles, with less (or no) harmful waste, as a long-term, affordable solution. This can drive innovation, and be more effective in reaching the goal of worldwide reductions in microplastic emissions, and not just in the world's richest countries. Making safe textiles available to all textile users on the planet would pay for itself because these textiles will be marketed, advertised, sold and bought by users. This approach avoids citizens again footing the gigantic bill for the negative externalities of the world's textile producers.

References

- [1] J. R. Jambeck, R. Geyer, C. Wilcox, T. R. Siegler, M. Perryman, A. Andrady, R. Narayan, and K. L. Law. "Plastic waste inputs from land into the ocean". In: *Science* 347.6223 (2015), pages 768–771 (cited on page 35).
- [2] J. Boucher and D. Friot. *Primary microplastics in the oceans: a global evaluation of sources*. IUCN Gland, Switzerland, 2017 (cited on page 35).
- [3] P. Kershaw. *Sources, fate and effects of microplastics in the marine environment: a global assessment*. Technical report. International Maritime Organization, 2015 (cited on page 35).
- [4] L. C. Lebreton, J. Van Der Zwet, J.-W. Damsteeg, B. Slat, A. Andrady, and J. Reisser. "River plastic emissions to the world's oceans". In: *Nature communications* 8 (2017), page 15611 (cited on page 35).
- [5] G. Gatidou, O. S. Arvaniti, and A. S. Stasinakis. "Review on the occurrence and fate of microplastics in Sewage Treatment Plants". In: *Journal of hazardous materials* 367 (2019), pages 504–512 (cited on page 35).
- [6] C. M. Rochman. "Microplastics research—from sink to source". In: *Science* 360.6384 (2018), pages 28–29 (cited on page 35).
- [7] K. Liu, T. Wu, X. Wang, Z. Song, C. Zong, N. Wei, and D. Li. "Consistent transport of terrestrial microplastics to the ocean through atmosphere". In: *Environmental science & technology* 53.18 (2019), pages 10612–10619 (cited on page 35).
- [8] F. Sommer, V. Dietze, A. Baum, J. Sauer, S. Gilge, C. Maschowski, and R. Gieré. "Tire abrasion as a major source of microplastics in the environment". In: *Aerosol and air quality research* 18.8 (2018), pages 2014–2028 (cited on page 36).

Measurement of nano- and microfibers in water and air: Physical and chemical methods.

Commercially available techniques

By: Louk Peffer¹, R. Martijn Wagterveld², Jan. C.M. Marijnissen³

- 1 – Delft Solids Solutions BV, Molenweer 2B, 2291 NR Wateringen, The Netherlands
- 2 – Wetsus, European Centre of Excellence for Sustainable Water Technology, Oostergoweg 9, 8911 MA Leeuwarden, The Netherlands
- 3 – Aerosolconsultancy, Zaart 11, 4819ED Breda, The Netherlands

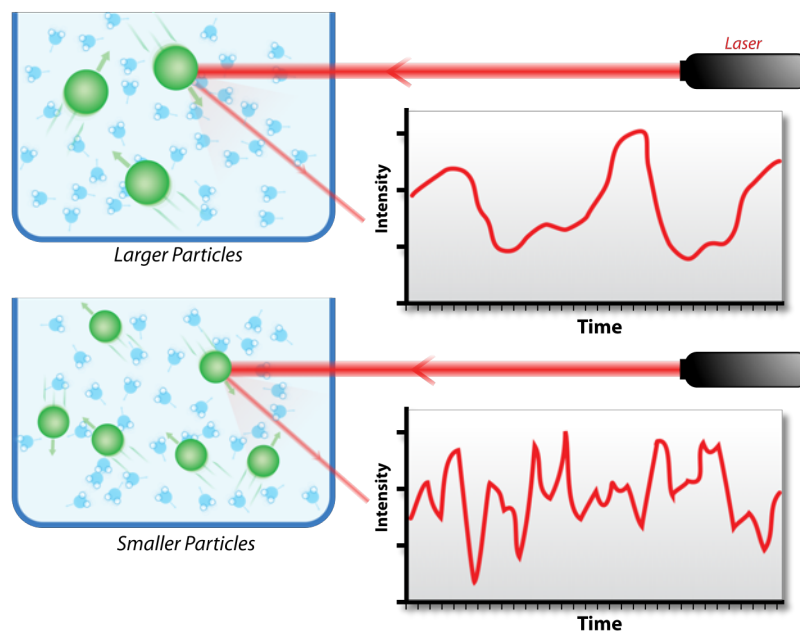


Figure 5.1.: Sketch of one of the measurement principles: Dynamic light scattering. By Mike Jones / CC BY-SA <https://creativecommons.org/licenses/by-sa/3.0>

Table 5.1.: Overview of commercially available techniques and their measurement properties

Measurement technique	Measurement parameter	Measurement range	Concentration	Sample type	Preparation	Name - Manufacturer
Product name	Principle	Size etc.	Distribution	Overall	Typical	
Dynamic light scattering (photon correlation spectroscopy)	Photon correlation spectroscopy (Brownian motion)	Light-scattering intensity-weighted average (hydrodynamic diameter)	Spherical hydrodynamic particle size distribution, monomodal and non-monomodal	0.5 to 10,000 nm	-	Nanophox - Sympatec
Dynamic light scattering (non-invasive back scattering) and Zeta potential	Photon correlation spectroscopy (Brownian motion), Laser Doppler electrophoresis	Light-scattering intensity-weighted average (hydrodynamic diameter) plus Zeta potential	Spherical hydrodynamic particle size distribution, monomodal, bi-modal (1:3) to poly-disperse	0.3 to 10,000 nm	1 to 5000 nm	Zetasizer Nano series - Malvern Pananalytical
Differential centrifugation - Photo centrifuge	Settling speed by centrifugal G-force according to Stokes' law	Hydrodynamic diameter	Volume or light extinction based	2 to 80,000 nm	10 to 1000 nm	CPS Disc Centrifuge - CPS instruments
Morphology and chemical identity	Optical microscopic imaging and Raman spectroscopy	Circular diameter, Shape descriptors and Identity	Number and Volume, and Shape distribution, Chemical classification	0.5 to 1300 μm , 1 to 1300 μm^a	0.5 to 1300 μm	Malvern Morphology G3 ID - Malvern Panalytical
Nano Tracking Analysis (NTA)	Monitoring displacement by Brownian motion of individual particles	Size (Particle's sphere equivalent hydrodynamic diameter)	Hydrodynamic number size distribution with single particle resolution	10 to 2000 nm	10 to 1000 nm	Nanosight NS300 - Malvern Panalytical

Continued on next page

Table 5.1 - continued from previous page

Measurement technique		Measurement Parameter		Measurement range		Concentration	Sample type	Preparation	Name - Manufacturer
Product name	Principle	Size etc.	Distribution	Overall	Typical				
Charger-Electrometer Aerosol Monitor	Diffusion charging	Size (number, area)	Average size, surface areas and number per unit volume	20 to 120 nm average particle diameter	10 to 300 nm	0 to 10 ⁶ particles cm ⁻³	Airborne ultra-fine and nanoparticles	None	NanoTracer XP - Oxil-ity
SEM-EDS, Scanning Electron Microscope, Energy Dispersive Spectroscopy	Electron microscopic imaging, morphology; Detection X-rays of all energies	Size, shape, morphology; elemental composition, area fraction	2D size and shape distribution, Multi-elemental (chemical) composition	< 50 nm to several mm ^b	-	≥ 1000 ppm	Dry	Representative sampling very important	TM3030 - Hitachi / Quantax EDS - Bruker
TEM, Transmission Electron Microscope	Electron microscopic imaging, morphology	Size, shape, morphology; area fraction	2D size and shape distribution	0.5 nm to 100 nm	-	-	Dry	Representative sampling very important, sample slice thickness < 300 nm	JEM-F200 - JEOL
SAXS, Small Angle X-Ray Scattering	Interaction (adsorption, scattering) of X-rays with matter	Size (volume), shape, surface, inner structure, porosity, crystallinity	-	0.15 to 310 nm	1 to 200 nm	-	Liquids, pastes, solids, powders	Depending on matter	SAXSpoint 2.0 - Anton Paar
Laser Diffraction - Static Light Scattering	Model based calculation of scattered laser light	Equivalent laser scatterer diameter	Volume based equivalent spheres	0.010 to 3500 μm	Dv50: 20 nm - 3.0 mm	mg to g	Suspensions, dispersed dry powder, emulsions	Concentration in range	Malvern MasterSizer 3000 - Malvern Pananalytical

Continued on next page

Table 5.1 - continued from previous page

Measurement technique	Measurement Parameter	Measurement range	Concentration	Sample type	Preparation	Name - Manufacturer
Product name	Principle	Size etc.	Distribution	Overall	Typical	
Volume Specific Surface Area (VSSA)	Physical monolayer adsorption of inert gas at low temperature, BET method	$\text{m}^2 \text{cm}^{-3}$	Mean equivalent sphere diameter	-	$100 \text{ nm} = 60 \text{ m}^2 \text{ cm}^{-3}$	$\approx 1 \text{ g}$
					Known density, dry physical clean surface	Autosorb iQ - Anton Paar / TriStar II 3020 - Micromeritics

a Chemical analysis (Raman) b Pixel size is $< 50 \text{ nm}$ (relevant for elemental analysis)

Measurement of nanofibers in the breathing air

By: George Biskos^{1,2}, Jan C.M. Marijnissen³

1 – Climate and Atmosphere Research Centre, The Cyprus Institute, Nicosia 2121, Cyprus

2 – Faculty of Civil Engineering and Geosciences, Delft University of Technology, 2628CN Delft, The Netherlands

3 – Aerosolconsultancy, Zaart 11, 4819ED Breda, The Netherlands

e-mail: g.biskos@cyi.ac.cy; g.biskos@tudelft.nl

abstract Aerosol instrumentation offers a wide range of online tools for characterising airborne nanoparticles. For the majority of these instruments, using the measurements to determine particle size and morphology remains a big challenge when probing non-spherical particles. Specifically for fibrous particles, online identification and counting can be achieved by optical methods, in combination with dielectrophoretic alignment, as well as dielectrophoretic and aerodynamic classification. These techniques, however, can characterise fibrous particles having diameters larger than ca. 0.5 μm in diameter and greater than ca. 2 μm in length. To measure smaller fibers, and particularly nanofibers, one has to use a combination of sizing techniques, including electrostatic classification, in order to determine both the size and the morphology of the sampled particles. At the same time, particle mass spectrometry techniques developed over the past decades can allow online chemical characterisation of the aerosol particles, providing great tools for fully analysing airborne fibers. This chapter provides an overview of these techniques for identifying, characterizing and counting micrometre- and nanometre-sized fibrous particles suspended in the breathing air. It also discusses the feasibility of these techniques and how they can be combined to determine exposure to fibrous particles, and provides an outlook based on recent efforts towards the development of cost-effective and miniaturized instruments for aerosol characterization.

6.1 Introduction

The health effects associated with exposure to asbestos fibrous particles has raised great concerns during the past decades on whether other fiber-like particles suspended in the breathing air can be threatening for humans. Of particular concern are nanofibers, defined as fibrous particles having diameters less than ca. 100 nm, that can potentially be more toxic (due to their smaller size) and able to penetrate deeper in our respiratory system compared to asbestos fibers.

The first steps towards assessing the impacts of airborne nanofibers is i. to distinguish them from the background natural or man-made particles, ii. determine their concentration, and iii. characterize their intrinsic properties including their size/morphology and composition. Traditionally, identification, counting and characterization of airborne fibrous particles is made by collecting samples from the breathing air and analyzing them under a microscope (typically a Scanning or a Transmission Electron Microscope). Such off-line measurements, however, provide qualitative results while at the same time they are tedious and time-consuming. Online identification and characterization of airborne fibrous particles is therefore highly desired for near real-time exposure assessments.

A number of techniques is available for the characterization of non-spherical aerosol nanoparticles, including fibers. For example, by measuring the migration velocity of a particle in a uniform electric field, one can determine their mobility diameter, which corresponds to the apparent diameter that the particle would have if it were a

6. Measurement of nanofibers in the breathing air

sphere. Apart from the size, the mobility diameter of an aerosol particle also depends on its morphology, but determining simultaneously these two properties (i.e., particle size and morphology) is challenging unless some a-priori information is available. For this reason different aerosol sizing techniques need to be combined in order to distinguish non-spherical from spherical/compact-shape particles before counting them in an online manner.

A unique property of fiber-shaped particles is that they can exhibit preferential orientation within a force field, and exhibit optical behavior that is considerably different compared to that of their spherical-shape counterparts. This phenomenon has been used to build instruments for identifying and counting fibrous particles based on their optical and electrophoretic properties. These instruments, however, are more effective for particles larger than a few hundred nanometers. To characterize fibrous particles having sizes in the nanometer range requires a combination of methods, typically resulting in more complex analytical systems.

This chapter provides an overview of aerosol instrument that can be used to identify, count, and measure the size, morphology and composition of non-spherical airborne nanoparticles, and particularly of fibers. Starting with a brief description of standard aerosol sizing principles (Sect. 6.2), the chapter continues by discussing how different operating principles can be combined to distinguish non-spherical from spherical/background particles and determine their concentration, size and morphology (Sect. 6.3). Sect. 6.4 provides a brief overview of particle analysis by mass spectrometry that can be used to determine the composition of aerosol particles including fibers. The last section of the chapter (Sect. 6.5) provides concluding remarks and an outlook based on recent developments with respect to the production of simple/cost-effective aerosol instruments that can be used for monitoring and characterization of fibrous nanoparticles.

6.2 Online physical characterization of nanofibers

Instruments for characterizing aerosol particles employ a range of principles, yielding different expressions of the particle concentration and/or size. The concentration of aerosol particles can be expressed in terms of their number, surface, or volume/mass depending on the measuring principles. Optical particle counters [1] for example, provide direct measurements of the number concentrations of the particles, whereas epifanometers [2] provide a signal that is directly proportional to the surface concentration of the sampled particles. The mass concentration of an aerosol can be determined directly by gravimetric measurements of particles collected on filters, or by measuring their capability to absorb radiation [3].

In a similar manner, the particle size can be expressed in different ways depending on the measuring principle employed. For instance, impactors and aerodynamic particle sizers can be used to determine the "aerodynamic diameter" of the particles, which apart from their size also depends on their shape and density. The "optical diameter" of aerosol particles can be determined by measuring the amount of light scattered by individual particles, which depends on their size, refractive index, and morphology. In a similar manner, electrostatic classifiers can be used to determine the "electrical mobility diameter" of the particles, which apart from their size depends on particle shape but not density.

The paragraphs that follow give an overview of the different measurement principles, and how information of the size and the shape of the particles is related.

6.2.1 Optical Sizing

Particles suspended in a gaseous medium can be counted and sized using their ability to scatter light. Optical Particle Spectrometer (OPSs) that can measure the light scattered by individual particles as they traverse a tightly focused beam of light, can determine their concentration through the counts of single scattering events (each event caused by a single particle), and size through the amplitude of the pulse they produce [4]. In single-particle OPSs the aerosol sample flow is sheathed with a particle-free flow and pulled through the optical detector. The sheath flow collimates

the particles in the aerosol sample flow in a narrow beam, causing them to pass one by one through the focused beam of light.

A fraction of the light scattered by the individual particles is collected by a photodetector that converts it to an electric pulse. The amplitude of this pulse (i.e., the pulse height) is proportional to the size and refractive index of the sampled particles, as well as to their morphology. Information on particle size can be extracted from the magnitude of the electric pulses using calibration curves that are obtained with particles of well-defined size and composition. If information on the size of the sampled particles is already known, the signal from the OPSs can be used to determine either their refractive index (under the assumption that the particles are spherical) or their morphology in the event that their composition, and specifically their refractive index, is known.

Typically, OPSs use a photodetector that is at a fixed angle with respect to the incident light. By measuring the light scattered by the sample particles within a range of angles, information on the shape and/or the refractive index of the particles can be inferred. This is because, apart from the counting events and the height of the resulting pulses, multi-angle detectors provide information on the scattering pattern by the sampled particles, which can differ substantially depending on their morphology. This has been demonstrated in a number of studies by Kaye and his co-workers in the 1990s [5–7], who showed that fibrous particles can easily be distinguished from their spherical-shaped counterparts by observing their scattering patterns as shown in Figure 6.1.

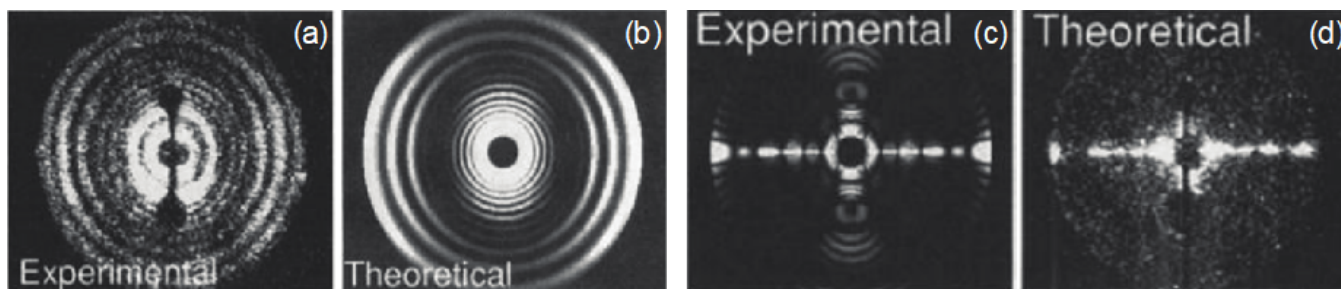


Figure 6.1.: Experimental and theoretical scattering profiles produced by spherical water droplets (a, b) and fibrous (c and d) particles. (Adopted by Hirst and Kaye [6])

It should be noted here that OPSs in general are effective sizers and counters for particles larger than a few hundreds of nanometers. For fibrous particles to be identified and counted by OPSs, they have to be at least a few hundred nanometers in diameter and at least a couple of micrometers in length. These are appropriate ranges for asbestos fibers, but any airborne fibers smaller than that would be practically invisible to OPSs.

6.2.2 Electrostatic Classification

Compared to optical sizing, electrostatic classification can be used to size effectively nanoparticles, and consequently nanofibers, having sizes down to the nanometer scale. There are two mechanisms for classifying nanofibers electrostatically: i. by charging and subsequently exposing them to an uniform electrostatic field, or ii. by polarizing and classifying them in a non-uniform electrostatic field. The first process can be broadly referred to as electrophoretic classification, whereas the second as dielectrophoretic classification. Instruments in the first category include the Differential Mobility Analyser (DMA), and the Aerosol Particle Mass (APM) Analyser, whereas the Fibre Length Classifier fall under the second category. Schematic layouts of these instruments are provided in Figure 6.2, whereas the sections below give a brief description of the associated methods.

6. Measurement of nanofibers in the breathing air

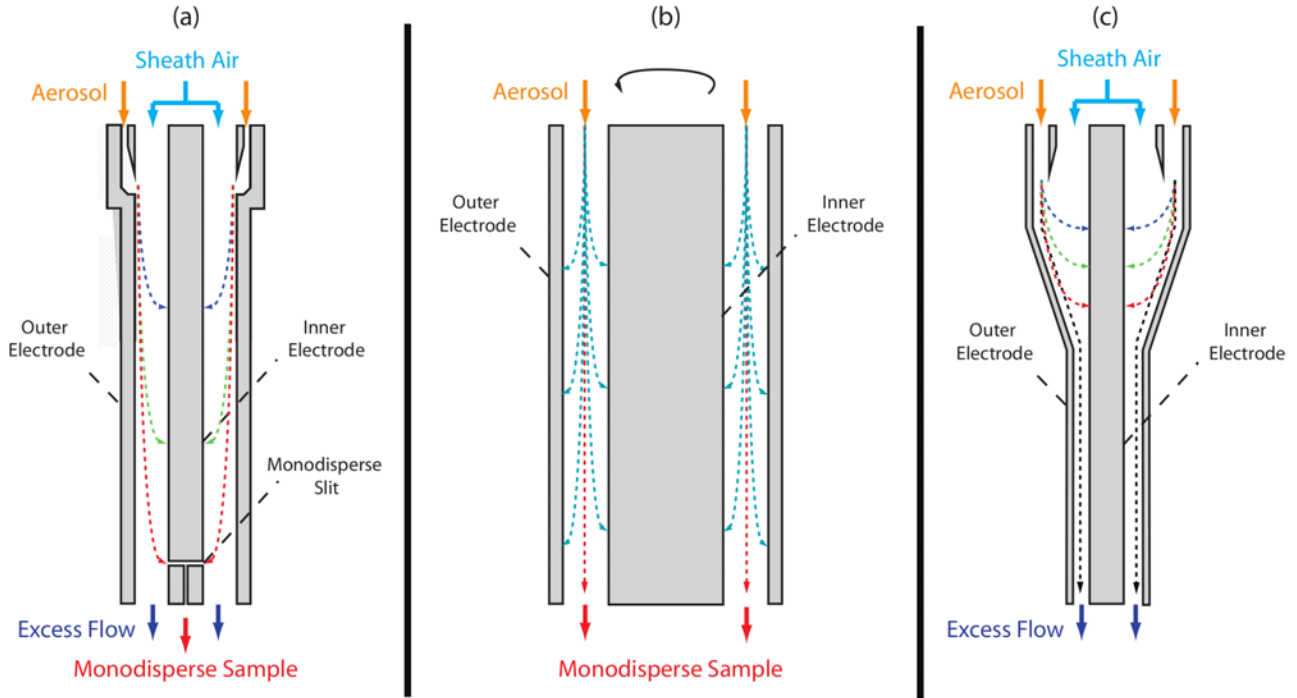


Figure 6.2.: Schematic layout of a Differential Mobility Analyser (a), an Aerosol Particle Mass analyser (b), and a Fibre Length Classifier (c).

Electrophoretic Classification

Electrophoresis describes the motion of charged particles in an electric field. Electrophoretic classification is widely used to determine the electrical mobility of particles, which is related to their size according to:

$$Z = \frac{neC_c(d_m)}{3\pi\eta d_m\chi} \quad (6.1)$$

Here n is the number of elementary charges carried by the particles, e is the charge of the electron, η the dynamic viscosity of the carrier gas, χ is the dynamic shape factor, whereas C_c is the Cunningham slip correction factor given by:

$$C_c = 1 + \frac{2\lambda}{d} \left[1.142 + 0.558 \exp\left(\frac{-0.999d}{2\lambda}\right) \right] \quad (6.2)$$

where λ is the gas mean free path, and d the size of the particles. It should be noted here that subscript m in d_m indicates the so called "mobility diameter" of the particles, which is derived by measuring their electrical mobility.

One of the most widely used electrophoretic classifiers is the Differential Mobility Analyser (DMA [8]). A DMA combines a uniform flow and electrostatic field within which charged aerosol nanoparticles are classified according to their electrical mobility. In brief, charged particles introduced adjacent to one of its electrodes (which is typically grounded) at the one side of the DMA classification column, follow different trajectories within a parallel particle-free sheath flow, ending up at different positions along the other electrode that is kept at high voltage (cf. Figure 6.2a). A narrow slit at the high-voltage electrode is used to pull from the classification zone a flow of particles having electrical

mobilities within a very narrow range (corresponding to the particles arriving at the position where the slit is located). This aerosol flow (i.e., the monodisperse aerosol flow) can then be sent to a counter to determine the concentration of the particles.

Assuming that all the particles carry one elementary charge (an assumption that can be safely made for nanoparticles passed through a bipolar charge neutralizer [9]), the electrical mobility depends only on their size and dynamic shape factor as indicated by Eq. 6.1. Thus, to determine particle size one has to know or assume the shape of the particles, or vice versa. It should be noted here that aspherical charged particles classified by a DMA, can align with the electric field as its strength increases [10]. As a result, they can exhibit a different dynamic shape factor, and thus electrical mobility, depending on the operating conditions of the instrument. This phenomenon has been used in instruments and setups to identify and count fiber-like particles as will be discussed in Sect. 6.3 below.

Particle Mass Classification

Alternatively to classifying charged particles with a DMA along a uniform electric field, one can balance the electrostatic force acting on the particles with a centrifugal force. This principle was first employed by Ehara et al. [11] who developed an instrument that is now commonly referred to as the Aerosol Particle Mass (APM) analyser. The APM consists of two concentric cylindrical electrodes, maintained at a potential difference, that rotate at a fixed angular speed. Charged particles passing through the annulus of the classifier are attracted to the one or the other electrode depending on whether the electrostatic or the centrifugal force acting upon them is stronger. Particles having a mass-to-charge ratio within a very narrow range are balanced and therefore exit the APM classification section in a flow that is typically directed to a particle counter as shown in Figure 6.2b. By adjusting the voltage and the angular velocity of the APM, particles of different mass-to-charge ratios can be selected.

The APM provides a direct measurements of the mass of the particles, determined as:

$$M = \frac{neV}{(2\pi\omega r_c)^2 \ln \frac{r_2}{r_1}} \quad (6.3)$$

where n is the number of elementary charges carried by the particles, e is the charge of the electron, V is the voltage applied between the two electrodes and ω their rotational speed, whereas r_c , r_1 and r_2 are the equilibrium radius (i.e., the radius at which the particles can be balanced), and the radii of the two cylindrical electrodes.

It should be noted here that the mass of the particles that can pass through the PMA does not depend on their morphology. However, when used in combination with electrical mobility classification (i.e., with a DMA upstream as described in Sect. 6.3 below), one can directly determine the shape factor of the particles provided that particle density is known.

Dielectrophoretic Classification

In contrast to electrophoresis, dielectrophoresis describes the motion of an uncharged particle in a non-uniform electrostatic field due to induced polarization. Using this principle, Baron et al. [12] developed an instrument to classify conductive fibrous particles based on their length. Similarly to the DMA, the Fibre Length Classifier (FLC) employs two axisymmetric cylindrical electrodes that are kept at a potential difference (cf. Figure 6.2c). Uncharged but conductive fiber-shaped particles entering the annulus between the two electrodes experience polarization by, and get aligned with, the electric field. As a result of the polarization, the one end of the fiber is attracted to the central electrode whereas the other is pushed away from it. If the electric field in the classifier were uniform, the opposing electrostatic forces at the two ends of fibers would have the same magnitude and thus would cancel each other. Due to the non-uniformity of the electric field in the FLC, however, the magnitude of the two opposing electrostatic forces at the ends of the aligned fibers is different and thus the fibers experience a net force towards the central electrode, where they are collected and subsequently counted.

6. Measurement of nanofibers in the breathing air

The ability of the nanofiber to polarize and migrate within a non-uniform electric field is proportional to their conductivity and size, and particularly to their length. Fully conductive fibers have an infinite dielectric constant, and thus can fully polarize within an electric field. In principle, non-conductive fibers are not polarizable, but they can polarize and consequently be classified in fiber-length classifiers when small amounts of water (which is highly polarizable) are condensed on them; this can be ensured by increasing the Relative Humidity of the sample and the sheath flow passing through the system.

6.2.3 The Fibre Aerosol Monitor

Using the ability of fiber-shaped particle to polarize upon exposure to an electric field, and the patterns of the scattered light they can cause, Lilienfeld et al. [13] developed a Fibrous Aerosol Monitor (FAM). The FAM employs a quadrupole to induce an electric field within its optical detector. This field induces a dipole charge separation on the fibers, and consequently aligns them as they pass through the focused beam of light of the detector. Distinction of the fibers from the background particles is achieved by analyzing the modulations of the scattered light (fibers have a distinctive scattering pattern compared to spherical particles as already discussed in Sect. 6.2.1; cf. Figure 6.1), while their concentration is determined by measuring the counting events.

The FAM is currently commercially available by TSI (Model 7400), and can determine the concentration of airborne fibers that have a minimum diameter of 0.5 μm and length of 2.0 μm , at concentrations up to 10 fibers cm^{-3} . Any fibers smaller than that would require using different techniques to identify and characterize. Description of such techniques are provided in the following section.

6.2.4 Aerodynamic classification

As described above, an impactor and an aerodynamic particle sizer can be used to determine the size of the particles. Both instruments separate the particles based on their inertia, with the impactor using the inertia of the particle to remove the larger/heavier ones from the sample flow and the aerodynamic particle sizer by accelerating the particles and measuring their velocities (i.e., measuring the time they need to travel between two laser beams placed at a small distance along the particle path) that differ depending on their size. In either case, the ability of the particles to follow the motion of the gas molecules is proportional to the so called "aerodynamic diameter" of the particles given by:

$$d_a = d_e \sqrt{\frac{\rho C_c(d_e)}{\chi \rho_0 C_c(d_a)}} \quad (6.4)$$

Here d_e is the diameter of a spherical particle that has an equivalent volume with the sampled particle, ρ and ρ_0 are respectively the density of the particle and the unit density, χ is the dynamic shape factor of the particle, and C_c is the Cunningham slip correction factor given by Eq. 6.2. It should be noted here that any equivalent diameter (e.g., equivalent volume, aerodynamic, electrical mobility diameter, etc.) can be used as d in Eq. 6.2.

Assuming that the aerodynamic diameter of the particles can be measured directly (e.g., by an aerodynamic particle sizer), Eq. 6.4 requires information of the volume equivalent diameter, and the density of the sample particles in order to determine their dynamic shape factor.

Specifically, for nanofibers in the continuum regime the aerodynamic diameter is defined as:

$$d_a = d_f \sqrt{\frac{\rho_f \beta_\alpha}{\chi \rho_0}} \quad (6.5)$$

where d_f and ρ_f are respectively the diameter and the density of the fiber, and β_α its aspect ratio. The dynamic shape

factor of fibrous particles depends on their orientation in the flow field. For random orientation, which typically occurs at low particle Reynolds numbers, the shape factor is given as:

$$\frac{1}{\chi_{ran}} = \frac{1}{3} \left(\frac{1}{\chi_{\parallel}} + \frac{2}{\chi_{\perp}} \right) \quad (6.6)$$

where χ_{\parallel} and χ_{\perp} are the shape factors when the fiber axis of symmetry is respectively parallel or perpendicular to the flow. Although aerodynamic classification at high and low Reynolds numbers can in principle be used to distinguish fibrous from spherical/compact-shaped particles, the technique has not yet been investigated to the best of our knowledge.

6.3 Integrated systems for determining the size and shape of aerosol nanoparticles

With the exception of the FAM and the multi-angle OPSs, the rest of the instruments alone cannot distinguish between non-spherical (fibrous in our case) and spherical/compact particles. It is therefore required to use a combination of methods in order to obtain additional information for the fibers. Brockmann and Rader [14] employed measurements by a cascade impactor and an aerodynamic particle sizer to obtain information on the size and morphology of non-spherical particles (see details in Sect. 6.2.4). Baron et al. [15] also combined a fiber length classifier with an aerodynamic sizer to determine the length and the diameter distribution of fibrous particles in near real time, whereas Canagaratna et al. [16] showed that tandem measurements of aerodynamic particle size and/or optical properties can more broadly provide information related to particle size and morphology.

As mentioned above, aerodynamic and optical classification is limited to fibers having sizes in the micron size range, and thus they are not effective for measuring nanofibers. In contrast, electrostatic classification (cf. Sect. 6.2.2) is the most effective way of sizing particles in the sub-micron and the nanometer size regime. As a result, systems that combine electrostatic classification with other techniques have proven highly useful for disentangling the size from the morphology of sampled aerosol particles in near real time. For example, by using in a tandem configuration a DMA and an inertial impactor, one can determine the particle size and the dynamic shape factor of the particles assuming their density [17]. Coupling electrostatic classification and vacuum aerodynamic particle sizing, one can also derive information both on the size and the dynamic shape factor of the sampled particles [18]. The same information can be obtained by measuring the mass (using an APM) and the electrical mobility (using a DMA) of the particles, provided that their density is known [19]. Last, but not least, tandem measurements involving two DMAs and an intermediate stage where particle morphology can change from that of the non-spherical particle to a more compact shape (e.g., through the adsorption of a working fluid that can "lubricate" - the primary particles in case of large agglomerates - or slightly dissolve or melt the particles), have also been used to determine simultaneously the size and the dynamic shape factor of airborne particles [20].

Park et al. [21] provide a thorough overview of tandem systems that include a DMA to determine a range of aerosol particle properties including their size and morphology. Here we envisage the combination of the above-mentioned techniques in a combo system as illustrated in Figure 6.3. The concept behind tandem measurements carried out by the combo system is that a DMA is used to produce a monodisperse aerosol sample, which is then fed to other sizers; namely an APM, an APS, an OPS and a second DMA coupled with an aerosol conditioner for restructuring the particles.

The paragraphs that follow provide a brief description of how the different components of this combo system can be combined to derive specific properties of the sampled aerosol particles, including fibrous particles.

The tandem DMA-APM: Electrical mobility sizing followed by particle mass classification can be used to determine particle hygroscopicity [22], density, or morphology. In this case the DMA is used to determine the

6. Measurement of nanofibers in the breathing air

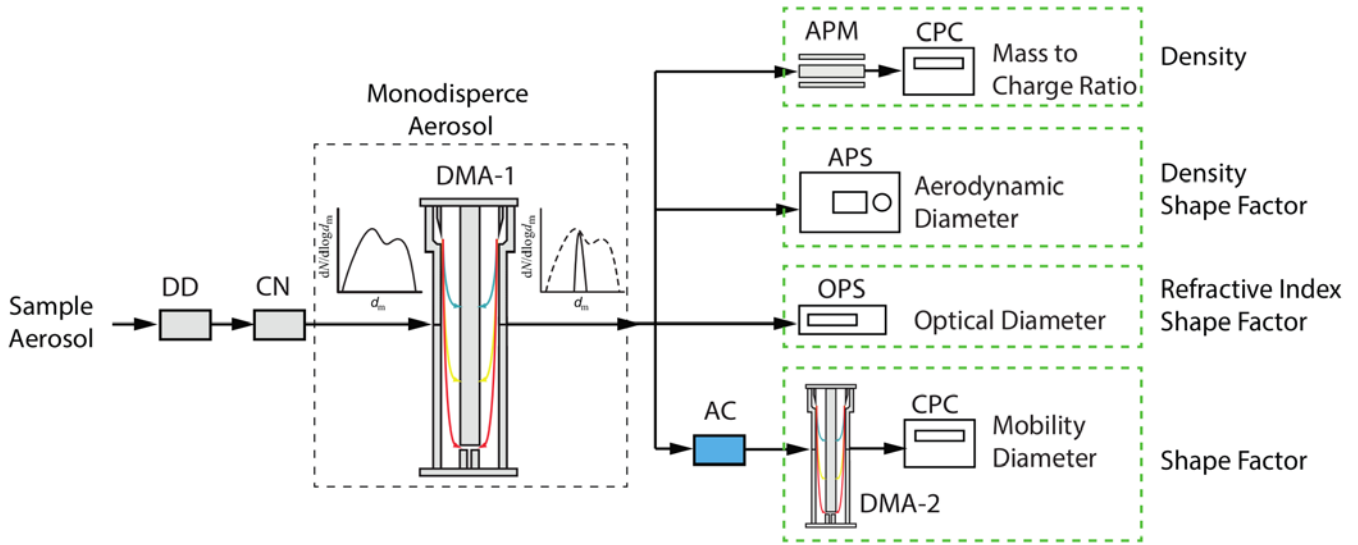


Figure 6.3.: Combination of instruments that can be used to determine the density, refractive index, and shape factor of sampled particles. Key: DD, Diffusion Dryer; CN, Charge Neutralizer; DMA, Differential Mobility Analyser; AC, Aerosol Conditioner; CPC, Condensation Particle Counter; OPS, Optical Particle Spectrometer; APS, Aerodynamic Particle Sizer; APM, Aerosol Particle Mass analyser.

electrical mobility equivalent diameter (cf. Eq. 6.1) of the particles, and the APM the mass of the particle (cf. Eq. 6.3). Assuming that the particles are spherical, the diameter determined by the DMA can be used to calculate the volume of the particles, which combined with the information of their mass can be used to determine their density. If the density of the particles is known, the two measurements can be used to determine the dynamic shape factor of the particles. In this case, information of the mass can be used to estimate an equivalent diameter corresponding to spherical particles having the same mass. This diameter can then be plugged in Eq. 6.1, in order to calculate the dynamic shape factor of the particles. This technique has been used to infer the morphology of cubic-shaped sodium chloride particles using an APM that can measure the mass of sub-10-nm particles [23].

The tandem DMA-APS: The DMA and the APS can be combined to determine the density, if the sampled particles are spherical [24], or the dynamic shape factor of the sampled particles. It should be noted here that traditional APSs operated at atmospheric, or near atmospheric, pressure can size particles having diameters larger than ca. 500 nm, and thus may not be applicable for the characterization of nanofibers as discussed above. Aerodynamic sizers operated at vacuum conditions that are typically employed with Aerosol Mass Spectrometers [16], however, can determine the size of smaller particles, and can thus be employed for the characterization of small aerosol fibers. It should be noted here that the vacuum aerodynamic diameter of non-spherical particles in such sizers is given by:

$$d_{va} = \frac{\rho_p d_e}{\rho_0 \chi} \quad (6.7)$$

Similarly, the mobility diameter can be expressed in terms of volume equivalent diameter as [18]:

$$d_m = \frac{c_c(d_m) \chi d_e}{c_c(d_e)} \quad (6.8)$$

The only unknowns in the two equations above are ρ_p, d_e , and χ . However, if the density of the particles is known, Eqs. 6.7 and 6.8 can be used to estimate the volume equivalent diameter and the shape factor of the particles.

The tandem DMA-OPS: The combinations of electrical mobility and optical measurements is typically used to determine the optical properties (i.e., the refractive index) of aerosol particles. If the composition (and thus the refractive index) of the sampled particles is known, their optical behavior can be used to infer their morphology. However, because a unique relationship between mobility diameter and optical response is difficult to obtain, the combination of these two measuring techniques may not always lead to interpretable results. For the particular case of characterizing fibrous particles, having the particles aligned in the optical detector (as it is done in the FAM described above) is required for distinguishing them from spherical/compact-shaped background particles. It should be also noted here that because typical OPSs can measure particles larger than a few hundreds of nanometers, the combination of these two techniques is limited to that size range.

The tandem DMA: An alternative to combining two instruments using different operating principles as described above, employing two DMAs in tandem can also provide information about the size and the morphology of the sampled particles. Traditionally, Tandem DMA (TDMA) systems have been used to measure the hygroscopicity [25] or the volatility (e.g., [26]) of aerosol particles, but attempts to probe information about the morphology have also been made (e.g., [27]). To extract information on particle morphology from TDMA measurements, the particles need to go complete (or nearly complete) restructuring between the two DMAs. This can be achieved for agglomerated particles by condensing some working fluid for "lubrication" (of the primary particles in case of large agglomerates) or by mild melting, thereby reducing open structures to more compact/spherical geometries. For the particular case of fibrous particles, unless those can be dissolved when small amounts of a solvent can be condensed on their surface, mild heating may be sufficient. Because this technique has not been extensively employed yet for the characterization of fiber-shaped particles, further proof-of-concept tests using fibrous particles of different composition are required.

6.4 Online chemical analysis

As described above, online techniques to determine the physical properties (i.e., the size and morphology) of fibrous particles already exist, while promising combinations of a number of methods can provide good alternatives for probing additional particle properties (e.g., density and refractive index). To determine the composition of synthetic nanofibers, or the composition of additives, adsorbed contaminants and biofilm compounds on nanofibers, however, one needs to employ a chemical analysis method. Of course this can be achieved by off-line analysis techniques on particles collected with samplers, but that requires a significant amount of time, for the collection of particles, and effort, for the preparation of the samples. To overcome these limitations, online methods to determine the composition of aerosol particles are indispensable, yielding the development of Aerosol Mass Spectrometers (AMSs) over the past decade [28–31].

Generally speaking, on-line systems consist of a specially designed inlet to introduce the particles from ambient conditions into the instrument, a step where they are evaporated and the resulting vapours are ionized, and finally a part where the mass of the ionized vapours is determined by a classical mass spectrometer (MS) system. For instance, in the instrument described by Kleefsman et al. [31], introduction of the sampled particles to the AMS is achieved via a nozzle and skimmers that are designed to suck the particles into the low-pressure chamber, while accelerating them on a narrow particle beam. The velocity of the accelerated particles is then determined by passing them through two laser beams located at a small distance along the path of the particles, providing information on their size in a similar manner as the aerodynamic particle sizer does (cf. Sect. 6.2.4). This information is also used to trigger a high energy laser to volatilize the particles (or part of the particles) and ionize the resulting vapours. Positive ions produced through this process then enter the MS part of the system. In a similar manner, Hinz et al. [29] employed two MS analyzers in order to detect simultaneously positively and negatively charged ions, to improve the specificity of the chemical characterization.

6. Measurement of nanofibers in the breathing air

It should be noted that particles smaller than a few tenths of a micrometer cannot be detected by the lasers employed for sizing in typical AMS systems. To overcome this limitation one can grow the particles by condensation of vapours before entering the vacuum chamber. If for the coating an appropriate material (i.e. a matrix) is applied on the fibers, adsorbed (bio)material can be analysed. This so called Matrix Assisted Laser Desorption/Ionization (MALDI) Mass Spectrometry technique can be used to analyse nanofibers or, as already mentioned, adsorbed (bio)material on the surface of fibers. The technique has been successfully employed to measure different polymers [32, 33], while more recently Geenen et al. [34] reported that Mass Spectrometry can be used to chemically analyse sampled polymer fibers and by using MALDI the fiber finish layer. It should be noted here that for the chemical analysis of liquids or particles (in our case fibers) in liquids, on-line aerosol mass spectrometry can be employed with a system for atomizing the liquid suspension and introducing the resulting droplets into the instrument.

6.5 Conclusions and future perspectives

Compared to probing spherical (or compact-shape) particles, for which it is sufficient to determine only their diameter, fiber-shaped particles require information of both their diameter and length. As discussed in Sects. 6.2 and 6.3, equivalent diameters that can be reported by different sizing techniques (i.e., optical, electrical mobility, and aerodynamic diameter) depend on the shape of the particles. Existing instruments that can be used to distinguish fibrous particles from compact-shaped particles include the multi-angle Optical Particle Counter, the Fibre Length Classifier, and the Fibrous Aerosol Monitor. It should be noted, however, that all these instruments require that the fibers are large enough (typically having diameters $> 0.5 \mu\text{m}$ and lengths $> 2.0 \mu\text{m}$ thereby becoming inappropriate for nanofibers.

To characterize airborne fibers having diameters smaller than ca. 100 nm requires use of a combination of techniques in order to determine both their size and morphology. In this respect, using a DMA in tandem with an APM, OPS or an APS can provide information on the density, the refractive index and the morphology (expressed as a shape factor) of the particles. Changes in particle shape can yield in large differences in mobility diameters, and thus tandem DMA systems, in which a process that can induce particle/fiber restructuring between the two classifiers, have also been effectively employed to determine their morphology.

A process employed in aerosol fiber characterization is their preferential electrostatic orientation during electrical mobility classification. In practice, aerosol fibers can align with the electric field depending on their aspect ratio. For instance, nanowires having diameters of 15 nm and aspect ratios less than 30 tend to rotate freely in electric fields up to 1 kV cm^{-1} , but when their aspect ratio is higher (i.e., if the fibers are longer) they tend to align with the electric field (e.g., [35]). In a similar manner, Zelenyuk and Imre [36] have shown that fiber-shaped chain aggregates can be aligned in mobility classifiers when the applied electric field is relatively high. As a result, identical particles in terms of size and shape, can have different apparent electrical mobilities depending on whether they are classified under a strong or a weak electric field in a DMA.

To use this phenomenon (i.e., alignment in strong electric fields) in order to characterize fibrous aerosol particles one can build a classification system for distinguishing not only between particles of different size but also between particles of different morphology. Although this can be performed by simultaneously employing two DMAs in tandem operated at different operating conditions (i.e., flow rates and electric field strengths), or with one DMA and altering the operating conditions in each measurement, an elegant and more accurate alternative is to have a DMA with two or more monodisperse-particle outlets [37]. By appropriately selecting the location of the monodisperse-particle outlets along the classification column of such a DMA so that particles having the same electrical mobility are classified at stronger and weaker electric fields, one can in principle determine variations in the shape factor of the particles induced by changes of their alignment when they are sampled under higher/lower electric field strengths through different outlets.

One limitation of tandem systems for characterizing airborne nanoparticles is their high complexity and cost,

which in turn limit their use for continuous monitoring. Using new methods of fabricating DMAs [38] can produce lightweight and inexpensive aerosol sizers without sacrificing their accuracy and precision. In addition, electrostatic segregators [39] that do not require controlled sheath flows can offer very compact, simple, and extremely inexpensive solutions that are much simpler to operate in the field; a characteristic that is extremely important when these instruments have to operate unattended for long periods of time. Incorporating these techniques in tandem systems described in Sect. 6.3, can certainly help towards the development of integrated compact nanofiber monitoring and characterization tools that can be used more easily and effectively to assess human exposure.

AMS systems are also available to determine the chemical composition of aerosol particles including fibers. Such systems can provide information of both the size and the composition of particles (and fibers) that are larger than a few tenths of a micrometer. To investigate smaller particles one can use the MALDI techniques, whereby the particles are grown via condensation before sampling. These techniques are successfully used to measure a number of polymers, providing promising ways for the characterization of aerosol nanofibers. Coupled with tools for determining the physical characterization of fibrous aerosol particles as described above, full characterization of aerosol nanofibers can well be realized.

References

- [1] J. Gebhart. “Aerosol Measurement: Principles, Techniques, and Applications”. In: edited by K. Willeke and P. Baron. Industrial Health & Safety. Van Nostrand Reinhold, 1993. Chapter Optical direct-reading techniques: light intensity systems, pages 419–454 (cited on page 42).
- [2] U. Baltensperger, H. Gäggeler, and D. Jost. “The epiphaniometer, a new device for continuous aerosol monitoring”. In: *Journal of Aerosol Science* 19.7 (1988), pages 931–934 (cited on page 42).
- [3] E. Triantafyllou, E. Diapouli, E. Tsilibari, A. Adamopoulos, G. Biskos, and K. Eleftheriadis. “Assessment of factors influencing PM mass concentration measured by gravimetric & beta attenuation techniques at a suburban site”. In: *Atmospheric environment* 131 (2016), pages 409–417 (cited on page 42).
- [4] W. R. Zinky. “A new tool for air pollution control: The aerosol particle counter”. In: *Journal of the Air Pollution Control Association* 12.12 (1962), pages 578–583 (cited on page 42).
- [5] P. H. Kaye, N. Eyles, I. Ludlow, and J. Clark. “An instrument for the classification of airborne particles on the basis of size, shape, and count frequency”. In: *Atmospheric Environment. Part A. General Topics* 25.3-4 (1991), pages 645–654 (cited on page 43).
- [6] E. Hirst and P. H. Kaye. “Experimental and theoretical light scattering profiles from spherical and nonspherical particles”. In: *Journal of Geophysical Research: Atmospheres* 101.D14 (1996), pages 19231–19235 (cited on page 43).
- [7] P. H. Kaye. “Spatial light-scattering analysis as a means of characterizing and classifying non-spherical particles”. In: *Measurement Science and Technology* 9.2 (1998), page 141 (cited on page 43).
- [8] E. Knutson and K. Whitby. “Aerosol classification by electric mobility: apparatus, theory, and applications”. In: *Journal of Aerosol Science* 6.6 (1975), pages 443–451 (cited on page 44).
- [9] A. Wiedensohler. “An approximation of the bipolar charge distribution for particles in the submicron size range”. In: *Journal of aerosol science* 19.3 (1988), pages 387–389 (cited on page 45).
- [10] H.-C. Hansson and M. S. Ahlberg. “Dynamic shape factors of sphere aggregates in an electric field and their dependence on the Knudsen number”. In: *Journal of aerosol science* 16.1 (1985), pages 69–79 (cited on page 45).
- [11] K. Ehara, C. Hagwood, and K. J. Coakley. “Novel method to classify aerosol particles according to their mass-to-charge ratio—aerosol particle mass analyser”. In: *Journal of Aerosol Science* 27.2 (1996), pages 217–234 (cited on page 45).
- [12] P. Baron, G. Deye, and J. Fernback. “Length separation of fibers”. In: *Aerosol science and technology* 21.2 (1994), pages 179–192 (cited on page 45).
- [13] P. Lilienfeld, P. B. Elterman, and P. Baron. “Development of a prototype fibrous aerosol monitor”. In: *American Industrial Hygiene Association Journal* 40.4 (1979), pages 270–282 (cited on page 46).
- [14] J. Brockmann and D. Rader. “APS response to nonspherical particles and experimental determination of dynamic shape factor”. In: *Aerosol Science and Technology* 13.2 (1990), pages 162–172 (cited on page 47).
- [15] P. Baron, G. Deye, J. Fernback, and W. Jones. “Direct-reading measurement of fiber length/diameter distributions”. In: *Advances in Environmental Measurement Methods for Asbestos*. ASTM International, 1999 (cited on page 47).

- [16] M. Canagaratna, J. Jayne, J. Jimenez, J. Allan, M. Alfarra, Q. Zhang, T. Onasch, F. Drewnick, H. Coe, A. Middlebrook, et al. “Chemical and microphysical characterization of ambient aerosols with the aerodyne aerosol mass spectrometer”. In: *Mass spectrometry reviews* 26.2 (2007), pages 185–222 (cited on pages 47, 48).
- [17] W. Kelly and P. H. McMurry. “Measurement of particle density by inertial classification of differential mobility analyzer-generated monodisperse aerosols”. In: *Aerosol Science and Technology* 17.3 (1992), pages 199–212 (cited on page 47).
- [18] P. F. DeCarlo, J. G. Slowik, D. R. Worsnop, P. Davidovits, and J. L. Jimenez. “Particle morphology and density characterization by combined mobility and aerodynamic diameter measurements. Part 1: Theory”. In: *Aerosol Science and Technology* 38.12 (2004), pages 1185–1205 (cited on pages 47, 48).
- [19] P. H. McMurry, X. Wang, K. Park, and K. Ehara. “The relationship between mass and mobility for atmospheric particles: A new technique for measuring particle density”. In: *Aerosol Science & Technology* 36.2 (2002), pages 227–238 (cited on page 47).
- [20] G. Biskos, D. Paulsen, L. Russell, P. Buseck, and S. Martin. “Prompt deliquescence and efflorescence of aerosol nanoparticles”. In: (2006) (cited on page 47).
- [21] K. Park, D. Dutcher, M. Emery, J. Pagels, H. Sakurai, J. Scheckman, S. Qian, M. R. Stolzenburg, X. Wang, J. Yang, et al. “Tandem measurements of aerosol properties—A review of mobility techniques with extensions”. In: *Aerosol Science and Technology* 42.10 (2008), pages 801–816 (cited on page 47).
- [22] S. Leinert and A. Wiedensohler. “A DMA and APS based technique for measuring aerodynamic hygroscopic growth factors of micrometer-size aerosol particles”. In: *Journal of aerosol science* 39.5 (2008), pages 393–402 (cited on page 47).
- [23] D. Broßell, M. Valenti, S. Bezantakos, A. Schmidt-Ott, and G. Biskos. “The nano-particle mass classifier (nano-PMC): Development, characterization, and application for determining the mass, apparent density, and shape of particles with masses down to the zeptogram range”. In: *Aerosol Science and Technology* 49.7 (2015), pages 495–507 (cited on page 48).
- [24] J. G. Slowik, K. Stainken, P. Davidovits, L. Williams, J. Jayne, C. Kolb, D. R. Worsnop, Y. Rudich, P. F. DeCarlo, and J. L. Jimenez. “Particle morphology and density characterization by combined mobility and aerodynamic diameter measurements. Part 2: Application to combustion-generated soot aerosols as a function of fuel equivalence ratio”. In: *Aerosol Science and Technology* 38.12 (2004), pages 1206–1222 (cited on page 48).
- [25] E. Swietlicki, H.-C. Hansson, K. Hämeri, B. Svenningsson, A. Massling, G. McFiggans, P. H. McMurry, T. Petäjä, P. Tunved, M. Gysel, et al. “Hygroscopic properties of submicrometer atmospheric aerosol particles measured with H-TDMA instruments in various environments—a review”. In: *Tellus B: Chemical and Physical Meteorology* 60.3 (2008), pages 432–469 (cited on page 49).
- [26] L. Mendes, K. Eleftheriadis, and G. Biskos. “Performance comparison of two thermodenuders in Volatility Tandem DMA measurements”. In: *Journal of Aerosol Science* 92 (2016), pages 38–52 (cited on page 49).
- [27] G. A. Kelesidis, F. M. Furrer, K. Wegner, and S. E. Pratsinis. “Impact of humidity on silica nanoparticle agglomerate morphology and size distribution”. In: *Langmuir* 34.29 (2018), pages 8532–8541 (cited on page 49).
- [28] J. Marijnissen, B. Scarlett, and P. Verheijen. “Proposed on-line aerosol analysis combining size determination, laser-induced fragmentation and time-of-flight mass spectroscopy”. In: *Journal of Aerosol Science* 19.7 (1988), pages 1307–1310 (cited on page 49).
- [29] K.-P. Hinz, R. Kaufmann, and B. Spengler. “Simultaneous detection of positive and negative ions from single airborne particles by real-time laser mass spectrometry”. In: *Aerosol Science and Technology* 24.4 (1996), pages 233–242 (cited on page 49).
- [30] K.-P. Hinz and B. Spengler. “Instrumentation, data evaluation and quantification in on-line aerosol mass spectrometry”. In: *Journal of Mass Spectrometry* 42.7 (2007), pages 843–860 (cited on page 49).
- [31] W. Kleefsman, M. Stowers, P. Verheijen, and J. Marijnissen. “Single particle mass spectrometry—bioaerosol analysis by MALDI MS”. In: *KONA Powder and Particle Journal* 26 (2008), pages 205–214 (cited on page 49).
- [32] A. P. Gies, M. Kliman, J. A. McLean, and D. M. Hercules. “Characterization of branching in aramid polymers studied by MALDI- ion mobility/mass spectrometry”. In: *Macromolecules* 41.22 (2008), pages 8299–8301 (cited on page 50).
- [33] G. R. Hilton, A. T. Jackson, K. Thalassinou, and J. H. Scrivens. “Structural analysis of synthetic polymer mixtures using ion mobility and tandem mass spectrometry”. In: *Analytical chemistry* 80.24 (2008), pages 9720–9725 (cited on page 50).

- [34] F. A. van Geenen, M. C. Franssen, A. H. Schotman, H. Zuilhof, and M. W. Nielen. “Ambient characterization of synthetic fibers by laser ablation electrospray ionization mass spectrometry”. In: *Analytical chemistry* 89.7 (2017), pages 4031–4037 (cited on page 50).
- [35] S. Kim, G. Mulholland, and M. Zachariah. “Understanding ion-mobility and transport properties of aerosol nanowires”. In: *Journal of aerosol science* 38.8 (2007), pages 823–842 (cited on page 50).
- [36] A. Zelenyuk and D. Imre. “On the Effect of Particle Alignment in the DMA”. In: *Aerosol science and technology* 41.2 (2007), pages 112–124 (cited on page 50).
- [37] M. Giamarelou, M. Stolzenburg, and G. Biskos. “The multiple monodisperse outlet differential mobility analyzer: derivation of its transfer function and resolution”. In: *Aerosol Science and Technology* 46.9 (2012), pages 951–965 (cited on page 50).
- [38] K. Barmounis, A. Maisser, A. Schmidt-Ott, and G. Biskos. “Lightweight differential mobility analyzers: Toward new and inexpensive manufacturing methods”. In: *Aerosol Science and Technology* 50.1 (2016), pages 2–5 (cited on page 51).
- [39] S. Bezantakos, L. Huang, K. Barmounis, M. Attoui, A. Schmidt-Ott, and G. Biskos. “A cost-effective electrostatic precipitator for aerosol nanoparticle segregation”. In: *Aerosol Science and Technology* 49.1 (2015), pages iv–vi (cited on page 51).

A human risk banding scheme for high aspect-ratio materials

By: Dirk Broßell¹, Asmus Meyer-Plath¹, Kerstin Kämpf¹, Sabine Plitzko¹, Wendel Wohlleben², Burkhard Stahlmecke³, Martin Wiemann⁴, Andrea Haase⁵

1 – Federal Institute for Occupational Safety and Health (BAuA), Nöldnerstr, 40-42, 10317 Berlin

2 – BASF SE, Geb. B7, 67056 Ludwigshafen

3 – Institute of Energy and Environmental Technology e.V., Bliersheimer Str. 58-60, 47229 Duisburg

4 – IBE R&D gGmbH, Mendelstr. 11, 48149 Münster

5 – German Federal Institute for Risk Assessment (BfR), Department of Chemical and Product Safety, Max-Dohrn-Str. 8-10, 10589 Berlin

abstract High aspect ratio materials (HARM) like carbon nanotubes (CNT) show material properties that enable innovative applications but also raise concerns about harmful effects to humans due to their asbestos-like morphology. A risk banding approach for HARM with hazard- and exposure-related parameters has been developed as a promising way to enable risk assessment and risk mitigation for an important family of advanced materials. It also provides guidance for a safer design of HARM and corresponding products.

Our scheme attributes HARM to three risk levels: low, moderate and high. The two-dimensional risk matrix builds on a hazard and an exposure banding. Parameters for hazard banding are the biopersistence and the fiber rigidity. The latter has been derived from an extension of the classic fiber principle with the intrinsic material property flexural rigidity, hypothesized to play a significant role in limiting the toxicity of inhaled fibers. Current research efforts of BAuA focus on further investigating the influence of flexural rigidity on fiber toxicity aiming at threshold values e.g. for fiber diameter, which can be used as band limits. In addition, we are developing methods for measurement of fiber rigidity.

For exposure banding, relevant parameters are the material dustiness, the propensity of release of fibers with a critical morphology and the degree of fiber agglomeration. fibers of critical morphology are defined according to the WHO fiber counting convention to be thinner than 3 µm, longer than 5 µm and exhibiting an aspect ratio greater than 3:1 [1]. To characterize the dustiness of fibrous materials, we have developed and evaluated the ‘fluidizer’ as an aerosol generator to adequately perform dustiness testing with powders of HARM [2]. In combining aerosol characterization and sampling with subsequent particle-morphological analysis, we enable the identification and characterisation of HARM with relevant potential for release of fibers with critical morphology.

We applied the new risk banding scheme to 15 different types of multi-walled CNTs (MWCNTs) by determining their hazard and exposure parameters and adapting risk bands in accordance to the current knowledge on the risk potential of MWCNTs. A central result of our work is that the tested MWCNT variants cover large parameter ranges and can be allocated to all three risk levels. Our risk banding scheme also enables identifying those properties that are relevant for low risk materials. This way, our risk banding scheme can support the development of safe by design strategies for HARM and other advanced materials.

7.1 Introduction

According to the fiber toxicology paradigm (FTP), the inhalative hazards of high aspect-ratio materials (HARM) are correlated to their aerodynamic properties, durability in the lung environment (bio-durability) and fiber length. It was first proposed by Pott et al., Stanton and Wrench [3, 4] on the basis of toxicological effects of asbestoses, man-made mineral fibers (MMMMF) and vitreous fibers (MMVF) and can be formulated as:

"The elongated shape of fibers is a carcinogenic principle, provided the fibers are respirable, long and bio-durable."

According to this paradigm, fiber-shaped (high aspect ratio > 3), respirable (diameter $< 3 \mu\text{m}$), long (length $> 5 \mu\text{m}$), and bio-durable (insoluble in tissue) fibers may cause harm to lungs.

Many other fiber materials, including polymer fibers, refractory ceramic fibers (RCF), carbon fiber fragments [5] and the broad spectrum of nanofiber variants including carbon nanotubes [6], exhibit combinations of properties being relevant for the FTP. Accordingly, the terms High "Aspect Ratio Materials" (HARM) or "High Aspect Ratio Nanomaterials" (HARN) have been introduced to categorize such materials also with the intention to indicate that they may be of particular concern when it comes to inhalation. However, only a minority of the currently available HARM materials have been actually toxicologically characterized and not all of the investigated materials were found to be hazardous. Thus, it appears necessary to review reports on fiber toxicology and to discuss the toxicity-governing principles in order to further differentiate the FTP.

The FTP links pulmonary toxicity to (1) inhalative uptake, (2) durability in lung tissue and (3) high aspect-ratio geometry. The present understanding can be briefly summarized as follows.

- (1) The alveolar uptake is governed by particle aerodynamics: In the laminar flow regime of the respiratory tract, fibers tend to align their longitudinal axis to the flow, thus minimizing their flow cross-sectional area. Elongated particles thus exhibit smaller aerodynamic diameters and higher penetration rate to the alveoli compared to spherical particles of equivalent mass. Even asbestos fibers with lengths of more than $50 \mu\text{m}$ appear with aerodynamic diameters smaller than $3 \mu\text{m}$ [7], which is the cut-off diameter for alveolar dust.
- (2) Once deposited in lung tissue, bio-durable materials retain their mass and shape rather than degrade. Many asbestos types exhibit low solubility in aqueous physiological media and also within the acidic environment of phagolysosomes of macrophages. A high bio-durability in physiological media and the lack of clearance from the lung due to the fiber geometry contribute to what is called the biopersistence of asbestos fibers. This term describes the long retention time which, in case of asbestos fibers, is typically reaching decades.
- (3) The high-aspect ratio geometry especially of long fibers has been found to inhibit the macrophage-mediated lung clearance mechanism [6]. The efficiency of HARM clearance by macrophages is lower compared to that of spherical particles. This is firstly believed to be partially due to a lower ingestion rate caused by the fact that phagocytosis can only start at a fiber's tip, which must be found by the macrophage prior to ingestion [8]. Secondly, phagocytosis will fail in case a fiber is too long with respect to the macrophage size. In an attempt to internalize long fibers, macrophages have to distort themselves until ingestion eventually gets stalled, a state called incomplete or frustrated phagocytosis. Depending on the type of macrophage, frustrated phagocytosis has been observed for fibers longer than $5 \mu\text{m}$ (pleural space) and $15 \mu\text{m}$ (lung) [9].

Acute pulmonary adverse effects of fibers are believed to be mainly due to frustrated macrophages releasing, e.g., hydrogen peroxide and superoxide anions intend to kill microorganisms. Also mediators such as interleukins and tumour necrosis factor α , both being part of the unspecific immune response, are released and foster local inflammation, also by attracting other phagocytes and immune cells. As a consequence, bio-durable HARM may lead to chronic inflammation, granuloma formation, fibrotic lesions, and possibly cause cancer.

7.2. Risk banding and material properties required for HARM risk banding

fibers of high-aspect ratio geometry may also translocate through the lung parenchyma and, after years, will reach the lung periphery. Eventually they will penetrate the mesothelium and protrude into the pleural cleft where they cause membrane lesions and chronic inflammation. Quite often this has culminated in the development a so-called mesothelioma, a malignant and highly aggressive tumour typical for asbestos exposed workers. Recognizing these processes has led many countries to ban the use of asbestos and also other respirable biopersistent MMMFs and MMVFs.

With the development of fibrous nanomaterials especially carbon nanotubes (CNTs), the FTP has led to appropriate toxicological studies confirming the pathogenicity of high aspect-ratio nanomaterials: Several animal studies on the carcinogenicity of the MITSUI MWNT-7 material showed asbestos-like effects as predicted by the FTP. This material, a vapour-grown carbon fiber [10, 11], comprises a high fraction of individualized multi-walled carbon nanotubes (MWCNTs) long enough to cause frustrated phagocytosis.

Animal studies on very thin MWCNTs however, showed low or no carcinogenicity. In fact, toxicity of such HARM seems to better comply with biopersistent granular particles, for which toxicity is associated with the volume load and lung-specific surface area rather than shape [12, 13]. These results were due to the high degree of agglomeration of the exposure material. Thin MWCNTs more likely entangle into ellipsoidal agglomerates, effectively losing their high aspect-ratio and thus the fiber-toxicological paradigm its applicability. Such not asbestos-like carcinogenicity suggests to extend the FTP, as will be discussed in the following.

Animal studies with thin multi-walled (MW) or even single-walled (SW) CNTs with an exposure dose comprising a high fraction of individual fibers longer than 5 μm are sparse. Rittinghausen et al. exposed rats via intraperitoneal injection to a defined number of long, individual fibers ($L > 5 \mu\text{m}$) for four different MWCNT materials with mean diameters between 37 nm and 85 nm [14]. Mesothelioma incidence in rats dropped for nanotubes with diameters around 37 to 40 nm. Thinner MWCNTs, disentangled and matching the WHO-criteria, could not be provided yet for toxicity testing to the authors' knowledge. Even if disentanglement and dispersion were achieved, fibers longer than 5 μm were not present or their fraction comprised in the exposure dose was not quantified [15], as is required for intraperitoneal testing (i.p.-testing) according to OECD standards. I.p.-testing results were nevertheless reported by several authors who observed no carcinogenicity for MWCNTs with diameters below 15 nm [16–19]. Still, the results of Rittinghausen et al. points towards a diameter threshold where the fiber paradigm loses its predictive value. Of note, Nagai et al. proposed that fiber rigidity may play a critical role in cell injury and carcinogenesis [16, 20].

7.2 Risk banding and material properties required for HARM risk banding

The risk related to hazardous material exposure is the product of the material's hazard and its exposure concentration: "No hazard, no risk; no exposure, no risk".

For practical risk assessment, it is necessary to assess specific concentrations of a hazardous material component. Such concentrations are generally not available, unless a material was actually handled in comparable processes and the resulting emissions were sampled and characterized with great care. The gargantuan task of detailed risk analysis, may be eased by not working with numerically predicted material- and handling-related hazard and exposure values but by applying a "fuzzy" approach relying on hazard and exposure "bands".

Banding decisions have generally to be made for multiple material- and process-related properties and require threshold values or exclusion/inclusion value ranges for each parameter. If data on relevant material hazard properties and exposure concentrations are at hand, risk banding sorts these data into distinct value ranges that are associated to band labels, e.g., "low", "intermediate" or "high" hazard and exposure. As shown below, these band labels can then be weighted numerically, summarized for hazard and exposure separately, and finally multiplied to attribute a material handled in a specific process a risk level. This however requires scientific consensus on the applied range limits that separate "low" from "intermediate" and "high" for all categorized properties, as well as on the numerical weights attributed to the labels.

7. A human risk banding scheme for high aspect-ratio materials

For both approaches, risk assessment and risk banding, it is important to develop strategies to predict or measure the exposure concentration of the toxicologically relevant fraction of a material. This requires real-world or laboratory data or, if missing, theoretical considerations or widely accepted concepts. Whenever real-world hazard or exposure data are missing for risk assessment or banding, systematic laboratory studies may help identifying key hazard properties and general exposure trends. The fiber toxicology paradigm will be used in the following as starting point for developing a concept that aims at risk banding of HARM-containing materials that are handled in specific processes.

For HARM risk banding, we are investigating, e.g., whether:

- a) a process exhibits a "high" or "low" propensity to release respirable constituents,
- b) whether a specific material contains a "high" or "low" fraction of particles with high-aspect ratio,
- c) whether the material contains a "high" or "low" concentration of long fibers etc.

The following properties and propensities of HARM are considered relevant for achieving their risk banding. In the following, both compact fibers and agglomerates in fiber shape are considered as toxicologically relevant. An example of an agglomerate fiber is chrysotile asbestos that is a bundle composed of nanoscale fibers of about 38 nm diameter. Table 7.1 shows material properties allocated to categories, stating the respective hypothesis for its relevance for fiber hazard. Likewise, exposure-affecting propensities are specified that result from a complex combination of material and process-related properties, including, e.g., interaction forces between agglomerated, attached or tangled fibers and processes to overcome them by slipping, bending or breaking of fibers.

Here we propose band limits for selected parameters that aim at enabling a HARM-specific hazard grouping. Selected parameters have been proven to affect the hazard potential of HARM according to the fiber-toxicological paradigm. The band limits are based either on threshold values found by literature review or on theoretical considerations aiming at bridging the experimental knowledge gap of available toxicity studies on disentangled, long and thin nanotubes.

As mentioned earlier, the FTP describes toxic effects of biopersistent fibers. As such, this hazard ranking scheme is limited to such HARM. For the sake of completeness, given in the next paragraph is a short review of toxic effects caused by reactive properties of HARM, i.e., not chemically inert materials.

HARM that are water soluble or exhibit surface reactivity can be harmful due to the toxicity of released ions or generated reactive-oxygen species (ROS), respectively. Examples include ion-releasing silver nanowires [21] and some mineral fibers producing ROS [22]. Even graphitic MWCNTs that, in principle, are chemically inert generally exhibit enhanced chemical reactivity due to tube curvature, defects in the graphitic structure, tube end terminal groups and dangling bonds. Substitution of carbon atoms by doping or ion implantation as well as covalent or non-covalent chemical functionalization has been used to convert CNTs into functional materials of modified reactivity [23–25]. Anionic functionalization, e.g. using carboxylate groups, has been used to mitigate toxicity by enhancing particle agglomeration [26]. In contrast, cationic functionalization, e.g., with polyetherimide has been observed to increase the inflammatory potential of CNTs [27]. Surface functionality and polarity plays a role in protein corona formation [28].

The aforementioned toxicological studies on MWCNTs underline the relevance of the individual fiber dose for toxicity assessment of HARM. A determination of the particle number or of mass concentrations in the exposure dose provides only a quantitative measure of the total exposure dose, not of the toxicologically relevant fiber fraction. HARM containing long fibers can appear less hazardous if the fibers remain in an entangled state during testing and thus cannot evoke individual fibers effects.

Exposure-related banding is therefore to be performed on the basis of material- and process-specific dustiness, the grade of agglomeration of released dust samples and the released concentration of harmful fibers.

In the following sections, we describe the parameters and propensities that are considered as risk governing together with the underlying hazard hypothesis. Also the methodology of band limit determination and benchmark materials are described.

Table 7.1.: Properties and propensities of HARM affecting fiber toxicity.

Hazard-affecting properties	
<i>Properties controlling particle or agglomerate respirability</i>	
Property	Hypothesis
Particle or agglomerate length	Affect respirability via aerodynamic properties
Particle or agglomerate width	
Particle material density	
Agglomerate density	
<i>Properties impeding ingestion of particles by macrophages</i>	
Property	Hypothesis
Particle or agglomerate length	Long particles may result in incomplete phagocytosis
Particle material's Young's modulus	Rigid fibers may result in incomplete phagocytosis and translocation
Particle or agglomerate width or, preferably, cross sectional shape	Governs flexural rigidity of fibers and fiber-shaped agglomerates
Bio-durability, water insolubility	Governs biopersistence in cells and tissue
Exposure-affecting propensities	
Propensity	Description
Dust release propensity	Overall dustiness comprising particles, fibers and agglomerate release
Individual fiber release propensity	Individual fiber-related dustiness
fiber-shaped agglomerate release propensity	fiber-shaped agglomerate-related dustiness
WHO-object release propensity	WHO-object related dustiness

7.2.1 Length

Hypothesis: The underlying hypothesis for hazard banding by fiber length is the validity of the fiber-toxicological paradigm for all chemically inert HARM. Essentially, respirable fibers are harmful, if they are biopersistent, long and rigid [6]. Clearance of respired materials, i.e. particles and fibers, from the lung is carried out by alveolar macrophages. They attempt to internalize respired materials into phagolysosomes that provide an acidic milieu intended for a defence against microbial invaders. Even if a particle or fiber may withstand chemical degradation inside the lysosome, the laden macrophage may migrate and reach the mucociliar escalator of the bronchial epithelium, and eventually become expelled or swallowed. However, this lung clearance mechanism fails if the macrophages (1) cannot internalize the respired particles due to overload, or (2) do not fully internalize fibers due an excessive fiber length, or (3) if an ingested material deteriorates the macrophage motility or viability. Thus, in case of long and rigid fibers which cannot be fully internalized, macrophages will be unable to carry their load. Instead it will enter into a stage referred to as incomplete or "frustrated" phagocytosis, where a fiber is only partly engulfed. This may lead to pronounced inflammatory responses and eventually fibrosis, asbestosis, or mesothelioma. Geometrical dimensions (length and aspect ratio) as well as the flexural rigidity of fibers are assumed to be pivotal material parameters governing toxic effects of HARM.

Chosen testing strategy: A new OECD technical guidance document for length and diameter determination of micro- and nanoscale fibers is currently under development, funded by the German Environment Agency (UBA),

7. A human risk banding scheme for high aspect-ratio materials

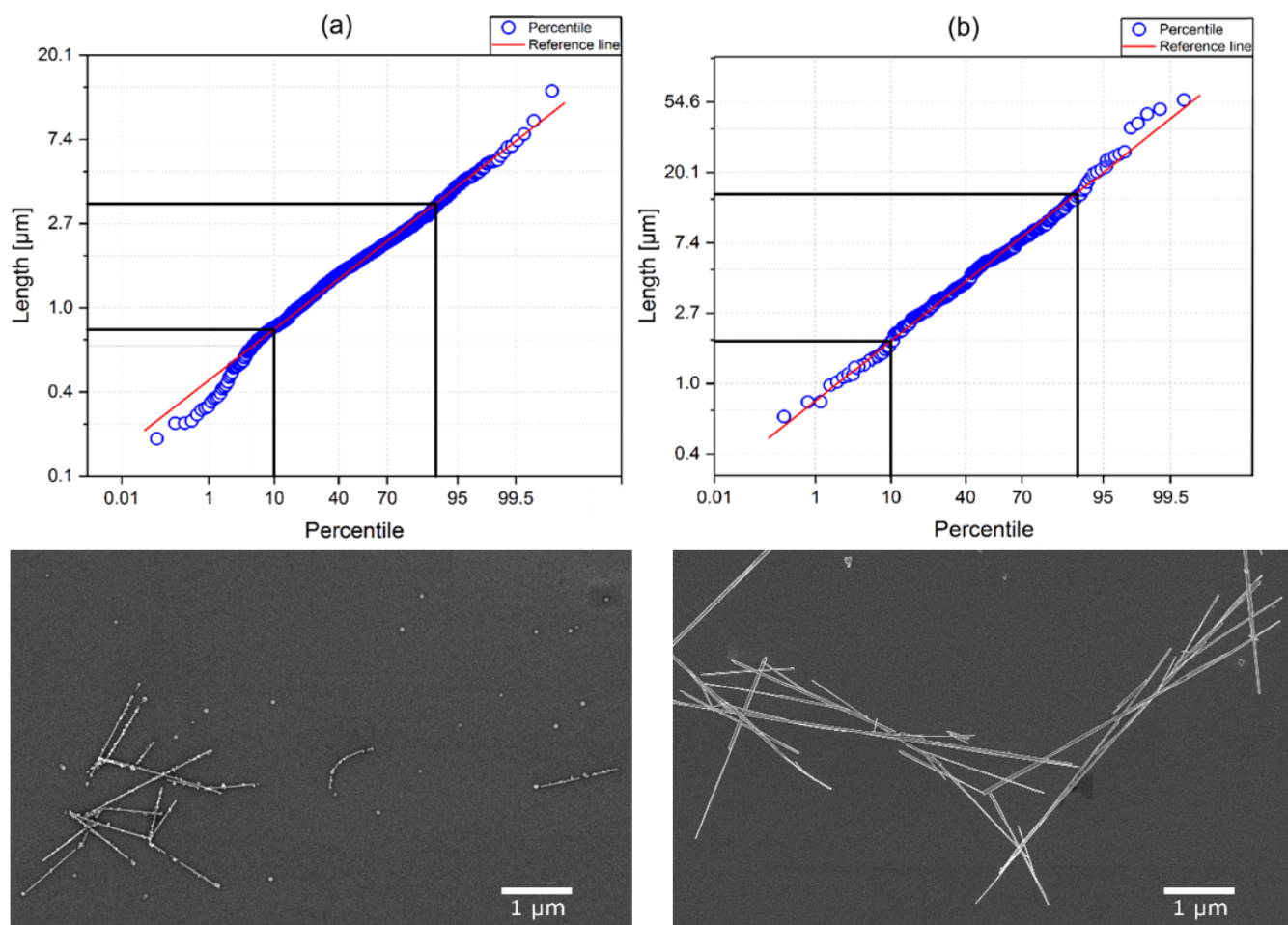


Figure 7.1.: Log-probability plots of the length distribution of the Ag nanowires (a) and ZnO fibers (b) (top) with respective SEM images for reference. The results of the 10th and 90th percentiles allocate Ag nanowires to the "Short" band and the 50th percentile ZnO fibers to the "Medium" band.

grant no. FKZ 3717 66 415 1. For sample preparation, material powder/suspension is dispersed in isopropanol with the help of an ultrasonic micro-tip for disentanglement. The suspension is then pipetted onto a silicon wafer. After evaporation of the medium, the wafer can be analysed via electron microscopy (EM), following a standard operation procedure that includes counting rules as well as measurement guidance for primary particles.

We propose that the decision whether a material is of "short", "medium" or "long" length is based on the percentiles of the probability plot of length, i.e. the linear percentile displacement of a cumulative length-fraction from the count median length (CML, 50th percentile). See books on particle size statistics for a more detailed description [29]. Important values for the decision are the 10th, 50th and 90th percentiles.

Note that this procedure cannot be applied for materials deviating significantly from lognormal distributions, such as: deliberate mixtures of particles and fibers, leading to multi-modal or discontinuous distributions. In case of mixtures of HARM, additional analytical methods might be necessary to distinguish between fibers, e.g. by energy-dispersive x-ray spectroscopy as part of the SEM imaging or by fiber-specific Raman spectra identifying the chemical bonds. This scenario might be of relevance for materials that consist of bundles of different polymer fibrils. One example is the so-called "Belima-X" fiber, consisting of a star-shaped nylon core with cone-shaped polyester fibrils embedded into the opening. Used to make microfiber cloth, these fibers break up easily to increase the effective

surface area during wiping.

Band limits: Proposed are the 10th, 50th, 90th percentiles of the length distribution as descriptors. The current consensus in the scientific community is that asbestos fibers with a length greater than 15 μm most likely cause the adverse effects in the lungs as described in [6]. However, inflammation and mesothelioma development was also being reported for asbestos fibers as short as 5 μm [30]. The World Health Organization (WHO) counting convention for fibers in air samples likewise sets a minimum length of 5 μm [1].

Figure 7.1 (a) and (b) provide examples for Ag nanowires (a) and ZnO fibers (b). Banding allocated the Ag nanowires to the "short" band whereas ZnO fibers are banded as "medium".

Benchmark-Materials: Data of MWCNT characterization on length distributions of aerosol samples from fiber dustiness tests identified suitable benchmark materials for the "Short" and "Medium" category [2]. These materials are also chosen due to their general availability as a OECD testing material from the repository of the Joint Research Center (JRC) by the European Commission [31]. The authors of this chapter have not yet found a "long" HARM based on length data sufficient for producing log-probability plots. Analysis of mineral fibers, polymer fibers and other micro-fibers might identify a "long" HARM and a suitable benchmark-material.

Table 7.2.: Length

Descriptor: Percentiles of the log-probability graph of the lognormal length distribution.

Band	Short	Medium	Long
Band limit	L90 < 5 μm	L10 < 5 μm AND L90 > 5 μm	L50 > 5 μm
Benchmark materials			
Material	Description	L value at percentiles	Band
NM-400	MWCNT, OECD Testing Material	L90 = 1.9 μm	Short
NM-401	MWCNT, OECD Testing Material	L10 = 1.1 μm , L90 = 8.1 μm	Medium
Not yet identified			Long

7.2.2 Respirability

This risk scheme banding proposed here applies to respirable fibers only. Particle respirability is determined by its aerodynamic diameter, the diameter of a sphere with unit density with equivalent terminal velocity. Therefore, the aerodynamic diameter depends on the inertia of the particle and its flow cross-sectional area. For fibers that align parallel to stream lines in the laminar flow of the pulmonary tract, the latter depends on the fiber diameter. The WHO set a cut-off-diameter for respirable fibers of 3 μm , based on experimental results [1]. The parameter respirability therefore does not need further consideration in the following since the WHO fiber fraction that is considered toxicologically relevant is the respirable one. It must be noted however, that the WHO convention excludes fibers thinner than 200 nm from counting even if they can be imaged during EM analysis. This is necessary to guarantee comparability of optical and electron microscopy fiber number results.

For fiber toxicology however, the findings on MWCNT materials presented in the next section have shown that also fibers thinner than 200 nm can be of very high toxicological relevance.

7.2.3 Thickness (Rigidity)

Hypothesis: The fiber toxicology paradigm is extended here by the parameter thickness. This is necessary to account for the hypothesized vanishing of fiber toxicity effects for fibers of low flexural rigidity [32]. Rigid fibers are defined as fibers that can maintain their fiber shape during phagocytosis whereas flexible fibers are bent by ingestion forces

7. A human risk banding scheme for high aspect-ratio materials

exerted by the macrophage. Highly flexible fibers may even spontaneously entangle during production or handling and lose their fiber character. Only rigid fibers are assumed to be able to cause frustrated phagocytosis or even pierce through cell membranes, whereas the latter ones can be fully internalized like a granular particle. Flexural rigidity R is defined as the product of the Young's modulus E of the fiber material and the second moment of area I_A that depends on the fiber cross-sectional shape:

$$R = EI_A \quad (7.1)$$

for a fiber of cross-section area A :

$$I_A = \int_A r^2 dA \quad (7.2)$$

For fibers of cylindrical cross-section this simplifies to:

$$R = E \frac{\pi d^4}{64} \quad (7.3)$$

While only linearly dependent on the elastic modulus, rigidity scales with the fourth power of fiber diameter. Currently, there is no validated method available to measure the rigidity of micro- and nanoscale fibers. Hence, based on this relationship, its quantification relies on the knowledge of the Young's modulus of the material from literature and the measurement of the mean fiber diameter. Note that flexural rigidity is derived theoretically as integral over the cross-section of a bundle of infinitesimal thin filaments [33]. Depending on the radius of bending of this bundle, flexural rigidity results from outer filaments being stretched and inner ones being compressed, assuming the existence of a central ("neutral") filament that is neither stretched nor compressed. For each filament, the stretching or bending force results from the Young's modulus of that filament and its length change that depends on its distance to the neutral filament. All forces are to be summed up. Consequently, fiber rigidity scales with the cross-sectional distribution of the filaments.

Anisotropic or nanoscale materials like CNTs are expected to show deviations from the Young's modulus approach of continuum mechanics, especially if they show buckling effects [34]. Therefore, literature values on Young's modulus determined on macroscopic materials are considered as only approximate when assigned to fibers of small diameters.

Apart from inflammatory effects most likely being related to rigid fibers, migration of fibers from the lung tissue to mesothelium is hypothesized to be more probable for highly rigid, needle-like fibers. Such translocation may eventually lead to the development of mesothelioma [6]. One hypothesised translocation route of fibers is via the para-cellular pathway in direction of the gradient for physiological absorption of lymphatic fluid, possibly supported by increased perforation of the alveolar epithelium because of inflammatory stimulation by frustrated macrophages [35]. Curvature has been demonstrated to significantly impact the penetration probability of fibers through pores [36, 37], since straight rods show a favoured orientation in capillary flows and have a high chance to enter such pores tip-first whereas curly fibers spin around. Other translocation pathways exist and translocation rates might also depend on fiber curvature [35]. The curvature along the longitudinal axis of fibers is hypothetically determined by rigidity [38]. However, the theoretical correlation of rigidity and curvature relies on fiber bending under the influence of thermal fluctuations and stems from the determination of bending behaviour of polymer chains in terms of the static bending persistence length. How this model applies for HARM like MWCNTs is currently subject of research. Deriving a threshold value of rigidity that ranks their translocation probability and allows identifying 'needle-like' fibers appears currently out of reach. The introduction of an additional band describing the translocation probability of fibers, using fiber curvature as a descriptor, might be more appropriate.

7.2. Risk banding and material properties required for HARM risk banding

Chosen testing strategy: The diameter distribution of individual fibers is determined by EM analysis of material samples. The mean of the diameter distribution is chosen as a descriptor instead of percentiles as was done before. This decision is made due to the following reasons.

Available data obtained during EM analysis of MWCNT-materials from the previously referred dustiness study showed normally-distributed diameters [2]. A log-probability graph analysis as applied above is not applicable, because the shape of the diameter distribution is unknown. Different to the fiber length band, we therefore propose to use the mean of the diameter distribution as a descriptor for thickness.

Band limits: Based on current knowledge, a threshold value of rigidity can only be estimated, after analysing the biophysics of phagocytosis. In short, during phagocytosis of filamentous objects, macrophages create a tubular phagocytic cup with a negative gradient of actin polymerization rate from the entrance towards the rear of the tube [39, 40]. By removing the actin network from the base of the cup, the macrophage invaginates the plasma membrane alongside the fiber. This mechanism exerts an inbound force on the object, called polymerization force, with a maximum value of about $f_p \sim 10$ nN. In case that a long fiber bumps into the cell membrane during phagocytosis, a compressive load is expected to build up along the fiber axis that leads to bending of the fiber provided Euler's critical load f_{cr} is being overcome:

$$f_{cr} = \frac{\pi^2 R}{(KL)^2} = \frac{\pi^2 EI_a}{(KL)^2} \quad (7.4)$$

K is the column effective length factor that depends on the conditions of the fiber ends (fixed or free). Here, it is assumed that $K = 1.2$ for one fixed and on freely translating fiber end, assuming the cell doesn't translocate the entrance of the phagocytic cup and that the tubular phagocytic cup can freely move at its base.

Considering that the critical load is equivalent to the polymerization force, ($f_{cr} = f_p = 10$ nN), one can calculate a critical rigidity that limits fiber bending under these conditions, which is in the order of $\sim 10^{-19}$ Nm².

For MWCNTs with E of approx. 360 to 1000 GPa [41–45], this rigidity threshold refers to a critical diameter of approx. 37 to 44 nm (40 nm mean). For a selection of other fibers, Table 7.3 correlates critical diameters of different materials to the rigidity threshold value of $\sim 10^{-19}$ proposed here. Values on the Young's modulus were taken from literature.

Table 7.3.: Estimated critical diameters for selected fibers, assuming a rigidity of 10^{-19} Nm².

Source for E	Material	E [GPa]	Threshold Diameter d [nm]
[41–45]	MWCNT	360-1000	44-37
[46]	ZnO nanorods	151	60
[47]	SWCNT	1250	35
[48]	SiO ₂ nanowire	47	81
[49]	Polyester fibers	0.9	218
[50]	SiC nanowire	430-660	47-42
[51]	PAN carbon fiber	200	56
[51]	Hydrated cellulose fiber	97	68
[52]	Diamond nanothreads	850	39
[53]	Chrysotile	160	60
[53]	Crocidolite	190	56

A rigidity band limit would be independent from the material. However, directly measuring rigidity (or elastic modulus) currently requires much experimental effort and no standard protocol exists. The authors of this chapter are

7. A human risk banding scheme for high aspect-ratio materials

currently working on developing a method based on the measurement of resonance frequencies of vibrating fibers visible by electron microscopy (BAuA research project F2365). Until an adequate method to directly determine fiber rigidity is available, the mean of the diameter distribution is to be used for banding and threshold values in table 7.3 apply for the respective material.

Following this theoretical considerations, a fiber diameter band limit is chosen to distinguish flexible from rigid fibers.

This approach is supported by results from animal intraperitoneal testing (i.p.-test). Figure 7.2 presents data of i.p.-test results for various MWCNT materials in a plot of the mean length versus the mean diameter. Numerical values between 0 and 1 annotating the points give the observed mesothelioma incidence in rats. In these studies, no cancer incidence has been observed for MWCNTs with mean diameters below 30 to 40 nm. Note that MWCNTs (9) and (11) were entangled into large agglomerates.

The hypothesis formulated above describes acute toxic effects on macrophages. Nevertheless, these acute effects may, on the long term, lead to mesothelioma development after translocation of fibers from the lung tissue to the pleura.

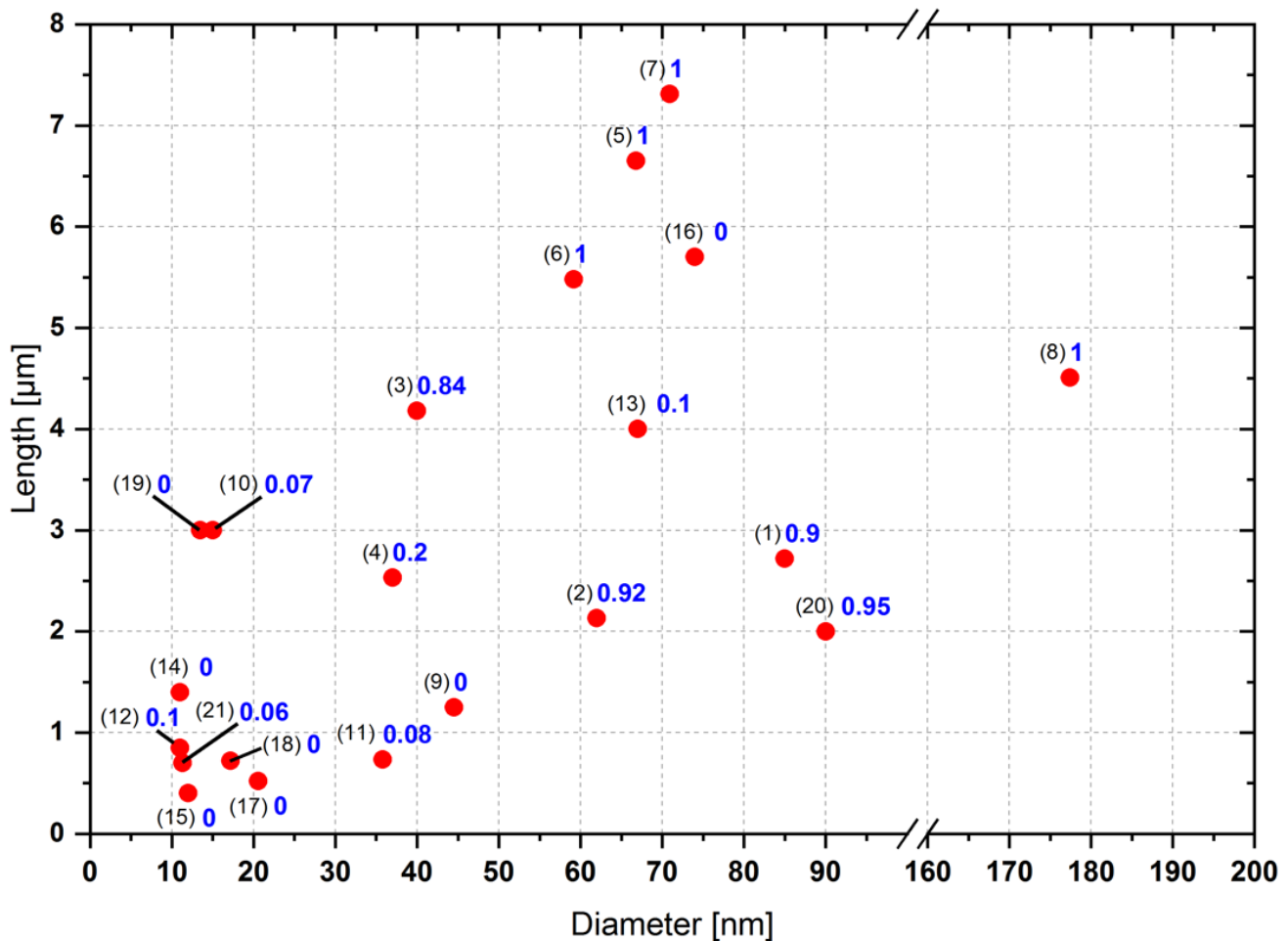


Figure 7.2.: Plot of the mean length versus the mean diameter of MWCNT materials used in the studies cited above. The numerical values specify the observed mesothelioma incidence in rats and mice. The black numbers in brackets indicate the respective studies: (1)-(4) Rittinghausen et al. [14], (5)-(11) Sakamoto et al. [54], (12)-(18) Knudsen et al. [55], (19) Nagai et al. [56], (20) Takagi et al. [57], (21) Muller et al. [16].

An additional thickness band limit for ‘needle-like’ fibers might exist in case the abovementioned hypothesis of fiber migration towards interstitial tissue is also limited by rigidity is supported by further evidence. Currently, fibers are only allocated to two bands.

Benchmark-Materials: Data on diameter distributions of aerosol samples from fiber dustiness tests identified suitable benchmark materials for the "flexible" and "rigid" category [2]. Note that the range of rigidity values were estimated assuming the lowest and the highest known Young’s modulus for the lower and higher range limit, respectively.

Table 7.4.: Rigidity (thickness)

Descriptor: Mean fiber flexural rigidity, mean of diameter distribution of primary particles as a surrogate until rigidity can be directly measured adequately.

Band	Flexible	Rigid	
Band limit	$< 10^{-19} \text{Nm}^2$, $< 40 \text{ nm}$	$> 10^{-19} \text{Nm}^2$, $> 40 \text{ nm}$	
Benchmark materials			
Material	Description	Mean rigidity (diameter)	Band
NM-400	MWCNT, OECD Testing Material	0.007×10^{-19} to $0.02 \times 10^{-19} \text{ Nm}^2$ ($11 \pm 3 \text{ nm}$)	Flexible
NM-401	MWCNT, OECD Testing Material	0.5×10^{-19} to $33.6 \times 10^{-19} \text{ Nm}^2$ ($67 \pm 24 \text{ nm}$)	Rigid

7.2.4 Biopersistence

Biopersistence describes the propensity of a substance to withstand degradation in biological tissue [58]. Such HARM materials remain their fibrous shape and may cause fiber-specific adverse health effects in lung tissue. Biopersistence can be tested by intratracheal instillation of a fibrous material into an animal, followed by fiber counting in lung tissue after defined time intervals to determine the fiber clearance rate [59], standardized under EN 18748 and German TRGS 905. The clearance half-life must not exceed 40 days to declare a HARM to be not biopersistent.

Here, we propose a much simpler testing strategy, by individually assessing the parameters that determine persistence of materials in tissue (excluding cellular clearance), water-solubility and bio-dissolution.

Water solubility

Hypothesis: Water-soluble fibers dissolve in the lung fluid once deposited in the respiratory tract so that they don’t retain their original shape. However, water-soluble materials may release toxic ions and cause ion-specific health effects. Such chemistry, not material related effects are however not subject of the risk banding scheme presented here.

Chosen testing strategy: The currently drafted OECD "guideline for the testing of dissolution rate of nanomaterial in aquatic media" describes a screening dissolution test for substances in 5 mM sodium bicarbonate buffered water (pH 7).

Band limits: The draft OECD Test Guideline declares substances that are completely dissolved after 24 h as water soluble. The lower detection limit of the ion detection method of choice (here ICPOES) is chosen to represent the band limit value. Only if no ions are detected, the material is regarded "insoluble".

Benchmark-Materials: A list of Benchmark-Materials is given by the drafted Test Guideline. Water solubility is not dependent from shape, so spherical particles can serve as benchmark materials here.

7. A human risk banding scheme for high aspect-ratio materials

Table 7.5.: Water insolubility

Descriptor: Ion concentration after 24 hours in 5 mM sodium bicarbonate buffered water (pH 7), after applying 10 mg l^{-1} particles

Band	Insoluble	Soluble	
Band limit	$< 0.1 \text{ } \mu\text{g l}^{-1}$ after 24 h	$> 0.1 \text{ } \mu\text{g l}^{-1}$ after 24 h	
Benchmark materials			
Material	Description	Water solubility	Band
CuO (SUN)	Copper(II)oxide, $< 50 \text{ nm}$, SA: $29 \text{ m}^2 \text{ g}^{-1}$, non-coated	$97 \text{ } \mu\text{g l}^{-1}$	Water soluble
NM-211	Cerium Dioxide, $< 20 \text{ nm}$, SA: $65 \text{ m}^2 \text{ g}^{-1}$, non-coated	$< 0.1 \text{ } \mu\text{g l}^{-1}$ [60]	Water insoluble

Bio-dissolution

Hypothesis: Bio-dissolution describes the degradation of fibers in relevant physiological media, like the acidic (pH 4.5) medium within lysosomes of macrophages. Under these conditions degradable fibers might lose their high aspect-ratio geometry by breaking up, a feature of non-biopersistent mineral fibers with engineered crystal defects.

Chosen testing strategy: A protocol for the dissolution at non-equilibrium conditions for nanomaterials can be found in the literature [61, 62]. It applies an abiotic flow-through testing system. The material is situated in a flow-through cell, traversed by a lysosomal simulation medium. During 7 days, the eluting ion concentration is measured by ICP-MS and remaining material examined by EM. The metric of dissolution was adapted to the k -rate [$\text{ng cm}^{-2} \text{ h}^{-1}$] that is conventional for WHO-fiber assessment.

Band limits: Currently proposed are $< 100 \text{ ng cm}^{-2} \text{ h}^{-1}$ for moderate and $< 1 \text{ ng cm}^{-2} \text{ h}^{-1}$ for low dissolution. This matches the findings on mineral fibers, which are biopersistent with fibrosis and cancer in the $1 \text{ ng cm}^{-2} \text{ h}^{-1}$ range [63], but not persistent in vivo with no adverse effects for rates above $100 \text{ ng cm}^{-2} \text{ h}^{-1}$ [64].

Table 7.6.: Bio-dissolution

Descriptor: Dissolution rate k in physiological simulant medium

Band	High	Moderate	Low
Band limit	$> 100 \text{ ng cm}^{-2} \text{ h}^{-1}$	$100 > k > 1 \text{ ng cm}^{-2} \text{ h}^{-1}$	$< 1 \text{ ng cm}^{-2} \text{ h}^{-1}$
Benchmark materials			
Material	Description	Dissolution rate in $\text{ng cm}^{-2} \text{ h}^{-1}$	Band
MMVF34	Bio-soluble stone wool	> 400	High
MMVF32	E-glass-wool	9	Moderate
Asbestos	Crocidilite, amosite	< 1	Low

7.2.5 Release propensity (dustiness)

Hypothesis: The term "dustiness" refers to the propensity of a material to release aerosol particles following agitation. Powder agitation can, e.g., result from pouring, dropping, stirring, vibration or blowing. The (inhalative) exposure to a material is more likely in case of high dustiness compared to a material with low dustiness.

Chosen testing strategy: Dustiness testing for HARM-powders is conducted following the protocol of the 'fluidizer dustiness test' [2]. In short, the fluidizer setup consists of a sample holder with a gas-permeable base that can be subject to vertical vibrations induced by a shaker. Both the vibration and a traversing laminar airflow agitate a column

of powder situated on the base. A fluidized bed is established. Aerosol generation first happens by removal of free particles in the powder bed, visible by a short spike in particle number concentration downstream. Subsequently, the particle number concentration settles at a level that is stable for a long period of time during which particle release is most likely due to continuous de-agglomeration happening by particle-particle collisions in the fluidized bed. See the cited study for a detailed description of the experimental setup [2]. Results obtained with the fluidizer dustiness test are reproducible and can be ranked with results obtained for other materials. In case dust emission did not show equivalent qualitative behaviour as described above, dust generation is assumed to be due to different mechanisms. Such results would not be subject to comparison for other materials by ranking. During the performance tests with 15 MWCNT materials in the study referred to above, only two materials showed different emission behaviour and were hence disregarded for the material ranking. Since the 13 MWCNT materials left were diverse in properties describing the primary particles and also powders and still showed similar behaviour, we consider that the method is principally applicable for most carbonaceous fibers, ceramic and inorganic fibers, metallic fibers or organic fibers not being allotropes of carbon (e.g. cellulose).

Dustiness is often measured as so-called dustiness coefficients, the ratio of the total mass of released particles in a specific time frame (or handling process) and the initial mass of the powder. The mass based metric is motivated by mass-based concentration values defining (occupational) exposure limits. In case of fibers, exposure limits in Europe are given in the metric of number concentration e.g. in the workplace ambient air. The performance of the fluidizer dustiness test allows the determination of an average particle number concentration in a chosen time frame at which the emission rate was stable, which is a better metric to assess the exposure potential on the basis of exposure limit values. Of course, measuring the number concentration is much more practicable since the emitted total mass is often too low to be easily determined by standard microgram balances.

The chosen testing strategy to determine fiber dustiness is currently by applying exclusively the fluidizer dustiness test. This is due to the unknown performance of other dustiness tests like the rotating drum or continuous drop, when HARM-powders are used. Another dustiness test called vortex shaker was critically reviewed for its applicability for dustiness testing of HARM [65]. The authors concluded that reproducible results were not achievable because of chaotic powder bed behaviour during agitation. However, reproducibility of results is a requirement for dustiness assessment using material rankings.

Band limits: Band limits are defined in a decadal manner based on the results of dustiness tests for 15 MWCNT materials [2]. More bands beyond "High" might be identified in case dustiness is determined with higher orders of magnitude. The band limits proposed here are applicable for results obtained with the fluidizer dustiness test. In case harmonization of dustiness tests is successful, method-specific band limits might be defined. The metric of choice for fiber dustiness is average number concentration on the basis that exposure limit values are usually number concentrations in the e.g. workplace atmosphere. Note that concentrations comprise particle sizes determined by the aerosol monitor. Taking the Condensation Particle Counter as an example, particles with sizes between 3 nm and 3 µm are detected and counted.

Benchmark-Materials: Based on the dustiness tests with MWCNTs performed with the fluidizer [2], benchmark-materials are chosen from the material ranking.

7.2.6 Dust agglomeration

Hypothesis: Dust particles in aerosols can occur as agglomerates of smaller particles, in particular when the pristine materials are in the nanoscale. Agglomeration brings alteration of several extrinsic aerosol properties e.g. size, surface area and volume. For fibers, agglomeration can have a significant effect on their toxicity as well, because agglomeration occurs in form of fiber entanglement and bundling. Often observed ball-like agglomerates have diameters in the micrometre-range and comprise a large number of individual fibers. Those fibers basically lose their fibrous nature. Note that low dustiness might correlate with strong dust agglomeration simply because particles are clustered and counted as one.

7. A human risk banding scheme for high aspect-ratio materials

Table 7.7.: Release propensity (dustiness)

Descriptor: Average particle number concentration (P) during fluidizer dustiness test

Band	Low	Moderate	High
Band limit	$< 100 \text{ #cm}^{-3}$	100 to 1000 #cm^{-3}	$> 1000 \text{ #cm}^{-3}$
Benchmark materials			
Material	Description	Dustiness	Band
NM-401	MWCNT, OECD Testing Material	$P = 44 \pm 3 \text{ #cm}^{-3}$ [2]	Low
NM-400	MWCNT, OECD Testing Material	$P = 179 \pm 1 \text{ #cm}^{-3}$ [2]	Moderate
ARIGM001	MWCNT, Arry Intl.	$P = 3656 \pm 10 \text{ #cm}^{-3}$ [2]	High

Chosen testing strategy: The grade of agglomeration is often of qualitative nature and refers to e.g. the composition of powder grains of the pristine material visualized by means of electron microscopy. Accordingly, the grade of agglomeration of dust describes the composition of the aerosol released during dust generation. Quantitative approaches to determine a grade of agglomeration also involve analysis by electron microscopy, by estimating the number of primary particles that are bound within agglomerates and counting individual primary particles.

The grade of agglomeration is determined by the ratio of the number of all agglomerated fibers and the number of all individual fibers found on an aerosol sample:

$$X_N = \frac{N_f^a}{N_f^a + N_f} \quad (7.5)$$

where N_f is the number of single fibers found on the sample and N_f^a is the number fibers comprised within agglomerates. Samples with a grade of agglomeration near 1 comprise mainly agglomerated fibers whereas a small grade of agglomeration is obtained for samples with mainly single fibers.

With EM alone, accurately determining the number of fibers per agglomerate is not possible since the 2D-projection of an agglomerate often does not allow deriving the agglomerate volume. In addition, internal voids of agglomerates are not visualized. Currently, we propose an estimation of the agglomerate volume based on its projected area, by applying volume shape factors, and by assuming an agglomerate volume void fraction, determined with the agglomerate density. Since the calculation is based on several assumptions, in particular modelling the non-spherical nature of agglomerates with spheres, it is error-prone.

Band limits: Band limits are defined based on analysis of aerosol samples collected during the dustiness tests for 15 MWCNT materials [2]. Volumes of agglomerates, and geometric properties of single fibers were determined as described above and the grade of agglomeration for the dust of each material calculated. The band limits were arbitrarily set to allocate a similar number of materials to each band.

Benchmark-Materials: Benchmark-materials can be identified from the list of MWCNTs for which the grade of agglomeration was determined for the dust collected during the fluidizer dustiness test.

7.2.7 WHO-fiber concentration

Hypothesis: It has been demonstrated in many studies that fibers longer than 15 μm have higher carcinogenicity compared to short fibers [3, 4, 66–68]. As a consequence, the WHO recommends for workplace exposure assessment that the diameter and length of inorganic fibers should be determined to extract the fraction of fibers with length $> 5 \mu\text{m}$, diameter $< 3 \mu\text{m}$ and aspect ratio $> 3:1$ [1, 69], WHO-fibers. The upper limit for the diameter is due to the assumption that thicker fibers are not respirable.

Table 7.8.: Dust agglomeration

Descriptor: Grade of agglomeration of dust released during fluidizer dustiness test

Band	Low	Moderate	High
Band limit	< 5	0.5 – 0.99	> 0.99
<i>Benchmark materials</i>			
Material	Description	χ_N	Band
ARIGM001	Arry Intl., $df \sim 30 \text{ nm}$, $L \sim 0.7 \mu\text{m}$, Industrial grade	0.259	Low
NM-400	MWCNT, OECD Testing Material	0.830	Moderate
Baytubes® C150P	Bayer Mat. Science, $df \sim 12 \text{ nm}$, $L \sim 0.4 \mu\text{m}$,	0.996	High

Chosen testing strategy: To assess the release propensity of potentially harmful fibers from a material, the concentration of fibers matching the WHO-criteria in the aerosol has to be determined. By measuring the length and diameter of each single fiber on the aerosol samples collected during dustiness testing, WHO-fibers can be identified. The extrapolation of the WHO-fiber concentration from counting results follows the VDI 3492 guideline for determining indoor aerosol concentrations at e.g. workplace sites, which is based on the ISO 14966:2002 standard.

In general, the question is raised how confident an extrapolation of the WHO-concentration in the aerosol is based on evaluating an aerosol sample. For a more detailed description, we refer to textbooks on statistics. The variance of the counting result n when the same number N of images was evaluated several times can be described by a Poisson distribution,

$$W(n, a) = \frac{a^n e^{-a}}{n!} \quad (7.6)$$

which gives an expected value a of the WHO-fiber concentration. The lower and upper limits of the confidence intervals, λ_L and λ_U respectively, are given by the relationship between the cumulative distribution functions of the Poisson and the chi-squared distribution functions. For a 95% confidence interval, the lower and upper limits of the confidence interval are given by:

$$\lambda_L = \frac{1}{2} \chi_{2(n+1), 0.025}^2 \quad \text{and} \quad (7.7)$$

$$\lambda_U = \frac{1}{2} \chi_{2(n+1), 0.975}^2 \quad (7.8)$$

with $\chi_{k,p}^2$ being the quantile function of the chi-squared distribution with k degrees of freedom and p being the result of the function, the probability value. Values for λ_L and λ_U can be taken from table 2 in ISO 14966:2002 and "Tabelle 5" in VDI 3492. The fiber concentration C that falls under the 95% confidence interval can be calculated by $C = \lambda_U / V_P$, where V_P is the total sample aerosol volume represented by the evaluated area.

For example, a WHO-fiber count of $n=10$ and an evaluated sample volume of 1 l would result in a concentration of 18391 WHO-fibers m^{-3} with 95% confidence.

Band limits: Band limits are defined based on the German national occupational safety limits for WHO-fibers, i.e. the "acceptance limit value" of 10^4 m^{-3} and the "tolerance limits value" of 10^5 m^{-3} (TRGS 517, 519, 910).

To accurately determine these two concentrations within the 95% confidence interval based on less than a fiber count of $n = 1$, a specific total aerosol volume has to be evaluated, represented by an area on the filter, that "has seen" this volume. For 10^4 m^{-3} , the band limit between "low" and "moderate", $5 \times 10^{-4} \text{ m}^3 = 0.5 \text{ l}$ has to be evaluated. For

7. A human risk banding scheme for high aspect-ratio materials

10^5 m^{-3} , the band limit between "moderate" and "high", 0.05 l has to be evaluated. Thereby, we propose to generally evaluate 0.5 l and accordingly the sample area that has to be subject to fiber counting. Note that by definition, a result of zero fiber counts would lead to an infinite sample volume in order to fit any confidence interval.

The required sample area that represents 0.5 l can be calculated from the filter size and the total sampled aerosol volume. For the aerosol samples from the fluidizer dustiness test that were collected for 60 min with 0.3 l min^{-1} sample volume flow rate on nuclear pore filters with 20 mm open diameter, 0.5 l are then represented by ca. 8.7 mm^2 filter area. Note, that the VDI 3492 guideline was formulated for mineral fibers with diameter in the $>200 \text{ nm}$ range. Since nanoscale fibers like MWCNT require high magnification, even for images with 20 megapixels (the highest image resolution contemporary EM deliver), the number of EM images to cover such an area can be inappropriately high for visual evaluation and fiber counting. For example, in order to image a MWCNT with a diameter of 10 nm, the pixel size in the image should be at least 10 nm. A 20 megapixels image would then cover $2 \times 10^{-3} \text{ mm}^2$ so that 4425 images must be evaluated in order to cover 8.7 mm^2 . This is a problem that must be considered and might require new conventions about fiber counting. Note that the VDI 3492 recommends using an aerosol sampling setup that allowing for 1 cm^2 of filter area to represent 2 l of samples air. The setup used during the dustiness tests clearly undercuts this value.

Benchmark-Materials: The WHO-fiber concentration was determined for the dust collected during the fluidizer dustiness test. However, the evaluated areas were too small, leading to extremely high concentrations for the upper limit of the confidence interval. Benchmark materials can currently not be identified due to the lack of confidence in the data.

Table 7.9.: WHO-fiber concentration

Descriptor: Average number concentration (P_{WHO}) extrapolated from fiber counting on aerosol samples collected during fluidizer dustiness test.

Band	Low	Moderate	High
Band limit	$< 1000 \text{ WHO-fibers m}^{-3}$	$1000 - 10000 \text{ WHO-fibers m}^{-3}$	$> 10000 \text{ WHO-fibers m}^{-3}$
Benchmark materials			
Material	Description	WHO-fiber concentration	Band
HARM	Short HARM with low release potential	$< 1000 \text{ WHO-fibers m}^{-3}$	Low
HARM	Medium HARM with moderate release potential	$1000 - 10000 \text{ WHO-fibers m}^{-3}$	Moderate
HARM	Long HARM with high release potential	$> 10000 \text{ WHO-fibers m}^{-3}$	High

7.3 Summary of human risk banding for high aspect-ratio materials

Table 7.10 presents a summary of all property bands that contribute to hazard and exposure banding.

Table 7.10.: Properties and bands for HARM risk banding together with proposed benchmark materials.

Property	Band	Band limit	Benchmark-Material (value)
Hazard banding			
Length <i>Descriptor: Percentiles of the log-probability graph of the lognormal AR distribution</i>	Short	L90 < 5 μm	NM-400 (L90 = 1.9 μm)
	Medium	L10 < 5 μm, L90 > 5 μm	NM-401 (L10 = 1.1 μm, L90 = 8.1 μm)
	Long	L10 > 5 μm	Long fiber with L10 > 5 μm
Thickness (Rigidity) <i>Descriptor: Mean of rigidity (diameter) distribution</i>	Flexible	$R < 10^{-19} \text{N m}^2$, $d < 40 \text{ nm}$	NM-400 (11 ± 3nm)
	Rigid	$R > 10^{-19} \text{N m}^2$, $d > 40 \text{ nm}$	NM-401 (67 ± 24nm)
Water solubility <i>Descriptor: Dissolution in water</i>	Soluble	Dissolved after 24 h	CuO (n.a.)
	Insoluble	Not dissolved after 24 h	NM-211 (< 1 μg l ⁻¹)
Bio-dissolution <i>Descriptor: Dissolution rate (k) in physiological simulant medium</i>	High	$k > 100 \text{ ng cm}^{-2} \text{ h}^{-1}$	MMVF34 (> 400)
	Moderate	$100 > k > 1 \text{ ng cm}^{-2} \text{ h}^{-1}$	MMVF32 (9)
	Low	$k < 1 \text{ ng cm}^{-2} \text{ h}^{-1}$	Crocidolite asbestos (< 1)
Exposure banding			
Dustiness <i>Descriptor: Average number concentration (P) in fluidizer dustiness test</i>	Low	$P < 100 \text{ \# cm}^{-3}$	NM-401 (44 ± 3 #cm ⁻³)
	Moderate	$100 \text{ \# cm}^{-3} < P < 1000 \text{ \# cm}^{-3}$	NM-400 (179 ± 1 #cm ⁻³)
	High	$P > 1000 \text{ \# cm}^{-3}$	ARIGM001 (3656 ± 10 #cm ⁻³)
Dust agglomeration <i>Descriptor: Grade of agglomeration (χ_N) on aerosol samples collected during fluidizer dustiness test</i>	Low	$\chi_N < 0.5$	ARIGM001 (0.259)
	Moderate	$0.5 > \chi_N > 0.99$	NM-400 (0.830)
	High	$\chi_N > 0.99$	Baytubes C150P (0.996)
WHO-fiber concentration <i>Descriptor: Average number concentration (P_{WHO}) extrapolated from fiber counting subsequent to fluidizer dustiness test</i>	Low	$P_{WHO} < 1000 \text{ \# m}^{-3}$	HARM ($P_{WHO} < 1000 \text{ \# m}^{-3}$)
	Moderate	$1000 \text{ \# m}^{-3} > P_{WHO} > 10000 \text{ \# m}^{-3}$	HARM ($1000 \text{ \# m}^{-3} > P_{WHO} > 10000 \text{ \# m}^{-3}$)
	High	$P_{WHO} > 10000 \text{ \# m}^{-3}$	HARM ($P_{WHO} > 10000 \text{ \# m}^{-3}$)

7.4 Matrix for risk banding

Risk matrices or risk diagrams are preferred tools for risk assessment in many industrial frameworks, because they visualize risk in an intuitive and simplistic way. The purpose of a risk matrix is to predict the risk associated with a specific scenario based on the probability, likelihood or frequency of a dangerous event and its severity, impact or consequences. Probability and severity are represented by rows or columns, a scheme representing the general consensus that "risk = probability × severity" commonly with numeric scores grading both traits of risk. Each pair of

7. A human risk banding scheme for high aspect-ratio materials

scores is associated with a specific level of risk, usually represented in traffic light colours: green for low risk, yellow for moderate risk and red for high risk. For example, the risk of injury for workers in mining operations is assessed by the frequency of mining injuries and the severity level (from no-days-lost injuries to fatalities). A risk matrix was developed incorporating yearly data to determine trends in workers' risks [70].

When applying a risk matrix for risk assessment of chemicals, the probability of an event is represented by the exposure to the chemical, and the severity with the hazard, i.e. toxicity [71]. This strategy has also been incorporated within proposed control banding tools for nanomaterials [72].

Hazard and exposure potential of HARM are scored based on the proposed parameter banding introduced in the sections before. Table 7.11 summarizes allocated scores to respective parameters bands and demonstrates how the resulting hazard and exposure score to be applied in the risk matrix is determined.

Table 7.11.: WHO-fiber concentration

Descriptor: Average number concentration (P_{WHO}) extrapolated from fiber counting on aerosol samples collected during fluidizer dustiness test.

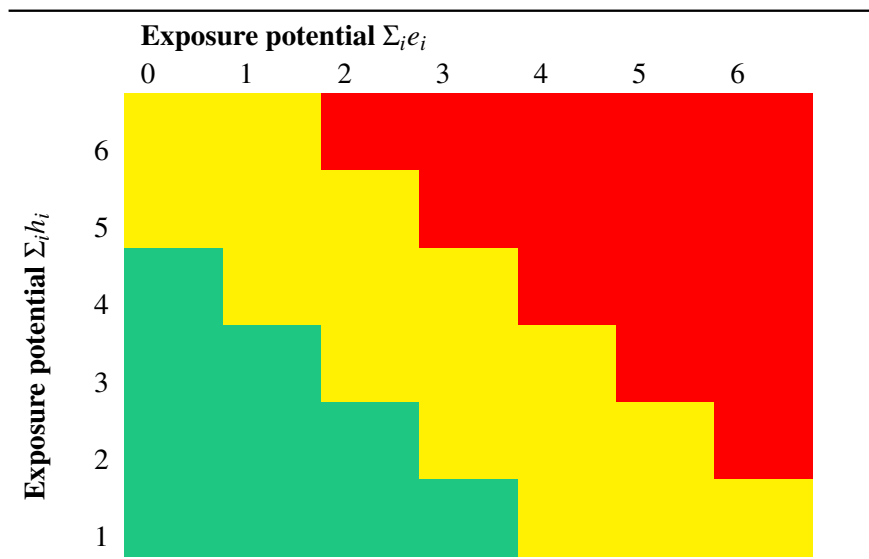
Hazard banding								
Parameter		Band and scores						
Length	h_1	Short	0	Medium	1	Long	2	
Rigidity	h_2	Flexible	0			Rigid	1	
Water solubility	h_3	Soluble	0			Insoluble	1	
Bio-dissolution	h_4	Low	0	Moderate	1	High	2	
Cumulative Score	$\Sigma_i h_i$	0	1	2	3	4	5	6
Exposure banding								
Dustiness	e_1	Low	0	Moderate	1	High	2	
Grade of Agglomeration	e_2	Low	0	Moderate	1	High	2	
WHO-fiber Concentration	e_3	Low	0	Moderate	1	High	2	
Cumulative Score	$\Sigma_i e_i$	0	1	2	3	4	5	6

The risk matrix determines the risk potential by juxtaposing the scores of hazard and exposure potential as shows in Table 7.12. Each scoring-pair leads to allocation of a traffic light colour, with green representing an acceptable, yellow an increased and red an unacceptable risk potential, respectively.

Acceptable risk potential indicates towards low toxicity and low to moderate exposure potential. For example, a fiber that is biopersistent, i.e. insoluble in water and durable in lysosomal fluid, but flexible and short, has an increased chance of not causing toxic effects in line with the FTP. If it also shows moderate dustiness, but the dust only contains agglomerates and a low concentration of fibers matching the WHO-criteria, then the chance of being exposed to harmful fibers is low during handling the HARM.

Increased risk potential is a vague term, since it means that characterization results cannot accurately predict whether handling the HARM is safe or highly risky. Taking a biopersistent, rigid and long HARM as an example, if its dustiness is low and its cardinality of the single fiber fraction in the dust and WHO-fiber concentration are low, exposure is simply improbable. A toxic material cannot cause effects if there is no exposure. However, a dustiness test is only mimicking powder agitation and currently it is unclear whether a different mode of agitation, i.e. a different dustiness test, leads to a different assessment relative to other materials (ranking). Consequently, this assessment cannot predict with certainty that exposure to the toxic material will not happen. Ergo, the risk potential is increased, motivating precautionary measures during manufacturing and handling of the material.

The result of an unacceptable risk potential can be the basis of a set of consequences, motivating strict precautionary

Table 7.12.: Matrix for risk banding. Green: Acceptable risk potential; Yellow: Increased risk potential; Red: Inacceptable risk potential.

measures during manufacturing and handling of the HARM or even discontinuing further material development and redesign the fiber material to accomplish risk mitigation.

7.5 Application in risk prediction for MWCNT

In a recent paper, we showed results of dustiness testing of 15 different commercially available MWCNTs (some have been taken of the market since) [2]. We apply the risk matrix based on the dustiness data and the results of the morphological characterization by SEM to perform the exposure banding as described here.

Since we did not perform morphological characterization of primary particles in the pristine powder material, length and diameter distributions of aerosolized fibers were measured instead, which can be viewed as representative for the material, assuming that the fibers did not break during agitation and the aerosol generator did not release fibers of favoured length. The mode of aerosol generator, powder grain surface de-agglomeration by colliding and subsequently slipping particles in the fluidized bed, is discussed in detail in the referenced study and lends credence to the assumption of no primary particle alteration occurring, since the energy required to break MWCNTs would be much larger than the energy applied during those collisions.

MWCNTs were regarded per se as biopersistent, since they are not water soluble ($< 2 \text{ mg l}^{-1}$ at 20°C in pH 7–9.2 according to the REACH dossier 936-414-1 of MWCNT) and do not dissolve or transform in artificial lysosomal fluid within 24h [31, 73].

Datasets for each MWCNT as stated by the manufacturer can be found in the study referenced above.

Table 7.13 shows physico-chemical characteristics relevant to hazard and exposure banding that were obtained for each material. Note that the WHO-fiber concentrations were calculated based on the morphological characterization of aerosol samples by two persons per sample. Presented are mean values and standard deviations that can be rather large. Subjectivity plays a large role for object classification. For example, one person could classify an object found on SEM images as a fibrous agglomerate which is rather long. Another person could count each individual fibers in this agglomerate which do not have dimensions matching the criteria for WHO-fibers. Such diverting decisions can lead to large errors in fiber counting. Generally, confidence in the extrapolation of counting results to determine WHO-fiber concentrations must be regarded low, since the evaluated areas in all cases were not sufficient according

7. A human risk banding scheme for high aspect-ratio materials

Table 7.13.: Evaluation parameters of 15 MWCNT materials relevant to for hazard and exposure banding.

Materials	Mean rigidity	Dustiness	Dust grade of agglomeration	Dust WHO-fibre concentration
Metric	[10^{-19} Nm ²]	[#cm ⁻³]	Dimensionless	[10 ⁵ m ⁻³]
Band limit	< 100 #cm ⁻³	100 to 1000 #cm ⁻³	> 1000 #cm ⁻³	
ARIGM001	0.26 ± 0.06	3656 ± 10	0.26 ± 0.03	1125.1 ± 375.3
ARIGM002	1.02 ± 0.01	1222 ± 8	0.29 ± 0.01	11.4 ± 2.0
ARM006	0.51 ± 0.01	1186 ± 12	0.96 ± 0.03	1210.8 ± 2.1
Baytubes C150P	0.08 ± 0.01	173 ± 1	0.99 ± 0.17	1.6 ± 0.3
C2148	0.04 ± 0.01	454 ± 4	0.98 ± 0.08	4.6 ± 0.2
C2154	1.26 ± 0.01	7539 ± 44	0.91 ± 0.01	4149.1 ± 150.9
C2158	1.84 ± 0.29	3947 ± 17	0.52 ± 0.01	6520.7 ± 799.7
CNT-MW	0.19 ± 0.01	422 ± 6	0.51 ± 0.01	94.4 ± 8.3
MRCSD	321.70 ± 103.81	478 ± 5	0.61 ± 0.06	5835.3 ± 54.8
MWCNT-7	20.11 ± 1.06	134 ± 7	0.41 ± 0.03	1554.6 ± 2355.8
NC 7000	0.03 ± 0.01	204 ± 2	0.99 ± 0.03	26.0 ± 9.1
NM 400	0.05 ± 0.09	179 ± 1	0.83 ± 0.01	132.8 ± 64.5
NM 401	28.12 ± 0.1	44 ± 3	0.58 ± 0.03	206.6 ± 281.2
NTX3	0.91 ± 0.19	8779 ± 54	0.99 ± 0.01	1306.1 ± 1349.2
SMW 100	0.03	204 ± 1	0.99 ± 0.01	2.1 ± 3.4

to VDI 3492, i.e. the calculated concentrations within the 95% confidence interval were significantly higher than the calculated average concentrations presented here.

Different to the assumption made in section 7.2.6, average number concentration and grade of agglomeration did not correlate here. One reason might be that the size of the agglomerates and number of primary particles comprised in agglomerates strongly differed between materials. For future further analysis, one might consider measuring emitted mass as well. A HAR material of high grade of agglomeration and high particle number concentration would emit much higher dust mass than a HAR material of low grade of agglomeration and comparable particle number concentration.

Based on these values, risk banding can be performed. Scoring and the application of the risk matrix leads to the allocations of the three risk bands to the materials, presented in Table 7.14.







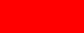


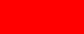





7.6 Conclusions and outlook

The risk banding scheme presented here is an important tool for assessing occupational risk related to handling HARM materials, identifying the material parameters that govern those risks and developing safety-by-design concepts for HARM to mitigate those risks.

The risk banding scheme was applied to a selection of 15 very different MWCNT materials and allowed grouping them into three distinct risk classes. This grouping is specific for the dust emission test procedure applied here. Other powder processing steps could generate different dust emission profiles and lead to a different risk ranking. In addition, release propensity over the life-cycle of the materials, e.g. release from composites, need to be considered.

The hypothesis that the flexural rigidity is of pivotal relevance for fiber-related hazards, which we call the extended fiber toxicology paradigm, was motivated by i.p.-test findings. For rigid HARM only those materials that do not

Table 7.14.: Scores and risk banding for the studied MWCNT-materials.

	Exposure	Toxicity	Risk
ARIGM001	6	3	
ARIGM002	4	3	
ARM006	5	3	
Baytubes C150P	1	3	
C2148	2	3	
C2154	5	3	
C2158	5	5	
CNT-MW	2	3	
MRCSD	4	5	
MWCNT-7	5	5	
NC 7000	2	3	
NM 400	4	3	
NM 401	3	5	
NTX3	4	3	
SMW 100	1	3	

contain long fibers or processes that do not emit those long fibers may end in the low risk class. For future interpretation of toxicological data on fibers, we propose to substitute the parameter "fiber diameter" by "fiber rigidity" and to develop reliable rigidity measurement techniques for sub-microscale fibers. This would allow extending the fiber toxicology paradigm, which intrinsically is a material-independent hypothesis, by the new hypothesis that in future should also include flexural rigidity (refer to the introduction):

*"The elongated shape of fibers is a carcinogenic principle, provided the fibers are respirable, long, **rigid** and bio-durable."*

Using this approach, it is planned to extend the risk banding scheme to HARM with other chemical and structural composition.

Other industrially relevant fiber materials were discussed in 7.2.3. To validate the material independence of the extended fiber toxicology paradigm and the critical diameters predicted from the critical rigidity derived from i.p.-test with MWCNTs will require systematic i.p.-testing of those materials. It will be a very costly task that will require a joint effort and much time to accomplish. Until then, we propose to use the proposed rigidity-extended fiber toxicology paradigm together with the present estimate for a critical rigidity of 10^{-19} Nm² to protect workers from presently un-assessed risks of biopersistent fibers with diameters below the WHO counting limit of 200 nm.

7.7 Acknowledgements

Part of this book chapter is based on results of the research project "InnoMat.Life" and was funded by the German Ministry for Education and Research, grant no. 03XP0216B.

References

- [1] W. H. Organization et al. *Determination of airborne fibre number concentrations: a recommended method, by phase-contrast optical microscopy (membrane filter method)*. World Health Organization, 1997 (cited on pages 55, 61, 68).
- [2] D. Broßell, E. Heunisch, A. Meyer-Plath, D. Bäger, V. Bachmann, K. Kämpf, N. Dziurawitz, C. Thim, D. Wenzlaff, J. Schumann, et al. “Assessment of nanofibre dustiness by means of vibro-fluidization”. In: *Powder technology* 342 (2019), pages 491–508 (cited on pages 55, 61, 63, 65–68, 73).
- [3] F. Pott et al. “Tumoren der Ratte nach ip-Injektion faserförmiger Stäube”. In: (1972) (cited on pages 56, 68).
- [4] M. F. Stanton and C. Wrench. “Mechanisms of mesothelioma induction with asbestos and fibrous glass”. In: *Journal of the National Cancer Institute* 48.3 (1972), pages 797–821 (cited on pages 56, 68).
- [5] D. Kehren, B. Simonow, D. Bäger, N. Dziurawitz, D. Wenzlaff, C. Thim, J. Neuhoff, A. Meyer-Plath, and S. Plitzko. “Release of Respirable Fibrous Dust from Carbon Fibers Due to Splitting along the Fiber Axis”. In: *Aerosol and air quality research* 19.10 (2019), pages 2185–2195+ (cited on page 56).
- [6] K. Donaldson, F. A. Murphy, R. Duffin, and C. A. Poland. “Asbestos, carbon nanotubes and the pleural mesothelium: a review of the hypothesis regarding the role of long fibre retention in the parietal pleura, inflammation and mesothelioma”. In: *Particle and fibre toxicology* 7.1 (2010), page 5 (cited on pages 56, 59, 61, 62).
- [7] R. Sturm and W. Hofmann. “A theoretical approach to the deposition and clearance of fibers with variable size in the human respiratory tract”. In: *Journal of hazardous materials* 170.1 (2009), pages 210–218 (cited on page 56).
- [8] J. A. Champion and S. Mitragotri. “Shape induced inhibition of phagocytosis of polymer particles”. In: *Pharmaceutical research* 26.1 (2009), pages 244–249 (cited on page 56).
- [9] M. Lippmann. “Toxicological and epidemiological studies on effects of airborne fibers: coherence and public health implications”. In: *Critical reviews in toxicology* 44.8 (2014), pages 643–695 (cited on page 56).
- [10] M. Endo. “Grow carbon fibers in the vapor phase”. In: *Chemtech* (1988) (cited on page 57).
- [11] G. Tibbetts. “Vapor-grown carbon fibers”. In: *Carbon fibers filaments and composites*. Edited by J. L. Figueiredo, C. A. Bernardo, R. Baker, and K. Hüttinger. Volume 177. Springer Science & Business Media, 1990 (cited on page 57).
- [12] L. Ma-Hock, S. Treumann, V. Strauss, S. Brill, F. Luizi, M. Mertler, K. Wiench, A. O. Gamer, B. Van Ravenzwaay, and R. Landsiedel. “Inhalation toxicity of multiwall carbon nanotubes in rats exposed for 3 months”. In: *Toxicological Sciences* 112.2 (2009), pages 468–481 (cited on page 57).
- [13] J. Pauluhn. “Subchronic 13-week inhalation exposure of rats to multiwalled carbon nanotubes: toxic effects are determined by density of agglomerate structures, not fibrillar structures”. In: *Toxicological Sciences* 113.1 (2010), pages 226–242 (cited on page 57).
- [14] S. Rittinghausen, A. Hackbarth, O. Creutzenberg, H. Ernst, U. Heinrich, A. Leonhardt, and D. Schaudien. “The carcinogenic effect of various multi-walled carbon nanotubes (MWCNTs) after intraperitoneal injection in rats”. In: *Particle and fibre toxicology* 11.1 (2014), page 59 (cited on pages 57, 64).
- [15] G. A. Westphal, N. Rosenkranz, A. Brik, D. Weber, I. Föhring, C. Monsé, N. Kaiser, B. Hellack, M. Mattenkloft, T. Brüning, et al. “Multi-walled carbon nanotubes induce stronger migration of inflammatory cells in vitro than asbestos or granular particles but a similar pattern of inflammatory mediators”. In: *Toxicology in Vitro* 58 (2019), pages 215–223 (cited on page 57).
- [16] J. Muller, M. Delos, N. Panin, V. Rabolli, F. Huaux, and D. Lison. “Absence of carcinogenic response to multiwall carbon nanotubes in a 2-year bioassay in the peritoneal cavity of the rat”. In: *Toxicological Sciences* 110.2 (2009), pages 442–448 (cited on pages 57, 64).
- [17] J. Muller, F. Huaux, N. Moreau, P. Misson, J.-F. Heilier, M. Delos, M. Arras, A. Fonseca, J. B. Nagy, and D. Lison. “Respiratory toxicity of multi-wall carbon nanotubes”. In: *Toxicology and applied pharmacology* 207.3 (2005), pages 221–231 (cited on page 57).
- [18] F. A. Murphy, C. A. Poland, R. Duffin, K. T. Al-Jamal, H. Ali-Boucetta, A. Nunes, F. Byrne, A. Prina-Mello, Y. Volkov, S. Li, et al. “Length-dependent retention of carbon nanotubes in the pleural space of mice initiates sustained inflammation and progressive fibrosis on the parietal pleura”. In: *The American journal of pathology* 178.6 (2011), pages 2587–2600 (cited on page 57).
- [19] J. Xu, D. B. Alexander, M. Futakuchi, T. Numano, K. Fukamachi, M. Suzui, T. Omori, J. Kanno, A. Hirose, and H. Tsuda. “Size- and shape-dependent pleural translocation, deposition, fibrogenesis, and mesothelial proliferation by multiwalled carbon nanotubes”. In: *Cancer science* 105.7 (2014), pages 763–769 (cited on page 57).

- [20] H. Nagai, Y. Okazaki, S. H. Chew, N. Misawa, Y. Yamashita, S. Akatsuka, T. Ishihara, K. Yamashita, Y. Yoshikawa, H. Yasui, et al. “Diameter and rigidity of multiwalled carbon nanotubes are critical factors in mesothelial injury and carcinogenesis”. In: *Proceedings of the national academy of sciences* 108.49 (2011), E1330–E1338 (cited on page 57).
- [21] C. Marambio-Jones and E. M. Hoek. “A review of the antibacterial effects of silver nanomaterials and potential implications for human health and the environment”. In: *Journal of Nanoparticle Research* 12.5 (2010), pages 1531–1551 (cited on page 58).
- [22] Q.-e. Wang, C.-h. Han, W.-d. Wu, H.-b. Wang, S.-j. Liu, and N. Kohyama. “Biological Effects of Man-Made Mineral Fibers (I)”. In: *Industrial health* 37.1 (1999), pages 62–67 (cited on page 58).
- [23] P. G. Collins. “Defects and disorder in carbon nanotubes”. In: *Oxford Handbook of Nanoscience and Technology Volume 2: Materials: Structures, Properties and Characterization Techniques*. Edited by A. V. Narlikar and Y. Y. Fu. Oxford University Press Oxford, 2009, pages 156–184 (cited on page 58).
- [24] S. Hanelt, J. F. Friedrich, G. Orts-Gil, and A. Meyer-Plath. “Study of Lewis acid catalyzed chemical bromination and bromoalkylation of multi-walled carbon nanotubes”. In: *Carbon* 50.3 (2012), pages 1373–1385 (cited on page 58).
- [25] S. Hanelt, G. Orts-Gil, J. F. Friedrich, and A. Meyer-Plath. “Differentiation and quantification of surface acidities on MWCNTs by indirect potentiometric titration”. In: *Carbon* 49.9 (2011), pages 2978–2988 (cited on page 58).
- [26] M. Allegri, D. K. Perivoliotis, M. G. Bianchi, M. Chiu, A. Pagliaro, M. A. Koklioti, A.-F. A. Trompeta, E. Bergamaschi, O. Bussolati, and C. A. Charitidis. “Toxicity determinants of multi-walled carbon nanotubes: the relationship between functionalization and agglomeration”. In: *Toxicology Reports* 3 (2016), pages 230–243 (cited on page 58).
- [27] R. Li, X. Wang, Z. Ji, B. Sun, H. Zhang, C. H. Chang, S. Lin, H. Meng, Y.-P. Liao, M. Wang, et al. “Surface charge and cellular processing of covalently functionalized multiwall carbon nanotubes determine pulmonary toxicity”. In: *ACS nano* 7.3 (2013), pages 2352–2368 (cited on page 58).
- [28] C. Gunawan, M. Lim, C. P. Marquis, and R. Amal. “Nanoparticle–protein corona complexes govern the biological fates and functions of nanoparticles”. In: *Journal of Materials Chemistry B* 2.15 (2014), pages 2060–2083 (cited on page 58).
- [29] W. C. Hinds. *Aerosol technology: properties, behavior, and measurement of airborne particles*. John Wiley & Sons, 1999 (cited on page 60).
- [30] Y. Suzuki, S. R. Yuen, and R. Ashley. “Short, thin asbestos fibers contribute to the development of human malignant mesothelioma: pathological evidence”. In: *International journal of hygiene and environmental health* 208.3 (2005), pages 201–210 (cited on page 61).
- [31] K. Rasmussen, J. Mast, P.-J. De Temmerman, E. Verleysen, N. Waegeneers, J. Van Steen, J. C. Pizzolon, L. De Temmerman, E. Van Doren, K. A. Jensen, et al. “Multi-walled carbon nanotubes, NM-400, NM-401, NM-402, NM-403: characterisation and physico-chemical properties”. In: *JRC Repository: NM-series of Representative Manufactured Nanomaterials* (2014) (cited on pages 61, 73).
- [32] A. B. Kane, R. H. Hurt, and H. Gao. “The asbestos-carbon nanotube analogy: an update”. In: *Toxicology and applied pharmacology* 361 (2018), pages 68–80 (cited on page 61).
- [33] I. Arias and M. Arroyo. “Size-dependent nonlinear elastic scaling of multiwalled carbon nanotubes”. In: *Physical review letters* 100.8 (2008), page 085503 (cited on page 62).
- [34] H. Shima. “Buckling of carbon nanotubes: a state of the art review”. In: *Materials* 5.1 (2012), pages 47–84 (cited on page 62).
- [35] G. Miserocchi, G. Sancini, F. Mantegazza, and G. Chiappino. “Translocation pathways for inhaled asbestos fibers”. In: *Environmental Health* 7.1 (2008), page 4 (cited on page 62).
- [36] E. Gavze and M. Shapiro. “Motion of inertial spheroidal particles in a shear flow near a solid wall with special application to aerosol transport in microgravity”. In: *Journal of Fluid Mechanics* 371 (1998), pages 59–79 (cited on page 62).
- [37] A. Shukla, M. Ramos-Nino, and B. Mossman. “Cell signaling and transcription factor activation by asbestos in lung injury and disease”. In: *The international journal of biochemistry & cell biology* 35.8 (2003), pages 1198–1209 (cited on page 62).
- [38] B. I. Yakobson and L. S. Couchman. “Persistence length and nanomechanics of random bundles of nanotubes”. In: *Journal of Nanoparticle Research* 8.1 (2006), pages 105–110 (cited on page 62).
- [39] J. A. Swanson. “The noodle defense”. In: *J Cell Biol* 203.6 (2013), pages 871–873 (cited on page 63).
- [40] E. Evans, A. Leung, and D. Zhelev. “Synchrony of cell spreading and contraction force as phagocytes engulf large pathogens”. In: *The Journal of cell biology* 122.6 (1993), pages 1295–1300 (cited on page 63).
- [41] P. Poncharal, Z. Wang, D. Ugarte, and W. A. De Heer. “Electrostatic deflections and electromechanical resonances of carbon nanotubes”. In: *science* 283.5407 (1999), pages 1513–1516 (cited on page 63).

- [42] B. G. Demczyk, Y. M. Wang, J. Cumings, M. Hetman, W. Han, A. Zettl, and R. Ritchie. “Direct mechanical measurement of the tensile strength and elastic modulus of multiwalled carbon nanotubes”. In: *Materials Science and Engineering: A* 334.1-2 (2002), pages 173–178 (cited on page 63).
- [43] E. W. Wong, P. E. Sheehan, and C. M. Lieber. “Nanobeam mechanics: elasticity, strength, and toughness of nanorods and nanotubes”. In: *science* 277.5334 (1997), pages 1971–1975 (cited on page 63).
- [44] S. Al-Harhi, M. Al-Barwani, M. Elzain, N. Al-Naamani, and T. Hysen. “Nanobubbles stability and multiwall carbon nanotubes straightening on few-layer graphene surfaces”. In: *Journal of Applied Physics* 110.4 (2011), page 044319 (cited on page 63).
- [45] M. Arroyo and T. Belytschko. “Nonlinear mechanical response and rippling of thick multiwalled carbon nanotubes”. In: *Physical Review Letters* 91.21 (2003), page 215505 (cited on page 63).
- [46] F. Xu, Q. Qin, A. Mishra, Y. Gu, and Y. Zhu. “Mechanical properties of ZnO nanowires under different loading modes”. In: *Nano Research* 3.4 (2010), pages 271–280 (cited on page 63).
- [47] A. Krishnan, E. Dujardin, T. Ebbesen, P. Yianilos, and M. Treacy. “Young’s modulus of single-walled nanotubes”. In: *Physical review B* 58.20 (1998), page 14013 (cited on page 63).
- [48] D. Dikin, X. Chen, W. Ding, G. Wagner, and R. Ruoff. “Resonance vibration of amorphous SiO₂ nanowires driven by mechanical or electrical field excitation”. In: *Journal of applied physics* 93.1 (2003), pages 226–230 (cited on page 63).
- [49] M. Naraghi, I. Chasiotis, H. Kahn, Y. Wen, and Y. Dzenis. “Novel method for mechanical characterization of polymeric nanofibers”. In: *Review of scientific instruments* 78.8 (2007), page 085108 (cited on page 63).
- [50] S. Perisanu, V. Gouttenoire, P. Vincent, A. Ayari, M. Choueib, M. Bechelany, D. Cornu, and S. Purcell. “Mechanical properties of SiC nanowires determined by scanning electron and field emission microscopies”. In: *Physical Review B* 77.16 (2008), page 165434 (cited on page 63).
- [51] L. Kobets and I. Deev. “Carbon fibres: structure and mechanical properties”. In: *Composites science and technology* 57.12 (1998), pages 1571–1580 (cited on page 63).
- [52] R. E. Roman, K. Kwan, and S. W. Cranford. “Mechanical properties and defect sensitivity of diamond nanothreads”. In: *Nano letters* 15.3 (2015), pages 1585–1590 (cited on page 63).
- [53] F. Liddell and K. Miller. *Mineral fibers and health*. CRC Press, 1991 (cited on page 63).
- [54] Y. Sakamoto, M. Hojo, Y. Kosugi, K. Watanabe, A. Hirose, A. Inomata, T. Suzuki, and D. Nakae. “Comparative study for carcinogenicity of 7 different multi-wall carbon nanotubes with different physicochemical characteristics by a single intraperitoneal injection in male Fischer 344 rats”. In: *The Journal of toxicological sciences* 43.10 (2018), pages 587–600 (cited on page 64).
- [55] K. B. Knudsen, T. Berthing, P. Jackson, S. S. Poulsen, A. Mortensen, N. R. Jacobsen, V. Skaug, J. Szarek, K. S. Hougaard, H. Wolff, et al. “Physicochemical predictors of Multi-Walled Carbon Nanotube–induced pulmonary histopathology and toxicity one year after pulmonary deposition of 11 different Multi-Walled Carbon Nanotubes in mice”. In: *Basic & clinical pharmacology & toxicology* 124.2 (2019), pages 211–227 (cited on page 64).
- [56] H. Nagai, Y. Okazaki, S. H. Chew, N. Misawa, Y. Miyata, H. Shinohara, and S. Toyokuni. “Intraperitoneal administration of tangled multiwalled carbon nanotubes of 15 nm in diameter does not induce mesothelial carcinogenesis in rats”. In: *Pathology international* 63.9 (2013), pages 457–462 (cited on page 64).
- [57] A. Takagi, A. Hirose, M. Futakuchi, H. Tsuda, and J. Kanno. “Dose-dependent mesothelioma induction by intraperitoneal administration of multi-wall carbon nanotubes in p53 heterozygous mice”. In: *Cancer Science* 103.8 (2012), pages 1440–1444 (cited on page 64).
- [58] W. Utembe, K. Potgieter, A. B. Stefaniak, and M. Gulumian. “Dissolution and biodurability: Important parameters needed for risk assessment of nanomaterials”. In: *Particle and fibre toxicology* 12.1 (2015), page 11 (cited on page 65).
- [59] D. M. Bernstein, C. Morscheidt, H.-G. Grimm, P. Thévenaz, and U. Teichert. “Evaluation of soluble fibers using the inhalation biopersistence model, a nine-fiber comparison”. In: *Inhalation Toxicology* 8.4 (1996), pages 345–385 (cited on page 65).
- [60] C. Singh, S. Friedrichs, G. Ceccone, N. Gibson, K. A. Jensen, M. Levin, H. Goenaga Infante, D. Carlander, and K. Rasmussen. “Cerium Dioxide, NM-211, NM-212, NM-213. Characterisation and test item preparation”. In: *JRC Repository: NM-Series of Representative Manufactured Nanomaterials* (2014) (cited on page 66).
- [61] W. Wohlleben, H. Waindok, B. Daumann, K. Werle, M. Drum, and H. Egenolf. “Composition, respirable fraction and dissolution rate of 24 stone wool MMVF with their Binder”. In: *Particle and fibre toxicology* 14.1 (2017), page 29 (cited on page 66).
- [62] J. Koltermann-Jülly, J. G. Keller, A. Vennemann, K. Werle, P. Müller, L. Ma-Hock, R. Landsiedel, M. Wiemann, and W. Wohlleben. “Abiotic dissolution rates of 24 (nano) forms of 6 substances compared to macrophage-assisted

- dissolution and in vivo pulmonary clearance: Grouping by biodissolution and transformation”. In: *NanoImpact* 12 (2018), pages 29–41 (cited on page 66).
- [63] IARC Working Group on the Evaluation of Carcinogenic Risks to Humans and International Agency for Research on Cancer and World Health Organization. *Man-made vitreous fibres*. 81. World Health Organization, 2002 (cited on page 66).
- [64] M. Guldborg, S. L. Jensen, T. Knudsen, T. Steenberg, and O. Kamstrup. “High-alumina low-silica HT stone wool fibers: A chemical compositional range with high biosolubility”. In: *Regulatory Toxicology and Pharmacology* 35.2 (2002), pages 217–226 (cited on page 66).
- [65] B. K. Ku, G. Deye, and L. A. Turkevich. “Characterization of a vortex shaking method for aerosolizing fibers”. In: *Aerosol Science and Technology* 47.12 (2013), pages 1293–1301 (cited on page 67).
- [66] E. D. Kuempel, M.-C. Jaurand, P. Møller, Y. Morimoto, N. Kobayashi, K. E. Pinkerton, L. M. Sargent, R. C. Vermeulen, B. Fubini, and A. B. Kane. “Evaluating the mechanistic evidence and key data gaps in assessing the potential carcinogenicity of carbon nanotubes and nanofibers in humans”. In: *Critical reviews in toxicology* 47.1 (2017), pages 1–58 (cited on page 68).
- [67] G. Boulanger, P. Andujar, J.-C. Pairen, M.-A. Billon-Galland, C. Dion, P. Dumortier, P. Brochard, A. Sobaszek, P. Bartsch, C. Paris, et al. “Quantification of short and long asbestos fibers to assess asbestos exposure: a review of fiber size toxicity”. In: *Environmental Health* 13.1 (2014), page 59 (cited on page 68).
- [68] D. B. Warheit, K. Reed, K. E. Pinkerton, and T. Webb. “Biodegradability of inhaled p-aramid respirable fiber-shaped particulates (RFP): mechanisms of RFP shortening and evidence of reversibility of pulmonary lesions”. In: *Toxicology letters* 127.1-3 (2002), pages 259–267 (cited on page 68).
- [69] WHO. *Workshop on “mechanisms of fibre carcinogenesis and assessment of chrysotile asbestos substitutes: summary consensus report”*. 2005 (cited on page 68).
- [70] D. Komljenovic, W. A. Groves, and V. J. Kecojevic. “Injuries in US mining operations—A preliminary risk analysis”. In: *Safety Science* 46.5 (2008), pages 792–801 (cited on page 72).
- [71] M. Dellarco, R. Zaleski, B. Gaborek, H. Qian, C. Bellin, P. Egeghy, N. Heard, O. Jolliet, D. Lander, N. Sunger, et al. “Using exposure bands for rapid decision making in the RISK21 tiered exposure assessment”. In: *Critical reviews in toxicology* 47.4 (2017), pages 317–341 (cited on page 72).
- [72] D. M. Zalk, S. Y. Paik, and P. Swuste. “Evaluating the control banding nanotool: a qualitative risk assessment method for controlling nanoparticle exposures”. In: *Journal of Nanoparticle Research* 11.7 (2009), page 1685 (cited on page 72).
- [73] Y. Zhao, B. L. Allen, and A. Star. “Enzymatic degradation of multiwalled carbon nanotubes”. In: *The journal of physical chemistry A* 115.34 (2011), pages 9536–9544 (cited on page 73).

Deposition of synthetic fibers in human respiratory tract

By: Yung Sung Cheng¹, Wei-Chung Su¹, Yue Zhou¹

¹ – Lovelace Respiratory Research Institute, 2425 Ridgecrest Dr. SE, Albuquerque, NM 87108, USA

abstract Inhalation exposure of fiber aerosol may have serious health consequences including lung cancer, fibrosis and mesothelioma. The deposition pattern in the respiratory tract as a function of fiber dimensions is the information critical to understanding respiratory dosimetry and defining the index of exposure for health protection purposes. Controlled studies of fiber deposition in human volunteers are not available because of ethical concerns. However, total and regional depositions of inhaled fibers have been estimated from post-mortem measurements and mathematical modeling. Increasingly, mathematical deposition models have been used to assess the dosimetry of inhaled man-made vitreous fibers. However, current lung dosimetric models for fibers in the human respiratory tract are based on theoretical equations, which have not been verified with experimental data. The objectives of this study are (1) to develop experimental information on the deposition of fibrous aerosols as a function of fiber diameter and length in realistic human respiratory tract replicas, (2) to verify and improve the prediction of fiber dose estimates in human lungs using both empirical data as well as computational fluid dynamic technique, and (3) to define a size-selective exposure index based on fiber penetration data. In the deposition experiment, a human nasal airway cast and oral/upper tracheobronchial airway replicas were used for the study. Carbon, glass fiber, and TiO₂ fibers were used as test materials. Deposition patterns in the oral airway, nasal airway, and the tracheobronchial region were obtained as a function of fiber dimensions and inspiratory flow rate. For the test fibers, deposition efficiency increased with flow rate and square of aerodynamic diameter, indicating that impaction is the main deposition mechanism of these fibers. Deposition efficiencies of fibers in the nasal, oral, and tracheobronchial airways were smaller than spherical particles of the same aerodynamic diameter. This appears to be a result of the tendency of a fiber to align with flow direction, resulting in lower drag in the axial flow direction and more easily penetrating the upper respiratory tract. Lower deposition efficiencies in the oral and nasal airways implied higher penetration of fibers into the lower airway regions. Experimental deposition efficiencies in the nasal and tracheobronchial airways are in agreement with fiber theoretical deposition equations. Fiber deposition equations in the nasal, oral, and tracheobronchial airways were developed and can be used in the fiber lung deposition model. Because lung diseases caused by inhaled fibers occur in the bronchial, alveolar, and parachymal regions, a thoracic fraction defined as the fraction of particles penetrating the larynx and reaching the lung was defined from the experimental data obtained in this study. The experimental data show that the thoracic fraction of fiber aerosol is different from that of spherical particles obtained in this study. This research also produced essential information on the dosimetry of inhaled fibers in the human lung, data for an improved mathematical lung deposition model, and a definition of the thoracic fraction of fibers for exposure assessment. Sampling devices based on this size-selection definition can be developed in the future for improved assessment of worker exposure.

8.1 Introduction

Inhalation exposure to asbestos causes (1) asbestosis, a diffuse fibrosis in the alveolar and pleural region of the lung, (2) bronchogenic lung cancer, and (3) mesothelioma in pleura and peritoneum [1, 2]. Evidence from epidemiological studies and animal experiments is substantial. Other mineral fibers such as erionite may have a similar effect on the

8. Deposition of synthetic fibers in human respiratory tract

exposed human population [3]. Man-made vitreous fibers (MMVFs), including glass fibers, ceramics, and carbides that replace asbestos in many applications, may have similar biological effects in laboratory animals [4–8]. Although the etiology of these diseases has not yet been clearly elucidated, fiber dimensions and durability play an essential role [9, 10].

Fiber materials contain elongated particles with an aspect ratio (length divided by diameter) over 3. The aerodynamic diameter of a fiber depends primarily on fiber diameter with a secondary dependence on the aspect ratio [11, 12]. Based on experimental evidence, Lippmann [13] argued that three diseases are associated with fibers of different dimensions, which may deposit at different locations in the respiratory tract. While occupational exposure to asbestos fibers has decreased because the material was replaced with synthetic vitreous fibers (SVFs), the main concerns of occupational exposure and health effects are on SVF now.

No human data are available from controlled experiments of inhaled fiber aerosols for the obvious reason that most fiber materials are potentially hazardous when inhaled. From the post-mortem examination of lung tissues in miners working in asbestos mines, Pooley and Clark [14] determined the size distribution of chrysotile, crocidolite, and amosite fibers. Based on post-mortem lung specimens of workers exposed to anthophyllite fibers, Timbrell [15] showed a bivariate presentation of retention curves for each worker. These results were used to infer the deposition of fibers with respect to fiber length and diameter after the clearance processes were considered.

Glass fiber deposition in the human airway has been observed directly in a single bifurcation tube [16, 17] and a more realistic silicon-rubber airway cast, including a simulated larynx, trachea, and bronchiole larger than 3 mm in diameter [18]. Deposition efficiency was higher with increasing flow rates, and deposition densities were much greater at the bifurcation than along the walls of the daughter tubes. An empirical equation that included the impaction and interception parameters was developed to describe the experimental data [19].

A mathematical deposition model of inhaled fiber aerosols in the human respiratory tract was first developed by Beeckmans [20] based on Weibel's morphological lung model [21]. This model was an extension of the lung deposition model of spherical particles [22]. Harris and Fraser [23] considered impaction, sedimentation, diffusion, and interception mechanisms and developed a more complete deposition model. A fiber in the airway was considered either in random orientation or parallel to the airflow, depending on flow conditions and the strength of the Brownian motion. The model also considered nasal deposition by interception and impaction mechanisms. These early works were an extension of spherical particle models and did not consider fiber rotation.

Asgharian and Yu [24, 25] recognized the importance of fiber orientation. In a shear flow of an airway tube, the fiber moves in the direction of the air flow, but also undergoes an end-to-end rotation as described by Jeffery [26]. The flow profile and Brownian motion of the particle [27] determine the particle movement. In lung airways, most fibers move with the long axis parallel to the axial flow in the parent and daughter tubes. Asgharian and Yu [28] extended their human deposition model to consider the airway structure and breathing patterns of rats. This model has been improved further [29–32].

Air sampling of particulate matter in the ambient and occupational environments are based on size-selective criteria [33]. Size-selective criteria have been defined based on the deposition of spherical particles in human volunteers [33]. All three size-selective exposure indices have been developed for compact or spherical particles with the aerodynamic diameter as the characteristic parameter. No size equivalent indices for fiber aerosols are specified in the sampling recommendations, although the specified inlet configurations of the sampler will impose some size-selection. A more definitive index based on quantitative information of fiber deposition in the lung is needed.

It is clear that the deposition of fibers in the bronchial and alveolar regions and the subsequent uptake and translocation to the nearby interstitium and other tissues play important roles in the etiology of fiber-associated lung diseases. Mechanisms of fiber deposition in various regions of the human respiratory tract have been proposed and mathematical equations developed. However, few experimental data confirm the model prediction, and there is no fiber deposition equation for the nasal and oral airways. Experimental data are needed on the deposition of fibers in human nasal and oral passages and in the TB trees to ascertain the importance of fiber dimension and flow rate on lung deposition. A consequence of insufficient deposition data is that the current sampling procedure may not be

adequate to assess exposure of fibers in occupational settings.

The goal of this manuscript was to measure deposition of fibers in realistic replicas of the human respiratory tract. Synthetic fibers of uniform diameters were generated so the effects of fiber dimensions and flow rate on the deposition efficiency can be determined accurately. The experimental data were used to compare with theoretical and numerical deposition models. With the verified theoretical results, improved deposition equations in the nasal, oral and tracheobronchial airways were developed. Deposition data were also used to define a thoracic fiber fraction as an index of exposure to fiber aerosols.

8.2 Materials and Methods

8.2.1 Human nasal airway cast

The nasal airway is the major entry to the human respiratory tract, and acts as a first line of defense and a filtration system in preventing hazardous aerosols from entering the lung. The fraction of the inhaled fiber acquired from the nasal airway due to deposition could directly indicate the remaining fraction of the inhaled fiber entering the lower respiratory airway. A replicate human nasal cast was used in this research for the fiber deposition study. This nasal airway cast was made based on the *in vivo* magnetic resonance imaging (MRI) of a nonsmoking Caucasian male (53 years of age, 73 kg in body mass, and 173 cm tall). The MRI images were taken every 3 mm in the nasal airway [34]. The original images obtained from these MRIs were digitized with a GRAF/PEN sonic digitizer (SAC, Southport, CT), and then three-dimensional surfaces were constructed for adjacent perimeter traces using a computer-assisted design software (SmartCAM, Point Control Co., Eugene, OR). The physical nasal airway cast was made by using 1.5 mm-thick acrylic plates and milling with a computer-controlled micro-milling machine (CAMM 3, Roland DG, Los Angeles, CA). The entire nasal airway cast contains 77 acrylic plates (115.5 mm total length) and consists of complete nasal airway structures including an anterior region (first 25 plates: 0 mm to 37.5 mm, with vestibule and nasal valve subregions), turbinate region (middle 32 plates: 37.5 mm to 85.5 mm, with front and rear turbinate subregions), and posterior region (last 20 plates: 85.5 mm to 115.5 mm, with entire nasopharynx region). The turbinate region was further divided into superior turbinate (also known as the olfactory area), middle turbinate (MT), and inferior turbinate (IT) sections. Figure 8.1 shows the structure and sections of the nasal airway cast used in this research. This nasal replica was used previously to study deposition of spherical particles and with similar deposition efficiencies obtained in the nasal airways of human volunteers [35]).

8.2.2 Human respiratory airway casts

Production models of human respiratory airways have been developed [36] from *in vivo* measurements (oral cavity) and cadavers (tracheobronchial airways). These production molds can reproduce human respiratory airway casts for deposition study with defined geometric dimension, which has been shown to provide reliable data in experiments of particle deposition in the human respiratory airway [36–39]. Therefore, these airway casts are ideal to be used in this research for the advanced fiber deposition studies.

Two different airway casts (LA and LB) were made from selected production modes. The only information available for these two casts are that the LA cast was made based on a 16-year-old male, and the LB cast was made based on a 21-year-old male. The airway casts were made from conductive silicone rubber (KE-4576, Shin-Etsu Chemical Co., Ltd., Tokyo, Japan). Using conductive material has an advantage for fiber deposition experiments since it can eliminate the unexpected fiber deposition in the airway caused by possible electrostatic effects. Figure 8.2 shows the structure and physical model for the two airway casts used in this research. Each airway cast consists of an oral cavity, oropharynx, larynx, trachea, and the tracheobronchial airways to the 4th (LA) or 3rd (LB) bifurcation.

8. Deposition of synthetic fibers in human respiratory tract

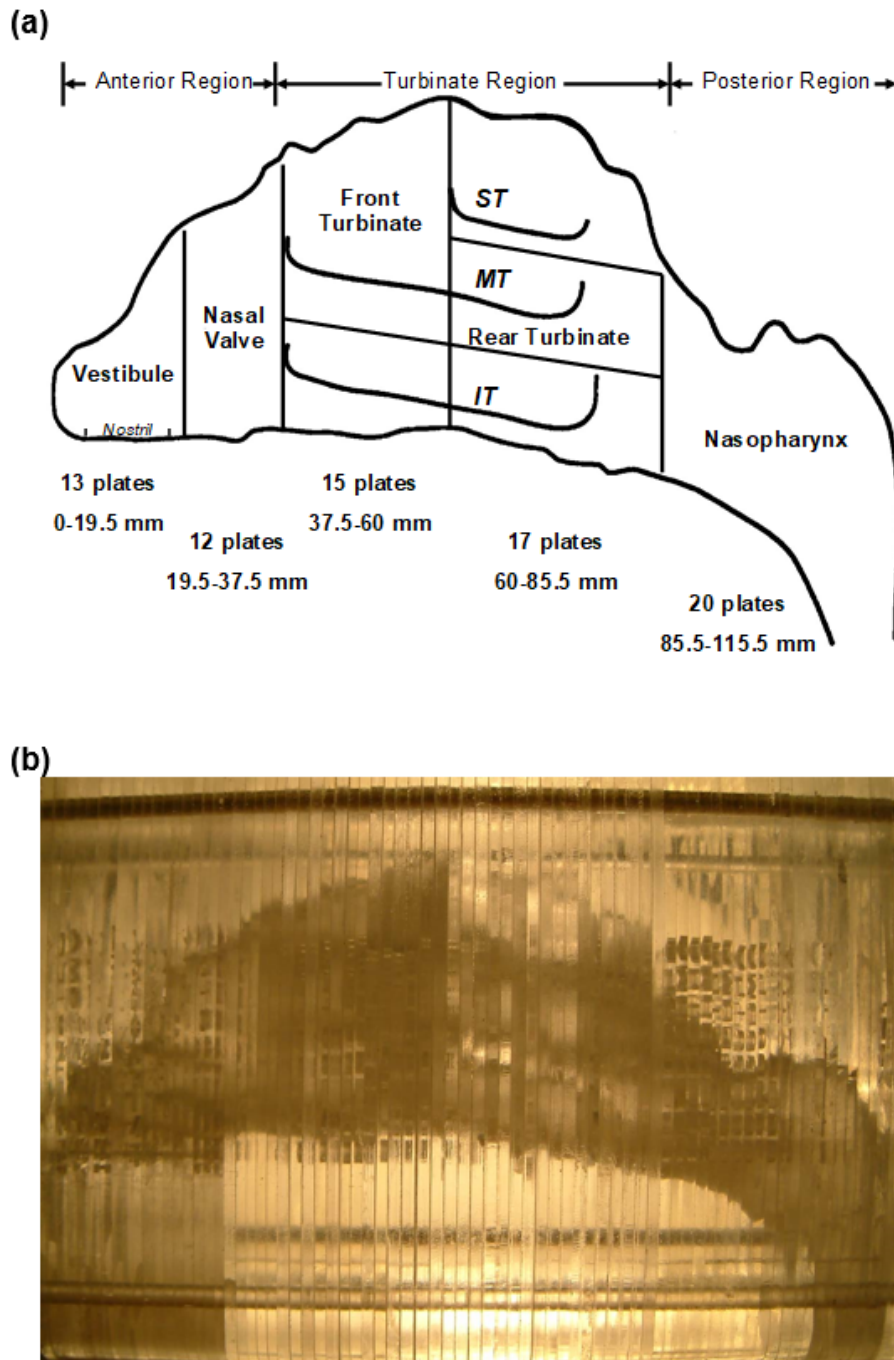
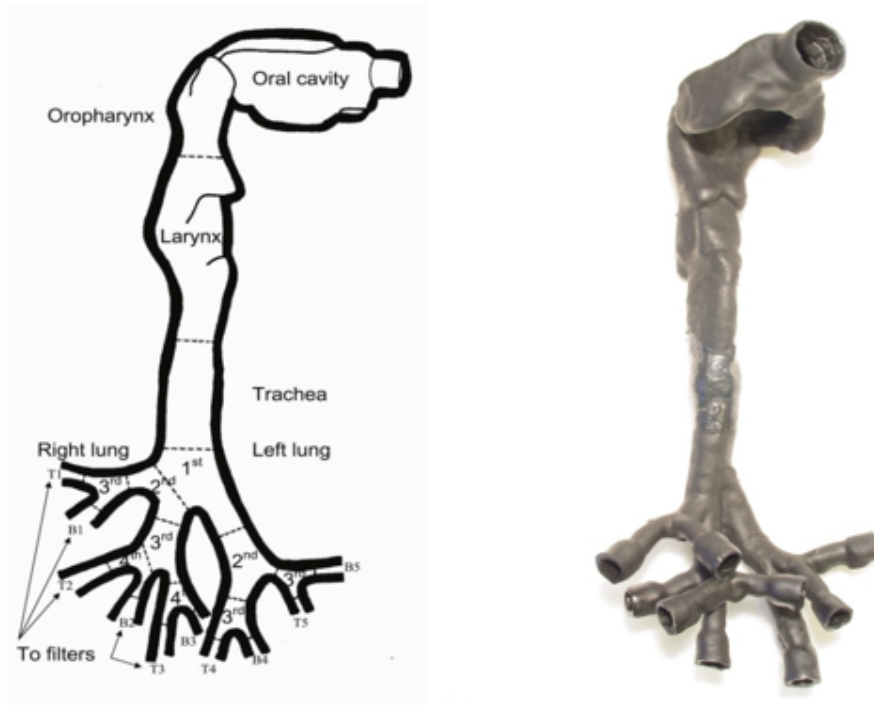


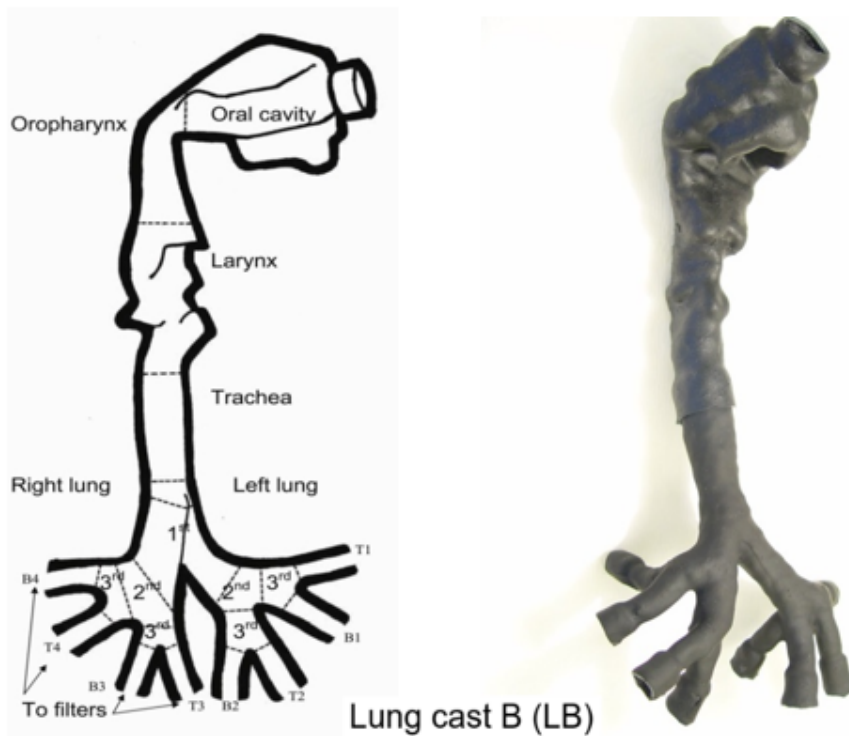
Figure 8.1.: Structure and regions of the human nasal airway replica (a) schematic diagram and (b) physical model

8.2.3 Fiber materials

Fiber is defined as elongated particles with an aspect ratio, β (the ratio of the length to the diameter), over 3 [40]. The fiber dimension is the key factor affecting the fiber deposition in the human airway. It has been reported that the aerodynamic diameter of a fiber in the air depends primarily on its diameter and only slightly on its length [11, 12]. The toxicity of a fiber is strongly related to the fiber length. For instance, it has been reported that long and thin



Lung cast A (LA)



Lung cast B (LB)

Figure 8.2.: Structure and regions of the human nasal airway replica.

8. Deposition of synthetic fibers in human respiratory tract

fibers have greater toxicity than short and thick fibers [15, 41–43]. Therefore, a variety of fiber material is needed for the fiber deposition study in order to determine the relationship between the fiber dimension and the associated deposition pattern in the human respiratory airway.

In this research, three man-made fiber materials were employed in the deposition experiments: carbon, titanium dioxide (TiO₂) and glass. These fiber materials were all uniform in diameter and diverse in length. Using fibers with uniform diameter is a new approach for fiber deposition studies since it provides a simple way to obtain the fiber dimension for the deposited fiber (length measurement only) and a sure way to determine the effect of fiber length or fiber diameter on the deposition pattern. The test carbon fibers were relatively large fiber which provided by Hercules, Inc. (Wilmington, DE). These carbon fibers are black in color, conductive, monodisperse in diameter (CMD = 3.66 μm, $\sigma_g = 1.11$), polydisperse in length (CML = 14.83 μm), and with a density measured at 1.83 g cm⁻³. The test carbon fiber material contains cylindrical fibers and fiber debris. In this research, only fibers with lengths larger than 10 μm were counted as contributing to the final deposition data.

The TiO₂ and glass fibers were short fibers compared to the carbon fibers. The TiO₂ fiber used in this research was made in the University of Florida with electro-spinning technology. The TiO₂ fiber is monodisperse in diameter (CMD = 0.59 μm, $\sigma_g = 1.18$) and polydisperse in length (CML = 3.20 μm) with a density of 4.23 g cm⁻³. The glass fiber (JM475/100, Johns Manville Co., Littleton, CO) is nearly monodisperse in diameter (CMD = 0.62 μm, $\sigma_g = 1.30$) and polydisperse in length (CML = 7.67 μm) with a density of 2.56 g cm⁻³. Similar criteria for fiber measurement were also applied to these two fiber materials: only TiO₂ fibers longer than 2.5 μm and glass fibers longer than 3.5 μm were counted in the deposition data due to the limitation of the visual measurement. Figure 8.3 shows images and statistics of these three man-made fibers. Table 8.1 lists the physical properties of the test fibers.

Table 8.1.: Comparison of the physical characteristics and aerodynamic diameter for three different man-made fiber materials.

Fiber	Density	Diameter [μm]	Length [μm]	d _{ae} [μm]
Carbon	1.83 g cm ⁻³	CMD = 3.66	CML = 14.83	7.6-12.8 ^a
		$\sigma_g = 1.11^c$	$\sigma_g = 4.00$	8.1-14.9 ^b
TiO₂	4.23 g cm ⁻³	CMD = 0.59	CML = 3.20	L = 10 – 300
		$\sigma_g = 0.17$	$\sigma_g = 0.42$	2.1-2.7
				2.2-3.0
Glass	2.56 g cm ⁻³	CMD = 0.62	CML = 7.67	L = 2.5 – 12.0
		$\sigma_g = 0.27$	$\sigma_g = 0.45$	1.8-2.3
				2.0-2.7
				L = 3.5 – 20.0

^a Fiber aerodynamic diameter with random orientation.

^b Fiber aerodynamic diameter with parallel orientation.

^c Geometric standard deviation.

The aerodynamic diameter (d_{ae}) of the test fiber could be approximately calculated by the equations below [44]:

$$d_{ae} = d_{ve} \sqrt{\frac{\rho}{\rho_0 \kappa}} \quad (8.1)$$

where d_{ve} is the fiber volume equivalent diameter, ρ is the density of fiber, ρ_0 is the density of water, and κ is the dynamic shape factor for a prolate spheroid. For a prolate spheroid flying in the air with its long axis orientating

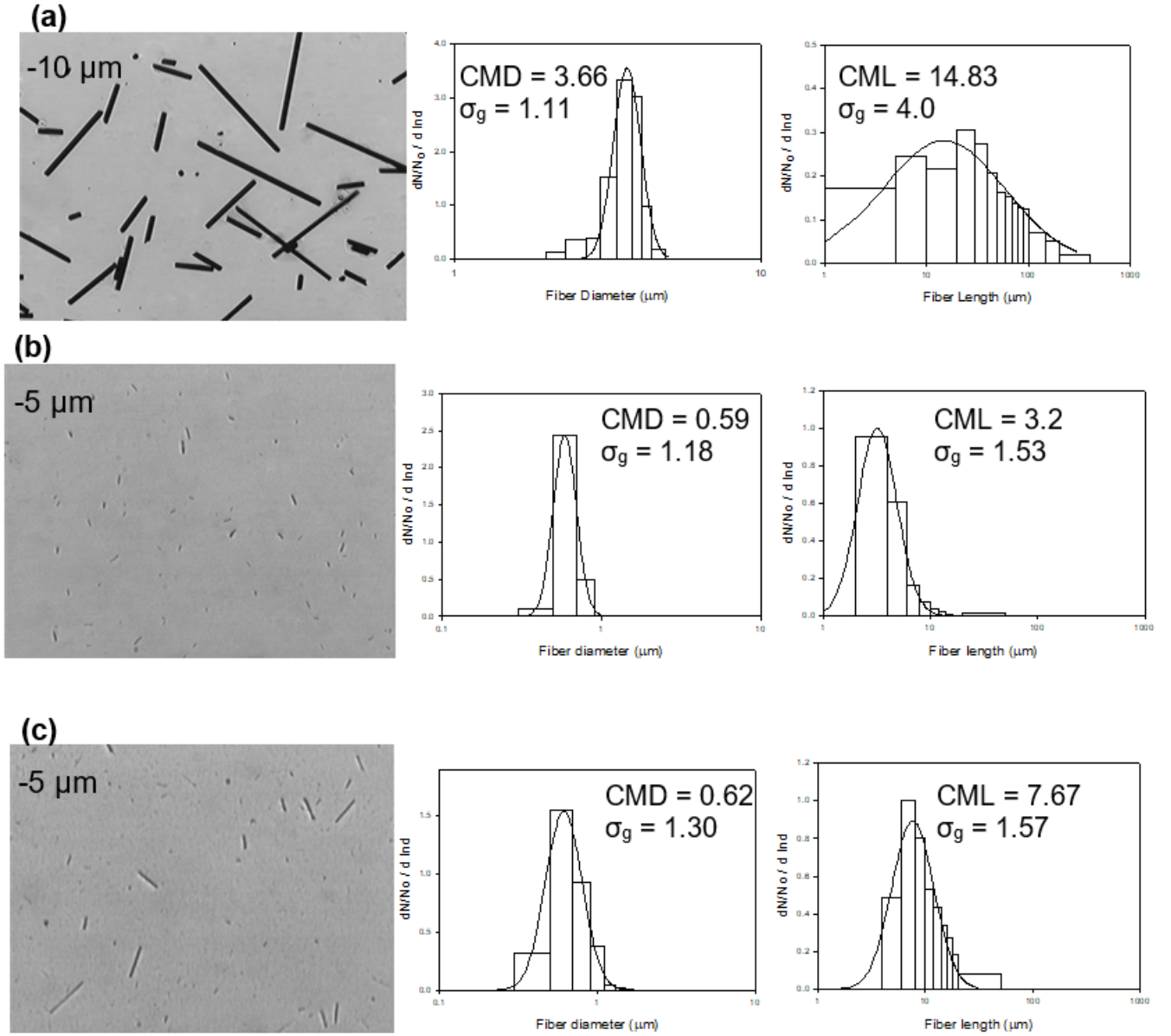


Figure 8.3.: The test man-made fiber materials (a) carbon fiber, (b) TiO_2 fiber, and (c) glass fiber.

perpendicular to the flow direction, the dynamic shape factor is κ_{\perp}

$$\kappa_{\perp} = \frac{\frac{8}{3} (\beta^2 - 1) \beta^{-\frac{1}{3}}}{\frac{2\beta^2 - 3}{\sqrt{\beta^2 - 1}} \ln (\beta + \sqrt{\beta^2 - 1} + \beta)} \quad (8.2)$$

where β is the aspect ratio. The dynamic shape factor is κ_{\parallel} , if the long axis of a prolate spheroid orientates parallel to

8. Deposition of synthetic fibers in human respiratory tract

the flow direction.

$$\kappa_{\parallel} = \frac{\frac{4}{3}(\beta^2 - 1)\beta^{-\frac{1}{3}}}{\frac{2\beta^2 - 1}{\sqrt{\beta^2 - 1}} \ln(\beta + \sqrt{\beta^2 - 1} + \beta)} \quad (8.3)$$

If the orientation of a prolate spheroid is random in the air, the dynamic shape factor is κ_r and can be written as [45]

$$\frac{1}{\kappa_r} = \frac{1}{3\kappa_{\parallel}} + \frac{2}{3\kappa_{\perp}} \quad (8.4)$$

Based on the equations shown above, for a 20- μm -long carbon fiber in the airflow (diameter = 3.66 μm) with its long axis orientating perpendicular to the flow direction (dynamic shape factor = κ_{\perp}), the aerodynamic diameter of the carbon fiber, $d_{ae(\perp)}$, is 8.4 μm . On the other hand, if the carbon fiber's long axis is parallel to the flow direction (dynamic shape factor = κ_{\parallel}), the aerodynamic diameter, $d_{ae(\parallel)}$, is 9.7 μm . However, if the carbon fiber orientates randomly in the air (dynamic shape factor = κ_r), the aerodynamic diameter, $d_{ae(r)}$, is 8.8 μm . In contrast, for a 100- μm long carbon fiber in the air, its $d_{ae(\perp)}$, $d_{ae(\parallel)}$, and $d_{ae(r)}$ are 10.4 μm , 13.0 μm , and 11.3 μm , respectively. Based on the calculation above, Table 8.1 summarizes the physical characteristics as well as the estimated d_{ae} for these three man-made fibers (all the measured data were obtained after the fiber materials passed through the aerosol generation devices).

8.3 Experimental setup

Two different setups were used in this research for the fiber deposition experiments due to the characteristics of the fiber material. The carbon and glass fiber materials were dry-powder-like. Therefore they could be aerosolized by a small-scale powder disperser (SSPD, Model 3433, TSI Inc., St. Paul, MN). The related experimental apparatus includes an SSPD, a charge neutralizer, the human airway cast, and the backup filter holder. 8.4 shows the experimental setup for the fiber deposition study using SSPD. For this experimental setup, the dispersed fibers were first delivered to the Kr⁸⁵ charge neutralizer. Fibers passing through the neutralizer were at Boltzmann equilibrium and then delivered to the airway cast. A filter holder was attached to the nasopharynx of the nasal airway cast (ten filter holders were connected to the ends of the bronchial airways for lung airway cast) for collecting fibers that passed through the entire cast. A typical experiment lasted from 5 to 20 minutes depending on the inspiratory flow rate selected, and the SSPD rotation plate was set to a speed of 2. All of these operation parameters have proved to provide a sufficient number of fibers for the deposition study.

The TiO₂ fiber aerosol was generated by a medication nebulizer (Up-Mist, Hospitak Inc., Farmingdale, NY) due to its material characteristics. The experimental apparatus included a nebulizer, several alumina drying columns, a charge neutralizer, and the filter holder. Figure 8.5 shows the experimental setup for the TiO₂ fiber deposition study. Before generating the TiO₂ fiber aerosol, the TiO₂ fiber plates were placed in alcohol and ultrasonicated for 30 s before the aerosol generation process. When generating TiO₂ fiber aerosol, the nebulizer generates TiO₂ fiber aerosol along with the alcohol aerosol (droplets). These aerosols were first transferred to several drying columns and a Kr⁸⁵ charge neutralizer. In this way, sufficient time was provided to ensure that the alcohol mist evaporated and only TiO₂ fiber aerosol remained prior to entering the airway cast.

Before the deposition experiment, silicon oil (550 Fluid, Dow Corning Co., Midland, MI) was applied to the inside surface of the airway casts to simulate the adhesive nature in a real human airway. The oil coating has another advantage that it can force fibers to remain on the place where they originally deposited. The deposition experiments were conducted with constant inspiratory flow rates. Four flow rates (7.5, 15, 30, and 43.5 lmin⁻¹) were used in the

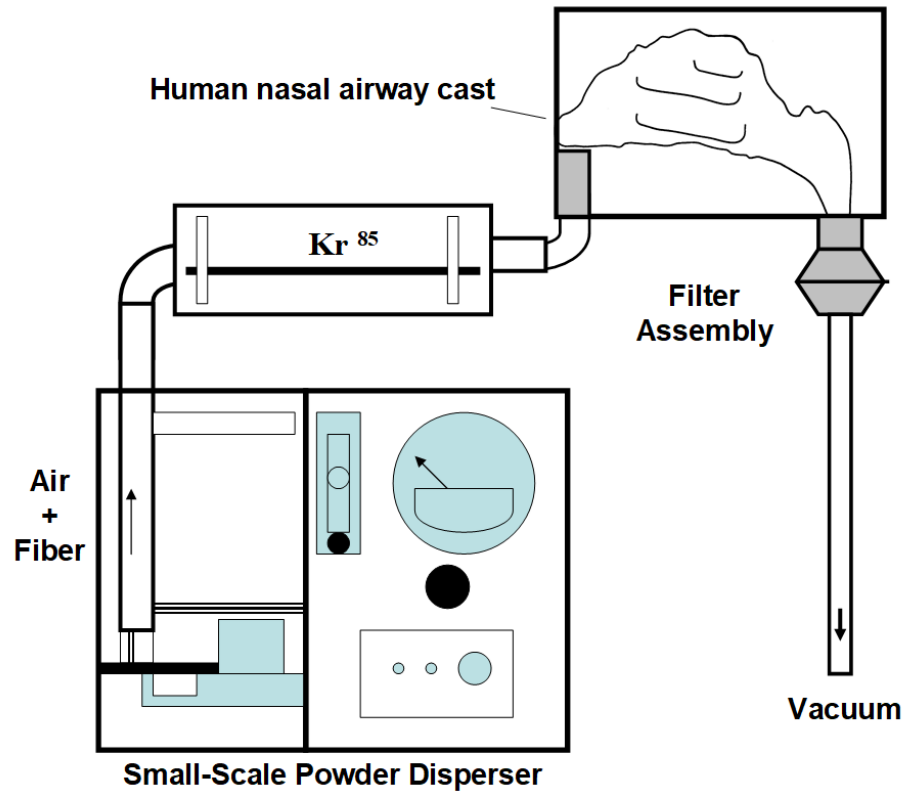


Figure 8.4.: Schematic diagram of the experimental setup for the fiber deposition study with a small-scale powder disperser.

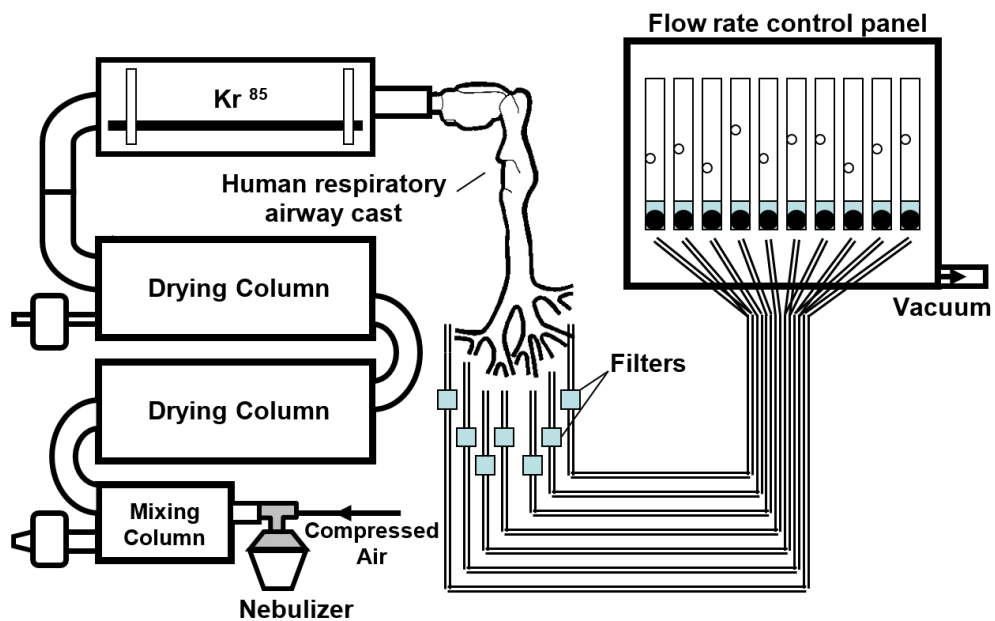


Figure 8.5.: Schematic diagram of the experimental setup for the fiber deposition study with a medication nebulizer.

nasal airway studies, and three flow rates (15, 43.5, and 60 lmin^{-1}) were used in the lung airway studies. These inspiratory flow rates ideally cover an adult breathing rate in different activities from at-rest to moderate work. Three

8. Deposition of synthetic fibers in human respiratory tract

experiments were carried out for each combination of inspiratory flow rate, fiber materials, and airway casts to obtain average deposition values. It is worth noting that in this research, the dimensions of the glottis openings in the respiratory airway casts (LA and LB) were modified based on the inspiratory flow rate conducting to virtually simulate the variation in the laryngeal airways under different respiratory flow rates. The modification of the glottis opening refers to the information reported in Martonen and Lowe [46].

8.4 Sample preparation, fiber counting and length measurement

After each run of the deposition experiments, the nasal airway cast or the lung airway cast was divided into regions/subregions based on the structure of the human nasal or lung airway. Care was taken when the airway cast was separated apart (nasal airway) or cut into segments (lung airway). Each divided section was flushed by alcohol jet or brushed several times with an artist's brush dipped in alcohol. The fiber-alcohol solution from individual airway sections was vacuum-filtered by a 25-mm filtration assembly to allow fibers to uniformly deposit on a 25-mm mixed cellulose ester membrane filter (GSWP, Millipore Co., Bedford, MA). The filters were then dried at room temperature in a dust-free environment and prepared as sample slides for later microscopic counting and measurement. In general, nine sample slides were acquired from each run of the nasal airway deposition experiment, and 22 to 26 sample slides were acquired from each run of the lung airway deposition experiment. Each sample slide represents the situation of fiber deposition in a specific region of the human airway.

The sample slides were then examined by an optical microscope (BH-2, Olympus Optical Co., Tokyo, Japan) with a G22 Walton-Beckett graticule (Pyser-SGI Ltd., Kent, UK). Figure 8.6 shows an example of deposited fibers in a microscopic viewing area (under 40x magnification). The number of fibers and the length of individual fibers in a viewing area were determined based on National Institute of Occupational Safety and Health (NIOSH) method 7400 (the fiber diameter was not measured in each sample slide due to the fact that the fiber materials used are assumed to be uniform). Each sample slide was counted/measured for 200 fibers or 200 viewing areas, depending on whichever came first. In this way, the averaged number of fiber in certain length categories in a specific human airway region could be obtained. When these deposited data are available for all regions of the airway cast, the deposition pattern for the entire airway cast as well as the deposition efficiency for a specific airway region could then be determined.

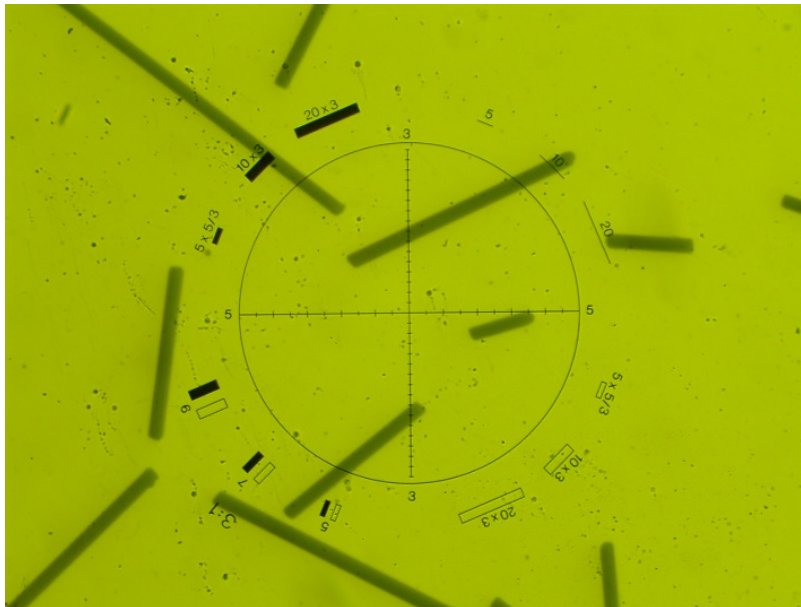


Figure 8.6.: Fiber counting and measurement with G22 Walton-Beckett graticule (under 40x magnification).

8.5 Results and discussion

8.5.1 Fiber deposition efficiency in the human nasal airway

Figure 8.7: Left shows the fiber deposition patterns as a function of fiber length. The subregions of the nasal airway are shown in Figure 8.7: Left. The deposition fraction for each subregion is an average value of three experiments. As shown in Figure 8.7: Left, the deposition pattern for an inspiratory flow rate of 7.5 lmin^{-1} indicates that most of the fibers passed through the nasal airway and were collected on the backup filter. The fiber deposition fraction in each nasal airway subregion was typically below 10% for every length category. Only one subregion, the inferior turbinate of the front turbinate, was slightly larger than 10% in the long fiber ($> 100 \mu\text{m}$) category (Figure 8.7: Left d). In addition, the number of fibers collected on the filter decreases as the fiber length increases, which implies that the longer the fiber, the harder it is for it to pass through the nasal airway.

8.7: Right shows the deposition pattern for a 15-lmin^{-1} inspiratory flow rate. A considerable percentage of fibers were deposited in the nasal airway. Most of the fibers were in the anterior region (vestibule and nasal valve) and some in the middle turbinate of the front turbinate. However, there were still a considerable percentage of short fibers found passing through the entire nasal airway (33%; 8.7: Right a). Similarly, as shown in 8.7: Left, the percentage of fibers passing through the nasal airway in 8.7: Right decreases as the fiber length increases. In the long fiber category ($> 100 \mu\text{m}$; 8.7: Right), only 11% of long fibers passed through the nasal airway and collected on the filter. In the turbinate region, very few fibers were found in the rear turbinate subregion and only a few fibers deposited in the front turbinate subregion, especially in the middle turbinate region. Almost no fibers were deposited in the posterior region (nasopharynx).

The deposition pattern for a 43.5-lmin^{-1} inspiratory flow rate is similar to that for an inspiratory flow rate of 30 lmin^{-1} , but relatively more long fibers (fibers $> 70 \mu\text{m}$) were found in the nasal valve and front turbinate subregions. Fibers were mainly deposited in the vestibule, nasal valve, and the front turbinate subregions. More than 99% of the fibers were deposited in these places for each fiber length category. Extremely few fibers ($< 0.5 \%$) passed the nasal airway and collected on the filter. Additional deposition data for other flow rates were reported elsewhere [47, 48].

Figure 8.8 shows the deposition efficiency as a function of the impaction parameter (fiber momentum) for man-made fibers in the nasal airway replica. The fiber deposition efficiency is determined by the fraction of the fiber entering the nasal airway that deposited within it. The d_{ae} used for calculating the impaction parameter $d_{ae}^2 Q$ is the fiber aerodynamic diameter in random orientation. As can be seen in Figure 8.8, the trend of the fiber deposition efficiency in the nasal airway is a smooth S-like shape. The lower end of the carbon fiber deposition efficiency is ideally connected to the higher end of the TiO_2 fiber deposition efficiency, which plainly shows the overall continuity between the data sets acquired. Figure 9 shows that the deposition efficiency of the carbon fiber increased proportionally with the impaction parameter. This result indicates that impaction is the main deposition mechanism for the carbon fiber used. The deposition efficiency of the carbon fiber can reach 1.0 when the impaction parameter is greater than $50000 \mu\text{m}^2 \text{ cm}^3 \text{ s}^{-1}$. To the contrary, there was no significant relationship found between the impaction parameter and the deposition efficiency for the TiO_2 and the glass fibers. The deposition efficiencies increased only slightly with an increase in the impaction parameter. In general, the impaction parameters of TiO_2 and glass fibers were both smaller than $6000 \mu\text{m}^2 \text{ cm}^3 \text{ s}^{-1}$, and partially overlapped. The deposition efficiencies of TiO_2 and glass fibers were shown to be similar, and were both less than 0.2.

The discrepancy of the deposition efficiencies between the three fiber materials shown in the Figure 8.8 might be due to the fact that the diameter and length of the carbon fiber are considerably large compared with those of TiO_2 and glass fibers. This large physical dimension gives carbon fibers a significant d_{ae} value and inertia. As a result, the impaction parameter (fiber momentum) as well as the associated deposition efficiency increases substantially when the fiber d_{ae} increased. As shown in Figure 8.8, most of the high-momentum fibers have a deposition efficiency of 1.0, which implies that high-momentum fibers do not pass through the nasal airway. Thus, the human nose appears to function well for filtering out large fibers such as carbon fibers and preventing them from entering the lower

8. Deposition of synthetic fibers in human respiratory tract

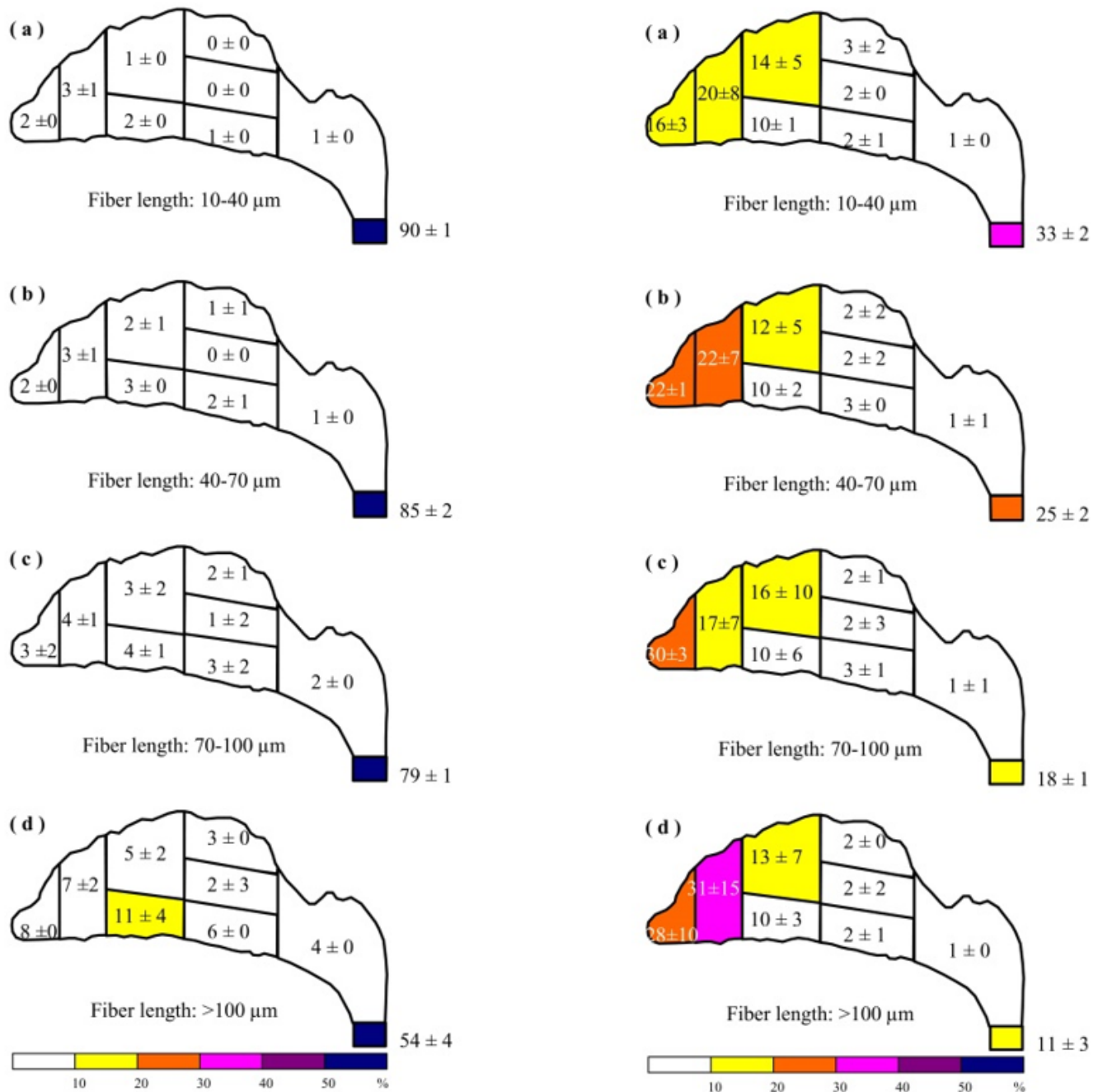


Figure 8.7.: Left: Deposition in the nasal airway for 7.5 l min⁻¹.; Right: Deposition in the nasal airway for 15 l min⁻¹.

respiratory tract.

On the other hand, the dimensions of the TiO₂ and the glass fibers are relatively small compared with the carbon fiber. Therefore, the fiber d_{ae} , the impaction parameter, and the associated fiber deposition efficiency are all consequently small. It is interesting to note that the diameters of the TiO₂ and the glass fibers are comparable, and the length distribution of the TiO₂ fiber is shorter than that of the glass fiber. However, the calculated d_{ae} and the related impaction parameters of the TiO₂ fibers are, in general, larger than those of the glass fibers. This result is due to the

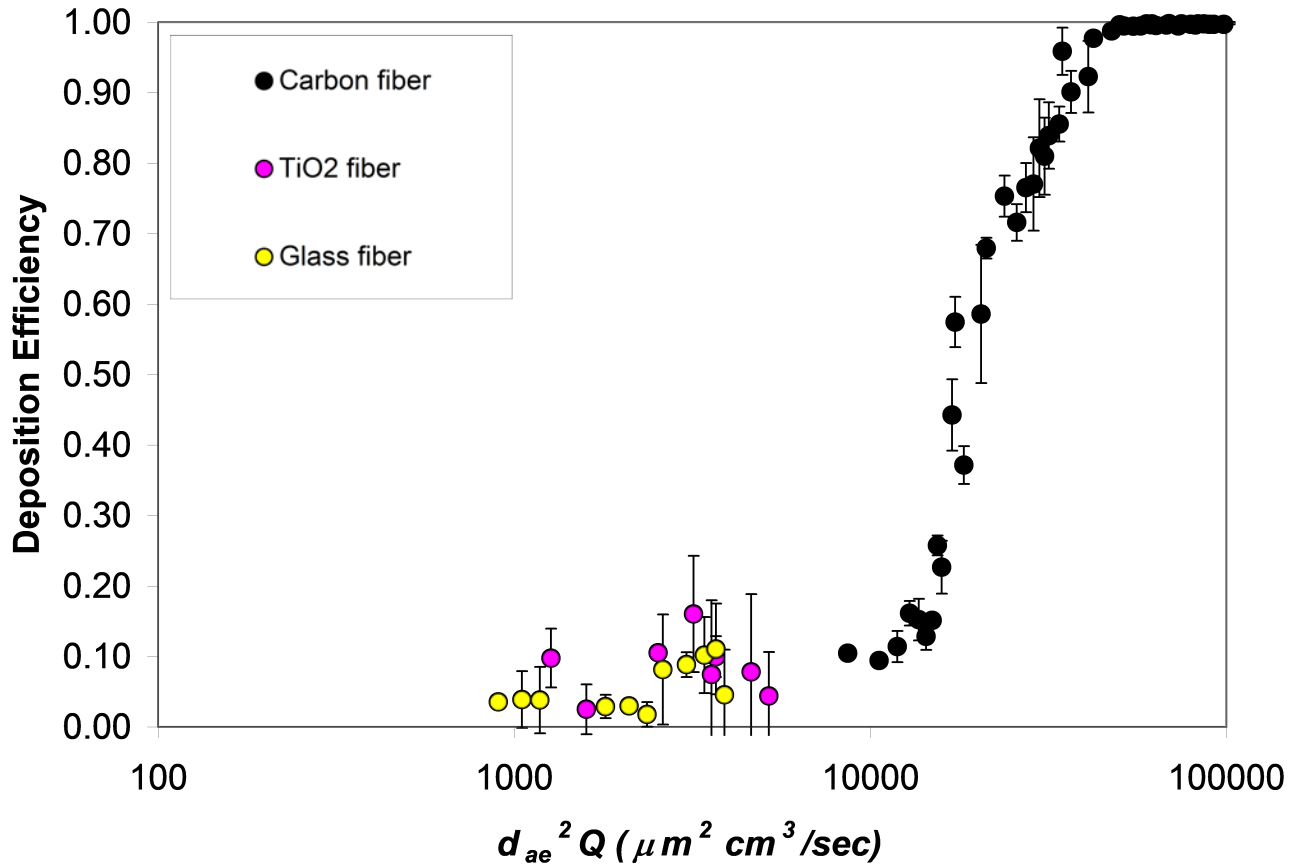


Figure 8.8.: Deposition efficiency as a function of the impaction parameter for different man-made fiber materials in the human nasal airway.

fact that the density of the TiO_2 fiber is greater than that of the glass fiber. Moreover, as mention before, the d_{ae} of a fiber depends primarily on its diameter and only slightly on its length [12, 15, 44]. Therefore, the TiO_2 fiber shows a relatively higher momentum in the nasal airway compared with the glass fiber, and the deposition efficiencies of the TiO_2 fiber agree well with those of the glass fiber where the values of the impaction parameters for these two fibers overlap. As shown in Figure 8.8, the deposition efficiencies of the TiO_2 and glass fibers all ranged from 0.02–0.2, which implies that small fibers have a high penetration rate (≥ 0.8) through the nasal airway. Therefore, small fibers may present a hazard to the human lower respiratory tract.

8.5.2 Comparison of nasal deposition between fibers and compact particles

Aerosol deposition experiments in the nasal airway have been conducted intensively with compact particles in the inertia regime [35, 37, 38, 49–51]. It has been shown that most of the experimental data acquired from those studies agree well with each other and the data are all located within a narrow band when the deposition efficiency is plotted against the impaction parameter. In this research, deposition experiments were also carried out with compact particles. The compact particles used had comparable aerodynamic diameters to carbon, TiO_2 and glass fibers in order to compare the coincident deposition efficiencies obtained from fibers. The test particles were fluorescent polymer microspheres (Duke Scientific Co., Palo Alto, CA) with sizes ranging from 2.1 to 10.0 μm ($d_{ae} = 2.2$ to 10.2 μm). Deposition experiments were conducted using a similar experimental method as for the fiber study, and the deposition

8. Deposition of synthetic fibers in human respiratory tract

result was acquired by measuring the florescence intensity in the washed-out solution for each nasal airway region. The deposition pattern and deposition efficiency of the compact particle were obtained with the same method as employed in the fiber study. Figure 8.9 shows the deposition efficiency and corresponding deposition patterns for fibers and compact particles in the nasal airway. As can be seen, for fibers and compact particles with a large impaction parameter ($\geq 15000 \mu\text{m}^2 \text{cm}^3 \text{s}^{-1}$), the deposition efficiencies are at least 0.5 and above, and the fiber deposition efficiencies are smaller than the compact particle deposition efficiencies. In this impaction parameter regime, the anterior region is the site of common deposition.

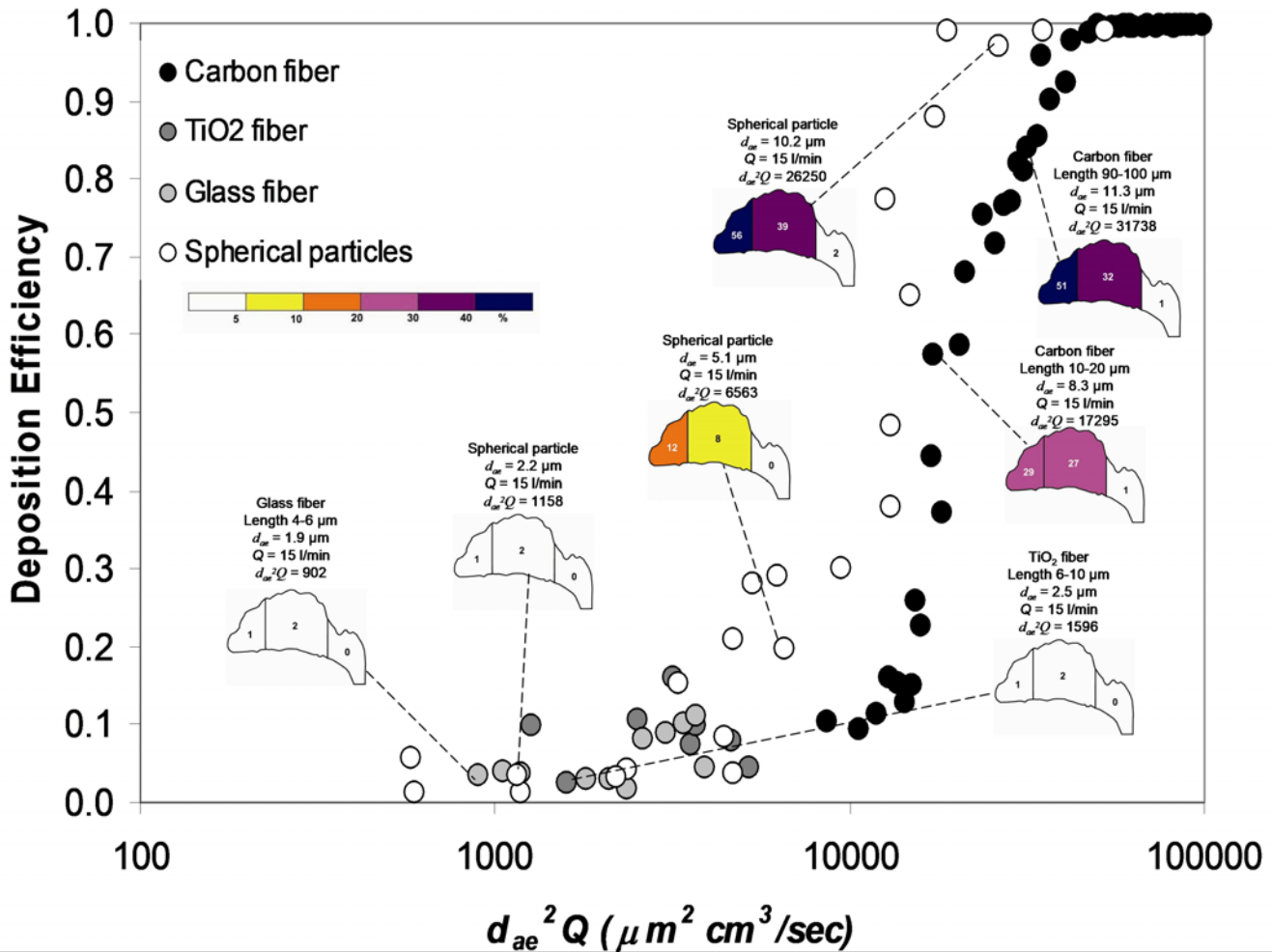


Figure 8.9.: Comparison of the deposition efficiencies and related deposition patterns between fibers and spherical particles.

On the other hand, for those TiO₂ fibers, glass fibers, and compact particles with a small impaction parameter ($\leq 5000 \mu\text{m}^2 \text{cm}^3 \text{s}^{-1}$), the deposition efficiencies are generally small in the nasal airway (less than 0.2), and relatively higher deposition was found in the turbinate region. However, in this small impaction parameter regime, no significant difference was found regarding the deposition efficiency between the fiber aerosol and the compact particles. The fiber deposition efficiencies were shown to be fairly close to those of compact particles. These results shown above imply that, in the inertia regime, fibers with low momentum would have similar deposition behavior as compact particles having comparable aerodynamic diameters in the human nasal airway, while fibers with high momentum would behave differently from compact particles having an equal aerodynamic diameter. The main cause that could account for this difference could be the fiber orientation in the inhaled air flow. As has been reported in some theoretical

calculations [52–54] and experimental observation [16], fibers tend to align themselves to the flow direction when they fly through the air. With fibers oriented parallel to the air streamline, it could reduce the deposition of fiber in the human airway to a certain extent. The deposition efficiency of fiber is therefore less than that of compact particles in the nasal airway. This might provide an explanation for the difference of the deposition efficiencies found between fibers and compact particles. More recently, a numerical simulation of fiber and spherical particle deposition in the human nasal airway using the nasal geometry of this study was published [55]. In the simulation, fiber moved with the main axis parallel to the flow. Theoretical calculations showed that fiber deposition efficiency was lower than that of spherical particles at the same impaction parameter.

8.5.3 Fiber Deposition in the Human Oral Airway

Figures 8.10-8.12 show the fiber deposition patterns for three inspiratory flow rates as a function of fiber length [56]. The deposition fraction for each region is an average value of three experiments. For a low inspiratory flow rate of 15 lmin^{-1} (Figure 8.10), the deposition pattern indicates that most fibers (at least 63%) passed through the entire human airway replica. The penetration decreased as the fiber length increased. Fiber depositions in each region of the replica were all below 10%, and the typical deposition fraction in the bronchial airways was below 2%. Overall, the oral cavity, larynx, and trachea had relatively higher deposition fractions compared to other regions. Long fibers were shown to have a higher deposition fraction than short fibers for any specific region in the human airway.

Figure 8.11 shows the deposition pattern for a 43.5-lmin^{-1} inspiratory flow rate. A considerable percentage of fibers were deposited in the human airway at this inspiratory flow rate. Most of the deposition was at the oropharynx to larynx area and some were at the first bifurcation. Approximately 30% of the short fibers still passed through the replica, but only 15% of the long fibers were able to penetrate through the replica. The deposition fraction for a specific region basically increased as the fiber length increased, which is similar to Figure 8.10. It is worth noting that the deposition fraction in the oropharynx gradually became significant.

The deposition pattern for a 60-lmin^{-1} inspiratory flow rate is shown in Figure 8.12, similar to that of the 43.5-lmin^{-1} inspiratory flow rate (Figure 8.11). The majority of the fibers were deposited at the area of oropharynx to larynx. The total deposition fraction in this area was around 40% to $\sim 50\%$ for different length categories. However, in contrast to Figures 8.10 and 8.11, the deposition “hot spot” in Figure 8.12 shifted from the larynx to the oropharynx. In addition, the fiber deposition in the trachea decreased slightly, which is believed due to the dimensional change of the glottis opening at this inspiratory flow rate. For long fibers ($> 100 \mu\text{m}$), the total deposition in the human airway was about 90%, which implies that long fibers had more difficulty passing through the entire replica at a high inspiratory flow rate.

The oral airway is the major air entry for some workers because of the need for a large respiratory flow rate while performing moderate-to-heavy work. However, aerosol collection in the human oral airway is less efficient compared with that in the nasal airway due to the smaller inhalation air velocity caused by the larger dimension of the oral airway. Therefore, when breathing by mouth, a considerable portion of the inhaled fibers are able to penetrate the oral airway and then enter the tracheobronchial airways. The fiber deposition efficiency found in the oral airway can be used as an index of the oral penetration rate of interest which can then indicate the amount of fibers that enters the lower respiratory airway. Figure 8.13 shows the fiber deposition efficiency as a function of the impaction parameter $d_{ae}^2 Q$ (d_{ae} is the fiber aerodynamic diameter calculated by parallel orientation, and Q is the inspiratory flow rate) in the oral airways for the two casts.

The oral airway here was defined as the regions from the oral cavity to the larynx in the airway casts. The fiber deposition efficiency in the oral airway was determined by the fraction of the fiber entering the oral airway that deposited within it. Also shown in Figure 8.13 are the deposition data of compact particles from our previous work for cast A [37] together with the new results from this study for cast B. Fluorescent polymer microspheres (Duke Scientific Co., Palo Alto, CA) with an aerodynamic diameter from 0.5 to $16.4 \mu\text{m}$ were used as the test particles. The deposition studies of the compact particles were carried out using the same experimental method as described in

8. Deposition of synthetic fibers in human respiratory tract

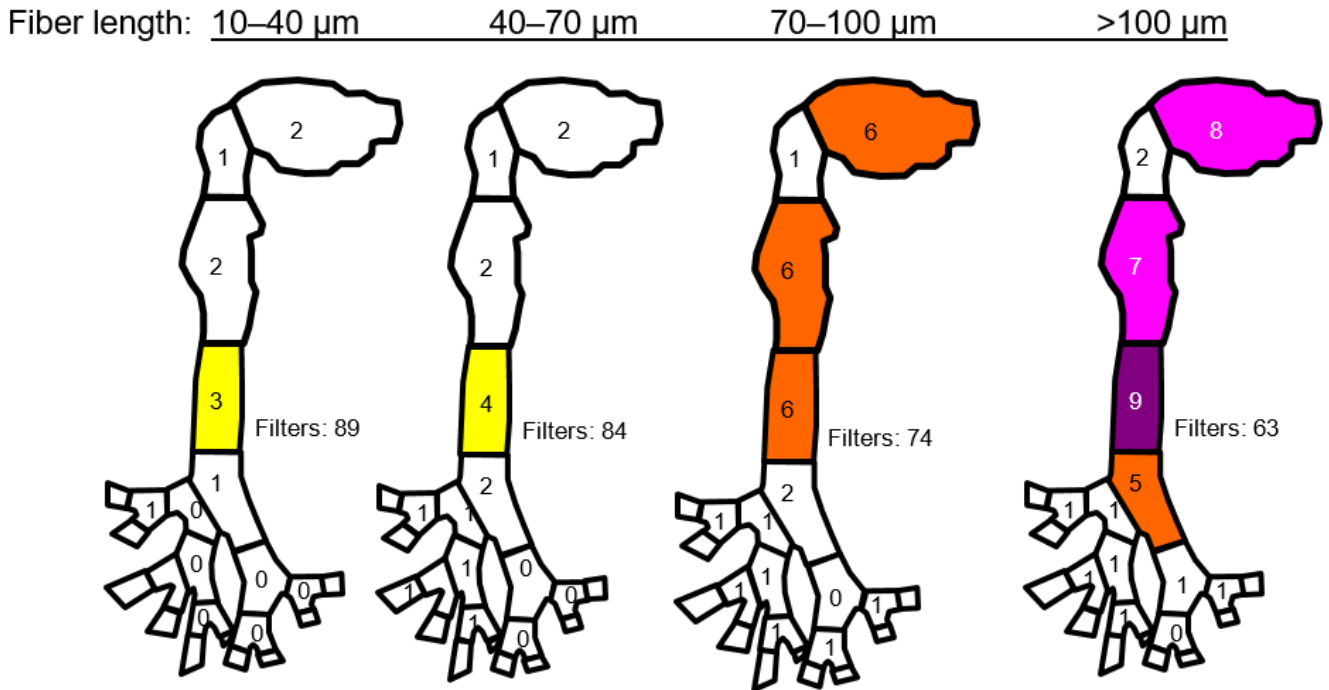


Figure 8.10.: Fiber deposition pattern in the oral airway for an inspiratory flow rate of 15 l min⁻¹.

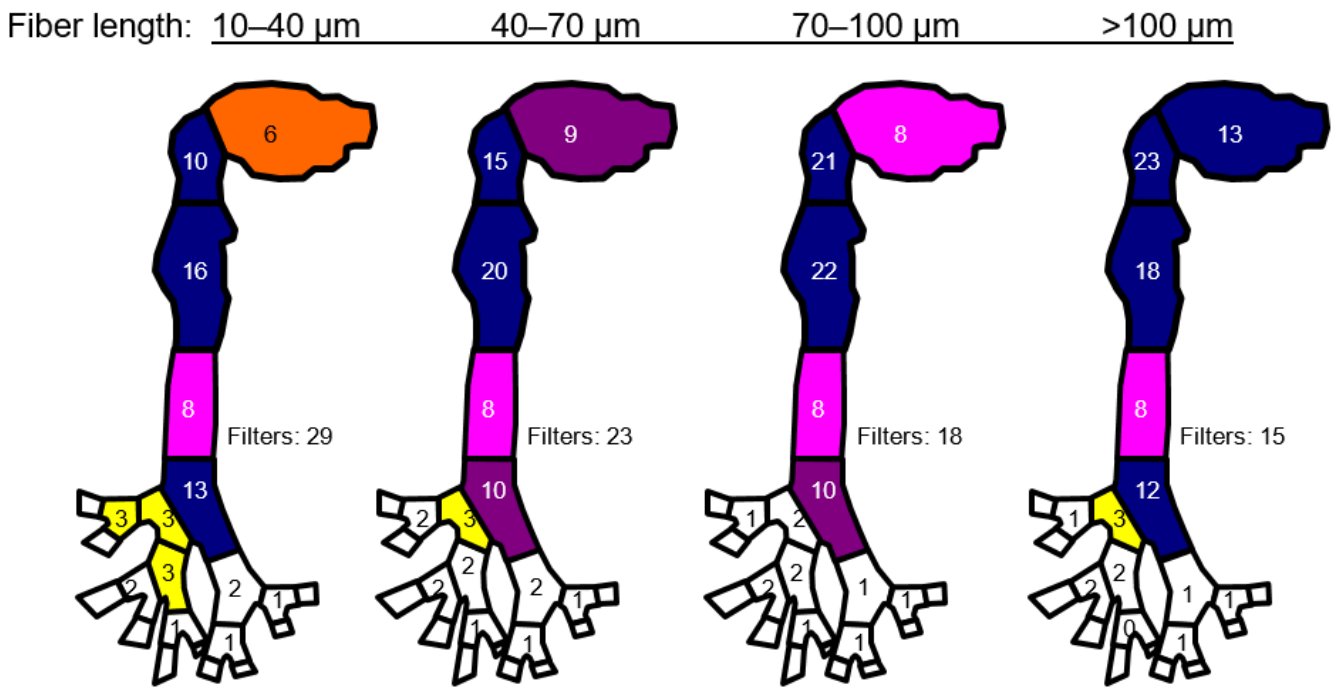


Figure 8.11.: Fiber deposition pattern in the oral airway for an inspiratory flow rate of 43.5 l min⁻¹.

the nasal airway deposition study. The particle deposition in the airway was acquired by measuring the fluorescence intensity in the washed-out solution of the oral airway.

As can be seen in Figure 8.13, the magnitudes and the configurations of the fiber deposition efficiencies in the

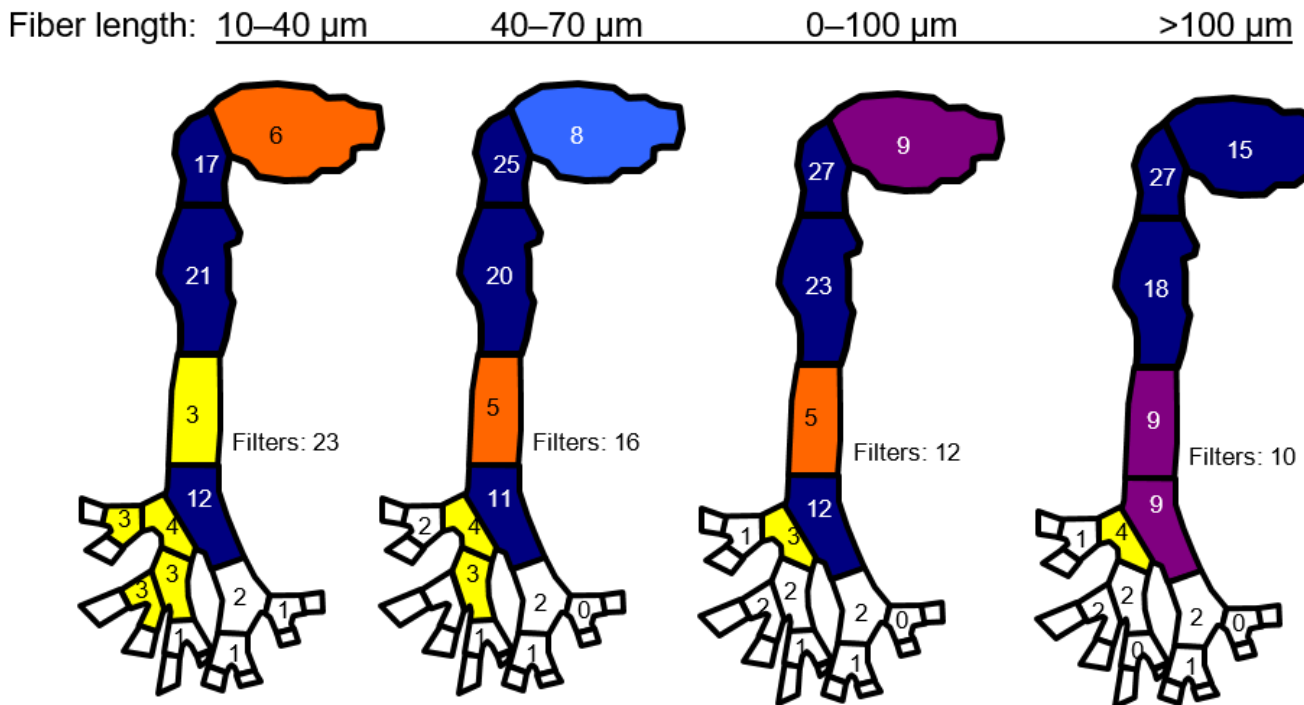


Figure 8.12.: Fiber deposition pattern in the oral airway for an inspiratory flow rate of 60 l min^{-1} .

oral airways were comparable in both casts, which indicates that the intersubject variability was insignificant in this study. For TiO_2 and glass fibers, there was no significant relationship shown between the impaction parameter and the deposition efficiency. The deposition efficiencies increased very slightly as the impaction parameter increased. The magnitudes of the deposition efficiencies were all similar and less than 0.1. This result indicates that thin man-made fibers could have a high penetration rate (≥ 0.9) in the human oral airway. In contrast, the deposition efficiency for carbon fiber increased proportionally with the impaction parameter and reached 0.6. This result implies that impaction is the major deposition mechanism in the oral airway for thick man-made fibers, and fibers with large momentum would have difficulty penetrating the oral airway. In general, Figure 8.13 reveals an overall continuous match between data obtained from different fiber materials in both airway casts, and a relationship between the deposition efficiency and the impaction parameter is clearly shown.

Figure 8.13 also shows that the deposition efficiencies of compact particles are comparable in the two casts in terms of magnitude and configuration, which is similar to the results found in the fiber deposition studies for insignificant intersubject variability. Cheng, Zhou, and Chen [37] suggested an empirical model for the deposition of compact particles in the oral airway based on the available *in vivo* data. The predicted values using the suggested model are also shown in Figure 8.13. It was interesting to note that the empirical model suggested by Cheng, Zhou, and Chen [37] agreed quite well with the experimental data acquired in this study for both airway casts. This result validated the practicability of this empirical model. When comparing the deposition efficiency of compact particles with that of fibers in both airway casts, the data showed that the deposition efficiencies of compact particles were generally higher than those of fibers. As was discussed above, this result is presumed to be attributed to the fiber alignment in the inhaled airflow. Here, this deposition phenomenon was shown again, which supported the fact that fibers tend to fly parallel to the air stream in the human respiratory airway. With prevailing parallel orientation for fibers flying in the human airway, it could be assumed that “interception” therefore, is not a critical deposition mechanism for fiber deposition in the oral airway (oral cavity, pharynx and larynx). The major deposition mechanism in the oral airway is still thought to be impaction solely. The interception would be an important deposition mechanism when

8. Deposition of synthetic fibers in human respiratory tract

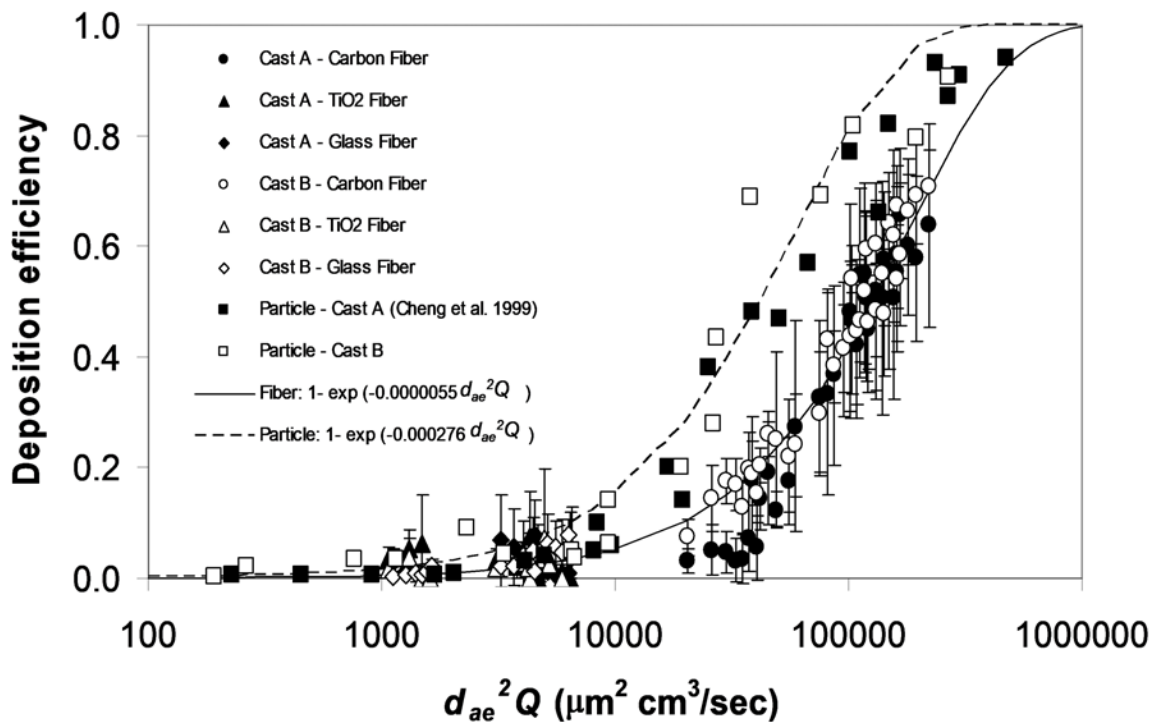


Figure 8.13.: Deposition efficiency as a function of the impact parameter for fibers and compact particles in the human oral airway.

the dimension of the airway has a similar scale as the fiber length (e.g., in the lower tracheobronchial airways).

8.5.4 Fiber deposition in the tracheobronchial airways

Figure 8.14 shows deposition efficiency of spheres and fibers in the first generation of airway in the upper TB region, plotted as a function of Stokes number, which is a dimensionless impact parameter, ($Stk = \frac{\rho d_{ev}^2 U}{18\mu d}$), where d_{ev} is the volume equivalent diameter of the fiber, U and d are the mean velocity and diameter of the parent airway, respectively, as defined by Zhang, Asgharian, and Anjilvel [57]. Despite differences in the airway structure, fiber depositions in each airway generations were similar for Cast A and B [58]. Similar to deposition in the human nasal/oral airways, we also show that deposition efficiencies of spherical particles are higher than those of fibers for the same impact parameter.

Figure 8.15 plots fibers deposition data in the third generation of bronchial airways showing good agreements with deposition data of asbestos fibers in the same airway generation in a different human airway cast [18]. Detailed comparison of fiber deposition in individual airway generation was reported previously [58]. We also compared experimental data with theoretical deposition equations derived based on a single bifurcation [59]. The best agreement was obtained with numerical calculations of fiber trajectory showing rotation of the fiber resulting in alignment of the fiber with the flow [57] (Figure 8.16).

Figure 8.17 shows comparisons with our experimental data and numerical simulation [57], which can be expressed

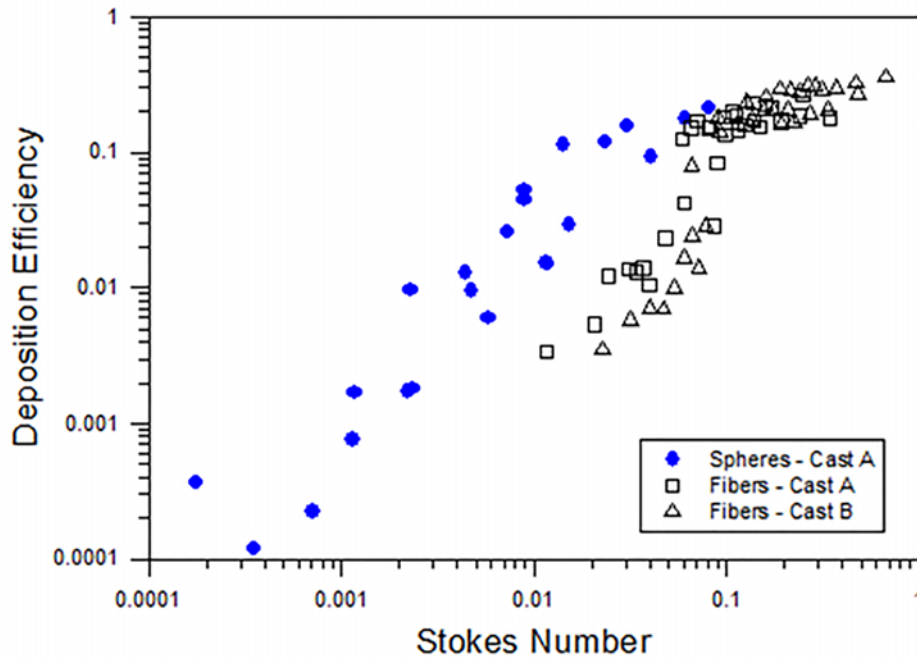


Figure 8.14.: Deposition efficiencies of fiber and spherical particles in the first generation.

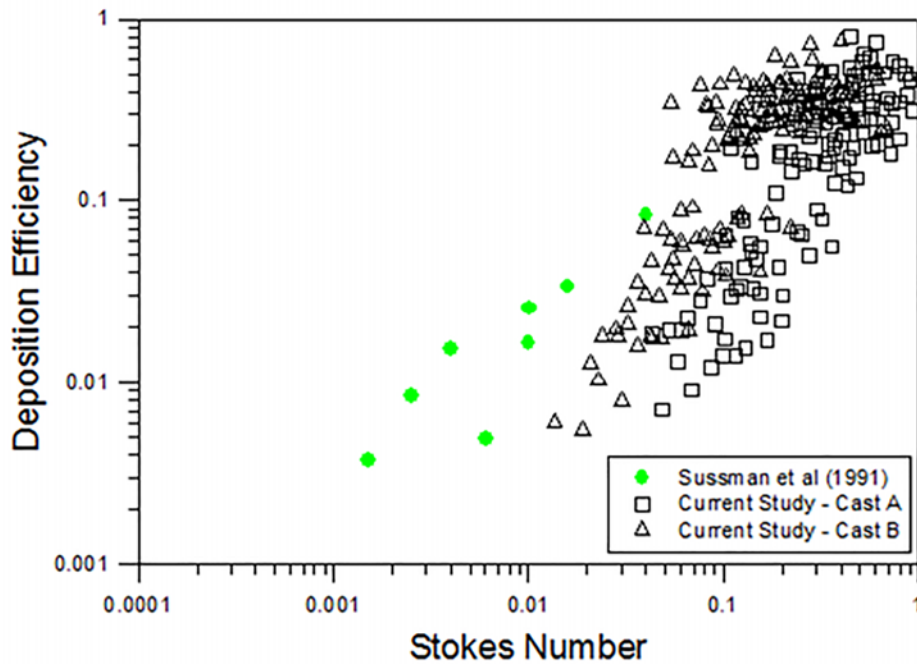


Figure 8.15.: Comparison of fiber deposition in the third generation with deposition of asbestos fibers [18].

as:

8. Deposition of synthetic fibers in human respiratory tract

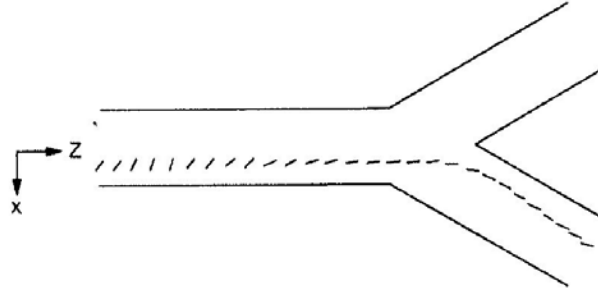


Figure 8.16.: Movement of a fiber in an airway bifurcation, showing rotation of the fiber resulting in alignment of the fiber with the flow [57].

$$DE = 0.0008e^{14.49\text{Stk}^{0.77}} \text{Re}^{\frac{1}{3} \sin \theta} \quad \text{for } \text{Stk} < 0.08 \quad (8.5)$$

$$DE = 0.1753 - 0.1769e^{-5.547\text{Stk}^{1.90}} \text{Re}^{\frac{1}{3} \sin \theta} \quad \text{for } \text{Stk} \geq 0.08 \quad (8.6)$$

where θ is the bifurcation angle. Experimental data including asbestos [18] show large variability but generally agree with the numerical simulation results. One of the contributing factors of this large variability of deposition efficiency in the TB airway is that the airway geometry is not symmetrical, which leads to uneven flow and aerosol distribution in the daughter airway as shown.

8.5.5 Empirical model for fiber deposition in the nasal airway

Based on all the fiber deposition data shown above, an attempt was made to find an empirical model for the practical estimation of the fiber deposition efficiency in the human nasal airway. As stated in Kelly, Asgharian, Kimbell, and Wong [51], nasal deposition can be expressed by the following expression:

$$DE = 1 - e^{-(ad_{ac}^2 Q)^b} \quad (8.7)$$

where a and b are constants to be determined from curve fitting process. In this research, Equation 8.1 was adopted for searching the best-fit equations for fiber and available compact particle data. A nonlinear fitting procedure in SigmaPlot (SPSS Inc., Chicago, IL) was used as the fitting tool. Recent published compact particle data from Kelly, Asgharian, Kimbell, and Wong [51], and from the current study were used in the fitting process. It is worth noting that the nasal airway cast used in Kelly, Asgharian, Kimbell, and Wong [51] was made from the same MRI scans. The best-fit curve obtained for the fiber deposition efficiency is $a = 4.262 \times 10^{-5}$, $b = 2.46$ with $R^2 = 0.98$. The best-fit curve found for compact particle is $a = 6.426 \times 10^{-5}$, $b = 1.89$, and $R^2 = 0.90$. Figure 8.18 shows the best-fit curves for the deposition of fiber and compact particles in the nasal airway plotted along with the related experimental data. It is clearly shown that, given the same impaction parameter, fibers deposit less in the human nasal airway compared with the compact particles. Therefore, it implies that compared with general particles in the ambient air, relatively more fibers could penetrate into the human lower respiratory tract, causing adverse health effects.

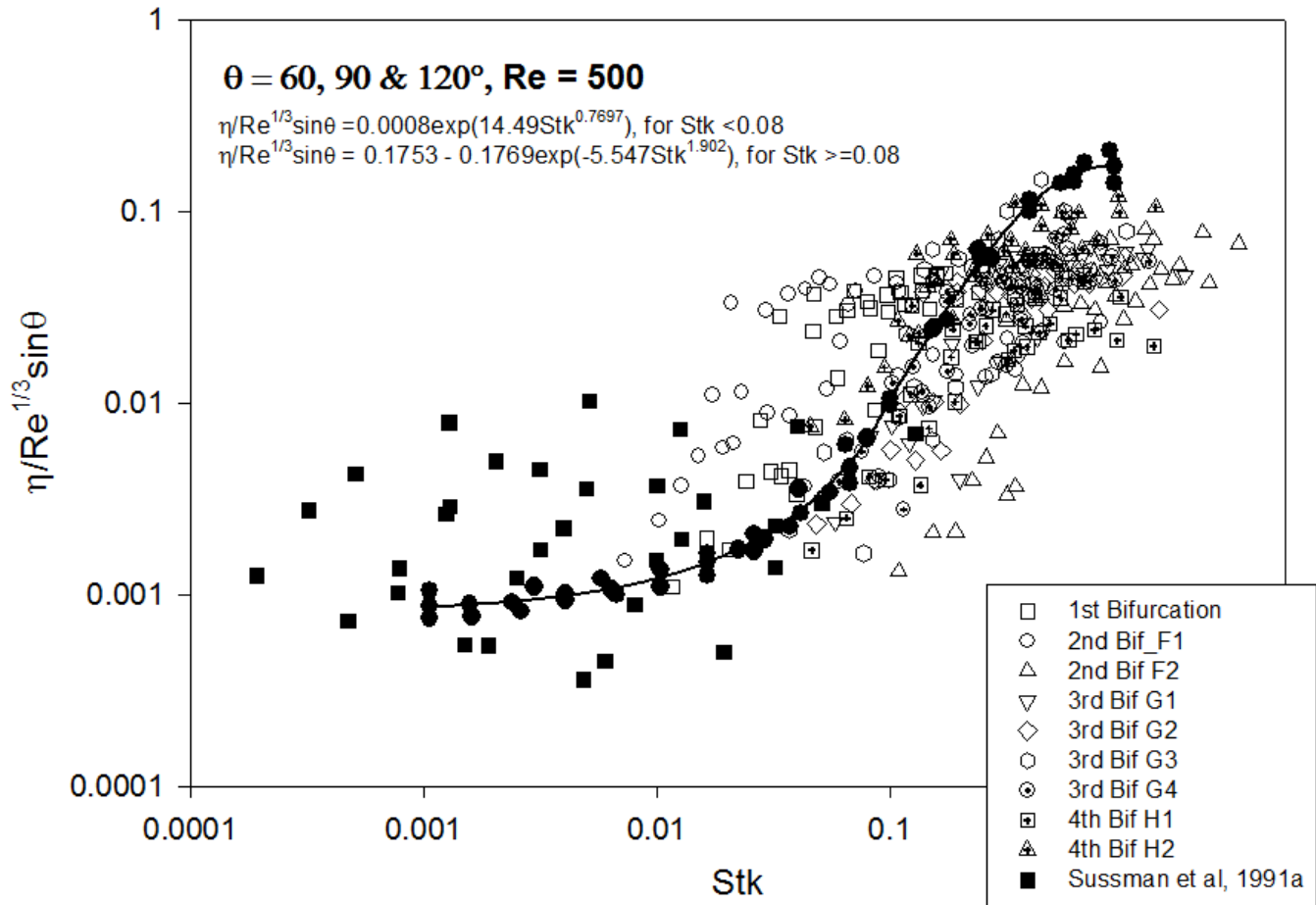


Figure 8.17.: Comparison of fiber deposition data in bronchial airways with numerical simulation in a simple bifurcation [57].

8.5.6 Empirical model for fiber deposition in the oral airway

An empirical model is proposed for fiber deposition in the oral airway based on the equation format suggested by Cheng, Zhou, and Chen [37].

$$DE_{oral} = 1 - e^{-(ad_{ae}^2 Q)} \quad (8.8)$$

where DE_{oral} is the fiber deposition efficiency in the oral airway, a is a constant needed to be determined, and $d_{ae}^2 Q$ is the fiber impaction parameter. The nonlinear regression program used in finding the nasal airway empirical model was employed again as the fitting tool. All fiber data shown in Figure 8.13 were used in the fitting process. The best-fitted parameter was $a = 5.47 \times 10^{-6}$ with $R^2 = 0.96$, and the result was plotted beside the experimental data in Figure 8.13. As can be seen, this proposed empirical model can fairly well predict the fiber deposition efficiency in the oral airway, and is believed to be useful in any given fiber exposure scenario (within similar experimental conditions) for estimating the fiber deposition in the human oral airway.

8. Deposition of synthetic fibers in human respiratory tract

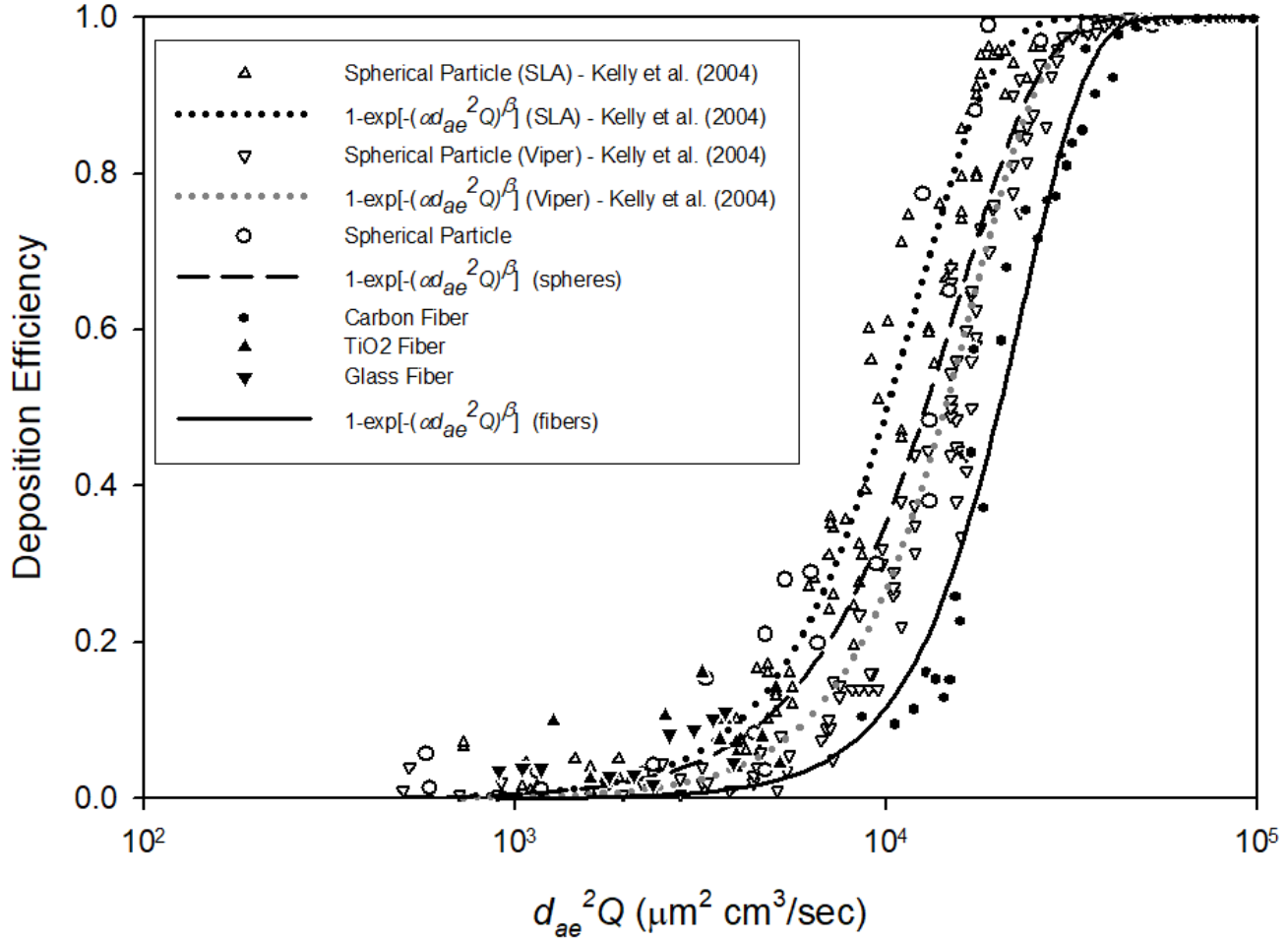


Figure 8.18.: The best-fit equations of the nasal deposition for fibers and spherical particles.

8.5.7 Empirical model for fiber deposition in the tracheobronchial airway

In order to predict the fiber deposition in human lungs, an empirical model was developed. The derivation of this empirical equation followed the approach we used for deposition of spherical particles [39]. The basic equation was considered as the same as described in Zhou and Cheng [39],

$$\eta = 1 - e^{-aStk^b} \quad (8.9)$$

where a and b are constant numbers for each individual bifurcation or trachea, the Stokes number Stk here is defined based on the volume equivalent diameter, diameter of parent tube, and velocity in the parent tube [57].

The experimental data in each bifurcation of cast A and B, which were obtained in our previous study [58], were used to obtain the fitted Equation 8.9. The result for the constant values of a and b is listed in Table 8.2. We treated b as a constant value as we did for spherical particles [39]. We found that the average value of b (1.34 ± 0.19) is exactly the same as we obtained for spherical particles although the standard deviation was relatively large. For value a , we plotted data of F as a function of a as we did for the spherical particle study [39]. F is a function of bifurcation angle

Table 8.2.: Constant values of a and b obtained by Equation 8.5 and 8.6 for each bifurcation.

	Bifurcation#*	F	a	b
Cast A	1_E	0.75	3.51	1.515
	2_F1	1.33	1.43	1.525
	2_F2	0.51	0.19	1.504
	3_G1	0.97	0.91	1.201
	3_G2	0.49	0.41	1.177
	3_G3	0.69	1.01	1.234
	3_G4	0.93	1.05	1.263
	4_H1	1.03	0.79	1.261
4_H2	1.09	2.41	1.222	
Cast B	1_E	0.72	2.45	1.605
	2_F1	0.93	2.27	1.53
	2_F2	0.80	1.00	1.036
	3_G1	1.30	11.44	1.719
	3_G2	0.79	1.51	1.191
	3_G3	1.03	2.53	1.256
	3_G4	1.43	2.13	1.26

* Details of the bifurcation number were described in Zhou, Su, and Cheng [58].

and ratio of parent to daughter radii [60]:

$$F = \frac{4 \sin \theta}{\pi \frac{R}{R_0}} \quad (8.10)$$

An equation of $a = 1.70F$ was obtained even though the linear relation was not as good as spherical particles. Thus, the empirical fiber deposition model for the different bifurcations is expressed as:

$$\eta = 1 - e^{-1.70F \text{Stk}^{1.34}} \quad (8.11)$$

8.5.8 Fiber exposure index

The thoracic fraction of particulate matter is defined by the American Council for Governmental Hygienists (ACGIH) as the particulate fraction that by virtue of aerodynamic size and behavioral properties is expected to penetrate the head airway and enter the lung airways during mouth breathing [33]. This thoracic fraction represents the worst-case potential exposure of the whole lung to particles. The definition of thoracic fraction is used as an index of exposure for particles that may have adverse effects in large and small airways in the lung [33]. Because the known adverse health effects of inhaled fibers are in the TB, alveolar, and parenchymal regions of the lung, a thoracic fraction will be used as the index of exposure. Similar to the thoracic fraction curve for spherical particles, experimental deposition data of fibers in the oral airways obtained at the flow rate of 43.5 l min^{-1} are used to develop the size-selective criteria. Figure 8.19 shows that fiber penetration through oral airways plotted as a function of aerodynamic diameter. Our data show that penetration of fibers is higher than those of spheres in human oral airways, because large fibers tend to align

8. Deposition of synthetic fibers in human respiratory tract

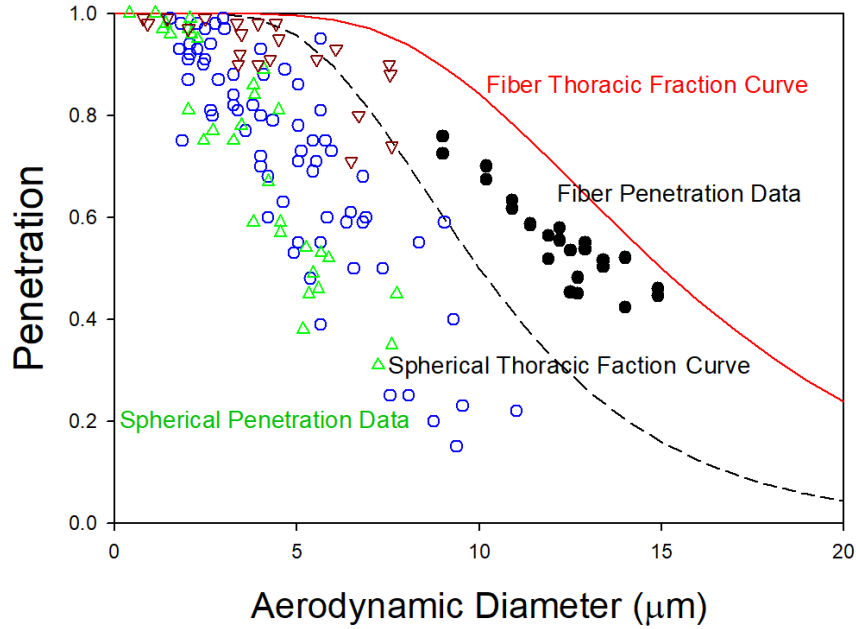


Figure 8.19.: Fiber penetration data for thoracic fraction curve.

with air flow as shown in Figure 8.16. Following the same procedure for spherical particles, we define a thoracic fraction for fiber (ST) as:

$$ST = 1 - F(x) \quad (8.12)$$

where $F(x) = \int_{-\infty}^x \frac{dy}{\sqrt{2\pi}} e^{-\frac{y^2}{2}}$, is a function of fiber aerodynamic diameter d_{ae} ; $y = \frac{\ln\left(\frac{d_{ae}}{d_{ae(50\%)}}\right)}{\ln \sigma_g}$, $d_{ae(50\%)} = 15 \mu\text{m}$; and $\sigma_g = 1.5$. The thoracic curve is to the right of experimental values to provide a conservative measure, because some individuals will have penetration values greater than the experimental data obtained here due to variability of airway geometry (ACGIH, 1985).

The proposed thoracic fraction is different from that of spherical particles in two aspects. First, the 50% aerodynamic diameter of the curve, $15 \mu\text{m}$, is larger than $10 \mu\text{m}$ for spherical particles. Second, the thoracic fraction of fiber is based on fiber count or number, whereas the thoracic fraction for spherical particles is based on mass. These differences will be reflected in air samplers designed to collect thoracic fraction of fibers and methods to analyze samples.

8.6 Conclusions

Fibers with diameter greater than $0.5 \mu\text{m}$ deposit in the nasal, oral, and tracheobronchial airways; the deposition efficiency increases with flow rate and square of aerodynamic diameter, indicating that impaction is the main deposition mechanism. Deposition efficiency of fiber aerosols in the nasal, oral, and tracheobronchial airways is lower than deposition efficiency of spherical particles of the same aerodynamic diameter. Penetration of fiber aerosol through the nasal, oral, and upper tracheobronchial regions is higher than spherical particles of the same aerodynamic diameter, indicating that even long fibers could penetrate to the lower portion of the lung. Comparison of experimental deposition data in tracheobronchial airways and theoretical models of fibers showed that a numerical calculation based on computational fluid dynamics [57] is in good agreement. The numerical simulation in the simple bifurcation

showed that rotation of a fiber cause the fiber to align with the flow stream, resulting in less deposition. Empirical deposition equations for nasal and oral airways were developed for lung dosimetry models. An empirical deposition equation in the tracheobronchial region was developed taking into account the bifurcation angle and diameter ratio of parent and daughter tubes. Finally, a thoracic fraction is defined based on penetration of fibers through the oral airways. The proposed fiber thoracic fraction is different from that of spherical particles in two aspects. First, the 50% aerodynamic diameter of the curve, 15 μm , is larger than 10 μm for spherical particles. Second, the thoracic fraction of fiber is based on fiber count or number, whereas the thoracic fraction for spherical particles is based on mass.

Acknowledgment

This research was sponsored by US NIOSH grant R01 OH003900.

References

- [1] P. Bogovski, V. Tmbrela, J. Gilson, J. Wagner, et al. “Biological effects of asbestos. Proceedings of a Working Conference held at the International Agency for Research on Cancer. Lyon. France, 2-6 October 1972”. In: *Biological effects of asbestos. Proceedings of a Working Conference held at the International Agency for Research on Cancer. Lyon. France, 2-6 October 1972*. International Agency for Research on Cancer. 1973 (cited on page 81).
- [2] I. J. Selikoff, D. H. K. Lee, et al. *Asbestos and disease*. Academic Press, Inc. 111 Fifth Avenue, New York, New York 10003, USA, 1978 (cited on page 81).
- [3] I. Baris, M. Artvinli, R. Saracci, L. Simonato, F. Pooley, J. Skidmore, and C. Wagner. “Epidemiological and environmental evidence of the health effects of exposure to erionite fibres: A four-year study in the cappadocian region of turkey”. In: *International Journal of Cancer* 39.1 (1987), pages 10–17 (cited on page 82).
- [4] B. G. Miller, A. Searl, J. M. Davis, K. Donaldson, R. T. Cullen, R. E. Bolton, D. Buchanan, and C. A. Soutar. “Influence of fibre length, dissolution and biopersistence on the production of mesothelioma in the rat peritoneal cavity”. In: *Annals of Occupational Hygiene* 43.3 (1999), pages 155–166 (cited on page 82).
- [5] T. W. Hesterberg and G. A. Hart. “Synthetic vitreous fibers: a review of toxicology research and its impact on hazard classification”. In: *Critical reviews in toxicology* 31.1 (2001), pages 1–53 (cited on page 82).
- [6] IARC Working Group on the Evaluation of Carcinogenic Risks to Humans and International Agency for Research on Cancer and World Health Organization. *Man-made vitreous fibres*. 81. World Health Organization, 2002 (cited on page 82).
- [7] O. Kamstrup, A. Ellehauge, C. Collier, and J. Davis. “Carcinogenicity studies after intraperitoneal injection of two types of stone wool fibres in rats”. In: *Annals of occupational hygiene* 46.2 (2002), pages 135–142 (cited on page 82).
- [8] M. Lippmann. “Toxicological and epidemiological studies on effects of airborne fibers: coherence and public health implications”. In: *Critical reviews in toxicology* 44.8 (2014), pages 643–695 (cited on page 82).
- [9] M. F. Stanton and C. Wrench. “Mechanisms of mesothelioma induction with asbestos and fibrous glass”. In: *Journal of the National Cancer Institute* 48.3 (1972), pages 797–821 (cited on page 82).
- [10] V. Timbrell. “Physical factors as etiological mechanisms”. In: *Biological effects of asbestos* (1973), pages 295–303 (cited on page 82).
- [11] W. Stöber, H. Flachsbart, and D. Hochrainer. “The aerodynamic diameter of latex aggregates and asbestos fibres”. In: *Staub-Reinhalt Luft* 30.1 (1970) (cited on pages 82, 84).
- [12] Y.-S. Cheng, Q. H. Powell, S. M. Smith, and N. F. Johnson. “Silicon carbide whiskers: Characterization and aerodynamic behaviors”. In: *American Industrial Hygiene Association Journal* 56.10 (1995), pages 970–978 (cited on pages 82, 84, 93).
- [13] M. Lippmann. “Asbestos exposure indices”. In: *Environmental research* 46.1 (1988), pages 86–106 (cited on page 82).
- [14] F. Pooley and N. Clark. “A comparison of fibre dimensions in chrysotile, crocidolite and amosite particles from samples of airborne dust and from post-mortem lung tissue specimens.” In: *IARC scientific publications* 30 (1980), pages 79–86 (cited on page 82).
- [15] V. Timbrell. “Deposition and retention of fibres in the human lung”. In: *Inhaled Particles V*. Elsevier, 1982, pages 347–369 (cited on pages 82, 86, 93).

- [16] T. Myojo. "Deposition of fibrous aerosol in model bifurcating tubes". In: *Journal of Aerosol Science* 18.3 (1987), pages 337–347 (cited on pages 82, 95).
- [17] T. Myojo. "The effect of length and diameter on the deposition of fibrous aerosol in a model lung bifurcation". In: *Journal of aerosol science* 21.5 (1990), pages 651–659 (cited on page 82).
- [18] R. G. Sussman, B. S. Cohen, and M. Lippmann. "Asbestos fiber deposition in a human tracheobronchial cast. I. Experimental". In: *Inhalation toxicology* 3.2 (1991), pages 145–160 (cited on pages 82, 98–100).
- [19] R. G. Sussman, B. S. Cohen, and M. Lippmann. "Asbestos fiber deposition in a human tracheobronchial cast. II. Empirical model". In: *Inhalation toxicology* 3.2 (1991), pages 161–179 (cited on page 82).
- [20] J. Beeckmans. "The deposition of asbestos particles in the human respiratory tract". In: *International Journal of Environmental Studies* 1.1-4 (1970), pages 31–34 (cited on page 82).
- [21] E. R. Weibel, A. F. Cournand, and D. W. Richards. *Morphometry of the human lung*. Volume 1. Springer, 1963 (cited on page 82).
- [22] J. Beeckmans. "The deposition of aerosols in the respiratory tract: I. Mathematical analysis and comparison with experimental data". In: *Canadian journal of physiology and pharmacology* 43.1 (1965), pages 157–172 (cited on page 82).
- [23] R. L. Harris and D. A. Fraser. "A model for deposition of fibers in the human respiratory system". In: *American Industrial Hygiene Association Journal* 37.2 (1976), pages 73–89 (cited on page 82).
- [24] B. Asgharian and C. Yu. "Deposition of inhaled fibrous particles in the human lung". In: *Journal of aerosol medicine* 1.1 (1988), pages 37–50 (cited on page 82).
- [25] B. Asgharian and C. Yu. "A simplified model of interceptional deposition of fibers at airway bifurcations". In: *Aerosol science and technology* 11.1 (1989), pages 80–88 (cited on page 82).
- [26] G. B. Jeffery. "The motion of ellipsoidal particles immersed in a viscous fluid". In: *Proceedings of the Royal Society of London. Series A, Containing papers of a mathematical and physical character* 102.715 (1922), pages 161–179 (cited on page 82).
- [27] B. Asgharian, C. Yu, and L. Gradon. "Diffusion of fibers in a tubular flow". In: *Aerosol science and technology* 9.3 (1988), pages 213–219 (cited on page 82).
- [28] B. Asgharian and C. Yu. "Deposition of fibers in the rat lung". In: *Journal of aerosol science* 20.3 (1989), pages 355–366 (cited on page 82).
- [29] C. Yu, L. Zhang, G. Oberdörster, R. Mast, L. Glass, and M. Utell. "Deposition modeling of refractory ceramic fibers in the rat lung". In: *Journal of aerosol science* 25.2 (1994), pages 407–417 (cited on page 82).
- [30] B. Asgharian and S. Anijilvel. "Movement and deposition of fibers in an airway with steady viscous flow". In: *Aerosol science and technology* 22.3 (1995), pages 261–270 (cited on page 82).
- [31] B. Asgharian and G. Ahmadi. "Effect of fiber geometry on deposition in small airways of the lung". In: *Aerosol science and technology* 29.6 (1998), pages 459–474 (cited on page 82).
- [32] J. Ding, C. Yu, L. Zhang, and Y. Chen. "Deposition modeling of fibrous particles in rats: Comparisons with available experimental data". In: *Aerosol science and technology* 26.5 (1997), pages 403–414 (cited on page 82).
- [33] R. F. Phalen, W. C. Hinds, W. John, P. J. Lioy, M. Lippmann, M. A. McCawley, O. G. Raabe, S. C. Soderholm, and B. O. Stuart. "Rationale and recommendations for particle size-selective sampling in the workplace". In: *Applied Industrial Hygiene* 1.1 (1986), pages 3–14 (cited on pages 82, 103).
- [34] R. Guilmette and T. Gagliano. "Construction of a model of human nasal airways using in vivo morphometric data". In: *The Annals of Occupational Hygiene* 38.inhaled_particles_VII (1994), pages 69–75 (cited on page 83).
- [35] Y. Cheng, T. Holmes, J. Gao, R. Guilmette, S. Li, Y. Surakitbanharn, and C. Rowlings. "Characterization of nasal spray pumps and deposition pattern in a replica of the human nasal airway". In: *Journal of Aerosol Medicine* 14.2 (2001), pages 267–280 (cited on pages 83, 93).
- [36] Y.-S. Cheng, S. Smith, and H.-C. Yeh. "Deposition of ultrafine particles in human tracheobronchial airways". In: *The Annals of Occupational Hygiene* 41.inhaled_particles_VIII (1997), pages 714–718 (cited on page 83).
- [37] Y.-S. Cheng, Y. Zhou, and B. T. Chen. "Particle deposition in a cast of human oral airways". In: *Aerosol Science & Technology* 31.4 (1999), pages 286–300 (cited on pages 83, 93, 95, 97, 101).
- [38] Y. Cheng, C. Fu, D. Yazzie, and Y. Zhou. "Respiratory deposition patterns of salbutamol pMDI with CFC and HFA-134a formulations in a human airway replica". In: *Journal of aerosol medicine* 14.2 (2001), pages 255–266 (cited on pages 83, 93).
- [39] Y. Zhou and Y.-S. Cheng. "Particle deposition in a cast of human tracheobronchial airways". In: *Aerosol Science and Technology* 39.6 (2005), pages 492–500 (cited on pages 83, 102).

- [40] N. I. for Occupational Safety and H. (NIOSH). *Asbestos and Other Fibers by PCM: Method 7400*. 1994 (cited on page 84).
- [41] M. Lippmann. “Effects of fiber characteristics on lung deposition, retention, and disease.” In: *Environmental health perspectives* 88 (1990), pages 311–317 (cited on page 86).
- [42] I. Hill, P. Beswick, and K. Donaldson. “Differential release of superoxide anions by macrophages treated with long and short fibre amosite asbestos is a consequence of differential affinity for opsonin.” In: *Occupational and environmental medicine* 52.2 (1995), pages 92–96 (cited on page 86).
- [43] M. Bernstein, J. M. R. Sintes, B. K. Ersboell, and D. Joachim Kunert. “Biopersistence of synthetic mineral fibers as a predictor of chronic intraperitoneal injection tumor response in rats”. In: *Inhalation toxicology* 13.10 (2001), pages 851–875 (cited on page 86).
- [44] W. Stöber. “Dynamic shape factors of nonspherical aerosol particles”. In: *Assessment of airborne particles* (1972), pages 249–289 (cited on pages 86, 93).
- [45] J. Happel, H. Brenner, and L. R. N. Hydrodynamics. “Noordhoff International Publishing”. In: *Leyden, Netherlands* (1973) (cited on page 88).
- [46] T. Martonen and J. Lowe. “Assessment of aerosol deposition patterns in human respiratory tract casts”. In: *Aerosols in the mining and industrial work environments* 1 (1983), pages 151–164 (cited on page 90).
- [47] W.-C. Su and Y. S. Cheng. “Deposition of fiber in the human nasal airway”. In: *Aerosol Science and Technology* 39.9 (2005), pages 888–901 (cited on page 91).
- [48] W.-C. Su, J. Wu, J. C. Marijnissen, and Y. S. Cheng. “Deposition of man-made fibers in a human nasal airway”. In: *Aerosol science and technology* 42.3 (2008), pages 173–181 (cited on page 91).
- [49] D. Swift. “Inspiratory inertial deposition of aerosols in human nasal airway replicate casts: implication for the proposed NCRP lung model”. In: *Radiation Protection Dosimetry* 38.1-3 (1991), pages 29–34 (cited on page 93).
- [50] G. Zwartz and R. Guilmette. “Effect of flow rate on particle deposition in a replica of a human nasal airway”. In: *Inhalation toxicology* 13.2 (2001), pages 109–127 (cited on page 93).
- [51] J. T. Kelly, B. Asgharian, J. S. Kimbell, and B. A. Wong. “Particle deposition in human nasal airway replicas manufactured by different methods. Part I: Inertial regime particles”. In: *Aerosol Science and Technology* 38.11 (2004), pages 1063–1071 (cited on pages 93, 100).
- [52] B. Asgharian. “Theoretical Deposition of Fibrous Particles in the Respiratory System of Humans and Rats”. PhD thesis. State University of New York at Buffalo, 1988 (cited on page 95).
- [53] Y. Chen and C. Yu. “Sedimentation of fibers from laminar flows in a horizontal circular duct”. In: *Aerosol science and technology* 14.3 (1991), pages 343–347 (cited on page 95).
- [54] B. Asgharian, L. Zhang, and C. P. Fang. “Theoretical calculations of the collection efficiency of spherical particles and fibers in an impactor”. In: *Journal of aerosol science* 28.2 (1997), pages 277–287 (cited on page 95).
- [55] K. T. Shanley, G. Ahmadi, P. K. Hopke, and Y.-S. Cheng. “Simulated airflow and rigid fiber behavior in a realistic nasal airway model”. In: *Particulate Science and Technology* 36.2 (2018), pages 131–140 (cited on page 95).
- [56] W. Su and Y. Cheng. “Deposition of fiber in the human respiratory tract”. In: *J Aerosol Sci* 37 (2006), pages 1429–1441 (cited on page 95).
- [57] L. Zhang, B. Asgharian, and S. Anjilvel. “Inertial and interceptional deposition of fibers in a bifurcating airway”. In: *Journal of aerosol medicine* 9.3 (1996), pages 419–430 (cited on pages 98, 100–102, 104).
- [58] Y. Zhou, W.-C. Su, and Y. S. Cheng. “Fiber deposition in the tracheobronchial region: Experimental measurements”. In: *Inhalation toxicology* 19.13 (2007), pages 1071–1078 (cited on pages 98, 102, 103).
- [59] Y. Zhou, W.-C. Su, and Y. S. Cheng. “Fiber deposition in the tracheobronchial region: Deposition equations”. In: *Inhalation toxicology* 20.13 (2008), pages 1191–1198 (cited on page 98).
- [60] F. Cai and C. Yu. “Inertial and interceptional deposition of spherical particles and fibers in a bifurcating airway”. In: *Journal of Aerosol Science* 19.6 (1988), pages 679–688 (cited on page 103).

Part II.
Day Two

9

Micro and nanoplastics in the aquatic environment with special reference to synthetic fibers

By: A. Dick Vethaak^{1,2}, C. Martínez-Gómez³

- 1 – Deltares, Marine and Coastal Systems, Boussinesqweg 1, 2629 HV Delft, the Netherlands
- 2 – Vrije Universiteit Amsterdam, Department of Environment and Health, De Boelelaan 1085, 1081 HV Amsterdam, the Netherlands
- 3 – Instituto Español de Oceanografía (IEO), Oceanographic Centre of Murcia, Varadero 1, PO BOX 22, 30740 San Pedro del Pinatar Murcia, Spain

9.1 Introduction

Plastics are polymers produced from synthetic solid petroleum- or bio-based materials and often mixed with chemical additives. The annual global production of these polymers has exponentially increased over the past decades, reaching 348 million tons in 2017, and is expected to double by 2050 [1, 2]. Such an increase is related with an important production of waste, of which a fraction will eventually end up in the environment due to poor waste management or inappropriate disposal. Plastics are insoluble in water and have (extremely) slow degradation rates after being discarded. Global leakage of persistent plastic waste flowing into rivers and waterways, and ultimately into the oceans, was estimated in the order of 10 million tonnes per year (Mt y^{-1}) [3], resulting in a widespread occurrence and accumulation of microplastic pollution.

Plastic particles in the micrometer-size range have been detected worldwide in virtually all aquatic compartments, such as surface waters, water column, sea floor, coastlines, polar ice, rivers, small waterways and lakes, as well as in a wide range of species (e.g., [4–9]). This raises scientific and public concern on their possible impact on aquatic populations, food webs, and food production for humans. The debate is fuelled by the persistence of the plastics and a projected future increase in microplastic pollution levels [10, 11]. The term microplastics (MPs), whether originating from intentional production (primary microplastics) or fragmentation of larger plastics (secondary microplastics), was coined by Thompson and co-workers in 2004 to describe the widespread occurrence of microscopic plastic particles and fibers in the oceans [12]. Since then, microplastic research has attracted increasing attention in environmental sciences, interlinking them between the fields of macro-plastic pollution and the field of nanoparticle toxicology [13].

Microplastic debris is heterogeneous in nature with a large variety of shapes, from spherical particles to angular fragments or films and long fibers [14]. All plastic particles or fibers in the size range 1–5000 μm (in their largest dimension) are referred to as microplastics (MPs) and those in the size range $< 1 \mu\text{m}$ (in their largest dimension) as nanoplastics (NPs) [14, 15]. Microplastic fibers are a specific type of microplastics defined as any artificial fibrous materials (e.g., acrylic, polyesters, nylon) of threadlike structure with a diameter less than 50 μm , length ranging from 1 to 5000 μm , and length to diameter ratio greater than 100 [16]. Some studies have used different morphological criteria to confirm a fibrous particle, for example "a length to diameter ratio of > 3 " [17] or "a length substantially longer than its width" [14].

9. *Micro and nanoplastics in the aquatic environment with special reference to synthetic fibers*

Field studies to date have mostly focused on plastic particles and fibers in the micro-size range. Due to analytical limitations, nano-sized plastic particles and fibers are not considered in field studies, but they have been commonly used in laboratory studies to understand the behavior and toxic effects of micro- and nanoplastics (MNPs) in aquatic organisms. The bulk of field and laboratory studies concerning environmental concentrations and effects to date have been performed for marine environments, but the impact of MNPs may be equally serious for freshwater and terrestrial environments. However, the occurrence, fate and ecological effects of this type of pollution are still poorly understood. In the past decade, a rapidly growing body of empirical research on aquatic microplastics has aimed at elucidating and understanding the ecological impact of MNPs to provide evidence to inform and support policy makers remediating plastic pollution (e.g., [4, 18–31]).

This chapter aims to present a summary of what is currently known about MNP pollution in aquatic ecosystems. Special attention will be given to synthetic fibers, which are a predominant type of MNP pollution. Factors influencing MNP uptake and absorption, their bioaccumulation and ecological effects will be considered as well. Case studies on phytoplankton and bivalves will be highlighted. We conclude by discussing important knowledge gaps that need to be addressed in future work.

9.2 Sources, pathways and sinks

9.2.1 Major sources of MNPs

MNPs enter the aquatic environment from a variety of sources. The weathering and fragmentation of large plastic pieces, such as containers, packaging materials, bottles, and ropes are the most important source of secondary MNPs throughout the world ocean (e.g., [22, 32, 33]). It is estimated that between 1.15 and 2.41 million tons of both macro- and micro-plastic debris enter the ocean every year from rivers, with the top 20 polluting rivers, mostly located in Asia, accounting for 67 per cent of the global total [34]. Wastewater treatment plants are significant sources of microplastics in river catchments with concentrations reaching up to 125 particles per liter [35]. In addition to this, sea-based sources of plastic litter (beach littering, shipping and fisheries) and atmospheric transport and deposition of MNPs, may also be important pathways [16, 22, 36].

Not all MNPs originate from the breakdown of larger plastic items or particles. MNPs can also be generated by erosion and abrasion during the production, maintenance, and use of plastic products. In this case, tyre wear and tear during driving and shredding of synthetic fibers from textiles during washing are relevant and major sources [3, 37]. In their review on wear and tear of tyres, Kole and co-workers estimated that the per capita emission ranges from 0.23 to 4.7 kg y⁻¹, with a global average of 0.81 kg y⁻¹ [38]. These estimates indicate that car wear and tear, consisting largely of elongated particles of rubber polymers [39], significantly contribute to the flow of (micro)plastics into the aquatic environment with a relative contribution of 5–10% of total global oceanic plastic.

Some portion of MNPs are manufactured as micro or nano-sized particles and directly released to the environment, such as pellets, powders, or microbeads in personal care products (PCP) [22]. However, these primary particles are probably only a small fraction of the total amount of MNPs in the aquatic environment [3].

Well-known are plastic preproduction resin pellets, usually 1 to 5 mm in size and of variable composition. They are found in aquatic samples and on beaches all over the world and their presence is often linked to spillage during transportation or industrial effluents. Other major, but lesser known sources of plastic particles and fibers emitting to the environment are abrasion of polymeric paints from shipping, water works, city dust, and household dust [3, 40]. Microplastic pollution by smaller size micropellets has also been observed. For example, micro-debris detected in European river (Rhine) sediments close to polymer plants contained overall 18% PS pellets (100–200 µm) showing visual and spectroscopic resemblance to primary preproduction pellets/powder [41]. Another very recent example is the shipping accident of the MSC Zoe in 2019 during a storm in the North Sea. The loss of 342 containers of goods, several of which contained 5 mm plastic preproduction pellets (polystyrene and HPPE), resulted in a wide spread

microplastic contamination of Dutch and German islands in the Wadden Sea (a protected area under European Natura 2000 law).

9.2.2 Sources of fibrous MNPs

Synthetic microfibers in the aquatic environment originate from primary textile microfibers that are used in the textile and clothing industry, and the fragmentation of larger fabrics originates during textile production, use, and from discarded textiles [16, 42, 43]. Other sources of fibrous microplastics are fishing nets, ropes, and certain polymeric paints and coatings. Microfibers are easily shed from clothes and household textiles with loose structures, such as fleece sweaters, during daily use [44]. Boucher and Friot [3] estimated that approximately 35% of microplastics in the world's oceans arise from laundry of synthetic textiles. Some estimates are lower, but even a value of 20% for 2014 as reported by Eunomia [45] means that the equivalent to 0.19 million tons of textile microfibers from the production and normal use of synthetic textiles, particularly household washing of clothing, enters the marine environment alone annually (see Henry et al. [43]). Browne et al. [46] found that a single piece of clothing can produce > 1900 synthetic microfibers per wash, while in a recent study by Napper and Thompson [44], it was estimated that the release of synthetic fibers from polyester, polyester-cotton blend and acrylic fabrics into waste water during each use of a washing machine could be as high as 700,000 microscopic fibers. Microplastics can be found in wastewater where approximately 35% of microplastics are thought to be fibers from synthetic clothes [47]. Although treated effluents only contain few microplastics per liter, the high volume of effluents constantly released constitutes a considerable source of microplastic contamination of aquatic systems. However, it is likely that globally over 80% of wastewater is released to the environment without treatment, resulting in an even much greater emission of synthetic fibers [48].

9.2.3 Pathways and sinks

Relevant pathways of MNPs into the aquatic environment are through littering of larger plastic items, road and land runoff, storm water, flooding, soil amendments and irrigation, wind transfer, and atmospheric outfall [3, 26, 49, 50]. Sewage Treatment Plants (STPs) are considered important pathways of MNPs to surface waters [4], especially in parts of the world where sewage water is treated less rigorously. Plastic particles and fibers contained in personal care products (PCPs) and those originating from laundry, tyre wear, etc., will at least partly end up in the STP effluents [6, 35, 51], and thus get released into receiving surface waters. Atmospheric deposition of suspended atmospheric microplastics, especially textile fibers, has been recently recognized as an important input pathway [16]. Marine systems, especially sediments, still appear to be the ultimate sink for microplastics in the environment, but freshwater systems such as estuaries and lakes are also important recipients and reservoirs of microplastics pollution (e.g., [6, 52, 53]). Relatively high levels of MPs can be found in oceanic gyres and enclosed sea water regions, remote mountain lakes, industrial effluents, sites near factories, estuaries, seabed and urban sediments, filter feeding biota, and household dust [24, 52–60]. Generally, aquatic biota, such as filter and deposition feeders may represent relevant reservoirs, as they will temporarily retain plastic particles from other environmental compartments [61].

From the information above, it can be concluded that sources of aquatic MNPs are diverse. A major source of plastic fibers originates from wear, tear, and maintenance of textile and apparel. In addition to direct emissions into surface waters through effluents and raw untreated wastewater, atmospheric transport and deposition is likely to play a role in the distribution of MNPs, notably fibers.

9.3 Composition of aquatic micro- and nanoplastic debris

MNPs in the aquatic environment are highly complex cocktails of contaminants, including polymeric materials, chemical additives, residual monomers, ambient chemical substances that sorb to plastic, and proteins (ecocorona) [62]. Furthermore, the plastic debris serves as a novel substrate for microbial community structures (biofilms) on

9. *Micro and nanoplastics in the aquatic environment with special reference to synthetic fibers*

their surfaces. The combinations of polymeric materials and associated chemical and biological contaminants are countless making each plastic particle or fiber having its own unique properties [63]. The polymeric, chemical, and biological components of plastic debris, in particular MNPs, are further described below.

9.3.1 Debris polymers

The distribution and abundance of MNPs is inseparably linked to macroplastic debris, largely via the degradation of bulk plastic into smaller particles down to the nanoscale [64]. Aquatic debris polymers, which are most commonly found, are mostly high production volume polymers (or mixtures thereof), such as polyethylene (as both high-density, HDPE, and low density, LDPE), polypropylene (PP), polystyrene (PS), polyvinylchloride (PVC), polyamide (nylon) (PA), polyurethane (PUR), polyethylene terephthalate (PET), polyester resin and glass fiber, and cellulose acetate (CA). Most debris-prone polymers contain a variety of chemical additives (chemicals which are used to polymerize, process or to modify end use properties of plastics), unpolymerized monomer residues and impurities, depending on polymer surface structure and affinity [23, 65, 66]. Less commonly reported debris polymers include polyvinyl alcohol (PVA), acrylic (AC), poly-methylmethacrylate (PMMA), alkyd (AKD), polyurethane (PU), styrene butadiene rubber (SBR) [41, 67, 68]. Polyamide 66 (nylon66), PVA, polyester, and PP are produced as synthetic monofilaments and used in fibrous materials in textiles and apparel [43], and for fishing lines and fishing nets [23]. Considering that overall 8000 different plastic grades are currently in the market, it is likely that the total number of debris polymers might add up to several hundreds (<https://www.campusplastics.com>).

9.3.2 Chemical additives

Besides synthetic polymers or mixtures thereof, a wide range of chemicals are present in plastic as a result of manufacturing specifications. Chemical additives in polymeric and plastic packaging materials include monomers (e.g., styrene), intermediates, solvents, surfactants, plasticizers (bisphenol-A and phthalates), stabilizers, biocides, flame retardants, accelerators, and colorants [69]. Also, the polymerization process may leave trace quantities of residual monomer or low-molecular-mass polymers in the plastic, especially in primary MNPs. Furthermore, upon aging/weathering, polymer degradation products are likely to be formed, for example, as result of UV-exposure. Many of these substances are not exclusively used by the plastic industry and have applications elsewhere as well, for example in textiles and food technology industry [70]. A considerable number of plastic additives have been listed as chemicals of very high concern because of their endocrine disrupting or carcinogenic properties and other toxicological hazards [71, 72]. Once in the water, hazardous additives might rapidly leach out of the plastics to the surroundings and into the food chain, as it degrades. As such, debris plastics, especially macro-sized objects, significantly contribute to chemical contamination of aquatic systems [73–75].

9.3.3 Adsorption of chemical contaminants

MNPs have a hydrophobic nature (i.e., low polarity) with relatively large ratio of surface to volume with a significant ability to highly accumulate a wide range of chemicals [76] either directly from the environment or as a result of biofouling. Under laboratory conditions, PE, PVC, PP, and PS display high sorption capacity for polycyclic aromatic hydrocarbons (PAHs), dichlorodiphenyltrichloroethane (DDT), hexachlorocyclohexanes, chlorinated benzenes, musks, pharmaceuticals, and personal care products [77–82]. Many of the contaminants adsorbed from the surrounding water have toxic, endocrine disrupting and/or immunomodulating properties [23, 83]. Examples are metals [84] and hydrophobic contaminants such as PCBs, PAHs and PBDEs [23, 85] and emerging contaminants such as PFAS [86] and pharmaceuticals [87]. Compared to microplastics, nanoplastics exhibit a large surface area with increased sorption capacity and are able to bind increased levels of organic contaminants [88] and metals [89]. The contaminants present in MNPs may migrate from the particles into the organism by equilibrium partitioning [88] and can cause chemical toxicity [71, 76]. Contaminant transfer is bi-directional and can either increase or decrease contaminant body burden

depending on polymer type, environmental conditions, and chemical fugacity/transport gradients [88, 90]. The above studies show that MNPs could be significant vectors of both organic and inorganic substances, potentially affecting bioavailability and chemical toxicity.

9.3.4 Eco-corona, biofilm and biofouling

In addition to polymers and chemical additives and adsorbed chemicals, MNPs can bind organic matter, nutrients, and also macromolecules (e.g., lipids, proteins, polysaccharides) and may serve as substrates for microbial biofilms, forming a so called eco-corona around the MNPs [62]. Subsequently, MNPs can be colonized by a distinct fouling community of aquatic microorganisms and small invertebrates, such as diatoms, bacteria, cyanobacteria, fungi, unicellular algae, ciliates, dinoflagellates, bryozoans, crustaceans, worms, and marine insect eggs [91–93].

Attracted by nutrients and depending on the polymer type, MNPs develop unique microbial community structures compared to their surrounding environment [93]. Main bacterial colonies found on MPs appear to be established by their adherence properties, such as hydrophobicity and surface roughness, rather than by the type of polymer itself [94], although species able to degrade the specific polymeric material or chemical additives usually also occur in the biofilm communities [95–97]. Thus, additional to weathering processes, some bacteria may also act as plastic degraders and accelerate MP degradation processes [98], although biodegradation in aquatic habitats is recognized to be low [97]. On the other hand, biofilm micro-organisms may produce exudates acting as infochemicals of food occurrence, potentially increasing the ingestion rate of MNPs [62].

An increasing number of studies on (micro)plastic-microbiological research indicate that aquatic (micro)plastics represent a distinct environmental niche that can potentially harbor and disperse pathogenic bacteria [92, 99–103], antibiotic resistant micro-organisms [104, 105], toxic dinoflagellates [106], toxic cyanobacteria [97], thus posing novel health risks to fish and other aquatic organisms and potentially humans as well [92, 99, 100, 103–105]. The long decomposition time coupled with lower density of MNPs favor their dispersal in aquatic systems compared to non-plastic particles [107].

It is becoming clear that eco-corona and biofilm formation and subsequent biofouling and plastic biodegradation may change the identity and density of MNPs, and could influence their behavior, fate, bioavailability, and effects [62, 108–112]. Overall, these interactions between MNPs and microbial ecology are far from being understood and require further research.

9.4 Factors that control degradation and fate of polymeric material

Physical and chemical processes, such as exposure to UV light (photodegradation), oxidation, leaching of additives, biofilm growth, and mechanical abrasion (with rocky shores and sandy beaches), initiate plastic degradation and fragmentation, consequently releasing numerous plastic particles from the surface of larger items or fragments [66, 113, 114]. The fragmentation process primarily depends on the type of plastic, the concentrations of antioxidants and stabilizers used as additives [115] and the physical-chemical environmental conditions including contact by biota [116]. Eco-corona and biofilm formation on plastic particles surfaces could prevent the plastic from photo-catalysis, either directly or via decreased buoyancy, thereby promoting microplastic sedimentation. Over time, the polymeric material itself degrades very slowly and consequently, MNPs will persist for decades and even centuries [113, 115, 117]. Decreasing particle size as a consequence of fragmentation will further result in a higher particle abundance and increase encounter probability with biota [23]. Further, nanoplastics can be generated from microplastics through digestive fragmentation by organisms such as Antarctic krill [118]. These effects have potential consequences as the number of particles that are sufficiently small for translocation into the body, but it introduces a new role for biota in the fate of plastic and nutrient cycling and biogeochemical processes. In fact, the likelihood that marine and freshwater biota has not been exposed to MNPs from any source is very low.

9. Micro and nanoplastics in the aquatic environment with special reference to synthetic fibers

The fate of microplastics in the aquatic environment primarily depends on polymer density, particle size and shape which influences buoyancy, and residence time (biofilm development and the potential interaction with detritus, living organisms, and inorganic matter) [18, 119]. Further, the fate of MNPs in the water column is highly affected by the aggregation of nano and microplastic with suspended solids [120]. The densities of the most encountered plastic materials, such as polyethylene, polypropylene, nylon, and polyester typically range between 0.9 and 1.4 g cm⁻³. Polymers less dense than (sea)water (e.g., PE and PP) will tend to float on or within the water surface layers, while those with higher density (e.g., PVC, polyester, acrylics, and polyamide) will sink. Settling/resuspension behavior of MPs is highly dependent on the particle shape (i.e., flat fragments may stay motionless and flexible threads and fibers can be easily captured by the flow) [121]. The transport and distribution of fibrous MNPs are intrinsically differently due to the low sinking rate, delayed settling and low re-suspension threshold compared to non-fibrous plastic particles [122]. Biofilm formation and the settlement of organisms on the plastic surface increase the weight of particles, thus increase their sinking velocity [123–125], with small-sized particles losing buoyancy much faster than larger ones, depending on the shape and especially specific density [126]. Other studies have shown that MPs flocculate and adhere to sticky exo-polymers [119] or be incorporated into faecal pellets [127], influencing their buoyancy and position in the water column. On the other hand, evidence indicates that aggregates in marine waters are involved in removing MPs from the ocean surface and facilitating their transfer to marine food webs [128].

9.5 Physical and chemical quantification and characterization of MNPs

9.5.1 Analysis of microplastics in aquatic matrices

There is currently no ideal analytic method to quantify and chemically characterize plastic particles in aquatic samples (< 5 mm). The major issues are the complexity of environmental samples – to adequately remove the organic fraction (e.g., biological tissues) – and the lower detection limit for particle size. Often one or more extraction and cleaning steps are needed to isolate the microplastics from the surrounding matrix prior to analysis. These extractions and cleaning techniques include visual sorting, density gradient-based separation, filtration, acid and alkaline cleaning, and enzymatic destruction [14, 129–131].

Microplastic measurement results rely strongly on good sampling and sample purification. Therefore, the combination of a separating and qualifying method has been widely used [132]. Visual sorting can lead to large error values (e.g., [67, 133, 134]) in determining the concentration of MPs. Other techniques reportedly generate much higher recovery and identification rates for MPs, although these rates generally decrease as the particle size decreases [135].

Analysis techniques commonly used for the identification of (micro)plastics include Fourier transform infrared microscopy (FTIR), Raman spectroscopy, scanning electron microscopy with energy dispersive x-ray spectroscopy (SEM-EDS), and pyrolysis-based gas chromatography mass spectrometry (GC-MS) [129, 130, 132, 133]. The spectroscopic FTIR and Raman techniques are currently best suited for the detection of plastic particles larger than about 10 and 1 µm respectively, depending on the equipment used [67]. Stimulated Raman Scattering (SRS) microscopy is a powerful spectroscopic imaging technique based on the synchronized action of two pulsed laser beams with a specific photon energy difference. Compared to conventional Raman spectroscopy, it allows a thousand-fold faster mapping of, for instance, particles on a filter surface. A multispectral SRS-approach of this method was recently developed for MPs in the low-micrometer size range from harbour sediment, although this technique needs improvement to be used for small sized particles in a high throughput mode [136].

The advantages and limitations of the various methods are discussed in detail elsewhere [14, 132, 137]. A major limitation in the analysis of MPs in complex environmental (organic rich and weathered plastics) matrices is the lack of standard operating procedures for detecting and quantifying microplastics. Clearly, there is a need for harmonized protocols for sampling, analysis, and identification of microplastic particles and fibers. Further research is required to determine whether any of the currently available analytical techniques can be developed to the extent where they can be routinely used for MNP exposure assessment the entire range of sizes. Most suitable methods for analyzing

microplastics reported in aquatic matrices have been reviewed and recommended by GESAMP [14].

Field studies on microplastic abundance reported in the literature contain mostly particle counts and less often quantitative data on polymer types. Environmental concentrations are usually expressed in particle number per unit (volume, surface area, mass) and rarely in mass per unit. The physico-chemical heterogeneity (i.e., in polymer type, size, shape) of MPs found in field samples implies that the conversion between particle and mass-based concentrations is fraught with imprecision. On the other hand, mass-based concentrations are commonly reported in laboratory studies using test MNPs, exhibiting more homogenous characteristics. It would be preferable, when possible, to record both number and mass (e.g., using pyrolysis GC-MS) to facilitate comparisons of quantities between micro-sized (high mass) and nano-sized (high numbers) debris. From a toxicological perspective, particle numerical concentrations are preferred, because these represent the number of MNPs biota are exposed to. For further discussion, see Skåre et al. [31].

9.5.2 Analysis of microplastic fibers and nanoplastics

Fibers may even be more difficult to count and qualify than non-fibrous particles and some recent reviews have questioned the effectiveness of microfiber identification [138–140]. There are several issues with the accurate identification of synthetic microfibers. Natural (e.g., cotton, flax, wool, linen, silk, and hair) and artificial (regenerated) cellulosic microfibers (e.g., viscose (or rayon), bamboo and acetate fibers) have similar morphological properties, but are not plastic [141]. For example, the difficulty of separating natural and synthetic microfibers following visual inspections may result in misidentification of synthetic microfibers to natural fibers [140] or misidentification of natural fiber (e.g., cotton, hemp) to manmade cellulosic fibers (e.g., viscose) [138]. Spectroscopic analysis is essential to ascertain the plastic nature and differentiate the different types of fibers. On the other hand, fibers are often too thin and their abundance in water samples taken with bigger net mesh sizes is therefore often likely to be underestimated [41]. A simple and effective step before spectroscopic analysis seems to be the use of Nile Red (9-diethylamino-5H-benzo[a]phenoxazine-5-one), offering the possibility of selective identification of plastics, based on surface polarity characteristics of plastic particles, including small MPs (< 100 µm) [142, 143]. For recommendations on how to accurately differentiate types of fibers, the reader is referred to the work of Woodall et al. [144] and Comnea-Stancu et al. [138].

Due to methodological challenges, the smaller sized MNPs, such as sub-micron or nano-sized plastics, are yet to be detected in environmental field samples or in tissues of field-collected organisms [14, 145–147]. Advanced separation techniques, such as asymmetric flow-field-flow fractionation (AF4), might also be applicable to nano-sized plastic particles and fibers. Similarly, electron microscopy-based analytical techniques might also be helpful in visualizing nano-sized particles and fibers, although this technique probably would have to be combined with other analytical techniques, such as pyrolysis GC-MS, for sub-micron-sized particle identification. Possible routes for developing adequate sampling preparation and analytical techniques for the detection of the yet unanalyzed MNPs could come from the field of engineered nanoparticles and fiber toxicology.

9.5.3 Uncertainties in aquatic MNP measurements

The reliability of some early microplastic results is questioned [134]. This is because cross-contamination is likely to occur at each stage of sampling, handling, and analysing microplastics samples, as demonstrated by various studies (e.g., [134, 144]). In most instances, investigations pinpoint that microplastics were most likely acquired from worker clothing, unwashed lab equipment, and general contamination from airborne microplastics in the laboratory. Recommendations on avoiding contamination and applying quality criteria for the analysis of microplastics in biota, including the use of procedural blank analysis and clean air devices, have been described by [134].

9.6 Occurrence of microplastics in aquatic systems

9.6.1 Microplastics in abiotic matrices

Concentrations reported in water vary from a few particles up to thousands of particles m^{-3} [26, 148]. Microplastic concentrations in suspended matter and sediment can reach several thousand particles kg^{-1} of dry sediment [148–151]. In a study in Dutch coastal and inland waters, microplastic analysis (particle sizes between 10–5000 μm) in major rivers Rhine and Meuse and urban water in and around Amsterdam in 2014, showed concentrations between 100 and 3600 particles kg^{-1} of dry sediment along the Dutch North Sea coast and between 68 and 10,500 MPs kg^{-1} in urban canal sediments. Amsterdam canal water samples contained microplastic concentrations (48–187 MPs l^{-1}) similar to those observed in treated wastewater effluent in the area. These data show that MPs do settle in urban waters, meaning that at least a part of the MPs is retained in freshwater systems. On the other hand, microplastic concentrations in riverine suspended particulate matter appearing to be high (1400–4900 MPs kg^{-1} dry weight (dw)) [6], substantiating previous studies that rivers are a key factor for microplastics to move towards the ocean [26, 152].

In aquatic samples, PE, PP and PS are the most frequently found polymers [24], but also a range of other polymer types have been occasionally identified, for example PET, nylon, polyether urethane, styrene acrylate, alkyd, styrene butadiene rubber, and polymethyl methacrylate [41, 136, 153]. Haave et al. [60] identified twenty different polymer types, at concentrations from 12,000 to 200,000 MPs kg^{-1} dw. Over 95% of the MPs were smaller than 100 μm and commonly consisted of polyurethane acrylate resins, while the larger MPs consisted mostly of polyamide fibers.

Several studies indicate fibers to be a most common type [23]. However, this may be partly due to cross contamination of samples as discussed above. Burns et al. [27] reported that the most abundant shape type in water and sediment is fibers (48.5%), followed by fragments (31%), spherical beads (6.5%), films (5.5%), and foam (3.5%). However, till date, published microplastic data for aquatic matrices are only partly complete and as previously explained, limited to the upper end of the particle size spectrum. In addition to this, published field and monitoring studies often do not mention any specific aspect ratio to distinguish fibrous from non-fibrous particles (e.g., irregular shaped thin fragments or films). As microplastic measurements can be fraught with uncertainties, the representativeness and reliability of obtained data can be compromised. Moreover, existing microplastic data collected from aquatic systems may vary considerably largely because different methods and level of QA have been applied [67], hampering useful comparison. Generally, methods that can sample or detect smaller particles, such as mesh size effects on sample composition, will result in higher concentrations [65, 154]. These studies indicate the significance of the unanalyzed MNP fraction and the need for improved methods for MNP sampling and analysis. To illustrate, microplastic measurements in marine and coastal surface waters have often been limited to manta trawl or neuston samples using nets with > 0.3 mm mesh, underestimating the actual concentrations of microplastics that are likely to accumulate at the sea surface.

Concentrations of MPs in marine and coastal sediments that reach from zero to several thousands of particles kg^{-1} (dw), show generally higher concentrations at more inland sites. For example, the average amount found across the SW North Sea and Channel region in 2014 ranged between 200 and approximately 700 particles kg^{-1} (dw), with levels up to 3,146 particles kg^{-1} in sediment in harbor areas (particle sizes between 10 and 5000 μm). In North Sea sediments, mainly fibers and spheres were found, whereas at the sea surface, fragments were dominant. Several studies have shown that the concentrations of microplastics at the sea surface are lower and more variable than in sediments, indicating that most microplastics including fibers eventually do sink to the seabed supporting the hypothesis that the seabed may act as an important long-term sink [36, 142].

Gago et al. [155] reviewed the presence of microfibers in marine water and sediments and concluded that their occurrence is worldwide and represent a dominant fraction of the total microplastics, in some samples up to 100%. Most common colors were blue (seawater and sediments), transparent and black (seawater), and black (sediments); most common polymers were Polypropylene (water and sediments), Polyethylene (water), Polyester (water and sediments), HD/LD polyethylene and cellophane (only in waters), and rayon (sediments). Concentrations ranged from

0 to 459681 items km⁻² in sea water and from 12 to 160 items kg⁻¹ (dw) in sediments, with blue and polypropylene microfibers as the most abundant microfiber type.

Several studies indicate that microfibers have reached the deep waters of the Mediterranean Sea (3500-meter-deep) and Atlantic (up to 4844-meter-deep) [156], and Indian and West Pacific Ocean (5768 meters deep) [157], where they can be found in similar concentrations as in coastal sediments [158], most likely via the supply of organic detritus "marine snow" containing these particles [55]. Long range transport of synthetic fibers from southern European coastal waters to open deep sea was investigated by Sanchez-Vidal et al. [33]. The measured abundances and composition of microfibers in sediments suggested a downslope transport from coastal seas via submarine canyons to deep open sea floor. They found abundances of 10–70 microfibers in 50 ml of sediment, including both natural and regenerated cellulose, and synthetic fibers; the plastic microfibers consisted of polyester, acrylic, polyamide, polyethylene, and polypropylene.

It can be concluded that microplastics, notably fibers, and also fragments, films and pellets, or granules, are found widespread in all abiotic compartments (surface water, water column, suspended matter, sediments) of marine and freshwater systems. Microplastic concentrations reported for fresh water systems and estuaries are mostly largely similar to those reported for marine and coastal environments, depending on the location, while in some deep-sea sediments microplastics have already reached concentrations similar to those reported for intertidal and shallow sub-tidal sediments [55, 57].

9.6.2 Microplastics in aquatic biota

The occurrence of MNPs in marine biota and commercial marine species have been well documented. Numerous studies show that MPs are ingested by an increasing number of marine species, including invertebrates (protists, small and large crustaceans, mollusks, annelids, echinoderms, cnidarian, and tunicates), pelagic and demersal fish [159], turtles [160] and large top predating marine fish, mammals [161], and penguins [162]. For more comprehensive reviews, the reader is referred to Kershaw et al., Wesch et al., Lusher et al., O'Connor et al. [23, 140, 163, 164].

Taylor et al. [158] provided convincing evidence that microplastics are present within deep-water organisms, and thus have become infiltrated into deep ocean ecosystems. Screening for microplastics and applying major quality control measures, they found 15 rather different plastic fibers ingested or internalized by diverse organisms with different feeding mechanisms. The fibers were made of modified acrylic, polypropylene, viscose, polyester, and acrylic. An increasing number of studies also reported MP consumption by freshwater species such as duck mussel [165], tadpoles [166], wild gudgeons [167], fish eating birds such and cormorants [168]. Overall, reported microplastic data indicate that almost all aquatic species and phyla analyzed to date show plastic particles in their digestive system or tissues. Further, it clearly shows that MNPs have infiltrated aquatic food chains through various pathways, ingestion, and trophic transfer [169].

The concentrations of microplastics in biota generally depend on the habitat and feeding modes [140, 163], but one study on fresh water invertebrates found MPs ubiquitous across different taxa and sites independent of feeding guild and biological traits [170]. Only few studies did not encounter any microplastics in a particular fish or invertebrate species [41, 158, 171].

Table 9.1.: Percentage of fibrous and other and not specified shapes in measurements of marine shellfish and fish (based on data from Barboza et al. [172], Table 2).

Marine food	No of species (No of measurements)	% Fiber/ filament	Other shapes	% Not specified
Shellfish (whole)	23 (25)	87.0	4.3	8.7
Fish (stomach)	69 (90)	78.8	19.1	2.1

9. Micro and nanoplastics in the aquatic environment with special reference to synthetic fibers

Analysis of large number of marine shellfish (whole organisms) and fish species (stomach content) showed the contribution of ingested microplastic fibers to total plastic to be 87% and 78.8% respectively (Table 9.1). A similar conclusion is reached for MP burden in freshwater biota where available field studies report microplastic fibers ranging from 46.6% to 100% (for references, see O'Connor et al. [164]).

Most species analyzed for microplastics contained plastic particles or fibers in their stomach content or tissues. For example, field analysis revealed that 8 out of 9 tested invertebrate species from five different phyla from the North Sea and 68% of analyzed individuals of brown trout (*Salmo trutta*) from the Swedish West Coast had microplastics in them (particle sizes between 10–5000 μm). Despite the poor analytical recovery of the used method, several trends emerged from these data. Among invertebrate species, highest concentrations were found in suspension and filter feeders, such as brittle star, sponges, and mollusks. Grazers analyzed for microplastic content, such as isopods, *Patella vulgate*, and *Littorina littorea*, and also secondary consumers (*Hemigrapsus sanguineus*), showed consistently lower concentrations, and in one species (*Patella sp.*), no microplastics were found. These findings compare well with those reported in other studies. Biota subsamples analyzed with FTIR confirmed various polymer types including PS, Alkyd resin, poly (methyl methacrylate) [41]. Other studies reported variable MP contents in various fish species, such as 36.5% of specimens of pelagic and demersal fish species in the English Channel [173]. Analyzing sprat from the Belgium coast, it was found that an average of 39% of individuals had ingested microplastic (78% synthetic fibers) (Figure 9.1). Individual whole shrimps from the North Sea contained 63% ingested or internalized microplastics (96.5% synthetic fibers) (Figure 9.1). In shrimps, blue fibers were found that could be related to shrimp trawl nets. These values are difficult to compare as they might be biased and use different identification and qualification methods. However, they support claims that in marine biota, fibers are an important and not rarely most common contaminant.

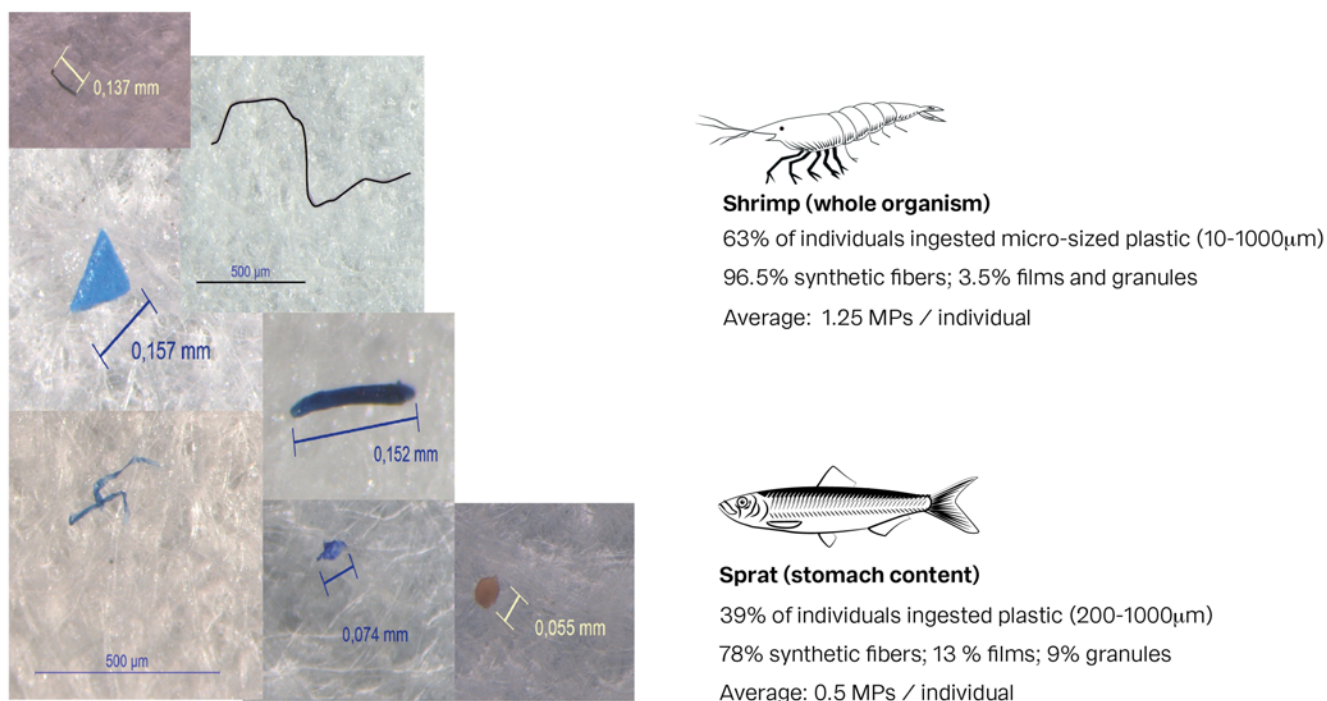


Figure 9.1.: Microplastic (MP) contamination in shrimp (*Crangon crangon*) and sprat (*Sprattus sprattus*) from the North Sea. Based on data from Devriese et al., Zoeter Vanpoucke [174, 175]. Photos ©ILVO.

Microplastics were analyzed in the freshwater duck mussel *Anodonta anatina* from a Swedish river by Berglund et al. [165]. All analyzed mussels contained both fibrous and nonfibrous microplastics. Higher abundances of microplastics were observed in larger mussels indicating a size-related uptake effect. The authors reported higher

concentrations of microplastics downstream urban areas with wastewater treatment plants and anthropogenic activities. Comparing the levels of MPs along a salinity gradient in Dutch waters, the MP concentrations from the North Sea coast to Lake IJssel was similar to the MP concentrations going inland wards. MP levels are approximately similar in freshwater mussels compared to marine mussels (Figure 9.2). In the Dutch study performed by [41], whole body concentrations reported in North Sea mussel ranged from 5–37 MPs per gram (dw) (particle sizes between 10–5000 μm), and 50% of the MPs were fibers. Based on the number of MPs per Kg (dw), the MP concentrations were approximately a factor 1000 higher than in surrounding surface water and sediment, with water, sediment and biota containing 51, 34 and 25% fibers respectively [41]. Several studies have indicated the spatial association in coastal and fresh waters and human activities [4, 5, 142, 148, 165, 176, 177]. A study on riverine macroinvertebrates (*Baetidae*, *Heptageniidae*, and *Hydropsychidae*) found that any increase in MP abundance in biota downstream of sewage treatment works, is possibly due to river flow dilution at the time of sampling [170].

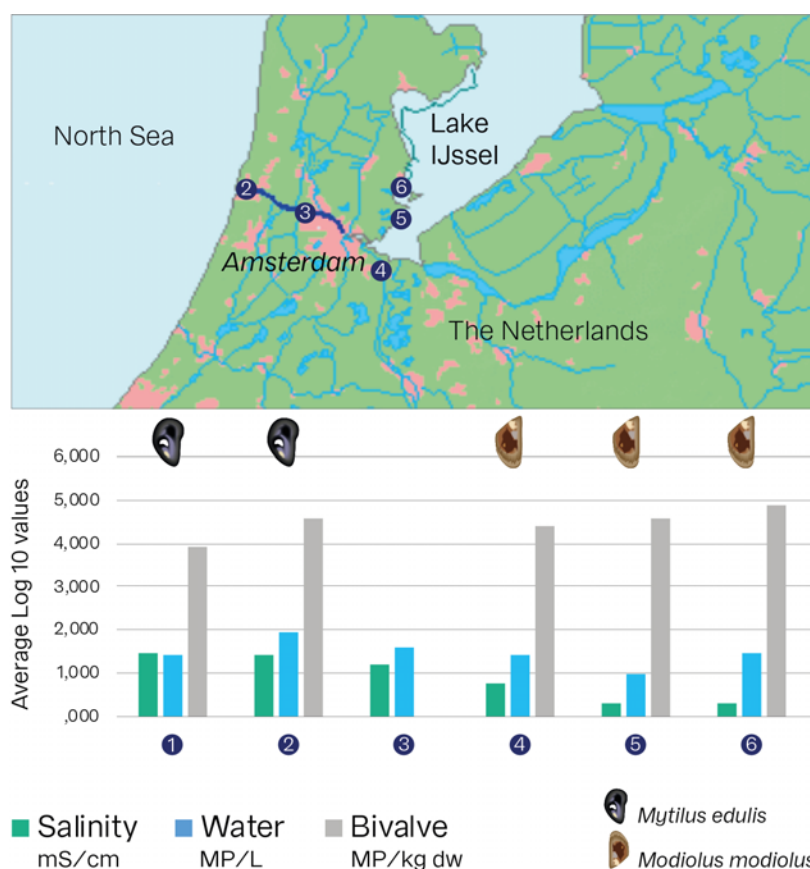


Figure 9.2.: Microplastic particle concentrations in water (MPs l^{-1}) and mussel (MPs kg^{-1} dw) along a salinity gradient. Microplastics contained 25% synthetic fibers. (Based on data from Karlsson [41, 178].

The relatively high concentrations of MPs found in commercial marine species such as fish and shellfish have raised important questions about potential risks in higher trophic level species and human food safety [28, 172, 179–182]. Commercial mussels and oysters especially appear to contain high levels of microplastics, and estimates indicate that, for example, European consumers of shellfish ingest 1800 - 11,000 microplastic particles (size range 5–1000 μm) per year [183]. Therefore, oral exposure to MNPs is believed to occur through the consumption of sea products, but may also occur through the consumption of livestock fed fishmeal [23], tap water [184], commercial salts across the world, and in several terrestrial foodstuffs such as honey, beer, and sugar (reviewed by Barboza et al., Yang et al., Joon [172, 185, 186] as well as inhalation of air-born MNPs [187]. It was recently demonstrated that the risk of plastic ingestion

via mussel consumption is minimal compared to the fiber exposure during a meal via indoor dust fallout [188]. On basis of currently available data, the risk of plastic ingestion via seafood consumption is relatively small, and at these levels, it is unlikely that MP exposure will represent a significant risk to human health.

To conclude, the current data clearly show that MPs are widespread among aquatic populations and have penetrated aquatic food chains and potentially, humans. Overall, fibers are the most prevalent microplastic type found in aquatic biota.

9.7 Uptake and effects of MNPs on aquatic biota

9.7.1 Uptake

The ingestion of MNPs by aquatic biota can occur either by directly ingesting the particles from the water or from the sediment or indirectly through trophic transfer. Not readily visible plastic particles or fibers are of special concern, because they can be ingested by biota more readily than larger particles. Organisms can either preferentially feed on MPs or can accidentally ingest them. Predators, detritivores, and scavengers may indirectly ingest plastic while consuming prey or scavenging detrital matter (e.g., marine snows) containing microplastic [128, 163]. Microplastics occupy the same size fraction as some planktonic organisms and may be ingested by a wide range of organisms as outlined above. There is evidence for both size-selective [189, 190] and non-selective ingestion [191], as well as avoidance of microplastics by different species [192]. Plastic particles may also adhere on gills, external appendages or stick to the outside of the body, as on algae and deep-sea coral.

Numerous laboratory studies show that particle size is key, but particle numbers, particle shape, charge, hydrophobicity, composition, and other factors such as aggregation of particles and presence of eco-corona may play an important role in causing effects [193, 194]. Once ingested and/or internalized, plastic particles and fibers, especially the nano-size fractions, can cross cell membranes and enter the circulation where they may reach tissues and cells and induce harm, i.e., particle toxicity, including cytotoxic, oxidative stress, DNA damage, and inflammatory responses. Major sites of entry upon ingestion of MNPs include the Peyer's patches in the intestine [195]. Some studies focused on the potential mechanism of uptake of MNPs. Phagocytosis or endocytosis is possible, whereas the paracellular transport can be excluded given the size of MNPs. Based on what we know from mammalian and aquatic model studies, it can be expected that micro-sized plastic particles, owing to their size, will largely remain in the intestinal tract and excreted through faeces, while smaller microplastics (< 20 µm) and submicro-sized particles can be absorbed by the gut and retain in circularly fluids; the very small particles (e.g., < 100 nm are readily absorbed by the gut and are capable to penetrate cells [195–197]). Once within the organism, MNPs interact with serum soluble components, forming a "protein corona", which may confer a biological identity to MNPs and affects their interactions with target cells [198, 199]. There is only limited evidence that MNPs can transfer from the gut into the circulation [200–202], cells [201], organs [203], and brain [203, 204]. Unfortunately, the size-fraction of MNPs capable of being internalized within fluids and tissues of aquatic organisms largely corresponds with the unanalysed fraction of these particles in field studies, thus seriously hampering risk assessment. Generally, smallest diameter particles have prolonged retention times and higher bioavailability [205]. Smaller MNPs, including nano-sized particles, which have the capability to be internalized by organisms, will have a higher probability of ingesting and biomagnifying up the food chain [169]. It is possible that larger fibrous MPs that have a higher risk of being entangled in the gut and intestines may result in a higher probability for trophic transfer than non-fibrous particles of similar size, but this requires further research. Ultimately, this implies that each plastic particle type exhibits different gut uptake rates and pathways.

Several studies provided insights into the biokinetics of MNPs. A study by Sendra and co-workers with Mediterranean mussels (*M. galloprovincialis*) showed size dependent accumulation of PS NPs (50 nm, 100 nm and 1 µm) in tissues and provided evidence for the translocation of these particles into the hemolymph [202]. The smallest PS NPs tested were detected in the digestive gland and muscle. A fast and size-dependent internalization of particles to the hemolymph was recorded after 3 h of exposure, and this process seemed to be controlled by different endocytic

pathways (i.e., caveolae and clathrin mediated endocytosis and phagocytosis). Al-Sid-Cheikh et al. [206] provided evidence that particle size influences the biokinetics of nanoplastics in a mollusk species. In their experiment the uptake, whole body distribution, and depuration were studied in *Pecten maximus* at environmentally realistic concentrations ($< 15 \mu\text{g MPsl}^{-1}$) using pulse exposures of ^{14}C -radiolabeled nanopolystyrene (24 and 250 nm). The results suggest relatively rapid uptake of both particle sizes after 6 h, with 250 nm particles present in intestine and 24 nm particles dispersing throughout the whole body, indicating possible translocation across epithelial membranes. Model extrapolations indicated that it could take 300 days to reach equilibrium in scallop body tissues, although the MP concentrations would still be below 2.7 mg g^{-1} . A comparison with a previous work, in which scallops were exposed to nonplastic (silver) nanomaterials of similar size (20 nm), suggests that nanoparticle composition may also influence the uptake. There are some further examples in the literature on how particle surface properties may influence uptake and associated effects. Proteins secreted by *Daphnia magna* around polystyrene nanoplastics with charged and modified surface created an eco-corona which increased the NP uptake, ecotoxicity, and caused a longer gut retention time with effects on feeding rate [111]. However, the environmental relevance of these surface modifications is questionable, since such modifications are not expected to be part of the natural weathering process of MNPs. Fotopoulou et al. [207] observed significant alteration of functional groups on the surface of eroded PE pellets, whereby the altered surface acquired a negative charge due to ketone groups. Particles of weathered PP, on the other hand, were reported by these authors to remain neutral. Severe toxicity was observed in sea urchin embryos (*Paracentrotus lividus*) after incubation with amine (PS-NH₂) polystyrene, and in a lesser extent with carboxylated (PS-COOH) polystyrene. Both nanoparticle types, notably PS-COOH, aggregated partially with time and only PS-COOH accumulated inside embryo's digestive tract [208]. However, when these NPs encountered biological fluids (i.e., coelomic), they became covered by a protein-corona, which conferred identical colloidal features to PS-NH₂ and PS-COOH particles, both acquiring a monodisperse size distribution and a negative potential in the coelomic fluid [209]. It has been also evidenced that NPs translocated to mussel hemolymph after ingestion may specifically bind to plasma proteins, forming a protein corona that can affect particle uptake and toxicity in target cells [198] (see above).

Overall, the extent to which MNP particle translocation occurs, the uptake mechanism, tissue distribution, and potential accumulation of particles are still poorly understood and represents a major obstacle in assessing their risk in aquatic organisms. The associated effects following intake of MNPs will be discussed further below.

9.7.2 Physical effects

Physical effects of MNPs

Although a few laboratory studies report little or no physical harm to aquatic biota [210–213], by far, most laboratory studies reveal adverse effects on marine and freshwater organisms at various levels of biological organization, from changes in gene expression, inflammation, and energy allocation to effects on reproduction, immune system, and central nerve system to death [23, 214, 215] (Table 9.2). In several of these cases, it is not clear if the effect is particle-related or caused by associated toxic co-contaminants or impurities. An example of a typical physical effect is perhaps the study of [18] exposing the polychaete worm, *Arenicola marina* (a deposit feeder) to unplasticised polyvinylchloride (UPVC) hold in sediments spiked at concentrations coinciding with high levels found in the environment. The worms showed reduced feeding activity, increased gut residence time of ingested particles, inflammation and significantly depleted energy stores by up to 50% compared to control. Such energy-reduced effects, in the above case mainly linked to a reduction in lipid reserves, can have an impact on growth, reproduction, and ultimately, survival. Other studies have shown similar effects on energy budget, but negative effects on the fecundity and reproductive, immune system, and behavior have also been reported. Immunological effects have been reported for micro- and nano-sized plastic particle interactions with marine invertebrates by several research groups, indicating that in marine invertebrates the immune function represents a potential target for plastic (polystyrene) nano-plastics [202, 216].

9. *Micro and nanoplastics in the aquatic environment with special reference to synthetic fibers*

Table 9.2.: Selected examples of frequently reported effects observed in marine and freshwater biota after exposure to MNPs in laboratory studies.

Species	Observed effect	Reference
MARINE BIOTA		
Marine bacteria	Effects on ecological function, oxidative stress, grow inhibition	[217]
Microalgae	Reduced chlorophyll content	[210]
	Lower feeding rates; negative effects on growth and photosynthesis	[218]
	Reduced growth	[219]
	Inhibition of photosynthesis and promotion of ROS	[220]
Ascidians	Slowed down metamorphosis, growth inhibition	[221]
Sea urchin	Developmental defects	[208]
Copepod	Reductions in fecundity	[222]
	Increased immune response, lower feeding rates	[223]
Blue Mussel	Oxidative stress, reduced lysosomal membrane stability, cell damage, inflammation, granuloma formation	[201]
	Damaged ecophysiological functions	[224]
Mediterranean mussel	Alterations of immunological responses, lysosomal compartment, peroxisomal proliferation, antioxidant system perturbations and genotoxicity; altered gene expression	[225]
Brown mussel	Impaired larval development	[226]
Asian green mussel	Reduced filtration behavior, respiration rate and byssus production	[227]
Pacific Oyster	Immune system modulation and alteration of homeostasis	[228]
	Decrease in fertilization and embryogenesis success	[229]
Pearl oyster	Impact on assimilation efficiency and energy balance, with negative repercussions on reproduction	[230]
Lugworm	Effects on fitness and bioaccumulation, reduced feeding capacity	[210]
	Reduced feeding, weight loss and oxidative stress	[224]
	Reduced growth, inflammation	[18]
Oyster, sea urchin, copepod	Decreased fecundity; negative impacts on subsequent generations	[223, 231–233]
FRESHWATER BIOTA		
Microalgae	Growth inhibition (enhanced by enhanced growth), oxidative stress	[234]
	Growth inhibition	[219]
	Inhibited algal photosynthesis and growth; promotion of ROS indicative of oxidative stress	[220]
Polyp	Significant changes in morphology	[235]
Copepod	Effects on fecundity, survival and feeding	[236]
Nematod	Significant reduction in survival, decreased body length and reproduction impairment	[237]
	Decreased survival	[238]
Water flea	Lower feeding and reproduction at high microplastic levels	[239]
	Inhibited reproduction and induced abnormal embryonic development	[240]
	Inhibition of hatching, decreased growth rates, and altered feeding preferences and innate behaviors	[241]
Crucian carp	Effects on behavioral and fat metabolism	[108]
	Brain damage, behavioral disorders	[204]
Common goby	Decrease in predatory performance	[242]

Continued on next page

Table 9.2 – continued from previous page

Species	Observed effect	Reference
Zebrafish	Increased activity of antioxidant enzymes inflammation and lipid accumulation in liver, altered metabolic profile in liver	[243]
	Intestinal damage, including cracking of villi and splitting of enterocytes	[237]
	Inhibited larvae locomotion	[244]

More toxic effects of smaller microplastics below 10 µm were reported in aquatic organisms, compared to plastic particles of larger size. The majority of lab exposure studies have used nano-sized plastic particles that appear to be more readily absorbed and accumulated in tissues of aquatic species [204, 245, 246]. Several studies indicate that microplastic fragments or irregular fluffy microplastics were readily ingested by different species [201, 247, 248], and in some cases effects of these irregular shaped microplastics were observed, while by comparison spherical microplastics did not reveal any effect [248], indicating that particle shape, in addition to their separate influence on uptake, can influence the effects of MNPs. In box 9.1 and 9.2, we have summarized laboratory studies of MNPs on phytoplankton and marine mussel respectively, which elucidate insights into possible mechanisms underlying the observed microplastic effects.

Box 9.1: Effects on phytoplankton

The risk that MNPs may affect autotrophic phytoplankton that form the basis of the aquatic food chains and represent the major global source of oxygen to the atmosphere is of particular concern. Several studies have demonstrated negative effects on marine and freshwater phytoplankton species under laboratory conditions. Negatively charged nano-PS can sorb to microalgae, inhibiting microalgal photosynthesis and promoting ROS [220]. Furthermore, nano-PS (0.22 and 103 mg l⁻¹) exposure to microalgae affects the growth and photosynthesis in terms of reduced chlorophyll content [210]. No effects of negatively charged and uncharged PS particles (0.05, 0.5 and 6 µm) on microalgal photosynthesis were noticed. However, microalgae growth was negatively affected (up to 45%) by uncharged PS particles, but only at high concentrations (250 mg l⁻¹). These effects were demonstrated to increase with decreasing particle size [219]. In another study a negative effect of PVC particles on growth (up to 39.7%) was seen only at high concentration (50 mg l⁻¹). Toxic effects were likely to be caused by absorption and aggregation [218]. The above findings are not always consistent, for example, Besseling et al. [210] found effects on the growth and photosynthesis, while Sjollem et al. [219] and Lagarde et al. [249] observed no changes in algal growth rate but a significant reduction in photosynthesis. These differences may be due to different experimental test conditions. Lagarde et al. [249] presented the first evidence on microplastic-induced molecular toxicity in freshwater microalgae, *Chlamydomonas reinhardtii*. Exposure to high density polyethylene (HDPE) and polypropylene (PP) particles induced hetero aggregates consisting of microplastics, microalgae, and exopolysaccharides, eventually leading to vertical pathway transfer of microplastics from surface water to sediment. This was evidenced by elevated expression of genes (UGD and UGE) involved in rhamnose and xylose synthesis representing exopolysaccharide biosynthesis pathway elevated gen-expression [249].

Box 9.2: Effects on marine bivalve mollusks

The biology of filter feeding bivalves such as mussels and oysters makes them particularly suitable models for investigating the fate and effects of MNPs in organisms. Bivalves have a highly developed phagocytosis process for the cellular internalization of particles from 0.1 to 100 µm to intracellular digestion and cellular immunity [250], and they can select their food particles using various criteria, including size [18, 251]. Internalization of

9. Micro and nanoplastics in the aquatic environment with special reference to synthetic fibers

MPs in bivalves can occur by means of two routes: i) MPs can be trapped by gills through microvilli activity and endocytosis processes, and; ii) they can be taken up via ciliary movement in the digestive system and subsequent translocation to the hemolymph (reviewed by Franzellitti et al. [29]). Bivalve pallial cavity is of vital importance as a portal and barrier to invade microorganism and microparticles, and the mucus layer secreted by pallial organs (gills, mantle, etc.) generally allows to effectively capture particles as small as 3–4 μm and smaller [18]. Therefore, bivalves are effective concentrators of MNPs from the surrounding environment.

The ingestion, bioaccumulation, and translocation of plastic microparticles by bivalves, with particular reference to mussels, has been demonstrated in numerous studies [252–255]. Physical blockages and biological changes have been described in *Ostrea edulis* by ingestion of MPs [256]. Polystyrene microspheres filtered by *Mytilus edulis* were found to be accumulated in gut and digestive tubules and subsequently translocated into hemolymph and hemocytes [200]. A significant reduction in the filtration rate was observed in mussels exposed to microplastic fibers (459 ± 2.25 (SE) μm), although more than 70% of fiber uptake by mussels were also found to be quickly rejected as pseudofeces, with approximately 9% ingested and < 1% excreted in feces [257]. There are evidences pointing that small MPs in the digestive gland are slower processed and eliminated than larger ones, and that a translocation of small MPs occurs from the digestive system to the gills [197]. Indeed, there is evidence indicating that bivalves are more likely to consume smaller MPs instead of larger microfibers [258]. More recently, microfibers have been observed in foot, mantle, and fused in to the byssus of mussels in experimental exposure experiments, and the adherence and fusion to these and other organs has been proposed as a novel way for mussels to uptake microplastics beyond ingestion, contributing about 50% of the microplastic uptake in mussels [259, 260].

Innate immune defence in mussels is comprised of cell-mediated and humoral mechanisms, in which hemocytes are primarily responsible for defence against parasites and pathogens. Consequently, immune functional parameters of bivalves are used as a model for investigating the major mechanisms involved, modes of actions and effects of MNPs on innate immune responses in organisms. Several *in vivo* studies have found that experimental exposure of *Mytilus galloprovincialis* to virgin MNPs may trigger upregulation of lysosome and immune-related functions, such as changes in hemolymph total cell counts, phagocytosis-related activities, extracellular lysozyme and oxyradical production and cause significant effects on the cellular (lysosomal membrane destabilization, genotoxic effects) and tissue level responses associated with infiltration of immune cells (suggestive of inflammatory processes) besides a modulation of antioxidant defenses and detoxification enzymes [201, 225, 261–263].

In vitro studies hemocytes of *M. galloprovincialis*, which have also evidenced immunomodulation (including increase in extracellular reactive oxygen species and nitric oxide production) and apoptotic processes induced by cationic polystyrene nanoparticles (PS-NH₂ NPs) [216]. The formation of a protein-corona complex around cationic polystyrene nanoparticles incubated in hemolymph serum has been described [264]. The authors found that cellular/lysosomal damage, ROS production, and p-p38MAPK levels were higher when cells were exposed to nanoplastics in hemolymph serum than in seawater, demonstrating that biological fluids can affect NP impact in marine species [264]. Lastly, it has been found that exposure to virgin micro-PS leads to an imbalance of energy reserves causing feeding alterations and reproductive disruption in oysters *Crassostrea gigas* (significant reductions in oocyte number and decreased sperm velocity) with impacts on offspring (significant reduced larval count and larval development) [231]. However, the ecological relevance of the observed sublethal effects under laboratory conditions is limited or remains unclear for reasons which are later discussed (see paragraph 9.7.5).

Physical effects of synthetic fibers

By far, most lab studies reported in the literature used regular shaped microplastics, i.e., microbeads of spheres, and not microfibers. Laboratory exposure studies using fibers are largely limited mostly to crustaceans, mostly small species (Table 9.3). Reported effects including mortality are limited to crustaceans, in particular amphipods and copepods. The majority of ingested microplastics reported in field studies were fibers, and several studies indicate that this shape of microplastics appear to have a higher potential than other forms of microplastics to enter the food chain (see above). It is unclear whether this shape is more bioavailable and may also influence the severity of resulting biological effects due to increased risk for entanglement and increased gut passage time. Differences in biological response due to the shape of microplastics, especially fibrous shapes, are however not well understood. Compared to other particle shapes, fibers may have (1) a greater potential to entangle the gut contents or externalities; (2) increased gut passage time; (3) increased chemical reactivity (and resulting effects) due to relatively large surface area to volume ratio. More research is needed to confirm whether entanglement of fiber-shaped microplastics could worsen adverse effects [13, 18].

Table 9.3.: Observed effects in marine and freshwater biota after exposure to synthetic fibers in laboratory studies.

Species	Exposure conditions	Observed effects	Reference
Marine lobster (<i>Nephrops norvegicus</i>)	PP fibers (from ropes) 3-5 mm in length and 0.2 mm in diameter; five fibers per feeding; uncertain what proportion of ingested plastic is retained in the foregut; fed and starved controls were used.	Reduced body mass and reductions in blood protein and stored lipids.	[265]
Marine crab (<i>Carcinus maenas</i>)	PP fibers (from ropes) (1-5 mm in length chronic 4 week feeding studies, crabs that ingested food containing microfibers (0.3-1.0 % plastic by weight).	Effect on food consumption and energy balance (scope for growth).	[266]
Marine copepod (<i>Calanus finmarchicus</i>)	Mixture of cultured microalgae (control), $\sim 50 \text{ ml}^{-1}$ of nylon granules (10-30 μm or nylon fibers (10 \times 30 μm), similar in shape and size to the microalgal prey.	Nylon fibers: altered prey selectivity ($P < 0.01$) and nonsignificant 40% decrease in algal ingestion rates. Nylon granules and fibers: premature moulting in juvenile copepods.	[267]
Freshwater amphipod (<i>Hyalella Azteca</i>)	PE particles and PP fibers; conducting 10-d and 42-d bioassays using individual 250 ml chambers.	Acute EC50: PE particle and PP fibers 4.64×10^4 and 71.43 particles/fibers per ml respectively. Observed chronic effects: decreased growth and reproduction.	[268]
Freshwater amphipod (<i>Gammarus fossarum</i>)	PA fibers; 50-200 μm ; exposure levels: 100, 540, 2680, 13,380 fibers cm^{-2} base area of glass beakers.	Reduced assimilation efficiency, reduced weigh. Found in gut after 0.5 hr of exposure; egestion in 16 h after exposure stop; No effects with PS 1.6 mm beads.	[269]
Freshwater crustacean (<i>Daphnia magna</i>)	PET textile microfibers (length range: 62-1400 μm , width 31-528 μm , thickness 1-21.5 μm).	Ingestion of very long microfibers (even 1400 μm long); increased mortality, even after 24 h of exposure in MP free medium following 48 h of MP exposure.	[13]

9. Micro and nanoplastics in the aquatic environment with special reference to synthetic fibers

Blarer et al. [269] found reduced assimilation efficiency and weight after ingestion of PA fibers (50-200 μm) in freshwater amphipod (*Gammarus fossarum*) while no effects were present after ingestion of 1.6 mm PS microbeads. Jemec and Drobne [13] exposed *Daphnia magna* to a size range of PET textile microfibers (62–1400 μm) and found that while the majority of ingested fibers were around 300 μm , some very large twisted microfibers even up to 1400 μm were present inside the gut. As noted above, several studies have shown that the size, shape, and surface physicochemical characteristics of MNPs are essential determinants of their fate and effects. However, this knowledge is mainly based on studies using spherical and other non-fibrous MNPs. Cole et al. [267], exposing marine copepods to nylon fibers vs nylon granules, found that shape and chemical profile of a MP can influence its bioavailability and toxicity. Exposure to nylon fibers caused significant shifts in prey selectivity resulting in a 40% decrease in algal ingestion rates, while nylon granules negatively affected lipid accumulation.

The limited use of plastic microfibers and nanofibers in experimental work has provided a very limited view on their fate and potential effects. In addition to this, there are several limitations related with the experimental design of published laboratory findings that hamper translation of the findings to the field situation in nature, which will be described in 9.7.6.

9.7.3 Chemical-mediated effects of MNPs

With the sorption of chemicals on MNPs, the transfer of harmful substances such as persistent organic pollutants (POPs), can lead to organic bioaccumulation of such contaminants within the upper part of the food chain [210]. Nevertheless, laboratory studies and model estimates indicate that the relative importance of MNPs as a carrier of hydrophobic organic chemicals is low compared to other media (for review, see Koelmans et al. [90, 270]). However, the bioaccumulation can vary depending on polymer nature, chemical type, and fish species traits [88]. Microfibers exhibit a high surface to volume ratio compared to non-fibrous microplastic shapes and thus may exhibit enhanced pollutant-sorption performance and bioavailability of toxic compounds. Thus, the combined effects of microplastics, in particular microfibers, and other pollutants, including persistent organic pollutants (POPs) and heavy metals, through aquatic food chains requires further attention. The real risk for aquatic and human consumers still needs to be elucidated [172, 181].

Mechanisms potentially contributing to chemical impacts of microplastic particles and microfibers on aquatic biota include leaching of plastic additives and transfer of sorbed compounds such as POPs and metals. The chemical effect on organisms mediated via the ingestion of MNPs depends on the amount and nature of both the polymeric materials and sorbed/desorbed hydrophobic pollutants. Uptake and negative effects of additives and sorbed contaminants attributed to leaching from plastics has been documented in several cases [224, 225, 232, 271–275]. Several of these studies showed that microplastics and sorbed chemicals had a greater effect than chemicals alone; other studies did not reveal such effects [276, 277]. This can be largely contributed to the different experimental test conditions used in these studies. The combined effect of microplastics and sorbed co-contaminants in aquatic organisms is still not well understood. Some studies found additive effects of microplastics and sorbed contaminants, others did not find such combined effects. For example, Rainieri et al. [275] exposed zebrafish to feed spiked with 2% microplastics (LD-PE 125–250 μm of diameter) or a sorbed mixture of PCBs, BFRs, PFCs and methylmercury and a combination of both. After 3 weeks of exposure, microplastics alone did reveal no relevant health effects on zebrafish, but the combined effect of microplastics and sorbed contaminants caused significant organ toxicity in a greater manner than the contaminants alone.

The above studies suggest that ingestion of microplastics can move additives and sorbed pollutants into the tissues of organisms at concentrations that are sufficient to cause health effects or ecophysical functions (e.g., [83, 224, 278]). However, in most of these cases, it will be difficult to separate physical effects of the polymeric material and chemical effects caused by desorption from the particles.

Several studies indicate that so-called virgin microplastics are toxic to the larval stage of aquatic organisms through the leaching of chemicals, with subsequent consequences for the evaluation of microplastic laboratory experiments.

Martínez-Gómez et al. [233] evaluated the effects of virgin, weathered, and leachate of PS 6 µm and HDPE fluff particles < 80 µm in the sea urchin, *Paracentrotus lividus*. During the 48-h exposure time, fertilization and larval development were significantly impaired. The authors concluded that sea urchin embryotoxicity was attributed to the chemical leachate of the exposed plastic particles. Major identified compounds likely responsible for the observed effects were aliphatic hydrocarbons (C14, C16, C18, C20, and C22) from HDPE and styrene monomers from PS particles [279]. Embryotoxicity and impairment of larval development was also reported after exposure of brown mussel to PP microplastic leachate [226]. This makes the point that previous studies using virgin microplastics may have difficulties of separating between physical and chemical effects, and that weathered microplastics should provide more realistic exposure scenarios. Cleaning the MP particles with organic solvent may be insufficient to stop continuous leakage of chemical co-contaminants or residual monomers, such as styrene, which is known to be toxic to aquatic organisms.

Despite this, there is some evidence for effects of MPs on organisms at environmentally relevant concentrations. Rochman et al. [83] demonstrated that the ingestion of plastic microdebris (PE particles and associated chemicals) by Japanese medaka (*Oryzias latipes*) at environmentally relevant concentrations in sea water is capable of altering endocrine system function. However, a critical review of published studies and empirical evidence by Koelmans et al. [270] concluded that the ingestion of contaminated microplastics was not likely to increase the overall exposure to and risk of hydrophobic organic chemicals in marine organisms, highlighting current uncertainty in impacts. In a study by our group, ingestion of PCB-spiked microplastics by Norway lobster (*Nephros norvegicus*) showed limited PCB bioaccumulation for polyethylene and negligible PCB bioaccumulation for polystyrene. No PCB depuration from lobster tissue to microplastics was observed [93]. A similar conclusion was reached independently using a modelling approach. Transfer of sorbed organic contaminants from microplastics was modelled to marine biota using the model OMEGA (Optimal Modelling for Ecotoxicological Applications) with different conditions of temperature, pH and gut surfactants. There was a negligible input from plastic compared to intake from food and water under both relevant and worst-case scenarios [280]. However, given the discrepancies in research results and the many uncertainties in risk assessment of microplastics and sorbed chemicals, more research is needed in this area.

9.7.4 Microbial effects of MNPs

An increasing number of studies provide ample evidence that potential pathogenic bacteria (e.g., *Vibrio spp.*, *Aeromonas salmonicida*) bind particularly strong to plastic debris [91, 100, 101, 281]. In several studies, for example, the bacterial richness including *Vibrio spp.* was higher on MPs than in the surrounding seawater, [102, 282, 283]. Other studies were unable to confirm an enrichment of *Vibrio spp.* with plastic [282–284]. Gene sequencing analysis has shown that the microbial assemblages associated with marine MPs are very diverse and different between geographical zones, the greater species richness found at lower latitudes [30, 97, 285]. Research on riverine microplastics showed that bacteria assembling differently on riverine microplastics have lower taxa richness, diversity, and evenness on plastic than on non-plastic substrates [286]. Especially, plastic polluted surface waters which directly receive urban storm water or raw sewage effluents may pose direct plastic associated microbial risks, including the spread of potential pathogens and antimicrobial resistance (AMR). It has been shown that microplastic particles and fibers passing through sewage treatment plants may become enriched with pathogens [100] and subsequently may then be dispersed to the marine environment [99]. However, so far there is no evidence that microplastic-associated pathogens, AMR, and biotoxins caused health effects in aquatic organisms. Extensive multidisciplinary research is needed to identify disease risks, ecological impacts and potential implications for human health [99]. A key question concerns whether and how long microbial pathogens may persist on aquatic MPs and whether they pose a potential risk to aquatic ecosystems.

9.7.5 Potential ecological effects of MNPs

Although hypothesized, the ubiquitous, persistent, and anticipated increase of microplastic pollution could in the long-term reach concentrations that physically alter ecologically significant processes. Several studies have proposed potential ecological impacts of microplastics that could provide avenues for future research. For example, the potential of MP pollution to alter ecosystem microbial function [287], whether MP pollution could affect the functioning and structure of sedimentary environments and the structure of benthic assemblages [288, 289], and the potential impact of microplastics on marine pelagic primary producers [290]. The assessment of potential ecological impacts strongly relies on predictions from experimental studies and modelling studies [291] and more thorough research is needed before refined and more reliable assessments can be made.

9.7.6 Field evidence and ecological relevance of laboratory studies

Biological effects of microplastics in the field have not been demonstrated, mainly due to the fact that the environmental concentrations detected are below laboratory effect thresholds and these effects are non-specific and difficult to separate from the effect of associated chemicals [27, 292] and similar effects caused by other multiple natural and anthropogenic stressors acting on aquatic animals and ecosystems. The many uncertainties and knowledge gaps as highlighted throughout this chapter seriously hamper an adequate MNP risk assessment.

In the absence of field evidence for MNPs, one must rely on the available laboratory exposure studies, which for several reasons are difficult to extrapolate meaningfully to effects likely to occur in the field. Most of the studies looking at the effects of microplastics on model organisms are fraught with one or more of the following limitations: (1) conducted at unrealistically high MP concentrations, using only one type of particular polymeric particle, while aquatic organisms in nature are exposed to much lower concentrations and also much larger diversity of plastic particles; (2) lack information on dose-response curves; (3) used particles smaller than those reported from the field; (4) used virgin particles not taking the physical-chemical weathering, eco-corona/microbial biofilm interactions into their effect assessment; (3) lack of reference natural (non-plastic) particles as control treatment; (5) laboratory studies are typically short term (and high concentration), whilst in reality exposure is of a chronic nature and at low concentration (high dose acute exposure versus low dose chronic exposure). Clearly, these experimental limitations hinder translation of the observed effects to the actual field situation. Moreover, not unimportantly, to date, only a handful of experiments with fibrous MNPs, the environmentally most prevalent plastic particle shape, have been conducted. It is evident that the experimental results derived of lab-based MNP studies have only limited ecological relevance and are difficult to translate to the real nature [293].

Adverse effects in biota have rarely been shown experimentally at environmentally relevant concentrations of MNPs. Still, despite their limitations, the majority of reported laboratory studies on MNP health effects are at levels that are sub-organismal or affect individual organisms. That said, it is clear that most of the observed toxicity endpoints, such as survival, growth, and reproduction are of high ecological relevance and can potentially impact ecosystem function [246]. Provisional risk assessments show that current MP levels likely do not pose a widespread ecological risk, except in some coastal locations [28]. However, as said previously, a full characterisation of the risk of MNPs in the aquatic environment is not yet feasible, due to large data gaps. Laboratory and field-derived data to inform more comprehensive ecological risks assessments of MNPs are needed and expected to rapidly grow, as the levels of MNP are expected to increase in the future and the subject will continue to attract significant scientific attention.

9.8 Key conclusions

- Micro and nanoplastics are highly complex mixtures of polymer materials, chemical contaminants, and biological agents. They exhibit variable properties (particle composition, size, density, charge, toxicity, aggregation

- state, age, associated epibiota), representing a diverse and complex class of environmental contaminants.
- Microplastics, often in the form of microfibers, are common in both marine and freshwater systems from around the world. Current field data generally document only the larger plastic particles and fibers, seriously limiting field assessments. PP, PE, polyester, PET, HDPE, LDPE, PVC, and cellophane are most common polymer types; rayon, polyacrylonitrile, nylon only occasionally reported.
 - Synthetic fibers are the most prevalent type of aquatic microplastics, and their occurrence appears to be related to effluents, fishing activity, and atmospheric deposition.
 - Heterogeneous sampling methodologies and units are often applied resulting in poor quality data, hampering comparison with other studies. Microfibers are particularly difficult to monitor as they are pervasive throughout environment and laboratory.
 - MNP debris is an emerging multi-stressor in the aquatic environment due to the physical hazards of the polymeric material, and the chemical and microbial hazards associated with it.
 - There is ample laboratory evidence that exposure to MNPs can impact aquatic species across many taxa at various levels of biological organization, albeit at high concentrations. But there is only limited evidence from nature with many gaps in our understanding. Smaller particles are more harmful than large particles and micro-fibers are more harmful than non-fibrous particles.
 - The fate and effects of synthetic and natural microfibers are understudied and poorly understood.

9.9 Key knowledge gaps and research priorities

Our overview of the current state of knowledge on aquatic MNPs displays important research gaps which need to be filled in order to investigate the possible risks posed by MNPs. Major knowledge gaps are summed up below.

- For all aquatic compartments, there is a pressing need for improved characterization and quantification of MNPs and standardized methods for sampling and analysis. Good quality data on microfibers deserves special attention.
- A particular challenge is the development of analytical methods for small microplastics up to several micrometers and down to the nanoscale in aquatic matrices.
- There is a clear need for chronic experiments with environmentally relevant concentrations, particle sizes, shapes and compositions relative to natural particles. Special attention deserves microfiber fate and effects.
- Given the ubiquity of microplastics in our aquatic environments, there is a need to assess population and ecosystem level effects of increasing MNP pollution.
- Another challenge is to better understand how MNPs are cycled through aquatic ecosystems, where they go and how they degrade.
- Future research should elucidate the role of MNPs as a transport vector of pathogens, antibiotic resistance and biotoxins and the potential for dispersing diseases in aquatic systems and humans.

References

- [1] C. Wilcox, E. Van Sebille, and B. D. Hardesty. “Threat of plastic pollution to seabirds is global, pervasive, and increasing”. In: *Proceedings of the national academy of sciences* 112.38 (2015), pages 11899–11904 (cited on page 111).
- [2] Statista. *Global production of plastics since 1950*. 2017. URL: <https://www.statista.com/statistics/282732/global-production-of-plastics-since-1950/> (cited on page 111).
- [3] J. Boucher and D. Friot. *Primary microplastics in the oceans: a global evaluation of sources*. IUCN Gland, Switzerland, 2017 (cited on pages 111–113).
- [4] D. Eerkes-Medrano, R. C. Thompson, and D. C. Aldridge. “Microplastics in freshwater systems: a review of the emerging threats, identification of knowledge gaps and prioritisation of research needs”. In: *Water research* 75 (2015), pages 63–82 (cited on pages 111–113, 121).

- [5] J. Li, H. Liu, and J. P. Chen. “Microplastics in freshwater systems: A review on occurrence, environmental effects, and methods for microplastics detection”. In: *Water research* 137 (2018), pages 362–374 (cited on pages 111, 121).
- [6] H. A. Leslie, S. H. Brandsma, M. J. M. Van Velzen, and A. D. Vethaak. “Microplastics en route: Field measurements in the Dutch river delta and Amsterdam canals, wastewater treatment plants, North Sea sediments and biota”. In: *Environment international* 101 (2017), pages 133–142 (cited on pages 111, 113, 118).
- [7] C. J. Foley, Z. S. Feiner, T. D. Malinich, and T. O. Höök. “A meta-analysis of the effects of exposure to microplastics on fish and aquatic invertebrates”. In: *Science of the total environment* 631 (2018), pages 550–559 (cited on page 111).
- [8] M. Wagner, S. Lambert, and M. W. Lambert. *Freshwater microplastics*. Springer International Publishing Cham, Switzerland, 2018 (cited on page 111).
- [9] W. Luo, L. Su, N. J. Craig, F. Du, C. Wu, and H. Shi. “Comparison of microplastic pollution in different water bodies from urban creeks to coastal waters”. In: *Environmental pollution* 246 (2019), pages 174–182 (cited on page 111).
- [10] J. R. Jambeck, R. Geyer, C. Wilcox, T. R. Siegler, M. Perryman, A. Andrady, R. Narayan, and K. L. Law. “Plastic waste inputs from land into the ocean”. In: *Science* 347.6223 (2015), pages 768–771 (cited on page 111).
- [11] P. Villarrubia-Gómez, S. E. Cornell, and J. Fabres. “Marine plastic pollution as a planetary boundary threat—The drifting piece in the sustainability puzzle”. In: *Marine policy* 96 (2018), pages 213–220 (cited on page 111).
- [12] R. C. Thompson, Y. Olsen, R. P. Mitchell, A. Davis, S. J. Rowland, A. W. John, D. McGonigle, and A. E. Russell. “Lost at sea: where is all the plastic?” In: *Science* 304.5672 (2004), pages 838–838 (cited on page 111).
- [13] A. Jemec and D. Drobne. “From nanoparticles to microplastics: retrospective and prospective views”. In: *Arhiv za higijenu rada i toksikologiju* 67 (2016), page 31 (cited on pages 111, 127, 128).
- [14] P. Kershaw, A. Turra, F. Galgani, et al. “Guidelines for the Monitoring and Assessment of Plastic Litter in the Ocean—GESAMP Reports and Studies No. 99”. In: *GESAMP Reports and Studies* (2019) (cited on pages 111, 116, 117).
- [15] N. B. Hartmann, T. Hüffer, R. C. Thompson, M. Hassellöv, A. Verschoor, A. E. Daugaard, S. Rist, T. Karlsson, N. Brennholt, M. Cole, M. P. Herrling, M. C. Hess, N. P. Ivleva, A. L. Lusher, and M. Wagner. “Are we speaking the same language? Recommendations for a definition and categorization framework for plastic debris”. In: *Environmental science & technology* 53.3 (2019), pages 1039–1047 (cited on page 111).
- [16] K. Liu, T. Wu, X. Wang, Z. Song, C. Zong, N. Wei, and D. Li. “Consistent transport of terrestrial microplastics to the ocean through atmosphere”. In: *Environmental science & technology* 53.18 (2019), pages 10612–10619 (cited on pages 111–113).
- [17] M. Cole. “A novel method for preparing microplastic fibers”. In: *Scientific reports* 6 (2016), page 34519 (cited on page 111).
- [18] S. L. Wright, R. C. Thompson, and T. S. Galloway. “The physical impacts of microplastics on marine organisms: a review”. In: *Environmental pollution* 178 (2013), pages 483–492 (cited on pages 112, 116, 123–127).
- [19] M. Cole, P. Lindeque, C. Halsband, and T. S. Galloway. “Microplastics as contaminants in the marine environment: a review”. In: *Marine pollution bulletin* 62.12 (2011), pages 2588–2597 (cited on page 112).
- [20] J. A. I. do Sul and M. F. Costa. “The present and future of microplastic pollution in the marine environment”. In: *Environmental pollution* 185 (2014), pages 352–364 (cited on page 112).
- [21] M. Wagner, C. Scherer, D. Alvarez-Muñoz, N. Brennholt, X. Bourrain, S. Buchinger, E. Fries, C. Grosbois, J. Klasmeier, T. Marti, et al. “Microplastics in freshwater ecosystems: what we know and what we need to know”. In: *Environmental sciences Europe* 26.1 (2014), pages 1–9 (cited on page 112).
- [22] P. Kershaw. *Sources, fate and effects of microplastics in the marine environment: a global assessment*. Technical report. International Maritime Organization, 2015 (cited on page 112).
- [23] P. J. Kershaw and C. M. Rochman. “Sources, fate and effects of microplastics in the marine environment: part 2 of a global assessment”. In: *Reports and studies-IMO/FAO/Unesco-IOC/WMO/IAEA/UN/UNEP Joint Group of Experts on the Scientific Aspects of Marine Environmental Protection (GESAMP) eng no. 93* (2015) (cited on pages 112, 114, 115, 118, 119, 121, 123).
- [24] K. Duis and A. Coors. “Microplastics in the aquatic and terrestrial environment: sources (with a specific focus on personal care products), fate and effects”. In: *Environmental sciences Europe* 28.1 (2016), page 2 (cited on pages 112, 113, 118).
- [25] H. Auta, C. Emenike, and S. Fauziah. “Distribution and importance of microplastics in the marine environment: a review of the sources, fate, effects, and potential solutions”. In: *Environment international* 102 (2017), pages 165–176 (cited on page 112).

- [26] A. A. Horton, A. Walton, D. J. Spurgeon, E. Lahive, and C. Svendsen. “Microplastics in freshwater and terrestrial environments: evaluating the current understanding to identify the knowledge gaps and future research priorities”. In: *Science of the total environment* 586 (2017), pages 127–141 (cited on pages 112, 113, 118).
- [27] E. E. Burns and A. B. Boxall. “Microplastics in the aquatic environment: Evidence for or against adverse impacts and major knowledge gaps”. In: *Environmental toxicology and chemistry* 37.11 (2018), pages 2776–2796 (cited on pages 112, 118, 130).
- [28] B. Koelmans, S. Pahl, T. Backhaus, F. Bessa, G. van Calster, N. Contzen, R. Cronin, T. Galloway, A. Hart, L. Henderson, et al. *A scientific perspective on microplastics in nature and society*. SAPEA, 2019 (cited on pages 112, 121, 130).
- [29] S. Franzellitti, L. Canesi, M. Auguste, R. H. Wathsala, and E. Fabbri. “Microplastic exposure and effects in aquatic organisms: A physiological perspective”. In: *Environmental toxicology and pharmacology* (2019) (cited on pages 112, 126).
- [30] J.-Q. Jiang. “Occurrence of microplastics and its pollution in the environment: A review”. In: *Sustainable production and consumption* 13 (2018), pages 16–23 (cited on pages 112, 129).
- [31] J. U. Skåre, J. Alexander, M. Haave, I. Jakubowicz, H. K. Knutsen, A. Lusher, M. Ogonowski, K. E. Rakkestad, I. Skaar, L. E. Sverdrup, et al. “Microplastics; occurrence, levels and implications for environment and human health related to food. Scientific opinion of the Scientific Steering Committee of the Norwegian Scientific Committee for Food and Environment”. In: *VKM Report* (2019) (cited on pages 112, 117).
- [32] S. Estahbanati and N. L. Fahrenfeld. “Influence of wastewater treatment plant discharges on microplastic concentrations in surface water”. In: *Chemosphere* 162 (2016), pages 277–284 (cited on page 112).
- [33] A. Sanchez-Vidal, R. C. Thompson, M. Canals, and W. P. de Haan. “The imprint of microfibrils in southern European deep seas”. In: *PloS one* 13.11 (2018) (cited on pages 112, 119).
- [34] L. C. Lebreton, J. Van Der Zwet, J.-W. Damsteeg, B. Slat, A. Andrady, and J. Reisser. “River plastic emissions to the world’s oceans”. In: *Nature communications* 8 (2017), page 15611 (cited on page 112).
- [35] G. Gatidou, O. S. Arvaniti, and A. S. Stasinakis. “Review on the occurrence and fate of microplastics in Sewage Treatment Plants”. In: *Journal of hazardous materials* 367 (2019), pages 504–512 (cited on pages 112, 113).
- [36] C. M. Rochman. “Microplastics research—from sink to source”. In: *Science* 360.6384 (2018), pages 28–29 (cited on pages 112, 118).
- [37] F. S. Cesa, A. Turra, and J. Baruque-Ramos. “Synthetic fibers as microplastics in the marine environment: a review from textile perspective with a focus on domestic washings”. In: *Science of the total environment* 598 (2017), pages 1116–1129 (cited on page 112).
- [38] P. J. Kole, A. J. Löhr, F. G. Van Belleghem, and A. M. Ragas. “Wear and tear of tyres: a stealthy source of microplastics in the environment”. In: *International journal of environmental research and public health* 14.10 (2017), page 1265 (cited on page 112).
- [39] F. Sommer, V. Dietze, A. Baum, J. Sauer, S. Gilge, C. Maschowski, and R. Gieré. “Tire abrasion as a major source of microplastics in the environment”. In: *Aerosol and air quality research* 18.8 (2018), pages 2014–2028 (cited on page 112).
- [40] R. Dris, J. Gasperi, C. Mirande, C. Mandin, M. Guerrouache, V. Langlois, and B. Tassin. “A first overview of textile fibers, including microplastics, in indoor and outdoor environments”. In: *Environmental pollution* 221 (2017), pages 453–458 (cited on page 112).
- [41] T. M. Karlsson, A. D. Vethaak, B. C. Almroth, F. Ariese, M. van Velzen, M. Hassellöv, and H. A. Leslie. “Screening for microplastics in sediment, water, marine invertebrates and fish: method development and microplastic accumulation”. In: *Marine pollution bulletin* 122.1-2 (2017), pages 403–408 (cited on pages 112, 114, 117–121).
- [42] K. Laitala, I. G. Klepp, and B. Henry. “Does use matter? Comparison of environmental impacts of clothing based on fiber type”. In: *Sustainability* 10.7 (2018), page 2524 (cited on page 113).
- [43] B. Henry, K. Laitala, and I. G. Klepp. “Microfibrils from apparel and home textiles: prospects for including microplastics in environmental sustainability assessment”. In: *Science of the total environment* 652 (2019), pages 483–494 (cited on pages 113, 114).
- [44] I. E. Napper and R. C. Thompson. “Release of synthetic microplastic plastic fibres from domestic washing machines: Effects of fabric type and washing conditions”. In: *Marine pollution bulletin* 112.1-2 (2016), pages 39–45 (cited on page 113).
- [45] Eunomia Research & Consulting Ltd. Bristol. *Plastics in the Marine Environment*. 2016. URL: <http://www.eunomia.co.uk/reports-tools/plastics-in-the-marine-environment/> (cited on page 113).

- [46] M. A. Browne, P. Crump, S. J. Niven, E. Teuten, A. Tonkin, T. Galloway, and R. Thompson. “Accumulation of microplastic on shorelines worldwide: sources and sinks”. In: *Environmental science & technology* 45.21 (2011), pages 9175–9179 (cited on page 113).
- [47] J. C. Prata. “Microplastics in wastewater: State of the knowledge on sources, fate and solutions”. In: *Marine pollution bulletin* 129.1 (2018), pages 262–265 (cited on page 113).
- [48] UNESCO. “The United Nations world water development report 2017: wastewater: the untapped resource; facts and figures.” In: (2017). URL: <https://unesdoc.unesco.org/ark:/48223/pf0000247153> (cited on page 113).
- [49] A. Verschoor, L. De Poorter, R. Dröge, J. Kuenen, and E. de Valk. *Emission of microplastics and potential mitigation measures: Abrasive cleaning agents, paints and tyre wear*. National Institute for Public Health and the Environment: Bilthoven, The Netherlands. 2016 (cited on page 113).
- [50] M. Bläsing and W. Amelung. “Plastics in soil: Analytical methods and possible sources”. In: *Science of the total environment* 612 (2018), pages 422–435 (cited on page 113).
- [51] S. Ziajahromi, P. A. Neale, L. Rintoul, and F. D. Leusch. “Wastewater treatment plants as a pathway for microplastics: development of a new approach to sample wastewater-based microplastics”. In: *Water research* 112 (2017), pages 93–99 (cited on page 113).
- [52] I. A. Kane and M. A. Clare. “Dispersion, accumulation and the ultimate fate of microplastics in deep-marine environments: A review and future directions”. In: *Frontiers in earth science* 7 (2019), page 80 (cited on page 113).
- [53] L. Simon-Sánchez, M. Grelaud, J. Garcia-Orellana, and P. Ziveri. “River Deltas as hotspots of microplastic accumulation: The case study of the Ebro River (NW Mediterranean)”. In: *Science of the total environment* 687 (2019), pages 1186–1196 (cited on page 113).
- [54] H. K. Imhof, N. P. Ivleva, J. Schmid, R. Niessner, and C. Laforsch. “Contamination of beach sediments of a subalpine lake with microplastic particles”. In: *Current biology* 23.19 (2013), R867–R868 (cited on page 113).
- [55] L. C. Woodall, A. Sanchez-Vidal, M. Canals, G. L. Paterson, R. Coppock, V. Sleight, A. Calafat, A. D. Rogers, B. E. Narayanaswamy, and R. C. Thompson. “The deep sea is a major sink for microplastic debris”. In: *Royal society open science* 1.4 (2014), page 140317 (cited on page 113, 119).
- [56] K. Zhang, J. Su, X. Xiong, X. Wu, C. Wu, and J. Liu. “Microplastic pollution of lakeshore sediments from remote lakes in Tibet plateau, China”. In: *Environmental pollution* 219 (2016), pages 450–455 (cited on page 113).
- [57] M. Bergmann, V. Wirzberger, T. Krumpfen, C. Lorenz, S. Primpke, M. B. Tekman, and G. Gerdt. “High quantities of microplastic in Arctic deep-sea sediments from the HAUSGARTEN observatory”. In: *Environmental science & technology* 51.19 (2017), pages 11000–11010 (cited on pages 113, 119).
- [58] I. Peeken, S. Primpke, B. Beyer, J. Gütermann, C. Kattlein, T. Krumpfen, M. Bergmann, L. Hehemann, and G. Gerdt. “Arctic sea ice is an important temporal sink and means of transport for microplastic”. In: *Nature communications* 9.1 (2018), pages 1–12 (cited on page 113).
- [59] R. Ambrosini, R. S. Azzoni, F. Pittino, G. Diolaiuti, A. Franzetti, and M. Parolini. “First evidence of microplastic contamination in the supraglacial debris of an alpine glacier”. In: *Environmental pollution* 253 (2019), pages 297–301 (cited on page 113).
- [60] M. Haave, C. Lorenz, S. Primpke, and G. Gerdt. “Different stories told by small and large microplastics in sediment—first report of microplastic concentrations in an urban recipient in Norway”. In: *Marine pollution bulletin* 141 (2019), pages 501–513 (cited on pages 113, 118).
- [61] B. D. Hardesty, J. Harari, A. Isobe, L. Lebreton, N. Maximenko, J. Potemra, E. van Sebille, A. D. Vethaak, and C. Wilcox. “Using numerical model simulations to improve the understanding of micro-plastic distribution and pathways in the marine environment”. In: *Frontiers in marine science* 4 (2017), page 30 (cited on page 113).
- [62] T. S. Galloway, M. Cole, and C. Lewis. “Interactions of microplastic debris throughout the marine ecosystem”. In: *Nature ecology & evolution* 1.5 (2017), pages 1–8 (cited on pages 113, 115).
- [63] C. M. Rochman, C. Brookson, J. Bikker, N. Djuric, A. Earn, K. Bucci, S. Athey, A. Huntington, H. McIlwraith, K. Munno, et al. “Rethinking microplastics as a diverse contaminant suite”. In: *Environmental toxicology and chemistry* 38.4 (2019), pages 703–711 (cited on page 114).
- [64] S. Mintenig, P. S. Bäumlein, A. Koelmans, S. Dekker, and A. Van Wezel. “Closing the gap between small and smaller: towards a framework to analyse nano-and microplastics in aqueous environmental samples”. In: *Environmental Science: nano* 5.7 (2018), pages 1640–1649 (cited on page 114).
- [65] R. Dris, H. Imhof, W. Sanchez, J. Gasperi, F. Galgani, B. Tassin, and C. Laforsch. “Beyond the ocean: contamination of freshwater ecosystems with (micro-) plastic particles”. In: *Environmental chemistry* 12.5 (2015), pages 539–550 (cited on pages 114, 118).

- [66] A. L. Andrady. “The plastic in microplastics: A review”. In: *Marine pollution bulletin* 119.1 (2017), pages 12–22 (cited on pages 114, 115).
- [67] V. Hidalgo-Ruz, L. Gutow, R. C. Thompson, and M. Thiel. “Microplastics in the marine environment: a review of the methods used for identification and quantification”. In: *Environmental science & technology* 46.6 (2012), pages 3060–3075 (cited on pages 114, 116, 118).
- [68] C. Munari, V. Infantini, M. Scoponi, E. Rastelli, C. Corinaldesi, and M. Mistri. “Microplastics in the sediments of Terra Nova Bay (Ross Sea, Antarctica)”. In: *Marine pollution bulletin* 122.1-2 (2017), pages 161–165 (cited on page 114).
- [69] V. Ambrogi, C. Carfagna, P. Cerruti, and V. Marturano. “Additives in polymers”. In: *Modification of Polymer Properties*. Elsevier, 2017, pages 87–108 (cited on page 114).
- [70] G. Pritchard. *Plastics additives: an AZ reference*. Volume 1. Springer Science & Business Media, 2012 (cited on page 114).
- [71] D. Lithner, Å. Larsson, and G. Dave. “Environmental and health hazard ranking and assessment of plastic polymers based on chemical composition”. In: *Science of the total environment* 409.18 (2011), pages 3309–3324 (cited on page 114).
- [72] K. J. Groh, T. Backhaus, B. Carney-Almroth, B. Geueke, P. A. Inostroza, A. Lennquist, H. A. Leslie, M. Maffini, D. Slunge, L. Trasande, et al. “Overview of known plastic packaging-associated chemicals and their hazards”. In: *Science of the total environment* 651 (2019), pages 3253–3268 (cited on page 114).
- [73] I. Langelaan, I. Nuyoen, and M. Jansen. “Microplastics in de Nederlandse zoete wateren”. In: *H20, januari* (2015) (cited on page 114).
- [74] J.-H. Kwon, S. Chang, S. H. Hong, and W. J. Shim. “Microplastics as a vector of hydrophobic contaminants: Importance of hydrophobic additives”. In: *Integrated environmental assessment and management* 13.3 (2017), pages 494–499 (cited on page 114).
- [75] H. L. De Frond, E. van Sebille, J. M. Parnis, M. L. Diamond, N. Mallos, T. Kingsbury, and C. M. Rochman. “Estimating the mass of chemicals associated with ocean plastic pollution to inform mitigation efforts”. In: *Integrated environmental assessment and management* 15.4 (2019), pages 596–606 (cited on page 114).
- [76] E. L. Teuten, J. M. Saquing, D. R. Knappe, M. A. Barlaz, S. Jonsson, A. Björn, S. J. Rowland, R. C. Thompson, T. S. Galloway, R. Yamashita, et al. “Transport and release of chemicals from plastics to the environment and to wildlife”. In: *Philosophical transactions of the royal society B: biological sciences* 364.1526 (2009), pages 2027–2045 (cited on page 114).
- [77] A. Bakir, S. J. Rowland, and R. C. Thompson. “Competitive sorption of persistent organic pollutants onto microplastics in the marine environment”. In: *Marine pollution bulletin* 64.12 (2012), pages 2782–2789 (cited on page 114).
- [78] H. Lee, W. J. Shim, and J.-H. Kwon. “Sorption capacity of plastic debris for hydrophobic organic chemicals”. In: *Science of the total environment* 470 (2014), pages 1545–1552 (cited on page 114).
- [79] C. Wu, K. Zhang, X. Huang, and J. Liu. “Sorption of pharmaceuticals and personal care products to polyethylene debris”. In: *Environmental Science and pollution research* 23.9 (2016), pages 8819–8826 (cited on page 114).
- [80] L. M. Ziccardi, A. Edgington, K. Hentz, K. J. Kulacki, and S. K. Driscoll. “Microplastics as vectors for bioaccumulation of hydrophobic organic chemicals in the marine environment: A state-of-the-science review”. In: *Environmental toxicology and chemistry* 35.7 (2016), pages 1667–1676 (cited on page 114).
- [81] N. B. Hartmann, S. Rist, J. Bodin, L. H. Jensen, S. N. Schmidt, P. Mayer, A. Meibom, and A. Baun. “Microplastics as vectors for environmental contaminants: exploring sorption, desorption, and transfer to biota”. In: *Integrated environmental assessment and management* 13.3 (2017), pages 488–493 (cited on page 114).
- [82] H. Zhang, Q. Zhou, Z. Xie, Y. Zhou, C. Tu, C. Fu, W. Mi, R. Ebinghaus, P. Christie, and Y. Luo. “Occurrences of organophosphorus esters and phthalates in the microplastics from the coastal beaches in north China”. In: *Science of the total environment* 616 (2018), pages 1505–1512 (cited on page 114).
- [83] C. M. Rochman, T. Kurobe, I. Flores, and S. J. Teh. “Early warning signs of endocrine disruption in adult fish from the ingestion of polyethylene with and without sorbed chemical pollutants from the marine environment”. In: *Science of the total environment* 493 (2014), pages 656–661 (cited on pages 114, 128, 129).
- [84] A. Turner and L. A. Holmes. “Adsorption of trace metals by microplastic pellets in fresh water”. In: *Environmental chemistry* 12.5 (2015), pages 600–610 (cited on page 114).
- [85] F. Wang, C. S. Wong, D. Chen, X. Lu, F. Wang, and E. Y. Zeng. “Interaction of toxic chemicals with microplastics: a critical review”. In: *Water research* 139 (2018), pages 208–219 (cited on page 114).
- [86] M. Llorca, G. Schirinzi, M. Martínez, D. Barceló, and M. Farré. “Adsorption of perfluoroalkyl substances on microplastics under environmental conditions”. In: *Environmental pollution* 235 (2018), pages 680–691 (cited on page 114).

- [87] R. M. Razanajatovo, J. Ding, S. Zhang, H. Jiang, and H. Zou. “Sorption and desorption of selected pharmaceuticals by polyethylene microplastics”. In: *Marine pollution bulletin* 136 (2018), pages 516–523 (cited on page 114).
- [88] A. A. Koelmans, E. Besseling, A. Wegner, and E. M. Foekema. “Plastic as a carrier of POPs to aquatic organisms: a model analysis”. In: *Environmental science & technology* 47.14 (2013), pages 7812–7820 (cited on pages 114, 115, 128).
- [89] M. Davranche, C. Veclin, A.-C. Pierson-Wickmann, H. El Hadri, B. Grassl, L. Roweczyk, A. Dia, A. Ter Halle, F. Blancho, S. Reynaud, et al. “Are nanoplastics able to bind significant amount of metals? The lead example”. In: *Environmental pollution* 249 (2019), pages 940–948 (cited on page 114).
- [90] A. A. Koelmans. “Modeling the role of microplastics in bioaccumulation of organic chemicals to marine aquatic organisms. A critical review”. In: *Marine anthropogenic litter*. Springer, Cham, 2015, pages 309–324 (cited on pages 115, 128).
- [91] E. R. Zettler, T. J. Mincer, and L. A. Amaral-Zettler. “Life in the “plastisphere”: microbial communities on plastic marine debris”. In: *Environmental science & technology* 47.13 (2013), pages 7137–7146 (cited on pages 115, 129).
- [92] J. Reisser, J. Shaw, G. Hallegraeff, M. Proietti, D. K. Barnes, M. Thums, C. Wilcox, B. D. Hardesty, and C. Pattiaratchi. “Millimeter-sized marine plastics: a new pelagic habitat for microorganisms and invertebrates”. In: *PloS one* 9.6 (2014) (cited on page 115).
- [93] C. De Tender, L. I. Devriese, A. Haegeman, S. Maes, J. Vangeyte, A. Catrijsse, P. Dawyndt, and T. Ruttink. “Temporal dynamics of bacterial and fungal colonization on plastic debris in the North Sea”. In: *Environmental science & technology* 51.13 (2017), pages 7350–7360 (cited on pages 115, 129).
- [94] C. D. Rummel, A. Jahnke, E. Gorokhova, D. Kühnel, and M. Schmitt-Jansen. “Impacts of biofilm formation on the fate and potential effects of microplastic in the aquatic environment”. In: *Environmental science & technology letters* 4.7 (2017), pages 258–267 (cited on page 115).
- [95] C. A. De Tender, L. I. Devriese, A. Haegeman, S. Maes, T. Ruttink, and P. Dawyndt. “Bacterial community profiling of plastic litter in the Belgian part of the North Sea”. In: *Environmental science & technology* 49.16 (2015), pages 9629–9638 (cited on page 115).
- [96] G. Oberdörster, A. Maynard, K. Donaldson, V. Castranova, J. Fitzpatrick, K. Ausman, J. Carter, B. Karn, W. Kreyling, D. Lai, et al. “Principles for characterizing the potential human health effects from exposure to nanomaterials: elements of a screening strategy”. In: *Particle and fibre toxicology* 2.1 (2005), page 8 (cited on page 115).
- [97] D. Debroas, A. Mone, and A. Ter Halle. “Plastics in the North Atlantic garbage patch: a boat-microbe for hitchhikers and plastic degraders”. In: *Science of the total environment* 599 (2017), pages 1222–1232 (cited on pages 115, 129).
- [98] A. K. Urbanek, W. Rymowicz, and A. M. Miłośnik. “Degradation of plastics and plastic-degrading bacteria in cold marine habitats”. In: *Applied microbiology and biotechnology* 102.18 (2018), pages 7669–7678 (cited on page 115).
- [99] S. Oberbeckmann, M. G. Löder, and M. Labrenz. “Marine microplastic-associated biofilms—a review”. In: *Environmental chemistry* 12.5 (2015), pages 551–562 (cited on pages 115, 129).
- [100] I. V. Kirstein, S. Kirmizi, A. Wichels, A. Garin-Fernandez, R. Erler, L. Martin, G. Gerdt, et al. “Dangerous hitchhikers? Evidence for potentially pathogenic *Vibrio* spp. on microplastic particles”. In: *Marine environmental research* 120 (2016), pages 1–8 (cited on pages 115, 129).
- [101] M. K. Viršek, M. N. Lovšin, Š. Koren, A. Kržan, and M. Peterlin. “Microplastics as a vector for the transport of the bacterial fish pathogen species *Aeromonas salmonicida*”. In: *Marine pollution bulletin* 125.1-2 (2017), pages 301–309 (cited on pages 115, 129).
- [102] L. Frère, L. Maignien, M. Chalopin, A. Huvet, E. Rinnert, H. Morrison, S. Kerninon, A.-L. Cassone, C. Lambert, J. Reveillaud, et al. “Microplastic bacterial communities in the Bay of Brest: Influence of polymer type and size”. In: *Environmental pollution* 242 (2018), pages 614–625 (cited on pages 115, 129).
- [103] M. M. Silva, G. C. Maldonado, R. O. Castro, J. de Sá Felizardo, R. P. Cardoso, R. M. dos Anjos, and F. V. de Araújo. “Dispersal of potentially pathogenic bacteria by plastic debris in Guanabara Bay, RJ, Brazil”. In: *Marine pollution bulletin* 141 (2019), pages 561–568 (cited on page 115).
- [104] J. P. Harrison, T. J. Hoellein, M. Sapp, A. S. Tagg, Y. Ju-Nam, and J. J. Ojeda. “Microplastic-associated biofilms: a comparison of freshwater and marine environments”. In: *Freshwater microplastics*. Springer, Cham, 2018, pages 181–201 (cited on page 115).
- [105] M. Imran, K. R. Das, and M. M. Naik. “Co-selection of multi-antibiotic resistance in bacterial pathogens in metal and microplastic contaminated environments: An emerging health threat”. In: *Chemosphere* 215 (2019), pages 846–857 (cited on page 115).

- [106] M. E. Larsson, O. F. Laczka, I. M. Suthers, P. A. Ajani, and M. A. Doblin. “Hitchhiking in the East Australian Current: rafting as a dispersal mechanism for harmful epibenthic dinoflagellates”. In: *Marine ecology progress series* 596 (2018), pages 49–60 (cited on page 115).
- [107] M. Kooi, E. H. v. Nes, M. Scheffer, and A. A. Koelmans. “Ups and downs in the ocean: effects of biofouling on vertical transport of microplastics”. In: *Environmental science & technology* 51.14 (2017), pages 7963–7971 (cited on page 115).
- [108] T. Cedervall, L.-A. Hansson, M. Lard, B. Frohm, and S. Linse. “Food chain transport of nanoparticles affects behaviour and fat metabolism in fish”. In: *PloS one* 7.2 (2012) (cited on pages 115, 124).
- [109] M. Lundqvist, J. Stigler, T. Cedervall, T. Berggård, M. B. Flanagan, I. Lynch, G. Elia, and K. Dawson. “The evolution of the protein corona around nanoparticles: a test study”. In: *ACS nano* 5.9 (2011), pages 7503–7509 (cited on page 115).
- [110] D. Docter, U. Distler, W. Storck, J. Kuharev, D. Wünsch, A. Hahlbrock, S. K. Knauer, S. Tenzer, and R. H. Stauber. “Quantitative profiling of the protein coronas that form around nanoparticles”. In: *Nature protocols* 9.9 (2014), page 2030 (cited on page 115).
- [111] F. Nasser and I. Lynch. “Secreted protein eco-corona mediates uptake and impacts of polystyrene nanoparticles on *Daphnia magna*”. In: *Journal of proteomics* 137 (2016), pages 45–51 (cited on pages 115, 123).
- [112] L. Canesi and I. Corsi. “Effects of nanomaterials on marine invertebrates”. In: *Science of the total environment* 565 (2016), pages 933–940 (cited on page 115).
- [113] A. L. Andrady. *Plastics and the Environment*. John Wiley & Sons, 2003 (cited on page 115).
- [114] A. Ter Halle, L. Ladirat, X. Gendre, D. Goudounèche, C. Pusineri, C. Routaboul, C. Tenailleau, B. Duployer, and E. Perez. “Understanding the fragmentation pattern of marine plastic debris”. In: *Environmental science & technology* 50.11 (2016), pages 5668–5675 (cited on page 115).
- [115] B. Gewert, M. M. Plassmann, and M. MacLeod. “Pathways for degradation of plastic polymers floating in the marine environment”. In: *Environmental science: processes & impacts* 17.9 (2015), pages 1513–1521 (cited on page 115).
- [116] D. Hodgson, A. Bréchon, and R. Thompson. “Ingestion and fragmentation of plastic carrier bags by the amphipod *Orchestia gammarellus*: effects of plastic type and fouling load”. In: *Marine pollution bulletin* 127 (2018), pages 154–159 (cited on page 115).
- [117] D. K. Barnes, F. Galgani, R. C. Thompson, and M. Barlaz. “Accumulation and fragmentation of plastic debris in global environments”. In: *Philosophical transactions of the royal society B: biological sciences* 364.1526 (2009), pages 1985–1998 (cited on page 115).
- [118] A. L. Dawson, S. Kawaguchi, C. K. King, K. A. Townsend, R. King, W. M. Huston, and S. M. B. Nash. “Turning microplastics into nanoplastics through digestive fragmentation by Antarctic krill”. In: *Nature communications* 9.1 (2018), pages 1–8 (cited on page 115).
- [119] S. Summers, T. Henry, and T. Gutierrez. “Agglomeration of nano-and microplastic particles in seawater by autochthonous and de novo-produced sources of exopolymeric substances”. In: *Marine pollution bulletin* 130 (2018), pages 258–267 (cited on page 116).
- [120] E. Besseling, J. T. Quik, M. Sun, and A. A. Koelmans. “Fate of nano-and microplastic in freshwater systems: A modeling study”. In: *Environmental pollution* 220 (2017), pages 540–548 (cited on page 116).
- [121] I. Isachenko, L. Khatmullina, I. Chubarenko, and N. Stepanova. “Settling velocity of marine microplastic particles: laboratory tests”. In: *EGU General Assembly Conference Abstracts*. Volume 18. 2016 (cited on page 116).
- [122] A. Bagaev, A. Mizyuk, L. Khatmullina, I. Isachenko, and I. Chubarenko. “Anthropogenic fibres in the Baltic Sea water column: Field data, laboratory and numerical testing of their motion”. In: *Science of the total environment* 599 (2017), pages 560–571 (cited on page 116).
- [123] S. Ye and A. L. Andrady. “Fouling of floating plastic debris under Biscayne Bay exposure conditions”. In: *Marine pollution bulletin* 22.12 (1991), pages 608–613 (cited on page 116).
- [124] D. Lobelle and M. Cunliffe. “Early microbial biofilm formation on marine plastic debris”. In: *Marine pollution bulletin* 62.1 (2011), pages 197–200 (cited on page 116).
- [125] I. Jalón-Rojas, X. H. Wang, and E. Fredj. “A 3D numerical model to Track Marine Plastic Debris (TrackMPD): Sensitivity of microplastic trajectories and fates to particle dynamical properties and physical processes”. In: *Marine pollution bulletin* 141 (2019), pages 256–272 (cited on page 116).
- [126] F. M. Fazey and P. G. Ryan. “Biofouling on buoyant marine plastics: An experimental study into the effect of size on surface longevity”. In: *Environmental pollution* 210 (2016), pages 354–360 (cited on page 116).
- [127] M. Cole, P. K. Lindeque, E. Fileman, J. Clark, C. Lewis, C. Halsband, and T. S. Galloway. “Microplastics alter the properties and sinking rates of zooplankton faecal pellets”. In: *Environmental science & technology* 50.6 (2016), pages 3239–3246 (cited on page 116).

- [128] S. Zhao, J. E. Ward, M. Danley, and T. J. Mincer. “Field-based evidence for microplastic in marine aggregates and mussels: implications for trophic transfer”. In: *Environmental science & technology* 52.19 (2018), pages 11038–11048 (cited on pages 116, 122).
- [129] M. G. Löder and G. Gerdt. “Methodology used for the detection and identification of microplastics—A critical appraisal”. In: *Marine anthropogenic litter*. Springer, 2015, pages 201–227 (cited on page 116).
- [130] E. Fries, J. H. Dekiff, J. Willmeyer, M.-T. Nuelle, M. Ebert, and D. Remy. “Identification of polymer types and additives in marine microplastic particles using pyrolysis-GC/MS and scanning electron microscopy”. In: *Environmental science: processes & impacts* 15.10 (2013), pages 1949–1956 (cited on page 116).
- [131] C. G. Avio, S. Gorb, and F. Regoli. “Experimental development of a new protocol for extraction and characterization of microplastics in fish tissues: first observations in commercial species from Adriatic Sea”. In: *Marine environmental research* 111 (2015), pages 18–26 (cited on page 116).
- [132] W. J. Shim, S. H. Hong, and S. E. Eo. “Identification methods in microplastic analysis: a review”. In: *Analytical methods* 9.9 (2017), pages 1384–1391 (cited on page 116).
- [133] T. Rocha-Santos and A. C. Duarte. “A critical overview of the analytical approaches to the occurrence, the fate and the behavior of microplastics in the environment”. In: *TrAC Trends in analytical chemistry* 65 (2015), pages 47–53 (cited on page 116).
- [134] E. Hermsen, S. M. Mintenig, E. Besseling, and A. A. Koelmans. “Quality criteria for the analysis of microplastic in biota samples: a critical review”. In: *Environmental science & technology* 52.18 (2018), pages 10230–10240 (cited on pages 116, 117).
- [135] C. G. Avio, S. Gorb, and F. Regoli. “Plastics and microplastics in the oceans: from emerging pollutants to emerged threat”. In: *Marine environmental research* 128 (2017), pages 2–11 (cited on page 116).
- [136] L. Zada, H. A. Leslie, A. D. Vethaak, G. H. Tinnevelt, J. J. Jansen, J. F. de Boer, and F. Ariese. “Fast microplastics identification with stimulated Raman scattering microscopy”. In: *Journal of Raman spectroscopy* 49.7 (2018), pages 1136–1144 (cited on pages 116, 118).
- [137] E. C. Eber, V. E. Ngozi, et al. “Microplastics, an emerging concern: A review of analytical techniques for detecting and quantifying microplastics”. In: *Analytical methods in environmental chemistry journal* 2.2 (2019), pages 13–30 (cited on page 116).
- [138] I. R. Comnea-Stancu, K. Wieland, G. Ramer, A. Schwaighofer, and B. Lendl. “On the identification of rayon/viscose as a major fraction of microplastics in the marine environment: discrimination between natural and manmade cellulosic fibers using Fourier transform infrared spectroscopy”. In: *Applied spectroscopy* 71.5 (2017), pages 939–950 (cited on page 117).
- [139] Y. Yu, D. Zhou, Z. Li, and C. Zhu. “Advancement and challenges of microplastic pollution in the aquatic environment: a review”. In: *Water, air, & soil pollution* 229.5 (2018), page 140 (cited on page 117).
- [140] C. Wesch, K. Bredimus, M. Paulus, and R. Klein. “Towards the suitable monitoring of ingestion of microplastics by marine biota: A review”. In: *Environmental pollution* 218 (2016), pages 1200–1208 (cited on pages 117, 119).
- [141] F. Remy, F. Collard, B. Gilbert, P. Compère, G. Eppe, and G. Lepoint. “When microplastic is not plastic: the ingestion of artificial cellulose fibers by macrofauna living in seagrass macrophytodebris”. In: *Environmental science & technology* 49.18 (2015), pages 11158–11166 (cited on page 117).
- [142] T. Maes, R. Jessop, N. Wellner, K. Haupt, and A. G. Mayes. “A rapid-screening approach to detect and quantify microplastics based on fluorescent tagging with Nile Red”. In: *Scientific reports* 7 (2017), page 44501 (cited on pages 117, 118, 121).
- [143] G. Erni-Cassola, M. I. Gibson, R. C. Thompson, and J. A. Christie-Oleza. “Lost, but found with Nile Red: a novel method for detecting and quantifying small microplastics (1 mm to 20 μ m) in environmental samples”. In: *Environmental science & technology* 51.23 (2017), pages 13641–13648 (cited on page 117).
- [144] L. C. Woodall, C. Gwinnett, M. Packer, R. C. Thompson, L. F. Robinson, and G. L. Paterson. “Using a forensic science approach to minimize environmental contamination and to identify microfibrils in marine sediments”. In: *Marine pollution bulletin* 95.1 (2015), pages 40–46 (cited on page 117).
- [145] A. A. Koelmans, E. Besseling, and W. J. Shim. “Nanoplastics in the aquatic environment. Critical review”. In: *Marine anthropogenic litter*. Springer, Cham, 2015, pages 325–340 (cited on page 117).
- [146] K. Mattsson, S. Jovic, I. Doverbratt, and L.-A. Hansson. “Nanoplastics in the aquatic environment”. In: *Microplastic contamination in aquatic environments*. Elsevier, 2018, pages 379–399 (cited on page 117).
- [147] J. Gigault, B. Pedrono, B. Maxit, and A. Ter Halle. “Marine plastic litter: the unanalyzed nano-fraction”. In: *Environmental science: nano* 3.2 (2016), pages 346–350 (cited on page 117).

- [148] S. Rezania, J. Park, M. F. M. Din, S. M. Taib, A. Talaiekhosani, K. K. Yadav, and H. Kamyab. “Microplastics pollution in different aquatic environments and biota: A review of recent studies”. In: *Marine pollution bulletin* 133 (2018), pages 191–208 (cited on pages 118, 121).
- [149] S. Klein, E. Worch, and T. P. Knepper. “Occurrence and spatial distribution of microplastics in river shore sediments of the Rhine-Main area in Germany”. In: *Environmental science & technology* 49.10 (2015), pages 6070–6076 (cited on page 118).
- [150] J. Wang, J. Peng, Z. Tan, Y. Gao, Z. Zhan, Q. Chen, and L. Cai. “Microplastics in the surface sediments from the Beijiing River littoral zone: composition, abundance, surface textures and interaction with heavy metals”. In: *Chemosphere* 171 (2017), pages 248–258 (cited on page 118).
- [151] R. R. Hurley, A. L. Lusher, M. Olsen, and L. Nizzetto. “Validation of a method for extracting microplastics from complex, organic-rich, environmental matrices”. In: *Environmental science & technology* 52.13 (2018), pages 7409–7417 (cited on page 118).
- [152] C. Schmidt, T. Krauth, and S. Wagner. “Export of plastic debris by rivers into the sea”. In: *Environmental science & technology* 51.21 (2017), pages 12246–12253 (cited on page 118).
- [153] S. Eo, S. H. Hong, Y. K. Song, J. Lee, J. Lee, and W. J. Shim. “Abundance, composition, and distribution of microplastics larger than 20 μm in sand beaches of South Korea”. In: *Environmental pollution* 238 (2018), pages 894–902 (cited on page 118).
- [154] J. A. Brandon, A. Freibott, and L. M. Sala. “Patterns of suspended and salp-ingested microplastic debris in the North Pacific investigated with epifluorescence microscopy”. In: *Limnology and oceanography letters* 5.1 (2020), pages 46–53 (cited on page 118).
- [155] J. Gago, O. Carretero, A. Filgueiras, and L. Viñas. “Synthetic microfibers in the marine environment: A review on their occurrence in seawater and sediments”. In: *Marine pollution bulletin* 127 (2018), pages 365–376 (cited on page 118).
- [156] L. Van Cauwenberghe, A. Vanreusel, J. Mees, and C. R. Janssen. “Microplastic pollution in deep-sea sediments”. In: *Environmental pollution* 182 (2013), pages 495–499 (cited on page 119).
- [157] V. Fischer, N. O. Elsner, N. Brenke, E. Schwabe, and A. Brandt. “Plastic pollution of the Kuril–Kamchatka Trench area (NW pacific)”. In: *Deep Sea Research Part II: Topical Studies in Oceanography* 111 (2015), pages 399–405 (cited on page 119).
- [158] M. Taylor, C. Gwinnett, L. Robinson, and L. Woodall. “Plastic microfibre ingestion by deep-sea organisms”. In: *Scientific reports* 6.1 (2016), pages 1–9 (cited on page 119).
- [159] S. E. Nelms, T. S. Galloway, B. J. Godley, D. S. Jarvis, and P. K. Lindeque. “Investigating microplastic trophic transfer in marine top predators”. In: *Environmental pollution* 238 (2018), pages 999–1007 (cited on page 119).
- [160] E. M. Duncan, A. C. Broderick, W. J. Fuller, T. S. Galloway, M. H. Godfrey, M. Hamann, C. J. Limpus, P. K. Lindeque, A. G. Mayes, L. C. Omeyer, et al. “Microplastic ingestion ubiquitous in marine turtles”. In: *Global change biology* 25.2 (2019), pages 744–752 (cited on page 119).
- [161] T. Romeo, B. Pietro, C. Pedà, P. Consoli, F. Andaloro, and M. C. Fossi. “First evidence of presence of plastic debris in stomach of large pelagic fish in the Mediterranean Sea”. In: *Marine pollution bulletin* 95.1 (2015), pages 358–361 (cited on page 119).
- [162] F. Bessa, N. Ratcliffe, V. Otero, P. Sobral, J. C. Marques, C. M. Waluda, P. N. Trathan, and J. C. Xavier. “Microplastics in gentoo penguins from the Antarctic region”. In: *Scientific reports* 9.1 (2019), pages 1–7 (cited on page 119).
- [163] A. Lusher, N. Welden, P. Sobral, and M. Cole. “Sampling, isolating and identifying microplastics ingested by fish and invertebrates”. In: *Analytical methods* 9.9 (2017), pages 1346–1360 (cited on pages 119, 122).
- [164] J. D. O’Connor, A. M. Mahon, A. F. Ramsperger, B. Trotter, P. E. Redondo-Hasselerharm, A. A. Koelmans, H. T. Lally, and S. Murphy. “Microplastics in freshwater biota: a critical review of isolation, characterization, and assessment methods”. In: *Global challenges* (2019), page 1800118 (cited on pages 119, 120).
- [165] E. Berglund, V. Fogelberg, P. Nilsson, and J. Hollander. “Microplastics in a freshwater mussel (*Anodonta anatina*) in Northern Europe”. In: *Science of the total environment* 697 (2019), page 134192 (cited on pages 119–121).
- [166] L. Hu, M. Chernick, D. E. Hinton, and H. Shi. “Microplastics in small waterbodies and tadpoles from Yangtze River Delta, China”. In: *Environmental science & technology* 52.15 (2018), pages 8885–8893 (cited on page 119).
- [167] W. Sanchez, C. Bender, and J.-M. Porcher. “Wild gudgeons (*Gobio gobio*) from French rivers are contaminated by microplastics: preliminary study and first evidence”. In: *Environmental research* 128 (2014), pages 98–100 (cited on page 119).

- [168] C. B. Brookson, S. R. De Solla, K. J. Fernie, M. Cepeda, and C. M. Rochman. “Microplastics in the diet of nestling double-crested cormorants (*Phalacrocorax auritus*), an obligate piscivore in a freshwater ecosystem”. In: *Canadian Journal of fisheries and aquatic sciences* 76.11 (2019), pages 2156–2163 (cited on page 119).
- [169] O. Setälä, M. Lehtiniemi, R. Coppock, and M. Cole. “Microplastics in marine food webs”. In: *Microplastic contamination in aquatic environments*. Elsevier, 2018, pages 339–363 (cited on pages 119, 122).
- [170] F. M. Windsor, R. M. Tilley, C. R. Tyler, and S. J. Ormerod. “Microplastic ingestion by riverine macroinvertebrates”. In: *Science of the total environment* 646 (2019), pages 68–74 (cited on pages 119, 121).
- [171] C. Wesch, A.-K. Barthel, U. Braun, R. Klein, and M. Paulus. “No microplastics in benthic eelpout (*Zoarces viviparus*): An urgent need for spectroscopic analyses in microplastic detection”. In: *Environmental research* 148 (2016), pages 36–38 (cited on page 119).
- [172] L. G. A. Barboza, A. D. Vethaak, B. R. Lavorante, A.-K. Lundebye, and L. Guilhermino. “Marine microplastic debris: An emerging issue for food security, food safety and human health”. In: *Marine pollution bulletin* 133 (2018), pages 336–348 (cited on pages 119, 121, 128).
- [173] A. Lusher, M. Mchugh, and R. Thompson. “Occurrence of microplastics in the gastrointestinal tract of pelagic and demersal fish from the English Channel”. In: *Marine pollution bulletin* 67.1-2 (2013), pages 94–99 (cited on page 120).
- [174] L. I. Devriese, M. D. van der Meulen, T. Maes, K. Bekaert, I. Paul-Pont, L. Frère, J. Robbens, and A. D. Vethaak. “Microplastic contamination in brown shrimp (*Crangon crangon*, Linnaeus 1758) from coastal waters of the Southern North Sea and Channel area”. In: *Marine pollution bulletin* 98.1-2 (2015), pages 179–187 (cited on page 120).
- [175] M. Zoeter Vanpoucke. “Impact of microplastic uptake: contamination in sprat and microplastic-mediated uptake of PAHs by European shore crab. Institute of Agricultural and Fisheries Research (ILVO) Ghent, EMBC+”. PhD thesis. MSc thesis, 2015 (cited on page 120).
- [176] A. Naji, Z. Esmaili, S. A. Mason, and A. D. Vethaak. “The occurrence of microplastic contamination in littoral sediments of the Persian Gulf, Iran”. In: *Environmental Science and pollution research* 24.25 (2017), pages 20459–20468 (cited on page 121).
- [177] A. Naji, M. Nuri, and A. D. Vethaak. “Microplastics contamination in molluscs from the northern part of the Persian Gulf”. In: *Environmental pollution* 235 (2018), pages 113–120 (cited on page 121).
- [178] T. Karlsson. “Can microliter in sediment and biota be quantified? Method development and analysis of microliter in field collected biota and sediment”. PhD thesis. Master thesis, University of Gothenburg and VU University of Amsterdam-IVM, 2015 (cited on page 121).
- [179] A. Vethaak and H. Leslie. “Plastic debris is a human health issue”. In: *Environmental science & technology* 50.13 (2016), pages 6825–6826 (cited on page 121).
- [180] A. Petersen. “Statement on the presence of microplastics and nanoplastics in food, with particular focus on seafood”. In: (2016) (cited on page 121).
- [181] M. Carbery, W. O’Connor, and T. Palanisami. “Trophic transfer of microplastics and mixed contaminants in the marine food web and implications for human health”. In: *Environment international* 115 (2018), pages 400–409 (cited on pages 121, 128).
- [182] W. Wang, H. Gao, S. Jin, R. Li, and G. Na. “The ecotoxicological effects of microplastics on aquatic food web, from primary producer to human: A review”. In: *Ecotoxicology and environmental safety* 173 (2019), pages 110–117 (cited on page 121).
- [183] L. Van Cauwenberghe and C. R. Janssen. “Microplastics in bivalves cultured for human consumption”. In: *Environmental pollution* 193 (2014), pages 65–70 (cited on page 121).
- [184] WHO (World Health Organization). *Microplastics in drinking-water*. ISBN: 9789241516198. Geneva, Switzerland: World Health Organization, 2019, 101 p. (Cited on page 121).
- [185] D. Yang, H. Shi, L. Li, J. Li, K. Jabeen, and P. Kolandhasamy. “Microplastic pollution in table salts from China”. In: *Environmental science & technology* 49.22 (2015), pages 13622–13627 (cited on page 121).
- [186] M. Joon. “Trophic transfer of microplastics in zooplanktons towards its speculations on human health: A review”. In: *Journal of biomedical and therapeutic sciences* 6.1 (2019), pages 8–14 (cited on page 121).
- [187] S. L. Wright and F. J. Kelly. “Plastic and human health: a micro issue?” In: *Environmental science & technology* 51.12 (2017), pages 6634–6647 (cited on page 121).
- [188] A. I. Catarino, V. Macchia, W. G. Sanderson, R. C. Thompson, and T. B. Henry. “Low levels of microplastics (MP) in wild mussels indicate that MP ingestion by humans is minimal compared to exposure via household fibres fallout during a meal”. In: *Environmental pollution* 237 (2018), pages 675–684 (cited on page 122).

- [189] J. van den Hoff, C. Eriksson, H. Burton, and M. Schultz. “Size-Selective Feeding by Mesopelagic Fish Can Impact Ocean Surface Abundance of Small Plastic Particles”. In: *Proceedings of the International Conference on Microplastic Pollution in the Mediterranean Sea*. Springer, 2018, pages 151–157 (cited on page 122).
- [190] C. Gebhardt and S. Forster. “Size-selective feeding of *Arenicola marina* promotes long-term burial of microplastic particles in marine sediments”. In: *Environmental pollution* 242 (2018), pages 1777–1786 (cited on page 122).
- [191] H. S. H. Chan, C. Dingle, and C. Not. “Evidence for non-selective ingestion of microplastic in demersal fish”. In: *Marine pollution bulletin* 149 (2019), page 110523 (cited on page 122).
- [192] M. G. Ryan, L. Watkins, and M. T. Walter. “Hudson River juvenile Blueback herring avoid ingesting microplastics”. In: *Marine pollution bulletin* 146 (2019), pages 935–939 (cited on page 122).
- [193] N. Hussain, V. Jaitley, and A. T. Florence. “Recent advances in the understanding of uptake of”. In: *Advanced drug delivery reviews* 50 (2001), pages 107–142 (cited on page 122).
- [194] D. A. Norris and P. J. Sinko. “Effect of size, surface charge, and hydrophobicity on the translocation of polystyrene microspheres through gastrointestinal mucin”. In: *Journal of applied polymer science* 63.11 (1997), pages 1481–1492. ISSN: 1097-4628 (cited on page 122).
- [195] T. S. Galloway. “Micro-and nano-plastics and human health”. In: *Marine anthropogenic litter*. Springer, Cham, 2015, pages 343–366 (cited on page 122).
- [196] A. L. Lusher, C. O’Donnell, R. Officer, and I. O’Connor. “Microplastic interactions with North Atlantic mesopelagic fish”. In: *ICES Journal of marine science* 73.4 (2016), pages 1214–1225 (cited on page 122).
- [197] B. Fernández and M. Albentosa. “Insights into the uptake, elimination and accumulation of microplastics in mussel”. In: *Environmental pollution* 249 (2019), pages 321–329 (cited on pages 122, 126).
- [198] L. Canesi, T. Balbi, R. Fabbri, A. Salis, G. Damonte, M. Volland, and J. Blasco. “Biomolecular coronas in invertebrate species: Implications in the environmental impact of nanoparticles”. In: *NanoImpact* 8 (2017), pages 89–98 (cited on pages 122, 123).
- [199] L. Marques-Santos, G. Grassi, E. Bergami, C. Faleri, T. Balbi, A. Salis, G. Damonte, L. Canesi, and I. Corsi. “Cationic polystyrene nanoparticle and the sea urchin immune system: biocorona formation, cell toxicity, and multixenobiotic resistance phenotype”. In: *Nanotoxicology* 12.8 (2018), pages 847–867 (cited on page 122).
- [200] M. A. Browne, A. Dissanayake, T. S. Galloway, D. M. Lowe, and R. C. Thompson. “Ingested microscopic plastic translocates to the circulatory system of the mussel, *Mytilus edulis* (L.)” In: *Environmental science & technology* 42.13 (2008), pages 5026–5031 (cited on pages 122, 126).
- [201] N. Von Moos, P. Burkhardt-Holm, and A. Köhler. “Uptake and effects of microplastics on cells and tissue of the blue mussel *Mytilus edulis* L. after an experimental exposure”. In: *Environmental science & technology* 46.20 (2012), pages 11327–11335 (cited on pages 122, 124–126).
- [202] M. Sendra, A. Saco, M. P. Yeste, A. Romero, B. Novoa, and A. Figueras. “Nanoplastics: From tissue accumulation to cell translocation into *Mytilus galloprovincialis* hemocytes. resilience of immune cells exposed to nanoplastics and nanoplastics plus *Vibrio splendidus* combination”. In: *Journal of hazardous materials* (2019), page 121788 (cited on pages 122, 123).
- [203] J. Ding, S. Zhang, R. M. Razanajatovo, H. Zou, and W. Zhu. “Accumulation, tissue distribution, and biochemical effects of polystyrene microplastics in the freshwater fish red tilapia (*Oreochromis niloticus*)”. In: *Environmental pollution* 238 (2018), pages 1–9 (cited on page 122).
- [204] K. Mattsson, E. V. Johnson, A. Malmendal, S. Linse, L.-A. Hansson, and T. Cedervall. “Brain damage and behavioural disorders in fish induced by plastic nanoparticles delivered through the food chain”. In: *Scientific reports* 7.1 (2017), pages 1–7 (cited on pages 122, 124, 125).
- [205] M. D. Prokić, T. B. Radovanović, J. P. Gavrić, and C. Faggio. “Ecotoxicological effects of microplastics: Examination of biomarkers, current state and future perspectives”. In: *TrAC Trends in analytical chemistry* 111 (2019), pages 37–46 (cited on page 122).
- [206] M. Al-Sid-Cheikh, S. J. Rowland, K. Stevenson, C. Rouleau, T. B. Henry, and R. C. Thompson. “Uptake, whole-body distribution, and depuration of nanoplastics by the scallop *Pecten maximus* at environmentally realistic concentrations”. In: *Environmental science & technology* 52.24 (2018), pages 14480–14486 (cited on page 123).
- [207] K. N. Fotopoulou and H. K. Karapanagioti. “Surface properties of beached plastic pellets”. In: *Marine environmental research* 81 (2012), pages 70–77 (cited on page 123).
- [208] C. Della Torre, E. Bergami, A. Salvati, C. Faleri, P. Cirino, K. Dawson, and I. Corsi. “Accumulation and embryotoxicity of polystyrene nanoparticles at early stage of development of sea urchin embryos *Paracentrotus lividus*”. In: *Environmental science & technology* 48.20 (2014), pages 12302–12311 (cited on pages 123, 124).

- [209] G. Grassi, C. Landi, C. Della Torre, E. Bergami, L. Bini, and I. Corsi. “Proteomic profile of the hard corona of charged polystyrene nanoparticles exposed to sea urchin *Paracentrotus lividus* coelomic fluid highlights potential drivers of toxicity”. In: *Environmental science: nano* 6.10 (2019), pages 2937–2947 (cited on page 123).
- [210] E. Besseling, A. Wegner, E. M. Foekema, M. J. Van Den Heuvel-Greve, and A. A. Koelmans. “Effects of microplastic on fitness and PCB bioaccumulation by the lugworm *Arenicola marina* (L.)”. In: *Environmental science & technology* 47.1 (2013), pages 593–600 (cited on pages 123–125, 128).
- [211] J. Hämer, L. Gutow, A. Köhler, and R. Saborowski. “Fate of microplastics in the marine isopod *Idotea emarginata*”. In: *Environmental science & technology* 48.22 (2014), pages 13451–13458 (cited on page 123).
- [212] K. L. Kaposi, B. Mos, B. P. Kelaher, and S. A. Dworjanyn. “Ingestion of microplastic has limited impact on a marine larva”. In: *Environmental science & technology* 48.3 (2014), pages 1638–1645 (cited on page 123).
- [213] A. A. Koelmans, E. Besseling, and E. M. Foekema. “Leaching of plastic additives to marine organisms”. In: *Environmental pollution* 187 (2014), pages 49–54 (cited on page 123).
- [214] C. M. Rochman, M. A. Browne, A. J. Underwood, J. A. Van Franeker, R. C. Thompson, and L. A. Amaral-Zettler. “The ecological impacts of marine debris: unraveling the demonstrated evidence from what is perceived”. In: *Ecology* 97.2 (2016), pages 302–312 (cited on page 123).
- [215] C. Barría, I. Brandts, L. Tort, M. Oliveira, and M. Teles. “Effect of nanoplastics on fish health and performance: A review”. In: *Marine pollution bulletin* (2019), page 110791 (cited on page 123).
- [216] L. Canesi, C. Ciacci, E. Bergami, M. Monopoli, K. Dawson, S. Papa, B. Canonico, and I. Corsi. “Evidence for immunomodulation and apoptotic processes induced by cationic polystyrene nanoparticles in the hemocytes of the marine bivalve *Mytilus*”. In: *Marine environmental research* 111 (2015), pages 34–40 (cited on pages 123, 126).
- [217] X. Sun, B. Chen, Q. Li, N. Liu, B. Xia, L. Zhu, and K. Qu. “Toxicities of polystyrene nano- and microplastics toward marine bacterium *Halomonas alkaliphila*”. In: *Science of the total environment* 642 (2018), pages 1378–1385 (cited on page 124).
- [218] C. Zhang, X. Chen, J. Wang, and L. Tan. “Toxic effects of microplastic on marine microalgae *Skeletonema costatum*: interactions between microplastic and algae”. In: *Environmental pollution* 220 (2017), pages 1282–1288 (cited on pages 124, 125).
- [219] S. B. Sjollem, P. Redondo-Hasselerharm, H. A. Leslie, M. H. Kraak, and A. D. Vethaak. “Do plastic particles affect microalgal photosynthesis and growth?”. In: *Aquatic toxicology* 170 (2016), pages 259–261 (cited on pages 124, 125).
- [220] P. Bhattacharya, S. Lin, J. P. Turner, and P. C. Ke. “Physical adsorption of charged plastic nanoparticles affects algal photosynthesis”. In: *The journal of physical chemistry C* 114.39 (2010), pages 16556–16561 (cited on pages 124, 125).
- [221] S. Messinetti, S. Mercurio, G. Scari, A. Pennati, and R. Pennati. “Ingested microscopic plastics translocate from the gut cavity of juveniles of the ascidian *Ciona intestinalis*”. In: *The European zoological journal* 86.1 (2019), pages 189–195 (cited on page 124).
- [222] K.-W. Lee, W. J. Shim, O. Y. Kwon, and J.-H. Kang. “Size-dependent effects of micro polystyrene particles in the marine copepod *Tigriopus japonicus*”. In: *Environmental science & technology* 47.19 (2013), pages 11278–11283 (cited on page 124).
- [223] M. Cole, P. Lindeque, E. Fileman, C. Halsband, R. Goodhead, J. Moger, and T. S. Galloway. “Microplastic ingestion by zooplankton”. In: *Environmental science & technology* 47.12 (2013), pages 6646–6655 (cited on page 124).
- [224] M. A. Browne, S. J. Niven, T. S. Galloway, S. J. Rowland, and R. C. Thompson. “Microplastic moves pollutants and additives to worms, reducing functions linked to health and biodiversity”. In: *Current biology* 23.23 (2013), pages 2388–2392 (cited on pages 124, 128).
- [225] C. G. Avio, S. Gorbi, M. Milan, M. Benedetti, D. Fattorini, G. d’Errico, M. Pauletto, L. Bargelloni, and F. Regoli. “Pollutants bioavailability and toxicological risk from microplastics to marine mussels”. In: *Environmental pollution* 198 (2015), pages 211–222 (cited on pages 124, 126, 128).
- [226] P. P. G. e Silva, C. R. Nobre, P. Resaffe, C. D. S. Pereira, and F. Gusmão. “Leachate from microplastics impairs larval development in brown mussels”. In: *Water research* 106 (2016), pages 364–370 (cited on pages 124, 129).
- [227] S. E. Rist, K. Assidqi, N. P. Zamani, D. Appel, M. Perschke, M. Huhn, and M. Lenz. “Suspended micro-sized PVC particles impair the performance and decrease survival in the Asian green mussel *Perna viridis*”. In: *Marine pollution bulletin* 111.1-2 (2016), pages 213–220 (cited on page 124).
- [228] C. Détrée and C. Gallardo-Escárate. “Single and repetitive microplastics exposures induce immune system modulation and homeostasis alteration in the edible mussel *Mytilus galloprovincialis*”. In: *Fish & shellfish immunology* 83 (2018), pages 52–60 (cited on page 124).

- [229] K. Tallec, A. Huvet, C. Di Poi, C. González-Fernández, C. Lambert, B. Petton, N. Le Goïc, M. Berchel, P. Soudant, and I. Paul-Pont. “Nanoplastics impaired oyster free living stages, gametes and embryos”. In: *Environmental pollution* 242 (2018), pages 1226–1235 (cited on page 124).
- [230] T. Gardon, C. Reisser, C. Soyeux, V. Quillien, and G. Le Moullac. “Microplastics affect energy balance and gametogenesis in the pearl oyster *Pinctada margaritifera*”. In: *Environmental science & technology* 52.9 (2018), pages 5277–5286 (cited on page 124).
- [231] R. Sussarellu, M. Suquet, Y. Thomas, C. Lambert, C. Fabioux, M. E. J. Pernet, N. Le Goïc, V. Quillien, C. Mingant, Y. Epelboin, et al. “Oyster reproduction is affected by exposure to polystyrene microplastics”. In: *Proceedings of the national academy of sciences* 113.9 (2016), pages 2430–2435 (cited on pages 124, 126).
- [232] C. Nobre, M. Santana, A. Maluf, F. Cortez, A. Cesar, C. Pereira, and A. Turra. “Assessment of microplastic toxicity to embryonic development of the sea urchin *Lytechinus variegatus* (Echinodermata: Echinoidea)”. In: *Marine pollution bulletin* 92.1-2 (2015), pages 99–104 (cited on pages 124, 128).
- [233] C. Martínez-Gómez, V. M. León, S. Calles, M. Gomáriz-Olcina, and A. D. Vethaak. “The adverse effects of virgin microplastics on the fertilization and larval development of sea urchins”. In: *Marine environmental research* 130 (2017), pages 69–76 (cited on pages 124, 129).
- [234] Y. Mao, H. Ai, Y. Chen, Z. Zhang, P. Zeng, L. Kang, W. Li, W. Gu, Q. He, and H. Li. “Phytoplankton response to polystyrene microplastics: perspective from an entire growth period”. In: *Chemosphere* 208 (2018), pages 59–68 (cited on page 124).
- [235] F. Murphy and B. Quinn. “The effects of microplastic on freshwater *Hydra attenuata* feeding, morphology & reproduction”. In: *Environmental pollution* 234 (2018), pages 487–494 (cited on page 124).
- [236] M. Cole, P. Lindeque, E. Fileman, C. Halsband, and T. S. Galloway. “The impact of polystyrene microplastics on feeding, function and fecundity in the marine copepod *Calanus helgolandicus*”. In: *Environmental science & technology* 49.2 (2015), pages 1130–1137 (cited on page 124).
- [237] L. Lei, S. Wu, S. Lu, M. Liu, Y. Song, Z. Fu, H. Shi, K. M. Raley-Susman, and D. He. “Microplastic particles cause intestinal damage and other adverse effects in zebrafish *Danio rerio* and nematode *Caenorhabditis elegans*”. In: *Science of the total environment* 619 (2018), pages 1–8 (cited on pages 124, 125).
- [238] K. Mattsson, K. Adolfsson, M. T. Ekvall, M. T. Borgström, S. Linse, L.-A. Hansson, T. Cedervall, and C. N. Prinz. “Translocation of 40 nm diameter nanowires through the intestinal epithelium of *Daphnia magna*.” In: *Nanotoxicology* 10 (2016), pages 1160–1167 (cited on page 124).
- [239] M. Ogonowski, C. Schür, Å. Jarsén, and E. Gorokhova. “The effects of natural and anthropogenic microparticles on individual fitness in *Daphnia magna*”. In: *PloS one* 11.5 (2016) (cited on page 124).
- [240] R. Cui, S. W. Kim, and Y.-J. An. “Polystyrene nanoplastics inhibit reproduction and induce abnormal embryonic development in the freshwater crustacean *Daphnia galeata*”. In: *Scientific reports* 7.1 (2017), pages 1–10 (cited on page 124).
- [241] O. M. Lönnstedt and P. Eklöv. “Environmentally relevant concentrations of microplastic particles influence larval fish ecology”. In: *Science* 352.6290 (2016), pages 1213–1216 (cited on page 124).
- [242] L. C. de Sá, L. G. Luís, and L. Guilhermino. “Effects of microplastics on juveniles of the common goby (*Pomatoschistus microps*): confusion with prey, reduction of the predatory performance and efficiency, and possible influence of developmental conditions”. In: *Environmental pollution* 196 (2015), pages 359–362 (cited on page 124).
- [243] Y. Lu, Y. Zhang, Y. Deng, W. Jiang, Y. Zhao, J. Geng, L. Ding, and H. Ren. “Uptake and accumulation of polystyrene microplastics in zebrafish (*Danio rerio*) and toxic effects in liver”. In: *Environmental science & technology* 50.7 (2016), pages 4054–4060 (cited on page 125).
- [244] C. Chen, A. D. Townsend, S. A. Sell, and R. S. Martin. “Microchip-based 3D-cell culture using polymer nanofibers generated by solution blow spinning”. In: *Analytical methods* 9.22 (2017), pages 3274–3283 (cited on page 125).
- [245] S. Bhargava, S. S. Chen Lee, L. S. Min Ying, M. L. Neo, S. Lay-Ming Teo, and S. Valiyaveetil. “Fate of nanoplastics in marine larvae: a case study using barnacles, *Amphibalanus amphitrite*”. In: *ACS Sustainable chemistry & engineering* 6.5 (2018), pages 6932–6940 (cited on page 125).
- [246] R. H. Waring, R. M. Harris, and S. C. Mitchell. “Plastic contamination of the food chain: A threat to human health?” In: *Maturitas* 115 (2018), pages 64–68 (cited on pages 125, 130).
- [247] R. J. Vroom, A. A. Koelmans, E. Besseling, and C. Halsband. “Aging of microplastics promotes their ingestion by marine zooplankton”. In: *Environmental pollution* 231 (2017), pages 987–996 (cited on page 125).

- [248] J. S. Choi, Y.-J. Jung, N.-H. Hong, S. H. Hong, and J.-W. Park. “Toxicological effects of irregularly shaped and spherical microplastics in a marine teleost, the sheepshead minnow (*Cyprinodon variegatus*)”. In: *Marine pollution bulletin* 129.1 (2018), pages 231–240 (cited on page 125).
- [249] F. Lagarde, O. Olivier, M. Zanella, P. Daniel, S. Hiard, and A. Caruso. “Microplastic interactions with freshwater microalgae: hetero-aggregation and changes in plastic density appear strongly dependent on polymer type”. In: *Environmental pollution* 215 (2016), pages 331–339 (cited on page 125).
- [250] M. Moore. “Do nanoparticles present ecotoxicological risks for the health of the aquatic environment?”. In: *Environment international* 32.8 (2006), pages 967–976 (cited on page 125).
- [251] E. P. Espinosa and B. Allam. “Reverse genetics demonstrate the role of mucosal C-type lectins in food particle selection in the oyster *Crassostrea virginica*”. In: *Journal of experimental biology* 221.6 (2018), jeb174094 (cited on page 125).
- [252] A. Mathalon and P. Hill. “Microplastic fibers in the intertidal ecosystem surrounding Halifax Harbor, Nova Scotia”. In: *Marine pollution bulletin* 81.1 (2014), pages 69–79 (cited on page 126).
- [253] L. Van Cauwenbergh, M. Claessens, M. B. Vandegheuchte, and C. R. Janssen. “Microplastics are taken up by mussels (*Mytilus edulis*) and lugworms (*Arenicola marina*) living in natural habitats”. In: *Environmental pollution* 199 (2015), pages 10–17 (cited on page 126).
- [254] J. Li, X. Qu, L. Su, W. Zhang, D. Yang, P. Kolandhasamy, D. Li, and H. Shi. “Microplastics in mussels along the coastal waters of China”. In: *Environmental pollution* 214 (2016), pages 177–184 (cited on page 126).
- [255] J. Li, C. Green, A. Reynolds, H. Shi, and J. M. Rotchell. “Microplastics in mussels sampled from coastal waters and supermarkets in the United Kingdom”. In: *Environmental pollution* 241 (2018), pages 35–44 (cited on page 126).
- [256] D. S. Green. “Effects of microplastics on European flat oysters, *Ostrea edulis* and their associated benthic communities”. In: *Environmental pollution* 216 (2016), pages 95–103 (cited on page 126).
- [257] M. N. Woods, M. E. Stack, D. M. Fields, S. D. Shaw, and P. A. Matrai. “Microplastic fiber uptake, ingestion, and egestion rates in the blue mussel (*Mytilus edulis*)”. In: *Marine pollution bulletin* 137 (2018), pages 638–645 (cited on page 126).
- [258] X. Qu, L. Su, H. Li, M. Liang, and H. Shi. “Assessing the relationship between the abundance and properties of microplastics in water and in mussels”. In: *Science of the total environment* 621 (2018), pages 679–686 (cited on page 126).
- [259] P. Kolandhasamy, L. Su, J. Li, X. Qu, K. Jabeen, and H. Shi. “Adherence of microplastics to soft tissue of mussels: a novel way to uptake microplastics beyond ingestion”. In: *Science of the total environment* 610 (2018), pages 635–640 (cited on page 126).
- [260] Q. Li, C. Sun, Y. Wang, H. Cai, L. Li, J. Li, and H. Shi. “Fusion of microplastics into the mussel byssus”. In: *Environmental pollution* 252 (2019), pages 420–426 (cited on page 126).
- [261] I. Paul-Pont, C. Lacroix, C. G. Fernández, H. Hégaret, C. Lambert, N. Le Goïc, L. Frère, A.-L. Cassone, R. Sussarellu, C. Fabioux, et al. “Exposure of marine mussels *Mytilus* spp. to polystyrene microplastics: toxicity and influence on fluoranthene bioaccumulation”. In: *Environmental pollution* 216 (2016), pages 724–737 (cited on page 126).
- [262] I. Brandts, M. Teles, A. Gonçalves, A. Barreto, L. Franco-Martinez, A. Tvarijonaviciute, M. Martins, A. Soares, L. Tort, and M. Oliveira. “Effects of nanoplastics on *Mytilus galloprovincialis* after individual and combined exposure with carbamazepine”. In: *Science of the total environment* 643 (2018), pages 775–784 (cited on page 126).
- [263] L. Pittura, C. G. Avio, M. E. Giuliani, G. d’Errico, S. H. Keiter, B. Cormier, S. Gorbi, and F. Regoli. “Microplastics as vehicles of environmental PAHs to marine organisms: combined chemical and physical hazards to the Mediterranean mussels, *Mytilus galloprovincialis*”. In: *Frontiers in marine science* 5 (2018), page 103 (cited on page 126).
- [264] L. Canesi, C. Ciacci, R. Fabbri, T. Balbi, A. Salis, G. Damonte, K. Cortese, V. Caratto, M. P. Monopoli, K. Dawson, et al. “Interactions of cationic polystyrene nanoparticles with marine bivalve hemocytes in a physiological environment: role of soluble hemolymph proteins”. In: *Environmental research* 150 (2016), pages 73–81 (cited on page 126).
- [265] N. A. Welden and P. R. Cowie. “Long-term microplastic retention causes reduced body condition in the langoustine, *Nephrops norvegicus*”. In: *Environmental pollution* 218 (2016), pages 895–900 (cited on page 127).
- [266] A. J. Watts, M. A. Urbina, S. Corr, C. Lewis, and T. S. Galloway. “Ingestion of plastic microfibers by the crab *Carcinus maenas* and its effect on food consumption and energy balance”. In: *Environmental science & technology* 49.24 (2015), pages 14597–14604 (cited on page 127).
- [267] M. Cole, R. Coppock, P. K. Lindeque, D. Altin, S. Reed, D. W. Pond, L. Sørensen, T. S. Galloway, and A. M. Booth. “Effects of nylon microplastic on feeding, lipid accumulation, and moulting in a coldwater copepod”. In: *Environmental science & technology* 53.12 (2019), pages 7075–7082 (cited on pages 127, 128).

- [268] S. Y. Au, T. F. Bruce, W. C. Bridges, and S. J. Klaine. “Responses of *Hyalella azteca* to acute and chronic microplastic exposures”. In: *Environmental toxicology and chemistry* 34.11 (2015), pages 2564–2572 (cited on page 127).
- [269] P. Blarer and P. Burkhardt-Holm. “Microplastics affect assimilation efficiency in the freshwater amphipod *Gammarus fossarum*”. In: *Environmental science and pollution research* 23.23 (2016), pages 23522–23532 (cited on pages 127, 128).
- [270] A. A. Koelmans, A. Bakir, G. A. Burton, and C. R. Janssen. “Microplastic as a vector for chemicals in the aquatic environment: critical review and model-supported reinterpretation of empirical studies”. In: *Environmental science & technology* 50.7 (2016), pages 3315–3326 (cited on pages 128, 129).
- [271] K. Tanaka, H. Takada, R. Yamashita, K. Mizukawa, M.-a. Fukuwaka, and Y. Watanuki. “Accumulation of plastic-derived chemicals in tissues of seabirds ingesting marine plastics”. In: *Marine pollution bulletin* 69.1-2 (2013), pages 219–222 (cited on page 128).
- [272] A. Bakir, S. J. Rowland, and R. C. Thompson. “Enhanced desorption of persistent organic pollutants from microplastics under simulated physiological conditions”. In: *Environmental pollution* 185 (2014), pages 16–23 (cited on page 128).
- [273] E. M. Chua, J. Shimeta, D. Nugegoda, P. D. Morrison, and B. O. Clarke. “Assimilation of polybrominated diphenyl ethers from microplastics by the marine amphipod, *Allorchestes compressa*”. In: *Environmental science & technology* 48.14 (2014), pages 8127–8134 (cited on page 128).
- [274] S. O’Donovan, N. C. Mestre, S. Abel, T. G. Fonseca, C. C. Carteny, B. Cormier, S. H. Keiter, and M. J. Bebianno. “Ecotoxicological effects of chemical contaminants adsorbed to microplastics in the clam *Scrobicularia plana*”. In: *Frontiers in marine science* 5 (2018), page 143 (cited on page 128).
- [275] S. Rainieri, N. Conlledo, B. K. Larsen, K. Granby, and A. Barranco. “Combined effects of microplastics and chemical contaminants on the organ toxicity of zebrafish (*Danio rerio*)”. In: *Environmental research* 162 (2018), pages 135–143 (cited on page 128).
- [276] S. Garrido, M. Linares, J. A. Campillo, and M. Albentosa. “Effect of microplastics on the toxicity of chlorpyrifos to the microalgae *Isochrysis galbana*, clone t-ISO”. In: *Ecotoxicology and environmental safety* 173 (2019), pages 103–109 (cited on page 128).
- [277] J. R. Rivera-Hernández, B. Fernández, J. Santos-Echeandia, S. Garrido, M. Morante, P. Santos, and M. Albentosa. “Biodynamics of mercury in mussel tissues as a function of exposure pathway: natural vs microplastic routes”. In: *Science of the total environment* 674 (2019), pages 412–423 (cited on page 128).
- [278] C. Peda, L. Caccamo, M. C. Fossi, F. Gai, F. Andaloro, L. Genovese, A. Perdichizzi, T. Romeo, and G. Maricchiolo. “Intestinal alterations in European sea bass *Dicentrarchus labrax* (Linnaeus, 1758) exposed to microplastics: preliminary results”. In: *Environmental pollution* 212 (2016), pages 251–256 (cited on page 128).
- [279] M. Björnsdotter. *Leaching of Residual Monomers, Oligomers and Additives from Polyethylene, Polypropylene, Polyvinyl Chloride, High-density Polyethylene and Polystyrene Virgin Plastics*. 2015 (cited on page 129).
- [280] A. Bakir, I. A. O’Connor, S. J. Rowland, A. J. Hendriks, and R. C. Thompson. “Relative importance of microplastics as a pathway for the transfer of hydrophobic organic chemicals to marine life”. In: *Environmental pollution* 219 (2016), pages 56–65 (cited on page 129).
- [281] M. Van der Meulen, L. De Vriese, J. Lee, T. Maes, J. Van Dalfsen, A. Huvet, P. Soudant, J. Robbens, and A. Vethaak. *Socio-economic impact of microplastics in the 2 Seas, Channel and France Manche Region. An initial risk assessment*. MICRO Interreg project Iva. 2014, p.10 (cited on page 129).
- [282] J. A. Bryant, T. M. Clemente, D. A. Viviani, A. A. Fong, K. A. Thomas, P. Kemp, D. M. Karl, A. E. White, and E. F. DeLong. “Diversity and activity of communities inhabiting plastic debris in the North Pacific Gyre”. In: *MSystems* 1.3 (2016), e00024–16 (cited on page 129).
- [283] C. Dussud, C. Hudec, M. George, P. Fabre, P. Higgs, S. Bruzard, A.-M. Delort, B. Eyheraguibel, A.-L. Meistertzheim, J. Jacquin, et al. “Colonization of non-biodegradable and biodegradable plastics by marine microorganisms”. In: *Frontiers in microbiology* 9 (2018), page 1571 (cited on page 129).
- [284] K. Keszy, S. Oberbeckmann, B. Kreikemeyer, and M. Labrenz. “Spatial environmental heterogeneity determines young biofilm assemblages on microplastics in Baltic Sea mesocosms”. In: *Frontiers in microbiology* 10 (2019), page 1665 (cited on page 129).
- [285] L. A. Amaral-Zettler, E. R. Zettler, B. Slikas, G. D. Boyd, D. W. Melvin, C. E. Morrall, G. Proskurowski, and T. J. Mincer. “The biogeography of the Plastisphere: implications for policy”. In: *Frontiers in ecology and the environment* 13.10 (2015), pages 541–546 (cited on page 129).

- [286] A. R. McCormick, T. J. Hoellein, M. G. London, J. Hittie, J. W. Scott, and J. J. Kelly. “Microplastic in surface waters of urban rivers: concentration, sources, and associated bacterial assemblages”. In: *Ecosphere* 7.11 (2016), e01556 (cited on page 129).
- [287] M. Arias-Andres, U. Klümper, K. Rojas-Jimenez, and H.-P. Grossart. “Microplastic pollution increases gene exchange in aquatic ecosystems”. In: *Environmental pollution* 237 (2018), pages 253–261 (cited on page 130).
- [288] D. S. Green, B. Boots, J. Sigwart, S. Jiang, and C. Rocha. “Effects of conventional and biodegradable microplastics on a marine ecosystem engineer (*Arenicola marina*) and sediment nutrient cycling”. In: *Environmental pollution* 208 (2016), pages 426–434 (cited on page 130).
- [289] D. S. Green, B. Boots, N. E. O’Connor, and R. Thompson. “Microplastics affect the ecological functioning of an important biogenic habitat”. In: *Environmental science & technology* 51.1 (2017), pages 68–77 (cited on page 130).
- [290] T. A. Troost, T. Desclaux, H. A. Leslie, M. D. van Der Meulen, and A. D. Vethaak. “Do microplastics affect marine ecosystem productivity?” In: *Marine pollution bulletin* 135 (2018), pages 17–29 (cited on page 130).
- [291] T. S. Galloway and C. N. Lewis. “Marine microplastics spell big problems for future generations”. In: *Proceedings of the national academy of sciences* 113.9 (2016), pages 2331–2333 (cited on page 130).
- [292] A. A. Koelmans, E. Besseling, E. Foekema, M. Kooi, S. Mintenig, B. C. Ossendorp, P. E. Redondo-Hasselerharm, A. Verschoor, A. P. Van Wezel, and M. Scheffer. “Risks of plastic debris: unravelling fact, opinion, perception, and belief”. In: *Environmental science & technology* 51.20 (2017), pages 11513–11519 (cited on page 130).
- [293] N. N. Phuong, A. Zalouk-Vergnoux, L. Poirier, A. Kamari, A. Châtel, C. Mouneyrac, and F. Lagarde. “Is there any consistency between the microplastics found in the field and those used in laboratory experiments?” In: *Environmental pollution* 211 (2016), pages 111–123 (cited on page 130).

Micro(nano)plastics in aquatic organisms, transferability of knowledge from nanowires

By: Martina G. Vijver¹, Willie Peijnenburg¹, Fazel Abdollahpur Monikh¹

¹ – Institute of Environmental Sciences, Leiden University, 2300 RA Leiden, The Netherlands

10.1 Introduction

Plastic pollution has attracted major political campaigns and media as well as scientific attention. It is reported that plastic production increased from 1.7×10^6 t in the mid 20th century to almost 3.2×10^8 t in 2015 [1]. These plastics eventually enter ecosystems. For example, it was estimated that around 10% of all plastics, deliberately and/or accidentally, end up as waste in different marine ecosystems [2, 3]. Plastic debris has pervaded even in remote areas such as Antarctica [4] and the deep ocean [5]. Plastic microfibres have been identified in ecosystems in all regions of the globe and have been estimated to comprise up to 35% of primary microplastics in marine environments, a major proportion of microplastics on coastal shorelines and to persist for decades in soils treated with sludge from waste water treatment plants. Most of the commonly used plastics are non-biodegradable and they remain in the environment for a long time [6, 7]. Over time, plastics fragment by biotic and abiotic processes. This produces plastic items or so-called plastic debris having different forms (particles, sheets and fibers) and different sizes and shapes, so called microplastics ($1 \mu\text{m} < \text{particle size} < 5 \text{ mm}$) and nanoplastics (particle size $< 1 \mu\text{m}$) (Figure 10.1).

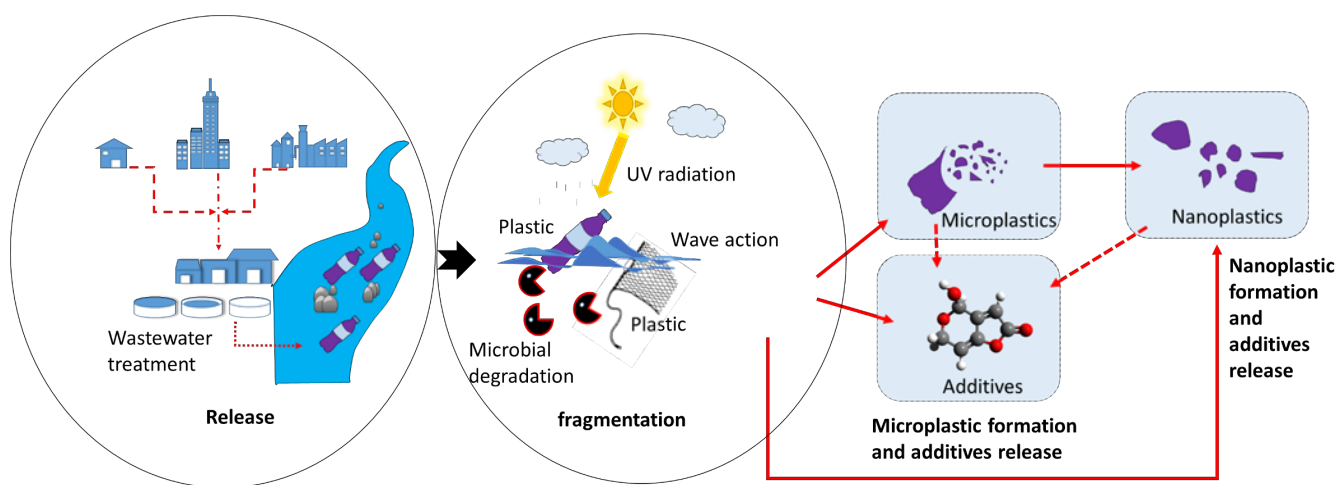


Figure 10.1.: An example of plastic emission through aquatic ecosystems and formation of microplastic and nanoparticle.

An increasing number of studies demonstrated that, due to their small size, microplastic are ingested by organisms [8–10], distributed in their body and cause toxicity to the organisms. A variety of responses have been recorded,

varying from anomalous embryonic development in sea urchins [11], to oxidative stress in rotifers [12] and increased histopathological damage and lysozyme mRNA levels in mussels [13]. To our understanding a limited number of studies are available on understanding the influences of fiber microplastics on organisms. Watts et al. [14] showed that in chronic 4 week feeding study, crabs that ingested food containing microfibers (0.3-1.0% plastic by weight) showed reduced food consumption (from 0.33 g d^{-1} to 0.03 g d^{-1}) and a significant reduction in energy available for growth (scope for growth) from $0.59 \text{ kJ crab}^{-1} \text{ d}^{-1}$ to $-0.31 \text{ kJ crab}^{-1} \text{ d}^{-1}$ in crabs fed with 1% plastic. The polypropylene microfibers were physically altered by their passage through the foregut and were excreted with a smaller overall size and length and amalgamated into distinctive balls. No study available to show even if nanofiber present in the environment.

Micro(nano)plastics (MNPs) contain chemical components which are used as additives (e.g. flame retardants, plasticizers, stabilizers and colorant etc.) to the plastics [15] or sorbed to the hydrophobic surface of the MNPs (e.g. metal and hydrophobic organic contaminants) during their journey to/in the environment. The uptake and accumulation of MNPs may lead to the uptake of the co-occurring contaminants. It is likely that the accumulated MNPs and their co-occurring contaminants by organisms not only increase the possible hazard to the organisms but enhance the risk of trophic transfer of the MNPs and their co-occurring contaminants [16, 17]. Humans as end users may be exposed by MNPs while consuming MNP-containing food [18], through inhalation [19] and/or application of MNP-containing consumer products.

10.2 Aims of the chapter

The aims of this chapter are:

1. To create a brief overview of the current understanding of MNPs in aquatic organisms which are used as food by humans. Most studies report ingestion or accumulation of MNPs, while the link of ingestion to effects is not often recorded in field experiments. To show that it is currently possible to unravel the sub-lethal effects of MNPs and extrapolate the outcome to natural conditions a recent published case study is summarized to link ingestion with key events that occur in zebrafish larvae. The limitation of this chapter is that we do not provide a full review on all response mechanisms that possibly can be induced by MNP exposure.
2. Since there is hardly any data available on shape-related toxicity of fiber-shaped MNPs in aquatic organisms, we discuss the impacts of nanowires (NWs) as a model of fiber-like materials to facilitate the development of hypotheses with regard to the adverse effects of the shape of fiber-like plastic fragments.

10.3 Human exposure to micro(nano)plastics through food

In this study, we searched the literature using Web of Science for peer-reviewed papers on MNPs in organisms (up to 2019) used for human consumption. The bibliographic search found that nearly 1120 papers were published on MNPs and 145 were on adverse effects (keywords: microplastic, nanoplastic, toxicology). Most of the studies focused on seafood, while crops, livestock and manufactured food products have been the subject of very few studies, yet comprise the majority of many diets globally [20]. This could be attributed to the limitation in the available methods to monitor MNPs in complex matrices and more specific within organisms.

Li et al. [21] found multiple types of microplastics (from 2.1 items g^{-1} to $10.5 \text{ items g}^{-1}$), including fibers, fragments and pellets, in the tissue of 9 commercial bivalves from a fishery market in China. They reported that fibers were the most common microplastics in each of the 9 species. De Witte et al. [22] demonstrated that the number of total microplastics in mussels collected from the field and at market varied from 2.6 to 5.1 fibres/10 g of mussel. They suggested that the higher incidence of orange fibres in market and field mussels is related to fisheries activities. Teng et al. [23] measured the concentration of microplastics in cultured oysters from different coastal areas in China. Their finding showed that the average number of microplastics in oysters was $0.62 \text{ items g}^{-1}$ (wet weight). Teng

et al. [23] also reported that fibers were the most common microplastics (81%) detected in the samples. In Germany, microplastics in the soft tissues of *Mytilus edulis* and *Crassostrea gigas* was measured [8]. The authors reported that *M. edulis* contain, on average, 0.36 ± 0.07 items g^{-1} ww and *C. gigas* contains, on average, 0.47 ± 0.16 items g^{-1} ww. These findings lead to the suggestion that the dietary exposure for European shellfish consumers (being humans) is around 11,000 microplastics per year. Baalkhuyur et al. [24] investigated microplastics in 26 commercial and non-commercial fish species from the Red Sea. They found 26 microplastic fragments of which 16 were films and 10 fishing thread. The mussels in coastal waters and local supermarkets in the United Kingdom [25] had microplastics in amounts varying from 0.7 items g^{-1} to 2.9 items g^{-1} of tissue and from 0.9 items g^{-1} to 1.4 items g^{-1} , respectively. Cho et al. [26] measured the concentration of microplastics in market bivalves from South Korea. They reported that the average number of microplastics in the bivalves was 0.15 ± 0.20 items g^{-1} and 0.97 ± 0.74 items individual $^{-1}$.

This summary shows that a wide variety of edible aquatic organisms are being exposed and able to take up MNPs directly or indirectly from their habitats. Fiber were reported as the commonly observed plastic fragments which may indicate that shape of MNPs play important role in their uptake and accumulation. No robust conclusion can be made yet because the existing limitations in monitoring methodologies for MNPs e.g. MNPs sampling and handling bias the final outcomes. For example, due to the limitation in sampling methods, most of the studies have used methods that are applicable for large size microplastic while disregarding the small size MNPs. Chemical composition of the MNPs also showed to have a striking effect on the accumulation of the MNPs in organisms. However, the comparison between the results of different studies is challenging as the results are laboratory-dependent, and the applied procedures and the reported data differ between studies due to the absence of standard operating protocols.

10.4 Responses attributed to additives in micro(nano)plastics

Plastics are usually mixed with various additives [27] to improve the functional properties of plastic products [28]. Phthalate plasticizers, brominated flame retardants (BFRs) and antioxidants (nonylphenol) are used in different quantities in plastics [29, 30]. For instance, additives in some PVC products make up to 50 % of the polymer weight [25, 31]. Apart from the effects induced by MNPs themselves, the additives can cause toxicity. Previous studies reported that plastic particles could transfer plastic-specific BFRs such as BDE-209 to seabirds upon ingestion of the plastic particles [32, 33]. Also, the transfer of organophosphorus flame retardants by microplastics to mouse tissues was documented [34], and ingestion of microplastics resulted in the accumulation of polybrominated diphenyl ethers (PBDEs) in fish [35, 36] and lugworms [37]. Rochman et al. [36] reported that there is a correlation between plastic contamination and the level of PBDEs in fish tissues. However the study performed by Horton et al. [38] did not show differences when daphnids were exposed to high versus low binding chemicals mixed with micron-sized plastics. These findings indicate that MPNs can act as a vector for transferring additives in organisms and probably humans. It is likely that the MNPs may change the toxicity profile of the additives by inducing the same mode of action while in a different location in organisms' bodies. This can be also applicable to other co-occurring chemicals that are sorbed to MNPs from the surrounding environment.

10.5 Understanding responses attributed to MNPs in laboratory setting

It is a huge quest how MNPs influence uptake, translocation and adverse effects to organisms. Although understanding these processes in environmental samples is at the moment a challenging task, performing laboratory experiments with model organisms can facilitate understanding the mechanisms behind the possible toxicity of MNPs, particularly MNPs of small size. A recent published case study is summarized to link ingestion of nano-sized plastics with key events leading to an adverse outcome pathway in zebrafish larvae. The zebrafish embryo is a useful small model for investigating vertebrate development because of its transparency, low cost, transgenic and morpholino capabilities, conservation of cell signaling, and concordance with mammalian developmental phenotypes. Given these advantages,

10. Micro(nano)plastics in aquatic organisms, transferability of knowledge from nanowires

the zebrafish embryo has been considered as an alternative model for traditional *in vivo* developmental toxicity screening whilst allowing to elucidate mechanisms and adverse outcome pathways for abnormal development. For example, the series of stages for development of the embryo of the zebrafish, *Danio (Brachydanio) rerio* are well described and understood (Figure 10.2), which allows providing insight into sub-lethal toxicity at each developmental stage.

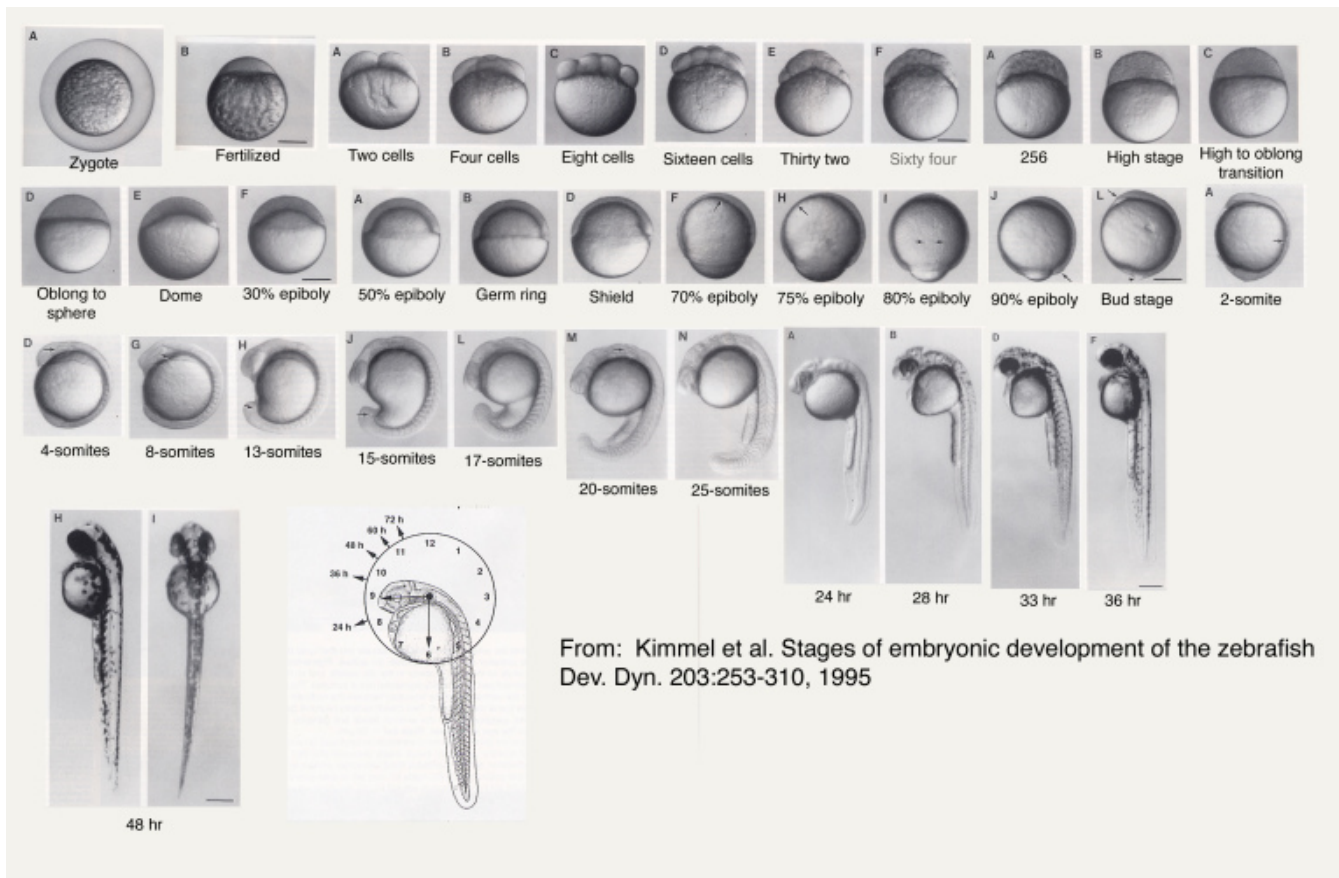


Figure 10.2.: Zebrafish embryo development: embryo in chorion till zebrafish larvae.

To date, several endpoints indicative of activation of metabolic processes to support energy-demanding activities were assessed in control and polystyrene nanoplastics-exposed larvae. Changes in metabolic rate are widely accepted as a proxy for stress response. Within the study performed by Brun et al. [39], effects of 25 nm polystyrene nanoplastics on glucose metabolism in larval zebrafish showed to follow a dose-dependent response. Transgenic zebrafish lines (Glucocorticoid receptor mutants) having an elevated glucose level as well as wild-type larvae with pharmacologically reduced activity (using mifepristone) did not appear to have affected glucose levels after the exposure. In a next step, Brun et al. [39] investigated the involvement of cortisol in the response to polystyrene nanoplastics exposure, cortisol levels in whole larvae were measured. Elevated cortisol secretion is a major hallmark of stress response. Cortisol was significantly increased in the wild-type strain AB/TL after exposure to the particles. The verification of this mechanism was obtained by using a transgenic zebrafish strain that has elevated cortisol levels. The treatment (exposure with polystyrene nanoplastics) versus the control here did not give differences within the cortisol levels.

In wild types, elevated cortisol levels induced by stress, starvation, or glucocorticoids can stimulate gluconeogenesis and thereby increase blood glucose levels. This was subsequently tested by using the wild types as well as the

transgenic lines, and showed to have indeed a strong chain reaction. Behavioral analysis often is chosen as an apical more sensitive toxicity endpoint. After an acclimation period the zebrafish larvae are subjected to the light–dark challenge test. Zebrafish larvae swim actively in the dark. In the light this activity will diminish. The zebrafish larvae that were exposed to nanoplastics had higher swimming activity and achieved a longer swimming distance as tracked for the control larvae (Figure 10.3, [39]). In brief, the study showed that 25 nm polystyrene nanoparticles disrupt glucose homeostasis with concurrent activation of the stress response system, eventually disrupting the swimming behavior.

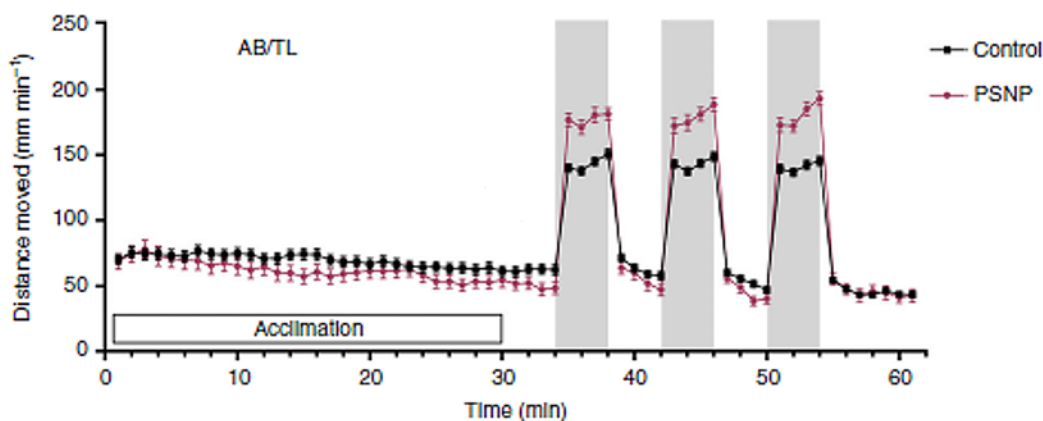


Figure 10.3.: Polystyrene NP exposure effects on larval behavior. Locomotor activity of control ($n = 165$, biologically independent replicates) and PSNP ($n = 91$, biologically independent replicates) exposed AB/TL larvae throughout behavioral tracking with 34 min acclimation and three times 4-min dark challenge phase followed by 4-min light recovery phases. Activity was measured as distance moved (mm) within 1 min per individual larvae.

These data may be transferable to MNPs of the same composition, size, and shape in the environment and may be transferable to other organisms.

10.6 Transferability of knowledge on nanowires to micro(nano)fibers

In this chapter we considered wire-shape micro/nanoscale materials to represent fibre-shaped MNPs. MNP fibers may be emitted into the environment (see previous chapters in this book) as they originate from dust, fragments and clothing. Only a few studies have reported acute and chronic ecological effects of wire-shape micro/nanoscale materials on aquatic and terrestrial organisms. The structural difference between wire-shape micro/nanoscale and other shapes of micro/nanoparticles has, unsurprisingly, resulted in the assumption of the existence of potential disparity in their distinct properties, behaviors, biological uptake and toxicity. Unlike nanoparticles which have attracted broad research attentions regarding their fate to effects among researchers, discussion on relevant topics of nanowires, for example, is still far away from being comprehensive. The absence of previous knowledge has largely hindered understanding the fate of MNPs fibers and their co-occurring contaminants in organisms and in the human body.

One attempt to measure nanoplastics and nanowires (carbon nanotubes) in complex biological media is published by Abdolapur Monikh et al. [40]. They reported the successful extraction of nanoplastics from biological media while facing challenges in extracting nanowires (recovery approx. 20%). This indicated the complexity of investigating MNP fibers in biota and the environment. In this chapter, we therefore extended literature search towards metal-based nanowires in order to extrapolate the knowledge obtained to date about metallic nanowires to understand the adverse effects regarding the shape of MNP fibers.

10. Micro(nano)plastics in aquatic organisms, transferability of knowledge from nanowires

A nanowire-specific literature search was performed using the Web search engine: Web of Science and an additional search within the the Online Chemical Modeling Environment (OCHEM, <http://ochem.eu>) database [41] as this includes information from grey literature. OCHEM is a web-based platform that provides tools for automation of typical steps necessary to create predictive models for assessing the fate and toxicity of chemicals. The platform consists of two major subsystems: a database of experimental measurements and a modeling framework. A total of seven studies were found. When summarizing the main findings of each of these seven studies, the following general conclusions may be drawn (Table 10.1).

Table 10.1.: Conclusions of the study.

Conclusions of the study	Reference
Algae were exposed to gold nanowires. However, the algal cells did not take up the gold nanowires. The wire also showed no membrane damage to the algal cells.	Abdolahpur Monikh et al. [40]
Nanowires do not cause mortality in exposed <i>Daphnia magna</i> . The nanowires fragmented in the body of the organisms and this could facilitate translocation across the intestinal epithelium.	Mattsson et al. [42]
Gallium phosphide nanowires are not taken up through dietary uptake into <i>Drosophila</i> tissues. The wires do not elicit a measurable immune response or changes in genome-wide gene expression and do not significantly affect life span or somatic mutation rate.	Adolfsson et al. [43]
A significant astrocyte response was observed in rat brain after one week exposure to nanowires as compared to controls. The nanowires are phagocytized by ED1 positive microglia, and some of them are degraded and/or transported away from the brain of the rat.	Eriksson Linsmeier et al. [44]
Silica nanowires did not cause toxicity at concentrations below 190 mg ml ⁻¹ to human epithelial cells but increased necrosis in cells exposed to high concentrations. In comparison to silica nanowires, silica nanoparticles showed very little cytotoxicity even at the highest concentrations.	Adili et al. [45]
Silicon carbide nanowires were toxic to amphipods, but no toxicity was observed in midges, oligochaete and mussels.	Mwangi et al. [46]
Silica nanomaterials with aspect ratios greater than 1 are highly toxic to zebrafish embryos and induce embryo deformities. Silica nanomaterials with an aspect ratio of 1 are neither toxic nor teratogenic at the same concentrations. Silica nanowires may interfere with neurulation and disrupt expression of sonic hedgehog, which encodes a key midline signaling factor.	Nelson et al. [47]

From the results of this literature search it is to be concluded that the toxicity of nanowires is limited as reported effect levels are in general quite high (up till 190 g l⁻¹). The aspect ratio is shown to be of importance in modulating adverse effects of nanowires. In addition to the key findings deduced from the database search of shorter nanowires in general being more toxic than nanowires of higher aspect ratio, it is stressed that fragmentation of nanowires is an issue to be considered during fate and effect testing. This implies that MNP fibers with similar aspect ratio may follow the same fate and toxicity pathways.

From the database OCHEM, eleven references were available [47–57]. A morphological comparison of CeO₂

nanowires and nanoparticles showed that CeO₂ nanoparticles mainly expose the stable plane on their surface, while the CeO₂ nanowires predominantly expose the reactive planes leading to the much higher catalytic activity of these materials [53]. This suggests that nanowires are more reactive than their corresponding nanoparticle analogues. This enhanced reactivity is not necessarily indicative of enhanced toxicity of nanowires as enhanced reactivity might primarily induce enhanced aggregation and hence lower bio-availability of reactive nanowires. It actually is the balance between enhanced chemical reactivity and enhanced interactions with biotic ligands which will determine whether reactive nanowires are more toxic than their nanoparticle-analogues. Unfortunately, quantitative information on this issue is not yet available.

A distinct difference between Ag nanowires and Ag nanoparticles and nanoplates with regard to particle aggregation in Holtfreter's medium was also reported, and was assumed to be caused by the high aspect ratio of nanowires [54]. Silica nanowires of high aspect ratio (> 1) were also evidenced to be highly toxic and teratogenic (LD50 = 110 µg g⁻¹ embryo) in developing zebrafish embryos [47]. The aspect ratio of 22 of CeO₂ nanowires is seen as allowing the nanowires to induce lysosomal damage, given the fact that the length of these NWs is below the critical length of ≈ 200 nm assessed by Ji et al. [55]. Meanwhile, shorter nanowires reportedly tend to be more toxic than longer ones based on the limited observations on Ag [52], CeO₂ [55], and Fe nanowires [56]. The efficiency of uptake of Au nanowires by fibroblast and HeLa cells was found to be higher for shorter nanowires [57] Uptake processes in cells may also differ for Fe nanowires with different lengths [56].

From the results of this database search it can overall be concluded that the aspect ratio is of importance in modulating adverse effects of nanowires. Shorter nanowires tend to be more toxic than nanowires of higher aspect ratio. Tentatively, nanowires above a critical length of ≈ 200 nm are assumed to be non-toxic. Further verification of this rule of thumb is however needed.

10.7 To summarize and recommend

MNPs are taken up in a variety of organisms. The water exposure pathway is of importance and transfer towards higher organism levels, e.g. from primary producers to consumers. Adverse effects of MNPs are also recorded, and a adverse outcome pathway is related to the energy budgets. Either observed from field and lab studies in which food ingestion reduced in organisms leading to lower energy levels, as well as in the case of zebrafish larvae where a chain reaction via the glucose metabolism pathway eventually leads to 50% more activity in a standard behavior test compared to larvae that were not exposed to MNPs. This type of systematic investigation of the chain of reactions initiated by MNPs can provide the building blocks to develop a more mechanistic understanding of responses. In general, toxicity of nanowires via water is limited as reported effect levels are in general quite high. Shorter nanowires are in general more toxic than nanowires of higher aspect ratio, and it is stressed that fragmentation of nanowires is an issue to be considered during fate and effect testing. Various detection techniques are not trained to work with nanowires but rather are able to measure spherical particles. The aspect ratio is shown to be of key importance in modulating adverse effects of nanowires.

References

- [1] P. Europe. "An analysis of European plastics production, demand and waste data". In: *Plastics—the facts* (2015) (cited on page 147).
- [2] J. R. Jambeck, R. Geyer, C. Wilcox, T. R. Siegler, M. Perryman, A. Andrady, R. Narayan, and K. L. Law. "Plastic waste inputs from land into the ocean". In: *Science* 347.6223 (2015), pages 768–771 (cited on page 147).
- [3] D. K. Barnes, F. Galgani, R. C. Thompson, and M. Barlaz. "Accumulation and fragmentation of plastic debris in global environments". In: *Philosophical transactions of the royal society B: biological sciences* 364.1526 (2009), pages 1985–1998 (cited on page 147).

- [4] C. L. Waller, H. J. Griffiths, C. M. Waluda, S. E. Thorpe, I. Loaiza, B. Moreno, C. O. Pachterres, and K. A. Hughes. “Microplastics in the Antarctic marine system: an emerging area of research”. In: *Science of the total environment* 598 (2017), pages 220–227 (cited on page 147).
- [5] W. Courtene-Jones, B. Quinn, S. F. Gary, A. O. Mogg, and B. E. Narayanaswamy. “Microplastic pollution identified in deep-sea water and ingested by benthic invertebrates in the Rockall Trough, North Atlantic Ocean”. In: *Environmental pollution* 231 (2017), pages 271–280 (cited on page 147).
- [6] B. C. Gibb. “Plastics are forever”. In: *Nature Chemistry* 11 (2019), pages 394–395 (cited on page 147).
- [7] E. D. Goldberg. “Diamonds and plastics are forever?” In: *Marine pollution bulletin* 28.8 (1994), page 466 (cited on page 147).
- [8] L. Van Cauwenberghe and C. R. Janssen. “Microplastics in bivalves cultured for human consumption”. In: *Environmental pollution* 193 (2014), pages 65–70 (cited on pages 147, 149).
- [9] M. A. Browne, A. Dissanayake, T. S. Galloway, D. M. Lowe, and R. C. Thompson. “Ingested microscopic plastic translocates to the circulatory system of the mussel, *Mytilus edulis* (L.)” In: *Environmental science & technology* 42.13 (2008), pages 5026–5031 (cited on page 147).
- [10] E. M. Chua, J. Shimeta, D. Nugegoda, P. D. Morrison, and B. O. Clarke. “Assimilation of polybrominated diphenyl ethers from microplastics by the marine amphipod, *Allorchestes compressa*”. In: *Environmental science & technology* 48.14 (2014), pages 8127–8134 (cited on page 147).
- [11] C. Nobre, M. Santana, A. Maluf, F. Cortez, A. Cesar, C. Pereira, and A. Turra. “Assessment of microplastic toxicity to embryonic development of the sea urchin *Lytechinus variegatus* (Echinodermata: Echinoidea)”. In: *Marine pollution bulletin* 92.1-2 (2015), pages 99–104 (cited on page 148).
- [12] C.-B. Jeong, E.-J. Won, H.-M. Kang, M.-C. Lee, D.-S. Hwang, U.-K. Hwang, B. Zhou, S. Souissi, S.-J. Lee, and J.-S. Lee. “Microplastic size-dependent toxicity, oxidative stress induction, and p-JNK and p-p38 activation in the monogonont rotifer (*Brachionus koreanus*)”. In: *Environmental science & technology* 50.16 (2016), pages 8849–8857 (cited on page 148).
- [13] I. Paul-Pont, C. Lacroix, C. G. Fernández, H. Hégaret, C. Lambert, N. Le Goïc, L. Frère, A.-L. Cassone, R. Sussarellu, C. Fabioux, et al. “Exposure of marine mussels *Mytilus* spp. to polystyrene microplastics: toxicity and influence on fluoranthene bioaccumulation”. In: *Environmental pollution* 216 (2016), pages 724–737 (cited on page 148).
- [14] A. J. Watts, M. A. Urbina, S. Corr, C. Lewis, and T. S. Galloway. “Ingestion of plastic microfibers by the crab *Carcinus maenas* and its effect on food consumption and energy balance”. In: *Environmental science & technology* 49.24 (2015), pages 14597–14604 (cited on page 148).
- [15] F. Gallo, C. Fossi, R. Weber, D. Santillo, J. Sousa, I. Ingram, A. Nadal, and D. Romano. “Marine litter plastics and microplastics and their toxic chemicals components: the need for urgent preventive measures”. In: *Environmental sciences Europe* 30.1 (2018), page 13 (cited on page 148).
- [16] O. Setälä, M. Lehtiniemi, R. Coppock, and M. Cole. “Microplastics in marine food webs”. In: *Microplastic contamination in aquatic environments*. Elsevier, 2018, pages 339–363 (cited on page 148).
- [17] A. Rudnicka and K. K. Hozyasz. “Choice of water in healthy baby nutrition-practical aspects”. In: *Pediatrics I Medycyna Rodzinna-Paediatrics and Family Medicine* 14.1 (2018), pages 33–46 (cited on page 148).
- [18] M. Carbery, W. O’Connor, and T. Palanisami. “Trophic transfer of microplastics and mixed contaminants in the marine food web and implications for human health”. In: *Environment international* 115 (2018), pages 400–409 (cited on page 148).
- [19] J. C. Prata. “Airborne microplastics: consequences to human health?” In: *Environmental pollution* 234 (2018), pages 115–126 (cited on page 148).
- [20] G. E. De-la-Torre. “Microplastics: an emerging threat to food security and human health”. In: *Journal of Food Science and Technology* (2019). DOI: 10.1007/s13197-019-04138-1 (cited on page 148).
- [21] J. Li, D. Yang, L. Li, K. Jabeen, and H. Shi. “Microplastics in commercial bivalves from China”. In: *Environmental pollution* 207 (2015), pages 190–195 (cited on page 148).
- [22] B. De Witte, L. Devriese, K. Bekaert, S. Hoffman, G. Vandermeersch, K. Cooreman, and J. Robbens. “Quality assessment of the blue mussel (*Mytilus edulis*): Comparison between commercial and wild types”. In: *Marine pollution bulletin* 85.1 (2014), pages 146–155 (cited on page 148).
- [23] J. Teng, Q. Wang, W. Ran, D. Wu, Y. Liu, S. Sun, H. Liu, R. Cao, and J. Zhao. “Microplastic in cultured oysters from different coastal areas of China”. In: *Science of the total environment* 653 (2019), pages 1282–1292 (cited on pages 148, 149).

- [24] F. M. Baalkhuyur, E.-J. A. B. Dohaish, M. E. Elhalwagy, N. M. Alikunhi, A. M. AlSuwailem, A. Røstad, D. J. Coker, M. L. Berumen, and C. M. Duarte. “Microplastic in the gastrointestinal tract of fishes along the Saudi Arabian Red Sea coast”. In: *Marine pollution bulletin* 131 (2018), pages 407–415 (cited on page 149).
- [25] W. C. Li. “The occurrence, fate, and effects of microplastics in the marine environment”. In: *Microplastic contamination in aquatic environments*. Elsevier, 2018, pages 133–173 (cited on page 149).
- [26] Y. Cho, W. J. Shim, M. Jang, G. M. Han, and S. H. Hong. “Abundance and characteristics of microplastics in market bivalves from South Korea”. In: *Environmental pollution* 245 (2019), pages 1107–1116 (cited on page 149).
- [27] A. A. Koelmans, E. Besseling, and E. M. Foekema. “Leaching of plastic additives to marine organisms”. In: *Environmental pollution* 187 (2014), pages 49–54 (cited on page 149).
- [28] J. N. Hahladakis, C. A. Velis, R. Weber, E. Iacovidou, and P. Purnell. “An overview of chemical additives present in plastics: migration, release, fate and environmental impact during their use, disposal and recycling”. In: *Journal of hazardous materials* 344 (2018), pages 179–199 (cited on page 149).
- [29] J. D. Meeker, S. Sathyanarayana, and S. H. Swan. “Phthalates and other additives in plastics: human exposure and associated health outcomes”. In: *Philosophical transactions of the royal society B: biological sciences* 364.1526 (2009), pages 2097–2113 (cited on page 149).
- [30] R. C. Thompson, C. J. Moore, F. S. Vom Saal, and S. H. Swan. “Plastics, the environment and human health: current consensus and future trends”. In: *Philosophical transactions of the royal society B: biological sciences* 364.1526 (2009), pages 2153–2166 (cited on page 149).
- [31] E. A. Coleman. “Applied plastics engineering handbook: processing, materials, and applications”. In: edited by M. Kutz. William Andrew, 2016. Chapter Plastics Additives, pages 489–500 (cited on page 149).
- [32] K. Tanaka, H. Takada, R. Yamashita, K. Mizukawa, M.-a. Fukuwaka, and Y. Watanuki. “Accumulation of plastic-derived chemicals in tissues of seabirds ingesting marine plastics”. In: *Marine pollution bulletin* 69.1-2 (2013), pages 219–222 (cited on page 149).
- [33] K. Tanaka, H. Takada, R. Yamashita, K. Mizukawa, M.-a. Fukuwaka, and Y. Watanuki. “Facilitated leaching of additive-derived PBDEs from plastic by seabirds’ stomach oil and accumulation in tissues”. In: *Environmental science & technology* 49.19 (2015), pages 11799–11807 (cited on page 149).
- [34] Y. Deng, Y. Zhang, R. Qiao, M. M. Bonilla, X. Yang, H. Ren, and B. Lemos. “Evidence that microplastics aggravate the toxicity of organophosphorus flame retardants in mice (*Mus musculus*)”. In: *Journal of hazardous materials* 357 (2018), pages 348–354 (cited on page 149).
- [35] C. M. Rochman, E. Hoh, T. Kurobe, and S. J. Teh. “Ingested plastic transfers hazardous chemicals to fish and induces hepatic stress”. In: *Scientific reports* 3 (2013), page 3263 (cited on page 149).
- [36] C. M. Rochman, R. L. Lewison, M. Eriksen, H. Allen, A.-M. Cook, and S. J. Teh. “Polybrominated diphenyl ethers (PBDEs) in fish tissue may be an indicator of plastic contamination in marine habitats”. In: *Science of the total environment* 476 (2014), pages 622–633 (cited on page 149).
- [37] M. A. Browne, S. J. Niven, T. S. Galloway, S. J. Rowland, and R. C. Thompson. “Microplastic moves pollutants and additives to worms, reducing functions linked to health and biodiversity”. In: *Current biology* 23.23 (2013), pages 2388–2392 (cited on page 149).
- [38] A. A. Horton, M. G. Vijver, E. Lahive, D. J. Spurgeon, C. Svendsen, R. Heutink, P. M. van Bodegom, and J. Baas. “Acute toxicity of organic pesticides to *Daphnia magna* is unchanged by co-exposure to polystyrene microplastics.” In: *Ecotoxicology and environmental safety* 166 (2018), pages 26–34. ISSN: 1090-2414 (cited on page 149).
- [39] N. R. Brun, P. van Hage, E. R. Hunting, A.-P. G. Haramis, S. C. Vink, M. G. Vijver, M. J. M. Schaaf, and C. Tudorache. “Polystyrene nanoplastics disrupt glucose metabolism and cortisol levels with a possible link to behavioural changes in larval zebrafish”. In: *Communications Biology* 2.1 (Oct. 2019), pages 1–9 (cited on pages 150, 151).
- [40] F. Abdolahpur Monikh, N. Grundschober, S. Romeijn, D. Arenas-Lago, M. G. Vijver, W. Jiskoot, and W. J. G. M. Peijnenburg. “Development of methods for extraction and analytical characterization of carbon-based nanomaterials (nanoplastics and carbon nanotubes) in biological and environmental matrices by asymmetrical flow field-flow fractionation.” In: *Environmental pollution* 255 (2019), page 113304 (cited on pages 151, 152).
- [41] I. Sushko et al. “Online chemical modeling environment (OCHEM): web platform for data storage, model development and publishing of chemical information”. In: *Journal of computer-aided molecular design* 25.6 (2011), pages 533–554 (cited on page 152).
- [42] K. Mattsson, K. Adolfsson, M. T. Ekvall, M. T. Borgström, S. Linse, L.-A. Hansson, T. Cedervall, and C. N. Prinz. “Translocation of 40 nm diameter nanowires through the intestinal epithelium of *Daphnia magna*.” In: *Nanotoxicology* 10 (2016), pages 1160–1167 (cited on page 152).

- [43] K. Adolfsson, M. Schneider, G. Hammarin, U. Häcker, and C. N. Prinz. “Ingestion of gallium phosphide nanowires has no adverse effect on Drosophila tissue function.” In: *Nanotechnology* 24 (2013), page 285101 (cited on page 152).
- [44] C. Eriksson Linsmeier, C. N. Prinz, L. M. E. Pettersson, P. Caroff, L. Samuelson, J. Schouenborg, L. Montelius, and N. Danielsen. “Nanowire biocompatibility in the brain—looking for a needle in a 3D stack.” In: *Nano letters* 9 (2009), pages 4184–4190 (cited on page 152).
- [45] A. Adili, S. Crowe, M. F. Beaux, T. Cantrell, P. J. Shapiro, D. N. McIlroy, and K. E. Gustin. “Differential cytotoxicity exhibited by silica nanowires and nanoparticles”. In: *Nanotoxicology* 2 (2008), pages 1–8 (cited on page 152).
- [46] J. N. Mwangi, N. Wang, A. Ritts, J. L. Kunz, C. G. Ingersoll, H. Li, and B. Deng. “Toxicity of silicon carbide nanowires to sediment-dwelling invertebrates in water or sediment exposures”. In: *Environmental Toxicology and Chemistry* 30.4 (2011), pages 981–987 (cited on page 152).
- [47] S. M. Nelson, T. Mahmoud, M. Beaux II, P. Shapiro, D. N. McIlroy, and D. L. Stenkamp. “Toxic and teratogenic silica nanowires in developing vertebrate embryos”. In: *Nanomedicine: Nanotechnology, Biology and Medicine* 6.1 (2010), pages 93–102 (cited on pages 152, 153).
- [48] J. Kwak and Y.-J. An. “A review of the ecotoxicological effects of nanowires”. In: *International journal of environmental science and technology* 12.3 (2015), pages 1163–1172 (cited on page 152).
- [49] M. Visnapuu, U. Joost, K. Juganson, K. Künnis-Beres, A. Kahru, V. Kisand, and A. Ivask. “Dissolution of silver nanowires and nanospheres dictates their toxicity to Escherichia coli”. In: *BioMed research international* 2013 (2013) (cited on page 152).
- [50] M. C. Artal, R. D. Holtz, F. Kummrow, O. L. Alves, and G. d. A. Umbuzeiro. “The role of silver and vanadium release in the toxicity of silver vanadate nanowires toward Daphnia similis”. In: *Environmental toxicology and chemistry* 32.4 (2013), pages 908–912 (cited on page 152).
- [51] M. J. Kim and S. Shin. “Toxic effects of silver nanoparticles and nanowires on erythrocyte rheology”. In: *Food and chemical toxicology* 67 (2014), pages 80–86 (cited on page 152).
- [52] L. D. Scanlan, R. B. Reed, A. V. Loguinov, P. Antczak, A. Tagmount, S. Aloni, D. T. Nowinski, P. Luong, C. Tran, N. Karunaratne, et al. “Silver nanowire exposure results in internalization and toxicity to Daphnia magna”. In: *Acs Nano* 7.12 (2013), pages 10681–10694 (cited on pages 152, 153).
- [53] M. Zhang, J. Li, H. Li, Y. Li, W. Shen, et al. “Morphology-dependent redox and catalytic properties of CeO₂ nanostructures: nanowires, nanorods and nanoparticles”. In: *Catalysis Today* 148.1-2 (2009), pages 179–183 (cited on pages 152, 153).
- [54] S. George, S. Lin, Z. Ji, C. R. Thomas, L. Li, M. Mecklenburg, H. Meng, X. Wang, H. Zhang, T. Xia, et al. “Surface defects on plate-shaped silver nanoparticles contribute to its hazard potential in a fish gill cell line and zebrafish embryos”. In: *ACS nano* 6.5 (2012), pages 3745–3759 (cited on pages 152, 153).
- [55] Z. Ji, X. Wang, H. Zhang, S. Lin, H. Meng, B. Sun, S. George, T. Xia, A. E. Nel, and J. I. Zink. “Designed synthesis of CeO₂ nanorods and nanowires for studying toxicological effects of high aspect ratio nanomaterials”. In: *ACS nano* 6.6 (2012), pages 5366–5380 (cited on pages 152, 153).
- [56] M.-M. Song, W.-J. Song, H. Bi, J. Wang, W.-L. Wu, J. Sun, and M. Yu. “Cytotoxicity and cellular uptake of iron nanowires”. In: *Biomaterials* 31.7 (2010), pages 1509–1517 (cited on pages 152, 153).
- [57] C.-W. Kuo, J.-J. Lai, K. H. Wei, and P. Chen. “Studies of Surface-Modified Gold Nanowires Inside Living Cells”. In: *Advanced Functional Materials* 17.18 (2007), pages 3707–3714 (cited on pages 152, 153).

11.1 . Health effects of synthetic fibers and nanoparticles: Advanced electron microscopy to determine nanoparticle and nanoplastic *in vivo*

By: Uschi M. Graham¹ , Günter Oberdörster²

- 1 – University of Kentucky Pharmaceutical Sciences, U.S.A.
- 2 – University of Rochester Medical Center, U.S.A.

11.1 Introduction

Environmental plastic pollution comes in numerous and diverse forms [1, 2]. The intake and resulting cellular effects of waterborne and airborne synthetic micro and nanoparticles, both fibrous and non-fibrous into biota and, more specifically, into the human body is a rapidly developing field [3]. Risk banding schemes are under development for gaining deeper insights into effects associated with micro and nanoplastics. Synthetic micro and nanoplastics are contaminating the environment [4]. Although the massive plastic debris floating in the oceans can be easily recognized as a manmade calamity, the micro and nanoparticle and fiber pollution cannot be seen and poses a ubiquitous challenge. Micro and nanoplastics comprise a broad range of polymeric particles/fibers (e.g., polyethylene, polystyrene, polyethylene terephthalate, etc.) that are below the 1 mm size threshold (1-1000 nm) and involve a multicomponent material that can consist of either primary or secondary plastics of diverse shapes. Nanofibers are characterized as materials that have at least one dimension that is 100 nm or less and high aspect ratios (> 1:3). Primary nanoplastics are generally derived from industrial processes that focused on the manufacture of such materials for various applications (e.g., cosmetics, fillers, laundry detergent powders, medical and diagnostics applications among others). Primary nanoplastics are made of a single type of polymer and are used in many niche markets as additives to enhance material properties. Although plastics are typically assumed to be not biodegradable, they can collapse and disintegrate and most secondary nanoplastics are derived from fragmentation of larger pieces and accumulate in water bodies including rivers, lakes, and oceans. Much of the micro and nanofiber load in water sources comes from laundering clothes that incorporate synthetic fibers.

Since plastics are generally derived from petroleum-based products, they can contain catalyst metals that were employed during the polymer synthesis processing steps [5]. In rivers and oceans, these organic and inorganic microscopic fragments become incorporated into plants and animals and ultimately merge in humans. The fate and effects of micro and nanoplastics in the environment and how to analyze the issues at hand are documented by Barcelo and Knepper [1]. Research that focuses on the ‘why and how’ micro and nanoplastics are harming the environment has been reviewed by Oliveira and Almeida [2], which shows how rapidly the number of studies reporting on plastic pollution is growing. Their overview on reported biological effects on mammalian species caused by micro and nanoplastics demonstrates that the adverse consequences are far ranging from altered metabolism and compromised

11. Advanced electron microscopy to determine nanoparticle and nanoplastic interactions in vivo

immune systems to neurotoxic effects. It is paramount to decrease the load and, and thereby impact of micro and nanoplastics worldwide. Inevitably, ultrafine plastics, both fibrous and non-fibrous, are encountered and taken in by humans and enter via different exposure routes (contaminated food, air and water pollution, etc.). Advanced manufacturing processes or filter technologies that reduce plastic pollution at the source have been addressed [6]. Proposed changes in legislature that would for example help a) mitigate micro and nanofiber pollution caused by laundering clothes [7] and, b) restrict plastic products with high production volumes but only single use which are starting to be implemented by governments around the globe. Case studies that investigated seawater including regions off the coast of British Columbia (Ocean Wise, Vancouver: <https://ocean.org/>) and in the Atlantic Ocean found evidence that the majority (70-90 %) of plastic debris involves fine fibers rather than spherical or irregularly formed particles with the bulk derived from synthetics (polyester, polyethylene, nylon, acrylic). Their high aspect ratio introduces an additional shape dependence on particle transport and uptake in the environment and related ecosystem, and human health effects are not yet understood. It is indisputable that the major impacts, prevalence and pervasive sources of synthetic micro and nanofibers in the oceans and inside biota demand immediate worldwide attention. Guidelines are needed on how best to analyze the enormous volumes of new data using standardized advanced methodologies. The micro and nanoplastics problem include both water and air contamination and their invasion, transport, and incorporation by and interaction with cells. A key issue that needs to be addressed is the interaction of ultrafine particulates (UFPs) with tissues after their translocation and potential bioprocessing. Bioprocessing refers to the physiochemical interaction of ultrafine fibrous and non-fibrous particles at the cellular and subcellular level which may or may not result in the modification of these invader substances or the alteration of tissues or both [8–10].

Mitigating pollution effects by focusing on air and water purification and, in particular the selective removal of micro and nano fibers using innovative filter techniques [6] has been outpacing the research efforts that are focused on understanding the damaging and cellular effects caused by the translocation and uptake of synthetic fibers and nanoparticles into living beings. This is partly because unlike with metal and metal oxide nanoparticles, polymeric nanoparticles and nanofibers are much more challenging to locate and visualize in low density organic tissue substrates which, in turn, makes it difficult to assign toxicological burdens to the micro and nanoplastics if their presence is uncertain. Therefore, analytical methods that focus on tissue specific fate of micro and nanoplastics of diverse shapes are needed to develop this field. The objective of this Chapter is to discuss the advanced analytical imaging techniques that are available and can distinguish nanosized particles in tissues at cellular and subcellular levels. This Chapter also addresses how to image the micro and nanoplastics after incorporation into biota including human organ tissues.

11.2 Background

Synthetic fibers and nanoparticles have many possible technological and commercial applications. They are used in water and air purification [11], lithium-air battery [12] and other energy storage systems, electronic devices [13], photonic structures [14], tissue engineering [15], and drug delivery [16], just to name some uses. The global plastic pollution crisis involves over 300 million tons of plastic every year, half of which is for single use only, and approximately 8 million tons of plastic contaminate the oceans every year (plasticoceans.org/the-facts). Unfortunately this is a reflection on our modern lifestyle choices but there are ample opportunities (<https://www.newplasticseconomy.org/projects/innovation-prize>) to reduce or redirect plastic waste. Attention has focused on the discontinuation of micro and nanosized plastics from pharmaceuticals, cosmetics, toothpaste and many other commodities since they are typically too small to be filtered by water treatment plants and work their way into rivers, lakes, oceans and into marine biota and, later, into humans [17]. Synthetic microfibers (less than 5 mm) and nanofibers (shorter than 1 μm) are released predominantly from garments during laundering (synthetic garments can shed large numbers of ultrafine fiber fragments during each washing cycle, pass unabated through filter systems in treatment plants [18] and ultimately accumulate in the oceans [4]).

Micro and nanofibers are derived from different polymers (polylactic acid, polycaprolactone, polyurethane,

polylactic-co-glycolic acid, poly3-hydroxybutyrate-co-3-hydroxyvalerate, polyethylene co-vinyl-acetate, etc.) and have different physiochemical properties. They also exhibit distinct exposure hazards [19]. Various methods can be applied to make plastic nanofibers including drawing, template-based synthesis, self-assembly, electrospinning and thermal-induced phase separation. Nanofibers may have different diameters depending on the nature and methods of formation of the precursor polymer used during production, but all micro and nanoplastics are unique for their high surface area-to-volume ratio compared with macro counterparts. Submicron-sized fibers typically range between 50 and 500 nanometers in length although shorter fibers have been produced [20]. To date, electrospinning is the most universally used method to generate nanofibers based on mass-production ease of continuous systems and polymer selectivity depending on expected product purposes [21]. Electrospinning allows for shape, size and structural control and can accommodate either natural or synthetic polymers and combine precursors to tune the functionality of the nanofiber products [22]. The electro-spun micro and nanofibers can be functionalized using various surface modification strategies, all of which will impact environmental transport, translocation, and potential incorporation of the nanofibers into biological hosts.

Ultrafine fibers, as opposed to nanoplastic beads, have irregular shape and mechanical strength that can pose threats to organisms during cellular uptake. Will the nanofiber pollution be to the textile industries what asbestos has been to the construction and building materials industries? Asbestos has been under intense inspection for decades [8] and there are clear health risks that have been identified such as fibrosis and cancer in the respiratory system in humans [23]. Even though, the impacts of synthetic micro and nanofiber pollution to the oceans and other ecosystems and the extent to which these fibers may inflict damage in living systems at the cellular and subcellular level has not been aptly gauged. Appropriately designed studies are needed to identify the extent to which synthetic ultrafine plastic fibers harm the ecosystem. This necessitates in depth expertise to distinguish which types of plastic micro/nanofibers interact with cellular systems and to what extent. In the following sections several important aspects will be discussed including a) a cellular stress response to invader (exogenous) nanoparticles with a focus on nanoplastics; b) advanced analytical imaging methods that help distinguish plastic components inside tissues and cells from other particulate inclusions; c) the fiber dilemma inside cells and a link to the formation of endogenous ferritin nanoparticles which could signal an inflammatory response; d) bioprocessing of the invader plastics.

11.3 Analytical imaging techniques for nanoparticles/fibers in tissues

Imaging nanoparticles at atomic resolution and coupled with analytical methods is a promising approach to investigate particle uptake, deposition, and bioprocessing inside tissues [24]. There are various techniques with different advantages, limitations, and varying degrees of expense that can be used to analyze particle location and potential reformation, ion concentration in tissues at or near dissolving particles. Advanced systems can deliver imaging resolution for particles trapped in cells at atomic level [25, 26]. In depth understanding of the cellular ultrastructure and nanoparticle tissue interactions are now possible because of advanced high-resolution analytical scanning electron microscopy HRSTEM [27–31]. The synthesis of secondary particles as a result of the tissue specific response and subsequent fate of nanomaterials and their interactions at the cellular and subcellular level can also be monitored. This will give in depth knowledge of tissue-particle interactions and helps identify effects that are caused by the environmental invader (pollutant) particles. HRSTEM provides a way to image local cellular milieus adjacent to a nanoparticle/fiber at molecular or near atomic resolution. Simultaneous application of energy dispersive spectroscopy (EDS) and electron energy loss spectroscopy (EELS) as described by Leapman and Ornberg [32] and Egerton [33] provides information on the tissue environment as well as the physiochemical nature of the invaders. HRSTEM can also identify invader particles/fibers (exogenous types) from those that form inside cells by a physiological cellular response mechanism (endogenous types). Examples will be shown in a later section. The HRSTEM with state-of-the art analytical imaging capabilities is routinely used to distinguish nanomaterials in technology fields such as catalysis, electronics, semiconductors and material synthesis, but when nanomaterials penetrated inside tissues the high-energy

11. Advanced electron microscopy to determine nanoparticle and nanoplastic interactions in vivo

electron beam can cause interactions and this requires unique sample preparation and handling [8, 34, 35]. The ultimate goal is to achieve a better understanding of the tissue structure [26, 36–38] and of the precise particle location at the cellular and subcellular level [8] and, at the same time, determine any structure-function relationships that may be due to the invasion of pollution particles. The important objective is to understand pollution nanoparticle effects inside cells and to determine toxicological outcomes [39, 40].

The crystal structure of tissue-trapped pollution nanoparticles inside a biological matrix may be analyzed by means of electron diffraction if the invader particles have a crystalline or semi-crystalline structure (example provided in later section). Individual crystalline fibrous or non-fibrous nanoparticles can be examined at a lattice resolution of down to 0.15 nm using aberration corrected STEM [31, 41] where advanced lens systems allow all electrons to enter the sample without scattering. However, if the fibrous or non-fibrous nanoparticles are amorphous as would be the case for most plastic micro particles (Figure 11.1) then electron diffraction would not yield information that could be used to identify the individual grains. Figure 11.1 shows side-by-side the high resolution TEM characteristics that typically apply to a wide range of inorganic nanoparticles (1-100 nm) versus nano plastic fibrous and non-fibrous particles (1-1000 nm).

Mineral and engineered NP (i.e., oxides, sulfides, nitrides, phosphates, carbonates, etc.) are distinguished in analytical TEM to be either crystalline or amorphous and by their morphologies (grains versus fibers or rods). They can also be characterized by either low or high density and distinct redox potentials (Figure 11.1). Metal NP (i.e., transition and noble metals, rare earth and alloys) are electron dense and under HRSTEM conditions appear bright due to the high degree of back scattered electrons. Different types of carbon nanoparticles (i.e., nanotubes/wires, graphene, carbon fibers, soot, etc.) can be either crystalline or amorphous, occur in a wide size range from nanodots (~ 1-3 nm) to long filaments (mm scale) and have high electron conductivity and low density. Industrially formed catalyst NP often are supported on either carbon or oxide structures. The inorganic nanoparticles after intake and translocation to different organ tissues including lung, liver, brain, blood, lymph, bone [39, 42] and to subcellular structures (macrophages and lysosomal regions) can be identified with HRSTEM based on their physiochemical properties (Figure 11.1). However, in case of micro/nano plastics (i.e., polyethylene, polypropylene, acrylics, polyesters and polystyrene, etc.) both low and high density polymers, the electron density is very similar to that of tissue and cellular structures and, hence, difficult to distinguish visually in HRSTEM in any organ tissue type (Figure 11.1). This applies to plastic foams, beads, sheets, fibers, and composites. They all have low electron densities and are x-ray amorphous. However, if the plastics have dissolved metal or metal oxide nanoparticle additives or crystalline carbon then the particle contrast versus tissue and cellular matrices in HRSTEM investigations would be greatly increased and can be distinguished optically and by performing chemical fingerprinting with EDS and EELS analysis (Figure 11.1). Advanced software technology including Gatan 'Digital Micrograph' and Oxford Instruments 'Aztec' are typically used to acquire elemental line profiles across particles or collect elemental maps (2D and 3D) in STEM mode with computerized EDS and EELS technology (www.gatan.com; <https://nano.oxinst.com>). Each scanned spot analyzes and collects a separate spectrum (either or both EDS and EELS) and collectively this provides spectrum images for a selected line profile or an entire area (mapping of tissue regions). This allows for elemental analysis even when particles/fibers are difficult to optically distinguish inside tissues. It also provides information on oxidative states via EELS analysis. Current scopes can image and acquire compositional as well as electronic data at the angstrom level [8, 43]. These HRSTEM analyses are of importance when investigating NPs that undergo bioprocessing which causes chemical and structural changes in the particles during tissue interactions. If nanoparticles transform in tissues, the EELS detector allows parent and daughter grains to be distinguished and elemental mapping can be used to identify the transformations [9]. Bioprocessing of inorganic nanoparticles has been documented in a host of organ tissues [8]. To our best knowledge, there is no HRSTEM information yet available that shows bioprocessing also occurs in case of plastics inside tissues and cells. However, this gaping hole in our knowledge is vital information that needs to be considered and examined if we want to understand the broader impacts plastic nanoparticles/fibers have after translocating to various organ tissues (Figure 11.1).

When it comes to toxicity, size matters. The smaller the particles that cells are exposed to, the higher their levels of

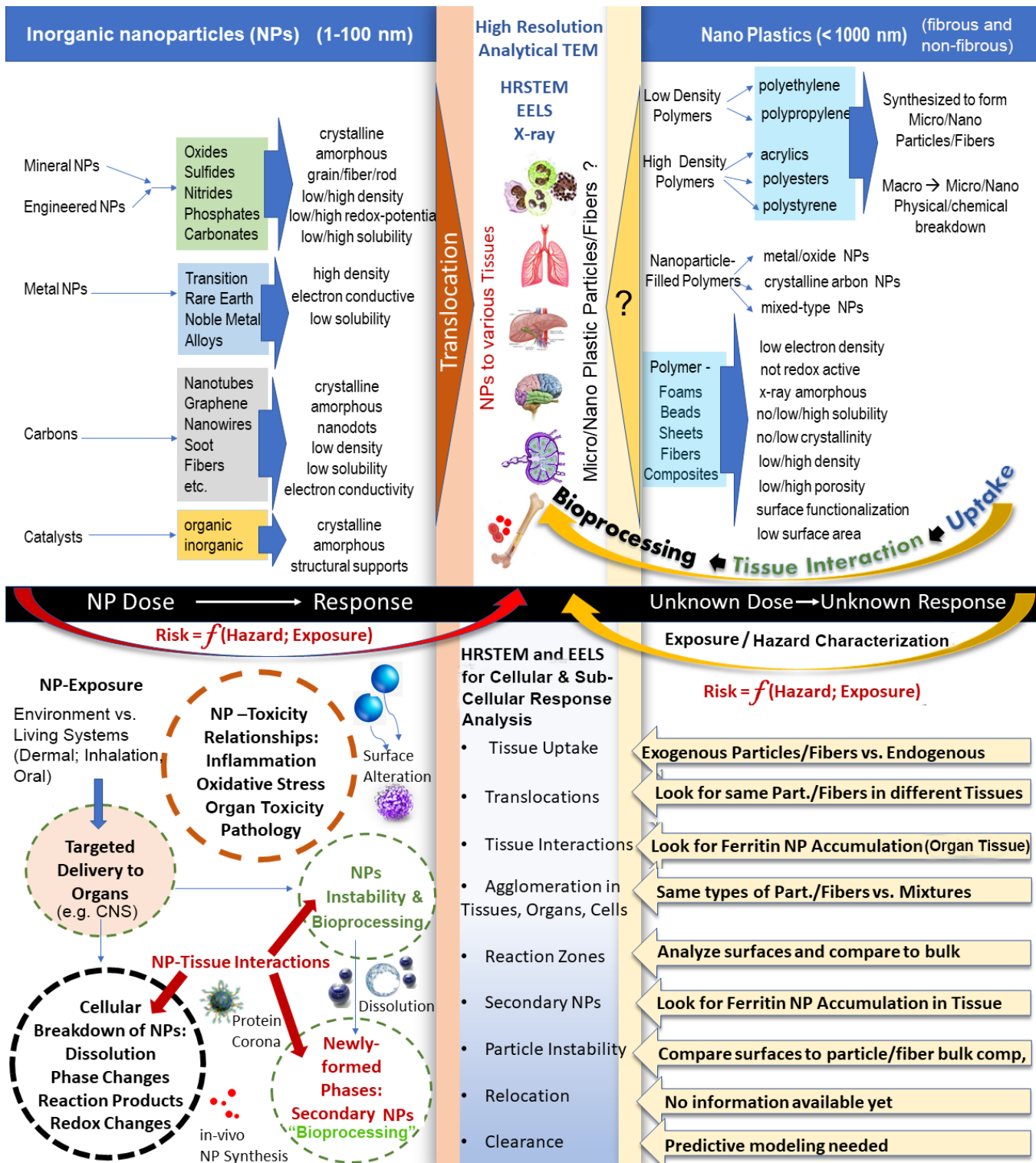


Figure 11.1.: Comparison of HRSTEM approach for engineered nanoparticles (left column) and micro/nano plastic particles/fibers (right column).

11. Advanced electron microscopy to determine nanoparticle and nanoplastic interactions in vivo

oxidative stress per mass, marked by the catalytic production of chemically reactive molecules such as peroxides, which, depending on the dose, could initiate inflammation and damage DNA. Analyzing plastic components at the nanoscale inside tissues is an emerging field and there are different and innovative experimental conditions that need to be accessed to optimize how to best use HRSTEM or aberration corrected STEM to fully characterize the nanoplastic fragments that potentially translocate to certain tissue regions or are part of macrophages after phagocytic uptake. Tissue materials typically have low contrast (low Z-contrast in HRSTEM) while any translocated metal (oxide, nitrate, phosphate, sulfide or sulphate NP, etc.) nanoparticles inside tissues (high Z-contrast for heavy atoms) appear as bright spots and can be readily located and analyzed with EDS or EELS [44]. Unfortunately, the Z-contrast is significantly reduced for plastic materials and it is, therefore, more difficult to discover and analyze nanoplastic particles inside tissues. If the nanoplastic particles are made of dense polymer, the contrast maybe more advantageous for HRSTEM and if the nanoplastic particles have adsorbed other elements to their surfaces then they may also be easier distinguishable from the host tissue [45]. Nanoplastics inside tissue matrices may be beam sensitive when the focused high-energy (200 keV) electron beam scans the sample. To alleviate some of the heat buildup from the beam interaction with the sample, thin tissue sections (~ 50 nm thickness) are secured onto carbon coated TEM grids. But any heat that is not conducted away from the sample may cause heat sensitive plastics to melt and potentially change their shape or vaporize which causes contamination onto the section. Contamination severely limits the ability to use EDS and EELS analytical capabilities of the HRSTEM. In this case, a cryo-transmission electron microscopy (cryo-TEM) application can be used to cool the sample to allow both imaging and elemental analysis of the translocated invader particles and fibers inside the tissue matrix. This also helps preserve the invader nanoplastic components within the biological host structure at the exact location without moving or rearranging any of the nanoplastic grains or fibers in the cellular regions. This is an important and growing area of research where new phenomena are being discovered related to the interaction of plastic nano-surfaces with cells or subcellular structures and improved sample preparation and analytical conditions are under development. It will help shed light on plastic particle uptake, tissue interactions and whether bioprocessing occurs (Figure 11.1).

For engineered nanoparticles and ambient aerosol particles various studies have been done to evaluate the exposure-dose-response relationship and the associated risk with ($\text{risk} = f(\text{hazard}; \text{exposure})$). For pollution fibrous and non-fibrous plastics both dose and response are unknown as of now, and therefore risk assessment studies need to be devised considering the full "Exposure-Dose-Response" paradigm. This involves exposure assessment (inhalation, oral, dermal; intake, uptake, translocation to target organs), hazard characterization (dose-exposure studies in vivo and in vitro) and risk characterization [46]. While this outlines the approach for designing toxicity studies in animals, for the purpose of risk assessment and identifying/providing target tissue samples for advanced HRSTEM analysis described here, there will be additional data from ongoing and planned epidemiological environmental and human studies to guide and support the design of toxicity studies of nanoplastics. This will help to develop greater knowledge of the targeted delivery of pollution plastics to organs (Figure 11.1). For engineered nanoparticles dose dependent inflammation, oxidative stress, cell toxicity, impaired organ function and pathology have been observed. Also, potential tissue interactions and cellular and subcellular breakdown of nanoparticles which depend on in vivo dissolution rates can cause formation of new reaction products (secondary NP) and redox changes all of which have been demonstrated to occur in vivo and in vitro and particle properties may be modified by protein surface coatings or other surface alterations.

In vivo nanoparticle synthesis that leads to the formation of phases separate from the invader particles or breakdown products such as the formation of ferritin nanoparticles (biomineralized iron) in the vicinity of translocated particles has been linked to inflammatory response mechanisms [9, 10, 27, 47]. Therefore, it will be vital to probe in future studies if ferritin nanoparticle formation can also be linked to the uptake and translocation of plastics into various organ tissues and related reactivities (Figure 11.1). Tissue uptake, interactions, translocations, agglomerations, reaction zones, instability, re-distribution, and clearance need to be determined for plastics in various tissues, organs and cells (Figure 11.1). It is important to distinguish between exogenous and endogenous particles when investigating tissue interactions with plastics. Also, when plastics translocated to different organ tissues the nature (chemistries, structures,

sizes, morphologies) of the plastics need to be compared in different organ tissues. Plastic surfaces in different tissue environments may be susceptible to forming reaction zones which can trigger protein adsorption [48, 49], ion leaching, pore formation among others, all of which are likely affecting the relocation and clearance potential of the pollution plastic components. HRSTEM investigations will need to be used to identify and characterize translocated plastics in different organ tissues to better understand the processes that alter plastics in biota. Collectively this information then can be used to build predictive modeling for plastics uptake into humans from environmental pollution (Figure 11.1).

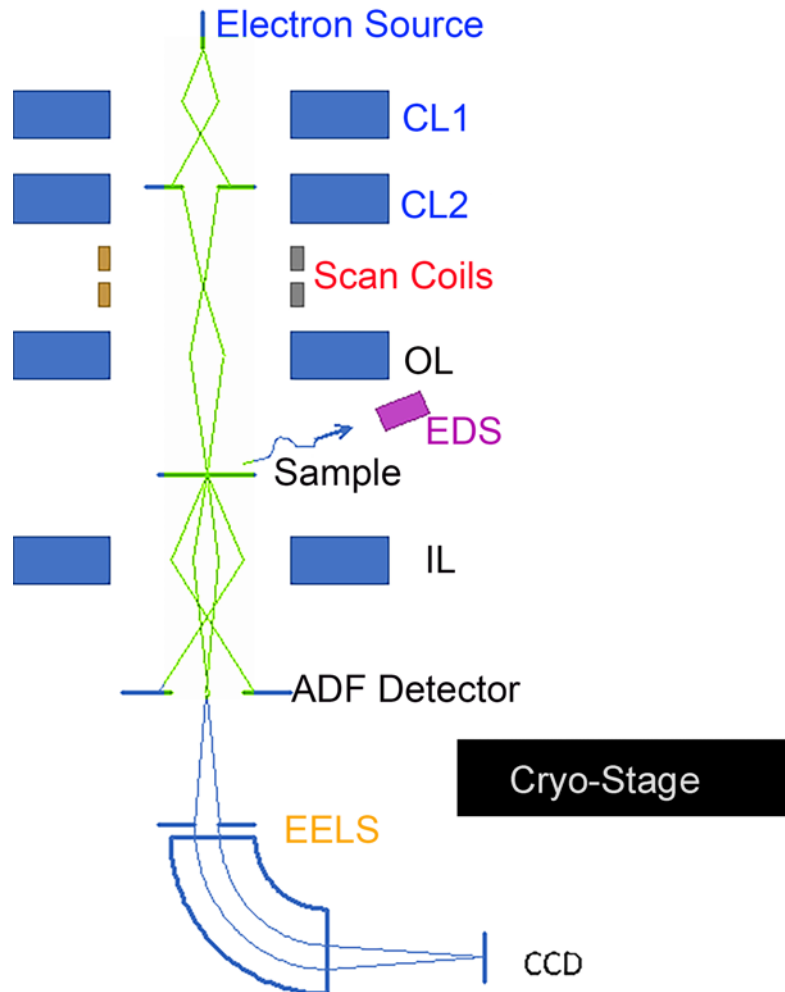


Figure 11.2.: Basic diagram of STEM mode for Dark Field imaging with EDS and EELS signal detectors.

A typical high-resolution microscope with analytical capabilities (Figure 11.2) would have both bright and dark field detectors in STEM mode operation and can analyze chemical information of the particles themselves but also detect metal ions that may have been released from the pollution particles into the surrounding tissue environments. Specialized methods of investigation are required. In STEM imaging mode the beam is focused by the condenser lenses and the objective lens pre-field to a point and scanned across the sample in a way comparable to a scanning electron microscope (SEM). The difference being that electrons transmitted through the specimen are imaged using either or both, a dark or bright field detector. Figure 11.2 is a simplified diagram of STEM operating mode. The condenser lens (CL) system focuses the electron beam into a spot on the specimen. The size of this spot is determined by the strength of the condenser lens 1. For high resolution work this requires the CL1 lens to be operated near maximum strength moving the CL crossover point closer to CL1. This reduces the magnification of CL2 and CL2 is

11. Advanced electron microscopy to determine nanoparticle and nanoplastic interactions in vivo

then adjusted to focus the spot on the polymer specimen Figure 11.2. For the nanoplastics, high-resolution analytical microscopy can be used to monitor a) changes in cell morphologies that may be caused by the translocation of the plastic particles/fibers into tissue regions and, b) changes (bioprocessing) in the plastic fibrous and non-fibrous parts that are triggered by the interaction with the cellular local environment. In other words, there are various cause and effect relationships between the plastic components and the cell that need to be considered and those studies can provide key insights into relationships between the plastic waste's synthetic identity and their biological reactivity which is also important for all other types of nanoparticle-cell interactions [50, 51]. Furthermore, these analyses help determine if particles react inside the tissue matrix and undergo aging (chemical or physical breakdown). The particle/fiber-tissue interface region may have elemental enrichments that can come from ions leached from the particle or ions including Fe, Ca, PO₄ that are upregulated due to cellular responses. STEM mode can detect elemental enrichments in the tissue at the tissue-particle interface region, in the particles (surface zone appears less dense, more porous with typical rounded edges that can form due to ion loss from corners or higher energy sites) and unaffected tissue regions for comparison. In STEM operation leached particle zones would look darker compared to the bulk particle since the leached zone contains less atoms. This information combined with spectroscopy computation and structure analyses can guide the observer to gain insights into chemical, structural and electronic nature of invader nanoparticles/fibers in tissues.

Exposure-Dose-Response relationships in the field of plastic nanoparticle/fiber toxicity are presently limited at best and probably not available for most plastic waste nanoparticles/fibers. Specifically, this includes detailed characterization of plastic waste nanoparticles/fibers after uptake and translocation into various tissues and their uptake and reactivity at the subcellular space. It is vital to obtain a more thorough knowledge of plastic waste bioprocessing in biological media to be able to make determinations of the long-term toxicological effects after exposure. This important task is further complicated by a fundamental shortage of data of the physicochemical changes plastic waste nanoparticles undergo inside cells and changes that occur inside the cells as a response to the plastic uptake. Polymer-based fibrous and non-fibrous nanoparticle interactions that occur inside a cellular environment will contribute individually and as groups of particles that determine the macro effects (health effects). It will be significantly more challenging to access the cellular effects of translocated plastics compared with inorganic crystalline nanoparticles, but there is also a great amount of know-how that can be gained from previous HRSTEM studies involving engineered nanoparticles.

11.4 Select case studies of nanoparticle-tissue interactions

The human CNS can be affected by inhaled ultrafine particles (UFPs) reaching the brain [52–55], which, of course, also include nanoplastics that could potentially translocate and reach the brain via the olfactory pathway (Figure 11.3). An increased risk for neurodegenerative diseases has been conjectured to be linked with exposure to particulate air pollution which involves neuronal nanoparticle transport from nasal deposits to the Central Nervous System (CNS) via olfactory and trigeminal pathways (Figure 11.3). The human nasal olfactory epithelium is a vital juncture where airborne pollutant deposition can occur over prolonged periods which could span a lifetime. Neurological disorders have been suspected to be related to long-term brain accumulation of toxicants. However, because of the minute size and concentration levels of UFPs translocated to olfactory bulb (OB) tissue it has been a challenge to determine the types of particles (shapes, sizes, chemistries, etc.) of UFPs that interact with the human olfactory system and deeper brain regions. Transport of spherical NPs will be different from needle or fiber-shaped invaders and this requires additional analyses to understand the health effects. Nose-to-brain transport of UFPs in mice induced activation of microglial cells and various NPs were shown in TEM along axonal pathways. Figure 11.3 provides an example of an autopsied human OB tissue and analytical HRSTEM imaging was used to identify the NPs that had translocated to the OB. Case in point, a thin section of the human OB tissue can be seen in Figure 11.3 that was imaged in STEM mode and reveals three discrete particle-rich regions which are distinguished as regions A, B and C. All the primary

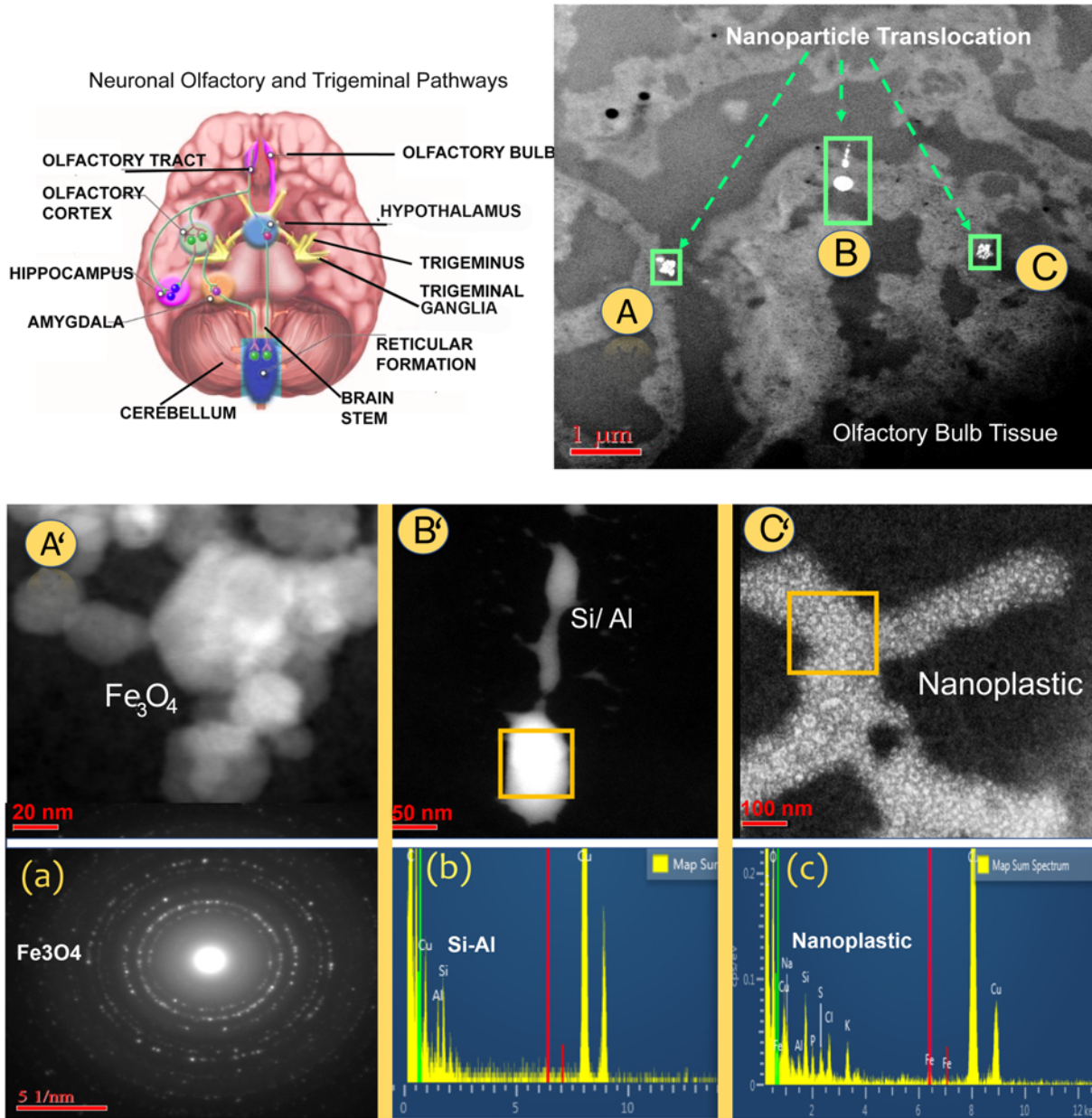


Figure 11.3.: Upper left shows the neuronal olfactory and trigeminal translocation pathways and CNS entry points for nanoparticles. Upper right shows the STEM image at low magnification shows the olfactory bulb tissue with 3 different regions where nanoparticles translocated to: A, B and C. A', B' and C' represent HRSTEM images of particles found in A, B and C with corresponding electron diffraction (a) and EDS analyses (b, c).

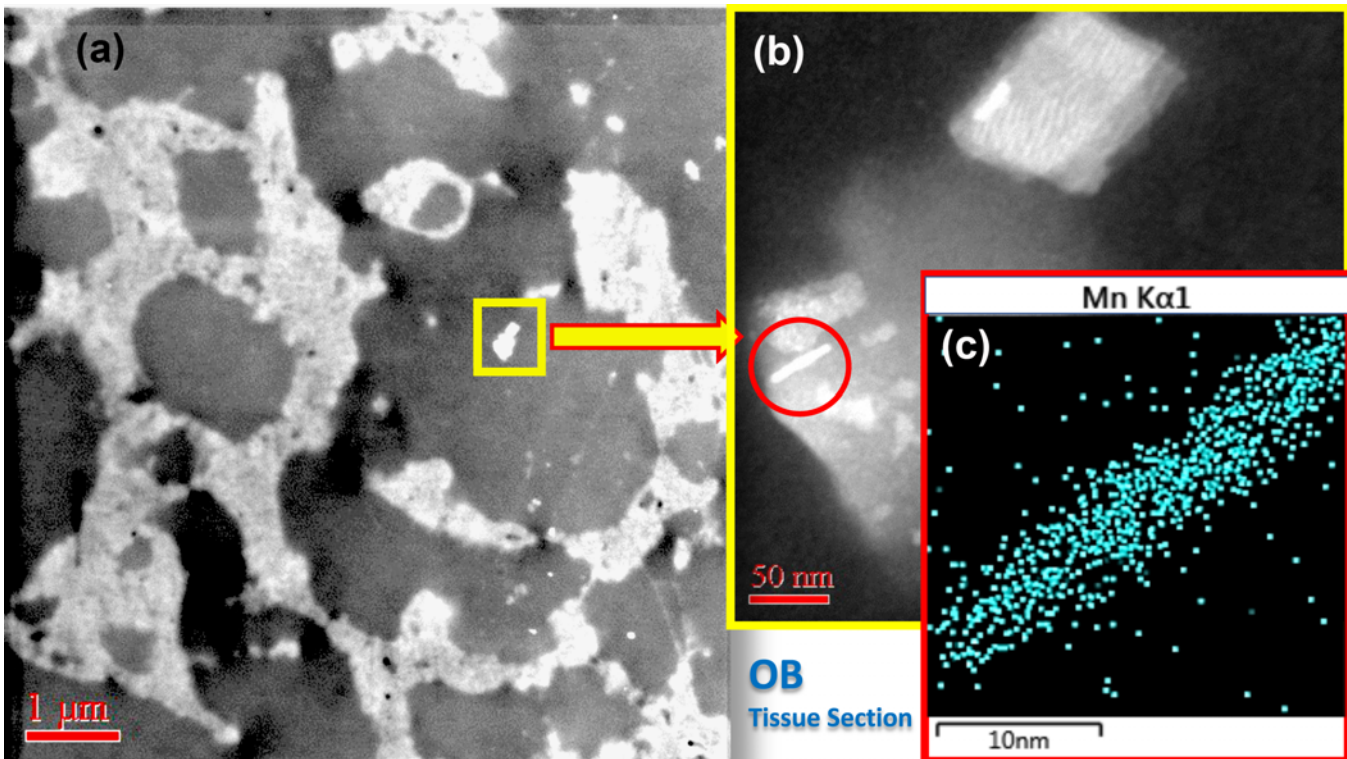


Figure 11.4.: (a) illustrates STEM image of human olfactory bulb tissue with translocated nanoparticles marked with the yellow squared area. The HRSTEM image in (b) shows a region with metal-encapsulated nanofiber (rod). EDS mapping of the nanofiber showed that it is composed of Mn (c).

NPs including their agglomerates are well below the micron size range. Figure 11.3 also compares and analyzes the different NPs at much greater magnification shown in A', B' and C' which allows identification of the particle shapes and sizes. The invader particles were then chemically and structurally distinguished by using either electron diffraction (a) or EDS-mapping (b and c) at the particle surfaces. In Figure 11.3 A' iron oxide (Fe_3O_4) NP represent a high degree of crystallinity with uniform morphology and narrow particle size range. The corresponding electron diffraction pattern corroborates the octahedral and cubic forms of the NP (Figure 11.3 a). Based on the crystallinity, the iron spinel (Fe_3O_4) includes both reduced (Fe_2^+) and oxidized (Fe_3^+) forms of iron, where the unpaired electrons from Fe_2^+ are located in the octahedral positions in the lattice and led the NP their magnetic moment. At a different region in the OB tissue, location B in Figure 11.3, spheres and semispherical NP (Figure 11.3 B') are identified with EDS analyses to correspond to a mixture of Si-Al oxides that are amorphous and potentially bioprocessed in the cellular matrix as can be seen by the leached surface features (Figure 11.3 b). Analyses were performed using a cryo-stage to minimize interactions of the tissue and translocated NP. The third region marked as "C" in Figure 11.3 shows an elongated fiber like structure that was analyzed with EDS and found to be beam sensitive. The beam interaction caused the NP surface roughness to be more pronounced, but the particle shape was preserved as illustrated in the HRSTEM image (Figure 11.3 C'). Electron diffraction of the nanofiber did not reveal any crystallinity which is characteristic of a polymeric fiber. During EDS mapping which is illustrated in Figure 11.3 c the beam was scanned across a squared region of the nanofiber and the spectra is C, N and O rich. The scanned region contained minor concentrations of Na, K and Cl suggesting that the particle adsorbed salts into its surface layers which also makes the nanofiber stand out more in STEM mode. Minute quantities of iron can also be identified in the EDS spectrum taken of the surface of the nanofiber (Figure 11.3 c). Unpublished analyses by the authors on metal-encapsulated systems showed the Si/Al host particles often carry heavy metal inclusions of Mn, Zn, Ti, Pb, Cu, Ru, Pd and Fe

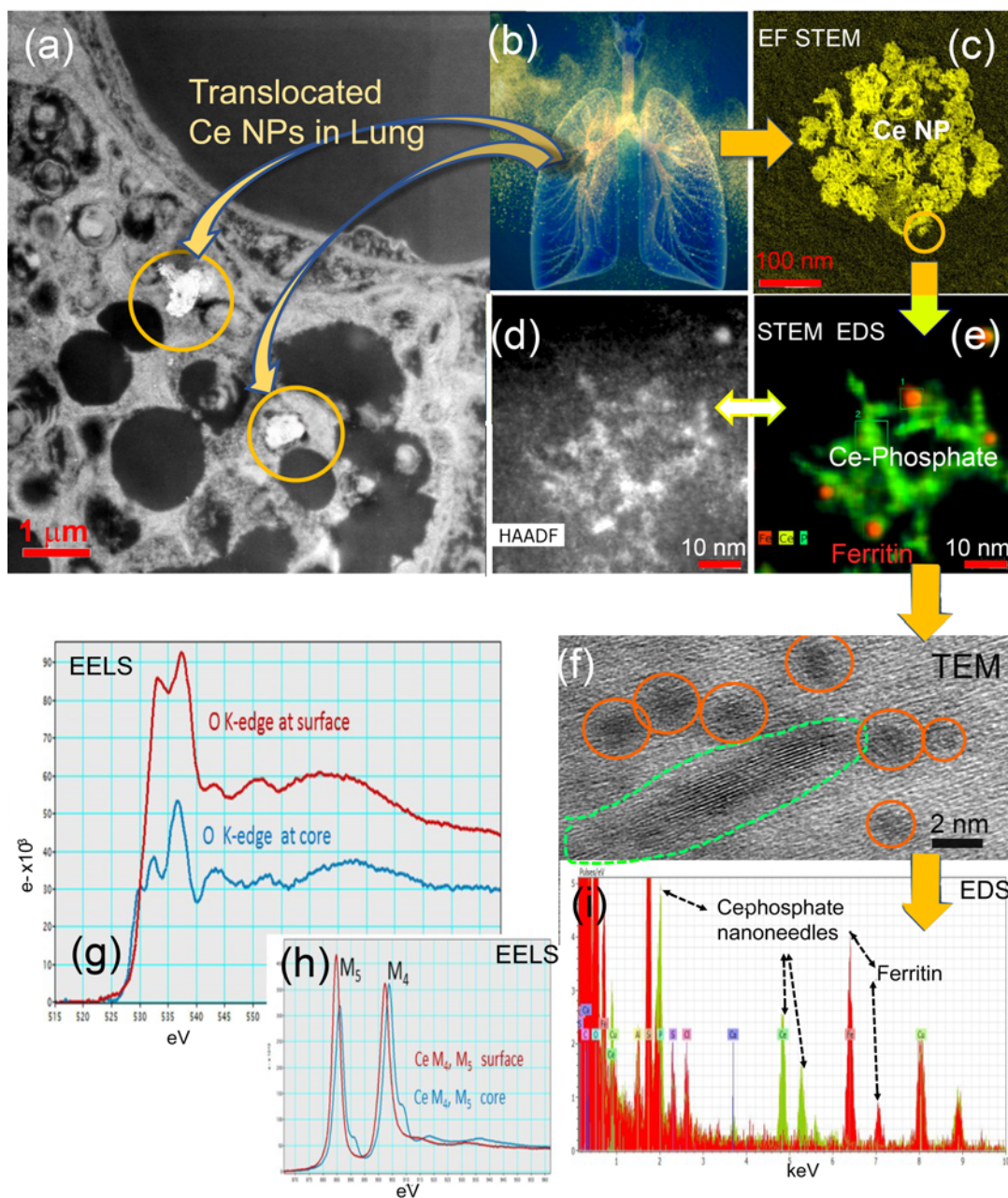


Figure 11.5.: a, b illustrates CeO_2 NP uptake in rat alveolar macrophages after inhalation; the arrows and yellow circles mark the agglomerates. Energy filtered (EF) STEM of a magnified region from (a) is shown in (c) where only Ce is mapped. An EDS map of a selected magnified region from (c) shows Ce, P and Fe-rich regions where the green and yellow overlap and represent Ce-Phosphate nanoneedles. The red dots mark the location of ferritin NP that surround the Ce-Phosphate needles. The high resolution TEM in (f) shows one single Ce-Phosphate nanoneedle circled in green with d-spacings. The red open circles mark the location of ferritin NP which are also crystalline. The EELS analyses with oxygen K-edges are shown in (g) and the cerium M5 and M4 edges are shown in (h) for the surface and the core of the Ce-phosphate needle. The EDS analysis shown in (f) was taken over the region shown in the TEM in (f) and marked are the peaks for Ce, P and Fe.

11. Advanced electron microscopy to determine nanoparticle and nanoplastic interactions in vivo

that translocated to OB tissue with the Si/Al NP via a Trojan Horse mechanism. It will be important in the future to focus also on the interfacial region between the invader particles and the tissue itself to understand if there are tissue interactions, ion transport to and from the tissue and the particle surfaces. Transport of iron in the body is tightly regulated but can fluctuate when inflammation is present as would be the case in the tissue regions affected by invader particles. Transport of iron in the form of particulate matter (Fe_3O_4 NP in Figure 11.3 A') involves entry of exogenous iron NP that initially accumulate in the OB, but also includes endogenous iron NP "ferritin" that form in tissue regions as an inflammatory or oxidative stress response mechanism. This will be discussed in detail later in the section. A third possible way to transport iron to the OB would be as a Trojan Horse mechanism where environmental Fe is adsorbed to the surfaces of nanoplastics as shown in the EDS analysis in Figure 11.3 c.

Unpublished analyses by the authors showed the Si/Al host particles often carry heavy metal inclusions of Mn, Zn, Ti, Pb, Cu, Ru, Pd and Fe that translocated to OB tissue with airborne environmental Si/Al NP via a Trojan Horse mechanism (metal-encapsulated systems). Ultrafine metal-rich particles that hide inside larger invader grains are shown in Figure 11.4. The larger agglomerate can be seen in the OB tissue in STEM mode (Figure 11.4 a) and at high resolution using HRSTEM imaging the inner "cargo" which happens to be Mn-rods or fibers can be seen (Figure 11.4 b). The diameter of these Mn-rods is only $\sim 3\text{-}4$ nm wide and HRSTEM is capable of analyzing these ultra-small metal inclusions inside an Si/Al oxide host grain that had translocated into OB tissue that was collected and stabilized as a thin tissue section for microscopic investigations. The application of analytical HRSTEM is a tool to study individual NP in the olfactory system and can help to form a greater understanding of potential neurodegeneration effects caused by pollution particles. Figure 11.4 c illustrates an EDS map of the nanofiber shown in (b) and identifies Mn throughout the particle. Mn has been shown to have neurotoxic effects when reaching the CNS [56]. Although Mn is an essential element, in excess it causes adverse effects manifested by neuroinflammation in those parts of the brain where it accumulates, e.g., in the substantia nigra, globus pallidus and corpus striatum; its presence in the human OB as shown in Figure 11.4 needs to be further investigated to understand the significance of exogenous UFP as host grains. Manganese oxide is a known catalyst and the smaller the particles that cells are exposed to, the higher their levels of oxidative stress that can be generated by the catalytic production per given mass of chemically reactive molecules such as peroxides, which could further damage DNA.

The majority of inhaled UFPs are deposited in the lung, an example is ceria (CeO_2) NP deposition and uptake into alveolar macrophages shown in Figure 11.5 using HRSTEM imaging coupled with analytical energy filtered (EF) STEM, EDS mapping and EELS analysis. Ceria has gained tremendous attention since it is auto-catalytically redox active and could, therefore, be useful as an inorganic antioxidant in future therapeutic treatments. But CeO_2 in vivo is not stable long-term and bioprocesses in the lung as well as in liver and spleen to form Ce-phosphate nanoneedles. The retention and clearance of CeO_2 NP in the respiratory tract as well as the release and transport of ions from the metal particle surfaces has been described extensively [9, 10, 57–60]. In vivo dissolution and ion release can trigger the formation of secondary NP in the vicinity of the dissolving parent grains. Since CeO_2 is a formidable redox mediator it is important to analyze and distinguish the primary and secondary Ce-NP, a task for which EELS measurements are ideal to determine the redox characteristics. The example in Figure 11.5 highlights this application to demonstrate how the physical and chemical transformations of air pollution NP at the cellular and subcellular space can be analyzed using a combination of HRSTEM/EDS/EELS methods. Specifically, Figure 11.5 a illustrates the CeO_2 NP retained in the alveolar region of the rat lung as bright lit areas against the grey cellular background since the metal particles are electron dense. This cannot be expected for polymeric particles which have electron densities comparable to the cellular matrix and would appear also grey. The CeO_2 NP have a strong tendency to agglomerate even before entry into the respiratory tract and bigger agglomerate size makes it easier to locate them in the tissue regions (Figure 11.5 a, b). At high magnification (HRSTEM) individual invader grains at the sub-cellular level can be analyzed using energy filtered (EF) STEM (Figure 11.5 c) and HAADF and EDS mapping (Figure 11.5 c, d). During EF STEM mapping, only a selected element (Ce in Figure 11.5 c) is mapped.

STEM EDS mapping of the high resolution HAADF visualized region in Figure 11.5 d shows all elements of interest, in this particular case Ce, P and Fe (Figure 11.5 e) since the CeO_2 NP bioprocessed to form Ce-phosphate

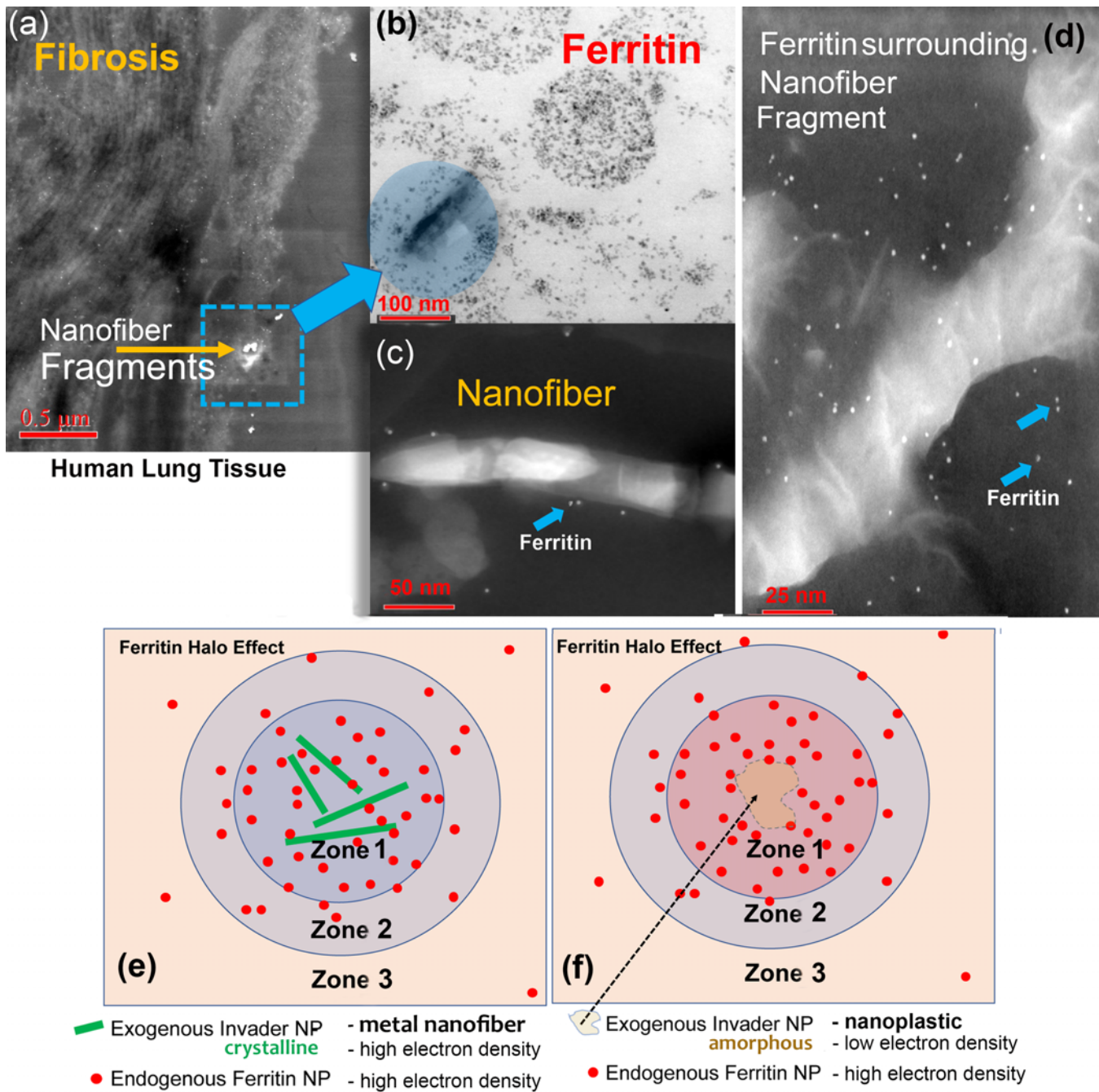


Figure 11.6.: (a) is a STEM image of a rat alveolar region with fibrosis indicated at the upper left side of (a) and the bright spots are nanofiber fragments shown inside the blue squared area. The fragments are crystalline mineral fibers that are surrounded by ferritin NP in the TEM image in (b) and the HRSTEM in (c) and (d) shows a different region of the nanofiber fragments at higher magnification with abundant ferritin NP surrounding the fiber fragment. The ferritin halo effect is illustrated in (e) and (f) for exogenous invader NP crystalline nanofibers (mineral fiber) and nanoplastics, respectively.

11. Advanced electron microscopy to determine nanoparticle and nanoplastic interactions in vivo

nanoneedles which are surrounded by copious ferritin (biomineralized iron) nanoparticles. At this point it was determined that the invader CeO_2 NP formed agglomerates in lung alveolar macrophages, bioprocessed to form Ce-phosphate nanoneedles ($\sim 5 - 30$ nm in length) and caused endogenous ferritin to form in the vicinity of the invader NP and secondary NP. What had not yet been determined was the structure of the secondary NP (Ce-phosphate nanoneedles) and the redox characteristics of the Ce in the new phases. Figure 11.5 f is a high resolution TEM of one Ce-phosphate nanoneedle which is ~ 2 nm in width and located inside an alveolar macrophage. The TEM image clearly shows the lattice spacing indicating that the needle is crystalline and the surrounding ferritin (indicated by red circles) are also crystalline. The corresponding EDS analysis shown in Figure 11.5 i shows peaks for Ce, P and Fe. The EELS analysis of the Ce-phosphate nanoneedle in Figure 11.5 f is demonstrated in g and h and shows the oxygen K-edge for the needle taken at the surface and also at the core (g) and the cerium M-edges (M5 and M4) in Figure 11.5 h. From the peak heights one can determine that the surface is enriched in oxygen vacancies which are balanced by an increase in Ce (III) in the crystal lattice. Although the NP are embedded in a biological matrix (lung tissue), atomic resolution imaging of the invader NPs and details of their chemical and physical fingerprints are still possible.

Fingerprinting of exogenous NP was also done with the help of HRSTEM in case of UFPs including nanofibers retained in lungs that were examined after autopsy of a worker who was exposed in an asbestos mining location [8, 23]. The nanofiber fragments are shown in Figure 11.6 and are in a region of the lung tissue with extensive interstitial fibrosis (Figure 11.6 a). At high magnification the crystalline exogenously derived nanofiber which trapped inside an alveolar macrophage was encircled by abundant endogenous ferritin NP that accumulated with vast density that was significantly distinct from those tissue regions that had no UFP uptake as seen in both TEM and STEM mode (Figure 11.6 b-d). The 3D morphology of a human hepatic ferritin mineral core is described by [61] using single ferritin particle analysis and HAADF-STEM imaging mode. The significance of high ferritin accumulation in the vicinity of invader NP is still to be understood. Because of this synergy it can be presumed that extraordinary high numbers of ferritin indicate a fundamental underlying issue reaction which could be used as a marker when looking for UFPs such as nanoplastics that have low contrast and electron densities to stand out in HRSTEM imaging and would, potentially, go unnoticed if it was not for the ferritin halo. A schematic of the ferritin halo effect is indicated in Figure 11.6 e and f for an electron dense (mineral fiber) and electron poor material (nanoplastics), respectively. This halo effect is independent of the type of invader NP or different organs where particles may translocate to or the exposure routes that may be involved such as inhalation, intravenous or dermal uptake. Since ferritin NP represent iron oxy nanoparticles (FeHO_2) with individual particles ranging from 5-8 nm diameter they would only be seen at high magnification in either TEM or STEM application as solitary dark or bright spots depending on the investigative mode. The halo effect (size and intensity of the region with accumulated ferritin) is controlled by the inflammatory response caused by the invader UFPs. If the UFP is a metal-rich (electron dense) crystal like a mineral nanofiber then the STEM image would show bright reflections for the UFP and for the electron dense ferritin (Figure 11.6 e). Both UFP and ferritin are easily seen in STEM mode. The ferritin halo can be separated into several zones where the inner Zone 1 is the closest to the UFP and has the highest number of precipitated ferritin NP. Therefore, Zone 1 appears brightest in STEM mode. The next Zone 2 is further away from the UFP and has a low density of ferritin NP while the outermost Zone 3 has only a limited number of ferritin NP above the concentration that would be characteristic in unaffected tissue regions. Contrary, when the UFP is a polymeric material such as a plastic nanofiber or flake (Figure 11.6 f) then the STEM image would show bright reflections for the electron dense ferritin, but where the nanoplastic particle is located there would be a shadow region. Because of the ferritin halo effect with Zone 1 being the brightest, the location of an electron poor invader "plastic" particle may be uncovered. The biomineralized iron (ferritin NP) is trapped inside the cage of the iron storage protein which together with ferroxidase catalytically regulates the storage of the iron [62–64]. Iron in biological systems is particularly important as it functions as a redox-mediator, free radical scavenger and provide antioxidant properties at the cellular and subcellular level. Because of the dense packing of iron atoms in the ferritin cage, individual 5 nm ferritin NP have high Z-contrast and are perfect candidates for HAADF-STEM mode applications (Figure 11.6 d).

11.5 Synopsis

A range of imaging and analytical methods are available to observe nanoparticles after uptake into organ tissues. These analyses can be performed at the cellular and subcellular levels. Using analytical scanning transmission electron microscopy (HRSTEM) can both image and measure the local cellular environments where fibrous and nonfibrous nanoparticles deposit in organ tissues. Analyzing plastic components inside organ tissues is an emerging field and there are experimental conditions that need to be accessed to optimize HRSTEM applications to fully characterize the nanoplastic fragments that potentially deposit in organ tissues. These studies are necessary for establishing 'Exposure-Dose-Response' relationships of plastics which are still limited at this time for most plastic types. HRSTEM studies can be adopted and appropriately modified for nanoplastic particles in tissues from previous experience with a wide range of inorganic environmental or manufactured nanoparticles.

Acknowledgement

Dr. Alan Dozier of NIOSH and Karen Bentley of the the University Rochester. Support of G.O. by NIH/NIEHS P30 ES001247 Center Grant (Dept. of Environmental Medicine/University of Rochester) and support of U.G. by Faraday Energy is acknowledged.

This Chapter is dedicated to Dr. Patricia Boone in respectful and fond memory of a devoted veterinarian, inspirational friend, and colleague, and in gratitude for her support towards discoveries in the field of environmental toxicology.

References

- [1] D. Barcelo and T. Knepper. *Analysis, Fate and Effects of Microplastics in the Environment: Preface to article collection*. 2019 (cited on page 157).
- [2] M. Oliveira and M. Almeida. "The why and how of micro (nano) plastic research". In: *TrAC Trends in analytical chemistry* (2019) (cited on page 157).
- [3] F. Ribeiro, J. W. O'Brien, T. Galloway, and K. V. Thomas. "Accumulation and fate of nano-and micro-plastics and associated contaminants in organisms". In: *TrAC Trends in analytical chemistry* 111 (2019), pages 139–147 (cited on page 157).
- [4] K. Conley, A. Clum, J. Deepe, H. Lane, and B. Beckingham. "Wastewater treatment plants as a source of microplastics to an urban estuary: Removal efficiencies and loading per capita over one year". In: *Water research X* 3 (2019), page 100030 (cited on pages 157, 158).
- [5] D. Lolla, A. Abutaleb, M. A. Kashfipour, and G. G. Chase. "Polarized Catalytic Polymer Nanofibers". In: *Materials* 12.18 (2019), page 2859 (cited on page 157).
- [6] Y. Akiyama, T. Egawa, K. Koyano, and H. Moriwaki. "Acoustic focusing of microplastics in microchannels: A promising continuous collection approach". In: *Sensors and Actuators B: Chemical* 304 (2020), page 127328 (cited on page 158).
- [7] Surfrider. *Plastic pollution*. Press Release. 2019. URL: <https://www.surfrider.org/programs/plastic-pollution> (cited on page 158).
- [8] U. M. Graham, G. Jacobs, R. A. Yokel, B. H. Davis, A. K. Dozier, M. E. Birch, M. T. Tseng, G. Oberdörster, A. Elder, and L. DeLouise. "From dose to response: in vivo nanoparticle processing and potential toxicity". In: *Modelling the Toxicity of Nanoparticles*. Springer, 2017, pages 71–100 (cited on pages 158–160, 170).
- [9] U. M. Graham, R. A. Yokel, A. K. Dozier, L. Drummy, K. Mahalingam, M. T. Tseng, E. Birch, and J. Fernback. "Analytical high-resolution electron microscopy reveals organ-specific nanoceria bioprocessing". In: *Toxicologic pathology* 46.1 (2018), pages 47–61 (cited on pages 158, 160, 162, 168).

- [10] U. M. Graham, G. Oberdörster, B. Case, and A. Dozier. “A case study of the translocation, bioprocessing and tissue interactions of EMP following inhalation exposure”. In: *Toxicology and applied pharmacology* 361 (2018), pages 81–88 (cited on pages 158, 162, 168).
- [11] M. R. Snowdon and R. L. Liang. “Electrospun filtration membranes for environmental remediation”. In: *Nanomaterials for Air Remediation*. Elsevier, 2020, pages 309–341 (cited on page 158).
- [12] H. Zhang, Z. Ji, T. Xia, H. Meng, C. Low-Kam, R. Liu, S. Pokhrel, S. Lin, X. Wang, Y.-P. Liao, et al. “Use of metal oxide nanoparticle band gap to develop a predictive paradigm for oxidative stress and acute pulmonary inflammation”. In: *ACS nano* 6.5 (2012), pages 4349–4368 (cited on page 158).
- [13] A. Luzio, E. V. Canesi, C. Bertarelli, and M. Caironi. “Electrospun polymer fibers for electronic applications”. In: *Materials* 7.2 (2014), pages 906–947 (cited on page 158).
- [14] J. L. Skinner, J. M. Andriolo, J. P. Murphy, and B. M. Ross. “Electrospinning for nano-to mesoscale photonic structures”. In: *Nanophotonics* 6.5 (2016), pages 765–787 (cited on page 158).
- [15] R. Vasita and D. S. Katti. “Nanofibers and their applications in tissue engineering”. In: *International Journal of nanomedicine* 1.1 (2006), page 15 (cited on page 158).
- [16] T. Garg, G. Rath, and A. K. Goyal. “Biomaterials-based nanofiber scaffold: targeted and controlled carrier for cell and drug delivery”. In: *Journal of drug targeting* 23.3 (2015), pages 202–221 (cited on page 158).
- [17] U.S. Centers for Disease Control and Prevention. *Per- and Polyfluorinated Substances (PFAS) Factsheet*. Factsheet. 2016. URL: https://www.cdc.gov/biomonitoring/PFAS_FactSheet.html (cited on page 158).
- [18] M. Eyvaz, S. Arslan, E. Gürbulak, and E. Yüksel. “Textile Materials in Liquid Filtration Practices. Current Status and Perspectives in Water and Wastewater Treatment”. In: *Textiles for Advanced Applications. InTech* 11 (2017), page 293 (cited on page 158).
- [19] P. Stapleton. “Toxicological considerations of nano-sized plastics”. In: *AIMS environmental science* 6.5 (2019), page 367 (cited on page 159).
- [20] S.-L. Liu, Y.-Z. Long, Z.-H. Zhang, H.-D. Zhang, B. Sun, J.-C. Zhang, and W.-P. Han. “Assembly of oriented ultrafine polymer fibers by centrifugal electrospinning”. In: *Journal of Nanomaterials* 2013 (2013) (cited on page 159).
- [21] D. Li and Y. Xia. “Electrospinning of nanofibers: reinventing the wheel?” In: *Advanced materials* 16.14 (2004), pages 1151–1170 (cited on page 159).
- [22] X. Wang, B. Ding, and B. Li. “Biomimetic electrospun nanofibrous structures for tissue engineering”. In: *Materials today* 16.6 (2013), pages 229–241 (cited on page 159).
- [23] C. W. Noonan. “Environmental asbestos exposure and risk of mesothelioma”. In: *Annals of translational medicine* 5.11 (2017) (cited on pages 159, 170).
- [24] I. Massie, M. Dziasko, A. Kureshi, H. J. Levis, L. Morgan, M. Neale, R. Sheth, V. E. Tovell, A. J. Vernon, J. L. Funderburgh, et al. “Advanced imaging and tissue engineering of the human limbal epithelial stem cell niche”. In: *Stem Cell Protocols*. Springer, 2015, pages 179–202 (cited on page 159).
- [25] R. D. Leapman and N. W. Rizzo. “Towards single atom analysis of biological structures”. In: *Ultramicroscopy* 78.1-4 (1999), pages 251–268 (cited on page 159).
- [26] R. Leapman. “Nanoscale Elemental Analysis by EELS in the Life Sciences”. In: *Microscopy and Microanalysis* 14.S2 (2008), pages 1378–1379 (cited on pages 159, 160).
- [27] U. M. Graham, M. T. Tseng, J. B. Jasinski, R. A. Yokel, J. M. Unrine, B. H. Davis, A. K. Dozier, S. S. Hardas, R. Sultana, E. A. Grulke, et al. “In vivo processing of ceria nanoparticles inside liver: Impact on free-radical scavenging activity and oxidative stress”. In: *ChemPlusChem* 79.8 (2014), pages 1083–1088 (cited on pages 159, 162).
- [28] Ł. Mielańczyk, N. Matysiak, O. Klymenko, and R. Wojnicz. “Transmission electron microscopy of biological samples”. In: *The transmission electron microscope-theory and applications* (2015) (cited on page 159).
- [29] L. H. Bryant Jr, S. J. Kim, M. Hobson, B. Milo, Z. I. Kovacs, N. Jikaria, B. K. Lewis, M. A. Aronova, A. A. Sousa, G. Zhang, et al. “Physicochemical characterization of ferumoxytol, heparin and protamine nanocomplexes for improved magnetic labeling of stem cells”. In: *Nanomedicine: Nanotechnology, Biology and Medicine* 13.2 (2017), pages 503–513 (cited on page 159).
- [30] Y. Kabiri, R. B. Ravelli, T. Lehnert, H. Qi, A. J. Katan, N. Roest, U. Kaiser, C. Dekker, P. J. Peters, and H. Zandbergen. “Visualization of unstained DNA nanostructures with advanced in-focus phase contrast TEM techniques”. In: *Scientific reports* 9.1 (2019), pages 1–9 (cited on page 159).
- [31] I. D. Pokrovskaya, S. Yadav, A. Rao, E. McBride, J. A. Kamykowski, G. Zhang, M. A. Aronova, R. D. Leapman, and B. Storrie. “3D ultrastructural analysis of α -granule, dense granule, mitochondria, and canalicular system arrangement

- in resting human platelets”. In: *Research and practice in thrombosis and haemostasis* 4.1 (2020), pages 72–85 (cited on pages 159, 160).
- [32] R. Leapman and R. Ornberg. “Quantitative electron energy loss spectroscopy in biology”. In: *Ultramicroscopy* 24.2-3 (1988), pages 251–268 (cited on page 159).
- [33] R. F. Egerton. *Electron energy-loss spectroscopy in the electron microscope*. Springer Science & Business Media, 2011 (cited on page 159).
- [34] C. Mühlfeld, B. Rothen-Rutishauser, D. Vanhecke, F. Blank, P. Gehr, and M. Ochs. “Visualization and quantitative analysis of nanoparticles in the respiratory tract by transmission electron microscopy”. In: *Particle and fibre toxicology* 4.1 (2007), page 11 (cited on page 160).
- [35] J. C. Andrews, F. Meirer, Y. Liu, Z. Mester, and P. Pianetta. “Transmission X-ray microscopy for full-field nano imaging of biomaterials”. In: *Microscopy research and technique* 74.7 (2011), pages 671–681 (cited on page 160).
- [36] R. Leapman. “Applications of electron energy-loss spectroscopy in biology: Detection of calcium and fluorine”. In: *40th Annual Proceedings of the Electron Microsc. Soc. Am* (1982) (cited on page 160).
- [37] M. Aronova and R. Leapman. “Development of electron energy-loss spectroscopy in the biological sciences”. In: *MRS bulletin* 37.1 (2012), pages 53–62 (cited on page 160).
- [38] R. Tomer, L. Ye, B. Hsueh, and K. Deisseroth. “Advanced CLARITY for rapid and high-resolution imaging of intact tissues”. In: *Nature protocols* 9.7 (2014), page 1682 (cited on page 160).
- [39] G. Oberdörster. “Toxicokinetics and effects of fibrous and nonfibrous particles”. In: *Inhalation toxicology* 14.1 (2002), pages 29–56 (cited on page 160).
- [40] A. Ostrowski, D. Nordmeyer, A. Boreham, C. Holzhausen, L. Mundhenk, C. Graf, M. C. Meinke, A. Vogt, S. Hadam, J. Lademann, et al. “Overview about the localization of nanoparticles in tissue and cellular context by different imaging techniques”. In: *Beilstein journal of nanotechnology* 6.1 (2015), pages 263–280 (cited on page 160).
- [41] S. J. Pennycook and M. Varela. “New views of materials through aberration-corrected scanning transmission electron microscopy”. In: *Journal of electron microscopy* 60.suppl_1 (2011), S213–S223 (cited on page 160).
- [42] J. C. Bonner, R. M. Silva, A. J. Taylor, J. M. Brown, S. C. Hilderbrand, V. Castranova, D. Porter, A. Elder, G. Oberdörster, J. R. Harkema, et al. “Interlaboratory evaluation of rodent pulmonary responses to engineered nanomaterials: the NIEHS Nano GO Consortium”. In: *Environmental health perspectives* 121.6 (2013), pages 676–682 (cited on page 160).
- [43] J. Wu, A. Kim, R. Bleher, B. Myers, R. Marvin, H. Inada, K. Nakamura, X. Zhang, E. Roth, S. Li, et al. “Imaging and elemental mapping of biological specimens with a dual-EDS dedicated scanning transmission electron microscope”. In: *Ultramicroscopy* 128 (2013), pages 24–31 (cited on page 160).
- [44] P. Nellist and S. Pennycook. “The principles and interpretation of annular dark-field Z-contrast imaging”. In: *Advances in imaging and electron physics*. Volume 113. Elsevier, 2000, pages 147–203 (cited on page 162).
- [45] D. M. Mitrano, A. Beltzung, S. Frehland, M. Schmiedgruber, A. Cingolani, and F. Schmidt. “Synthesis of metal-doped nanoplastics and their utility to investigate fate and behaviour in complex environmental systems”. In: *Nature nanotechnology* 14.4 (2019), pages 362–368 (cited on page 162).
- [46] G. Oberdörster, A. Maynard, K. Donaldson, V. Castranova, J. Fitzpatrick, K. Ausman, J. Carter, B. Karn, W. Kreyling, D. Lai, et al. “Principles for characterizing the potential human health effects from exposure to nanomaterials: elements of a screening strategy”. In: *Particle and fibre toxicology* 2.1 (2005), page 8 (cited on page 162).
- [47] J. G. Keller, U. M. Graham, J. Koltermann-Jully, R. Gelein, L. Ma-Hock, R. Landsiedel, M. Wiemann, G. Oberdörster, A. Elder, and W. Wohlleben. “Predicting dissolution and transformation of inhaled nanoparticles in the lung using abiotic flow cells: the case of barium sulfate”. In: *Scientific reports* 10.1 (2020), pages 1–15 (cited on page 162).
- [48] D. Docter, S. Strieth, D. Westmeier, O. Hayden, M. Gao, S. K. Knauer, and R. H. Stauber. “No king without a crown—impact of the nanomaterial-protein corona on nanobiomedicine”. In: *Nanomedicine* 10.3 (2015), pages 503–519 (cited on page 163).
- [49] J. S. Gebauer, M. Malissek, S. Simon, S. K. Knauer, M. Maskos, R. H. Stauber, W. Peukert, and L. Treuel. “Impact of the nanoparticle–protein corona on colloidal stability and protein structure”. In: *Langmuir* 28.25 (2012), pages 9673–9679 (cited on page 163).
- [50] W. G. Kreyling, M. Semmler-Behnke, J. Seitz, W. Scymczak, A. Wenk, P. Mayer, S. Takenaka, and G. Oberdörster. “Size dependence of the translocation of inhaled iridium and carbon nanoparticle aggregates from the lung of rats to the blood and secondary target organs”. In: *Inhalation toxicology* 21.sup1 (2009), pages 55–60 (cited on page 164).
- [51] H. F. Krug. “Nanosafety research—are we on the right track?” In: *Angewandte Chemie International Edition* 53.46 (2014), pages 12304–12319 (cited on page 164).

- [52] G. Oberdörster, Z. Sharp, V. Atudorei, A. Elder, R. Gelein, W. Kreyling, and C. Cox. “Translocation of inhaled ultrafine particles to the brain”. In: *Inhalation toxicology* 16.6-7 (2004), pages 437–445 (cited on page 164).
- [53] G. Oberdörster, A. Elder, and A. Rinderknecht. “Nanoparticles and the brain: cause for concern?”. In: *Journal of nanoscience and nanotechnology* 9.8 (2009), pages 4996–5007 (cited on page 164).
- [54] G. S. Ajmani, H. H. Suh, K. E. Wroblewski, D. W. Kern, L. P. Schumm, M. K. McClintock, J. D. Yanosky, and J. M. Pinto. “Fine particulate matter exposure and olfactory dysfunction among urban-dwelling older US adults”. In: *Environmental research* 151 (2016), pages 797–803 (cited on page 164).
- [55] M. C. Power, S. D. Adar, J. D. Yanosky, and J. Weuve. “Exposure to air pollution as a potential contributor to cognitive function, cognitive decline, brain imaging, and dementia: a systematic review of epidemiologic research”. In: *Neurotoxicology* 56 (2016), pages 235–253 (cited on page 164).
- [56] T. V. Peres, M. R. C. Schettinger, P. Chen, F. Carvalho, D. S. Avila, A. B. Bowman, and M. Aschner. “Manganese-induced neurotoxicity: a review of its behavioral consequences and neuroprotective strategies”. In: *BMC Pharmacology and Toxicology* 17.1 (2016), page 57 (cited on page 168).
- [57] R. A. Yokel, T. C. Au, R. MacPhail, S. S. Hardas, D. A. Butterfield, R. Sultana, M. Goodman, M. T. Tseng, M. Dan, H. Haghazadeh, et al. “Distribution, elimination, and biopersistence to 90 days of a systemically introduced 30 nm ceria-engineered nanomaterial in rats”. In: *Toxicological Sciences* 127.1 (2012), pages 256–268 (cited on page 168).
- [58] R. M. Molina, N. V. Konduru, R. J. Jimenez, G. Pyrgiotakis, P. Demokritou, W. Wohlleben, and J. D. Brain. “Bioavailability, distribution and clearance of tracheally instilled, gavaged or injected cerium dioxide nanoparticles and ionic cerium”. In: *Environmental science: nano* 1.6 (2014), pages 561–573 (cited on page 168).
- [59] P. Laux, C. Riebeling, A. M. Booth, J. D. Brain, J. Brunner, C. Cerrillo, O. Creutzenberg, I. Estrela-Lopis, T. Gebel, G. Johanson, et al. “Biokinetics of nanomaterials: The role of biopersistence”. In: *NanoImpact* 6 (2017), pages 69–80 (cited on page 168).
- [60] R. A. Yokel, M. L. Hancock, B. Cherian, A. J. Brooks, M. L. Ensor, H. J. Vekaria, P. G. Sullivan, and E. A. Grulke. “Simulated biological fluid exposure changes nanoceria’s surface properties but not its biological response”. In: *European Journal of Pharmaceutics and Biopharmaceutics* 144 (2019), pages 252–265 (cited on page 168).
- [61] Y.-H. Pan, K. Sader, J. J. Powell, A. Bleloch, M. Gass, J. Trinick, A. Warley, A. Li, R. Brydson, and A. Brown. “3D morphology of the human hepatic ferritin mineral core: New evidence for a subunit structure revealed by single particle analysis of HAADF-STEM images”. In: *Journal of structural biology* 166.1 (2009), pages 22–31 (cited on page 170).
- [62] K. H. Ebrahimi, E. Bill, P.-L. Hagedoorn, and W. R. Hagen. “The catalytic center of ferritin regulates iron storage via Fe (II)-Fe (III) displacement”. In: *Nature chemical biology* 8.11 (2012), page 941 (cited on page 170).
- [63] T. Tosha, R. K. Behera, H.-L. Ng, O. Bhattasali, T. Alber, and E. C. Theil. “Ferritin protein nanocage ion channels gating by N-terminal extensions”. In: *Journal of Biological Chemistry* 287.16 (2012), pages 13016–13025 (cited on page 170).
- [64] J. M. Bradley, G. R. Moore, and N. E. Le Brun. “Mechanisms of iron mineralization in ferritins: one size does not fit all”. In: *JBIC Journal of Biological Inorganic Chemistry* 19.6 (2014), pages 775–785 (cited on page 170).

12. The intake of synthetic fibers into the human body, by food, water and air

By: Ingeborg M. Kooter¹, Heleen Lanter¹, Wilma Middel¹, Harrie Buist²

- 1 – Department of Environmental Modelling, Sensing & Analysis, Nederlandse Organisatie voor Toegapast Natuurwetenschappelijk Onderzoek - TNO, PO Box 80015, 3508TA Utrecht, The Netherlands
- 2 – Department of Risk Analysis for Products In Development, Nederlandse Organisatie voor Toegepast Natuurwetenschappelijk Onderzoek - TNO, PO Box 80015, 3508TA Utrecht, The Netherlands

12.1 Introduction

12.1.1 The origin of plastics

The history of manmade plastics goes back to the late 19th century, when Parkesine, the first member of the Celluloid class of compounds, was invented and patented by Alexander Parkes [1]. The world's first fully synthetic plastic was Bakelite, invented in New York in 1907, by Leo Baekeland [2]. After World War I, improvements in chemical technology led to an explosion in new forms of plastics, with mass production beginning in the 1940s and 1950s [3]. Nowadays, mankind cannot imagine a world without plastic products and materials.

Because of the exponential growth in usage of plastics, the worldwide production has increased from 0,35 million metric tons in 1950 to 348 million metric tons in 2017, see Figure 12.1 [4]. Nowadays, the market is mainly dominated by polyethylene (PE, high and low density), polyethylene terephthalate (PET), polypropylene (PP), polyvinyl chloride (PVC), polystyrene (PS, including expanded EPS), polyurethane (PUR), and styrene-butadiene rubber (SBR) [5].

12.1.2 Plastics, blessing or curse

Despite all advantages that the use of several types of plastic yields for both consumers and producers, there is a big disadvantage as well. According to Jambeck et al. [6] 4.8-12.7 million metric tons of plastic debris, originating from a large number of land based sources [5], entered the oceans in 2010, see Figure 12.2. When in the environment, plastic debris degrades as a consequence of various physical and chemical processes. As a consequence, numerous small plastic particles are released to water, soil and air. Microplastics are more and more considered to be a threat to ecological life [7, 8] and potentially also to human health [9, 10].

12.1.3 What are microplastics and microfibers

Microplastics are small parts of plastic in all different types of shapes (fragments, fibers, flakes, granules, spheres) and sizes (small, fine, ultrafine). The term microplastics is associated with a classification based on size. Although there is still no general consensus about which size particles are considered to be microplastics, a value of < 5 mm

12. The intake of synthetic fibers into the human body, by food, water and air

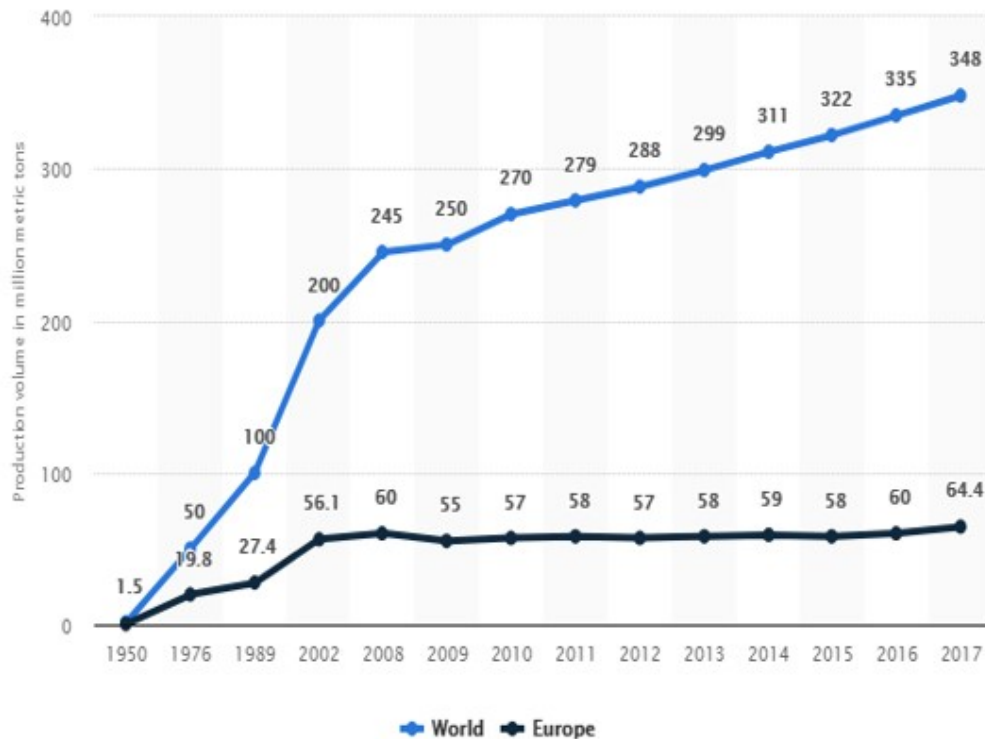


Figure 12.1.: Global plastic production from 1950 to 2017.

is often used. This value has for example been accepted by the Joint Group of Experts on the Scientific Aspects of Marine Environmental Protection [5] and the United Nations Environment Program.

A subgroup of microplastics is formed by synthetic microfibers. fibers are characterized by a high aspect ratio. As is the case with microplastics in general, an exact and general accepted definition is still not formulated. Because the cross-sectional shape of synthetic microfibers can differ from circular as a consequence of for example wear, external forces during processing etc, Salvador Cesa et al. [11] recommend to use the length of the fiber as a criterion for the classification of fibers [11]. This results in the suggestion that fibers < 5 mm are considered to be microfibers. Alternatively, synthetic microfibers can be defined as particles with a length four times the diameter [12], or particles with a width of 6 μm to 175 μm and a length of 250 μm to 6250 μm [13].

12.1.4 Are microplastics and synthetic microfibers a threat to human health?

With microplastics and synthetic microfibers present all over in environment, humans are likely be expected to be exposed to these particles via all different sources like the food they eat, the various drinks they consume, the air they breathe in and for examples cosmetics they use on their skin. Until now, little knowledge about the influence of microplastics on human health has been developed. A few papers have addressed the potential human health effects from exposure to microplastics [3, 5]. Even less is known about on the one hand the pathway of microplastics, see Figure 12.3, leading to exposure and on the other hand the effects of exposure (hazard). Knowledge of both is needed to assess the risk he microplastics are for human health, see Figure 12.4. The effect of synthetic fibers, as a subgroup of microplastics, is even less well understood. A possible way to assess the influence of synthetic microfibers upon human health, is to compare the properties and possible influence with fibers we do know (a lot) about, like asbestos fibers, diesel exhaust particulate etc.

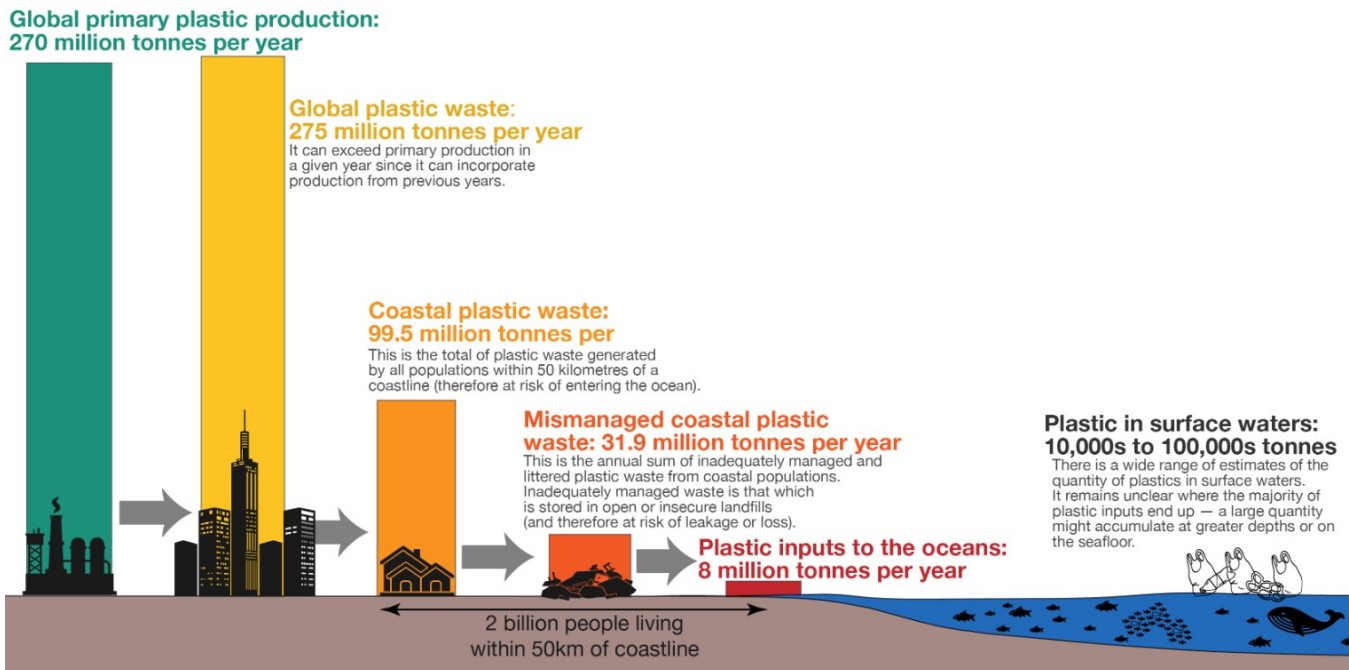


Figure 12.2.: Pathway by which plastic enters the marine environment from land based sources [14].

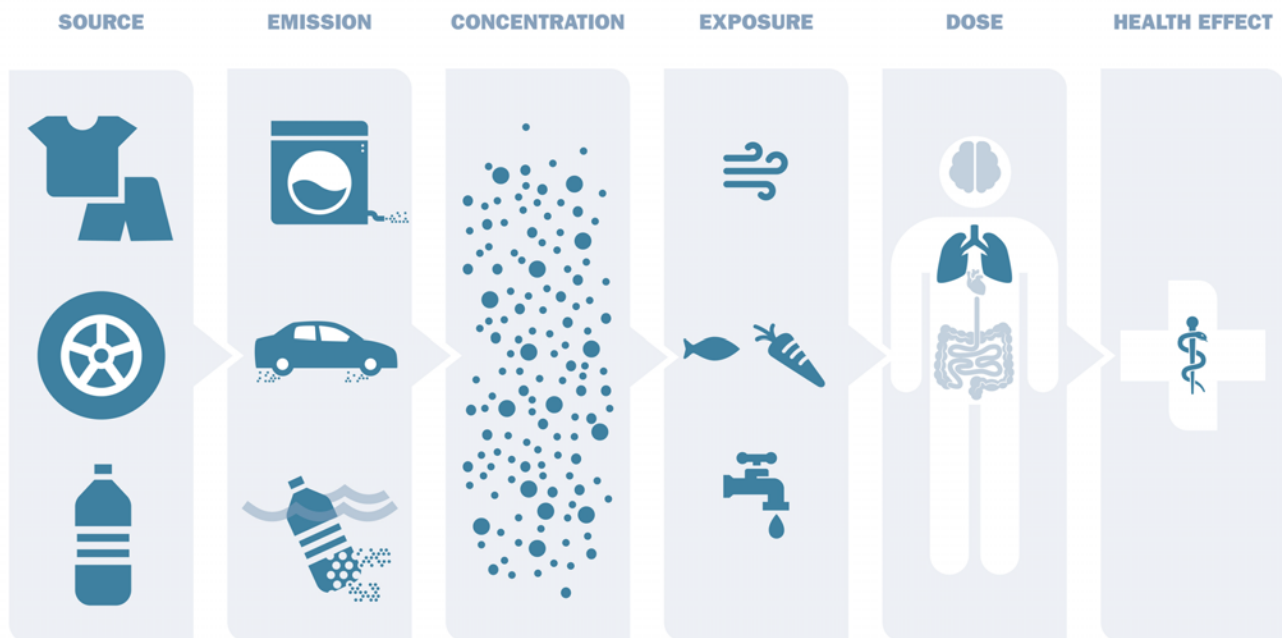


Figure 12.3.: Pathway from source to effect.

12.1.5 Reading guide

In this chapter, the intake of synthetic fibers in to the human body by food, water and air will be addressed. Firstly, the main sources of microplastics and synthetic fibers will be discussed, followed by an assessment of the emissions.

12. The intake of synthetic fibers into the human body, by food, water and air



Figure 12.4.: Risk = exposure x hazard.

After that, the internal exposure (routes) and doses will be discussed. The chapter finishes with recommendations on further research.

12.2 Sources of synthetic microfibers

Microplastics, like synthetic microfibers, can be divided into primary and secondary microplastics. Microplastics are considered to be primary when they are directly emitted as such into the environment, and secondary when they are degradation products from larger plastic objects (macroplastics) already in the environment. For example, macroplastics can break down due to UV-light, thermal changes and oxidative weathering, resulting in secondary microplastics [11, 13]. Every plastic product can end up in the environment and is therefore potentially a source of microplastics. Sources of primary and secondary microplastics can be grouped together into different activities and processes. A few examples are agriculture, tire erosion and landfills. An overview of the different sources can be found in 12.5. Of all the plastics found in the ocean, 80% has its source on land. The other 20% comes into the seawater via aquaculture and fishing equipment [11].

When looking into the sources of synthetic microfibers, it seems that only domestic washing of clothing results in a (significant) emission of synthetic microfibers to the environment. Not that there is a study concluding this, but the studies researching synthetic microfibers sources do not mention any other than the textile industry as a source [11–13, 15–20]. Of all the plastic sources depicted in Figure 12.6 the textile industry is fourth largest producer of primary plastics, making up 11.5% of the total amount produced (see Figure 12.6) and clothing is the foremost market for synthetic fibers [21].

Textiles or textile fibers can be natural or manmade, natural fabric sources are for example cotton, silk or wool 12.7.

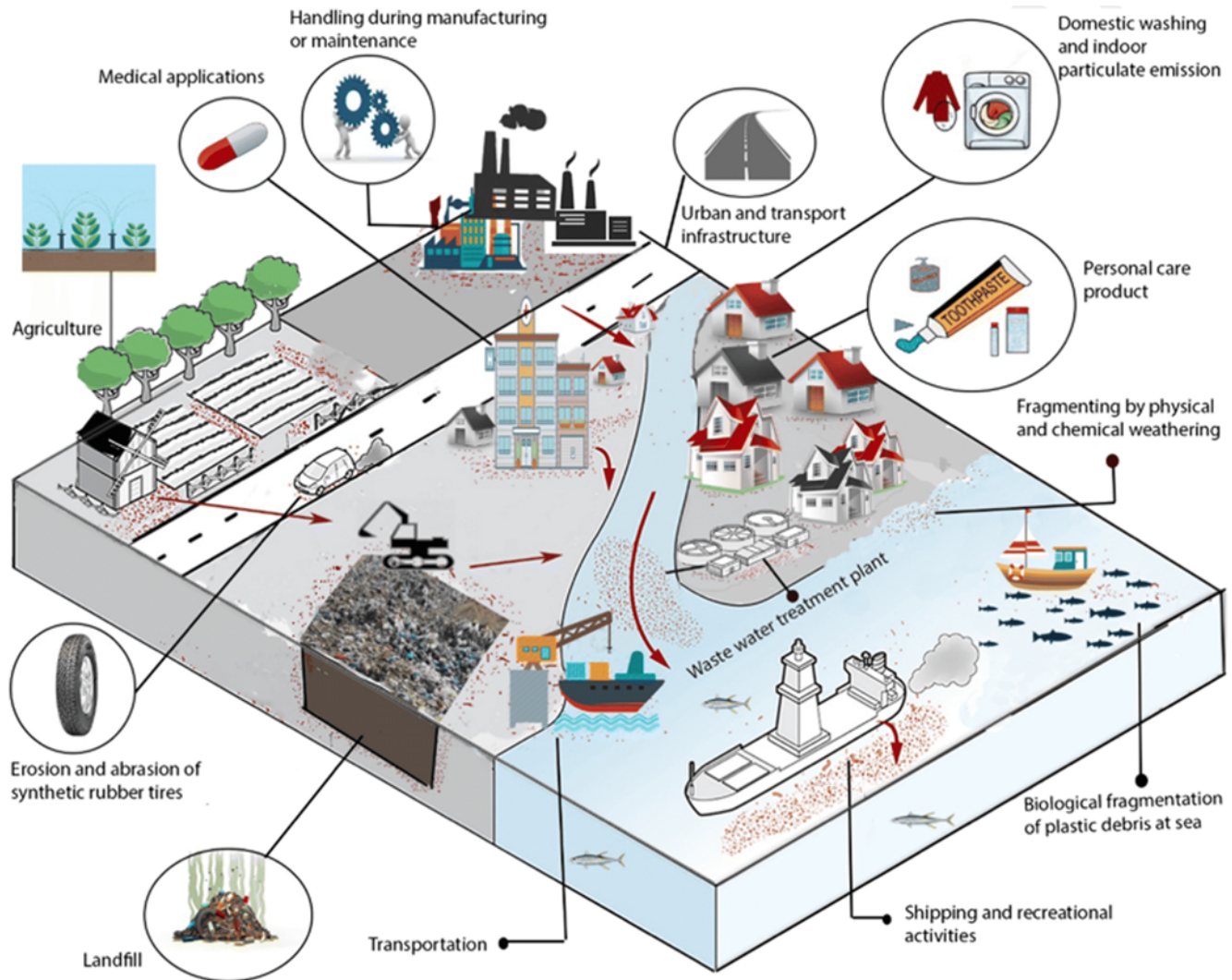


Figure 12.5.: Different sources of microplastics emission into the environment [15].

Synthetic textile fibers have become more and more popular, and in 2016 67% the fibers used in textile were synthetic (see Table 12.1 and Figure 12.8).

Every textile made with synthetic material is a source of synthetic microfibers, since fibers are released with the wear and tear of the fabric. This includes fishing nets, sails, ropes and flags for example. Domestic synthetic microfibers sources are the wear and tear of synthetic clothes, synthetic rugs and curtains by use and cleaning. The synthetic microfibers are either released into the air or end up in the wastewater stream (e.g. by washing). Both a hand-wash by hand and machine wash will release synthetic (micro)fibers into the wastewater stream. There are several parameters that influence the amount of fibers released from a fabric during a washing cycle (Table 2). A cut or tear in the fabric seems to have the most influence on the amount of fibers released. According to one paper, the release of fibers reduced and stabilized after five washings, while in another paper stabilizing was reported after eight washings and yet two other papers registered an increase of the release with increasing number of washings (reviewed by Salvador Cesa et al. [11]). Introducing a cut or tear also increased the amount of fibers released [12]. Considering the second scenario as most realistic, fiber release will also continue after several washings [12, 19]. In view of these results and the number of factors influencing the degree to which synthetic microfibers are shed (see Table 12.2), it is

12. The intake of synthetic fibers into the human body, by food, water and air

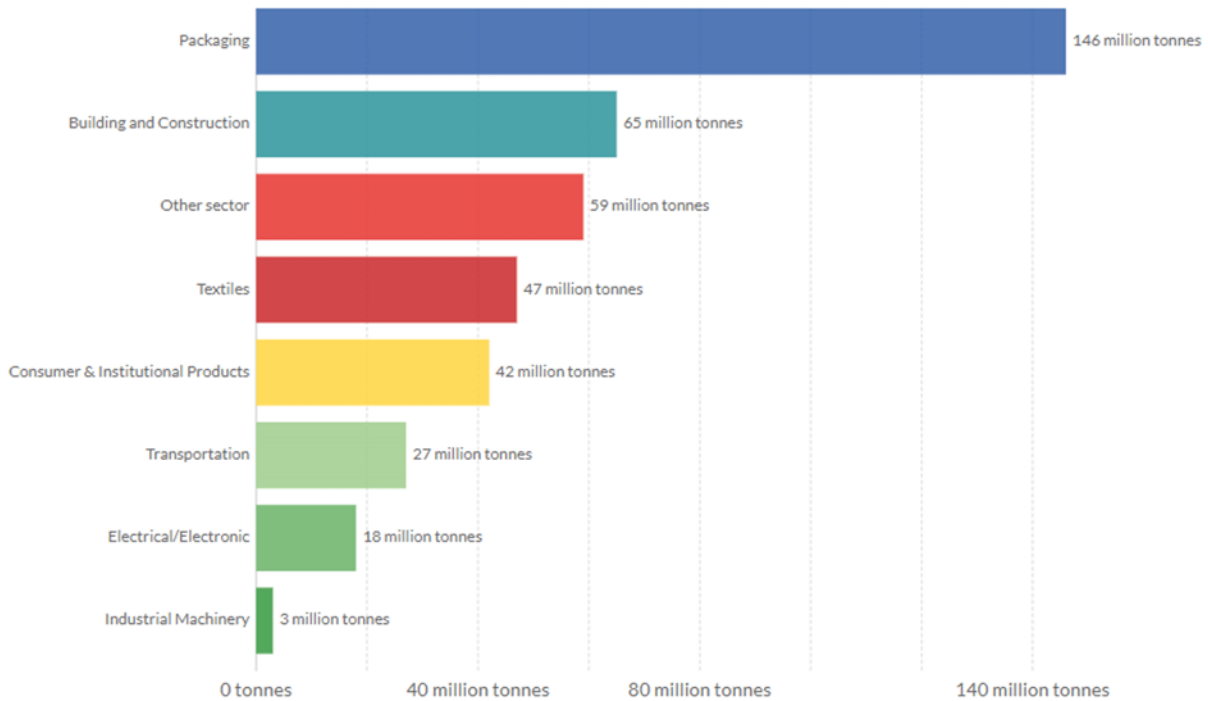


Figure 12.6.: Amount of plastic produced by the industrial sector worldwide in 2015 [14].

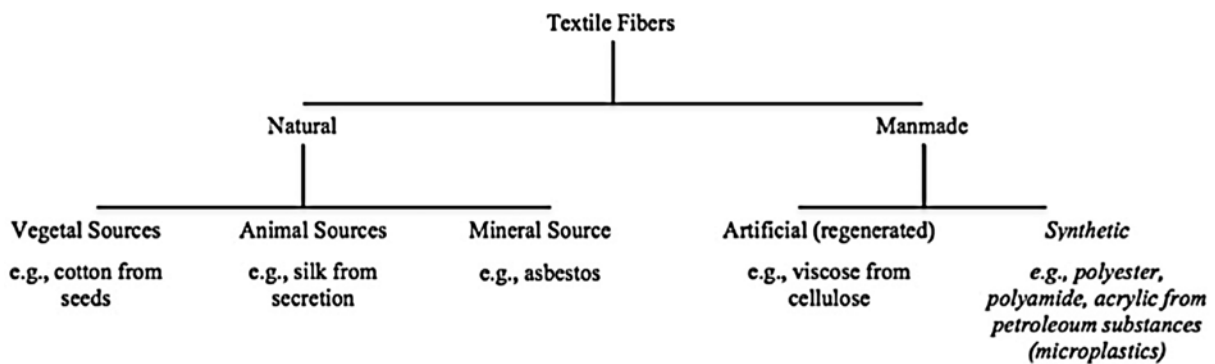


Figure 12.7.: Classification of textile fibers [11].

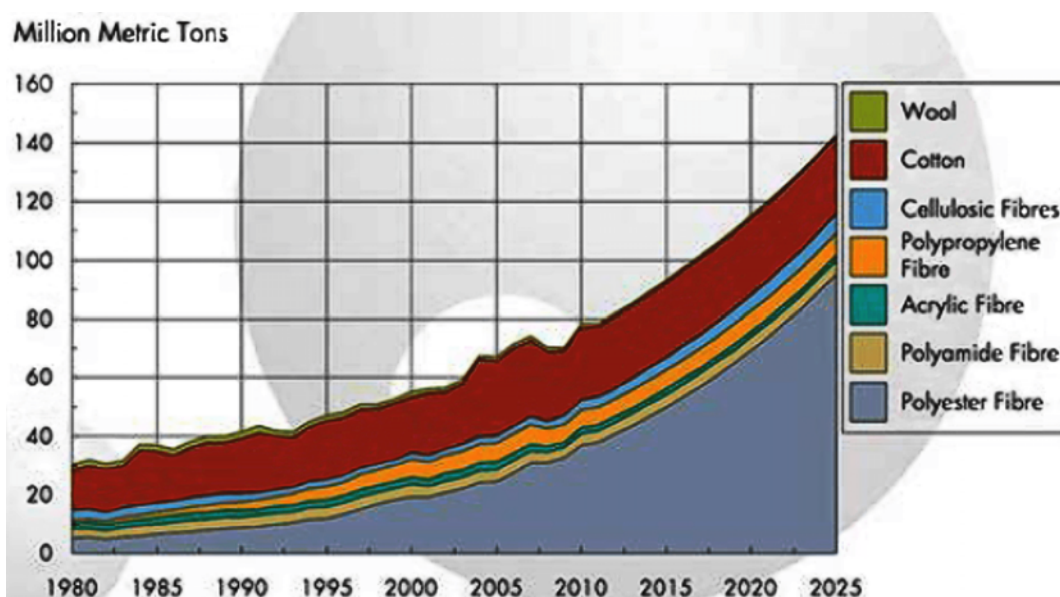
as yet difficult to come with a reliable quantitative estimate without sizeable margins of uncertainty.

The importance of the textile industry as a contributor to the release of microplastics in general is unclear, accounts vary from it being one of the largest contributors with 0.5 million tonnes of microplastic emissions a year to only being a small contributor [12]. Anyway, since this industry is the major user of synthetic fibers, its relative contribution to the prevalence of synthetic microfibers in the environment is bound to be significant.

What happens to synthetic microfibers that end up in the water depends on the characteristics of the fiber. Several studies suggest the fibers will be retained by wastewater treatment plants (WWTPs) [11, 13, 17, 23], though other studies that found synthetic microfibers to be present in the effluent of WWTPs suggest the contrary [15, 19, 24]. De Falco et al. [19] reviewed the role of WWTPs in the fate of synthetic microfibers and noted that indeed it is an open debate if synthetic microfibers can, and in what proportion, be blocked by WWTPs. It seems clear that WWTPs in different sites behave differently, either because of their characteristics or because of the properties of their influent and the synthetic microfibers contained in it or a combination of all these factors. In the end, even if

Table 12.1.: World textile fiber production in 2016 (JCFA as cited by Zwart et al. [22]).

Type of natural fibers	Production (millions of tonnes; 2016)	Type of man-made fibers	Production (millions of tonnes; 2016)
		Synthetic:	
Cotton	22.48	Polyester staple	16.21
Wool	1.10	Polyester filament	36.19
Silk	0.19	Nylon	4.79
		Acrylic	1.79
		Others	0.96
		Total synthetic fibers	59.94
		Cellulosic	5.35
Total natural fibers	23.77	Total man-made fibers	65.29
Grand total	89.06		

**Figure 12.8.:** World-wide historic and projected textile fiber production [22].

only low concentrations of synthetic microfibers can pass through WWTPs, they still can contribute significantly to their release into the aquatic environment in view of the large volumes of effluents discharged [19].

Other causes of these discrepancies may be that synthetic microfibers are difficult to detect and the lack of a standardized detection method. Therefore, results of different studies vary greatly and are difficult to compare. For example, the amount of fibers shed per washed garment as determined in two similar studies had very different results, namely 120 particles [12, 25] and 728,289 particles [12, 16]. Apart from detection methods, studies differ in definition of synthetic microfibers, which may also (partly) explain diverging results.

Although the exact routes and the relative contribution of various sources and processes may not yet be clear, still synthetic microfibers are found in relatively significant numbers in the various environmental compartments (see section 12.3).

12. The intake of synthetic fibers into the human body, by food, water and air

Table 12.2.: Parameters of influence on the shedding of synthetic microfibers of synthetic fabrics [12].

Parameter	Examples of values
Polymer type	Polyester, Nylon, Acrylics
Polymer origin	Virgin fossil, mechanically recycled, chemically recycled, bio-based
Yarn size	Micro-sized, medium-sized
Yarn length	Filament, staple
Brightness	Bright, semi-dull, dull
Twist	High twist, low twist
Fabric construction, knitted	Single jersey, interlock, rib knit, warp knit
Fabric construction, woven	Plain weave, satin, twill
Fabric finishing, mechanical	Shearing, brushing
Fabric finishing, chemical	Softeners
Cutting	Mechanical, laser, ultrasound
Sewing	Mechanical, ultrasound
Storage	Storage at the factory/store/at home
Washing	Time, temperature, equipment, detergents, softeners
Drying	Time, temperature, equipment

12.3 External exposure to synthetic microfibers

12.3.1 Introduction

Data on microplastics and especially synthetic microfibers are scarce, sometimes contradictory and therefore not easy to generalize. According to PlasticsEurope, the association of plastics manufacturers in Europe, the most widely used polymers in Europe (EU28+Norway and Switzerland) are polyethylene (29.4%), polypropylene (19.1%), polyvinylchloride (10.1%), polyurethane (7.5%), polyethylene-terephthalate (PET, 7.1%), polystyrene (6.9%) and others (19.1%) [26], but these data do not include fibers. The world production of synthetic fibers was about 63 million tonnes in 2015, of which most consisted of PET (approx. 8%) [27], of which most is destined for the manufacture of clothing [21]. The most important synthetic fiber for clothing production is also PET, others are polyacrylonitrile and aramid fibers (polyamide) [27]. In the sections below, some data on the prevalence and nature of synthetic microfibers in environmental compartments are presented. These data do not give a complete and consistent picture, but do illustrate the importance of synthetic microfibers within the broader microplastics issue.

12.3.2 Air

According to a review by Prata [28], little information on airborne microplastic concentrations is available: In a deposition study conducted in Greater Paris, a fall-out of 15 to 118 microplastic fibers $\text{m}^{-2} \text{d}^{-1}$ were detected. The majority of particles observed in this study were fibres, and approximately 30% of the counted particles were confirmed to be plastic [29]. In contrast, deposition of fibers measured over a period of one year in the catchment area of the river Trent in England consisted mainly of natural fibers; median deposition was 81 fibers $\text{m}^{-2} \text{d}^{-1}$ for natural fibers and 2 fibers $\text{m}^{-2} \text{d}^{-1}$ for synthetic fibers (Table S2 of the supplementary data of reference [30]).

In another Parisian study, indoor concentrations of 0.1 to 30 synthetic microfibers m^{-3} were measured, and outdoor concentrations of 0.3 to 1.5 microfibers m^{-3} [28]. It should be noted the detection limit for inhalable fibers in this study was 50 μm and that therefore smaller fibers are not included in these numbers. Half of the analysed outdoor fibers were natural fibers (50%), mainly cotton or wool. Some 20% of the total fibers were modifications of natural polymers (rayon or acetate from cellulose) and 17% synthetic microfibers, mainly polyethylene-terephthalate. The

remaining 12% fibers were a mixture of synthetic and natural microfibers [31]. Of the indoor microfibers 67% were made of natural material, the remaining 33% were synthetic microfibers, being mainly polypropylene, but polyamide fibers and copolymers of polypropylene and polyethylene were also detected [32].

In principle, occupational exposure to air-borne synthetic microfibers, e.g. in the manufacturing industry, will be substantially higher than environmental exposure. A scan of public literature did not produce any study quantifying such occupational exposure to synthetic (plastic) microfibers in terms of numbers per volume of air. For man-made synthetic fibers such data are available, and in a recent review it was concluded that concentrations of such fibers in occupational settings did not exceed 500,000 respirable fibers m^{-3} [33]; e.g. in a manufacturing plant of vitreous fibers personal and area sampling showed concentrations ranging from 500 to 1,500 respirable fibers m^{-3} [34]. In the Netherlands, the legally binding occupational limit value for asbestos, a potent carcinogenic mineral fiber, is 2,000 respirable fibers m^{-3} (according to WHO-convention defines as fibers with a length $> 5 \mu\text{m}$, a diameter $< 3 \mu\text{m}$ and an aspect ratio $> 3 : 1$). In this context, the outdoor and indoor environmental concentrations of synthetic microfibers can be considered low.

12.3.3 Water

Seawater

The oceans are an important sink of microplastics in which they are distributed between five main compartments: the ocean surface, the water column, the seafloor, the shoreline and, the biota [5]. Very little data are available on the MP concentrations in these compartments, with the exception of the surface ocean and seafood (but not other important organisms in the oceanic food web). Lusher et al. [35] microplastics in the Northeast Atlantic and found particles numbers ranging from 0 m^{-3} to 22.5 m^{-3} Figure 12.10), comprising four different types of particles (fiber, fragment, bead, foam) with the majority (count) being fibers (96%), and sizes mainly between 1.25 and 5 mm (see Figure 12.9). Synthetic microfibers such as nylon filaments from fishing nets, ropes or clothing are the most abundant microplastics in the sea, of which poly-ethylene, polypropylene, and polystyrene are most frequently found polymers [36].

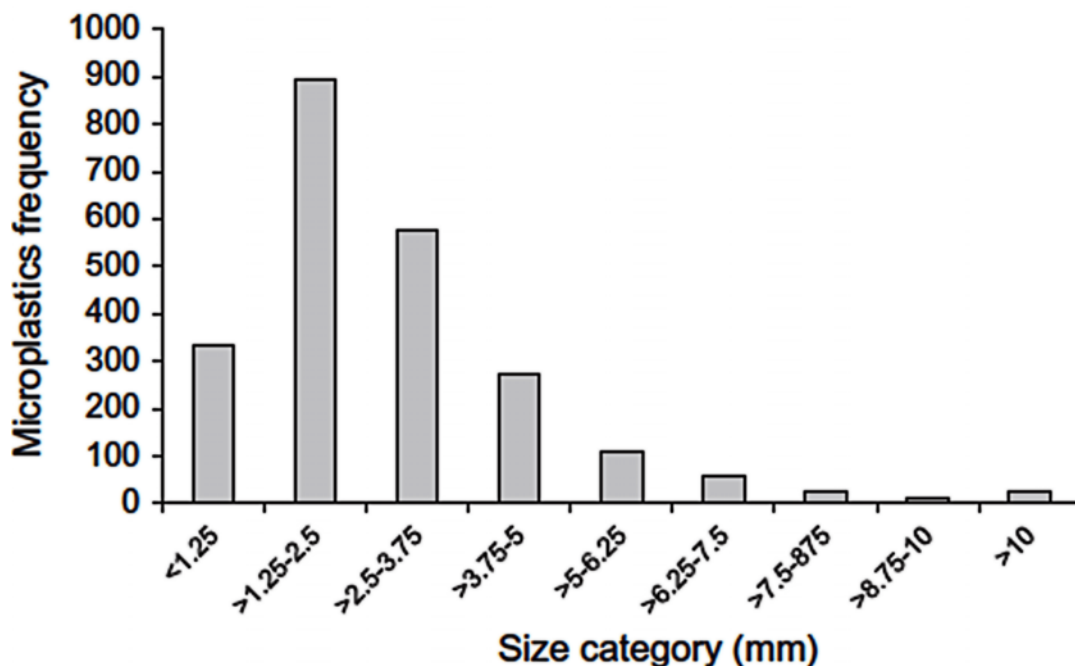


Figure 12.9.: Size frequency of microplastics in the Northeast Atlantic (reproduced from Lusher et al. [35]).

12. The intake of synthetic fibers into the human body, by food, water and air

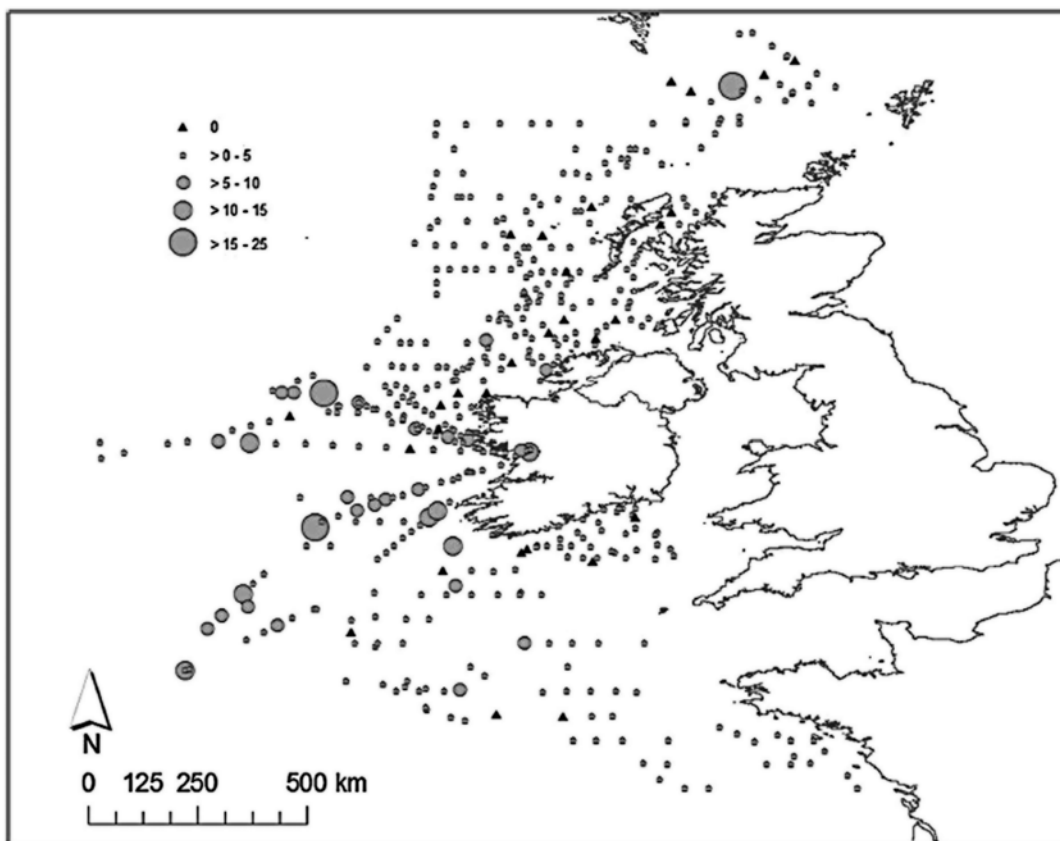


Figure 12.10.: Microplastics concentrations in the Northeast Atlantic (reproduced from Lusher et al. [35]).

Salvador Cesa et al. [11] have made an overview of field studies on microplastics in which a high percentage synthetic microfibers were measured, which mainly addressed the marine environment. These are listed in Table 12.3.

Table 12.3.: Concentration of microplastics in marine samples where textile fibers were considered dominant [11].

Sample	MPs definition (µm)	MPs size range (µm)	MPs shapes	Concentration range	Concentration average	Unit	Fiber (%)	MPs chemical identification	Reference cited in paper
Subsurface waters from western English channel	< 5000 (diameter)	6 to 175 (diameter) > 250 (length)	Bead, fiber, planar, fragment, granular	0.24 to 0.27, 0.27 to 0.35	0.26 (site 1), 0.31 (site 2)	item m ⁻³	61	yes	[37]
Subsurface seawater from north-eastern Pacific Ocean	333 to < 5000	64.8 to 5810	Fiber, fragment	8.51 to 9180	2080 ± 2190	particles m ⁻³	75	no	[38]

Continued on next page

Table 12.3 – continued from previous page

Sample	MPs definition (μm)	MPs size range (μm)	MPs shapes	Concentration range	Concentration average	Unit	Fiber (%)	MPs chemical identification	Reference cited in paper
Surface and sub-surface waters from North Sea (Germany)	< 5000	< 100 to 1000 ^a	Fiber, granular particle	0 to 1770, 0 to 650	64 \pm 194, 88 \pm 82	granules l ⁻¹ , fibers l ⁻¹	> 50	no	[39]
Subsurface seawater from north-eastern Pacific Ocean	333 to < 5000	64.8 to 5810	Fiber, fragment	8.51 to 9180	2080 \pm 2190	particles m ⁻³	75	no	[38]
Deep sea sediments from northwest Pacific Ocean	< 1000	< \pm 300 (majority)	Fiber, paint chip, small cracked piece	60 to 2020	Not specified	piece m ⁻²	75	no	[40]
Coastal sediments from Southern Portuguese water	Not specified	< 500	Fiber, fragment	0 to 0.2628	0.01 \pm 0.001	pieces Mg	\pm 80	yes ^b	[41]
Subsurface waters in northeast Atlantic Ocean	< 5000 (length)	200 to 43,200	Bead, fiber, foam, fragment	0 to 22.5	2.46 \pm 2.43	particles m ⁻³	96	yes ^c	[35]
Surface and sub-surface Arctic waters from Norway	< 5000	250 to 7710	Fiber, film, fragment	0 to 1.31 ^d , 0 to 11.5 ^e	0.34 \pm 0.31 ^d , 2.68 \pm 2.95 ^e	particles m ⁻³	95	yes ^b	[42]
Beach sediments and surf-zone water from south-eastern coastline of South Africa	< 5000	65 to 5000 ^f , 80 to 8000 ^g	Fiber, fragment	689 \pm 348 to 3308 \pm 1449 ^f , 258 \pm 53 to 1215 \pm 277 ^g	Not specified	particles m ⁻² , particles m ⁻³	> 90	no	[43]
Mangrove coastal sediments from Singapore	< 5000	< 20 (majority)	Fiber, film, granule	12.0 \pm 8.0 to 62.7 \pm 27.2	36.8 \pm 23.6	particles kg ⁻¹ , of dry sediment	72	yes	[44]
Arctic Sea ice	< 5000 (diameter)	< 2000 (fiber length), < 200 (chips, other)	Chip, fiber, other	28 to 234	not specified	particles m ⁻³	> 54	yes ^b	[45]

Continued on next page

12. The intake of synthetic fibers into the human body, by food, water and air

Table 12.3 – continued from previous page

Sample	MPs definition (μm)	MPs size range (μm)	MPs shapes	Concentration range	Concentration average	Unit	Fiber (%)	MPs chemical identification	Reference cited in paper
Sandy, estuarine and subtidal sediments around Plymouth (UK)	Not specified	± 20 (diameter)	Fiber, fragment	Not specified	$< 1^h, < 3^i, < 7^j$	fiber 50 ml^{-1}	> 50	yes	[46]
Deep sea sediments from Atlantic and Indian Ocean and Mediterranean Sea	Not specified	2000 to 3000 (length) < 100 (diameter)	Fiber	1.4 to 40	13.4 ± 3.5	piece 50 ml^{-1}	100	yes ^b	[47]
Coastal waters of the Eastern Chinese sea	< 5000	> 500 to 5000	Fiber, film, granule, spherule	0.030 to 0.455	0.167 ± 0.138	m^{-3}	83.2	no	[48]

^a Longer fibers were occasionally found. ^b Rayon (artificial man-made fiber) was identified and considered in results. ^c Rayon (artificial man-made fiber) was identified but removed from final count. ^d Surface samples. ^e Subsurface samples. ^f Beach. ^g Water column.

Freshwater

Microplastic particles have also been found across a range of freshwater environments worldwide, including lakes and rivers [49]: Concentrations varied several orders of magnitude; in rivers from 0.00005 to 0.32 particles l^{-1} , in lakes from 0.00012 to 26 particles l^{-1} , in riverine sediments from 70 to 3800 particles kg^{-1} and in lake sediments from 1.2 to 980 particles kg^{-1} . However, it should be noted that in a quality review performed by Koelmans et al. [50], the surface water investigations did not meet all quality criteria formulated, obtaining only half or less of the maximum quality score.

Stanton et al. [30] measured fiber concentrations in the river Trent in England over a period of one year and found mainly of natural fibers; median concentration was 0.1 fibers l^{-1} for natural fibers (mean 0.17) and 0 fibers l^{-1} for synthetic fibers (mean 0.02) [30].

Soil

Also in terrestrial ecosystems many different MPs can be found, but so far these have only been considered as a source for freshwater and marine environments since analytical techniques for identifying microplastics in soils are not yet advanced enough for a proper assessment [15]. Wang et al. [51] reviewed the presence of microplastics in soils and concluded that the concentration in human-impacted soils is unlikely to be higher than 0.1%. The application of plastic mulch in agriculture introduces by wear and tear polyethylene MPs into the soil and the application of sewage sludge on arable lands may introduce synthetic microfibers from clothing as MPs from these sludges consist for 67% of polyester microfibers and for 17% of acrylic microfibers [51].

12.4 Human exposure routes

12.4.1 Introduction

In sections 12.2 and 12.3, it was discussed how synthetic microfibers originate and are distributed over the different environmental compartments (air, seawater, surface water, groundwater, soil). It is believed that synthetic microfibers might play a role in potential health effects in three different ways. First, the plastic particles as such; second, the chemicals they are composed of or that are adsorbed to them; and third, the micro-organisms that may grow on them [52]. Since the plastic particle will act as a vector and exposure to the chemicals or micro-organisms will be a function of the exposure to the particles, we will focus on the exposure routes of the particles. When in the consulted literature particle shapes are specified, often non-fibrous particles are concerned. As in principle the routes will not differ greatly between fibrous and non-fibrous particles, all microplastics are considered here, be it with a special emphasis on synthetic microfibers, when possible. Anyway, fibers are the most abundant type of microplastic in sediments, seawater, fresh surface waters, atmospheric fall-out and indoor air [53]. It is apparent that humans are very likely to be exposed to microplastics via the environmental compartments indicated above. However, data for a proper exposure assessment are scarce, fragmentary and, due to methodological shortcomings, incomplete [5, 54, 55]. One of the issues currently hampering a proper exposure assessment of microplastics in the environment is a lack of standardized sampling, isolation, extraction, and analytical techniques that can cover the entire microplastic particle size range. Therefore the data on the exposure pathways presented in the sections below are mainly qualitative in nature and sometimes even speculative.

12.4.2 Inhalation pathway

The degree of respiratory exposure to air-borne synthetic microfibers is directly proportional to their concentration in the ambient air, be it indoor or outdoor. Very few data are available on these air concentrations (see section 12.3.2), which in principle depend how much of the synthetic microfibers is emitted from the primary and secondary sources into the air and the subsequent fate of these fibers. Since investigations on the sources of synthetic microfibers and microplastics in general have mainly focused on aquatic material streams (see section 12.2), also little is known about the start of this pathway. More research on the fate of synthetic microfibers with respect to their emission into air and the subsequent physical transport processes is needed in order to fill this knowledge gap. In section 5.2 is discussed what determines the uptake of synthetic microfibers once they are present in ambient air.

12.4.3 Oral pathway

Exposure via ingestion to microplastics present in the various environmental compartments may occur either directly or indirectly via the food chain or drinking water. Direct oral exposure to microplastics suspended in the air may occur when deposited inhaled microplastics are removed from the lungs by the mucociliary escalator, end up in the oropharynx and are eventually ingested. microplastics present in surface waters may be ingested accidentally when swimming or when drinking from streams, e.g. during a hike. microplastics in soils may be ingested through hand/mouth contact or by eating soil, a behavior that may be observed in young children. Eventually the plastic particles in contaminated soils may infiltrate into groundwater and subsequently enter public water supplies [56]. However, most likely the main oral pathways of human exposure are indirect, via microplastics that have accumulated in plants and animals that are subsequently eaten or that are present in drinking water obtained from groundwater or surface water. Therefore, this section will focus on these indirect pathways.

The contamination of seafood with microplastics has been extensively investigated and micro-sized microplastics were shown to be present in relatively high concentrations in the guts of fish caught amongst others in the Atlantic Ocean, the North Sea, the English Channel, the Adriatic sea, the Pacific Ocean, the Indian Ocean, the coastal waters of the USA, Brazil, Indonesia and Australia, and shellfish (reviewed by Kershaw[54]). With respect to human intake

12. The intake of synthetic fibers into the human body, by food, water and air

of synthetic microfibers only shellfish are of interest, since the weak parts of this seafood are eaten in its entirety while from fish usually only muscle tissue is consumed, which has not been shown to contain synthetic microfibers, or even microplastics in general (see also section 12.5.3).

Despite this sometimes high contamination levels in freshwater bodies, the ingestion of microplastics by biota in this environment has been much less extensively studied than in the marine environment. Still a number of studies on microplastics in fish from various corners of the earth is available, from freshwater drainages and an estuary of the Gulf of Mexico [55], from Poyang Lake, the largest freshwater lake of China [57], from the Parisian conurbation [58], from rivers and lakes Baden-Württemberg, Germany [59], from the Rio de la Plata estuary in Argentina [60], from lake Victoria, straddling the borders of Uganda, Tanzania and Kenya [61], from the Brazos River Basin, Texas, USA [62], from the Pajeú river, in the Northeast of Brazil [63], to name a few. Some specifically mentioned the presence of synthetic microfibers: in the Parisian conurbation the majority of the microplastics encountered in fish were microfibers [58], in Baden-Württemberg microfibers made up 39% of the microplastics from fish [59], in the Rio de la Plata estuary microfibers represented the 96% of the total number of microplastics extracted from fish [60] and in Pajeú river fish microfibers were the most frequent type of microplastics (46.6%) [63].

Also drinking water, both from the tap and from bottles, may contain microplastic particles in concentrations ranging from 0 to a few hundred particles l^{-1} (a.o. reviewed by Koelmans et al. [50]). The origin of these particles may not always be environmental in nature, as single-use plastic bottles contained, on average, approx. 8 times less microplastic particles than returnable bottles, suggesting they may have originated from the bottles themselves [50]. Since tap water may contain microplastics, it is no surprise also a beverage like beer can contain them (12-109 fragments l^{-1} as reported by Rainieri et al. [64], although no correlation was found between the contamination and the corresponding municipal tap water supply [65], indicating processing may be more important a source than the tap water used.

Commercial salts for human consumption from 38 different countries, representing five continents and 128 different brands and both of terrestrial and sea origin, may contain microplastics, ranging from 0 to 19,800 kg^{-1} (about half of the investigated salts $< 100 kg^{-1}$, about half $> 100 kg^{-1}$) with sizes between 4 and 5,000 μm [66].

An indication of the relevance of the presence of microplastics in soils may be that have also been detected in honey and sugar (32 fragments kg^{-1} , see [64]) and chicken crop and gizzards [56]. No data on the uptake by plants in the field have been encountered, but in lab experiments [67] demonstrated that lettuce could take up polystyrene (PS) microbeads sized 0.2 and 1 μm from a 0.005% suspension, and [68] showed that tobacco cells can incorporate nanoscale fluorescent PS beads through endocytosis.

Therefore, oral exposure to microplastics may occur due to the consumption of shellfish, but may also result from the consumption of livestock fed fishmeal as fishmeal is historically used in for example poultry and pig feed. Since humans are at the end of a long food web in which accumulation of microplastics might have occurred, bioaccumulation over the food chain may result in prominent exposure [69]. This concern about potential risks to higher trophic level species and human food safety [5, 54, 55, 70–72]. Still, there are (yet?) no data demonstrating their bioaccumulation or biomagnification [53].

Human exposure data are still very scarce and restricted to the consumption of marine bivalves and shrimps in Europe. These studies report that dietary exposure for Belgium and Dutch mussel consumers can range from 11,000 microplastics (size range 5 - 1000 μm) [73] up to 100,000 microplastics (size range 10 - 5000 μm) per person/year [5, 74]. Shrimp consumers (90% removed by peeling) may be exposed to much lower levels of 175 microplastics per person/year [75]. Most of the microplastics encountered in these species were synthetic fibers. GESAMP concluded that so far the numbers of identified micro-sized microplastics per seafood product are relatively small [5, 54, 55].

Table 12.4 presents an overview of food (products) that haven demonstrated to contain microplastics in their edible parts. Fish were not included in this list because so far no microplastics have been demonstrated to be present in muscle tissue (see section 12.5.3).

Table 12.4.: Concentration of microplastics in food (products) whose edible parts contain microplastics (compiled from table 2 and 3 in Toussaint et al. [65])

Study	Food (product)	Type	Mean [kg ⁻¹]	Range [kg ⁻¹] ^{\$}
1	Honey	Fibers	166	40-600
		Fragments	9	0-38
2	Honey	Fibers		10-336
		Fragments		2-82
3	Honey	Fibers		32-108
		Particles		8-28
4	Sea salt	Particles		16-84
	Lake salt	Microplastic		8-102
	Rock salt	Particles		9-16
5	Salt	Particles	212	47-806
6	Salt	Microplastic		1-10
7	Sea salt	Microplastics		50-280
8	Sea salt	Particles		550-680
	Lake salt	Particles		43-364
	Rock/well salt	Particles		7-204
9	Sugar	Fibers	217	
		Fragments	32	
10	Sardines and sprat, canned	Microplastic (0.001 - 1 mm)		0-9*
		Mesoplastic (1-10 mm)		0-12*
11	Beer	Fibers		2-79
		Fragments		12-109
		Granules		2-66
12	Beer	Fibers	16	0-30
		Fragments	21	5-50
		Granules	27	15-40
13	Beer	Fibers	4	0-14
14	Bottled water	Particles (> 100 µm)	10	
		Particles (0.5 - 100 µm)	325	
15	Bottled water (returnable bottles)	Particles	118	30-210
	Bottled water (single use plastic bottle)	Particles	14	0-25
	Bottled water (beverage cartons)	Particles	11	3-20
	Bottled water (glass bottles)	Particles	50	0-100
16	Tap water	Microplastic	5	0-61
17	Tap water	Microplastic > 100 µm	0.3	
18	Mussel, brown	Microplastic	±370 [#]	
19	Mussel, Mediterranean	Microplastic	2500	1000-4000
20	Mussel, Mediterranean	Microplastic		4400-11400
21	Mussel, blue	Microplastic	360	290-430

Continued on next page

12. The intake of synthetic fibers into the human body, by food, water and air

Table 12.4 – continued from previous page

Study	Food (product)	Type	Mean [kg ⁻¹]	Range [kg ⁻¹] [§]
22	Mussel, blue	Microplastic	200	0-500
23	Mussel, blue	Microplastic		700-2900

[§] Data for which no numbers per kg were available or could be calculated, were left out.

* Calculated from figure 1 of main text and table 3 of supplementary data from Karami et al. [76].

Same numbers and descriptions also mentioned for Mediterranean and blue mussel; these were left out to avoid redundant information.

Concluding, in view of this scarcity of data and the lack of harmonized, well-defined analytical methods, there is no reliable basis to calculate dietary intakes of microplastics [65]. Furthermore, it is not clear whether dietary intake of food products containing microplastics will significantly contribute to the total ingestion of microplastics, as it was observed that when eating mussels contaminated with microplastics, far more microfibers had been consumed that had settled on the food from the indoor air than that were contained in the mussels [53].

12.4.4 Dermal pathway

Dermal contact may occur when people wear synthetic clothes or are exposed to soils, surface water or bathing water contaminated with microplastics. Furthermore, air-borne microplastics may deposit on exposed skin.

Release of fibers from textiles in washing machines is recognized as a potential large source of micro-sized microplastics (see section 12.2), releasing 1,900 to 700,000 synthetic microfibers per wash [16, 25]. Therefore, it may be assumed that also some synthetic microfibers will be released onto the skin when wearing clothing containing synthetic fibers.

In the Netherlands, a recently much debated source of microplastic exposure is synthetic turf used on sport fields [77]. Also in other countries exposure to possibly toxic particles via synthetic turfs has been an issue [78, 79]. These sport fields contain polymeric grass fibers (monofilaments made of polyethylene) and rubber infill granules that are made from recycled rubber tyres. Although the synthetic grass may release fibers due to wearing, the discussion focused on the granules, which will probably release particles rather than fibers, and the toxic contaminants that may leach from them, like PAHs, phthalates, phenols and metals (see a.o. [77]). External exposure to microplastic for all routes considered was highest via the skin, on weight basis [77].

Use of skin care cosmetic products, like facial cleansers and scrubs, body scrubs and shower gels, can result in dermal exposure to MPs, as many of them nowadays contain microbeads instead of natural materials like inorganic powders, crushed shells or fruit stones in order to convey abrasive properties to the cosmetic product concerned [80]. However, MPs in skin care products are spherical particles rather than fibers [53, 80].

Concluding, few data are available on skin exposure to microplastics. Anyway, this route may be of limited relevance as the skin appears to be an effective barrier against their uptake (see section 12.5.4).

12.5 Internal exposure and human uptake routes

12.5.1 Introduction

As explained in chapter 12.4, three possible portals of entry need to be considered: the oral, the respiratory and the dermal portal. In absence of microplastic specific data, knowledge from engineered nanoparticles (ENP), especially the nanofibers, may be read-across to synthetic fibrous microplastics. More knowledge of the transfer of polymeric particles through biological membranes, can also be gained from the drug delivery research literature. There are many studies of how the bio-availability, uptake and delivery of medicines can be improved by using micro- or

nano-particulate carriers (e.g. [81, 82]). Furthermore, as convincingly demonstrated for ENPs, agglomeration of microplastics can affect the likelihood of their uptake (e.g. [81, 82]).

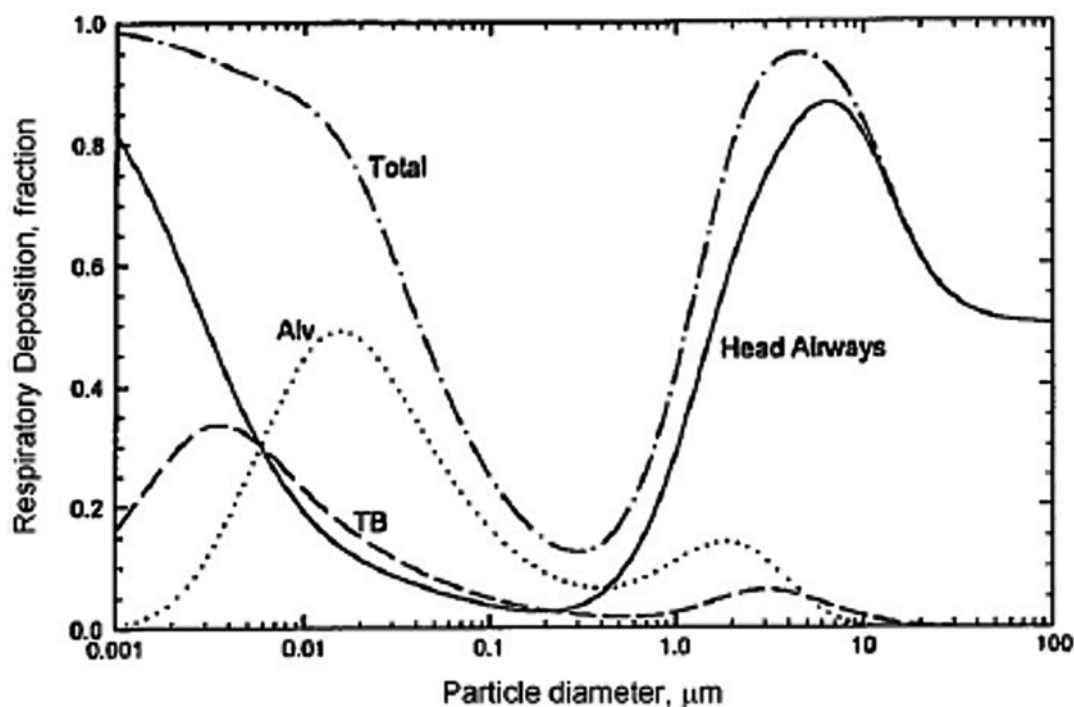


Figure 12.11.: Average predicted total and regional deposition for light exercise (nose breathing), based on the ICRP deposition model. Alv = alveoli; TB = tracheobronchial region (reproduced from [83]).

12.5.2 Uptake via inhalation

Before particles can cause local lung effects or enter into systemic circulation, they need to deposit in the lungs, otherwise they will be exhaled to the surrounding atmosphere. If and how they are taken up will depend on where in the airways the particles will deposit. In general, the size of the inhaled particle determines the location of its deposition, i.e. how deep a particle can enter into the airways (see Figure 12.8). Particles with a mass median aerodynamic diameter (MMAD) above 100 μm will deposit in the upper airways, whereas particles in the range of 10 to 100 μm will deposit in the oropharynx [84]. Particles with an MMAD between 5 and 10 μm will deposit in the central airways mucus layer, upon which ciliary movement of the endothelium will remove the particles from the airways (muco-ciliary clearance) [84]. Only particles below approx. 5 μm will be able to reach the alveoli, upon which clearance from the lung by macrophage phagocytosis usually takes place [84, 85]. Particles with an MMAD between approximately 0.2 and 0.5 μm are not deposited to a great degree, while particles in the 5 to 100 nm range mainly deposit in the alveoli and even smaller nanoparticles deposit in the trachea-bronchial region and the upper airways [85] (see Figure 12.11). These empirical laws are valid for particles, but fibers, which deposit by interception, tend to enter deeper into the lungs, even if as long as 250 μm (Prata 2018). This is expressed in the aerodynamic diameter of a particle, which is defined as the diameter of the spherical particle with a density of 1 g cm^{-3} that has the same settling velocity as the particle concerned [86]. For spherical particles the aerodynamic diameter is equal to the product of the square root of its density expressed in g cm^{-3} and its measured diameter, while for fibers the relationship is more complex, depending on its width, aspect ratio and density [87]. As can be seen from the examples presented in 12.5, the aerodynamic diameter of microfibers depends more on its cross-sectional diameter than its

12. The intake of synthetic fibers into the human body, by food, water and air

length, which can be considerable bigger than its cross-section. This means that non-fibrous, micron-sized MPs will rarely deposit in the alveoli, while nanoplastic particles and synthetic microfibers will deposit there upon inhalation.

Table 12.5.: Aerodynamic diameters of fibers at selected aspect ratios and densities [87]

Fiber cross-sectional diameter μm	Fiber density g cm^{-3}	Aerodynamic diameter at aspect ratio:		
		10 μm	20 μm	30 μm
1	1	1.89	2.08	2.20
1	1	1.99	2.20	2.32
1	2.5	2.99	3.30	3.47

When deposited, particles can be cleared from the lungs by mechanical means (from the upper airways, sneezing), by the mucociliary escalator (from the tracheobronchial compartment), macrophagic phagocytosis and subsequent migration (from the alveoli) and by lymphatic transport (Prata 2018) (see Figure 12.12). After transport to the oropharynx by the mucociliary escalator, the particles may be ingested after which they could become systemically available (see Figure 12.12). Once present in the lymph, particles may enter the bloodstream via the thoracic duct and thus reach other organs.

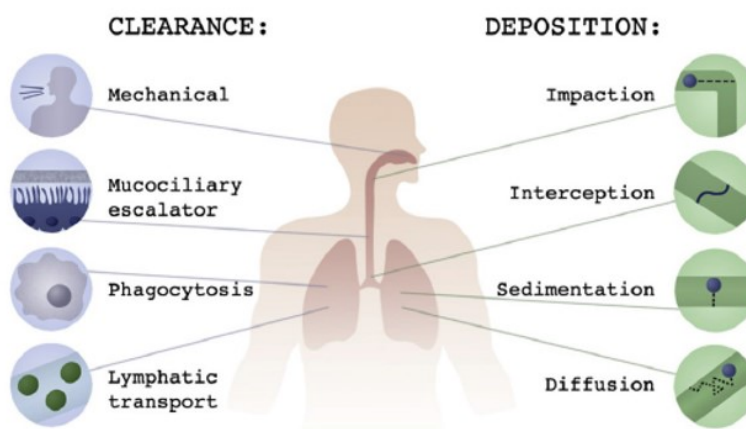


Figure 12.12.: Mechanisms of deposition, clearance and uptake of inhaled particles (reproduced from [28]).

The size of the particle is highly relevant in determining the extent to which the particle may become systemically available and how far the particle is able to penetrate into the human body. When the size of the plastic particle is smaller than about a quarter of a mm they may be taken up in endosomes, lysosomes, the lymph, circulatory systems and the lungs (e.g. see reviews by Kershaw et al. [54] and Leslie et al. [74]).

Studies of (ultra)fine solid particles in air, like diesel exhaust particulate, have demonstrated that these particles are capable to cross membranes, circulate in the body and invade human and mammalian tissues (see e.g. Hesterberg et al. [88]). Moreover, other factors than size, such as surface properties, particle solubility and aggregation state may affect the uptake of particles [89–91]. Inhaled particles may be retained within the pulmonary system for months [92]. Inhaled ultrafine particles ($< 0.1 \mu\text{m}$) may also be translocated along the olfactory nerve to the central nervous system in the brain [91].

Currently, no quantitative studies on the bioavailability of microplastics via inhalation seem to be available. Quite a number of studies on the bioavailability of nano-sized drug carriers are available, but these are designed to be bioavailable (when directed against a systemic disease) and hence the drug or even the carrier itself will dissolve in

biofluids, which will not be the case for microplastics, being plastic polymers. However, a review by [93] discusses, amongst others, the bioavailability of biodurable granular nanomaterials, which can give an indication of to what extent nanoplastic microplastics may become bioavailable. From the reviewed studies it was concluded in summary, that after inhalation exposure biodurable nanoparticles may translocate to a rather low extent via the circulatory, lymphatic, or nervous system to different tissues and organs, including the brain [93], but no quantitative estimations relative to e.g. inhaled dose were provided. The critical toxic effects of respiratory exposure to biopersistent granular nanoparticles but also of biopersistent nanofibers like carbon nanotubes tend to be local lung effects (see e.g. [94]). Therefore, it may be that also for nano-microplastics, and even more for micro-microplastics because of their bigger size, systemic absorption is a minor issue as local toxic effects will be manifest long before systemic ones.

Of course, there remains the potential for leaching of chemical substances from the microplastics retained in the lungs, particularly with longer retention times, e.g. for particles or fibers that deposit deep in the lungs, that is in the alveoli. For metals and metalloids associated with particulate matter, leaching by lung fluid has been studied in many papers, although there still is a lack of standardization and often the conditions applied and particles investigated are not representative of real-life exposure (see reviews by Wiseman and Kastury et al. [95, 96]). At this very moment, no studies addressing leaching of toxicants from microplastics seem to exist, so most likely this is an issue which warrants further research.

12.5.3 Uptake via ingestion

Once ingested, microplastics may pass the gut barrier. Several studies have proven transport of microplastics (sized between 0.1-150 μm) across the mammalian gut into the lymphatic system [54, 81]. Smaller particles are more easily and faster absorbed than larger particles [97]. For example, the uptake of polystyrene particles in the gastrointestinal system of rats increased as the particle size decreased [98, 99]. Exposure to fluorescent polystyrene (PS) microplastics (5 μm , $1.5 \times 10^6 \text{ d}^{-1}$ and 20 μm , $2.3 \times 10^4 \text{ d}^{-1}$) by gavage in mice showed size dependent accumulation in liver, kidney and gut [90]. This study clearly shows that PS particles in the lower micron size range, which are widely detected in the environment and food, become systematically available in mice after ingestion, and therefore may as well be absorbed from the gut by humans. Unfortunately, the mass balance deduced from the data from this study does not seem to be reliable, as after 28 days more 5 μm particles appeared to have accumulated in e.g. the kidney than had been administered by gavage ($28 \times 0.1 \text{ mg} = 2.8 \text{ mg}$ had been administered while $0.95 \text{ mg g}^{-1} \text{ bw}$ had allegedly accumulated in the kidney (equivalent to 28.5 mg in a 30 g animal)).

A laboratory experiment with seafish (mullets) held for 7 days in water containing 33.8 mg l^{-1} of PE or PS particles with a size of 0.1–1 mm (nearly $2500 \text{ particles l}^{-1}$), microplastics were mainly found in the gastrointestinal tract (approx. 10 PE particles and 90 PS particles per fish) and only a few in the liver of the fish (approx. 1–2 particles per fish for both PE and PS) (no other organs examined) [53]. Translocation to the liver of micro-sized microplastics was also observed in freshwater fish caught from the wild (European anchovie) and in lab experiments [100].

The uptake and fate of a particle is determined by the combination of the size of the particle, its surface properties, its charge, its hydrophobicity, and other factors such as aggregation of particles, presence of a corona around the particle, and chemical properties of its surface [81, 97, 101]. Ultimately, this implies that each different plastic particle type may exhibit different gut uptake rates and pathways.

Major sites of entry upon ingestion of microplastics are probably the Peyer's patches in the intestine [102]. Some studies focused on the potential mechanism of uptake of microplastics. Phagocytosis or endocytosis is possible, but the paracellular route of uptake can be excluded given the size of microplastics. According to Bouwmeester et al. [103] less than 1% of ingested micro-microplastics is absorbed, based on in vivo rodent studies, and even if they pass to the blood circulation via the lymph, they will probably be eliminated from the blood via the spleen [102, 103]. So far the presence of micro-sized microplastics has not been demonstrated in muscle tissue of fish, only in the digestive tract (the major site) and in organs, such as brain and liver, which are not commonly eaten [100].

For nano-sized microplastics, however, this may be different [102, 103]. Generally, nanoparticles may reach the

12. The intake of synthetic fibers into the human body, by food, water and air

circulation and spread to different tissues and organs because they are able to cross the gut epithelium and may also accumulate in tissues [69]. The largest particles were mainly found in the liver and spleen [98, 104, 105]. Smaller particles, for instance ≈ 200 nm polystyrene particles, were shown to translocate from the blood to the bone marrow [98, 106], where they can remain in cells for at least 4 days [89]. Furthermore, 50-240 nm particles have shown the ability to cross the human maternal-foetal placental barrier in an ex-vivo model [107], while 10 nm gold nanoparticles that were intravenously injected to rats were subsequently found in the brain [105] (De Jong and Borm 2008b). According to Bouwmeester et al. [103] 0.2 to 10% of ingested nano-sized particles may be absorbed from the gut, depending on the type and size of the particles.

Concluding, although no research has been done specifically on nano-sized plastic particles and most of the micro-sized microplastics will be excreted with faeces, nano-microplastics may become systemically available. Once plastic or non-plastic nanoparticles are systemically available, they may distribute through the entire body including reproductive organs and the brain.

Of course, there remains the potential for leaching of chemical substances. For example, Oomen et al. [77] a migration experiment in a simulated gastrointestinal system with rubber granulates from artificial sport turfs. This experiment showed that about 20 percent of the phthalates and 9 % of the PAHs present in the rubber granulate samples were released in the gastro-intestinal juices, and that a maximum of 9 μg lead and 2 μg cobalt per gram rubber granulate was released, while no cadmium was not detected. In comparison, leaching of these chemicals into sweat was negligible (see 12.5.4).

12.5.4 Uptake via the skin

In general, the available literature suggests that solid nanoparticles used in sunscreens or drug delivery systems do not penetrate into or through intact or compromised human skin nor produce local or systemic exposure or adverse health effects in humans (e.g. reviewed by Borm et al., Nohynek et al., Crosera et al. [108–110]. Alvarez-Román et al. [111] studied the dermal uptake of polymeric nanoparticles across porcine skin and showed accumulation of 20-100 nm polystyrene particles in the follicular openings. However, the PS particles were not able to cross the horny layer and pass the skin barrier of normal skin. In general, dermal penetration of micro-sized particles cannot be expected either, simply due to their large size.

Still, there remains the potential for leaching of chemical substances, particularly if there is prolonged contact with the skin due to retention in hair follicles for example. However, for substances enclosed within the particles this may be a minor pathway: In migration experiments with rubber granulate from recycled car tyres only a few substances were present above the detection limit in the artificial sweat used, amongst others five PAHs, of which 0.02% had migrated to the sweat, and lead, cobalt and cadmium (between 0.02 and 0.48 μg from 1 gram of granulate) and thus would be available for dermal uptake [77].

12.6 Conclusion

Like microplastics in general, synthetic microfibers can be found in marine and freshwater environments all over the globe and are often a sizeable fraction of the number of microplastics encountered. The atmosphere and the terrestrial environment have been less extensively investigated, but in view of the fact that 80% of all the plastics in the ocean have been generated on land, certainly in the latter synthetic fibers may occur wide-spread and in sizeable numbers. Since most of the microplastics taken up by biota do not translocate from the gastro-intestinal tract and microplastics do not appear to bioaccumulate or biomagnify in the food chain, consumption of food incorporating synthetic microfibers does not appear to be a significant route of human exposure to these microfibers. As a consequence, Indoor deposition of synthetic microfibers on food may contribute more to human dietary exposure to these fibers than their transfer in the food chain. Skin appears to be an effective barrier against the uptake of microplastics in general and, therefore, this route may also be of limited relevance in relation to exposure to synthetic microfibers.

Still these conclusions are tentative and qualitative at most, since due to the scarcity of data and the lack of harmonized, well-defined analytical methods, there is no reliable basis to calculate intakes of microplastics nor synthetic microfibers via dietary or respiratory routes. Therefore, there is an urgent need for standardization of sampling and analysis methods to enable a meaningful comparison across environmental compartments, different exposure routes and different sources of synthetic microfibers. Furthermore, quick and easy detection methods for microplastics including fibers smaller than 1 μm and particles in the nanorange (1-100 nm).

References

- [1] A. Parkes. *Improvements in the manufacture of parkesine or compounds of pyroxyline, and also solutions of piroxiline, known as collodion*. Patent 1313. 1865 (cited on page 175).
- [2] L. H. Baekeland. *Method of making insoluble products of phenol and formaldehyde*. US Patent 942,699. 1909 (cited on page 175).
- [3] R. C. Thompson, S. H. Swan, C. J. Moore, and F. S. Vom Saal. *Our plastic age*. The Royal Society Publishing, 2009 (cited on pages 175, 176).
- [4] Statista. *Global plastic production from 1950 to 2017 (in Million Metric Tons)*. en. 2018. URL: <https://www.statista.com/statistics/282732/global-production-of-plastics-since-1950/> (cited on page 175).
- [5] P. Kershaw. *Sources, fate and effects of microplastics in the marine environment: a global assessment*. Technical report. International Maritime Organization, 2015 (cited on pages 175, 176, 183, 187, 188).
- [6] J. R. Jambeck, R. Geyer, C. Wilcox, T. R. Siegler, M. Perryman, A. Andrady, R. Narayan, and K. L. Law. “Plastic waste inputs from land into the ocean”. In: *Science* 347.6223 (2015), pages 768–771 (cited on page 175).
- [7] J. G. Derraik. “The pollution of the marine environment by plastic debris: a review”. In: *Marine pollution bulletin* 44.9 (2002), pages 842–852 (cited on page 175).
- [8] W. C. Li, H. F. Tse, and L. Fok. “Plastic waste in the marine environment: A review of sources, occurrence and effects”. In: *Science of the total environment* 566 (2016), pages 333–349 (cited on page 175).
- [9] C.-L. Chen. “Regulation and management of marine litter”. In: *Marine anthropogenic litter*. Springer, Cham, 2015, pages 395–428 (cited on page 175).
- [10] S. L. Wright and F. J. Kelly. “Plastic and human health: a micro issue?” In: *Environmental science & technology* 51.12 (2017), pages 6634–6647 (cited on page 175).
- [11] F. Salvador Cesa, A. Turra, and J. Barúque-Ramos. “Synthetic fibers as microplastics in the marine environment: a review from textile perspective with a focus on domestic washings”. In: *Science of the total environment* 598 (2017), pages 1116–1129 (cited on pages 176, 178–180, 184).
- [12] C. Jönsson, O. Levenstam Arturin, A.-C. Hanning, R. Landin, E. Holmström, and S. Roos. “Microplastics shedding from textiles—Developing analytical method for measurement of shed material representing release during domestic washing”. In: *Sustainability* 10.7 (2018), page 2457 (cited on pages 176, 178–182).
- [13] S. A. Carr. “Sources and dispersive modes of micro-fibers in the environment”. In: *Integrated environmental assessment and management* 13.3 (2017), pages 466–469 (cited on pages 176, 178, 180).
- [14] R. Geyer, J. R. Jambeck, and K. L. Law. “Production, use, and fate of all plastics ever made”. In: *Science advances* 3.7 (2017), e1700782 (cited on pages 177, 180).
- [15] S. Karbalaei, P. Hanachi, T. R. Walker, and M. Cole. “Occurrence, sources, human health impacts and mitigation of microplastic pollution”. In: *Environmental science and pollution research* 25.36 (2018), pages 36046–36063 (cited on pages 178–180, 186).
- [16] I. E. Napper and R. C. Thompson. “Release of synthetic microplastic plastic fibres from domestic washing machines: Effects of fabric type and washing conditions”. In: *Marine pollution bulletin* 112.1-2 (2016), pages 39–45 (cited on pages 178, 181, 190).
- [17] K. Conley, A. Clum, J. Deepe, H. Lane, and B. Beckingham. “Wastewater treatment plants as a source of microplastics to an urban estuary: Removal efficiencies and loading per capita over one year”. In: *Water research X* 3 (2019), page 100030 (cited on pages 178, 180).
- [18] B. M. C. Almroth, L. Åström, S. Roslund, H. Petersson, M. Johansson, and N.-K. Persson. “Quantifying shedding of synthetic fibers from textiles; a source of microplastics released into the environment”. In: *Environmental Science and pollution research* 25.2 (2018), pages 1191–1199 (cited on page 178).

- [19] F. De Falco, E. Di Pace, M. Cocca, and M. Avella. “The contribution of washing processes of synthetic clothes to microplastic pollution”. In: *Scientific reports* 9.1 (2019), pages 1–11 (cited on pages 178–181).
- [20] M. Smith, D. C. Love, C. M. Rochman, and R. A. Neff. “Microplastics in seafood and the implications for human health”. In: *Current environmental health reports* 5.3 (2018), pages 375–386 (cited on page 178).
- [21] MarketWatch. *Synthetic Fibres Market Global Industry Statistics, Revenue Growth, Cost Structure, Robust Expansion in CAGR by Forecast 2023*. Press Release. 2019. URL: <https://www.marketwatch.com/press-release/synthetic-fibres-market-global-industry-statisticsrevenue-growthcost-structure-robust-expansion-in-cagr-by-forecast-2023-2019-01-09>. (cited on pages 178, 182).
- [22] M. H. Zwart and E. L. de Valk. “Microplasticvezels uit kleding: Achtergrondrapport mogelijke maatregelen”. In: (2019) (cited on page 181).
- [23] J. Talvitie, M. Heinonen, J.-P. Pääkkönen, E. Vahtera, A. Mikola, O. Setälä, and R. Vahala. “Do wastewater treatment plants act as a potential point source of microplastics? Preliminary study in the coastal Gulf of Finland, Baltic Sea”. In: *Water Science and Technology* 72.9 (2015), pages 1495–1504 (cited on page 180).
- [24] A. J. Underwood, M. G. Chapman, and M. A. Browne. “Some problems and practicalities in design and interpretation of samples of microplastic waste”. In: *Analytical methods* 9.9 (2017), pages 1332–1345 (cited on page 180).
- [25] M. A. Browne, P. Crump, S. J. Niven, E. Teuten, A. Tonkin, T. Galloway, and R. Thompson. “Accumulation of microplastic on shorelines worldwide: sources and sinks”. In: *Environmental science & technology* 45.21 (2011), pages 9175–9179 (cited on pages 181, 190).
- [26] OSPAR Commission. “Assessment document of land-based inputs of microplastics in the marine environment”. In: *The Convention for the Protection of the Marine Environment of the North-East Atlantic. Environmental Impact of Human Activities Series*. 2017 (cited on page 182).
- [27] B. Piribauer and A. Bartl. “Textile recycling processes, state of the art and current developments: A mini review”. In: *Waste Management & Research* 37.2 (2019), pages 112–119 (cited on page 182).
- [28] J. C. Prata. “Airborne microplastics: consequences to human health?” In: *Environmental pollution* 234 (2018), pages 115–126 (cited on pages 182, 192).
- [29] S. L. Wright, J. M. Levermore, and F. J. Kelly. “Raman Spectral Imaging for the Detection of Inhalable Microplastics in Ambient Particulate Matter Samples”. In: *Environmental science & technology* 53.15 (2019), pages 8947–8956 (cited on page 182).
- [30] T. Stanton, M. Johnson, P. Nathanail, W. MacNaughtan, and R. L. Gomes. “Freshwater and airborne textile fibre populations are dominated by ‘natural’, not microplastic, fibres”. In: *Science of the total environment* 666 (2019), pages 377–389 (cited on pages 182, 186).
- [31] R. Dris, J. Gasperi, M. Saad, C. Mirande, and B. Tassin. “Synthetic fibers in atmospheric fallout: A source of microplastics in the environment?” en. In: *Marine pollution bulletin* 104.1 (2016), pages 290–293 (cited on page 183).
- [32] R. Dris, J. Gasperi, C. Mirande, C. Mandin, M. Guerrouache, V. Langlois, and B. Tassin. “A first overview of textile fibers, including microplastics, in indoor and outdoor environments”. In: *Environmental pollution* 221 (2017), pages 453–458 (cited on page 183).
- [33] E. Mansour, C. Loxton, R. M. Elias, and G. A. Ormondroyd. “Assessment of health implications related to processing and use of natural wool insulation products”. In: *Environment international* 73 (2014), pages 402–412 (cited on page 183).
- [34] W. E. Fayerweather, W. Eastes, F. Cereghini, and J. G. Hadley. “Quantitative risk assessment of durable glass fibers”. In: *Inhalation toxicology* 14.6 (2002), pages 553–568 (cited on page 183).
- [35] A. L. Lusher, A. Burke, I. O’Connor, and R. Officer. “Microplastic pollution in the Northeast Atlantic Ocean: validated and opportunistic sampling”. In: *Marine pollution bulletin* 88.1-2 (2014), pages 325–333 (cited on pages 183–185).
- [36] J. Hämer, L. Gutow, A. Köhler, and R. Saborowski. “Fate of microplastics in the marine isopod *Idotea emarginata*”. In: *Environmental science & technology* 48.22 (2014), pages 13451–13458 (cited on page 183).
- [37] M. Cole, H. Webb, P. K. Lindeque, E. S. Fileman, C. Halsband, and T. S. Galloway. “Isolation of microplastics in biota-rich seawater samples and marine organisms”. In: *Scientific reports* 4 (2014), page 4528 (cited on page 184).
- [38] J.-P. W. Desforges, M. Galbraith, N. Dangerfield, and P. S. Ross. “Widespread distribution of microplastics in subsurface seawater in the NE Pacific Ocean”. In: *Marine pollution bulletin* 79.1-2 (2014), pages 94–99 (cited on pages 184, 185).
- [39] F. Dubaish and G. Liebezeit. “Suspended microplastics and black carbon particles in the Jade system, southern North Sea”. In: *Water, air, & soil pollution* 224.2 (2013), page 1352 (cited on page 185).
- [40] V. Fischer, N. O. Elsner, N. Brenke, E. Schwabe, and A. Brandt. “Plastic pollution of the Kuril–Kamchatka Trench area (NW pacific)”. In: *Deep Sea Research Part II: Topical Studies in Oceanography* 111 (2015), pages 399–405 (cited on page 185).

- [41] J. P. G. L. Frias, J. Gago, V. Otero, and P. Sobral. “Microplastics in coastal sediments from Southern Portuguese shelf waters”. In: *Marine environmental research* 114 (2016), pages 24–30 (cited on page 185).
- [42] A. L. Lusher, V. Tirelli, I. O’Connor, and R. Officer. “Microplastics in Arctic polar waters: the first reported values of particles in surface and sub-surface samples”. In: *Scientific reports* 5 (2015), page 14947 (cited on page 185).
- [43] H. A. Nel and P. W. Froneman. “A quantitative analysis of microplastic pollution along the south-eastern coastline of South Africa”. In: *Marine pollution bulletin* 101.1 (2015), pages 274–279 (cited on page 185).
- [44] N. H. M. Nor and J. P. Obbard. “Microplastics in Singapore’s coastal mangrove ecosystems”. In: *Marine pollution bulletin* 79.1-2 (2014), pages 278–283 (cited on page 185).
- [45] R. W. Obbard, S. Sadri, Y. Q. Wong, A. A. Khitun, I. Baker, and R. C. Thompson. “Global warming releases microplastic legacy frozen in Arctic Sea ice”. In: *Earth’s Future* 2.6 (2014), pages 315–320 (cited on page 185).
- [46] R. C. Thompson, Y. Olsen, R. P. Mitchell, A. Davis, S. J. Rowland, A. W. John, D. McGonigle, and A. E. Russell. “Lost at sea: where is all the plastic?” In: *Science* 304.5672 (2004), pages 838–838 (cited on page 186).
- [47] L. C. Woodall, A. Sanchez-Vidal, M. Canals, G. L. Paterson, R. Coppock, V. Sleight, A. Calafat, A. D. Rogers, B. E. Narayanaswamy, and R. C. Thompson. “The deep sea is a major sink for microplastic debris”. In: *Royal society open science* 1.4 (2014), page 140317 (cited on page 186).
- [48] S. Zhao, L. Zhu, T. Wang, and D. Li. “Suspended microplastics in the surface water of the Yangtze Estuary System, China: first observations on occurrence, distribution”. In: *Marine pollution bulletin* 86.1-2 (2014), pages 562–568 (cited on page 186).
- [49] A. A. Horton, A. Walton, D. J. Spurgeon, E. Lahive, and C. Svendsen. “Microplastics in freshwater and terrestrial environments: evaluating the current understanding to identify the knowledge gaps and future research priorities”. In: *Science of the total environment* 586 (2017), pages 127–141 (cited on page 186).
- [50] A. A. Koelmans, N. H. M. Nor, E. Hermesen, M. Kooi, S. M. Mintenig, and J. De France. “Microplastics in freshwaters and drinking water: Critical review and assessment of data quality”. In: *Water research* (2019) (cited on pages 186, 188).
- [51] J. Wang, X. Liu, Y. Li, T. Powell, X. Wang, G. Wang, and P. Zhang. “Microplastics as contaminants in the soil environment: A mini-review”. In: *Science of the total environment* (2019) (cited on page 186).
- [52] A. Vethaak and H. Leslie. “Plastic debris is a human health issue”. In: *Environmental science & technology* 50.13 (2016), pages 6825–6826 (cited on page 187).
- [53] K. Duis and A. Coors. “Microplastics in the aquatic and terrestrial environment: sources (with a specific focus on personal care products), fate and effects”. In: *Environmental sciences Europe* 28.1 (2016), page 2 (cited on pages 187, 188, 190, 193).
- [54] P. J. Kershaw and C. M. Rochman. “Sources, fate and effects of microplastics in the marine environment: part 2 of a global assessment”. In: *Reports and studies-IMO/FAO/Unesco-IOC/WMO/IAEA/UN/UNEP Joint Group of Experts on the Scientific Aspects of Marine Environmental Protection (GESAMP) eng no. 93* (2015) (cited on pages 187, 188, 192, 193).
- [55] EFSA Panel on Contaminants in the Food Chain (CONTAM). “Presence of microplastics and nanoplastics in food, with particular focus on seafood”. In: *EFSA Journal* 14.6 (2016), e04501 (cited on pages 187, 188).
- [56] E. Huerta Lwanga, H. Gertsen, H. Gooren, P. Peters, T. Salánki, M. van der Ploeg, E. Besseling, A. A. Koelmans, and V. Geissen. “Microplastics in the terrestrial ecosystem: implications for *Lumbricus terrestris* (Oligochaeta, Lumbricidae)”. In: *Environmental science & technology* 50.5 (2016), pages 2685–2691 (cited on pages 187, 188).
- [57] W. Yuan, X. Liu, W. Wang, M. Di, and J. Wang. “Microplastic abundance, distribution and composition in water, sediments, and wild fish from Poyang Lake, China”. In: *Ecotoxicology and environmental safety* 170 (2019), pages 180–187 (cited on page 188).
- [58] F. Collard, J. Gasperi, B. Gilbert, G. Eppe, S. Azimi, V. Rocher, and B. Tassin. “Anthropogenic particles in the stomach contents and liver of the freshwater fish *Squalius cephalus*”. In: *Science of the total environment* 643 (2018), pages 1257–1264 (cited on page 188).
- [59] S. Roch, T. Walter, L. D. Ittner, C. Friedrich, and A. Brinker. “A systematic study of the microplastic burden in freshwater fishes of south-western Germany-Are we searching at the right scale?” In: *Science of the total environment* 689 (2019), pages 1001–1011 (cited on page 188).
- [60] R. S. Pazos, T. Maiztegui, D. C. Colautti, A. H. Paracampo, and N. Gómez. “Microplastics in gut contents of coastal freshwater fish from Río de la Plata estuary”. In: *Marine pollution bulletin* 122.1-2 (2017), pages 85–90 (cited on page 188).
- [61] F. R. Khan, B. S. Mayoma, F. J. Biginagwa, and K. Syberg. “Microplastics in inland African waters: presence, sources, and fate”. In: *Freshwater microplastics*. Springer, Cham, 2018, pages 101–124 (cited on page 188).

- [62] C. A. Peters and S. P. Bratton. “Urbanization is a major influence on microplastic ingestion by sunfish in the Brazos River Basin, Central Texas, USA”. In: *Environmental pollution* 210 (2016), pages 380–387 (cited on page 188).
- [63] J. S. Silva-Cavalcanti, J. D. B. Silva, E. J. de França, M. C. B. de Araújo, and F. Gusmão. “Microplastics ingestion by a common tropical freshwater fishing resource”. In: *Environmental pollution* 221 (2017), pages 218–226 (cited on page 188).
- [64] S. Rainieri and A. Barranco. “Microplastics, a food safety issue?” In: *Trends in food science & technology* 84 (2019), pages 55–57 (cited on page 188).
- [65] B. Toussaint, B. Raffael, A. Angers-Loustau, D. Gilliland, V. Kestens, M. Petrillo, I. M. Rio-Echevarria, and G. Van den Eede. “Review of micro-and nanoplastic contamination in the food chain”. In: *Food Additives & Contaminants: Part A* 36.5 (2019), pages 639–673 (cited on pages 188–190).
- [66] D. Peixoto, C. Pinheiro, J. Amorim, L. Oliva-Teles, L. Guilhermino, and M. N. Vieira. “Microplastic pollution in commercial salt for human consumption: A review”. In: *Estuarine, Coastal and Shelf Science* (2019) (cited on page 188).
- [67] L. Li, Q. Zhou, N. Yin, C. Tu, and Y. Luo. “Uptake and accumulation of microplastics in an edible plant”. In: *Chinese Science Bulletin* 64.9 (2019), pages 928–934 (cited on page 188).
- [68] V. Bandmann, J. D. Müller, T. Köhler, and U. Homann. “Uptake of fluorescent nano beads into BY2-cells involves clathrin-dependent and clathrin-independent endocytosis”. In: *FEBS letters* 586.20 (2012), pages 3626–3632 (cited on page 188).
- [69] K. Mattsson, L.-A. Hansson, and T. Cedervall. “Nano-plastics in the aquatic environment”. In: *Environmental science: processes & impacts* 17.10 (2015), pages 1712–1721. ISSN: 2050-7895 (cited on pages 188, 194).
- [70] C. M. Rochman, A. Tahir, S. L. Williams, D. V. Baxa, R. Lam, J. T. Miller, F.-C. Teh, S. Werorilangi, and S. J. Teh. “Anthropogenic debris in seafood: Plastic debris and fibers from textiles in fish and bivalves sold for human consumption”. In: *Scientific reports* 5 (2015), page 14340 (cited on page 188).
- [71] J. Li, D. Yang, L. Li, K. Jabeen, and H. Shi. “Microplastics in commercial bivalves from China”. In: *Environmental pollution* 207 (2015), pages 190–195 (cited on page 188).
- [72] N. Seltnerich. “New link in the food chain? Marine plastic pollution and seafood safety”. In: *Environmental Health Perspect* 123.A34 (2015) (cited on page 188).
- [73] L. Van Cauwenberghe and C. R. Janssen. “Microplastics in bivalves cultured for human consumption”. In: *Environmental pollution* 193 (2014), pages 65–70 (cited on page 188).
- [74] H. A. Leslie, S. H. Brandsma, M. J. M. Van Velzen, and A. D. Vethaak. “Microplastics en route: Field measurements in the Dutch river delta and Amsterdam canals, wastewater treatment plants, North Sea sediments and biota”. In: *Environment international* 101 (2017), pages 133–142 (cited on pages 188, 192).
- [75] L. I. Devriese, M. D. van der Meulen, T. Maes, K. Bekaert, I. Paul-Pont, L. Frère, J. Robbens, and A. D. Vethaak. “Microplastic contamination in brown shrimp (*Crangon crangon*, Linnaeus 1758) from coastal waters of the Southern North Sea and Channel area”. In: *Marine pollution bulletin* 98.1-2 (2015), pages 179–187 (cited on page 188).
- [76] A. Karami, A. Golieskardi, C. K. Choo, V. Larat, S. Karbalaie, and B. Salamatina. “Microplastic and mesoplastic contamination in canned sardines and sprats”. In: *Science of the total environment* 612 (2018), pages 1380–1386 (cited on page 190).
- [77] A. G. Oomen and G. M. De Groot. “Evaluation of health risks of playing sports on synthetic turf pitches with rubber granulate”. In: (2017) (cited on pages 190, 194).
- [78] D. Brown. *Exposures to recycled rubber tire crumbs used on synthetic turf fields, playgrounds and gardening mulch*. 2007 (cited on page 190).
- [79] L. Anderson, P. Fleming, and A. Ansarifar. “Recent Advances in Understanding the Behavior of Shockpads for Outdoor Synthetic Sports Pitches”. In: *The Engineering of Sport* 6. Springer, 2006, pages 97–102 (cited on page 190).
- [80] C. Guerranti, T. Martellini, G. Perra, C. Scopetani, and A. Cincinelli. “Microplastics in cosmetics: Environmental issues and needs for global bans”. In: *Environmental toxicology and pharmacology* (2019) (cited on page 190).
- [81] N. Hussain, V. Jaitley, and A. T. Florence. “Recent advances in the understanding of uptake of”. In: *Advanced drug delivery reviews* 50 (2001), pages 107–142 (cited on pages 191, 193).
- [82] A. Verma and F. Stellacci. “Effect of surface properties on nanoparticle–cell interactions”. In: *small* 6.1 (2010), pages 12–21 (cited on page 191).
- [83] W. C. Hinds. “Respiratory deposition”. In: *Aerosol technology: properties, behavior, and measurement of airborne particles* (1999), pages 233–259 (cited on page 191).
- [84] A. F. Tena and P. C. Clarà. “Deposition of inhaled particles in the lungs”. In: *Archivos de Bronconeumología (English Edition)* 48.7 (2012), pages 240–246 (cited on page 191).

- [85] T. C. Carvalho, J. I. Peters, and R. O. Williams III. "Influence of particle size on regional lung deposition—what evidence is there?" In: *International journal of pharmaceutics* 406.1-2 (2011), pages 1–10 (cited on page 191).
- [86] W. C. Hinds. "Particle size statistics". In: *Aerosol Technology: Properties, Behavior, and Measurement of Airborne Particles* (1999), pages 69–103 (cited on page 191).
- [87] G. D. Nielsen and I. K. Koponen. "Insulation fiber deposition in the airways of men and rats. A review of experimental and computational studies". In: *Regulatory Toxicology and Pharmacology* 94 (2018), pages 252–270 (cited on pages 191, 192).
- [88] T. W. Hesterberg, C. M. Long, C. A. Lapin, A. K. Hamade, and P. A. Valberg. "Diesel exhaust particulate (DEP) and nanoparticle exposures: what do DEP human clinical studies tell us about potential human health hazards of nanoparticles?" In: *Inhalation toxicology* 22.8 (2010), pages 679–694 (cited on page 192).
- [89] A. Nemmar, B. Nemery, P. H. Hoet, J. Vermylen, and M. F. Hoylaerts. "Pulmonary inflammation and thrombogenicity caused by diesel particles in hamsters: role of histamine". In: *American journal of respiratory and critical care medicine* 168.11 (2003), pages 1366–1372 (cited on pages 192, 194).
- [90] Y. Deng, Y. Zhang, B. Lemos, and H. Ren. "Tissue accumulation of microplastics in mice and biomarker responses suggest widespread health risks of exposure". In: *Scientific reports* 7.1 (2017), pages 1–10. ISSN: 2045-2322 (cited on pages 192, 193).
- [91] A. Elder, R. Gelein, V. Silva, T. Feikert, L. Opanashuk, J. Carter, R. Potter, A. Maynard, Y. Ito, and J. Finkelstein. "Translocation of inhaled ultrafine manganese oxide particles to the central nervous system". In: *Environmental health perspectives* 114.8 (2006), pages 1172–1178 (cited on page 192).
- [92] G. Oberdörster, A. Maynard, K. Donaldson, V. Castranova, J. Fitzpatrick, K. Ausman, J. Carter, B. Karn, W. Kreyling, D. Lai, et al. "Principles for characterizing the potential human health effects from exposure to nanomaterials: elements of a screening strategy". In: *Particle and fibre toxicology* 2.1 (2005), page 8 (cited on page 192).
- [93] M. Moreno-Horn and T. Gebel. "Granular biodurable nanomaterials: no convincing evidence for systemic toxicity". In: *Critical reviews in toxicology* 44.10 (2014), pages 849–875 (cited on page 193).
- [94] H. E. Buist, R. Hischier, J. Westerhout, and D. H. Brouwer. "Derivation of health effect factors for nanoparticles to be used in LCIA". In: *NanoImpact* 7 (2017), pages 41–53 (cited on page 193).
- [95] C. L. Wiseman. "Analytical methods for assessing metal bioaccessibility in airborne particulate matter: a scoping review". In: *Analytica chimica acta* 877 (2015), pages 9–18 (cited on page 193).
- [96] F. Kastury, E. Smith, and A. L. Juhasz. "A critical review of approaches and limitations of inhalation bioavailability and bioaccessibility of metal (loid) s from ambient particulate matter or dust". In: *Science of the total environment* 574 (2017), pages 1054–1074 (cited on page 193).
- [97] L. Szentkuti. "Light microscopical observations on luminally administered dyes, dextrans, nanospheres and microspheres in the pre-epithelial mucus gel layer of the rat distal colon". In: *Journal of Controlled Release* 46.3 (1997), pages 233–242 (cited on page 193).
- [98] P. Jani, G. W. Halbert, J. Langridge, and A. T. Florence. "The uptake and translocation of latex nanospheres and microspheres after oral administration to rats". In: *Journal of pharmacy and pharmacology* 41.12 (1989), pages 809–812 (cited on pages 193, 194).
- [99] P. U. Jani, A. T. Florence, and D. E. McCarthy. "Further histological evidence of the gastrointestinal absorption of polystyrene nanospheres in the rat". In: *International Journal of Pharmaceutics* 84.3 (1992), pages 245–252 (cited on page 193).
- [100] F. Ribeiro, J. W. O'Brien, T. Galloway, and K. V. Thomas. "Accumulation and fate of nano- and micro-plastics and associated contaminants in organisms". In: *TrAC Trends in analytical chemistry* 111 (2019), pages 139–147 (cited on page 193).
- [101] D. A. Norris and P. J. Sinko. "Effect of size, surface charge, and hydrophobicity on the translocation of polystyrene microspheres through gastrointestinal mucin". In: *Journal of applied polymer science* 63.11 (1997), pages 1481–1492. ISSN: 1097-4628 (cited on page 193).
- [102] T. S. Galloway. "Micro- and nano-plastics and human health". In: *Marine anthropogenic litter*. Springer, Cham, 2015, pages 343–366 (cited on page 193).
- [103] H. Bouwmeester, P. C. Hollman, and R. J. Peters. "Potential health impact of environmentally released micro- and nanoplastics in the human food production chain: experiences from nanotoxicology". In: *Environmental science & technology* 49.15 (2015), pages 8932–8947 (cited on pages 193, 194).

- [104] S. A. Kulkarni and S.-S. Feng. “Effects of particle size and surface modification on cellular uptake and biodistribution of polymeric nanoparticles for drug delivery”. In: *Pharmaceutical research* 30.10 (2013), pages 2512–2522 (cited on page 194).
- [105] W. H. De Jong and P. J. Borm. “Drug delivery and nanoparticles: applications and hazards”. In: *International journal of nanomedicine* 3.2 (2008), page 133 (cited on page 194).
- [106] S. Gibaud, M. Demoy, J. P. Andreux, C. Weingarten, B. Gouritin, and P. Couvreur. “Cells involved in the capture of nanoparticles in hematopoietic organs”. In: *Journal of pharmaceutical sciences* 85.9 (1996), pages 944–950 (cited on page 194).
- [107] P. Wick, A. Malek, P. Manser, D. Meili, X. Maeder-Althaus, L. Diener, P.-A. Diener, A. Zisch, H. F. Krug, and U. von Mandach. “Barrier capacity of human placenta for nanosized materials”. In: *Environmental health perspectives* 118.3 (2010), pages 432–436 (cited on page 194).
- [108] P. J. Borm, D. Robbins, S. Haubold, T. Kuhlbusch, H. Fissan, K. Donaldson, R. Schins, V. Stone, W. Kreyling, J. Lademann, et al. “The potential risks of nanomaterials: a review carried out for ECETOC”. In: *Particle and fibre toxicology* 3.1 (2006), page 11 (cited on page 194).
- [109] G. J. Nohynek, E. K. Dufour, and M. S. Roberts. “Nanotechnology, cosmetics and the skin: is there a health risk?” In: *Skin pharmacology and physiology* 21.3 (2008), pages 136–149 (cited on page 194).
- [110] M. Crosera, M. Bovenzi, G. Maina, G. Adami, C. Zanette, C. Florio, and F. F. Larese. “Nanoparticle dermal absorption and toxicity: a review of the literature”. In: *International archives of occupational and environmental health* 82.9 (2009), pages 1043–1055 (cited on page 194).
- [111] R. Alvarez-Román, A. Naik, Y. Kalia, R. H. Guy, and H. Fessi. “Skin penetration and distribution of polymeric nanoparticles”. In: *Journal of Controlled Release* 99.1 (2004), pages 53–62 (cited on page 194).

13.

An overview of the effects of synthetic micro(nano)fibers following exposure, with a focus on humans

By: Stephanie Wright¹

1 – MRC Centre for Environment and Health, King's College London, London SE1 9NH, UK.

13.1 Introduction

Since their mass production began in the 1950s, synthetic fibers, characterized as being manmade from oil or cellulose [1], have been intrinsic in the progression of a range of technologies and industries, with applications as broad as clothing, upholstery and other textiles to car tyres to concrete. A key feature underpinning the popularity of synthetic fibers is durability, although it has become evident over the last 15 years that, whilst persistent, they are not resistant to deterioration. Through shedding and fragmentation, a global burden of microscopic synthetic fibers has penetrated far-reaching environments (see Chapters 4 and 9 for details). Considered a type of microplastic (microscopic plastic particle < 5 mm maximum dimension), synthetic fibers often comprise upward of 60% of the total microplastics observed in samples, from biota [2] to foodstuff [3] to air [4] and dust [5], and in solid matrices like sludge and soils [6]. Hence, it is likely that the general population has been exposed to synthetic fibers for decades and there is rising concern amongst both the public and policymakers regarding their impacts. However, without quantitatively assessing both exposure and hazards, it is challenging to infer risk, disease pathways and health outcomes. It is therefore timely to reflect on the potential hazards that synthetic fibers present and this chapter shall address existing evidence from fiber toxicology, occupational disease and *in vivo* case studies. This chapter is by no means exhaustive in describing the potential for microplastic toxicity but presents available evidence on the plausibility for health impacts due to synthetic fiber exposure. There is very little evidence available on the toxicity of ingested synthetic fibers, presumably since the primary exposure pathway anticipated up to now has been via inhalation of airborne fibers. Therefore, most of this chapter will focus on respiratory toxicology and health.

13.2 Inferences from fiber toxicology

Humans have been exposed to natural fibers, such as those originating from plants and animals, via diet and air throughout evolutionary history. As covered in Chapter 12, the human body has consequently developed clearance mechanisms and processing pathways to deal with them. It is also recognized that an unnatural influx of fibers can be harmful. For fibers, such harm is driven by composition and/or physical structure. Natural organic fibers, for example, are associated with health effects and morbidity and it is hypothesized that harmful toxic and/or allergenic proteins on their surface are responsible for these effects [1]. Perhaps the most famous fiber toxicant is asbestos, for which one of

13. An overview of the effects of synthetic micro(nano)fibers following exposure, with a focus on humans

the most well-established and accepted paradigms in particle toxicology exists [7]. A brief summary discussing the effects is given here, more details can be found in Chapter 7.

Asbestos exposure is associated with asbestosis (a disease characterized by chronic inflammation and scarring of the lower airway with an abundance of asbestos inclusions), lung cancer (predominantly adenocarcinoma) and mesothelioma (cancer of the plural lining) (reviewed in [8]). The interplay between dose, durability and dimension is shown to play a role in these aetiologies. For example, fiber dimensions influence aerodynamic behavior and therefore where along the airway a fiber deposits. Should inhaled fibers deposit in the tracheobronchial region, they will be transported to the pharynx via mucociliary clearance. However, if respirable fibers deposit in the distal region of the airway lacking a cilia-lined epithelium and thick mucus, they will be cleared via airway macrophages. Coughing is an effective mechanism for clearing asbestos from the lungs; just a fraction of the fibers an individual is exposed to accumulate and/or penetrate macrophages. Nevertheless, that fraction is enough to exert effects, which is why impacts can occur long after exposure. If a fiber is $> 15 \mu\text{m}$ in length, it will not be completely engulfed by a macrophage, leading to frustrated phagocytosis (see Chapter 7). Thus, long, respirable-sized fibers biopersist and can accumulate in the lung, increasing the local dose or burden. Frustrated phagocytosis leads to cell death and lowered pH by leakage of the cell content and, if prolonged, causes chronic inflammation, which can progress to a disease state. Fiber geometry has therefore been considered a significant contributor to pathogenicity throughout decades of research, culminating in the formulation of this widely accepted structure-activity paradigm [7], with toxicity increasing with length (reviewed in [8]). This gives rise to the question ‘*do particles of different composition with a fibrous shape conform to this paradigm?*’. Similar pathogenicity has been observed in rodents following exposure to carbon nanotubes (reviewed in [8]). However, male rats exposed to ‘finish-free’ nylon i.e. synthetic respirable fibers ($9.8 \times 1.6 \mu\text{m}$) for 6 h d^{-1} and 5 d week^{-1} for 4 weeks showed no significant impact on lung weights, pulmonary inflammation or macrophage function up to the highest concentration tested ($57 \text{ fibers cm}^{-3}$) compared to control animals [9], further emphasizing the importance of dimensions and composition.

13.3 Plausible toxic properties of synthetic fibers

At the time Burdett and Bard [1] published a fiber inventory to classify their hazard in 2006, synthetic fibers were not considered a public health risk due to their larger dimensions, dictated by the conventional machinery at the time. However, finer fibers are produced today to achieve silk-like, smooth and soft textiles, e.g., Taffeta, an artificial silk made from ultrafine ($< 1 \mu\text{m}$) polyester fibers. Combined with the low density of synthetic polymers, it is likely that synthetic fibers will behave aerodynamically smaller than their physical dimensions. Additionally, during production processes and use, fibrillation may occur, whereby thin fibers shear from the surface of a parent fiber or individual fibers split from a main structure compiled of smaller fibers. Para-aramid (Kevlar, p-aramid), polyacrylonitrile, polypropylene, polyhydroquinone-diimidazopyridine, polybenzobisoxazole and rayon (Lyocell) fibers were found to fibrillate following testing, highlighting a potential to shed thinner fibers (Figure 13.1 [1]). P-aramid fibrils generally have diameters of 0.3 to $0.7 \mu\text{m}$, whilst the origin fibers are ≈ 12 to $15 \mu\text{m}$ [9]. The following paragraphs assume exposure has already occurred, as per the fundamental presuppositions described in Chapter 12. It will be important to establish shedding and emission rates from the everyday use of synthetic textiles to understand of likelihoods of exposure.

The acidic environment (pH 4.6) of the phagolysosomal fluid within a macrophage may weaken a partially engulfed fiber, eventually breaking it into smaller constituents which can be completely engulfed and transported away, but this is influenced by the durability of the fiber material [1]. In 1990, Law et al. [10] the durability of manmade mineral-based and polymeric organic fibers (synthetic) in physiological fluid (Gamble’s Solution). In a 180 day leaching test, silica rapidly dissolved from the borosilicate fibers; surface area increased by 1800 to 22,000% whilst weight decreased by 37 to 75%. The synthetic fibers (polypropylene, polyethylene and polycarbonate) showed no dissolution, no significant changes to surface area and a very slight weight gain, suggesting they may persist in lung

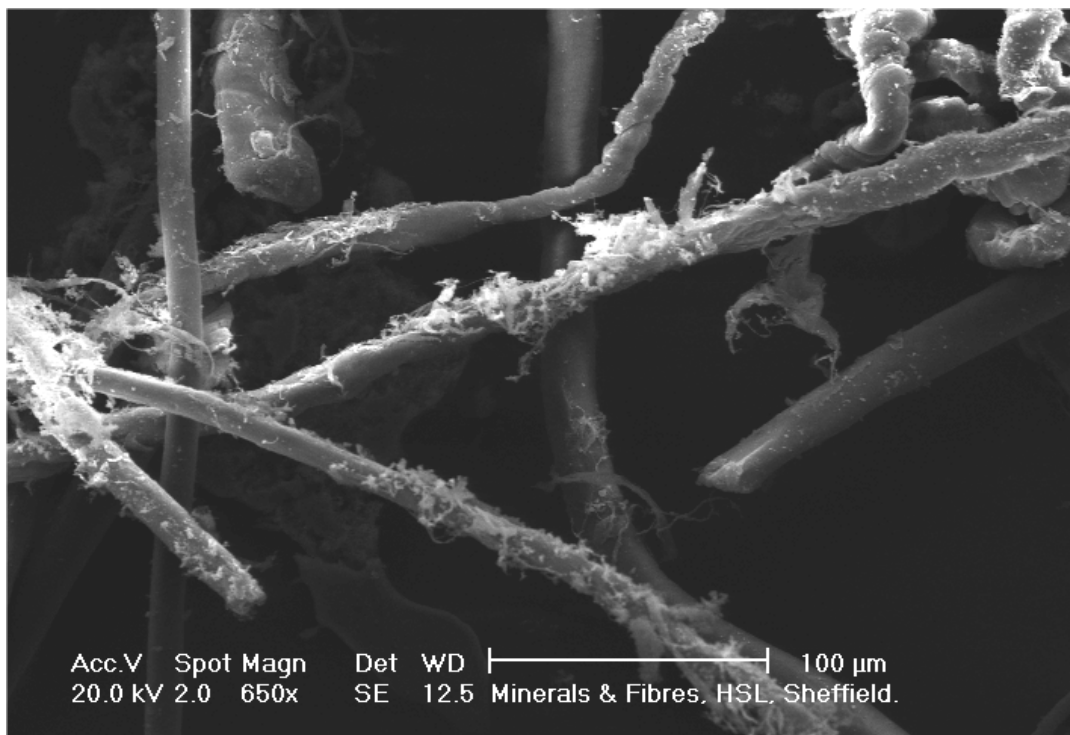


Figure 13.1.: A scanning electron micrograph of polypropylene fibers showing fibrils on the surface after testing [1]. Contains public sector information published by the Health and Safety Executive and licensed under the Open Government Licence.

lining fluid in the airway [10]. This is further supported by findings from [1], in which little weight loss was observed in para-aramid, rayon, nylon and polyacrylonitrile fibers, also in Gamble's solution. However, there is a lack of evidence on the dissolution of synthetic fibers in other physiological fluids; it is possible that pH and temperature, as well as enzymatic presence, may chemically attack polymers, facilitating degradation and elimination.

P-aramid (a synthetic polyamide) fibers are perhaps the most widely studied synthetic fiber in the field of toxicology due to their susceptibility to fibrillate, emitting respirable particles in the workplace (reviewed by [7]). Rapid clearance *in vivo* is consistently observed in controlled laboratory studies, which follows a pattern whereby p-aramid fibers are shortened in the lung over time. It has been hypothesized that lung fluid coats the fibers, catalyzing enzymatic attack and enabling biodegradation of inhaled p-aramid fibers in the lungs [9]. The shorter fibers are then completely phagocytosed and effectively cleared. This low biopersistence has led to their low hazard classification [7]. Degradation has also been observed for inhaled polypropylene fibers in rats, which increased with exposure concentration and time [11]. Whether this is apparent for other synthetic fibers is largely unknown and experiments are needed to assess their solubility. What is noteworthy, is that cellulose fibers were found to be more persistent than p-aramid fibers *in vivo* [9], and thus manmade cellulose fibers should be included in synthetic fiber hazard assessments.

An outstanding parameter intrinsic to mineral fibers and carbon nanotubes but lacking in synthetic fibers is rigidity (covered in Chapter 2 and 7). It is essential to determine whether flexibility lends respirable synthetic fibers a low hazard ranking.

13.4 Occupational epidemiology of synthetic fibers

Whilst there are no controlled human synthetic fiber exposure studies, there is literature on occupational epidemiology of synthetic textile workers. In these cases, it is likely that workers are exposed to a high concentration of a mixture of fibers and non-fibrous particles [12] in addition to chemicals (dyes, additives). In 1975, the earliest disease outbreak in relation to synthetic fiber exposure via inhalation was reported in workers in the textile (nylon, polyester, polyolefin, acrylic) industry. Patients presented with clinical symptoms similar to allergic alveolitis [13].

Since then, there have been outbreaks of a rare work-related interstitial lung disease in nylon flock manufacturing plants [14–19]. Flock refers to short-cut fibers which are applied to create velvet-like textiles and upholstery. When cut using a rotary mill, a substantial amount of respirable nylon dust is generated, leading to average exposure concentrations of 2.2 mg m^{-3} [20]. Otherwise healthy often young workers develop respiratory symptoms including chest pain, shortness of breath and cough [21]. Although these can evolve to fibrosis and respiratory failure [15, 16, 18], usually, removal from exposure is effective, stabilizing and ultimately improving respiratory symptoms [15, 16]. This contradicts the analogue of asbestos, which has prolonged latency periods and different disease outcomes. However, it is important to note that the respirable nylon flock dust, whilst fibrous, does not have the same dimensions as asbestos fibers making a direct comparison tenuous.

Pathologically, bronchoalveolar lavage fluid displays an abnormal cellular profile. Nonspecific interstitial pneumonia establishes, with accumulations of lymphocytes, in some cases where the lymphocytes are proliferating in the tissue, and lymphocytic inflammation of the bronchiole airway. Interestingly, similar pathologies and symptoms have been reported for workers exposed to other synthetic flock such as polyethylene [22], polypropylene [23] and rayon [24], raising concern that exposure to high levels of non-specific polymeric organic fibers increases the risk of interstitial lung disease. Long-term occupational exposure to respirable cotton (and flax and hemp) fibers is also associated with lung disease, with respiratory symptoms and loss of pulmonary function similar to asthma and chronic obstructive pulmonary disease. An understanding of the underlying cause for this is still not conclusive, although believed to be triggered by endotoxin secreted from gram negative microbes contaminating the surface of cotton fibers (reviewed in [25]). A case of diffuse lung disease due to cotton fiber inhalation has also been reported [26].

The underlying biochemical mechanisms leading to interstitial lung disease in response to synthetic fiber dust exposure remain unstudied, as do the physicochemical properties which trigger it. Whilst additives have been implicated in disease aetiology [27], there is also an evident propensity for washed nylon flock dust to be highly inflammatory [12, 27]. It has been hypothesized that the polycationic nature (i.e., the presence of multiple positive charges on the nitrogen atoms) of nylon flock could influence its pathogenicity [28]. This is supported by previous interstitial lung disease outbreaks following inhalation of other polycationic compounds e.g. Acramin-based spray paint [29, 30], mirrored *in vivo* [28], and by the suppression of polycationic paint toxicity by heparin, which has multiple negative charges [31].

There is suggestion that exposures in the nylon flocking industry increase the risk of lung cancer; a retrospective study on a nylon flocking plant cohort ($n = 162$) found risk to increase threefold [32]. Moreover, workers from a polyester and polyamide fiber factory in France were also found to be at statistically greater relative risk of mortality from various cancers (1.42 ($n = 79$, 95% CI 1.06 to 1.89) for high exposure or 1.38 ($n = 105$, CI 1.05 to 1.81) for former exposure to polymer dust). This group were at statistically greater risk of lung cancer mortality, irrespective of the level or duration of polymer dust exposure [33]. However, these findings are all worthy of an update with a larger cohort, confounding for individual smoking histories. In contrast, there was no association between synthetic fiber exposure and lung cancer risk in female textile workers in China [34].

Early histopathological analyses of lung biopsies from synthetic textile workers across a range of polymers showed, in addition to interstitial fibrosis, foreign-body-containing granulomatous lesions, believed to be acrylic, polyester and/or nylon dust [13]. There are no reports on whether frustrated phagocytosis occurs in the distal lung and no links to mesothelioma, although the diameter and aspect ratios of this synthetic fiber dust are likely very different to asbestos and carbon nanotubes. Flock dust was found to contain fibers 10 to 15 μm diameter and $\approx 1000 \mu\text{m}$ long),

respirable particles and elongated shreds of nylon (aerodynamic diameters of 4 to 8 μm) [20]. Whilst a proportion of the shreds were classified as fibers due to an aspect ratio of $> 3 : 1$ [20], they are morphologically distinct to the high aspect ratio asbestos and carbon fibers due to a heterogenous width and surface. No studies to date have assessed whether high aspect ratio flexible synthetic fibers matching the morphology and dimensions of asbestos fibers conform to the fiber toxicology paradigm. Considering their flexibility, it may be that other physicochemical properties, such as durability or (positive) surface charge, are more important for pathogenicity. It is essential to determine this for synthetic fibers in both indoor and outdoor environments and how this differs with fiber ‘age’ and weathering state.

13.5 *In vivo* evidence

13.5.1 Mammalian models

Few studies have assessed the toxicity of synthetic fibers *in vivo* and of these existing studies, most use p-aramid fibers for reasons mentioned earlier. Since Donaldson [7] comprehensively reviewed the toxicology of inhaled p-aramid fibers and there has been little update in the field since (assessed via a scoping search on databases ‘Pubmed’ and ‘Web of Science’ using ‘(p-aramid OR para-aramid) AND (toxicity OR toxicology)’), this section shall focus on other synthetic fibers. The toxicity of nylon flock (average particle dimensions 2 μm x 14 μm) *in vivo* has been assessed in controlled laboratory studies following occupational interstitial lung disease outbreaks in flock manufacturing plants. Following exposure via intratracheal instillation (10 mg kg^{-1} body weight, single dose), rats presented increased pulmonary inflammation and tissue injury at day 1 post-exposure. Significant differences to the control group had subsided by day 29 post-exposure, although localized areas of inflammation surrounding nylon fibers were still observed [27]. Contrasting findings were found in an industry-led study [9], which observed no significant effects and a NOEL (no observed effect limit) of 57 fibers m^{-3} , equivalent to 20 mg m^{-3} . The differences in fiber dimensions and dosing could explain these contradictory findings. Inhalation exposure to polypropylene fibers (1.6 x 30.3 μm ; 6 h d^{-1} , 5 day/week, for 90 d) resulted in a dose-dependent (15, 30, or 60 mg m^{-3}) increase in pulmonary macrophages across all tested time points. These increases were ‘mild’ and reversible, especially $< 30 \text{ mg m}^{-3}$. Additionally, no fibrosis was observed [11]. These few studies should be interpreted with caution. They each employ different exposure regimes; exposure is not necessarily representative (e.g. intratracheal instillation delivers a high, localized dose); and there are uncertainties in interspecies translation relative to humans. Considering the limited literature available, more research is needed to reach a conclusive evidence base, including chronic exposure studies to low doses.

13.5.2 Human studies

There are very few studies to address the effects of synthetic fibers on humans outside of the workplace. Both cellulosic and plastic fibers have been observed in non-neoplastic and malignant lung tissue from patients with different types of lung cancer [35]. However, with absent scale bars on the micrographs presented in the publication, it is difficult to discern their size and, in comparison to surrounding macrophages, they look too large to have reached such anatomical locations. For example, one fiber found was 135 μm in length. Even though this is one quarter of the diameter of a generation 17 bronchiole (540 μm diameter, 1410 μm length, where it was found), it is unlikely that this fiber was aerodynamically able to reach here (as presented in Chapter 2 and 8). The authors also highlight the lack of deterioration of the fibers observed [35]. Whilst they conclude this illustrates biopersistence, it could also be due to the fibers being freshly introduced into the tissue as an artefact of surgery. This is further supported by the absence of a Ferruginous body - a ferritin-protein coating from macrophage processing typically observed for asbestos fibers - and a lack of a foreign body tissue response presented.

Should the observations by Pauly et al. [35] be accurate, inhaled fibers were present in 83% of nonneoplastic lung samples ($n = 67/81$) and 97% of malignant lung samples ($n = 32/33$); there was a greater incidence of cellulosic and

plastic fibers in cancerous tissue. Whether this is a cause or effect remains to be determined and follow-up studies replicating this research are needed to address the inaccuracies mentioned above.

13.6 A potential for chemical effects?

Environmental synthetic fibers present complex mixture toxicology due to both their physical entity and associated chemicals. Synthetic fibers may contain unreacted monomers, additives, dyes and pigments [36] although there is a lack of data available on this. The contamination of house settled dust with brominated flame retardants (BFR) or phthalates [37] is widely documented worldwide. Abraded particles and fibers from treated upholstery has been found to enhance the concentration of BFR in household dust [38]. An estimated 15% of BFR exposure derives from household dust [39], yet the synthetic fiber proportion of dust is unknown. What is further unknown is if synthetic fibers contribute to this burden. Fibers of different ‘ages’ (time since manufacture and duration in the environment) will have different chemical burdens. Synthetic fibers have the potential to carry hydrophobic persistent organic pollutants adsorbed from the surrounding environment, due to their hydrophobic surface [40]. Many of these associated chemicals are reprotoxic, carcinogenic and mutagenic [36]. The key knowledge gap lies in the bioavailability of these chemicals *in vivo* and whether the contribution from synthetic fibers would ever be significant in relation to other sources of exposure. This becomes a question of toxicokinetics, which is beyond the scope of this chapter.

13.7 Discussion

This chapter has presented an overview of the current knowledge on synthetic fiber effects in humans. It highlights an array of knowledge gaps, which require address as our understanding of exposure develops. Most studies concerning the effects of synthetic fibers focus on respiratory health as, until recently, inhalation was perceived to be the primary exposure pathway. It is only now that evidence has emerged demonstrating that ingestion is another key exposure route (see Chapters 9 and 12). Does frustrated phagocytosis occur in intestinal macrophages or are other mechanisms here predominantly at play? This appears unstudied, yet macrophages of the gastrointestinal tract have important functional roles in inflammation and tissue homeostasis [41]. Both the airway and the gut are dynamic environments; the airways distend with breathing (e.g. in Chapter 8), whilst the intestines undergo peristalsis. Both have large surface areas, and both consist of hair-lined epithelial barriers with mucus layers. Both are exposed to the external environment and both have evolved to cope with exogenous particles. The two are even connected; particles cleared via the mucociliary escalator of the airway are swallowed, and therefore transported to the gut. There are also clear anatomical and physiological differences, but the applicability of some of the effects of synthetic fibers observed in the airway is worthy of interrogation in the gut.

Considering the duration of synthetic fiber mass production (almost 70 years ago) and use; the potential for synthetic fibers to shed and, in some cases, fibrillate; and the growing knowledge of synthetic fibers in the environment, one might question why related diseases are not observed in the general population. Firstly, since the presence of synthetic fibers in ambient air, dietary products and water is only just emerging, human exposure has not been comprehensively assessed and monitored; without knowledge on exposure concentrations, it is difficult to examine associations with diseases. Hesterberg et al. [11] exposed rats to a minimum dose of 13 mg of respirable polypropylene fibers m^{-3} for 6 h d^{-1} , 5 d week^{-1} , which induced minimal (but some) macrophage response after 30 d. This dose equates to 12 fibers cm^{-3} . Vianello et al. [42] reported a maximum average inhaled concentration of 16 microplastics m^{-3} in indoor air. Assuming these microplastics were respirable fibers, this concentration is seven orders of magnitude lower than that used by Hesterberg et al. [11]. Hence, current exposure estimates are substantially lower than the effective dose. These assumptions are crude, as the field of microplastics is technologically limited and Vianello et al. [42] could not identify particles $<10\ \mu\text{m}$ in size. Until researchers can robustly quantify health-relevant size fractions, the

relevance of these *in vivo* endpoints will not be realized. Furthermore, the effects of chronic exposures to low doses are unknown. Secondly, fine and ultrafine synthetic fiber fabrication is a recent technological development. Some fiber-related diseases have a long (15-30 year) latency period between exposure and onset. Thirdly, diseases due to elevated particulate matter (PM) exposure are known. What is unknown is the component of PM comprised of or originating from synthetic fibers and whether this plays a role in these. Whilst disease is observed in occupational cases, these synthetic fiber exposures are much greater than that experienced by the general population. However, these diseases do indicate the plausibility for environmental synthetic fibers to trigger localized biological responses.

13.8 Conclusions, limitations and future work

Knowledge on human exposure to synthetic fibers is gaining and a comprehensive understanding of the consequential health impacts is needed. The studies reviewed in this chapter have reaffirmed the conclusions of Chapter 7; that the impacts of fibers are influenced by the properties shape, length and chemical composition.

There is an evident lack of *in vivo* and *in vitro* studies on synthetic fiber toxicity, especially considering oral exposure pathways. Furthermore, there is no evidence on the bioavailability of additives from fibers and their relative contribution to human chemical burdens compared to other sources of exposures. Future work should follow a tiered approach using synthetic fibers composed of the polymers which are representative of common exposures. Cell-free *in vitro* biopersistence assays in different physiological fluids are needed, including an analysis of their degradation products and subsequent hazard identification. Ultimately, these would need to be replicated in *in vivo* fluids due to the enzymatic role in degradation. *in vitro* cell toxicity screens are required to assess local toxicity potential, cellular uptake and bio-transformation (Chapter 11), ensuring physiologically relevant dimensions are tested in lung models. This is also especially required in macrophage cell types to examine the applicability of the fiber toxicology paradigm to flexible synthetic fibers. A key limitation is the provision of test material for these studies and there is a need for cross-disciplinary and cross-industry collaboration to address these knowledge gaps. Nano-sized synthetic fiber toxicology is absent from the literature, yet considering the fabrication of fine and ultrafine fibers, is needed. Ultimately, whilst there are more outstanding questions than answers on the effects of synthetic fibers, what is clear is that any attempt to improve air and water quality via the development of effective filtration systems will be beneficial to environmental and human health.

References

- [1] G. Burdett and D. Bard. “An Inventory of fibres to classify their potential hazard and risk”. In: *Sudbury: Health and Safety Executive* (2006), pages 1–116 (cited on pages 201–203).
- [2] M. Compa, A. Ventero, M. Iglesias, and S. Deudero. “Ingestion of microplastics and natural fibres in *Sardina pilchardus* (Walbaum, 1792) and *Engraulis encrasicolus* (Linnaeus, 1758) along the Spanish Mediterranean coast”. In: *Marine pollution bulletin* 128 (2018), pages 89–96 (cited on page 201).
- [3] J. Li, C. Green, A. Reynolds, H. Shi, and J. M. Rotchell. “Microplastics in mussels sampled from coastal waters and supermarkets in the United Kingdom”. In: *Environmental pollution* 241 (2018), pages 35–44 (cited on page 201).
- [4] K. Liu, X. Wang, T. Fang, P. Xu, L. Zhu, and D. Li. “Source and potential risk assessment of suspended atmospheric microplastics in Shanghai”. In: *Science of the total environment* 675 (2019), pages 462–471 (cited on page 201).
- [5] C. Liu, J. Li, Y. Zhang, L. Wang, J. Deng, Y. Gao, L. Yu, J. Zhang, and H. Sun. “Widespread distribution of PET and PC microplastics in dust in urban China and their estimated human exposure”. In: *Environment international* 128 (2019), pages 116–124 (cited on page 201).
- [6] F. Corradini, P. Meza, R. Eguiluz, F. Casado, E. Huerta-Lwanga, and V. Geissen. “Evidence of microplastic accumulation in agricultural soils from sewage sludge disposal”. In: *Science of the total environment* 671 (2019), pages 411–420 (cited on page 201).
- [7] K. Donaldson. “The inhalation toxicology of p-aramid fibrils”. In: *Critical reviews in toxicology* 39.6 (2009), pages 487–500 (cited on pages 202, 203, 205).

- [8] E. Felley-Bosco and M. MacFarlane. “Asbestos: modern insights for toxicology in the era of engineered nanomaterials”. In: *Chemical research in toxicology* 31.10 (2018), pages 994–1008 (cited on page 202).
- [9] D. B. Warheit, K. Reed, K. E. Pinkerton, and T. Webb. “Biodegradability of inhaled p-aramid respirable fiber-shaped particulates (RFP): mechanisms of RFP shortening and evidence of reversibility of pulmonary lesions”. In: *Toxicology letters* 127.1-3 (2002), pages 259–267 (cited on pages 202, 203, 205).
- [10] B. Law, W. Bunn, and T. Hesterberg. “Solubility of polymeric organic fibers and manmade vitreous fibers in Gambles solution”. In: *Inhalation Toxicology* 2.4 (1990), pages 321–339 (cited on pages 202, 203).
- [11] T. Hesterberg, E. McConnell, W. Miiller, R. Hamilton, and W. Bunn. “Pulmonary toxicity of inhaled polypropylene fibers in rats”. In: *Toxicological Sciences* 19.3 (1992), pages 358–366 (cited on pages 203, 205, 206).
- [12] J. Burkhardt, W. Jones, D. W. Porter, R. M. Washko, and W. L. Eschenbacher. “Hazardous occupational exposure and lung disease among nylon flock workers”. In: *American journal of industrial medicine* (1999), pages 145–146 (cited on page 204).
- [13] J. C. Pimentel, R. Avila, and A. Lourenco. “Respiratory disease caused by synthetic fibres: a new occupational disease.” In: *Thorax* 30.2 (1975), pages 204–219 (cited on page 204).
- [14] A. H. Boag, T. V. Colby, A. E. Fraire, C. Kuhn III, V. L. Roggli, W. D. Travis, and V. Vallyathan. “The pathology of interstitial lung disease in nylon flock workers”. In: *The American journal of surgical pathology* 23.12 (1999), page 1539 (cited on page 204).
- [15] W. L. Eschenbacher, K. Kreiss, M. D. Lougheed, G. S. Pransky, B. Day, and R. M. Castellan. “Nylon flock-associated interstitial lung disease”. In: *American journal of respiratory and critical care medicine* 159.6 (1999), pages 2003–2008 (cited on page 204).
- [16] D. G. Kern, R. S. Crausman, K. T. Durand, A. Nayer, and C. Kuhn III. “Flock worker’s lung: chronic interstitial lung disease in the nylon flocking industry”. In: *Annals of internal medicine* 129.4 (1998), pages 261–272 (cited on page 204).
- [17] D. G. Kern. “The unexpected result of an investigation of an outbreak of occupational lung disease”. In: *International journal of occupational and environmental health* 4.1 (1998), pages 19–32 (cited on page 204).
- [18] D. G. Kern, C. Kuhn III, E. W. Ely, G. S. Pransky, C. J. Mello, A. E. Fraire, and J. Müller. “Flock worker’s lung: broadening the spectrum of clinicopathology, narrowing the spectrum of suspected etiologies”. In: *Chest* 117.1 (2000), pages 251–259 (cited on page 204).
- [19] S. E. Turcotte, A. Chee, R. Walsh, F. C. Grant, G. M. Liss, A. Boag, L. Forkert, P. W. Munt, and M. D. Lougheed. “Flock worker’s lung disease: natural history of cases and exposed workers in Kingston, Ontario”. In: *Chest* 143.6 (2013), pages 1642–1648 (cited on page 204).
- [20] J. Burkhardt, C. Piacitelli, D. Schwegler-Berry, and W. Jones. “Environmental study of nylon flocking process”. In: *Journal of Toxicology and Environmental Health Part A* 57.1 (1999), pages 1–23 (cited on pages 204, 205).
- [21] R. M. Washko, B. Day, J. E. Parker, R. M. Castellan, and K. Kreiss. “Epidemiologic investigation of respiratory morbidity at a nylon flock plant”. In: *American journal of industrial medicine* 38.6 (2000), pages 628–638 (cited on page 204).
- [22] E. Barroso, M. Ibañez, F. Aranda, and S. Romero. “Polyethylene flock-associated interstitial lung disease in a Spanish female”. In: *European Respiratory Journal* 20.6 (2002), pages 1610–1612 (cited on page 204).
- [23] S. Atis, B. Tutluoglu, E. Levent, C. Ozturk, A. Tunaci, K. Sahin, A. Saral, I. Oktay, A. Kanik, and B. Nemery. “The respiratory effects of occupational polypropylene flock exposure”. In: *European Respiratory Journal* 25.1 (2005), pages 110–117 (cited on page 204).
- [24] V. C. Antao, C. A. Piacitelli, W. E. Miller, G. A. Pinheiro, and K. Kreiss. “Rayon flock: a new cause of respiratory morbidity in a card processing plant”. In: *American journal of industrial medicine* 50.4 (2007), pages 274–284 (cited on page 204).
- [25] P. S. Lai and D. C. Christiani. “Long term respiratory health effects in textile workers”. In: *Current opinion in pulmonary medicine* 19.2 (2013), page 152 (cited on page 204).
- [26] H. Kobayashi, S. Kanoh, K. Motoyoshi, and S. Aida. “Diffuse lung disease caused by cotton fibre inhalation but distinct from byssinosis”. In: *Thorax* 59.12 (2004), pages 1095–1097 (cited on page 204).
- [27] D. W. Porter, V. Castranova, V. Robinson, A. F. Hubbs, R. R. Mercer, J. Scabilloni, T. Goldsmith, D. Schwegler-Berry, L. Battelli, R. Washko, et al. “Acute inflammatory reaction in rats after intratracheal instillation of material collected from a nylon flocking plant”. In: *Journal of Toxicology and Environmental Health Part A* 57.1 (1999), pages 25–45 (cited on pages 204, 205).
- [28] B. Nemery and P. H. Hoet. “Humidifier disinfectant-associated interstitial lung disease and the ardystil syndrome”. In: *American journal of respiratory and critical care medicine* 191.1 (2015), pages 116–117 (cited on page 204).

- [29] C. Moya, J. Antó, and A. Newman Taylor. “Collaborative Group for the Study of Toxicity in Textile Aerographic Factories. Outbreak of organising pneumonia in textile printing sprayers”. In: *Lancet* 344.8921 (1994), pages 498–502 (cited on page 204).
- [30] F. Ould Kadi, B. Mohammed-Brahim, A. Fyad, S. Lellou, and B. Nemery. “Outbreak of pulmonary disease in textile dye sprayers in Algeria”. In: *The Lancet* 344.8927 (1994), pages 962–963 (cited on page 204).
- [31] P. H. Hoet, L. Gilissen, and B. Nemery. “Polyanions protect against the in vitro pulmonary toxicity of polycationic paint components associated with the Ardystil syndrome”. In: *Toxicology and applied pharmacology* 175.2 (2001), pages 184–190 (cited on page 204).
- [32] D. G. Kern, E. Kern, R. S. Crausman, and R. W. Clapp. “A retrospective cohort study of lung cancer incidence in nylon flock workers, 1998–2008”. In: *International journal of occupational and environmental health* 17.4 (2011), pages 345–351 (cited on page 204).
- [33] M. Hours, J. Fevotte, S. Lafont, and A. Bergeret. “Cancer mortality in a synthetic spinning plant in Besançon, France”. In: *Occupational and environmental medicine* 64.9 (2007), pages 575–581 (cited on page 204).
- [34] H. Checkoway, R. Ray, J. Lundin, G. Astrakianakis, N. Seixas, J. Camp, K. Wernli, E. Fitzgibbons, W. Li, Z. Feng, et al. “Lung cancer and occupational exposures other than cotton dust and endotoxin among women textile workers in Shanghai, China”. In: *Occupational and environmental medicine* 68.6 (2011), pages 425–429 (cited on page 204).
- [35] J. L. Pauly, S. J. Stegmeier, H. A. Allaart, R. T. Cheney, P. J. Zhang, A. G. Mayer, and R. J. Streck. “Inhaled cellulose and plastic fibers found in human lung tissue.” In: *Cancer Epidemiology and Prevention Biomarkers* 7.5 (1998), pages 419–428 (cited on page 205).
- [36] D. Lithner, Å. Larsson, and G. Dave. “Environmental and health hazard ranking and assessment of plastic polymers based on chemical composition”. In: *Science of the total environment* 409.18 (2011), pages 3309–3324 (cited on page 206).
- [37] V. Sukiene, N. von Goetz, A. C. Gerecke, M. I. Bakker, C. J. Delmaar, and K. Hungerbühler. “Direct and air-mediated transfer of labeled SVOCs from indoor sources to dust”. In: *Environmental science & technology* 51.6 (2017), pages 3269–3277 (cited on page 206).
- [38] C. Rauert, S. Harrad, G. Suzuki, H. Takigami, N. Uchida, and K. Takata. “Test chamber and forensic microscopy investigation of the transfer of brominated flame retardants into indoor dust via abrasion of source materials”. In: *Science of the total environment* 493 (2014), pages 639–648 (cited on page 206).
- [39] C. Li, Z. Zhao, B. Lei, J. An, X. Zhang, and Y. Yu. “Polybrominated diphenyl ethers in the air and comparison of the daily intake and uptake through inhalation by Shanghai residents with those through other matrices and routes”. In: *Environmental science and pollution research* 22.3 (2015), pages 1750–1759 (cited on page 206).
- [40] S. Endo, M. Yuyama, and H. Takada. “Desorption kinetics of hydrophobic organic contaminants from marine plastic pellets”. In: *Marine pollution bulletin* 74.1 (2013), pages 125–131 (cited on page 206).
- [41] Y. R. Na, M. Stakenborg, S. H. Seok, and G. Matteoli. “Macrophages in intestinal inflammation and resolution: a potential therapeutic target in IBD”. In: *Nature Reviews Gastroenterology & Hepatology* (2019), page 1 (cited on page 206).
- [42] A. Vianello, R. L. Jensen, L. Liu, and J. Vollertsen. “Simulating human exposure to indoor airborne microplastics using a Breathing Thermal Manikin”. In: *Scientific reports* 9.1 (2019), pages 1–11 (cited on page 206).

14. Mechanics of fibrous particles immersed in selected flow conditions

Applications for air and water cleaning

By: Rafał Przekop¹, Leon Gradoń¹

¹ – Warsaw University of Technology, Faculty of Chemical and Process Engineering, ul. Waryńskiego 1, 00-645 Warsaw, Poland
e-mail: rafal.przekop@pw.edu.pl

14.1 Introduction

When the transport of spherical aerosol particle is considered, it is sufficient in most cases to take into account only the translation of the particle mass-centre. The same governing transport equations may be used to approximately describe motion of non-spherical isometric particles (e.g. cubes, octahedrons, compact aggregates), but require different expression for drag force. Various correlations of the drag coefficient for non-spherical particle were reviewed by Cheng [1], Ganser [2], and Chhabra, Agarwal, and Sinha [3]. These methods are, however, inappropriate for non-isometric particles, having significantly different major dimensions (discs, spheroids, cylinders). First, the drag force on a non-isometric particle is strongly dependent on particle orientation with respect to the fluid flow. Secondly, the rotation of a non-spherical particle plays a significant role in the determination of particle edge position in relation to the external boundary position. The interception become very important effect of fibrous particle deposition. Finally, for long particles drag force should be calculated rather locally, taking into account the fact that local velocity of different parts of the particle as well as the local fluid velocity may be significantly different. Thus, modelling of the transport of non-isometric particles is much more complex than of spherical or compact ones.

Fibrous particles are commonly met in the environment, in many technologies and in the workplace. They are also very important from a health standpoint. Materials that can be a source of fibrous aerosols include: a) a variety of natural mineral fibres (e.g., asbestos, zeolite); b) man-made fibres (glass, ceramic, carbon, polypropylene, nylon etc.); c) organic fibres (cotton, wool, wood and other cellulosic materials, caffeine, sugar cane); d) inorganic chain aggregates (iron and copper oxides) [4].

Several serious diseases are related to the inhalation of fibrous aerosol particles: fibrosis, mesothelioma and lung cancer. Besides other, widespread applications including thermal and acoustic isolators, friction materials, fire-proof clothes and ropes, floor tiles, laboratory equipment, asbestos was also used as a filtering material in protective respiratory masks for coal miners. Although such respirators had very good filtering properties, they themselves emitted respirable fibres. Examination of the size distribution of the fibres deposited in the lungs of miners with fibrosis showed that the fibre length was between 0.5 and 100 micrometers and the fibre diameter - between 0.1 and 2.5 micrometers [5]. Thus, surprisingly long fibres can penetrate into the alveolar region of the lungs. This is the result of the specific behavior of fibrous particles in a flow. They tend to align the major axis parallel to the streamlines, hence, the fibre diameter rather than the length mainly decides about the particle deposition. Longer

14. Mechanics of fibrous particles immersed in selected flow conditions

fibres are much more dangerous for health, since alveolar macrophages cannot completely engulf particles with a dimension larger than 17 micrometers [4–8].

Most theoretical analyses concerning the transport and deposition of fibrous aerosol particles consider the simplest mechanical model, that is the rigid body. It may be applicable to fibres made of some materials (e.g., asbestos, ceramic, carbon), but cannot be used for fibres which undergo deformation. For some kinds of fibres (e.g. cotton), the second limiting mechanical model, i.e., a thread-like particle, which is perfectly flexible but simultaneously inextensible, may be a reasonable approximation. However, for many fibrous particles (e.g. synthetic polymers), neither of these two limiting models is applicable as the fibre has a non-zero but a finite stiffness.

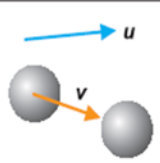
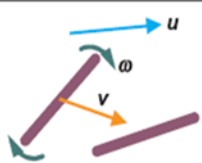
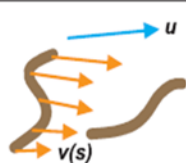
BEHAVIOUR OF AEROSOL PARTICLE IN FLUID		
SPHERICAL	FIBROUS	
	RIGID	DEFORMABLE
		
MATHEMATICAL DESCRIPTION OF MOTION		
ODE for linear acceleration of particle mass center	Set of ODEs for linear and angular accelerations of the entire particle	Set of PDEs for linear and angular accelerations of particle elements

Figure 14.1.: Schematic comparison of motion of spherical and fibrous (stiff and deformable) aerosol particles.

The method of mathematical description of motion of an aerosol particle depends on the particle shape and its mechanical properties (Fig. 14.1). For solid spherical (and compact, non-spherical) particles, it is sufficient to consider translation of the mass centre which is described by the single (in the vector form) ordinary differential equation (ODE). For a stiff fibre, its motion may be still described by set of ODEs for translation of the mass centre and additionally for rotation around its main axes. Otherwise, when a fibrous particle is deformable, instead of analyzing the motion of the entire object we have to consider motion of its subsequent elements, which leads to a set of partial differential equations (PDE); in this case, the numerical effort for modelling the fibre motion increases tremendously.

Many aspects of elongated aerosol particles have been investigated in recent decades. The influence of the particle size on its settling velocity was studied by Timbrell [9] and Ogden and Walton [10] considered the effect of fibre orientation. Krushkal and Gallily [11] and Griffiths [12] studied the effect of fibre orientation on the drag force. The diffusion of fibrous particles was investigated by Gentry, Spurny, Soulen, and Schörmann [13] and Asgharian, Yu, and Gradon [14]. Other studies concerned electrostatic problems for elongated aerosol particles, such as charge distribution on the fibre Wang, Pao, and Gentry [15] and deposition due to Coulombic attraction [16–18]. The behavior of fibrous particles in the turbulent flow was investigated by Shapiro and Goldenberg [19] and Bernstein and Shapiro [20]. Kvasnak and Ahmadi [21] measured the deposition rate of glass and paper fibrous particles in a horizontal wind tunnel. The results of mathematical modelling of the deposition of fibrous aerosol particles in vertical stagnation flows were presented by Broday, Fichman, Shapiro, and Gutfinger [22]. The deposition of fibrous aerosol particles in a granular bed was analysed theoretically by Podgórski, Zhou, Bibo, and Marijnissen [23] and investigated experimentally by Yue, Marijnissen, Lemkowitz, Podgorski, and Bibo [24]. All these works were concerned with the special case of a stiff, straight fibres.

The problem is even more complex when a particle is deformable. The second limiting case, the opposite of a model of stiff body, is a model of a perfectly flexible fibre. Theoretical works in this area started with the paper by Hinch [25], who considered the motion of a perfectly flexible, inextensible, weightless fibre neglecting inertia and

external forces other than drag. This description was extended by Podgórski and Gradoń [26] who derived governing transport equations for a perfectly flexible fibre taking into account inertia and any external forces and creeping gas flow field. This formulation became the standard method of description of flexible fibre motion and it was used to analyse the particle transport in various systems (e.g., deposition onto a circular collector [27, 28], sedimentation in laminar flow through a pipe [26], deposition in human airways [28], sampling of fibrous particles [29], deposition in turbulent flow in a rectangular duct [30]). The next step in the development of the theory of fibrous deformable aerosols particles considering the mechanical properties of the fibre [31].

14.2 Modelling of fibrous particle deposition in a fibrous filter

The general theory of fibrous, deformable aerosol particle mechanics formulated by Podgórski [31] was used for theoretical studies of motion and deposition of such particles. For this purpose, the single cell deposition efficiency, E_{cell} , was calculated as the ratio of the distance between the limiting trajectories, Y , to the unit cell height, h , (Fig. 14.2). The limiting trajectories were determined iteratively by integration of the equations of motion for various starting positions of particles at the cell inlet. Note that such a definition of the single cell efficiency is unique only for spherical particles. For fibrous ones, deposition efficiency depends also on particle orientation, which is characterized here by the angle of the initial orientation of the fibre main axis with respect to the direction of gas flow (Fig. 14.2).

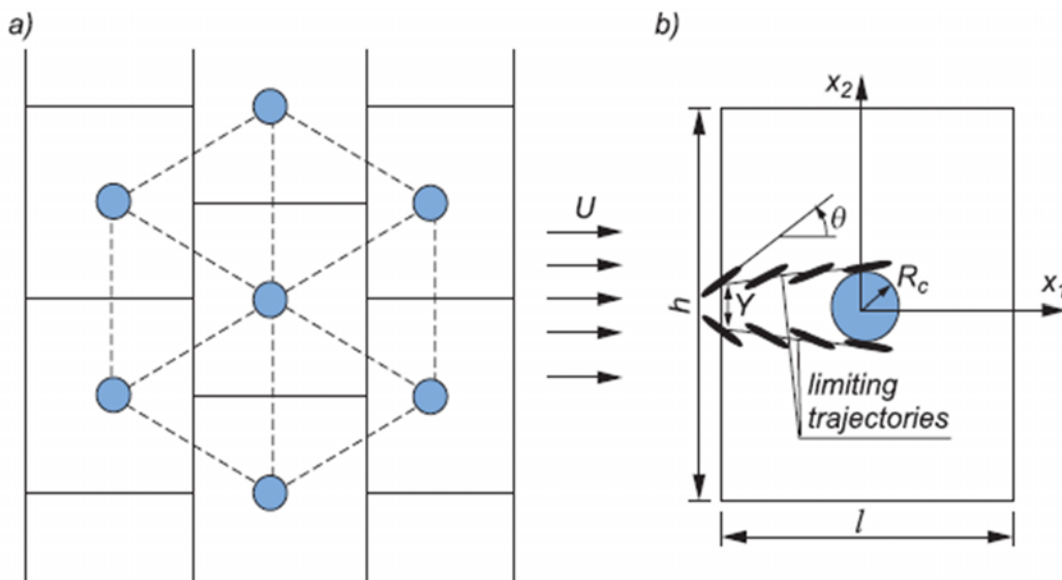


Figure 14.2.: a) model of fibrous filter structure; b) definition of single cell deposition efficiency, $E_{cell} = Y/h$.

The particles trajectories shown in Fig. 14.3 were calculated for a stiff fibre and for a perfectly flexible one. In both cases, we can observe the specific feature of the elongated aerosol particle motion: the fibrous particle tends to follow the fluid streamlines continuously changing its orientation in a gas flow field. This preferential alignment results from the fact that the drag force on the fibre is strongly dependent on its orientation. It is therefore of a great practical importance to understand that the deposition efficiency of large, oblong fibres in a porous filter is primarily related to the diameter of the particle cross-section, which can be very small even for fibres of relatively large volume. This phenomenon explains qualitatively why the deposition efficiency for long fibrous particles is usually lower than that for spherical particles of the same mass. On the other hand, the effect of fibre length is not negligible as it strongly affects particle inertia. Consequently, one should not expect that deposition efficiency for a fibrous particle could be estimated from well-known correlations for a spherical particle using a single characteristic dimension (e.g.,

14. Mechanics of fibrous particles immersed in selected flow conditions

equivalent sphere volume diameter or equivalent aerodynamic diameter). Let us also note, that a flexible fibre, which can change its shape, has a better possibility of adaptation to the local pattern of gas streamlines than a stiff one, which can achieve it by rotation only. Thus, it may be expected that the deposition efficiency for a flexible fibre should be lower than that for a stiff fibrous particle of the same dimensions and density.

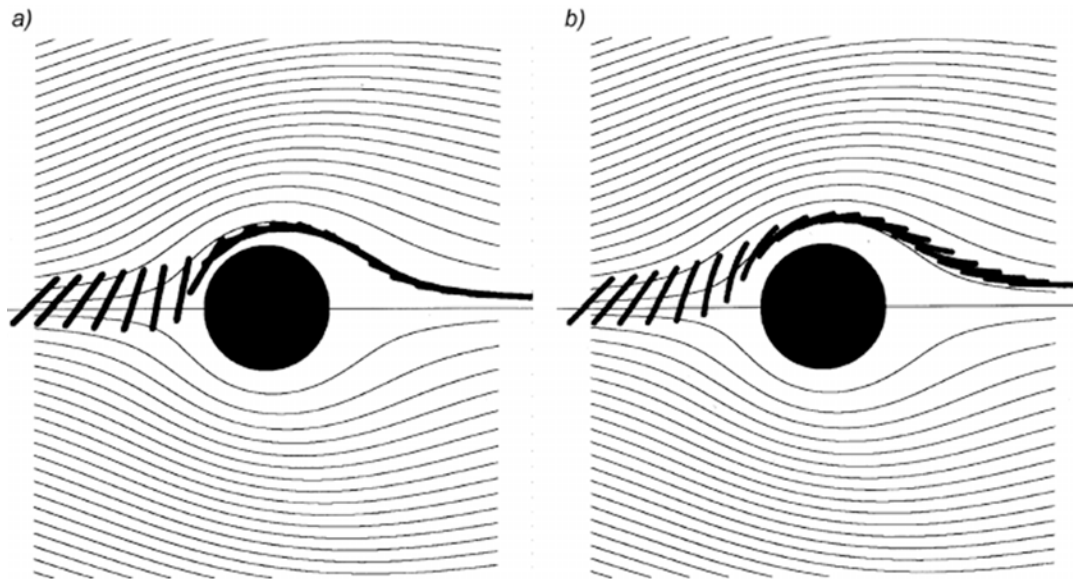


Figure 14.3.: Examples of fibrous particles trajectories in air flow around cylindrical obstacle. a) stiff particle; b) perfectly flexible particle.

14.2.1 The effect of gas velocity and fibre orientation on deposition efficiency

The two subsequent plots (Figs. 14.4 and 14.5) show the influence of gas velocity and initial fibre orientation on the single cell deposition efficiency for flexible and stiff fibres as compared to a spherical particle of the same volume. The characteristic minimum of the relationship shown in Fig. 14.4 reflects an opposite influence of the gas velocity on various mechanisms of particle deposition. For low velocity range, an increase of flow velocity causes a drop of the predominating deposition efficiency mechanism due to sedimentation, whilst for high gas velocities, the increase in velocity is favorable because of the enhancement of the inertial deposition. In addition, the torque on a fibrous particle is higher at a higher airflow rates, causing a faster rotation of a stiff fibre or the quicker deformation of a flexible fibre. Finally, as shown in Fig. 14.5, these phenomena are strongly affected by the initial orientation of the fibrous particle (located far from the collector). It is seen that a stiff fibrous particle has the highest deposition efficiency, and usually the lowest one is found for a flexible fibre; the deposition efficiency for an equivalent spherical particle is intermediate for almost all values of gas velocity. In the case, when a fibre is already aligned to the fluid streamlines far from the collector, the transverse force is very weak; thereupon rotation of a large, rigid fibre is almost negligible and the fibre falls mainly due to gravity. This explains a higher deposition efficiency of a rigid fibre compared to that of an equivalent sphere. Simultaneously, a weak lateral force is sufficient to cause a continuous deformation of a flexible fibre, which follows very closely the fluid streamlines. This is the reason why the deposition efficiency of a deformable aerosol particle being initially parallel to the direction of gas flow is lower compared to both stiff fibre and the equivalent sphere for low and intermediate air velocities. Only for high gas velocities, when inertial effects are very strong, the deposition efficiency becomes comparable for all considered types of aerosol particles. In the second limiting case of initial orientation of the fibre, the perpendicular one (Fig. 14.5) the results of simulations are somewhat different. As seen, the deposition efficiency for a spherical particle is always the highest, compared to that

for both flexible and stiff fibrous particles. Moreover, the efficiency for one and the other fibre is almost the same in this case. The explanation of this finding is relatively simple. For a fibre initially perpendicular to the gas flow direction, the transverse drag force, and consequently the torque on the particle, are much larger than for initially parallel fibre. This results in a rapid change of fibre orientation caused by its rotation (and, in addition, by a slight deformation of the flexible fibre). Hence, both kinds of fibre follow a similar trajectory aligning their major axis to the fluid streamlines in the vicinity of the collector. Such a preliminary analysis clearly indicates how strong and complicated is the combined influence of initial fibre orientation and gas velocity on the deposition efficiency. This complexity is even more emphasized by the results which present the influence of the initial fibre orientation on deposition efficiency. Local minima and maxima of the relationships can be observed, which reflect the different influence of fibrous particle orientation with respect to gas flow on various transport mechanisms (longitudinal vs. lateral convective-inertial motion, particle sedimentation, torque on the fibre, and, in turn, its rotation as well as shape deformation for a flexible fibre).

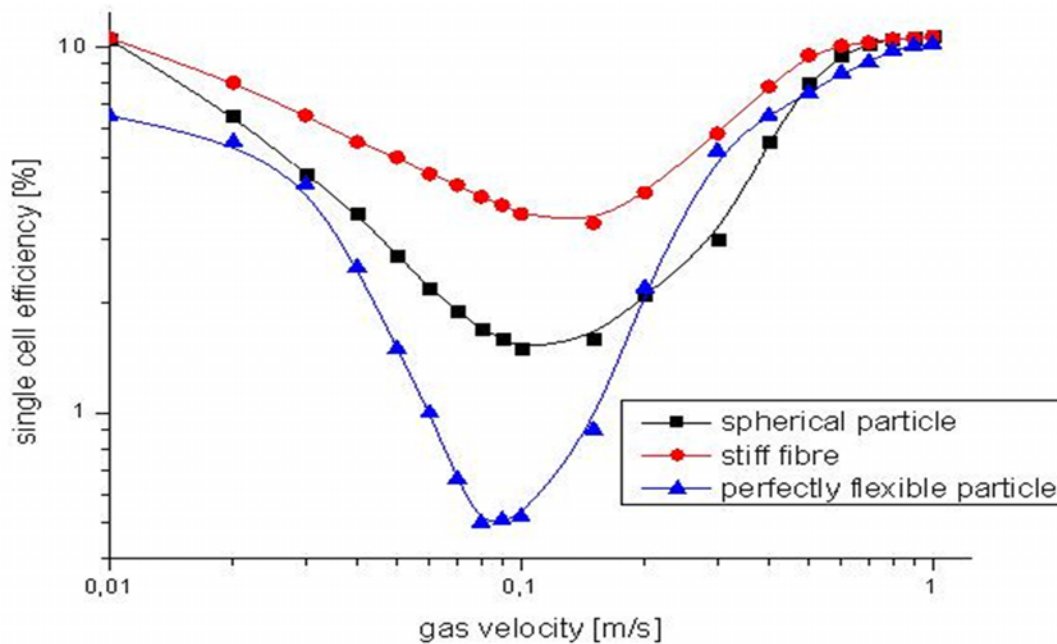


Figure 14.4.: Effect of gas velocity on single cell deposition efficiency for fibrous (flexible and stiff) and spherical (of the same volume) particles for initial fibre orientation $\theta = 0$

14.2.2 The effect of particle volume and slenderness ratio on the deposition efficiency

An example of the influence of particle size on the deposition efficiency are shown in Fig. 14.7. Since the diffusional mechanism of deposition (important for submicron particles) is not considered, we observe an enhancement of the deposition with the increase of the particle size, as this is predominating over all other mechanisms (sedimentation, interception, inertial impaction). The deposition efficiencies for fibrous particles are lower than those for spherical particles of the same volume. Deposition of stiff fibre of the same volume is higher than of a flexible one. The differences in the deposition efficiency of various aerosol particles are more notable for smaller particles. Fig. 14.6 shows the effects of fibre slenderness on the on the deposition efficiency of fibrous particles of fixed volume. For stiff fibre the deposition efficiency continuously decreases with increase of a slenderness far below the efficiency of the equivalent spherical particle. The efficiency of a flexible fibre is in this case always the lowest and it exhibits a local minimum. It is not easy to interpret these results qualitatively, since the deposition efficiency is the final result of many

14. Mechanics of fibrous particles immersed in selected flow conditions

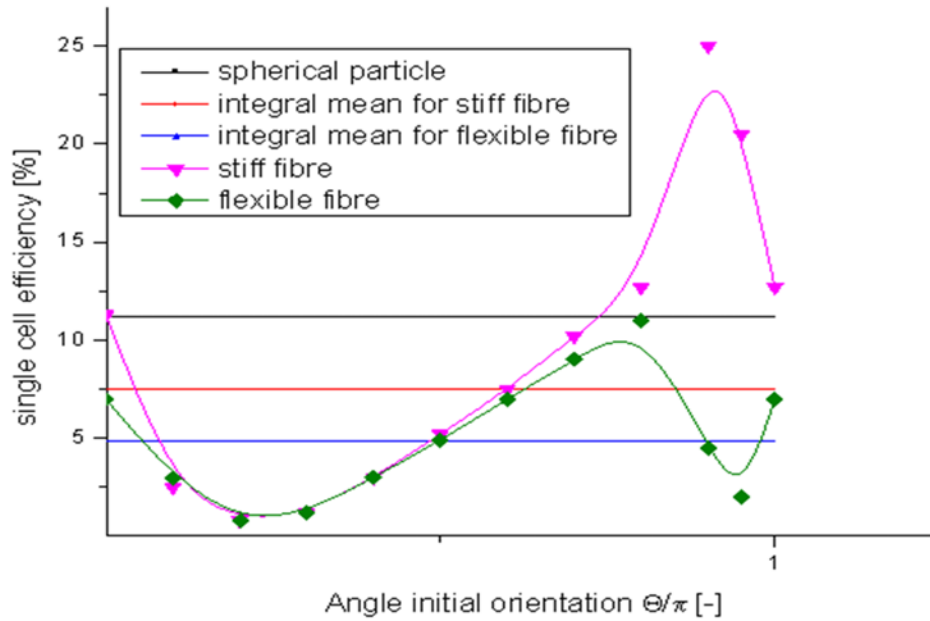


Figure 14.5.: Effect of the initial fibre orientation on deposition efficiency, $u = 0.01 \text{ ms}^{-1}$

phenomena occurring simultaneously: a) particle inertia, related to gas velocity and both, fibre length and diameter; b) particle interception, which may be mainly influenced either by the fibre length or by its diameter, depending on the fibre configuration with respect to the collector during collision; (this configuration is in turn related to the initial fibre orientation with respect to the flow far from the obstacle, gas velocity and particle mechanical properties); c) particle rotation and deformation, which depend on the dimensions of the fibre, its mechanical properties and gas velocity; d) particle sedimentation, depending mainly on the mass and configuration of the fibre. Nevertheless, the results obtained clearly indicate that an elongated fibrous particle will usually be less effectively captured compared to a compact particle of the same mass.

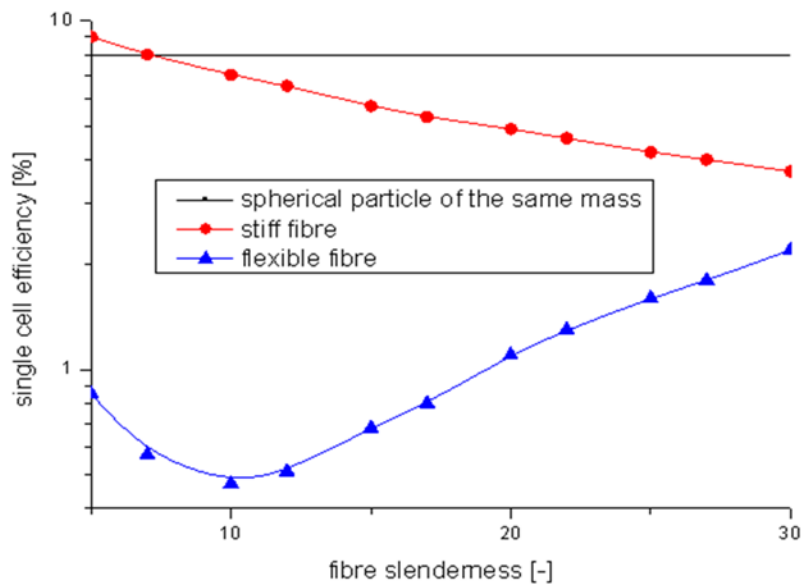


Figure 14.6.: Effect of particle slenderness on deposition efficiency, $u = 0.5 \text{ ms}^{-1}$, $\theta = \pi/2$

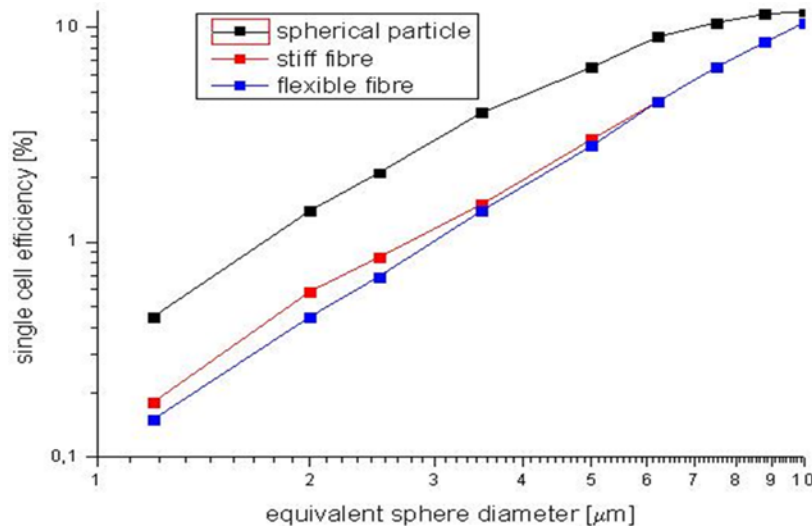


Figure 14.7.: Effect of particle size on deposition efficiency, $u = 0.5 \text{ m s}^{-1}$

14.2.3 Effect of collectors orientation

Although, the single cell deposition efficiency for fibrous particles is usually lower than for spherical particles of the same volume, it may be increased by the proper design of filter structure. Let us first consider a system of two cylindrical collectors. Przekop and Podgórski [32] have proposed a solution to the Oseen problem for the case of two cylindrical collectors. The authors noticed that an approximate analytical solution can easily be obtained using the method of complex disturbance velocity [33], which was used by Podgórski [34] to obtain a solution to the Oseen problem in case of a single fibre. Fig. 14.8 shows the fluid velocity vectors for the system of two cylinders. A strong influence of the cylinders mutual orientation can be observed, especially in the region between the collectors.

Fig. 14.10 shows the relation between the collection efficiency of stiff fibrous particles and angle, ϕ , which describes the orientation between the main direction of fluid flow and a line connecting centres of the cylinders (Fig. 14.9). As one can see, the maximum of deposition efficiency is observed for $\phi = \pi/6$. It can be explained by the fact that for this orientation the second fibre is not shadowed by the first one and, at the same time, the direction of fluid flow changes rapidly. Therefore, the fluid velocity in the region between the cylinders is relatively high, what results in an increased deposition efficiency due to the inertial mechanism. For higher values of ϕ particles can easily bypass in the region between the fibres.

Taking into account the real structure of a deep-bed filter, behavior of fibrous particles described above can occur more or less frequently. We expect that fibrous particle immersed in the fluid with periodically variable velocity gradient caused by neighboring collector fibres, changes its temporary orientation increasing the probability of interception with the collector's surface. Finally, the deposition of fibrous particles increases in comparison with the case of flow around single isolated fibre. Having such tools for the analysis of fibrous particle behavior at complex deep-bed structure we are able to design the filter for efficient removal of fibrous particles from a fluid.

14.2.4 Flexible aggregate model

Harmonic oscillator equation was applied to determinate interactions between the particles in aggregate [32, 35], which can represent a partially deformable fibrous particle. The aggregate's particles are modelled as material points

14. Mechanics of fibrous particles immersed in selected flow conditions

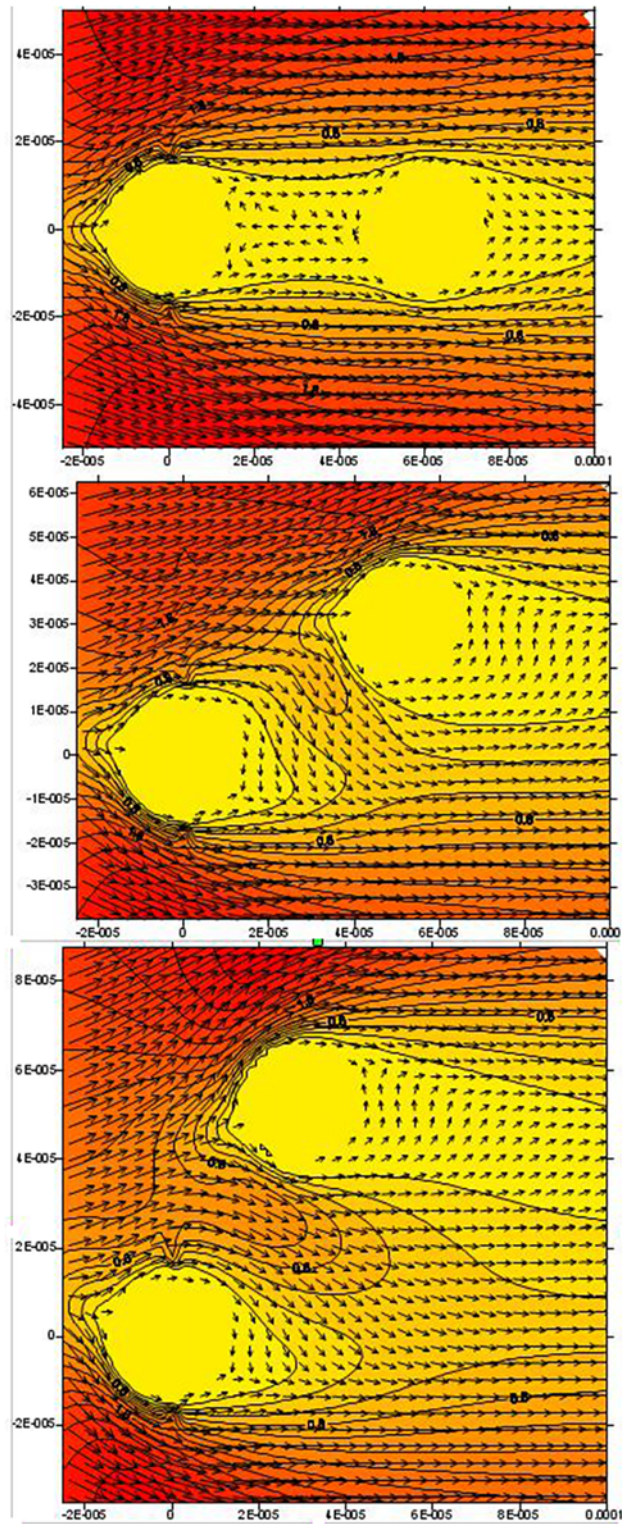


Figure 14.8.: Fluid velocity vectors in the system of two cylinders, $Re = 0.5$

connected by extensible spring with imposed damping factor.

$$m_{pi} \frac{d^2 r_i}{dt^2} = -k_s (r_{ij} - r_{0ij}) - f_d \frac{dr_i}{dt} \quad (14.1)$$

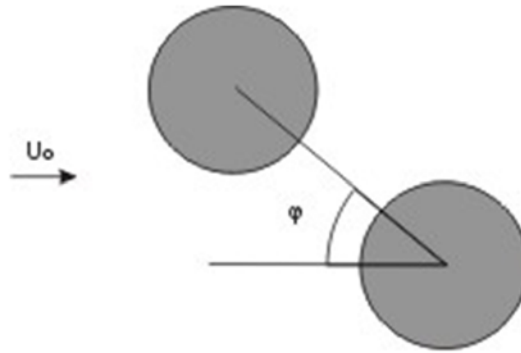


Figure 14.9.: Definition of the orientation angle, ϕ .

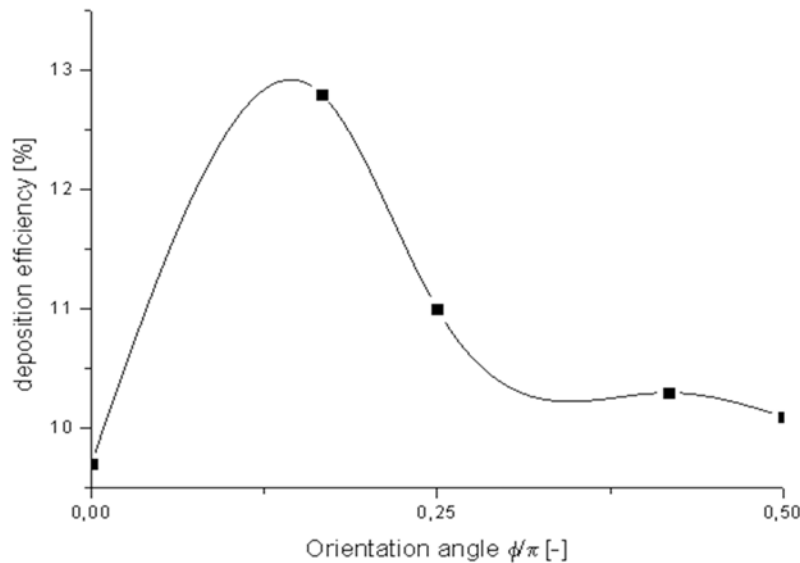


Figure 14.10.: Deposition efficiency as a function of collectors. Orientation angle $\theta = 0$, fluid velocity $u = 0.5 \text{ ms}^{-1}$, equivalent sphere diameter $d_p = 5 \mu\text{m}$, aspect ratio - 10.

where m_{pi} is primary particles mass, k_s is spring constant, f_d is a damping factor for oscillations, r_{ij} is the distance between geometrical centres of joined particles and r_{0ij} is initial distance between geometrical centres of joined particles. Equation 14.1 was extended to give a full mathematical description of vibrations commonly encountered in structures of fractal-like aggregates [36]. The following configurations of primary particles in fractal-like aggregates can be distinguished (Fig. 14.11):

- Pairs of bonded particles $i - j$, Fig 14.11(a);
- Tees (triplets) of particles $i - j - k$ and two pairs of bonded particles, $i - j$ and $k - j$, connected via one common particle j , Fig. 14.11(b);
- Quadruple of particles $i - j - k - l$ and two pairs of bonded particles, $i - j$ and $l - k$, connected via a middle pair $j - k$, Fig. 14.11(c);
- Quadruple of particles $i - j - k - l$ and triplet of particles $i - j - k$ connected with the last particle l via a bond with the middle particle j , Fig. 14.11(d).

Quantitative relations that describe the interactions between particles in the above-mentioned configurations are represented by five potential energy functions [36]. Determining the motion of an aggregate and evaluating its internal

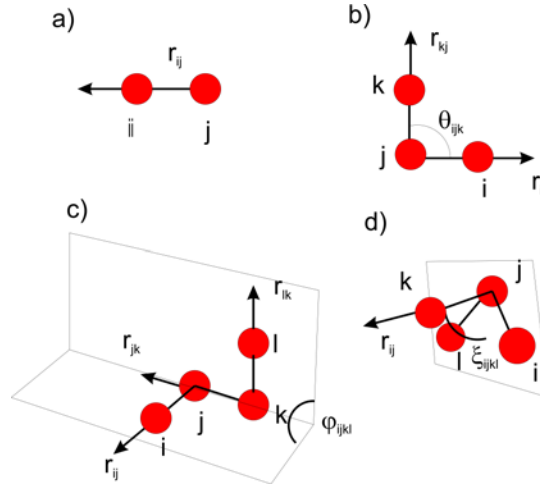


Figure 14.11.: Various configurations of connected particles.

forces are complex mathematical problems. Nevertheless, solving the motion equations for each constituent spherical particle of the aggregate allows to follow the evolution of the aggregate structure. The set of the equations combines translational with rotational Newton's second law equations of motion. Conveniently, Equation 14.2 represents a sum of all of the forces contributing to the movement of the i -th particle of aggregate in the single time step:

$$m_{pi} \frac{dv_i}{dt} = \sum_{i=1}^N F_i^S + \sum_{i=1}^N F_i^{dpp} + \sum_{i=1}^N F_i^b + \sum_{i=1}^N F_i^t + \sum_{i=1}^N F_i^p + \sum_{i=1}^N F_i^{ub} + \sum_{i=1}^N F_i^{dub} + \sum_{i=1}^N F_i^{ps} + \sum_{i=1}^N F_i^{dps} + F_g \quad (14.2)$$

where v_i is the velocity of primary particle, F_i^S , F_i^b , F_i^t , F_i^p are the bond (spring), bending, torsion and inversion internal interaction forces in aggregate's structure, F_g is the gravity force, F_i^{ps} is surface-particle interaction force, F_i^{ub} is the Urey-Bradley force which supports bending force in each tee configuration, F_i^{dpp} is a damping force of the harmonic oscillations between connected particles in aggregate, F_i^{dps} is a damping force of the harmonic oscillations between particle and collectors surface and F_i^{dub} is damping of Urey-Bradley force. Each particle in the aggregate is subjected to the Brownian force which can be described by the equation derived by Iwan and Mason Jr [37] regarding single spherical particle modified by inclusion of accessibility factor.

14.3 Lattice-Boltzmann modelling

To model mutual interactions between fluid flow and moving fibres the lattice-Boltzmann algorithm can be used. It allows to apply easily the moving boundary conditions and update the system geometry related to displacement and deformation of fibres. Complete information on the statistical description of a gas at, or near, thermal equilibrium is assumed to be contained in the one-particle phase-space distribution function $f(x, t, \Gamma)$ for the atomic constituents of the system. The variables x and t are the space and time coordinates of the atoms and Γ stands for all other phase-space coordinates e.g. momentum, momentum flux. Since collisions preserve conservation laws, the equations describing the macro dynamics of the system can be derived by integration of the Boltzmann equation. To build the cellular-space picture with dynamics of the collective motion predicted by the Navier-Stokes equation, a lattice on which particles move, collision rules and other restrictions characteristic for a chosen model should be defined. In this work a 3-dimensional lattice with 19 allowed directions of movement, usually referred as D3Q19 was used. The

evolution of the system is described by the expression:

$$f(x + e_i, t + 1) - f(x, t) = \Omega_i(f) \quad (14.3)$$

where x is position, e is lattice spacing, t is time and Ω is a collision operator. The outcome of collision can be approximated by assuming that the momentum of interacting particles will be redistributed at some constant rate toward an equilibrium distribution f_i^{eq} [38]. This simplification is called single-time-relaxation approximation and can be expressed by the equation:

$$\Omega_i = \frac{1}{\tau} [f_i^{eq}(x, t) - f_i(x, t)] \quad (14.4)$$

where τ is relaxation time. In the single-time-relaxation approximation, the momentum distribution at each lattice site is forced toward the equilibrium distribution at each time step. In the absence of external forces, the equilibrium distribution of a state with zero net momentum is just equal to momentum in each direction. The rate of change toward the equilibrium is the inverse of the relaxation time, and is chosen to produce the desired value of fluid viscosity, ν .

$$\nu = \frac{c_s^2}{2} (2\tau - 1) \quad (14.5)$$

where c_s is sound speed. The equilibrium distribution f_i^{eq} is given as follows:

$$f_i^{eq} = \rho \alpha_i \left(1 + \frac{e_i u}{c_s^2} + \frac{1}{2} \left(\frac{e_i u}{c_s^2} \right)^2 - \frac{u^2}{c_s^2} \right) \quad (14.6)$$

where α_i are the model dependent constants and u is fluid velocity. The plug fluid flow with an assumed mean velocity and equilibrium distribution was applied at the cell inlet. At the outlet and collector surface, zero-stress and bounce-back conditions were applied, respectively. The boundary conditions on the surface of a moving object (fibre) were applied according to the method proposed by Lallemand and Luo [39]. It is a simple extension of the treatment for a curved boundary proposed by Bouzidi, Firdaouss, and Lallemand [40], which is a combination of the standard bounce-back condition on the solid level and interpolations. When a grid point moves out of the non-fluid region into the fluid region to become a fluid node, one must specify some number of unknown distribution functions on this node. We use a second order extrapolation to compute the unknown distribution functions along the direction of a chosen discrete velocity e_i which maximizes the quantity of ne_i , where n is the out-normal vector of the wall at the point, through which the node moves to the fluid region.

14.4 Results and discussion

The efficiency of deposition of flexible fibres with fractal dimension $D_f = 1.2$ has been investigated. First, the collection efficiency of particle deposition modelled by Żywczyk and Moskal [36] model combined with lattice-Boltzmann algorithm was compared for results obtained with steady flow field. The example of calculations is shown in Fig. 14.12. For small values of maximum radius of the aggregate, the differences between both fluid flow models are not significant, but they increase with fibre size.

The deposition efficiency of fibres is influenced by bond constant k_s . Increasing the value of spring constant produces a stiffer bonds between primary particles of aggregate. A relation was found for a fibre-like aggregate,

14. Mechanics of fibrous particles immersed in selected flow conditions

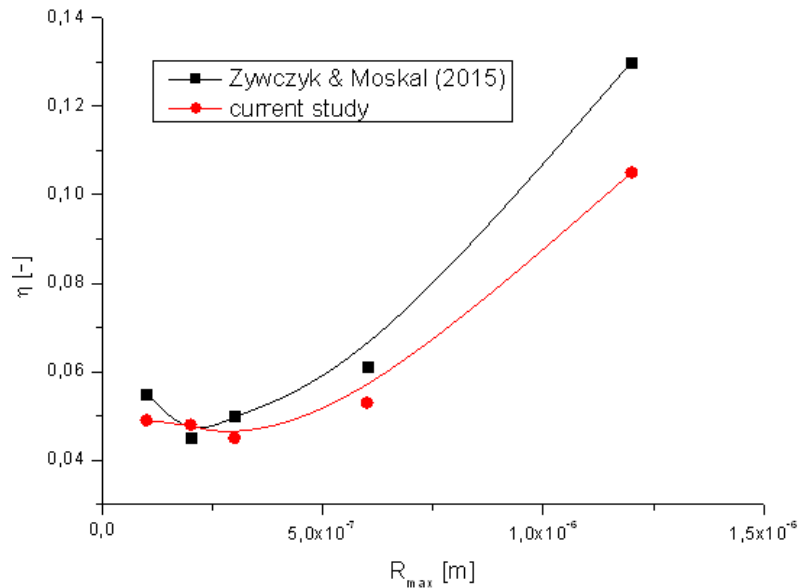


Figure 14.12.: Deposition efficiency as a function of maximal radius of aggregate, $u = 0.2 \text{ m s}^{-1}$, $k_s = 0.1$

composed of different numbers of primary particles, with fractal dimension $D_f = 1.2$ in function of k_s . As one can observe, the aggregate's deposition is influenced by the value of imposed harmonic constant, k_s (Fig. 14.13). Results indicate that aggregates with $k_s = 100$ deposit with higher efficiency than those with $k_s = 10$. However, the aggregates with imposed $k_s = 0.1$ deposit more effectively. This is due to the fact that bonds between primary particles can stretch producing longer aggregate fibres.

Differences in deposition ratios of flexible fibre-like aggregates can be clearly seen for different velocities (Fig. 14.14). With a decreasing velocity of air, increased collection efficiency is observed for all investigated aggregates. This is caused mainly by increased residence time of the fibre near the surface of the collector. According to the classical filtration theory, bigger particles deposit more effectively while the fluid velocity is higher. The reason of this discrepancy is a different behavior of fibre-like particles.

14.5 Conclusions

Modelling of a transport of a flexible deformable fibrous particle is much more complex than that of a stiff fibre or a spherical particle. It requires the integration of partial differential equations of motion of coupled with the set of boundary value problems for the momentary distribution of internal forces and moments along the particle, which have to be solved during the time-step. Moreover, the transport equations are "stiff" from the numerical point of view. The deposition efficiency depends strongly, and in very complex way, on gas velocity, initial fibre orientation, the fibre volume and its slenderness as well as on particle mechanical properties. One cannot expect to estimate a reliable deposition efficiency for a fibrous particle from the easily available data for spherical particles using any single equivalent dimension (equivalent volume diameter, aerodynamic diameter, etc.) as both the diameter and the length are important and must be taken into consideration. Flexible and stiff particles of the same dimension may behave in a quite different manner. The fibrous particles have usually lower deposition efficiency than spherical particles of the same volume. Consequently much longer than sphere fibres can penetrate through filters or human lungs better than spherical particles. Possibility of analysis of the behavior of fibrous particle at any flow condition makes also possible the design of depth filter structure which extort the desired particle orientation for its efficient removal from the fluid particle is immersed in.

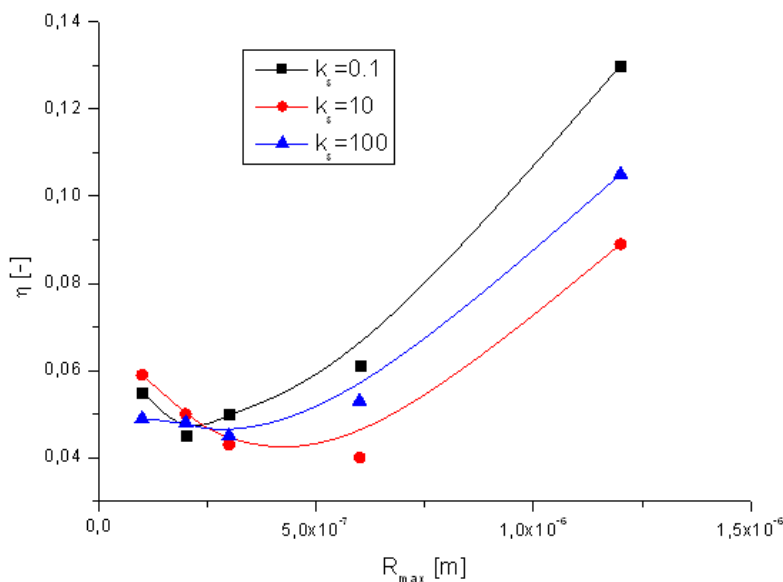


Figure 14.13.: Deposition efficiency as a function of maximal radius for three different spring constants, k_s , $u = 0.2 \text{ m s}^{-1}$.

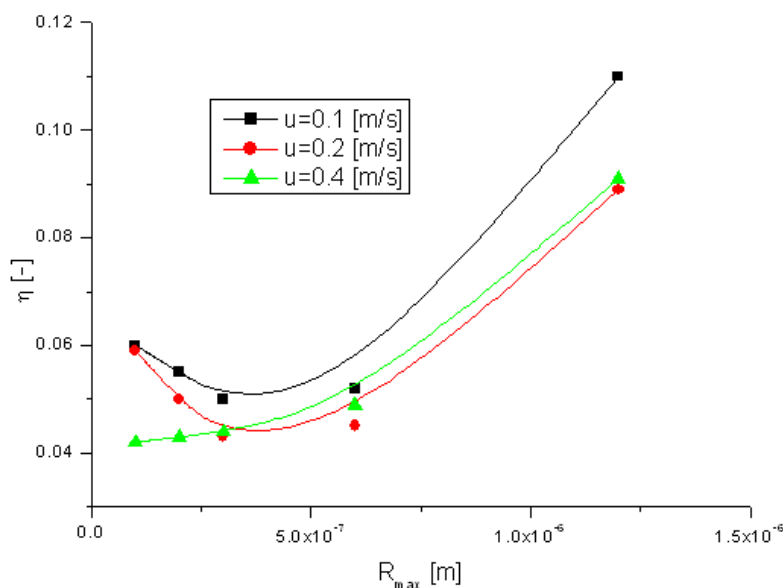


Figure 14.14.: Deposition efficiency as a function of maximal radius for three different fluid velocities, u .

References

- [1] Y.-S. Cheng. "Drag forces on nonspherical aerosol particles". In: *Chemical Engineering Communications* 108.1 (1991), pages 201–223 (cited on page 211).
- [2] G. H. Ganser. "A rational approach to drag prediction of spherical and nonspherical particles". In: *Powder Technology* 77.2 (1993), pages 143–152 (cited on page 211).
- [3] R. Chhabra, L. Agarwal, and N. K. Sinha. "Drag on non-spherical particles: an evaluation of available methods". In: *Powder technology* 101.3 (1999), pages 288–295 (cited on page 211).

- [4] P. Baron, C. Sorensen, and J. Brockmann. “Nonspherical particle measurements: shape factors, fractals, and fibers”. In: *Aerosol measurement: Principles, techniques, and applications* (2001), pages 705–749 (cited on pages 211, 212).
- [5] V. Timbrell. “Deposition and retention of fibres in the human lung”. In: *Inhaled Particles V*. Elsevier, 1982, pages 347–369 (cited on pages 211, 212).
- [6] K. Friedrichs. “Particles and Fibres in Human Lungs”. In: *Physical and Chemical Characterization of Individual Airborne Particles* (1986), page 212 (cited on page 212).
- [7] P. Holt. *Inhaled dust and disease*. John Wiley and Sons Inc., New York, NY, 1988 (cited on page 212).
- [8] D. B. Warheit. *Fiber toxicology*. Academic Press, 1993 (cited on page 212).
- [9] V. Timbrell. “The inhalation of fibrous dusts”. In: *Annals of the New York Academy of Sciences* 132.1 (1965), pages 255–273 (cited on page 212).
- [10] T. Ogden and W. Walton. “The descent angle of inclined cylinders—a possible means of separating fibres by length”. In: *The Annals of occupational hygiene* 18.2 (1975), pages 157–160 (cited on page 212).
- [11] E. Krushkal and I. Gallily. “On the orientation distribution function of nonspherical aerosol particles in a general shear flow: I. The laminar case”. In: *Journal of colloid and interface science* 99.1 (1984), pages 141–152 (cited on page 212).
- [12] W. Griffiths. “The shape selective sampling of fibrous aerosols”. In: *Journal of aerosol science* 19.6 (1988), pages 703–713 (cited on page 212).
- [13] J. Gentry, K. Spurny, S. Soulen, and J. Schörmann. “Measurements of the diffusion coefficients of ultrathin asbestos fibers”. In: *Journal of Aerosol Science* 19.7 (1988), pages 1041–1044 (cited on page 212).
- [14] B. Asgharian, C. Yu, and L. Gradon. “Diffusion of fibers in a tubular flow”. In: *Aerosol science and technology* 9.3 (1988), pages 213–219 (cited on page 212).
- [15] C. Wang, J. Pao, and J. Gentry. “Calculations and measurements of the charge distribution for non-spherical particles”. In: *Journal of Aerosol Science* 19.7 (1988), pages 805–808 (cited on page 212).
- [16] M. Schamberger, J. Peters, and K. Leong. “Collection of prolate spheroidal aerosol particles by charged spherical collectors”. In: *Journal of aerosol science* 21.4 (1990), pages 539–554 (cited on page 212).
- [17] P. Grzybowski and L. Gradoń. “Analysis of motion and deposition of fibrous aerosol particles flowing around a single filter element: the electrostatic effect”. In: *Chemical engineering science* 47.6 (1992), pages 1453–1459 (cited on page 212).
- [18] J. Marijnissen and R. Roos. “A dust reduction system based on corona discharge and electric wind”. In: *22nd European Aerosol Conference, September 4th-9th*. Tours, France: ACM Press, Sept. 2016, P1-AT-EE-006 (cited on page 212).
- [19] M. Shapiro and M. Goldenberg. “Deposition of glass fiber particles from turbulent air flow in a pipe”. In: *Journal of aerosol science* 24.1 (1993), pages 65–87 (cited on page 212).
- [20] O. Bernstein and M. Shapiro. “Direct determination of the orientation distribution function of cylindrical particles immersed in laminar and turbulent shear flows”. In: *Journal of Aerosol Science* 25.1 (1994), pages 113–136 (cited on page 212).
- [21] W. Kvasnak and G. Ahmadi. “Fibrous particle deposition in a turbulent channel flow—an experimental study”. In: *Aerosol science and technology* 23.4 (1995), pages 641–652 (cited on page 212).
- [22] D. Broday, M. Fichman, M. Shapiro, and C. Gutfinger. “Motion of diffusionless particles in vertical stagnation flows—II. Deposition efficiency of elongated particles”. In: *Journal of aerosol science* 28.1 (1997), pages 35–52 (cited on page 212).
- [23] A. Podgórski, Y. Zhou, H. Bibo, and J. Marijnissen. “Theoretical and experimental study of fibrous aerosol particles deposition in a granular bed”. In: *Journal of Aerosol Science* 27 (1996), S479–S480 (cited on page 212).
- [24] Z. Yue, J. Marijnissen, S. Lemkowitz, A. Podgorski, and H. Bibo. “A deposition model for fibrous particles in granular bed filters”. In: *Journal of Aerosol Science* 1001.28 (1997), S397–S398 (cited on page 212).
- [25] E. Hinch. “The distortion of a flexible inextensible thread in a shearing flow”. In: *Journal of Fluid Mechanics* 74.2 (1976), pages 317–333 (cited on page 212).
- [26] A. Podgórski and L. Gradoń. “Motion and deposition of fibrous flexible particles in laminar gas flow through a pipe”. In: *Journal of aerosol science* 21.7 (1990), pages 957–967 (cited on page 213).
- [27] L. Gradoń and A. Podgórski. “Flexible fibrous particle behaviour in the carrier gas flow around cylindrical obstacle”. In: *Chemical engineering science* 45.12 (1990), pages 3435–3441 (cited on page 213).
- [28] A. Podgórski, L. Gradoń, and P. Grzybowski. “Theoretical study on deposition of flexible and stiff fibrous aerosol particles on a cylindrical collector”. In: *The Chemical Engineering Journal and the Biochemical Engineering Journal* 58.2 (1995), pages 109–121 (cited on page 213).
- [29] S. Dunnett. “A study of the behaviour of fibrous flexible particles during the aspiration process”. In: *Journal of aerosol science* 24.1 (1993), pages 89–101 (cited on page 213).

- [30] M. Shams, G. Ahmadi, and H. Rahimzadeh. “Transport and deposition of flexible fibers in turbulent duct flows”. In: *Journal of aerosol science* 32.4 (2001), pages 525–547 (cited on page 213).
- [31] A. Podgórski. “Mechanics of a Deformable Fibrous Aerosol Particle: General Theory and Application to the Modeling of Air Filtration”. In: *Advances in Aerosol Filtration* (1998) (cited on page 213).
- [32] R. Przekop and A. Podgórski. “Effect of shadowing on deposition efficiency and dendrites morphology in fibrous filters”. In: *Inżynieria Chemiczna i Procesowa* 25.3 (2004), pages 1563–1568 (cited on page 217).
- [33] I. Imai. “On the asymptotic behaviour of viscous fluid flow at a great distance from a cylindrical body, with special reference to Filon’s paradox”. In: *Proceedings of the Royal Society of London. Series A. Mathematical and Physical Sciences* 208.1095 (1951), pages 487–516 (cited on page 217).
- [34] A. Podgórski. “Analytical description of gas flow around a fiber for modelling of aerosol filtration”. In: *Journal of Aerosol Science* 24 (1993), S277–S278 (cited on page 217).
- [35] R. Przekop, K. Grzybowski, and L. Gradoń. “Energy-balanced oscillatory model for description of particles deposition and re-entrainment on fiber collector”. In: *Aerosol science and technology* 38.4 (2004), pages 330–337 (cited on page 217).
- [36] Ł. Żywczyk and A. Moskal. “Modelling of deposition of flexible fractal-like aggregates on cylindrical fibre in continuum regime”. In: *Journal of Aerosol Science* 81 (2015), pages 75–89 (cited on pages 219, 221).
- [37] W. Iwan and A. Mason Jr. “Equivalent linearization for systems subjected to non-stationary random excitation”. In: *International Journal of Non-Linear Mechanics* 15.2 (1980), pages 71–82 (cited on page 220).
- [38] Y.-H. Qian, D. d’Humières, and P. Lallemand. “Lattice BGK models for Navier-Stokes equation”. In: *EPL (Europhysics Letters)* 17.6 (1992), page 479 (cited on page 221).
- [39] P. Lallemand and L.-S. Luo. “Lattice Boltzmann method for moving boundaries”. In: *Journal of Computational Physics* 184.2 (2003), pages 406–421 (cited on page 221).
- [40] M. Bouzidi, M. Firdaouss, and P. Lallemand. “Momentum transfer of a lattice Boltzmann fluid with boundaries”. In: *Physics of fluids* 13 (2001), pages 3452–9 (cited on page 221).

By: R. Martijn Wagterveld¹, Inez J.T. Dinkla¹

1 – Wetsus, European Centre of Excellence for Sustainable Water Technology, Oostergoweg 9, 8911 MA Leeuwarden, The Netherlands
e-mail: martijn.wagterveld@wetsus.nl

15.1 Introduction

Plastics are an increasing environmental problem. Most plastics particulates do not (bio-)degrade easily, which results in accumulation in the environment. It is without doubt that plastics have an impact on aquatic ecosystems. Images of aquatic birds showing ingested plastic paint a strong picture. Most attention in the media goes to the larger pieces of plastic, as these are easy to see, manipulate, measure and identify. However, shape and size does have an impact on many aspects of the plastic in water predicament. The smaller the particles, the more difficult to measure and identify the occurrence of plastics. Morphological differences further complicate manipulation of particles for both detection and removal. Nano- and microfibers are of importance because of their small size and high aspect ratio. The large surface to volume ratio also makes fibers more prone to adsorption of toxic compounds.

To get a comprehensive picture of the impact of nano- and microfibers in water, one has to identify the sources and routes to the aquatic ecosystem. Measurement and identification is an essential step in this assessment. When the occurrence is mapped, the human and environmental impact should be carefully evaluated. This serves as input to develop counter-measures. The survey identifies the importance and need for counter measures. Avoiding introduction and spread seems to be a logical next step. But as plastics are accumulating in the aquatic environment, treatment of water should be considered. Here we will discuss the current situation and the state of the art in water treatment. Some innovative techniques being developed in the scientific world could bring some important new solutions to difficulties that arise when considering removal of nano- and microfibers.

15.2 Nano- and microfibers in aquatic ecosystems

Plastics are encountered in the world's oceans, lakes and rivers. It is estimated that around 93% of this plastics are in the micrometer size (and smaller) [1]. According to research, fibers make up 20% of the plastics in environmental waters [2]. From all primary microplastics released in aquatic ecosystems, 35% are micrometer sized fibers released from textiles during laundering [3] (Fig. 15.1). These fibers enter the environment either through waste water treatment plants (developed countries), or directly through home laundering effluents (less developed countries). Up to around 85% of the microplastics released by waste water treatment plants is fibershaped and is attributed to laundry processes [4]. These synthetic microfibers are typically manufactured from nylon, polyethylene terephthalate, polypropylene, polyester, polyamide and polyacrylic [5, 6].

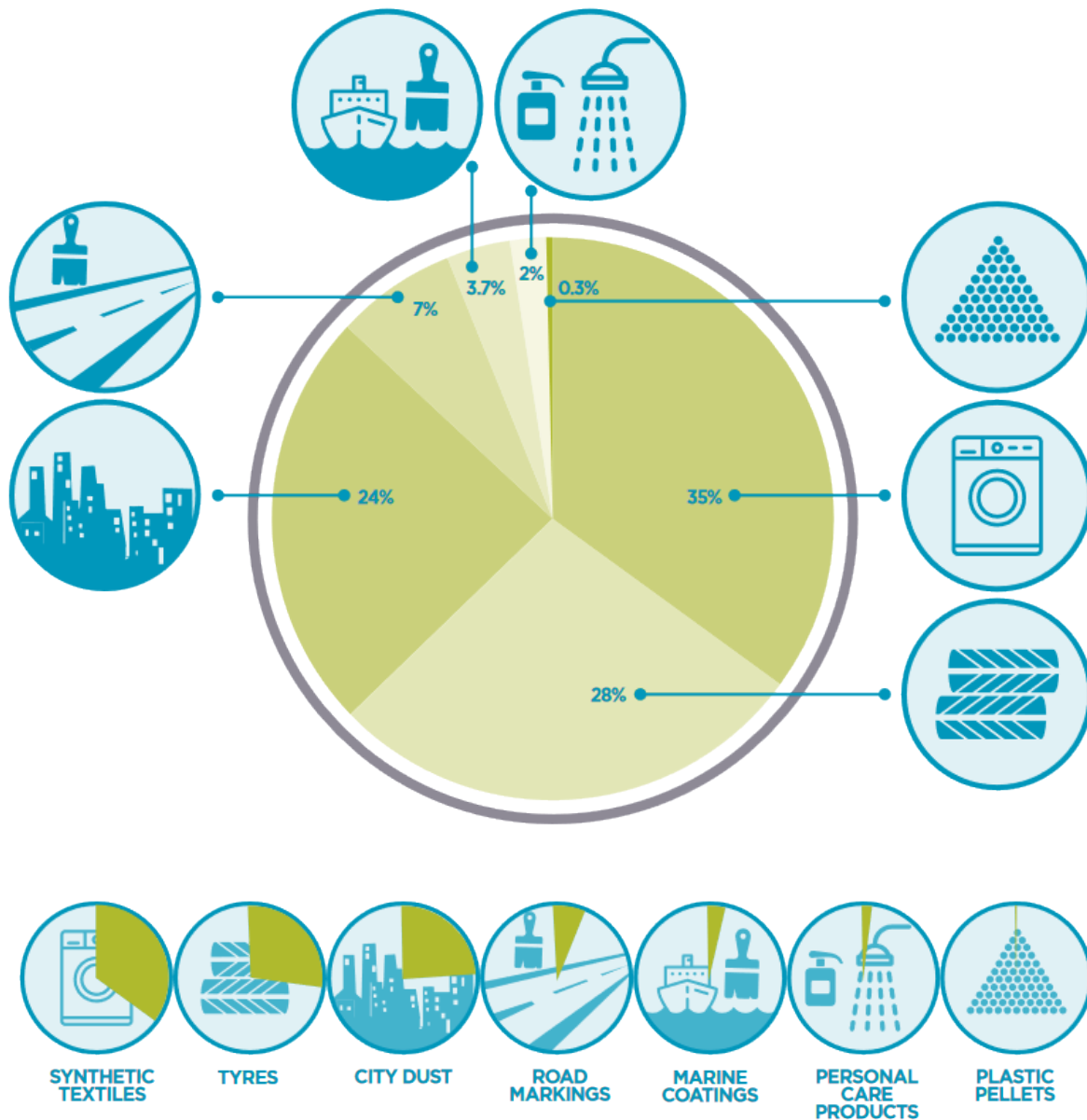


Figure 15.1.: Global releases of primary microplastics. Primary microplastics are manufactured in the micrometer size range. Textiles take the largest part. Reproduced with permission of the copyright owner, from Boucher and Friot [3].

Fiber and yarn physicochemical properties play a major role in the microfiber generation. Fabrics with high abrasion resistance, low hairiness and high breaking strength have a lower risk of releasing microfibers. The use of detergent increases the risk as surfactants promote the release of microfibers significantly [7]. Fibers from textiles from garments are thus an important source, but are not the only source. For example fibers from fishing nets and lines, carpets, furniture, curtains, fibers from filters, membranes, car tire fragments, etc also shed synthetic fibers into the environment, but it is unclear how large the impact is. Fibers are the most important constituents of indoor dust [5], and might also find their way via this route to aquatic ecosystems.

Little is known about the fate of fibers in aquatic environments. Most research focusses on (bio)degradation of microplastics in general, while the specific degradation of nano- and microfibers specifically remains unclear. The

general assumption is that synthetic microfibers do not (bio)degrade easily resulting in accumulation.

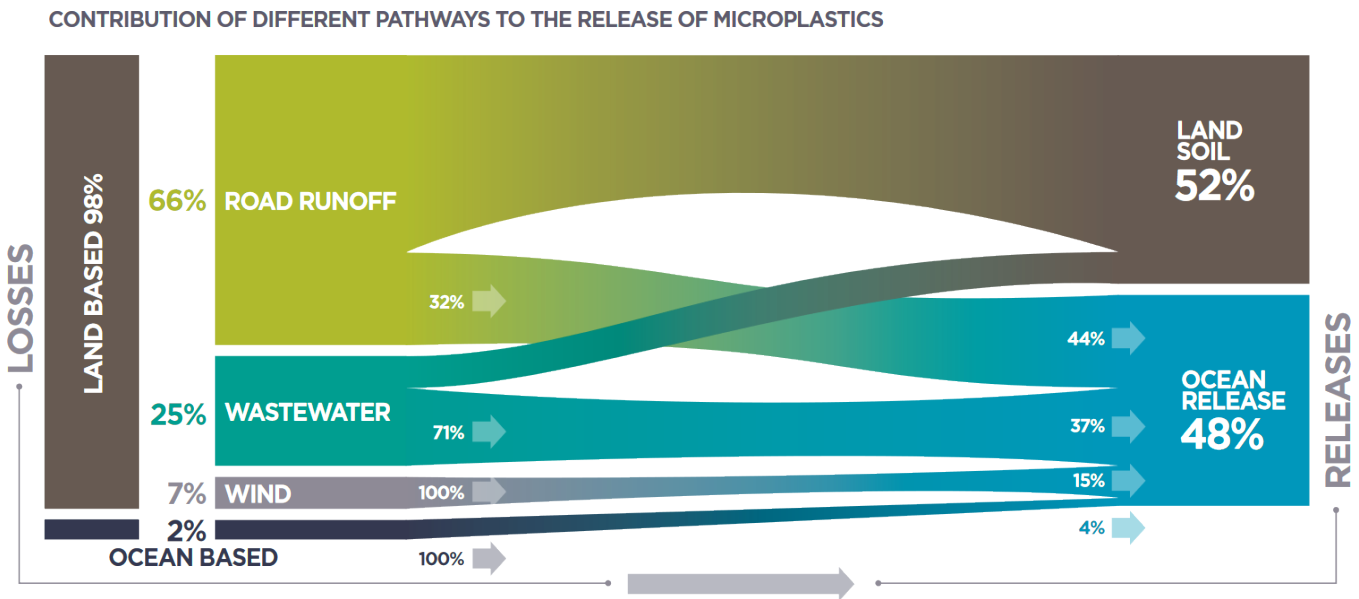


Figure 15.2.: Global releases of microplastics. Wastewater takes a considerable part of 44% to the ocean release. Reproduced with permission of the copyright owner, from Boucher and Friot [3].

15.3 Techniques to remove nano- and microfibers

15.3.1 Separation at source

A first approach is to prevent nano- and microfibers from entering aquatic ecosystems. As most fibers seem to come from laundry processes, taking measures here would be the most obvious direction. The easiest would be to no longer use non-(bio)degradable synthetic fibers in the clothing industry. This requires new policies and will have an enormous impact on the industry, both on processes but also economical. Synthetic fibers will give garments certain unique properties that might not be met by application of (bio)degradable synthetic fiber alternatives. Creating new (bio)degradable alternative materials with similar properties is essential for this route to be successful. It is unlikely that this route is favoured by policy makers, as it requires large adaptations of the industry and new technological development.

Synthetic nano- and microfibers that do enter the aquatic ecosystem come via laundry processes. Filtering during this process would cover a relatively large part of the fibers that would otherwise enter the environment. Unfortunately a relatively large part will still enter the environment via other sources e.g. fishing gear, carpets, car tire fragments, etc., but also as indoor dust that is discharged with cleaning water ending up in (municipal) waste water. This does not make it the preferred solution for removal, but might aid in public awareness. There are currently several technical solutions on the market to reduce the fiber content released in laundry processes. Several different technical solutions are currently on the market.

Environment Enhancements supplies the Lint LUV-R system, a filtration system that needs to be placed in the water discharge line of a washing machine (fig. 15.3A). This system is not specifically designed to remove microfibers, but serves as protection of septic tanks. A stainless steel sieve with holes of 1.6 mm removes around 87 % of microfibers [8]. In a common household the filter needs to be cleaned every three weeks. The sieve can be cleaned by removing the collected debris from the surface. The sieve has relatively large holes, that are inefficient for removal of the small

15. Cleaning water from nano- and microfibers

microfibers. This design choice is probably based on the presence of much larger debris in the effluent of the washing machine. Smaller holes will lead to faster clogging and necessity for cleaning.

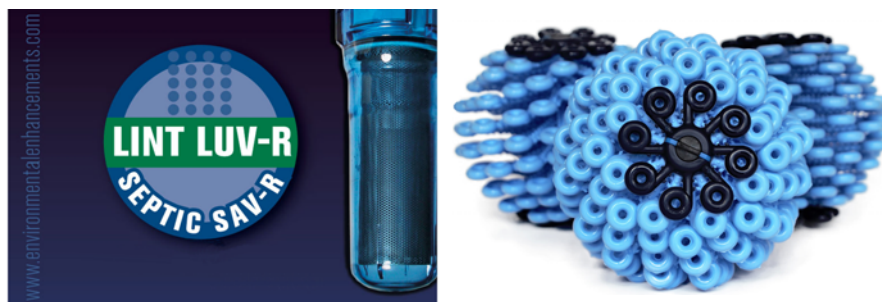


Figure 15.3.: Commercially available technologies for separation of microfibers at the source. A) Lint LUV-R (by Environment systems), a filter to be placed in the water discharge line of a washing machine. B) Cora Ball (by the Rozalia project), a ball that filters water inside the washing machine drum.)

The Rozalia Project supplies the Cora Ball, a ball that needs to be placed inside the washing machine. It is specifically designed to capture microfibers and is based on how coral filters water. It has stretchy plastic features with pores (fig 15.3B). This technique removes 26 % of microfibers [8]. Cleaning the ball is also very tedious, as the debris is entangled in the stretchy plastic features. Removing debris will result in disturbed fibers and a significant portion might end up outside the waste bin. Although this technology was specifically designed to remove microfibers, it still need significant improvement to have a serious impact.

Langbrett supplies the Guppyfriend which is a laundry-bag designed for microfiber removal. Laundry needs to be placed inside the bag, and put as a whole in the washing machine. The bag is made of recyclable polyamide and works as a filter. The fibers are collected inside the bag and can be manually removed and discharged in the waste bin. Unfortunately there are no scientific numbers for the removal efficiency of this bag, although it seems to be inherently more effective than the Lint LUV-R system. The filter-bag has an intrinsic self-cleaning mechanism due to the tumbling, working as a back-washing of the filter. This makes it possible to apply much smaller pores. This might go at the cost of effective cleaning as it might also screen the entrance of soap and water. The exact applied pore-size is unknown. The company claims a removal efficiency 86 % of microfibers. This is comparable to the external filtration technique.

All available techniques aim for microfiber removal and do not mention removal of nanofibers. This makes sense since for application of nanomaterial, filtration does not seem to be the ideal method of choice. Nanofiber removal requires much smaller pores, increasing energy use, clogging and thus cleaning frequency. A multistage approach can be taken here where filters with decreasing pore-size are applied in series. Due to the high aspect ratio of fibers, removal by conventional filtration remains challenging. The morphology of fibers enable them to pass longitudinally through the pores [9]. This can explain the relatively low removal rates obtained with the aforementioned techniques.

15.3.2 Waste water treatment plants

Conventional technology

A second approach is to prevent discharge of micro- and nanofibers via discharge effluents. Conventional wastewater treatment facilities already remove microplastics efficiently. In the best case, around 98 % of the incoming microplastics are removed [9]. However, due to the large volumes of water involved the effluent still contains a significant amount of micro- and nanoplastics [2, 10]. The effluent is discharged on surface waters introducing large numbers of microplastics to the environment, aiding to the spread. In numbers, a single waste water treatment plant releases between 2×10^6 particles/d and 1×10^{10} particles/d, of which over 50 % has the shape of a fiber [9]. Conventional

wastewater treatment facilities are not optimized for micro- and nanofiber removal, as it has never been a requirement for water boards and waste water treatment companies.

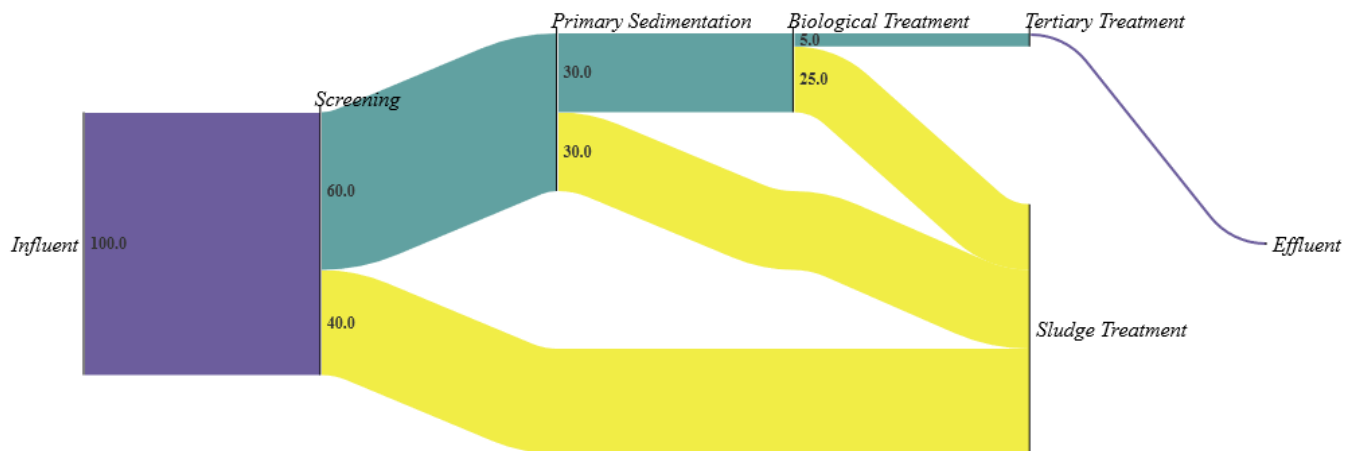


Figure 15.4.: Microparticle distribution in conventional waste water treatment.

The first step in a conventional waste water treatment plant is the preliminary and primary treatment (also pre-treatment). This step already removes the largest part of the microplastics from wastewater 50 % to 98 %. In the primary clarifiers, light floating microplastics are removed by skimming the grease from the surface. The heavier microplastics settle and are trapped in flocs and are removed during grit removal and gravity separation. Most of the removed microplastic at this stage are of the larger size. It is speculated that fibers are more easily trapped in flocs than solid particles, resulting in better removal of fibers than the particles with a smaller aspect ratio [9].

The secondary treatment usually is of a biological nature. Bacteria in aeration tanks produce extracellular polymers resulting in sludge flocs. Microplastics get trapped in these flocs and end up in the sludge bed. Chemical flocculants can be added at this stage to enhance the clarifying process. It is speculated that these chemicals negatively impact the uptake of microplastics in sludge flocs [9].

In the end, most of the removed microplastics end up in the generated sludge and consists up to 80% of fibrous material [11]. Adding an extra treatment step (tertiary treatment), e.g. techniques such as sand or cloth filtration, flotation or membrane bioreactors, shows significant improvement of effluent quality mainly for larger microplastics. Particles below 100 μm are still passing to the effluent and require alternative removal methods. This specifically holds for fibers as they can easily pass small pores due to the high aspect ratio and flexibility [9].

Most microplastic will end up in sludge. Sludge is exported from the waste water treatment plant. Sludge is either incinerated, or applied on land. With incineration, microplastics will be burnt together with the sludge. However, with land application microplastics end up in the environment and eventually leach into aquatic ecosystems, frustrating the initial removal.

15.3.3 Alternatives to conventional treatment techniques

There is still room for improvement to optimize conventional wastewater treatment facilities to remove micro- and nanoplastics. Though, especially for the smaller sized particles, an improvement of several orders of magnitude is not expected. The specific characteristics of fibers ask for additional cleaning techniques. The high aspect ratio's and deformability make normal filtration methods challenging. Innovative techniques such as acoustic separation [12] and improved (micro)filtration techniques, e.g. sieve based lateral displacement [13], can assist in aligning fibers, and improve separation of deformable particles.

Conventional membrane filtration techniques suffer from pore blocking and fouling, resulting in increasing pressure and thus high energy demand during operation and require regular cleaning. This is predominantly because membrane pores pass particles smaller than the pores, but block particles larger than the pores. Particles slightly larger than a pore will form a cake layer on top of the surface. This cake layer can reversibly be removed by chemical cleaning and/or back-washing the filter. However, irregularly shaped and deformable particles with a size close to the pore-size, will be pushed inside the pore. They can get stuck which leads to irreversible fouling which cannot be removed. Performance drops and eventual replacement of the membranes is inevitable.

Deterministic lateral displacement

Deterministic lateral displacement is a technique that deals with this limitation of conventional membrane filtration. Deterministic lateral displacement shapes hydrodynamic conditions, such that particles *smaller* than the pore-size are blocked by the filtration system. This results in no or much slower cake layer built up, and prevents irreversible blocking of the pores. Pressure drops and energy use is therefore much lower and less cleaning is required [13].

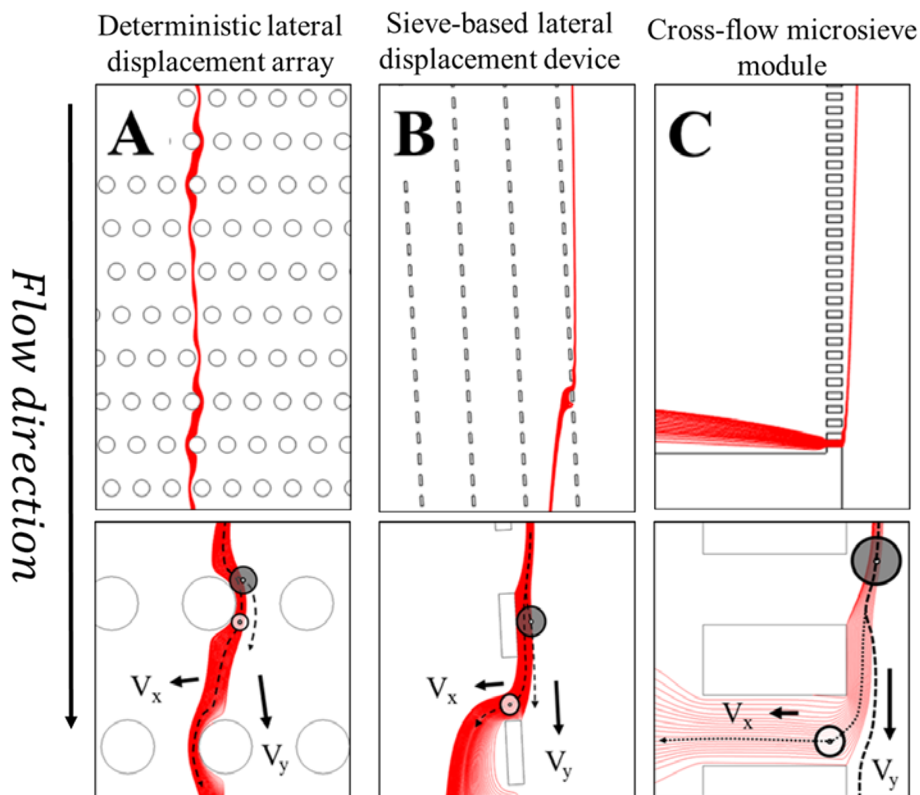


Figure 15.5.: Three geometries are shown with flow lanes (red) that allow deterministic displacement of particles. In (A) the original deterministic lateral displacement (DLD) array, in (B) a sieve-based lateral displacement (SLD) device and in (C) a cross-flow microsieve (CFM) module. A close up illustrates the separation principle in all three systems. The grey particle has a radius that is larger than the width of a flow lane and the white particle a radius that is smaller than the width of a flow lane. Particles with a radius larger than the flow lanes (grey) are physically excluded by particle-structure interactions. Particles with a radius smaller than the flow lane are dragged into the pore by the flow lane. Thus, separation depends on the flow lane width, which can be adapted via the ratio of V_y and V_x .

The technique has its roots in microfluidic analysis and started with a microfluidic device containing a forest

of pillars. These pillars generate flow lanes, which are essential for the separation (Fig. 15.4A). By choosing the dimensions properly, larger particles, but smaller than the gap between the pillars, can be separated from smaller particles. This approach works very well for small microfluidic systems, but does not scale well for larger volume flows. Recently the technique has been translated to a sieve-based lateral displacement device, capable of handling larger flows. By controlling the flow rates in the system, flowlane sizes could be controlled, leading to separation of particles smaller than the pores of the sieve (Fig. 15.4B). This was further optimized in a cross-flow microsieve module. Here it was proven that, by controlling the flow-rates, separation of particles *smaller* than the pore-size is possible with conventional microsieves (Fig. 15.4C).

The actual separation takes place before particles enter the pores of the sieve. Deformable particles are no longer pushed into pores and the required pressures with this technique are much lower compared to conventional systems resulting in gentle filtration. The performance of the separation of 0.1 wt% solid PMMA particles was equal to the separation of 0.1 wt% oil in water emulsions. This property makes it a promising technique for separation of soft fibers.

The hydrodynamics might help aligning fibers preventing them to slip through the pores because of their high aspect ratio. However, it remains unclear if and to what extent this takes place, as this has not been investigated for cross-flow microsieves modules. The technique works well for low and intermediate particle concentrations (below 1 wt%). At too high concentrations, particle-particle interactions come in to play, disturbing the distribution of particles in flow lanes. In terms of size, the separation of nano- and micrometer sized particles seems feasible in nano- or microfluidics [14], but has not been shown for larger flow volumes.

Acoustic separation

Deterministic lateral displacement reduces the cleaning issue of conventional filtration, but does not yet provide a clear answer to the high aspect ratio of fibers. Alignment of fibers inside the filtration module might help preventing fibers to pass through pores with their short end first. Acoustic (sound) fields can be used to manipulate particles, a field known as acoustophoresis or acoustofluidics. This field has its roots in nano- and microfluidics analysis as well.

Acoustic fields, applied to nano- and microfluidic flow channels, usually generate a standing wave. In a standing wave, a pattern of nodes and anti-nodes is created. A node is a region of high pressure; an antinode a region of low pressure. It has been shown that by manipulating standing wave patterns, the orientation of high aspect ratio particles in solution can be manipulated in any (2D-)direction [15]. Alignment takes place in the pressure nodal pattern of the acoustic standing wave. This method can be added to conventional and innovative filtration techniques to prevent slipping of fibers through pores. Acoustic alignment is still at its infancy and up-scaling of manipulable standing waves seems challenging. It is also unclear how much energy is required to have sufficient alignment. The acoustic force decreases with decreasing size, while the brownian motion of the particle increases, suggesting a particle size-limit for manipulation.

Very recent simulation results from our group show that fibers can be aligned. Fiber rigidity plays an important role. Very flexible fibers will buckle and eventually be folded by the acoustic forces. This process depends on fiber length and wavelength of the acoustic wave pattern.

Another application of acoustic waves is to selectively separate particles based on their size, density and/or compressibility. With this method filtration takes place without the need of pores, and thus circumvents the issue of fouling and cake layer formation on the filtration surface. Depending on the particle properties an acoustic standing wave pattern can selectively trap particles in nodal lines. This has been developed for separation in nano- and microfluidics, but has recently been scaled up to a centimeter sized system [12]. The method has a very clear size cut-off. Selectivity could either be obtained by changing the flow velocity, or the acoustic intensity. A smaller flow velocity, or a larger acoustic intensity, results in a smaller cut-off size. Acoustic separation of deformable particles works very well but is thus limited by fiber flexibility.

15. Cleaning water from nano- and microfibers

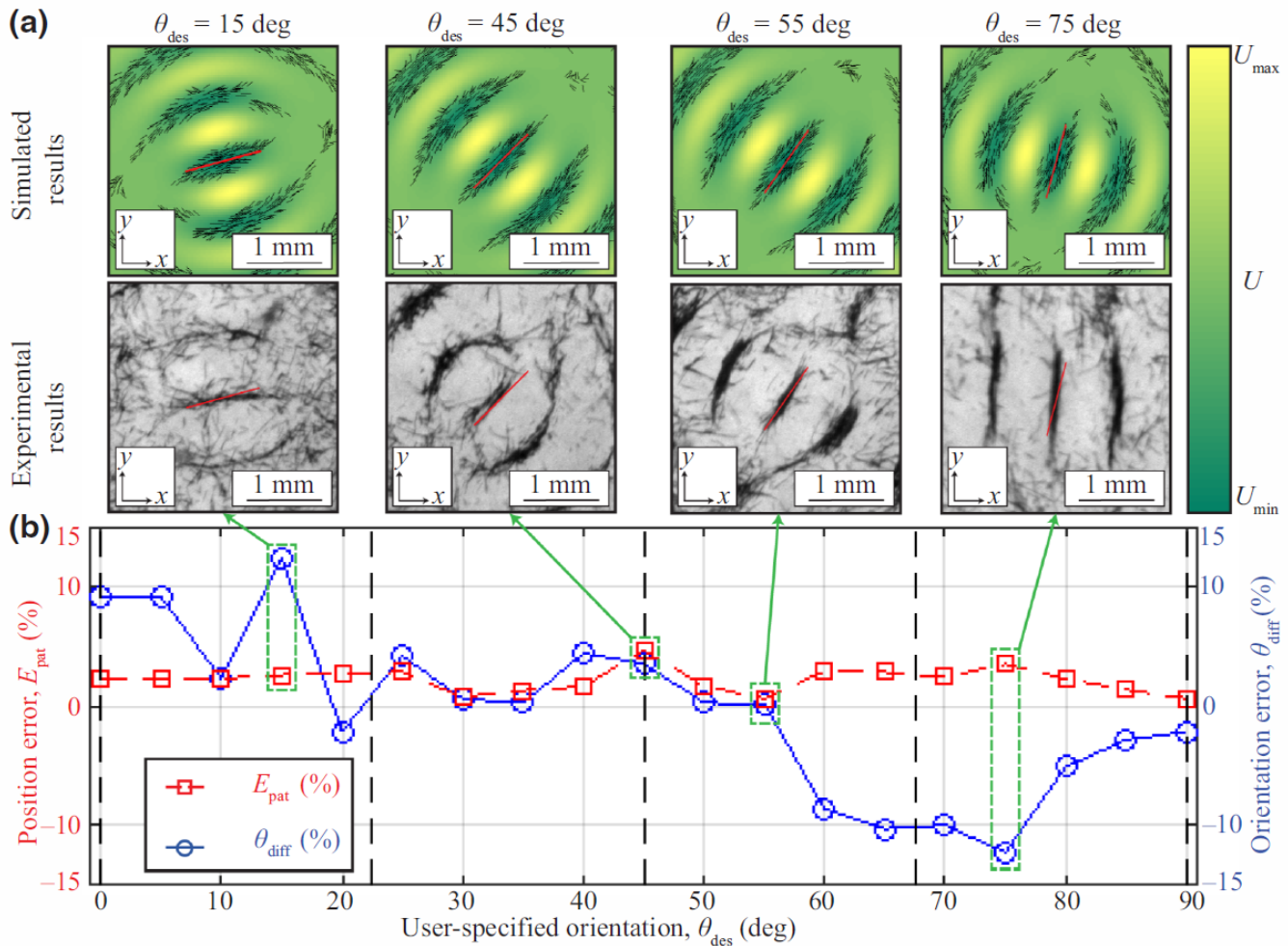


Figure 15.6.: Acoustic manipulation of high aspect ratio particles in solution. Reprinted Figure 4 with permission from: M. Prisbrey and B. Raeymaekers, *Physical Review Applied*, 12 1, 014014 2019 [15]. Copyright (2019) by the American Physical Society.

15.3.4 Approaches for nanofiber removal

Nanofiber removal remains challenging, even with the discussed improved filtration techniques. Due to their small size and resulting large Brownian motion, physical manipulation is challenging. The energy required increases with decreasing particle size. Nanofiber removal might require an additional step to increase their size for physical separation. Nanofiber coagulation or flocculation will result in larger structures and can be achieved by dosing chemicals as coagulant or flocculant. The formed constructs need to be mechanically stable to be removed with conventional filtration techniques. When the formed larger constructs are fragile and deformable, cleaning water from agglomerated nanomaterial benefits from the innovative alternative techniques mentioned above.

Another approach is to degrade the nanoplastics. Several techniques have been developed to remove so called micropollutants from waste water in waste water treatment plants. These techniques are usually placed at the end of the treatment train. The techniques are designed to remove molecules that are not degraded sufficiently in conventional water treatment systems, to be able to safely discharge the effluent on surface water. This typically holds for molecules used as pharmaceuticals and pesticides.

The technologies that degrade these molecules are advanced oxidation techniques such as ozone and UV-peroxide.

It was already shown that ozone treatment outperformed coagulation and membrane or sand filtration, for the removal of microplastics [16]. Nanoparticles were not part of the analysis (as is the case for most research), but it is logical that degradation techniques function better for nanoparticle removal than for microparticle removal due to the larger surface to volume ratio.

15.4 Future perspective for waste water treatment

There is a lot to gain in conventional waste water treatment plants by tweaking operational parameters to increase the performance of nano- and microfiber removal. Although, already up to 98 % is currently removed by conventional treatment techniques, an increase of several orders of magnitude is required to have a significant impact on aquatic ecosystems. Additional treatment techniques can increase the removal efficiency significantly.

Filtration is a logical choice trying to reach the required orders of magnitude improvement. However, fiber shaped, deformable material tends to cross membranes, significantly reducing the overall efficiency. Innovations such as deterministic displacement, acoustic alignment or acoustic filtration can aid in improving filtration but it is unclear at what cost. Research is necessary to evaluate the performance of filtration and the innovative solutions. Moreover, most of the removed fibers end up in sludge, or after filtration, in a concentrated stream. The nano- and microfibers that are now removed from the bulk, need to be dealt with in a better way to avoid reintroduction in the environment.

More promising are advanced oxidation techniques. Synthetic Nano- and microfibers, or nano- and microplastics in general, are not the only upcoming accumulating micropollutants. There are many more organic molecules that are hard to degrade. Applying treatment techniques such as advanced oxidation for degradation of these molecules could achieve two aims at once. Being successful for the removal of microplastics as well as many of these micropollutants, it is only logical that nanoplastics are very susceptible to this form of treatment.

15.5 Conclusion

Plastics are an increasing environmental problem as they are encountered in the world's oceans, lakes and rivers. Wastewater contributes a considerable part of 44% to the ocean release. Nano- and microfibers deserve special attention because of their small size, high aspect ratio and large surface to volume ratio. Morphology and size are important aspects for both detection and removal. As a first approach separation at source is a logical step. There are already several commercial technologies available to remove microfibers from washing machine effluent. The impact of these technologies is rather limited. Their removal efficiency is much lower than the already existing removal efficiency (up to 98%) of conventional waste water treatment plants. Especially fibers are difficult to remove with conventional methods. Additional innovative cleaning techniques are required to improve removal efficiencies with several orders of magnitude. Alternative filtration methods have been discussed, such as deterministic lateral displacement and acoustic separation. These methods can remove soft, flexible particles and align fibers so that they do not slip through pores in filtration. Nanofiber removal remains challenging. Coagulation or flocculation can be used to form larger constructs that can be removed with the described innovative methods. Additionally, advanced oxidation technologies can be applied after filtration to remove residual particles, together with other persistent molecules (e.g pharmaceuticals and pesticides).

Acknowledgement

This work was performed in the cooperation framework of Wetsus, European Centre of Excellence for Sustainable Water Technology (www.wetsus.nl). Wetsus is co-funded by the Dutch Ministry of Economic Affairs and Ministry of Infrastructure and Environment, the European Union Regional Development Fund, the Province of Fryslân and the Northern Netherlands Provinces.

References

- [1] M. Eriksen, L. C. Lebreton, H. S. Carson, M. Thiel, C. J. Moore, J. C. Borerro, F. Galgani, P. G. Ryan, and J. Reisser. “Plastic pollution in the world’s oceans: more than 5 trillion plastic pieces weighing over 250,000 tons afloat at sea”. In: *PLoS one* 9.12 (2014), e111913 (cited on page 227).
- [2] F. Murphy, C. Ewins, F. Carbonnier, and B. Quinn. “Wastewater treatment works (WwTW) as a source of microplastics in the aquatic environment”. In: *Environmental science & technology* 50.11 (2016), pages 5800–5808 (cited on pages 227, 230).
- [3] J. Boucher and D. Friot. “Primary microplastics in the oceans: a global evaluation of sources”. In: (2017) (cited on pages 227–229).
- [4] L. Yang, K. Li, S. Cui, Y. Kang, L. An, and K. Lei. “Removal of microplastics in municipal sewage from China’s largest water reclamation plant”. In: *Water research* 155 (2019), pages 175–181 (cited on page 227).
- [5] J. Gago, O. Carretero, A. Filgueiras, and L. Viñas. “Synthetic microfibers in the marine environment: a review on their occurrence in seawater and sediments”. In: *Marine pollution bulletin* 127 (2018), pages 365–376 (cited on pages 227, 228).
- [6] T. Bond, V. Ferrandiz-Mas, M. Felipe-Sotelo, and E. van Sebille. “The occurrence and degradation of aquatic plastic litter based on polymer physicochemical properties: A review”. In: *Critical reviews in environmental science and technology* 48.7-9 (2018), pages 685–722 (cited on page 227).
- [7] M. C. Zambrano, J. J. Pawlak, J. Daystar, M. Ankeny, J. J. Cheng, and R. A. Venditti. “Microfibers generated from the laundering of cotton, rayon and polyester based fabrics and their aquatic biodegradation”. In: *Marine pollution bulletin* 142 (2019), pages 394–407 (cited on page 228).
- [8] H. K. McIlwraith, J. Lin, L. M. Erdle, N. Mallos, M. L. Diamond, and C. M. Rochman. “Capturing microfibers—marketed technologies reduce microfiber emissions from washing machines”. In: *Marine pollution bulletin* 139 (2019), pages 40–45 (cited on pages 229, 230).
- [9] J. Sun, X. Dai, Q. Wang, M. C. van Loosdrecht, and B.-J. Ni. “Microplastics in wastewater treatment plants: Detection, occurrence and removal”. In: *Water research* 152 (2019), pages 21–37 (cited on pages 230, 231).
- [10] J. Talvitie, A. Mikola, A. Koistinen, and O. Setälä. “Solutions to microplastic pollution—Removal of microplastics from wastewater effluent with advanced wastewater treatment technologies”. In: *Water Research* 123 (2017), pages 401–407 (cited on page 230).
- [11] A. M. Mahon, B. O’Connell, M. G. Healy, I. O’Connor, R. Officer, R. Nash, and L. Morrison. “Microplastics in sewage sludge: effects of treatment”. In: *Environmental Science & Technology* 51.2 (2016), pages 810–818 (cited on page 231).
- [12] M. Kandemir, R. Wagterveld, D. Yntema, and K. Keesman. “selective particle Filtering in a Large Acoustophoretic serpentine Channel”. In: *Scientific reports* 9.1 (2019), page 7156 (cited on pages 231, 233).
- [13] J. Dijkshoorn, R. Wagterveld, R. Boom, and M. Schutyser. “Deterministic displacement of particles and oil droplets in a cross-flow microsieve module”. In: *Journal of membrane science* 566 (2018), pages 435–441 (cited on pages 231, 232).
- [14] T. Salafi, Y. Zhang, and Y. Zhang. “A Review on Deterministic Lateral Displacement for Particle Separation and Detection”. In: *Nano-Micro Letters* 11.1 (2019), page 77 (cited on page 233).
- [15] M. Prsbrey and B. Raeymaekers. “Aligning High-Aspect-Ratio Particles in User-Specified Orientations with Ultrasound-Directed Self-Assembly”. In: *Physical Review Applied* 12.1 (2019), page 014014 (cited on pages 233, 234).
- [16] H. Hidayatullah and T.-G. Lee. “A study on characteristics of microplastic in wastewater of South Korea: Identification, quantification, and fate of microplastics during treatment process”. In: *Marine pollution bulletin* 146 (2019), pages 696–702 (cited on page 235).

By: Stephanie Wright¹, Uschi M. Graham², Arkadiusz Moskal³

1 – MRC Centre for Environment and Health, King's College London, London SE1 9NH, UK.

2 – University of Kentucky Pharmaceutical Sciences, U.S.A.

3 – Warsaw University of Technology, Faculty of Chemical and Process Engineering, ul. Waryńskiego 1, 00-645 Warsaw, Poland

The 2019 workshop and forum on SYNTHETIC NANO- AND MICROFIBERS took place in Leeuwarden, The Netherlands and was hosted at Wetsus. Twenty participants from The Netherlands, Germany, Poland, the United Kingdom and the United States came together to discuss a broad range of topics related to synthetic nano- and microfibers (SNMFs) and particles. The 2019 workshop was organized by Jan C. M. Marijnissen from Delft University of Technology and Leon Gradoń from the Warsaw University of Technology in collaboration with Wetsus. This meeting was a continuation of a series of workshops focused on aerosols, which have been organized periodically since they began in the 1980s. **The fundamental goal of this workshop was to understand the environmental and health impacts of synthetic (plastic) fibers in water and atmospheric media, specifically nano- (NFs) and microfibers (MFs) with a high aspect ratio and measuring less than 100 µm**, as described from various scientific points of view.

The presence of plastic fibers in air and water is unquestionable, and hence one asks: Are fibers dangerous? Do they affect our health? What we can do about it? How do we prevent this pollution? Should we reduce the production of plastic goods? Many more questions arose as we learnt about fibers in oceans and ambient air. During the workshop, specialists from various fields tried to answer those questions and shed some light on the complex and multidisciplinary subject. There are two different methods in science to describe reality; one is based on observations and experiments and a second based on theoretical exploration. The first requires sophisticated experimental equipment, the second needs mathematical models to describe phenomena. Both approaches were represented during the workshop, which spanned two days and featured two sessions with a total of 15 presentations, concluding with an open forum discussion. Round table introductions by the participants highlighted the multidisciplinary backgrounds of the attendees:

- Nanoplastics, Microplastics
- Fiber Technology
- Powder Technology
- Separation Technology
- Sensor Technology
- Aerosol Sciences
- Instrument Development
- Risk Assessment
- Political Sciences
- Toxicology / Ecotoxicology
- Environmental Health

16. Workshop Summary and Conclusions

- Surface Sciences
- Food sciences
- Genomics
- Non-Governmental Organisation
- Analytical Chemistry

To understand the behavior, transport, fate and therefore potential impacts of SNMFs in both the external environment and internal environment of the body, it is important to first understand fiber dynamics. In atmospheric and aquatic environments, the dynamic behavior of SNMFs will be heavily influenced by both particle properties and external forces. To add an extra layer of complexity, flexible SNMFs can rotate in a fluid stream and change shape, which also need to be accounted for when modelling fiber dynamics. The behavior of flexible (plastic) fibers in viscous fluid and at the interfacial region (between water or lung surfactant and air) is more complex than rigid fibers, but can be modelled using modern techniques such as computational fluid dynamics, the Lattice Boltzmann approach and viscoelastic models for deformable bodies. Ultimately, this knowledge can be exploited to improve filter capture efficiency to reduce exposures. Results from recent work by workshop participants informed a conclusion that is interesting but concerning: compared to spherical particles, fibers are more difficult to remove from a stream of viscous fluid and, moreover, rigidity is a key parameter whereby the more flexible the fiber, the harder to separate. Therefore, **for better protection against fibers in water and air, new filters or sophisticated separation systems should be designed to replace old systems, which were designed for the separation of spherical particles and therefore may not work efficiently against flexible fibers.** Here, fiber technology can contribute to the solution; NF) fabricated via melt blowing, electrospinning, centrifugal spinning or solution blow spinning are being applied to advanced filtration systems. This has broad-reaching applications, from personal protective equipment (mask, respirators) to municipal and industrial wastewater treatment plants (WWTPs).

Wastewater is perceived as one of the main pathways for synthetic MFs to enter the environment. WWTPs remove synthetic MFs from influent with up to 72% efficiency, incorporating them into sludge. In many countries, sludge is then applied to agricultural land. The proportion of synthetic MFs which evades capture at WWTPs enters the wider environment via waterways, contaminating rivers and canals and forming the majority of microplastics. **WWTPs therefore present a vehicle for entry to both aquatic and terrestrial environments.** It was concluded that, whilst the above NF technology can contribute toward an end-of-pipe-solution, rethinking the use of plastic for a circular economy should take precedence. This should involve removal or simply using less plastic susceptible to degradation; an important challenge is to utilise chemical engineering and fiber technology to design smarter fibers in global systems. Synthetic fiber emissions result from design choices and there may be a need for implementing new policy to enforce and/or regulate this.

In addition to reducing the use of synthetic fibers in our economy, SNMFs in water and the atmosphere should be comprehensively characterised and monitored, with focus on fiber morphology and size. However, this is inhibited by methodological challenges. To characterize fibers, a variety of sophisticated measurement techniques and apparatus can be used, generating different information including surface area, composition, size/size distribution, crystallinity, shape and/or aspect ratio. Depending on the instrument, these can analyse particles down to tens of nanometers. However, all these methods require a degree of sample preparation and **there is not a 'one-fits-all' technological approach.** For example, scanning electron microscopy (SEM) coupled to energy dispersive spectroscopy (EDS) can analyze size and structural data as well as coarse chemical composition, but is time intensive and cannot discriminate between carbon-based particles. There are online solutions for measuring fibers directly in aerosols. The differing dynamics of fibers compared to spherical particles can be exploited using a DMA (Differential Mobility Analyzer). However, only conductive particles can be analyzed using a DMA; the applicability to environmental SNMFs needs testing. Additionally, it does not provide real-time data on composition, although DMA systems can be made using 3D-printer technology, substantially reducing resource costs. This could lead to the implementation of 3D-printed instruments that can be mass produced, of a portable size enabling in situ measurements. In certain applications it is also possible to use this for submersed particles (aqueous dispersions) and DMA presents a promising avenue for

future fiber monitoring. It was concluded that **for the field to progress, especially by way of exposure assessment, an online approach which can provide concentration, size distribution and compositional data is needed.**

In the environment, synthetic MFs join other plastic particles (measuring < 5 mm) to form a pollutant class known as microplastic. The ubiquity of microplastic particles in the environment combined with their large surface area has raised concern for biota. Microplastic particles have been recovered from biota collected in situ, including mussels; freshwater varieties contained three orders of magnitude more microplastic than marine. Shrimp have also been found to contain microplastic, the majority of which were fibers. Measuring microplastic content in biota presents a snapshot in time but the bioavailability and therefore accumulation potential of microplastic particles is important for predicting effects. Two photon laser tracking of gold nanoparticles and macrophage tracking provide alternative approaches for assessing translocation and, in zebrafish, suggest **most particles, including rods akin to fibers, reach the pancreas.** Microplastic particles present both **particle and chemical stressors**; styrene monomers and aliphatic hydrocarbons leached from test microplastics during a sea urchin embryo toxicity screen. Chronic exposure experiments using juvenile oysters observed mortality at the highest concentrations and modelling studies predict that current microplastic concentrations in the North Sea are affecting ecosystem productivity. Presently, the impacts of SNMFs on organisms are less understood in comparison to spherical particles. It was concluded that **there is a need to generate quality data on SNMF toxicity from chronic experiments** in aquatic biota.

To understand the **risk** SNMFs pose to humans, one must characterize and quantify both **exposure and hazard.** Humans are exposed to particles via three main routes: Inhalation, ingestion and skin contact. In order to fully quantify intake, improved methods and standardization are required. The route investigated most comprehensively is inhalation, driven by the potential risks of occupational exposure to respirable mineral-based fibers. In order to further understand exposure and toxicity, it is important to define fiber dynamics in the internal environment of the respiratory tract, inferred by deposition. There is a lack of experimental data on fiber deposition in the respiratory tract of human subjects, however, experiments have been performed on casts of human respiratory tracts. Using human nasal casts made from MRI scan data, and aerosolized carbon and asbestos fibers, it was concluded that **fibers can more easily penetrate the nose than spherical particles**, just as is the case in a filter system (high aspect ratio dependency), **and can penetrate into deeper parts of the respiratory tract.**

Aside from exposure at the point of contact (lung, gastrointestinal tract (GIT) and skin), exposure could also occur away from these sites should translocation and redistribution of SNMFs occur. A variety of imaging and analytical methods have been developed to study nanoparticles after uptake into organs and tissues at the cellular and subcellular levels, which are applicable to SNMFs. High Resolution Analytical Scanning Transmission Electron Microscopy (HRSTEM) has the unique ability to image local cellular environments adjacent to translocated nanoparticles and -fibers at near atomic resolution. Energy dispersive spectroscopy (EDS) and electron energy loss spectroscopy (EELS) can be used to determine particle location, translocation, potential reformation or bioprocessing, ion dispersion from particle solution inside cells and *in vivo* synthesis of second-generation nanoparticles. This can provide an in-depth qualitative understanding of tissue-particle interactions and effects that are caused by the environmental “invader” nano-objects. In all those techniques, sample preparation is critical in obtaining meaningful data that can be compared, which means that **working with fibers are more difficult than work with spherical particles.** There is another critical aspect; the costs of the instruments mentioned are very high. Therefore, their availability, especially in developing countries, is limited.

Following exposure, toxicity can arise. The presence of high aspect ratio materials in the lung are known to lead to inflammatory responses. Long NFs can cause frustrated phagocytosis. Fibers that are shorter than the typical diameter of an alveolar macrophage may become internalized, while longer fibers may damage the macrophage due to partial internalisation leading to cell leakage and inflammatory responses. There are no studies on the whether SNMFs cause frustrated phagocytosis. Here, biopersistence is an important parameter; high aspect low-durability particles will shorten in the lung, leading to effective phagocytosis and macrophage clearance. Synthetic fibers comprised of polypropylene, polyethylene and polycarbonate show no signs of deterioration in simulated lung fluid and are considered persistent. However, para-aramid fibers, another synthetic polymer, are classified as low-risk due to their

16. Workshop Summary and Conclusions

degradation into smaller pieces in the lung milieu *in vivo*, leading to macrophage clearance, similar to chrysotile fibers.

The critical length for pleural macrophages is 5 microns while fibers of ~15-25 microns will become part of alveolar macrophages. Ongoing studies show that the length of multiwalled carbon nanotubes (MCNTs) is related to the incidence of cancer development in treated mice. Therefore, it is critically important to distinguish regions of short, medium and long dimensions of MCNTs. One can conclude that there is an empirical 40 nm fiber length region that represents the transition from “safe” to “non-safe”. Additionally, flexible fibers with biopersistent and high aspect ratio properties have been classified as a low risk to humans. Hence rigidity (or flexibility) - a previously overlooked factor – should be incorporated in the fiber toxicology structure-activity paradigm (in addition to biopersistence and dimensions) and future human health hazard assessments on SNMFs. This may be particularly applicable to SNMFs. The toxicity of some fibers in the lung is unquestionable but there is a **lack of data and experiments on SNMF**.

Efforts to reduce exposure to SNMFs in the environment should be adopted as a cautious, preventative approach whilst we fill the experimental data gaps over the coming years. As mentioned at the start, modelling flexible fiber dynamics is a complex but necessary exercise for understanding deposition and therefore filtration efficiency. Filtration efficiency is greatest for spherical particles, and lowest for flexible fibers, with rigid fibers in between. **Understanding the minutiae details of the local dynamics will aid future filter design**, improving filtration efficiency for SNMFs in air and water. Other future technological advances could focus on minimising SNMF release to the environment, such as WWTP improvements including fiber alignment using microfluidics and nano-coagulation. This must be executed in parallel to efforts to implement a circular plastic economy.

During the final roundtable session at the end of the workshop it was apparent that synthetic (plastic) MFs, and potentially NFs, in air and water are of increasing concern and a challenge for scientists all over the world. **Only through cooperation with other specialists, sometimes from distant fields of science, can we better improve our understanding** of the dangers we face, or lack thereof. This will enable the introduction of countermeasures, such as advance filtration systems, which will contribute to protecting human health and maintaining ecosystem health. This workshop in Leeuwarden was a step in the right direction.

- Aerosol, 41
- Air liquid interface, 5
- Analytical methods, 37, 157
- Aquatic biota, 111
- Aquatic environment, 111
- Aquatic organisms, 111

- Centrifugal spinning, 19
- Characterization, 41
- Classification, 41

- Deep bed filtration, 211
- Deformable particles, 211
- Deposition, 5
- Dermal, 175

- Electrospinning, 19
- Environment, 3
- Exposure, 55, 147, 175

- Fiber, 55
- Fiber particle, 5
- Fiber toxicology, 201
- Fibers, 3, 81
- Fibrous particles, 211
- Filtration, 227
- Flexible particle, 5
- Fractal-like, 211

- Hazard, 55
- Health effects, 157
- House dust, 35
- HRSTEM, 157

- Inhalation, 175

- Lattice-Boltzmann, 211

- Marine, 111
- Measurement parameter, 37
- Measurement principle, 37
- Measurement range, 37
- Microfibers, 19
- Microplastics, 3, 111
- Mitigation of emissions, 35
- Morphology, 41

- Nanofibers, 19
- Nanoparticles, 157
- Nanowires, 147
- Nasal airway, 81
- Nylon flock, 201

- Occupational health, 201
- On-line measurement, 41
- Oral, 175
- Oral airway, 81
- Organisms, 147

- Plastic soup, 3
- Plasticene, 3
- Preparation, 37

- Removal, 227
- Respiratory deposition, 81
- Rigidity, 55
- Risk banding scheme, 55

- Separation at source, 227
- Solution blow spinning, 19
- Synthetic fiber, 201
- Synthetic fibers, 175

- Technology, 227
- Textiles, 35

Index

Tissue, 157

Toxicity, 147

Tracheobronchial Airways, 81

Transport, 5

Waste water treatment, 227

Wastewater treatment plants, 35

Water sector, 35

Zebrafish, 147

Authors (1): Maria Westerbos, **(2)** Arkadiusz Moskal, Tomasz R. Sosnowski, **(3)** Michał Wojasiński, Tomasz Ciach, **(4)** Heather A. Leslie, Ed. R. Martijn Wagterveld, **(5)** Louk Peffer, R. Martijn Wagterveld, Jan. C.M. Marijnissen, **(6)** George Biskos, Jan C.M. Marijnissen, **(7)** Dirk Broßell, Asmus Meyer-Plath, Kerstin Kämpf, Sabine Plitzko, Wendel Wohlleben, Burkhard Stahlmecke, Martin Wiemann, Andrea Haase, **(8)** Yung Sung Cheng, Wei-Chung Su, Yue Zhou, **(9)** A. Dick Vethaak, C. Martínez-Gómez, **(10)** Martina G. Vijver, Willie Peijnenburg, Fazel Abdolahpur Monikh, **(11)** Uschi M. Graham, Günter Oberdörster, **(12)** Ingeborg M. Kooter, Heleen Lanters, Wilma Middel, Harrie Buist, **(13)** Stephanie Wright, **(14)** Rafał Przekop, Leon Gradoń, **(15)** R. Martijn Wagterveld, Inez J.T. Dinkla, **(16)** Stephanie Wright, Uschi M. Graham, Arkadiusz Moskal

Abstract: Global production of fibrous material is significantly growing reaching an expected 145 million metric tons in 2030. Fiber production includes mostly synthetic polymers, cotton and man-made cellulose (viscose). The main uses are in clothing, household and furnishing, industrial construction, automotive and other.

Increasing consumption of fabric material causes the accumulation of single fibers into the natural environment. Significant numbers are discharged via wastewater from washing clothes, deposition from atmosphere or by other ways of transport. Fibers are now the most prevalent type of anthropogenic particles found by microplastic pollution surveys around the world. Substantial fiber concentrations are found in surface water, deep-sea and fresh water ecosystems. Consequently, fibers are present in food, drinking water, human lungs and digestive tracts of aquatic animals. Currently, there is great concern for the release of plastic nano- and micro fibers and microparticles (microplastics) to the natural environment for which nobody knows, so far, the ultimate consequences for health and ecological homeostasis.

The potential risk introduced by the presence of fibers in the environment induces significant interest. These challenges were the source of inspiration for organizing our workshop. A group of scientists from different parts of the world met on Nov 4/5 2019 at Wetsus, European Centre of Excellence for Sustainable Water Technology in Leeuwarden, The Netherlands, to discuss all known aspects of synthetic nano- and microfibers. This included morphology, physicochemical properties, production and origin of nano/micro fibers entering the atmosphere, water and food chain; the potential consequences of inhalation and ingestion for human health; exposure and ingress via life cycle for aquatic biota; analytical and measurement methods; techniques to clean air and water, and protection means against inhalation or other ways to enter the human body.

